Université de Strasbourg

UNIVERSITÉ DE STRASBOURG

École Doctorale des Sciences de la Vie et de la Santé STRASBOURG

ÉCOLE DOCTORALE DES SCIENCES DE LA VIE ET DE LA SANTÉ

Institut de Génétique et de Biologie Moléculaire et Cellulaire

Thèse présentée par :

Julian OBID

soutenue le : **22 juin 2026**

pour obtenir le grade de : **Docteur de l'université de Strasbourg**

Discipline/ Spécialité : Sciences de la Vie et de la Santé

Targeting transcriptional addiction and DNA repair in cancer: From super-enhancer inhibition to synthetic lethality

THÈSE dirigée par :

M. COIN Frédéric	Directeur de recherche CNRS, IGBMC, Illkirch

RAPPORTEURS :

Mme. CHARAFE-JAUFFRET Emmanuelle	PU-PH, Aix-Marseille Université, CRCM, Marseille
M. BALLOTTI Robert	Directeur de recherche INSERM, C3M, Nice

AUTRES MEMBRES DU JURY :

Mme. DANTZER Françoise	Directrice de recherche CNRS, ESBS, Illkirch

---

MEMBRES INVITÉS :

Mme. CHAN Susan	Directrice de recherche CNRS, IGBMC, Illkirch
M. WEBER Michaël	Directeur de recherche CNRS, ESBS, Illkirch

“When you have eliminated the impossible, whatever remains, however improbable, must be the truth.”

- Sherlock Holmes

“You look at science, or at least talk of it, as some sort of demoralizing invention of man, something apart from real life, and which must be cautiously guarded and kept separate from everyday existence. But science and everyday life cannot and should not be separated.”

- Rosalind Franklin

“The scientist is not a person who gives the right answers, he is one who asks the right questions.”

- Claude Lévi-Strauss

“Tu sais, je ne pense pas que tu sois bête, mais tu ne travailles pas assez.”
“You know, I do not think you are stupid, but you do not work hard enough.”

- Jean-Marc Egly, to me, on Christmas Day,
25 December 2023, while I was working alone in the lab

Table of contents:

Acknowledgments: **4**

Publications and oral communications: **7**

Résumé en français: **9**

List of abbreviations: **16**

List of figures: **22**

Introduction **28**

I- Cancer biology and therapeutic challenges: **30**

a. Hallmarks of cancer driven by transcriptional plasticity and genomic instability ... 30

i. Sustaining proliferative signaling 32

ii. Genome instability and mutations 34

iii. Non-mutational epigenetic reprogramming 36

iv. Phenotype plasticity: Enabling invasion and therapy resistance 40

b. Conventional cancer therapies: historical foundations and limitations 44

II- Gene expression and transcriptional dysregulations in cancer: **48**

a. Gene expression regulation in normal cells 48

i. Chromatin organization and regulatory architecture 48

ii. The multi-steps process of transcription: from initiation to termination 54

b. Gene expression dysregulation in cancer 58

i. Deregulation of trans-acting transcriptional regulators 60

ii. Deregulation of cis-regulatory architecture: emergence of super-enhancers and transcriptional condensates 66

c. Targeting transcriptional addiction in cancer: current strategies and limitations 74

III- DNA damage and repair pathways in cancer: **84**

a. Sources of DNA damage and major DNA repair pathways 86

b. Double-strand break repair and the role of homologous recombination in cancer .. 92

c. Synthetic lethality and therapeutic targeting of homologous recombination deficiency in cancer 100

i. PARP inhibitors: discovery and clinical development 100

ii. Molecular mechanisms of PARP inhibitor cytotoxicity 106

iii. Resistance mechanisms to PARP inhibitors 112

iv. BRCAness: expanding PARPi utility beyond BRCA mutations 118

IV- Synthetic ecteinascidins: DNA-binding transcriptional inhibitors as promising anti-cancer agents: **128**

a. Ecteinascidins: from natural compounds to clinically relevant synthetic derivatives.. ……128
b. Transcription-dependent mechanisms of action of synthetic ecteinascidins..... 132
V- Cutaneous melanoma: a powerful model of transcriptional addiction and plasticity: 138
a. Epidemiology, risk factors, and clinical classification of cutaneous melanoma.... 140
b. Currently approved treatments for cutaneous melanoma..... 148
c. Therapeutic resistance to targeted therapy and immune checkpoint inhibitors 154
d. Phenotype switching as a transcription-driven mechanism of resistance and invasion ……162
Results 174
Part I: Targeting super-enhancer-driven transcriptional addiction in melanoma 176
Preface to Article 1: 177
Article 1 – Pan-inhibition of super-enhancer-driven oncogenic transcription by next-generation synthetic ecteinascidins yields potent anti-cancer activity..... 178
Part II: Induction of BRCAness-like state through transcription elongation inhibition 230
Preface to Article 2: 231
Article 2 – Ecteinascidin-induced transcription elongation defects trigger a BRCAness-like state and sensitize HR-proficient tumors to PARP inhibitors..... 232
General discussion..... 297
Annexes 307
Preface to annexed Articles 3, 4, and 5:..... 309
Article 3 – Les Ecteinascidines: Quand la pharmacologie marine cible la dépendance transcriptionnelle du cancer 310
Article 4 – Super-enhancer-driven expression of BAHCC1 promotes melanoma cell proliferation and genome stability..... 314
Article 5 – Cancer cell transcriptional landscape primes the development of resistance to synthetic ecteinascidins 358
References 411

Acknowledgments:

Wow, it has been a very long ride. When I look back on the past few years, I feel that I sacrificed a large part of my twenties in the lab: planning experiments, analyzing results, reading articles, and melting my brain trying to understand cancer out of curiosity, while most people my age were enjoying their youth, travelling, partying, and making the most of it. I have to say, though, that it was a lot of fun, and most importantly, it paid off. All of this, however, would not have been possible without the important people who surrounded me throughout this journey, and to whom I am deeply thankful.

First of all, I would like to thank the members of my PhD committee, Dr. Emmanuelle Charafe-Jauffret, Dr. Robert Ballotti, Dr. Françoise Dantzer, Dr. Michaël Weber, and Dr. Susan Chan, for taking the time to evaluate this work.

In the lab, I have to start with my supervisor, Frédéric, who welcomed me into his lab for my Master's internship and then gave me the honor of pursuing a PhD. When I first joined, I was still a young student, full of motivation, but lacking confidence. I often tell myself that without the trust you placed in me, I would never have gained the self-confidence I have today, which allowed me to do science without fear. Thank you for trusting me from day one, for giving me the complete freedom to build projects from scratch and pursue my ideas without limitations, and for providing endless support, even when I was looking for postdoctoral opportunities in the USA. I will always be grateful for that.

When speaking about supervision, I cannot forget to mention Max Cigrang, who mentored me during my Master's internship and became my partner in crime during my PhD. Thank you for teaching me all about how to think and work in the lab. Scientifically, I am who I am today thanks to your guidance. It was an honor to co-lead two wonderful projects with you, and to share so many stimulating scientific discussions. I hope that life will give us the opportunity to work together again in the future.

In addition to Max, I must also express my sincere gratitude to our lab engineer, Maguelone Nogaret, who has been a tremendous help and never refused to share her precious technical expertise whenever I needed support with my experiments. This work would never have advanced so quickly, and perhaps would not have been possible at all, without you. You are an equal player in this success. Thank you.

I also have to thank Clara Capelli, whom I had the pleasure of supervising during her Master's internship, and who has now become a PhD student leading her own project. Beyond all the great movies we watched together at the cinema (although, to be fair, a few of them were terrible), thank you for your important help with the BRCAness project, and for always correcting my choice of statistical tests (I hope I can do that on my own now). I also want to thank Anthony Hannus, with whom I always had the most amazing scientific discussions, and with whom we built a project from scratch on SWI/SNF in melanoma, which he is now leading in the best possible way. I hope to see you joining Dana-Farber at the end of your PhD, so that we can continue working together as postdocs and, most importantly, continue taking endless coffee breaks.

I would also like to thank all the current and former members of the lab, especially Philippe Catez, for his scientific advice and all the funny discussions we had every morning, as well as Léane Seno, with whom I started my Master's internship and then made it into a PhD. Thank you for always being available to talk about science or life in general, and for the wonderful barbecue nights you organized for us every summer.

Furthermore, I think I owe a big part of my success to all the cups of coffee I had to drink over the past few years to stay awake. With that in mind, I will never forget the people who shared these coffee moments with me: the "team café" – Alexandre, Antonin, Julie, Anthony, and Maxime. Thank you for all the funny discussions that made it possible to disconnect a little from work, and for reminding me that it is also possible to have fun in the lab. I hope that one day we will be able to reunite and laugh together again, somewhere other than the couch on the fourth floor of the IGBMC.

Beyond the lab, I would like to thank everyone else who was involved in my academic journey, starting with all the amazing professors I had at university, the wonderful people from the IGBMC platforms without whom this work would not have been possible, with a special mention to Guillaume Davidson and Tao Ye for their help with the bioinformatic analyses. Lastly, I would like to thank the science educators on YouTube; Ahmed El-Ghandour, Hank Green, Derek Muller, Cleo Abram, Michael Stevens, and Neil deGrasse Tyson, who inspired me to get into research in the first place, and who continue to inspire me today.

Outside the institute, I am the luckiest person in the world to be surrounded by wonderful people who always supported me and kept me from going crazy during this intense period. First of all, I have to mention my great old friends, Joffrey, Clément, and Pierre, whom I met during my

studies in Reims, and with whom I managed to keep a strong friendship throughout the years. I also want to thank the amazing group of friends I made during my Master's: Maxime, Léa, Elsa, Morgane, Jade, Joffrey, Valentina, and Mégane. Thank you for all the wonderful nights, fun parties, and beautiful trips we shared together. I had some of the best moments of my life with you.

Finally, I cannot imagine being where I am today without my family. To my aunt Regina, who has always been like a second mother to me; to my two brothers, Jeries and Majd; and to my brother's wife, Hanady: thank you for always being by my side and for supporting me endlessly.

Above all, and most importantly, to my Mom and Dad… I have thought a lot about what I could possibly say to you, and I have reached the conclusion that no matter what I write, words will never be enough to thank you for everything you have done for me, from the day I was born until today. You have always supported me in my good times and protected me in my bad times. You always believed in me, and you made me understand that the sky was the limit.

All of this – the person I am today, succeeding in my studies, pursuing a PhD, publishing articles, and soon starting my postdoctoral journey at Harvard, would never have been possible without you. Not even close. So, although I can never thank you enough, all I can say is this: this is for you. My success is your success. I could never have asked for better parents.

I love you so much. بحبكو كثير!

Publications and oral communications:

Published articles:

[1] Max Cigrang*, **Julian Obid***, Maguelone Nogaret, Léane Seno, Tao Ye, Guillaume Davidson, Philippe Catez, Pietro Berico, Clara Capelli, Clara Marechal, Amélie Zachayus, Clémence Elly, Tsai Kun Li, Emanuel Compe, Pablo Avilés, Irwin Davidson, Jean-Marc Egly, Carmen Cuevas and Frédéric Coin (2025). **Pan-inhibition of super-enhancer-driven oncogenic transcription by next-generation synthetic ecteinascidins yields potent anti-cancer activity.** *Nat Commun* 16, 512. https://doi.org/10.1038/s41467-024-55667-z
* Co-first author

[2] Pietro Berico, Maguelone Nogaret, Max Cigrang, Antonin Lallement, Fatemeh Vand-Rajabpour, Amanda Florst-Yanke, Giovanni Gambi, Guillaume Davidson, Léane Seno, **Julian Obid**, Bujamin Vokshi, Stephanie Le Gras, Gabrielle Megnus, Tao Ye, Carlos Fernandez Codero, Mélanie Dalmasso, Emmanuel Compe, Corine Bertolotto, Eva Hernando, Irwin Davidson, Frédéric Coin (2023). **Super-enhancer-driven expression of BAHCC1 promotes melanoma cell proliferation and genome stability.** *Cell Reports* 42. https://doi.org/10.1016/j.celrep.2023.113363

[3] Max Cigrang, **Julian Obid**, Frédéric Coin (2025). **Les ecteinascidines – Quand la pharmacologie marine cible la dépendance transcriptionnelle du cancer.** *Med Sci (Paris)* 41, 10. https://doi.org/10.1051/medsci/2025155

Articles in preparation:

[1] **Julian Obid***, Max Cigrang*, Clara Capelli, Anthony Hannus, Tao Ye, Guillaume Davidson, Frédéric Coin. **Ecteinascidin-induced transcription elongation defects trigger BRCAness and sensitize HR-proficient tumors to PARP Inhibitors.**
* Co-first author

[2] Clara Marechal, **Julian Obid**, Philippe Catez, Maguelone Nogaret, Clara Capelli, Max Cigrang, Frédéric Coin. **Cancer cell transcriptional landscape primes the development of resistance to synthetic ecteinascidins.**

Presentations at international conferences:

[1] Poster – **Julian Obid**, Max Cigrang, Maguelone Nogaret, Frédéric Coin. **Targeting phenotype plasticity in melanoma with the transcriptional inhibitor LD2.** *2nd Edition of Tumor Heterogeneity, Plasticity, and Therapy* (2023, Leuven, Belgium).

[2] Poster – **Julian Obid**, Max Cigrang, Maguelone Nogaret, Frédéric Coin. **Targeting super-enhancer-driven oncogenic transcription in melanoma with a novel synthetic ecteinascidin.** *Annual Congress of the European Association for Cancer Research (EACR)* (2024, Rotterdam, Netherlands).

[3] Poster – **Julian Obid**, Max Cigrang, Maguelone Nogaret, Frédéric Coin. **Pan-inhibition of super-enhancer-driven oncogenic transcription by novel synthetic ecteinascidins yields potent anti-cancer activity.** *Annual Meeting of the American Association for Cancer Research (AACR)* (2025, Chicago, USA).

[4] Poster – **Julian Obid**, Max Cigrang, Maguelone Nogaret, Frédéric Coin. **Pan-inhibition of super-enhancer-driven oncogenic transcription by novel synthetic ecteinascidins yields potent anti-cancer activity.** *Keystone Symposia on Epigenetics and Gene Regulation* (2026, Geneva, Switzerland).

Résumé en français:

Le cancer est une maladie complexe caractérisée par l'accumulation progressive d'altérations génétiques, épigénétiques et transcriptionnelles permettant aux cellules tumorales de proliférer, d'échapper aux mécanismes de contrôle physiologiques, d'envahir les tissus et de résister aux traitements. Malgré les progrès considérables réalisés au cours des dernières décennies, notamment avec le développement des thérapies ciblées et de l'immunothérapie, l'émergence de résistances reste l'un des principaux obstacles à l'efficacité durable des traitements anticancéreux. Cette résistance repose en grande partie sur la capacité des cellules tumorales à s'adapter à la pression thérapeutique, soit par sélection de clones génétiquement résistants, soit par reprogrammation transcriptionnelle et phénotypique réversible. Ainsi, au-delà des mutations oncogéniques elles-mêmes, les programmes d'expression génique qui maintiennent les états cellulaires tumoraux représentent aujourd'hui des vulnérabilités thérapeutiques majeures.

Dans ce contexte, le concept d'addiction transcriptionnelle a émergé pour décrire la dépendance particulière des cellules cancéreuses à une activité transcriptionnelle élevée de gènes essentiels à leur prolifération, leur survie ou leur identité cellulaire. Cette addiction est fréquemment soutenue par des régions régulatrices appelées super-enhancers (super-amplificateurs). Ces derniers correspondent à de larges domaines enrichis en facteurs de transcription, coactivateurs et marques chromatiniennes actives, capables de soutenir l'expression très élevée d'oncogènes ou de facteurs d'identité cellulaire. Les super-enhancers jouent ainsi un rôle central dans de nombreux cancers, en maintenant des programmes transcriptionnels oncogéniques et en contribuant à la plasticité phénotypique. Leur activité dépend de régulateurs transcriptionnels tels que BRD4, CDK7, CDK12, EP300 ou le complexe Médiateur, qui peuvent s'accumuler localement sous forme de condensats transcriptionnels. Cette organisation permet de concentrer la machinerie transcriptionnelle autour des gènes critiques pour les cellules tumorales, mais rend également ces programmes particulièrement sensibles à certaines perturbations transcriptionnelles.

Le mélanome cutané constitue un modèle particulièrement pertinent pour étudier cette dépendance transcriptionnelle. Bien que les inhibiteurs de la voie MAPK et les inhibiteurs de points de contrôle immunitaire aient profondément amélioré la prise en charge de cette maladie, une proportion importante de patients ne répond pas aux traitements ou développe une résistance. Cette résistance est favorisée par la grande plasticité des cellules de mélanome, capables de basculer entre différents états transcriptionnels. Les cellules mélanocytaires

différenciées expriment fortement des facteurs d'identité tels que MITF et SOX10, alors que les cellules mésenchymateuses ou dédifférenciées expriment davantage des gènes associés à l'invasion, à la survie et à la résistance thérapeutique, tels que AXL, EGFR ou des facteurs AP-1/TEAD. Ces états cellulaires reposent sur des programmes transcriptionnels distincts, souvent associés à des super-enhancers spécifiques. Il existe donc un besoin important d'identifier des stratégies capables de cibler simultanément ces différents programmes transcriptionnels, indépendamment de l'état phénotypique ou du statut mutationnel des cellules tumorales.

Parallèlement à ces altérations transcriptionnelles, les cellules cancéreuses présentent fréquemment des défauts ou des dépendances particulières vis-à-vis des mécanismes de réparation de l'ADN. L'instabilité génomique est une caractéristique majeure des cancers, mais elle peut également constituer une vulnérabilité thérapeutique. L'exemple le plus marquant est celui des inhibiteurs de PARP, qui exploitent un principe de létalité synthétique dans les tumeurs déficientes pour la recombinaison homologue, notamment celles portant des mutations de BRCA1 ou BRCA2. Dans ces cellules, l'inhibition de PARP entraîne l'accumulation de lésions non réparées, des défauts de réplication et finalement la mort cellulaire. Cependant, l'utilisation clinique des inhibiteurs de PARP reste limitée à une fraction restreinte de patients, principalement ceux présentant des altérations génétiques de la recombinaison homologue. De plus, des résistances aux inhibiteurs de PARP apparaissent fréquemment. Une stratégie prometteuse consiste donc à induire pharmacologiquement un état de « BRCAness », c'est-à-dire une déficience fonctionnelle de la recombinaison homologue en l'absence de mutation de BRCA1/2, afin d'étendre l'efficacité des inhibiteurs de PARP à des cancers initialement compétents pour cette voie de réparation.

Cette thèse s'inscrit à l'interface entre ces deux axes : l'addiction transcriptionnelle et la réparation de l'ADN. L'objectif général de mon travail a été d'étudier les effets anticancéreux d'une classe particulière d'inhibiteurs transcriptionnels d'origine marine, les ecteinascidines synthétiques, et d'évaluer leur capacité à cibler à la fois les programmes transcriptionnels oncogéniques dépendants des super-enhancers et les voies de réparation de l'ADN. Les ecteinascidines, dont la trabectédine et la lurbinectédine sont les membres les mieux caractérisés, sont des molécules capables de se lier de manière covalente à l'ADN et d'interférer avec la transcription. La lurbinectédine est déjà approuvée pour le traitement du cancer du poumon à petites cellules en rechute, ce qui rend cette famille de molécules particulièrement intéressante d'un point de vue translationnel. Au cours de cette thèse, j'ai étudié plusieurs

ecteinascidines synthétiques, notamment la lurbinectédine, l'écubectédine et PM54, en collaboration avec la société pharmaceutique espagnole PharmaMar.

Le premier axe de ma thèse a porté sur la caractérisation du mécanisme d'action des ecteinascidines synthétiques dans le mélanome, en particulier leur capacité à inhiber les programmes transcriptionnels dépendants des super-enhancers. Ce travail a été publié dans *Nature Communications*, un article sur lequel je suis co-premier auteur, et a permis de montrer que ces molécules exercent une activité anticancéreuse très puissante sur des cellules de mélanome présentant des états phénotypiques distincts. Contrairement aux inhibiteurs ciblant la voie MAPK, dont l'efficacité dépend fortement du statut mutationnel et de l'état cellulaire, les ecteinascidines synthétiques se sont révélées cytotoxiques à des concentrations nanomolaires dans des modèles mélanocytaires et mésenchymateux, y compris dans des cellules résistantes aux thérapies ciblées. Ces effets ont été observés dans des modèles 2D, 3D, ainsi que dans des modèles de xénogreffes murines, où les traitements ont entraîné une inhibition importante de la croissance tumorale.

Afin de comprendre le mécanisme moléculaire sous-jacent, nous avons combiné des approches transcriptomiques, épigénomiques et de cartographie directe de la liaison des molécules au génome. Une partie importante de ma contribution a consisté à mettre en place et optimiser l'approche de Chem-Map, utilisant des dérivés biotinylés des ecteinascidines afin d'identifier leurs sites de liaison à l'échelle du génome. Ces analyses ont montré que les ecteinascidines ne se lient pas de manière aléatoire à l'ADN, mais ciblent préférentiellement des régions de chromatine ouverte riches en CpG, notamment des promoteurs et des enhancers actifs. Les sites de liaison des molécules étaient fortement associés à des marques de transcription active telles que H3K27ac, à l'accessibilité chromatinienne et à la présence de l'ARN polymérase II, mais peu associés à des régions répressives marquées par H3K27me3.

De manière intéressante, les ecteinascidines synthétiques ciblent à la fois des régions communes entre différents états cellulaires et des régions spécifiques de chaque phénotype. Ainsi, dans les cellules mélanocytaires, elles se lient aux régions régulatrices de gènes tels que MITF ou SOX10, alors que dans les cellules mésenchymateuses elles ciblent davantage des gènes associés à l'état invasif ou résistant. Cependant, au-delà de ces programmes spécifiques, les ecteinascidines inhibent également l'expression de régulateurs transcriptionnels plus ubiquitaires, tels que BRD4, CDK7, CDK12, CDK13, EP300 ou certaines sous-unités du complexe Médiateur. Ces facteurs étant nécessaires au maintien des super-enhancers, leur diminution provoque une désorganisation des condensats transcriptionnels et une inhibition

secondaire des oncogènes dépendants des super-enhancers. Ainsi, les ecteinascidines agissent selon un mécanisme en deux niveaux : une liaison directe à des régions actives du génome, et une perturbation indirecte de la machinerie transcriptionnelle qui soutient les programmes oncogéniques.

Ce premier travail a donc permis de proposer les ecteinascidines synthétiques comme une nouvelle classe d'inhibiteurs capables de cibler de manière large les programmes transcriptionnels dépendants des super-enhancers. Cette stratégie se distingue des inhibiteurs classiques de BRD4 ou CDK7 par le fait qu'elle repose sur une interaction directe avec l'ADN au niveau de régions transcriptionnellement actives. Elle permet ainsi d'affecter simultanément plusieurs régulateurs transcriptionnels et plusieurs programmes oncogéniques, ce qui pourrait être particulièrement intéressant dans des tumeurs caractérisées par une forte hétérogénéité transcriptionnelle, comme le mélanome. Ces résultats ont également fourni une base mécanistique expliquant l'efficacité des ecteinascidines dans d'autres cancers transcriptionnellement dépendants, notamment le cancer du poumon à petites cellules.

Le second axe de ma thèse est né de l'observation que, au-delà des oncogènes associés aux super-enhancers, les ecteinascidines répriment de manière récurrente l'expression de nombreux gènes impliqués dans la réparation de l'ADN. Nous avons donc cherché à déterminer si cette répression pouvait induire une déficience fonctionnelle de la recombinaison homologue et sensibiliser des tumeurs initialement compétentes pour cette voie aux inhibiteurs de PARP. Pour cela, nous avons étendu nos analyses à plusieurs modèles de cancers HR-proficients, incluant des cellules de mélanome, de cancer du poumon à petites cellules, de cancer du poumon non à petites cellules, de cancer du sein et de cancer de l'ovaire. Des traitements par la lurbinectédine ou PM54 ont révélé une signature transcriptionnelle commune, caractérisée par la répression coordonnée de gènes impliqués dans la recombinaison homologue et la voie de Fanconi, tels que BRCA1, BRCA2, PALB2, RAD51, BLM, WRN, ATM ou ATR.

Les analyses transcriptomiques et protéiques ont confirmé que cette diminution d'expression ne se limite pas à quelques gènes isolés, mais correspond à une répression plus globale de programmes associés à la réparation des cassures double brin et des pontages interbrins de l'ADN. Ces effets étaient particulièrement marqués pour les gènes de grande taille, suggérant un lien entre la longueur des gènes, la dynamique d'élongation transcriptionnelle et la sensibilité aux ecteinascidines. Des analyses fonctionnelles ont ensuite montré que cette répression s'accompagne d'une diminution de la capacité des cellules à réaliser la recombinaison homologue, indiquant que les ecteinascidines ne provoquent pas uniquement une signature

transcriptionnelle de BRCAness, mais bien un état fonctionnel de déficience en recombinaison homologue.

Sur le plan mécanistique, nous avons montré que les ecteinascidines perturbent principalement l'élongation transcriptionnelle. Le traitement entraîne une diminution rapide de plusieurs facteurs clés de l'élongation, dont CDK7, CDK9, CDK12 et BRD4, accompagnée d'une accumulation de l'ARN polymérase II au niveau des régions promotrices et d'une perte de signal dans les corps des gènes. Les analyses de transcription naissante ont confirmé une diminution de la production d'ARN le long des gènes, compatible avec une baisse de la processivité de l'ARN polymérase II. Ces défauts d'élongation favorisent vraisemblablement des événements de terminaison prématurée, notamment au niveau de sites de polyadénylation introniques, ce qui affecte préférentiellement les gènes longs. Or, de nombreux gènes de la recombinaison homologue et de la voie de Fanconi appartiennent précisément à cette catégorie de gènes longs et fortement dépendants d'une élongation efficace. Ce travail établit ainsi un lien mécanistique entre stress transcriptionnel, architecture génique et vulnérabilité des voies de réparation de l'ADN.

La conséquence thérapeutique majeure de cette induction de BRCAness est la sensibilisation des cellules cancéreuses aux inhibiteurs de PARP. Nous avons montré que des doses sublétales d'ecteinascidines, combinées à des inhibiteurs de PARP tels que l'olaparib ou le talazoparib, entraînent une forte diminution de la viabilité cellulaire dans plusieurs modèles initialement HR-proficients. Cette synergie s'accompagne d'une accumulation importante de dommages à l'ADN, détectée notamment par l'augmentation du signal γH2AX, ainsi que d'une induction de l'apoptose. Il est important de souligner que cette synergie ne doit probablement pas être interprétée comme la simple conséquence d'une répression des gènes de recombinaison homologue. Les ecteinascidines induisent également des lésions de l'ADN au niveau de régions transcriptionnellement actives, et l'inhibition de PARP pourrait empêcher la réparation de ces lésions, amplifiant ainsi l'accumulation de dommages. Le modèle le plus cohérent est donc celui d'un double effet : d'une part, une augmentation de la charge de lésions induite par les ecteinascidines au niveau de la chromatine active ; d'autre part, une diminution de la capacité des cellules à réparer ces lésions en raison d'une répression transcriptionnelle des voies HR/FA. Cette combinaison crée une vulnérabilité létale dans des cellules qui, en condition basale, ne sont pas nécessairement sensibles aux inhibiteurs de PARP.

Un résultat particulièrement important est que cette stratégie semble également capable de restaurer la sensibilité aux inhibiteurs de PARP dans des modèles ayant acquis une résistance.

Dans des cellules BRCA1-mutées rendues résistantes à l'olaparib ou au talazoparib, les ecteinascidines répriment des programmes de recombinaison homologue réactivés et rétablissent une déficience fonctionnelle de réparation, permettant à nouveau une réponse aux inhibiteurs de PARP. Ces résultats suggèrent que les ecteinascidines pourraient non seulement étendre l'utilisation des inhibiteurs de PARP à des tumeurs BRCA-sauvages, mais aussi contribuer à surmonter certaines formes de résistance dans des tumeurs initialement sensibles.

En parallèle de ces deux axes principaux, j'ai contribué à plusieurs projets collaboratifs du laboratoire, présentés en annexes de cette thèse. Le premier correspond à un article de vulgarisation scientifique publié dans médecine/sciences, rédigé à la suite de notre article dans *Nature Communications*, afin de présenter en français les principaux résultats concernant les ecteinascidines et le ciblage de la dépendance transcriptionnelle. Ma contribution à ce travail a principalement porté sur la préparation des figures et la révision du texte. Le second projet, publié dans *Cell Reports*, a identifié BAHCC1 comme un régulateur associé aux super-enhancers, surexprimé dans le mélanome métastatique et impliqué dans la prolifération cellulaire et la réparation de l'ADN. L'inhibition de BAHCC1 perturbe la croissance des cellules de mélanome, retarde la réparation de l'ADN et coopère avec les inhibiteurs de PARP pour induire la mort cellulaire. J'ai contribué à ce travail en réalisant des expériences explorant la synergie entre l'inhibition de BAHCC1 et les inhibiteurs de PARP. Enfin, j'ai également participé à un projet portant sur les mécanismes de résistance aux ecteinascidines. Dans ce travail, nous avons identifié le transporteur d'efflux ABCB1 comme un mécanisme majeur de résistance, associé à une amplification focale et à l'activation de facteurs AP-1/TEAD. Ma contribution a notamment consisté à identifier l'augmentation d'expression d'ABCB1 par RNA-seq, à la valider au niveau protéique, et à montrer fonctionnellement que l'invalidation d'ABCB1 restaure la sensibilité aux ecteinascidines.

En conclusion, les travaux présentés dans cette thèse montrent que les ecteinascidines synthétiques constituent une classe originale d'inhibiteurs transcriptionnels capables de cibler plusieurs vulnérabilités majeures des cellules cancéreuses. D'une part, elles perturbent les programmes oncogéniques dépendants des super-enhancers, permettant de cibler des états tumoraux transcriptionnellement hétérogènes, comme ceux observés dans le mélanome. D'autre part, elles induisent des défauts d'élongation transcriptionnelle qui affectent préférentiellement les longs gènes impliqués dans la recombinaison homologue et la voie de Fanconi, conduisant à un état fonctionnel de BRCAness. Cette double activité permet de relier

directement la perturbation de l'addiction transcriptionnelle à l'exploitation thérapeutique des défauts de réparation de l'ADN.

Ces résultats fournissent une base mécanistique solide pour le développement de combinaisons thérapeutiques associant ecteinascidines et inhibiteurs de PARP. Une telle approche pourrait permettre d'élargir l'utilisation de la létalité synthétique à des cancers actuellement exclus des indications des inhibiteurs de PARP, mais aussi de restaurer la sensibilité dans certains contextes de résistance acquise. Plus largement, cette thèse met en évidence l'importance de considérer la transcription non seulement comme un moteur de l'identité tumorale, mais aussi comme un déterminant majeur de la capacité des cellules cancéreuses à maintenir l'intégrité de leur génome. En ciblant les mécanismes transcriptionnels qui soutiennent à la fois les programmes oncogéniques et les voies de réparation de l'ADN, les ecteinascidines ouvrent ainsi de nouvelles perspectives pour le traitement de cancers transcriptionnellement dépendants et thérapeutiquement résistants.

List of abbreviations:

53BP1 = Tumor suppressor p53-binding protein 1

6-4 PP = 6-4 photoproduct

ABCB1 = ATP-binding cassette sub-family B member 1

ABCG2 = ATP-binding cassette sub-family G member 2

ACTH = Adrenocorticotropic hormone

AMBRA1 = Autophagy and beclin 1 regulator 1

ARID2 = AT-rich interactive domain-containing protein 2

ATM = Ataxia telangiectasia mutated

ATP = Adenosine triphosphate

ATR = Ataxia telangiectasia and Rad3-related protein

BER = Base excision repair

BET = Bromodomain and extraterminal proteins family

BLM = Bloom syndrome protein

BRCA1/2 = Breast cancer gene 1/2

BRD4 = Bromodomain-containing protein 4

CAF = Cancer-associated fibroblast

CBP = CREB-binding protein

CDK = Cyclin-dependent kinase

CDKN2A = Cyclin-dependent kinase inhibitor 2A

Chk1/2 = Checkpoint kinase 1/2

CIN = Chromosomal instability

CPD = Cyclobutane pyrimidine dimers

CpG = Cytosine-phosphate-guanine

CSA/B = Cockayne syndrome group A/B

CSC = Cancer stem cell

CSD = Chronically sun-damaged

CTCF = CCCTC-binding factor

CTD = Carboxy-terminal domain

CtIP = CtBP-interacting protein

CTLA-4 = Cytotoxic T-lymphocyte associated protein 4

DDR = DNA damage response

DDX3X = DEAD-box helicase 3 X-linked

DNA = Deoxyribonucleic acid

DNA-PKcs = DNA-dependent protein kinase catalytic subunit

DNMT = DNA methyltransferase

DSB = Double-strand break

DSBR = Double-strand break repair

DSIIF = DRB sensitivity inducing factor

DTP = Drug-tolerant persister

ecDNA = Extrachromosomal DNA

EGFR = Epidermal growth factor receptor

EMT = Epithelial-to-mesenchymal transition

ERK1/2 = Extracellular signal-regulated kinase ½

EXO1 = Exonuclease 1

FA = Fanconi anemia repair pathway

FAK1 = Focal adhesion kinase 1

FANCD2 = Fanconi anemia group D2

FANCI = Fanconi anemia complementation group I

GATA6 = GATA-binding factor 6

GG-NER = Global genome nucleotide excision repair

GRPR = Gastrin-releasing peptide receptor

GTF = General transcription factor

HAT = Histone acetyltransferase

HER2 = Human epidermal growth factor receptor 2

HGF = Hepatocyte growth factor

HMGB2 = High-mobility group protein B2

HOXA5 = Homeobox A5

HR = Homologous recombination

HRD = Homologous recombination-deficiency

HSP90 = Heat shock protein 90

ICI = Immune checkpoint inhibitors

IDR = Intrinsically disordered regions

IPA = Intronic polyadenylation

IPRES = Innate anti-PD-1 resistance

KMT2D = Histone-lysine N-methyltransferase 2D

LIG4 = DNA ligase IV

LLPS = Liquid-liquid phase separation

MAPK = Mitogen activated protein kinase

MAPKi = Mitogen activated protein kinase inhibitor

MC1R = Melanocortin 1 receptor

MED1/12 = Mediator complex subunit 1/12

MEK = MAPK/ERK Kinase

mESC = Mouse embryonic stem cells

MET = Mesenchymal-to-epithelial transition

MHC-I = Major histocompatibility complex class I

MIC = Metastasis-initiating cells

MITF = Microphthalmia-associated transcription factor

MLH = MutL protein homolog

MMR = Mismatch repair

MRD = Minimal residual disease

MRN = MRE11-RAD50-NBN

mRNA = Messenger RNA

MSH2/6 = MutS homolog 2/6

mTOR = Mammalian target of rapamycin

NCSC = Neural crest stem cell

NELF = Negative elongation factor

NER = Nucleotide excision repair

NGFR = Nerve growth factor receptor

NHEJ = Non-homologous end joining

OCT4 = Octamer-binding transcription factor 4

PALB2 = Partner and localizer of BRCA2

PARG = Poly(ADP-ribose) glycohydrolase

PARP = Poly (ADP-ribose) polymerase

PARPi = Poly (ADP-ribose) polymerase inhibitor

PARylation = Poly(ADP-ribosyl)ation

PAS = Polyadenylation signal

PAX3 = Paired box gene 3

PCNA = Proliferating cell nuclear antigen

PD-1 = Programmed cell death protein 1

PD-L1 = Programmed death ligand 1

PI3K = Phosphoinositide 3-kinase

PIC = Pre-initiation complex

PMEL = Premelanosome protein

POMC = Proopiomelanocortin

PPRX1 = Paired related homeobox 1

PRC2 = Polycomb repressive complex 2

PROTAC = Proteolysis targeting chimera

P-TEFb = Positive transcription elongation factor b

PTEN = Phosphatase and tensin homolog

PTF1 = Pancreas transcription factor-1

RAS = Rat sarcoma viral oncogene homolog

RB = Retinoblastoma protein

REST = RE1-silencing transcription factor

RNA = Ribonucleic acid

RNAPII = RNA polymerase II

ROSE = Ranking order of super-enhancer

RPA = Replication protein A

SE = Super-enhancer

Ser2/5 = Serine 2/5

SOX2/4/10 = SRY-box Transcription Factor 2/4/10

SSB = Single-strand break

SSBR = Single-strand break repair

STAT3 = Signal transducer and activator of transcription 3

SWI/SNF = Switch/sucrose nonfermenting chromatin remodeling complex

TAD = Topologically associating domains

TBP = TATA-box binding protein

TCF4/7 = Transcription factor 4/7

TC-NER = Transcription-coupled nucleotide excision repair

TERT = Telomerase reverse transcriptase

TET = Ten eleven translocation

TF = Transcription factor

TFIIA/B/D/E/F/H = Transcription factor II A/B/D/E/F/H

TGFβ = Transforming growth factor-β

TP53 = Transformation-related protein 53

TSS = Transcription start site

VEGF = Vascular endothelial growth factor

XPB = Xeroderma pigmentosum type B

XPC/D/F/G = Xeroderma pigmentosum complementation group C/D/F/G

XRCC1/4 = X-ray repair cross-complementing 1

XRN2 = 5'-3' Exoribonuclease 2

ZEB = Zinc-finger E-box binding homeobox

αMSH = α-melanocyte stimulating hormone

γH2AX = Phospho-gamma-H2AX

List of figures:

Figure 1. The updated hallmarks of cancer (2022). 31

Figure 2. Regulation of G1/S transition by the CDK4/6-RB-E2F axis. 33

Figure 3. Types of chromosomal instability (CIN). 35

Figure 4. Oncogene-induced replication stress as a driver of genomic instability. 37

Figure 5. Inflammation-driven mutagenesis and tumor initiation. 37

Figure 6. Epigenetic reprogramming in cancer. 39

Figure 7. Frequency of mutations in SWI/SNF chromatin remodeling complex subunits across cancer types. 39

Figure 8. Cellular plasticity: differentiation, dedifferentiation, and transdifferentiation. 41

Figure 9. Epithelial-mesenchymal transition (EMT) and mesenchymal-epithelial transition (MET). 43

Figure 10. Emergence of drug-tolerant persister cells and therapy resistance. 43

Figure 11. Limitations of conventional cancer therapies. 45

Figure 12. Historical development of major cancer therapies. 47

Figure 13. Common mechanisms of therapeutic resistance in cancer. 49

Figure 14. Enhancers as distal regulators of gene expression. 49

Figure 15. Hierarchical organization of chromatin and the 3D genome. 51

Figure 16. Models of enhancer-mediated transcriptional regulation. 53

Figure 17. Distinct promoter architectures and transcription initiation patterns. 55

Figure 18. Regulation of RNA polymerase II initiation, pausing, and elongation. 57

Figure 19. Transcription termination by exonuclease-mediated RNA degradation. 59

Figure 20. Master transcription factors control cell identity and lineage specification. .. 61

Figure 21. Mechanisms of transcription factor dysregulation in cancer. 63

Figure 22. Cohesin- and CTCF-mediated chromatin organization and its alteration in cancer. 65

Figure 23. SWI/SNF chromatin remodeling and its role in regulating gene expression programs. 65

Figure 24. TERT promoter mutations create de novo transcription factor binding sites. 67

Figure 25. Disruption of CTCF-mediated insulation drives oncogene activation. 67

Figure 26. Super-enhancers drive high transcriptional output through clustered regulatory activity. 69

Figure 27. Super-enhancers are defined by large genomic domains and high co-activator occupancy. 69

Figure 28. Mechanisms of super-enhancer formation and hijacking in cancer. 71

Figure 29. Identification of super-enhancers based on signal enrichment and ranking. . 71

Figure 30. Transcriptional condensates at super-enhancers driven by phase separation. 73

Figure 31. Disruption of transcriptional condensates preferentially affects super-enhancer activity. 73

Figure 32. Spatial coupling between super-enhancer condensates and target genes regulates transcriptional bursting. 75

Figure 33. Integration of cis-regulatory elements and trans-acting factors in transcriptional control. 75

Figure 34. Targeting transcription factor activity through nuclear receptor modulation and disruption of protein-protein interactions. 77

Figure 35. Targeted protein degradation using PROTACs. 77

Figure 36. BET inhibition disrupts super-enhancer function and suppresses tumor growth. 79

Figure 37. CDK7 inhibition selectively disrupts super-enhancer-driven transcription. .. 81

Figure 38. Proposed mechanisms underlying super-enhancer sensitivity to transcriptional inhibitors. 83

Figure 39. Overview of DNA damage sources, lesions, and repair pathways. 85

Figure 40. Mechanism of nucleotide excision repair (NER). 87

Figure 41. Mechanisms of base excision repair (BER) and mismatch repair (MMR). 89

Figure 42. Mechanism of single-strand break repair (SSBR). 91

Figure 43. Mechanism of non-homologous end joining (NHEJ). 93

Figure 44. Mechanism of homologous recombination (HR). 95

Figure 45. Cell-cycle and resection-dependent regulation of DSB repair pathway choice. 97

Figure 46. Chromatin context influences DSB repair pathway choice. 97

Figure 47. DNA damage response signaling pathways coordinating DNA repair and cell-cycle checkpoints. 99

Figure 48. Therapeutic targeting of DNA damage response (DDR) signaling pathways. 101

Figure 49. Structural and functional classification of the PARP protein family. 103

Figure 50. Synthetic lethality induced by PARP inhibition in homologous recombination-deficient cells. 105

Figure 51. Summary of FDA-approved PARP inhibitors and their clinical indications. 107

Figure 52. PARP inhibitor cytotoxicity is not solely due to inhibition of single-strand break repair. 108

Figure 53. Differential PARP-trapping potency of PARP inhibitors. 109

Figure 54. Differential PARP1 trapping induced by PARP inhibitors. 109

Figure 55. PARP inhibition alters replication fork dynamics. 111

Figure 56. PARP1 regulates transcription-replication conflicts. 111

Figure 57. Major mechanisms of resistance to PARP inhibitors. 113

Figure 58. Regulation of DNA repair pathway choice by 53BP1. 115

Figure 59. Replication fork stabilization as a mechanism of resistance to PARP inhibitors. 115

Figure 60. PARG loss promotes resistance to PARP inhibitors. 117

Figure 61. Gradual emergence of PARP inhibitor resistance through phenotypic adaptation. 117

Figure 62. Concept of BRCAness and its clinical implications. 119

Figure 63. Regulation of homologous recombination through Fanconi anemia and ATM-dependent pathways. 121

Figure 64. Examples of pharmacological induction of BRCAness through targeting transcription, chromatin regulation, and DNA damage response pathways. 123

Figure 65. CDK12 inhibition induces preferential downregulation of long DNA damage response genes through premature transcriptional termination. 125

Figure 66. BET inhibition impairs homologous recombination through repression of end resection factors. 127

Figure 67. Natural origin and semi-synthetic production of ecteinascidins. 129

Figure 68. Structural comparison of trabectedin and lurbinectedin. 131

Figure 69. Lurbinectedin targets active promoters and induces RNAPII degradation. . 133

Figure 70. Transcription-coupled NER mediates ecteinascidin-induced DNA damage. 135

Figure 71. Integrated mechanism of action of synthetic ecteinascidins. 137

Figure 72. Transcriptional plasticity and phenotypic heterogeneity in melanoma. 139

Figure 73. UV-induced melanogenesis and MITF-dependent transcriptional regulation in melanocytes. ……...…….. 141

Figure 74. UV-induced DNA photolesions and mutagenic consequences. 143

Figure 75. Clinical and molecular distinction between CSD and non-CSD melanomas. 145

Figure 76. ARID2 loss promotes enhancer activation and metastatic transcriptional programs in melanoma. 147

Figure 77. Histopathological progression of melanoma. 149

Figure 78. MAPK pathway activation and targeted inhibition in melanoma. 151

Figure 79. Immune checkpoint inhibition in melanoma. 153

Figure 80. Personalized neoantigen-based vaccination and mRNA-induced anti-tumor immunity in melanoma. 155

Figure 81. Major mechanisms of resistance to MAPK pathway inhibition in melanoma. 157

Figure 82. Selected mechanisms of resistance to immune checkpoint blockade in melanoma. 159

Figure 83. TGF-β-mediated immune evasion in melanoma. 161

Figure 84. Tumor-intrinsic transcriptional programs contribute to resistance to immune checkpoint blockade in melanoma. 161

Figure 85. Melanosome-mediated immune evasion through decoy MHC-I presentation. 163

Figure 86. Transcriptional plasticity and phenotype switching in melanoma. 165

Figure 87. Transcriptional states and hierarchical organization of melanoma cell plasticity. 167

Figure 88. Therapy-induced transcriptional reprogramming and selection of resistant melanoma cell states. 167

Figure 89. TCF4-driven dedifferentiation and resistance to immune checkpoint blockade in melanoma. 169

Figure 90. Microenvironmental control of melanoma phenotype switching. 171

Introduction

I- Cancer biology and therapeutic challenges:

a. Hallmarks of cancer driven by transcriptional plasticity and genomic instability

Cancer is the second leading cause of death worldwide, accounting for an estimated 20 million new cancer cases and 9.7 million deaths in 2022, according to World Health Organization data. Despite substantial advances in our understanding of cancer etiology, improvements in prevention strategies, and the development of sophisticated therapeutic options, both cancer incidence and mortality are projected to continue rising, reaching approximately 35 million new cases and 18.5 million deaths annually by 2050 (Bizuayehu *et al*, 2024). These projections underscore cancer as a persistent and growing global health challenge, and highlight the urgent need for continued research efforts to identify more effective and durable therapeutic strategies.

The National Cancer Institute defines cancer as a disease characterized by uncontrolled cell division with potential to invade and spread to distant organs (Brown *et al*, 2023). While operationally useful, this definition is overly simplistic, as cancer is now recognized as a generic term encompassing large groups of biologically and clinically distinct diseases, each with unique molecular drivers, cellular origins, evolutionary trajectories, and responses to therapy (Swanton *et al*, 2024). In an effort to provide a unifying conceptual framework, Hanahan and Weinberg proposed the "hallmarks of cancer". Initially formulated in 2000, this framework identified six core hallmarks that enable tumor initiation and progression (Hanahan & Weinberg, 2000). Subsequent updates expanded this model to incorporate additional hallmarks and enabling characteristics, reflecting advances in cancer biology and an increasing appreciation of regulatory, metabolic, and immune-related processes (Hanahan & Weinberg, 2011). The most recent revision further emphasized cancer cell plasticity and epigenetic reprogramming of tumor behavior, highlighting the dynamic and adaptive nature of malignant cells, largely driven by non-genetic and transcriptional mechanisms (Figure 1) (Hanahan, 2022).

As will be developed throughout this thesis, cancer cells exhibit extensive alterations in transcriptional regulation and DNA damage repair pathways, which contribute to tumor initiation and progression, but also create vulnerabilities that may be therapeutically exploited. Therefore, rather than providing an exhaustive overview of all currently described cancer hallmarks, this section will focus on those most relevant to the central themes of this work: hallmarks driven by transcriptional dysregulation and loss of genome integrity.

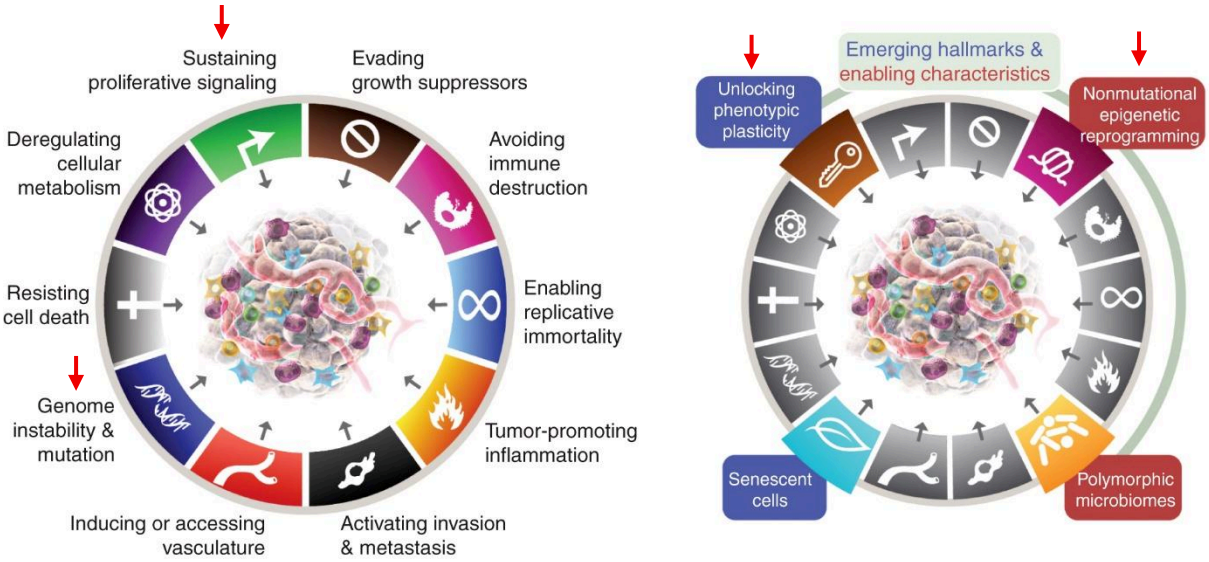

Figure 1. The updated hallmarks of cancer (2022). These include 10 functional and 4 enabling hallmarks. Red arrows indicate the hallmarks highlighted in this introduction, which are associated with alterations in transcriptional regulation and DNA repair. Reproduced from *Hanahan, Cancer Discov (2022)*.

i. Sustaining proliferative signaling

In normal tissues, cell proliferation is tightly regulated by complex signaling and transcriptional control mechanisms that ensure appropriate cell-cycle entry in response to extracellular stimulations. Commitment to proliferation is closely linked to the activation of the E2F-dependent transcriptional programs that promote transition from G1 to S phase, thereby initiating DNA replication and preparing cells for division. Under physiological conditions, these transcriptional programs are activated downstream of growth factor signaling pathways, in which ligand binding to cell-surface receptors triggers intracellular signaling cascades that ultimately lead to E2F activation and cell cycle progression (Figure 2) (Matthews *et al*, 2022).

Cancer cells acquire the ability to sustain proliferation by deregulating these tightly controlled pathways, resulting in proliferation rates that far exceed cell death and enable progressive tumor growth. This deregulation can occur through multiple mechanisms. For instance, tumor cells may produce growth factor ligands themselves, establishing autocrine proliferative loops (Wrenn *et al*, 2026), or stimulate surrounding stromal cells to supply them with various growth factors (Monteran *et al*, 2024). In parallel, cancer cells frequently increase the expression or activity of growth factor receptors at the cell surface, rendering them hyper-responsive to otherwise limiting growth factor concentrations. A well characterized example is estrogen receptor-positive breast cancer, in which amplification or overactivation of estrogen receptor α leads to ligand-dependent nuclear translocation and recruitment of transcriptional coactivators that drive proliferation-associated gene expression programs (Carroll, 2016). In this context, therapeutic interference with this transcriptional output, notably through selective estrogen receptor modulators such as 4-hydroxytamoxifen, has proven clinically effective (Howell & Howell, 2023).

In many cancers, proliferative signaling becomes independent of extracellular growth factors through constitutive activation of downstream signaling pathways. For example, approximately 50% of human melanomas harbor activating mutations in BRAF, resulting in persistent activation of the MAPK pathway (Davies & Samuels, 2010). Similarly, loss-of-function mutations in negative-regulators of proliferative signaling, such as the tumor suppressor PTEN, lead to hyperactivation of the PI3K/AKT/mTOR pathway and uncontrolled cell-cycle progression (Carracedo & Pandolfi, 2008).

These insights have motivated the development of therapeutic strategies targeting core components of the cell-cycle transcriptional machinery. Among the most prominent examples

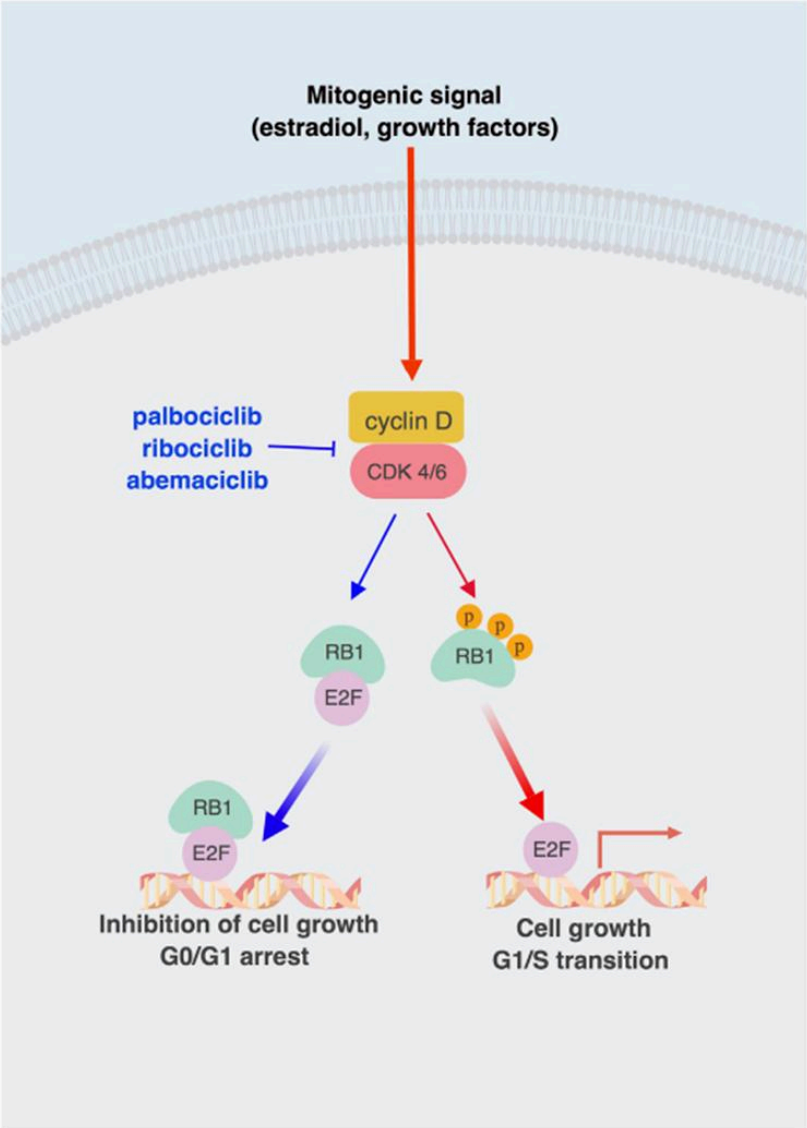

Figure 2. Regulation of G1/S transition by the CDK4/6-RB-E2F axis. Mitogenic signals activate Cyclin D-CDK4/6 complexes, leading to phosphorylation and inactivation of the retinoblastoma protein (RB), thereby releasing E2F transcription factors and promoting transcription of genes required for S-phase entry. CDK4/6 inhibitors (palbociclib, ribociclib, abemaciclib) prevent RB phosphorylation, maintaining E2F repression and inducing G1 cell-cycle arrest. Reproduced from *Dean et al., Oncogene (2010)*.

are CDK4/6 kinase inhibitors, such as palbociclib and ribociclib, which prevent phosphorylation and thereby maintain the activity of the E2F-negative regulator, the retinoblastoma protein (RB) (Dean *et al*, 2010). While these agents have shown significant efficacy in preclinical tumor models, their variable effectiveness and the frequent emergence of resistance in clinical contexts highlight the limitations of targeting proliferative signaling alone in highly adaptable cancers (Lynce *et al*, 2018).

ii. Genome instability and mutations

Genomic instability is prevalent feature of most human cancers and is considered a driving force of tumor initiation and progression (Martínez-Jiménez *et al*, 2020). During multistep tumorigenesis, cancer cells acquire genetic alterations that confer selective advantages over neighboring cells, enabling clonal expansion through a Darwinian evolutionary process. These advantageous alterations, commonly referred to as driver mutations, promote tumor growth and survival, while additional passenger mutations accumulate as a consequence of ongoing genomic instability (McGranahan & Swanton, 2017).

Among the different forms of genomic instability in cancer, chromosomal instability (CIN) is the most common and is characterized by structural and numerical chromosome alterations (Figure 3) (Hosea *et al*, 2024). Despite extensive research efforts, the precise molecular origins of genomic instability in cancer remain unclear. Historically, two major models have been proposed: the mutator hypothesis and the oncogene-induced DNA replication stress model. The mutator hypothesis postulates that genomic instability arises from early mutations in caretaker genes, whose main function is to preserve genome integrity, including DNA repair factors and mitotic checkpoint regulators (Negrini *et al*, 2010). Germline mutations in such genes are well documented in hereditary cancers, with BRCA1 and BRCA2 mutations predisposing to breast and ovarian cancer being a classical example (King *et al*, 2003). Similarly, the tumor suppressor gene TP53, which plays a central role in cell-cycle control and DNA damage response, is frequently mutated in cancer (Chen *et al*, 2022). Nonetheless, large genomic analyses of sporadic tumors proposed that the majority of cancers did not harbor mutations in caretaker genes (Chae *et al*, 2016). In addition, evidence from mouse models demonstrates that deletion of TP53 alone does not lead to structural chromosomal alterations (Bunz *et al*, 2002). Collectively, these findings suggest that loss of caretaker gene function alone is insufficient to account for the widespread genomic instability observed in most cancers.

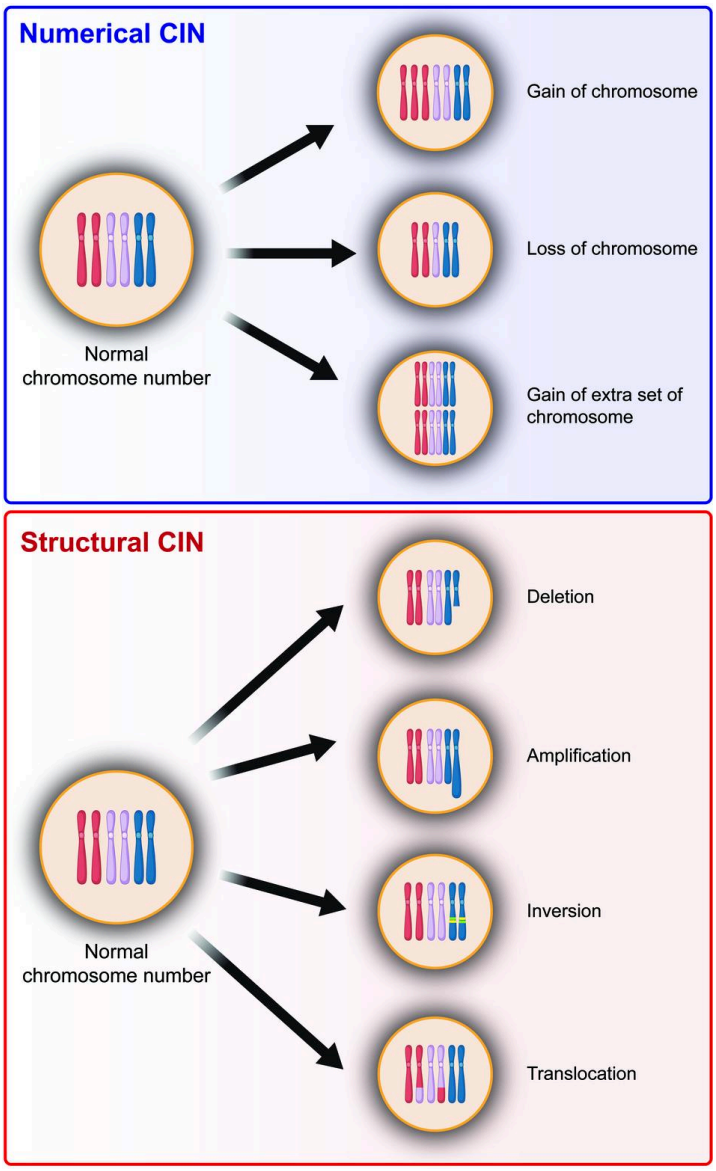

Figure 3. Types of chromosomal instability (CIN). Numerical CIN involves whole-chromosome gains or losses, whereas structural CIN comprises alterations affecting chromosome segments, including deletions, amplifications, inversions, and translocations. Reproduced from *Hosea et al., Signal Transduct Target Ther (2024)*.

An alternative and now widely supported model proposes that genomic instability in sporadic cancers primarily arises from oncogene-induced DNA replication stress. Aberrant activation of oncogenes such as MYC, BRAF, or EGFR, through mutation, amplification or epigenetic deregulation, drives sustained proliferative signaling and excessive E2F-dependent transcriptional activity. This accelerates S-phase entry and DNA replication, overwhelming replication machinery and leading to replication fork stalling and collapse, which in turn generates DNA double-strand breaks and chromosomal aberrations (Figure 4) (Bester *et al*, 2011). In support of this model, experimental activation of oncogenic RAS or MYC in cellular and xenograft models demonstrates loss of heterozygosity and increased chromosomal instability (Gilad *et al*, 2010; Hubbard *et al*, 2016).

As tumors progress, elevated genomic instability contributes to phenotypic heterogeneity through the continuous generation of genetic diversity, which fuels clonal evolution and selection of variants with enhanced invasive, metastatic, and therapy-resistant properties (Bozic & Nowak, 2014; Bakhoum & Landau, 2017). Inflammatory signaling within tumor microenvironment can further enhance this process by increasing exposure to reactive oxygen species (ROS), thereby accelerating mutagenesis (Figure 5) (Grivennikov *et al*, 2010).

Despite its role in carcinogenesis, genomic instability also creates therapeutic vulnerabilities that can be selectively exploited. A notable example is the clinical use of PARP inhibitors in BRCA1/2-mutant breast and ovarian cancers, which rely on defects in homologous recombination repair (Lee *et al*, 2014). Furthermore, genomic instability can serve as a predictive biomarker for therapeutic response. For instance, TP53-mutant tumors display increased sensitivity to DNA-damaging agents such as cisplatin (Fransson *et al*, 2016), while high tumor mutational burden has been associated with improved responses to immunotherapy due to increased neoantigen presentation (Strickler *et al*, 2021).

iii. Non-mutational epigenetic reprogramming

Early cancer research primarily focused on genetic origins of tumorigenesis, emphasizing how mutational activation of oncogenes and inactivation of tumor suppressor genes drive malignant transformation. Nevertheless, since the 1990s, it has become increasingly clear that epigenetic alterations, defined as heritable but reversible changes in gene regulation that do not involve alterations in DNA sequence, play a critical role in cancer development and progression (Baylin & Jones, 2011). While some epigenetic abnormalities arise secondary to mutations in genes encoding epigenetic regulators, microenvironmental factors such as hypoxia, inflammation, and

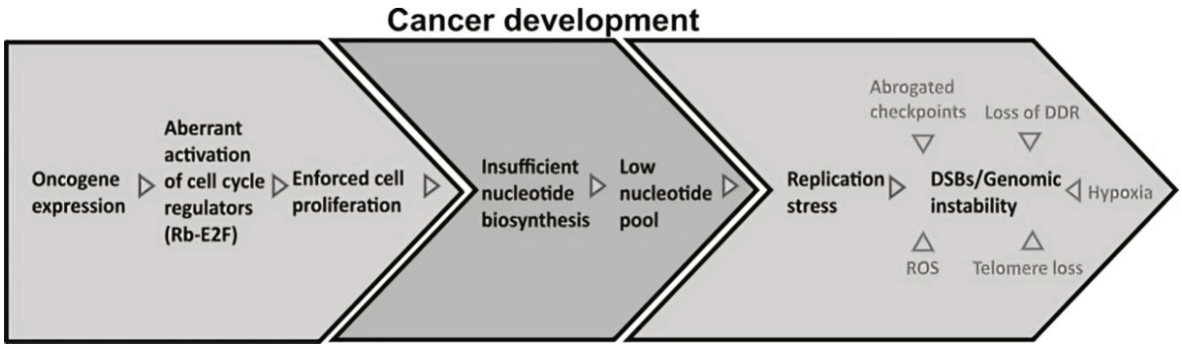

Figure 4. Oncogene-induced replication stress as a driver of genomic instability. Aberrant oncogene activation promotes sustained proliferative signaling and deregulated E2F-dependent transcription, leading to enforced S-phase entry and increased replication demand. This results in nucleotide depletion and replication stress, causing replication fork stalling and collapse, which ultimately generates DNA double-strand breaks (DSBs) and chromosomal instability. Reproduced from *Bester et al., Cell (2011)*.

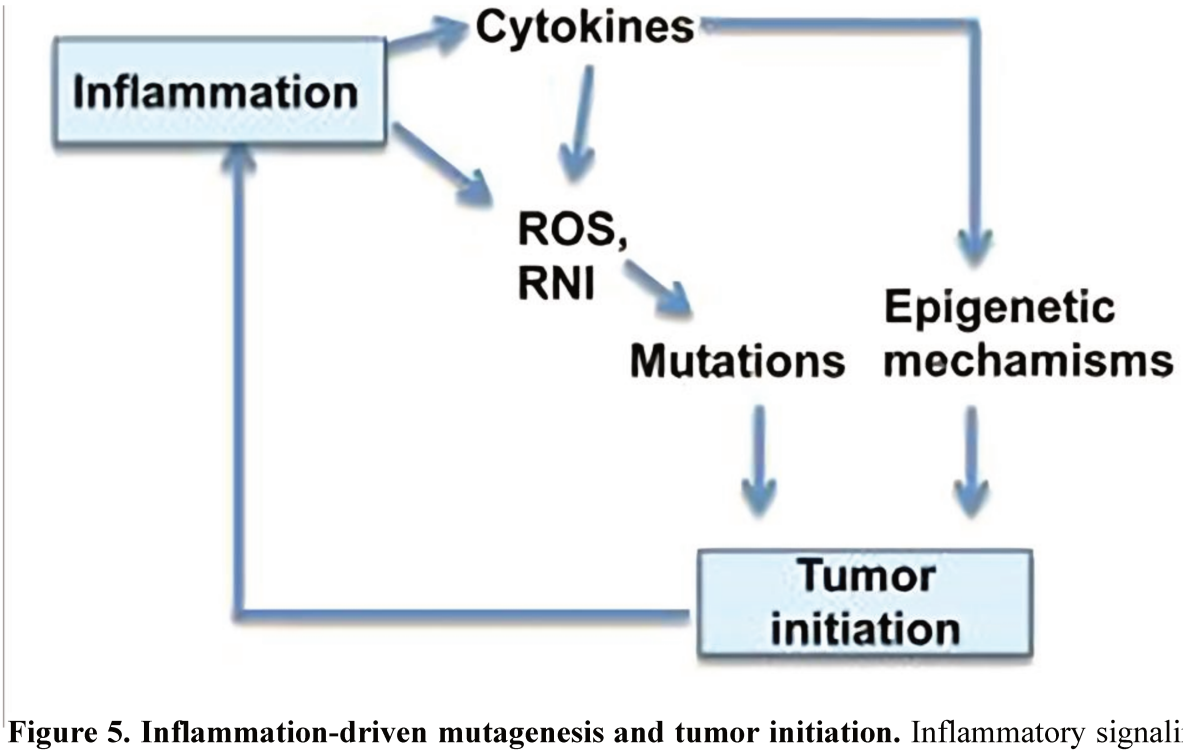

Figure 5. Inflammation-driven mutagenesis and tumor initiation. Inflammatory signaling promotes the production of cytokines and reactive oxygen and nitrogen species (ROS/RNI), which induce DNA damage and mutations. In parallel, inflammation can modulate epigenetic mechanisms, together contributing to tumor initiation and progression. Reproduced from *Grivennikov et al., Cell (2010).*

metabolic stress can also result in substantial abnormalities in the cancer epigenome, notably through signaling-driven transcriptional reprogramming and modulation of chromatin-modifying enzyme activity (Hanahan, 2022).

Epigenetic reprogramming in cancer occurs primarily through three main processes: abnormal DNA methylation, altered histone posttranslational modifications (PTMs), and dysregulations of ATP-dependent chromatin remodeling complexes (Figure 6) (Baylin & Jones, 2016). DNA methylation involves the addition of a methyl group to cytosine residues within the CpG dinucleotide, a process catalyzed by methyltransferases (DNMTs) and reversed by TET enzymes (Greenberg & Bourc'his, 2019). Cancer cells display a paradoxical redistribution of DNA methylation, marked by widespread hypomethylation across the genome alongside focal hypermethylation at CpG-rich gene promoters (Nishiyama & Nakanishi, 2021). While global hypomethylation has historically been associated with chromosomal instability and oncogene activation, a recent study suggests that the large-scale hypomethylation and its associated chromatin compartment alterations in tumors predominantly arise as a consequence of extensive cell proliferation and replicative history, rather than acting as direct drivers of oncogenic progression (Johnstone *et al*, 2020). In contrast, promoter hypermethylation of tumor suppressor genes, including MLH1, CDKN2A, and RB, is directly linked to transcriptional silencing and functional inactivation, contributing to tumor initiation and progression (Ng & Yu, 2015).

Histone alterations also play a central role in shaping cancer transcriptional programs. In particular, histone acetylation by the histone acetyltransferases (HATs) neutralizes the positive charge of lysine residues, loosening histone-DNA interactions and promoting transcriptional activation (Yang *et al*, 2022). Pathological acquisition of acetylation-driven regulatory elements has been described in multiple cancers. For example, in acute lymphoblastic leukemia, non-coding mutations upstream of the TAL1 oncogene create aberrant transcription factor binding sites that recruit the HAT CBP, resulting in hyperacetylation and oncogenic TAL1 overexpression (Mansour *et al*, 2014).

ATP-dependent chromatin remodeling complexes (CRCs) further modulate gene accessibility by repositioning nucleosomes and modulating histone-DNA interactions (Clapier *et al*, 2017). Among these, alterations of the SWI/SNF complex represent one of the most frequent chromatin-associated abnormalities in cancer, with loss-of-function mutations affecting at least one of its subunits in over 20% of human tumors (Figure 7) (Kadoch *et al*, 2013).

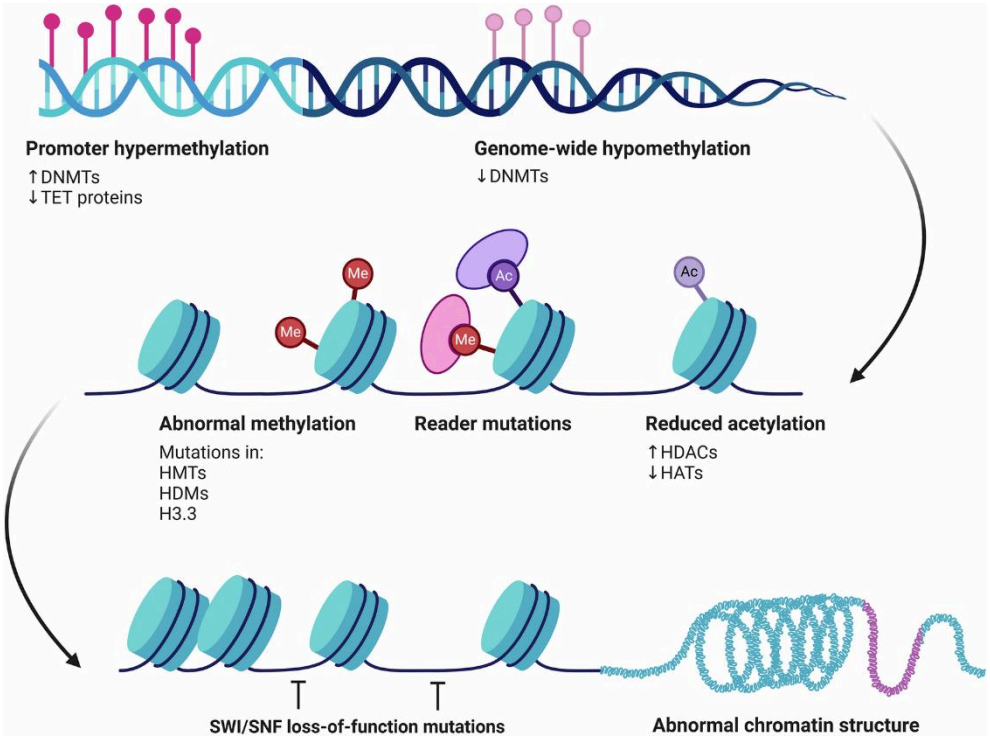

Figure 6. Epigenetic reprogramming in cancer. Cancer-associated epigenetic alterations arise through coordinated changes in DNA methylation, histone post-translational modifications, and chromatin remodeling. These include promoter hypermethylation and genome-wide hypomethylation, altered histone acetylation and methylation states, mutations in epigenetic "reader" proteins, and loss-of-function mutations in chromatin remodeling complexes such as SWI/SNF. Reproduced from *Marei et al., NPJ Precis Oncol (2025)*.

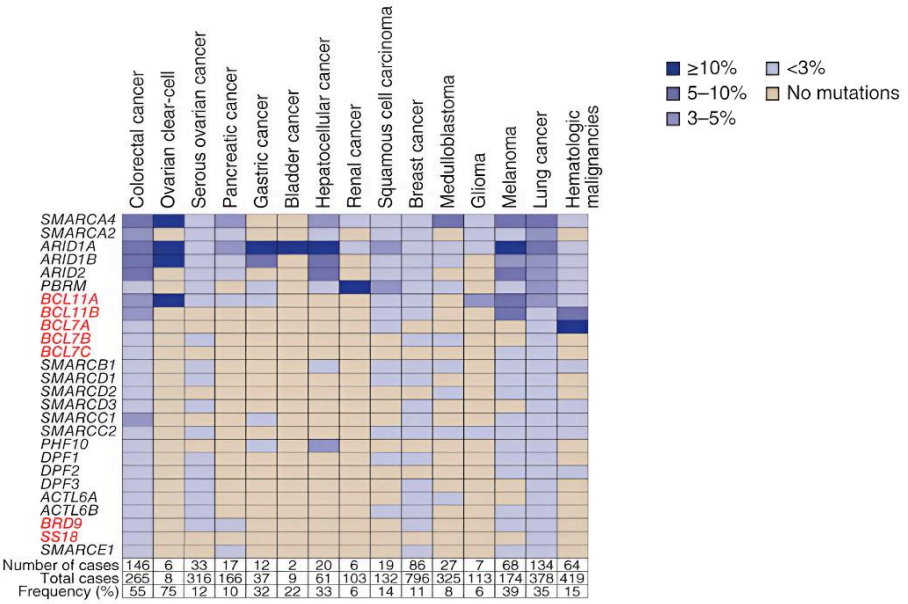

Figure 7. Frequency of mutations in SWI/SNF chromatin remodeling complex subunits across cancer types. Adapted from *Kadoch et al., Nat Genet (2013)*.

Although context-dependent, SWI/SNF dysregulation primarily drives tumorigenesis by perturbing transcriptional programs governing cell differentiation and growth control. Notably, SWI/SNF complexes also participate in DNA damage response (DDR) by remodeling chromatin at sites of DNA lesions, such that their disruption can indirectly exacerbate genome instability (Mittal & Roberts, 2020).

Unlike genetic mutations, epigenetic alterations are inherently reversible, rendering epigenetic regulators attractive therapeutic targets. Therefore, inhibitors of DNMTs (e.g., Azacitidine and Decitabine) and histone deacetylase (e.g., Vorinostat) have demonstrated the capacity to reprogram aberrant transcriptional states in cancer cells. However, their clinical efficacy has often been limited by toxicity, lack of specificity, and the adaptive capacity of cancer cells, underscoring the need for more selective strategies targeting transcriptional dependencies rather than global epigenetic modulation (Marei, 2025).

iv. Phenotype plasticity: Enabling invasion and therapy resistance

Cancer is increasingly recognized as heterogenous disease in which tumor cells can dynamically transition between distinct phenotypic states. This phenotypic plasticity enables cancer cells to reversibly reprogram transcriptional and epigenetic programs in response to intrinsic or extrinsic alterations from the tumor microenvironment, thereby facilitating adaptation to environmental stress and therapeutic pressure (Pérez-González *et al*, 2023).

Tumor cell plasticity can arise through several non-mutually exclusive mechanisms. One major form is dedifferentiation, defined as the loss of lineage-specific identity and specialized cellular functions by a transition toward a progenitor or stem-like state (Figure 8), often referred to as cancer stem cells (CSCs) (Chu *et al*, 2024). This process is associated with repression of differentiation markers and activation of stemness-associated transcriptional programs, including OCT4 and SOX2 (Karras *et al*, 2024). A prominent example is observed in colorectal cancer, where loss of the epithelial lineage regulator HOXA5 is linked to acquisition of stem-like traits, while its re-induction eliminates CSCs and reduces tumor progression (Ordóñez-Morán *et al*, 2015).

Loss of lineage-specific programs doesn't always result in dedifferentiation but can also lead to transdifferentiation, whereby cells are converted into an alternative differentiated lineage. For instance, in pancreatic cancer, acinar cells transdifferentiate into ductal-like cells during early tumorigenesis through repression of the lineage-defining transcription factors, PTF1 and MIST1 (Jiang *et al*, 2016).

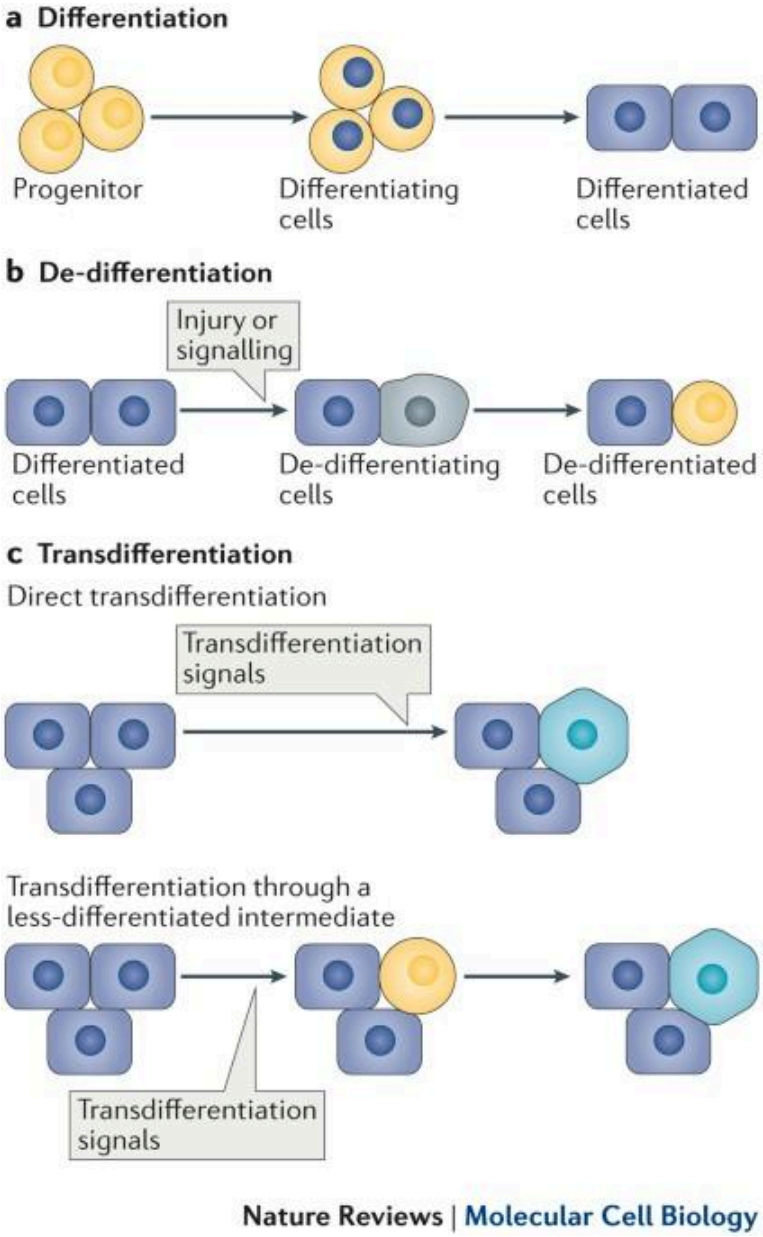

Figure 8. Cellular plasticity: differentiation, dedifferentiation, and transdifferentiation. Cancer cells can transition between distinct identity states through multiple mechanisms. Differentiation involves the progression from progenitor to specialized cell types. In contrast, dedifferentiation refers to the reversion of differentiated cells toward a less specialized, progenitor-like state. Alternatively, transdifferentiation describes the direct or indirect conversion of one differentiated cell type into another. Reproduced from *Merrell and Stanger, Nat Rev Mol Cell Biol (2016)*.

Besides, perhaps the most extensively studied form of phenotype plasticity is epithelial-to-mesenchymal transition (EMT), a reversible process characterized by loss of epithelial features, including cell-cell junctions and adhesion, and acquisition of mesenchymal traits that enhance migration and invasiveness (Dongre & Weinberg, 2019). EMT is driven by the co-option of developmental transcriptional programs, mainly regulated by core EMT transcription factors of the SNAIL and ZEB families, which can act redundantly or cooperatively. Importantly, EMT is reversible, and mesenchymal cells can revert to an epithelial state through mesenchymal-to-epithelial transition (MET), highlighting the dynamic nature of this process (Figure 9). EMT and MET are strongly influenced by microenvironment signals such as hypoxia, nutrient deprivation, and inflammatory cues, as well as by interactions with tumor associated stromal and immune cells through pathways such as TGF-β and Notch (Yang *et al*, 2020).

Phenotypic plasticity has long been implicated in metastasis, as a small subpopulation at the origin of metastatic lesions, termed metastasis-initiating cells (MICs), display high plasticity and different degrees of stemness and EMT (Pérez-González *et al*, 2023). However, the precise role of phenotypic plasticity in metastasis remains debated. While circulating tumor cells were found to contain CSC-like features, depletion of CSC in colorectal cancer did not reduce metastatic progression (de Sousa e Melo *et al*, 2017). Moreover, recent evidence suggests that cancer cells expressing full EMT programs are not optimal for metastatic colonization. Instead, cells occupying intermediate or hybrid EMT states appear more efficient at seeding distant organs (Pastushenko *et al*, 2018; Simeonov *et al*, 2021), underscoring the complexity and context dependence of plastic phenotypes in metastasis.

Beyond metastasis, phenotypic plasticity is now widely recognized as a major contributor to therapy resistance. Highly plastic subpopulations, often referred to as drug-tolerant persister (DTP) cells, are characterized by slow proliferation, flexible transcriptional programs, and enhanced stress tolerance (Figure 10) (Pérez-González *et al*, 2023). EMT-associated programs have been linked to resistance to cytotoxic and targeted therapies. For example, reversal of EMT through activation of the protein kinase A in breast cancer models restored sensitivity to several therapeutic agents, including doxorubicin and EGFR inhibitors (Pattabiraman *et al*, 2016). Similarly, CSC-like states have been implicated in immune evasion by reducing antigen presentation and altering their cell-cycle dynamics (Agudo *et al*, 2018). It is important to note that DTP cells may pre-exist prior to treatment, enabling their selective enrichment under therapeutic pressure (Shen *et al*, 2020).

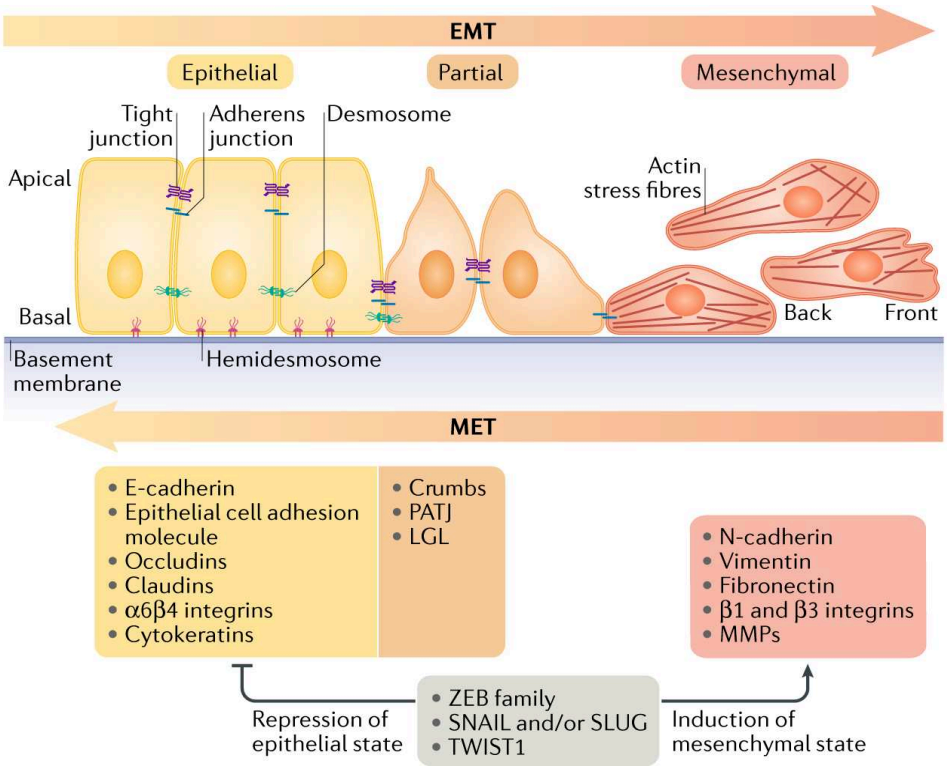

Figure 9. Epithelial-mesenchymal transition (EMT) and mesenchymal-epithelial transition (MET). EMT is a reversible process in which epithelial cells lose polarity and cell-cell adhesion, and acquire mesenchymal traits associated with increased motility and invasiveness. This transition is driven by transcription factors such as SNAIL, SLUG, ZEB, and TWIST. The reverse process, MET, restores epithelial characteristics. Adapted from *Dongre and Weinberg, Nat Rev Mol Cell Biol (2019)*.

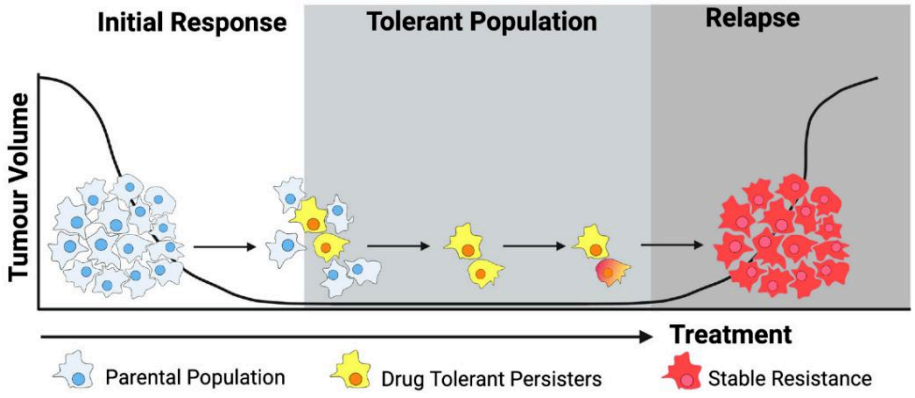

Figure 10. Emergence of drug-tolerant persister cells and therapy resistance. Upon treatment, a subset of cells, referred to as drug-tolerant persisters (DTPs), survive through reversible, non-genetic adaptive mechanisms. These cells exhibit slow proliferation, transcriptional plasticity, and increased stress tolerance. Over time, DTPs can give rise to stable, genetically resistant populations, ultimately driving tumor relapse. Adapted from *Davis et al., genes. (2024)*.

Despite their central role in cancer progression and resistance, there are currently no clinically validated strategies to specifically target phenotypic plasticity. This limitation reinforces the need to identify context-specific transcription dependencies that can be therapeutically exploited to overcome resistance and prevent disease progression.

b. Conventional cancer therapies: historical foundations and limitations

The earliest attempts to treat cancer date back to antiquity, with descriptions found in the Ebers Papyrus (~1500 BC), where tumors were treated using substances such as salt and arsenic paste (Hajdu, 2011). Advances in anatomical knowledge during the Renaissance established surgery as the primary curative option for cancer, a role it continues to play today in the management of localized, early-stage disease (Zafar *et al*, 2025). Despite the success of excision surgery in achieving complete tumor clearance, in some cases, residual cancer cells may persist as minimal residual disease (MRD) or undetectable micrometastases, which can rapidly drive relapse following surgery (Boukouris *et al*, 2025).

The discovery of X-rays at the beginning of the twentieth century introduced radiotherapy as an additional therapeutic option for local tumors. Radiotherapy relies on high-energy ionizing radiation to induce DNA damage, ultimately triggering cell death through apoptosis, necrosis, or autophagy (Jaffray *et al*, 2023). It is widely used in cancers such as head and neck, prostate, and breast cancer, either alone or in combination with surgery. However, despite its high efficacy, its clinical use is constrained by toxicity to surrounding healthy tissues and by the emergence of radioresistance, which is associated with activation of hypoxia-related survival pathways and adaptive DNA damage response mechanisms, including enhanced DNA double-strand break repair (Wu *et al*, 2023).

For advanced and systemic tumors, the mid-twentieth century marked the advent of chemotherapy, following observations made during World War II that nitrogen mustards suppressed rapidly dividing cells (Smith, 2017). Chemotherapeutic agents broadly target highly proliferating cells by interfering with DNA replication and transcription and by inducing DNA damage. Commonly used agents include platinum-based alkylating compounds such as cisplatin, antimetabolites such as 5-fluorouracil, and topoisomerase inhibitors such as doxorubicin (Zafar *et al*, 2025). Despite their widespread use and cost-effectiveness, chemotherapy is limited by substantial toxicity to normal tissues and by the frequent emergence of resistance (Figure 11). Resistance mechanisms mainly include enhanced drug efflux through overexpression of ATP-binding cassette (ABC) transporters, metabolic rewiring, and the

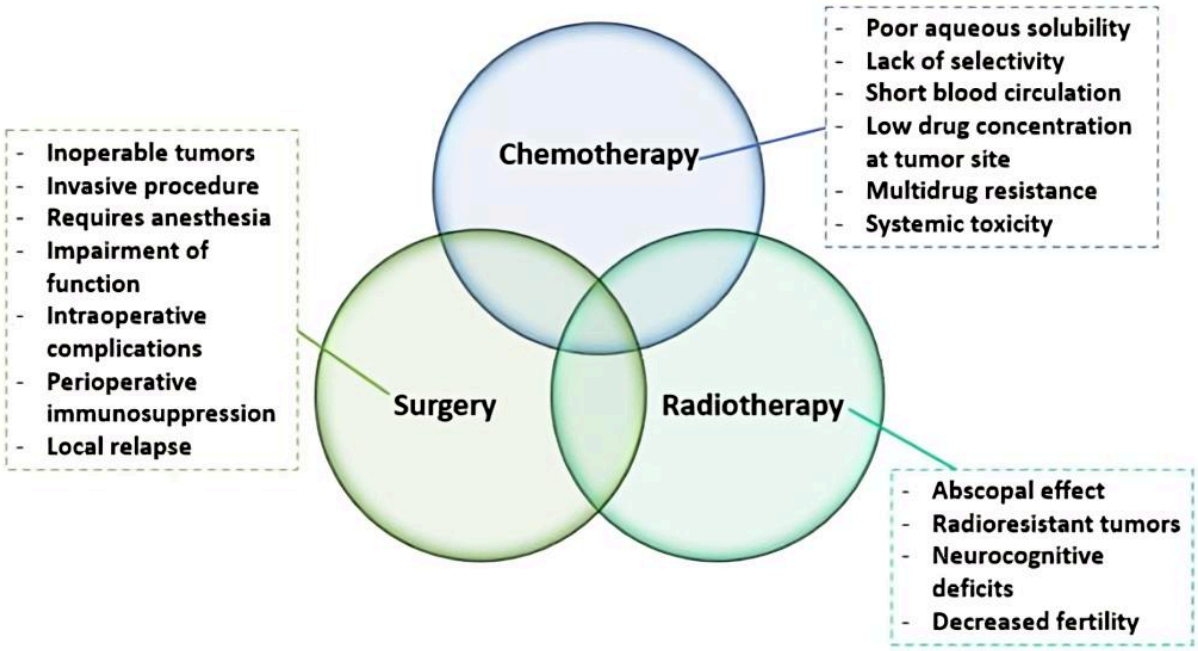

Figure 11. Limitations of conventional cancer therapies. Major treatment modalities, including surgery, radiotherapy, and chemotherapy, are associated with distinct and overlapping limitations. Surgery is constrained by incomplete tumor resection and potential postoperative complications. Radiotherapy effectiveness is limited by toxicity to surrounding tissues and the emergence of radioresistance. Chemotherapy is hindered by lack of selectivity, systemic toxicity, and the development of multidrug resistance. These limitations contribute to treatment failure and disease relapse. Reproduced from *Ion et al., Pharmaceutics (2021)*.

selection of slow-cycling, transcriptionally plastic tumor cell subpopulations (Tufail *et al*, 2024).

Efforts to overcome the nonselective action of chemotherapy led to the development of molecular targeted therapies, inspired by the "magic bullet" concept introduced in the 1890s by the German physician Paul Ehrlich to describe treatments that selectively target disease-causing agents without systemic toxicity (Strebhardt & Ullrich, 2008). Targeted therapies include hormone receptor-based approaches, such as monoclonal antibodies that modulate membrane receptors, exemplified by trastuzumab targeting HER2 in breast cancer. A second class of targeted therapies consists of small-molecule kinase inhibitors (SMKIs), which inhibit oncogenic signaling pathways by binding to the ATP-binding pocket of kinases in either their active or inactive conformations (Min & Lee, 2022). For instance, the recently FDA-approved SMKI sotorasib targets the KRAS G12C mutation in non-small cell lung cancer and has demonstrated promising outcomes in clinical trials (Skoulidis *et al*, 2021). Although these treatments display improved specificity and initial efficacy compared to chemotherapy, durable responses are frequently undermined by tumor heterogeneity and acquired resistance mechanisms, including hyperactivation of compensatory signaling pathways, secondary mutations in kinase domains, and isoform switching (Sabnis & Bivona, 2019).

More recently, immunotherapy has transformed cancer treatment by enhancing the immune system's capacity to recognize and eliminate tumor cells. The concept of immunotherapy dates back more than 140 years, when German physicians Busch and Fehleisen observed tumor regression in patients infected with Streptococcus pyogenes, concluding that infection could stimulate antitumor immune responses (Dobosz & Dzieciątkowski, 2019). Subsequent advances in tumor immunology led to the development of immune checkpoint inhibitors (ICIs), which limit tumor immune evasion by targeting negative regulators of T-cell activation such as CTLA-4 and PD-1. Accordingly, monoclonal antibodies targeting CTLA-4 (ipilimumab) and PD-1 (pembrolizumab) are among the FDA-approved immunotherapies that have shown durable clinical responses in subsets of cancer patients (Figure 12) (Zhang *et al*, 2025). Despite these advances, immunotherapy is effective only in a limited fraction of tumors with high mutational burdens and antigen presentation, such as melanoma and lung cancer. In contrast, tumors with low mutational burdens, such as pancreatic cancer and certain breast cancer subtypes, generate fewer neoantigens, rendering them largely unresponsive to immunotherapy (Strickler *et al*, 2021).

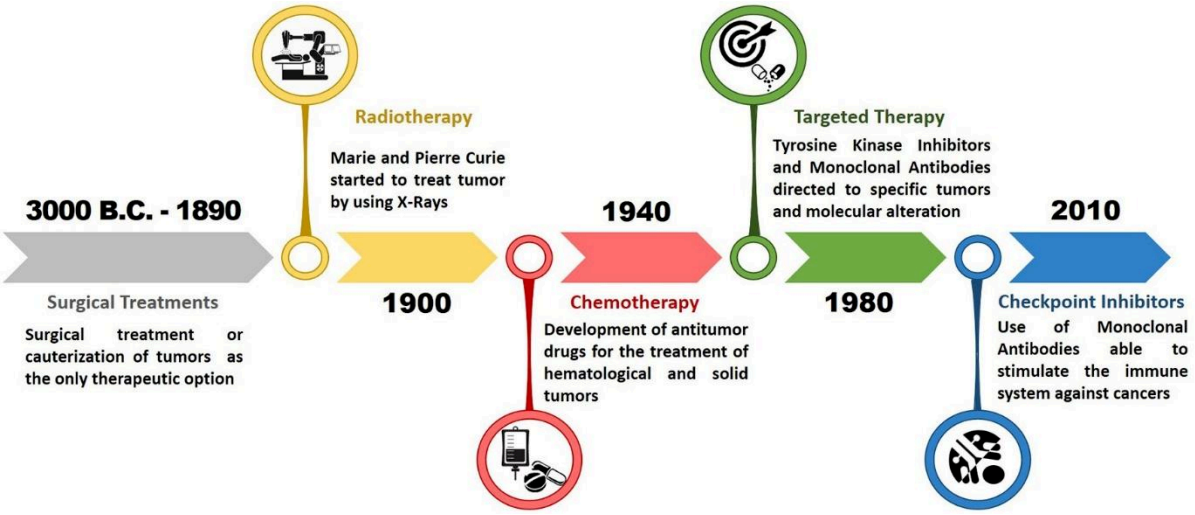

Figure 12. Historical development of major cancer therapies. Overview of the major classes of cancer treatment, from early surgical approaches to the introduction of radiotherapy and chemotherapy, followed by the emergence of targeted therapies and immune checkpoint inhibitors. These advances reflect the progressive shift toward more precise and mechanism-based therapeutic strategies. Adapted from *Falzone et al., Front Pharmacol (2018)*.

Moreover, the tumor microenvironment is a critical determinant of immunotherapy efficacy: so-called "hot tumors," characterized by high immune cell infiltration, respond more favorably to ICIs, whereas "cold tumors," such as pancreatic cancer, glioblastoma, and ovarian cancer, exhibit limited immune infiltration and reduced responsiveness (Wu *et al*, 2024). In addition, acquired resistance to ICIs (Sharma *et al*, 2017) and immune-related adverse events resulting from excessive immune activation (Conroy & Naidoo, 2022) can further limit treatment efficiency and tolerability.

Collectively, these therapeutic advances have significantly improved cancer outcomes. However, resistance, toxicity, and disease relapse remain pervasive challenges. Across treatment modalities, a common limitation is the inability to durably suppress the adaptive capacity of cancer cells (Figure 13), driven by transcriptional plasticity and altered DNA damage responses. Addressing these vulnerabilities represents a critical need in cancer therapy. Accordingly, this thesis focuses on developing strategies to target dysregulated transcriptional programs and DNA repair pathways, with the aim of overcoming therapeutic resistance. The following sections will provide an overview of transcriptional regulation and DNA repair mechanisms in cancer and discuss how their deregulation can be exploited therapeutically.

II- Gene expression and transcriptional dysregulations in cancer:

a. Gene expression regulation in normal cells

i. Chromatin organization and regulatory architecture

Gene expression is a fundamental process by which genetic information encoded in DNA is transcribed into RNA and ultimately translated into functional products. Tight regulation of gene expression is essential for maintaining cellular identity, homeostasis, and appropriate responses to environmental cues (Cramer, 2019). Historically, transcription was thought to be primarily controlled by gene promoters, which are DNA regions located near transcription start sites (TSSs) where RNA polymerase II (RNAPII) and the basal transcription machinery assemble to initiate transcription (Haberle & Stark, 2018). This promoter-centric view was revised with the discovery of enhancers in 1981, defined as distal regulatory DNA elements capable of activating transcription independently of their orientation and distance relative to the promoter (Banerji *et al*, 1981). Enhancers can be located tens to hundreds of kilobases away from their target genes and have since been recognized as major determinants of cell-type-specific gene expression programs (Figure 14).

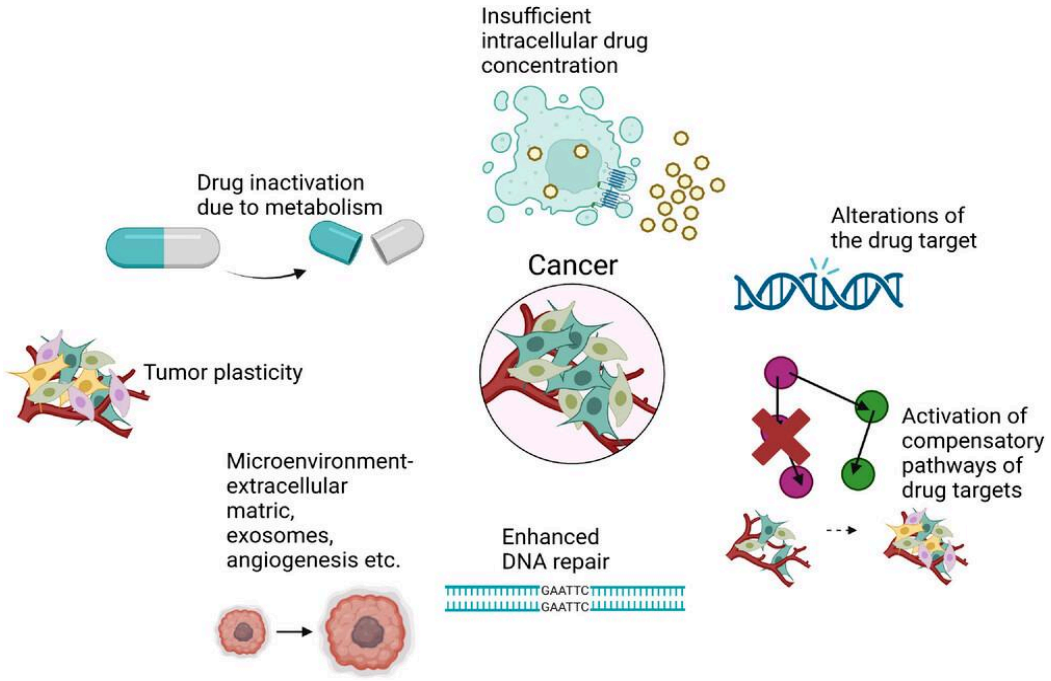

Figure 13. Common mechanisms of therapeutic resistance in cancer. Cancer cells evade therapeutic pressure through multiple adaptive mechanisms shared across treatment modalities. These include reduced intracellular drug accumulation, drug inactivation, and alterations of drug targets, as well as activation of compensatory signaling pathways. Tumor plasticity and interactions with the tumor microenvironment further contribute to resistance. In addition, enhanced DNA damage response and repair mechanisms promote survival following genotoxic stress. Reproduced from *Lei et al., MedComm (2023)*.

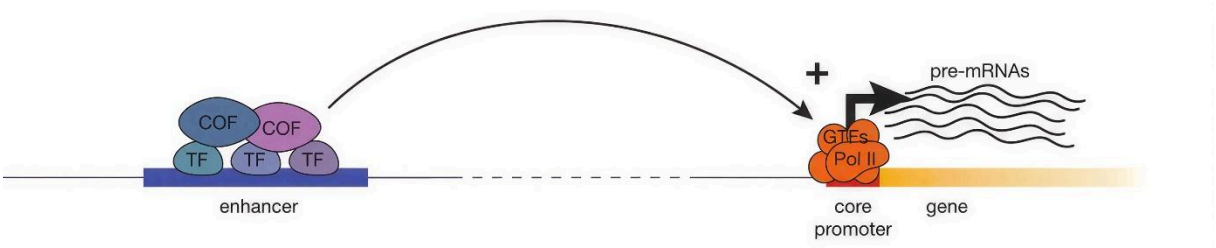

Figure 14. Enhancers as distal regulators of gene expression. Enhancers are distal regulatory DNA elements that control gene expression by activating transcription at target gene promoters. They recruit transcription factors and co-factors to stimulate RNA polymerase II activity and promote transcription. Adapted from *Haberle and Stark, Nat Rev Mol Cell Biol (2018)*.

At a higher organizational level, transcriptional regulation is tightly linked to the spatial organization of the genome. In human cells, approximately two meters of DNA are compacted within the nucleus through multiple hierarchical layers of chromatin organization, each directly influencing gene expression (Figure 15) (Misteli, 2020). At the most fundamental level, chromatin fibers are made up of ~146 base pairs of DNA wrapped around nucleosomes consisting of eight histone octamers (Dekker & Misteli, 2015). Nucleosome positioning and chromatin accessibility are dynamically regulated by ATP-dependent chromatin remodelers, as well as by histone-modifying enzymes such as histone acetyltransferases and methyltransferases, which together modulate chromatin compaction and thereby influence transcriptional permissiveness (Martire & Banaszynski, 2020).

Beyond the nucleosomal level, chromatin fibers can fold into higher-order structures to form chromatin loops, which enable long-range interactions between regulatory elements. For example, chromatin looping allows distal enhancers to physically interact with gene promoters across distances ranging from several to hundreds of kilobases, facilitating transcriptional regulation at a distance. Larger chromatin loops, spanning megabase-scale regions, also contribute to global genome folding and coordinated regulation of gene clusters (Kadauke & Blobel, 2009).

An additional level of topological organization is provided by chromatin domains, often referred to as topologically associating domains (TADs). TADs are genomic regions typically hundreds of kilobases in size, within which chromatin interactions occur more frequently than with neighboring regions (Dixon *et al*, 2012). TADs are thought to be formed primarily through a loop extrusion mechanism driven by the cohesin complex in an ATP-dependent manner, with boundaries frequently enriched in the architectural protein CTCF (Dekker & Mirny, 2016). While several studies have shown that co-regulated genes tend to reside within the same TADs, other work has challenged this view by demonstrating that disruption or loss of TAD boundaries can have limited effects on steady-state gene expression, suggesting that TADs may facilitate, but are not strictly required for transcriptional regulation (Ghavi-Helm *et al*, 2019).

At a larger scale, individual chromatin domains assemble into compartments that reflect global chromatin states. Genomic regions are broadly partitioned into A and B compartments, corresponding to transcriptionally active euchromatin and inactive, tightly packaged heterochromatin, respectively (Lieberman-Aiden *et al*, 2009). Finally, the highest layer of genome organization consists of chromosome territories, which occupy distinct spatial regions within the nucleus and typically measure 2-3 μm in diameter in mammalian cells

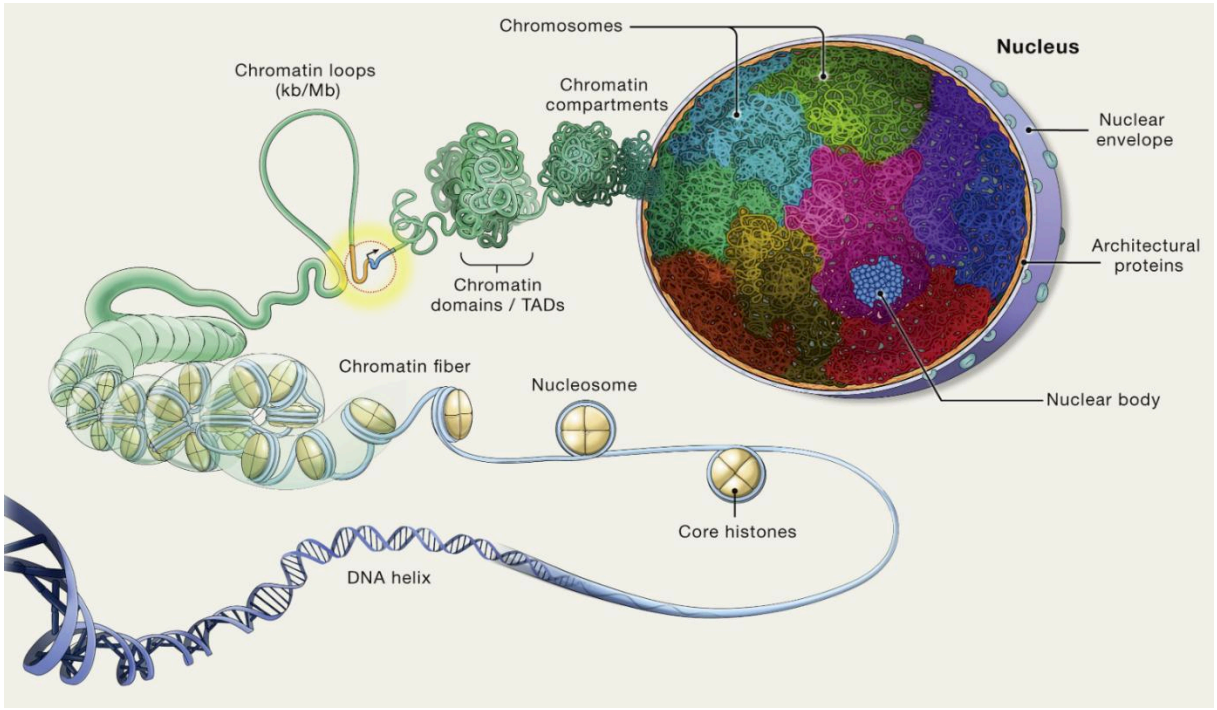

Figure 15. Hierarchical organization of chromatin and the 3D genome. Genomic DNA is organized into multiple hierarchical layers within the nucleus, from nucleosomes and chromatin fibers to chromatin loops, topologically associating domains (TADs), higher-order compartments, and chromosome territories. This spatial organization facilitates long-range interactions between regulatory elements and contributes to the control of gene expression. Reproduced from *Misteli, Cell (2020)*.

(Cremer & Cremer, 2010). The radial positioning of chromosomes and gene loci within the nucleus further correlates with transcriptional activity, with inactive genes often located near the nuclear periphery and active genes preferentially positioned toward the nuclear interior (Misteli, 2020).

Together, these topological layers of chromatin organization collaborate to ensure accurate and context-specific regulation of gene expression. A central outcome of this organization is the establishment of functional interactions between enhancers and gene promoters, enabling activation of the transcriptional machinery. Despite extensive investigation, the precise mechanisms by which enhancers selectively activate their target promoters remain debated, particularly given the observation that not all enhancer-promoter contacts are strictly required for transcriptional activation (Yang & Hansen, 2024).

Several models have been proposed to explain enhancer-mediated transcriptional regulation (Figure 16). One model involves the direct transfer of enhancer-recruited proteins to promoters, supported by studies suggesting that enhancers can act as reservoirs for RNAPII, transcription factors, and chromatin remodelers (Li *et al*, 2019; Thomas *et al*, 2021). A second model proposes that, rather than a direct transfer, the DNA-sequence specific transcription factors (TFs) bound at enhancers facilitate recruitment of co-activators that activate transcription at promoters. In this context, the bromodomain-containing protein BRD4, enriched at acetylated enhancers, has been shown to recruit the positive transcription elongation factor b (P-TEFb), as well as the Mediator complex, thereby promoting correct RNAPII positioning and productive transcription elongation (Narita *et al*, 2021).

A third and increasingly influential model involves transcriptional activation through liquid-liquid phase separation (LLPS). In this framework, high local concentrations of transcription factors, co-activators, and RNAPII at enhancers drive the formation of transcriptional condensates that spatially concentrate the transcriptional machinery near target genes, potentially without requiring stable direct enhancer-promoter contacts (Cho *et al*, 2018; Boija *et al*, 2018). Such condensates are particularly prominent at super-enhancers (SEs), which will be discussed in detail in subsequent sections of this thesis. Finally, another proposed model suggests that enhancers activate transcription through enzymatic post-translational modification of promoter-bound transcriptional components, such as phosphorylation of the RNAPII carboxy-terminal domain (CTD) by associated kinases, thereby enabling productive elongation (Soutourina, 2018). While these models are not mutually exclusive, their relative contributions to transcriptional regulation likely depend on gene context, cell type, and

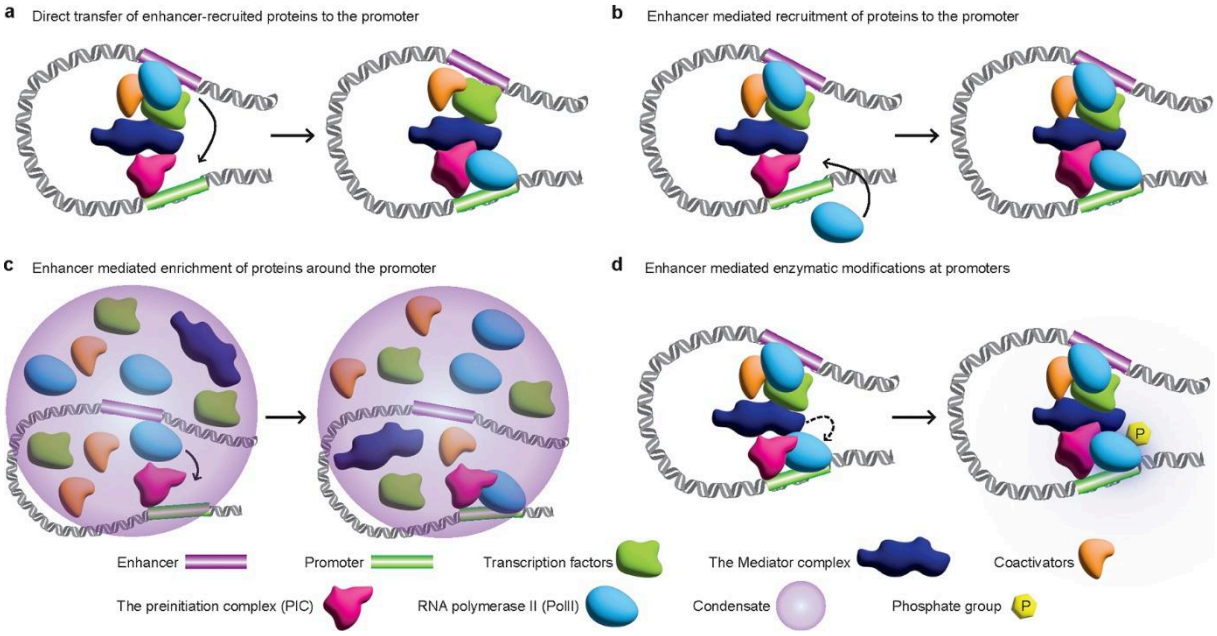

Figure 16. Models of enhancer-mediated transcriptional regulation. Multiple mechanisms have been proposed to explain how enhancers activate gene transcription. These include direct transfer of enhancer-bound factors to promoters, recruitment of transcriptional co-activators, formation of transcriptional condensates that concentrate the transcriptional machinery, and enzymatic modification of promoter-associated components such as RNA polymerase II. Reproduced from *Yang and Hansen, Nat Rev Mol Cell Biol (2024)*.

regulatory architecture. Importantly, single-cell transcriptional studies have revealed substantial heterogeneity in gene expression even among genetically identical cells, with many genes exhibiting transcriptional bursting, characterized by dynamic transitions between transcriptionally active and inactive states, leading to intermittent RNA production (Shah *et al*, 2018; Rodriguez *et al*, 2019). This functional heterogeneity suggests that distinct regulatory mechanisms may govern transcription across different gene populations.

In the following sections, transcriptional regulation will be further explored at the level of initiation, elongation, and termination in normal cells, before addressing how dysregulation of these fundamental processes contributes to oncogenic transcriptional programs and creates vulnerabilities that can be exploited for therapeutic intervention.

ii. The multi-steps process of transcription: from initiation to termination

Transcription is a multi-step process consisting of initiation, elongation, and termination, with each step subject to tight regulation. Transcription initiation occurs at the transcription start site (TSS) located at the 5′ end of genes. For initiation to occur, RNA polymerase II (RNAPII) must recognize the promoter core, spanning approximately 50 base pairs upstream and downstream of the TSS (Haberle & Stark, 2018). Different classes of promoters with distinct sequence features exist. For example, one major class contains CpG islands, characterized by high GC content and elevated CpG dinucleotide density, and is commonly associated with housekeeping genes and key developmental transcription factors (Deaton & Bird, 2011). Another class contains an AT-rich sequence (TATA box) upstream of the TSS and is generally linked to cell-type-specific genes activated during differentiation (Figure 17) (Haberle & Lenhard, 2016).

Access of RNAPII to promoters is constrained by nucleosomes, which must be repositioned or removed to allow transcription initiation (Lorch *et al*, 1987). RNAPII alone cannot recognize promoter sequences and requires the action of six general transcription factors (GTFs) that bridge RNAPII to the promoter, forming the pre-initiation complex (PIC) (Malik & Roeder, 2023). PIC assembly begins with recognition of the core promoter by TFIID, which contains the TATA-box binding protein (TBP) that binds upstream promoter DNA (Louder *et al*, 2016). This is followed by recruitment of TFIIA, which stabilizes the TBP-DNA interaction, and TFIIB, which facilitates recruitment of RNAPII escorted by TFIIF (Sainsbury *et al*, 2013). Subsequent binding of TFIIE enables recruitment of TFIIH, a multi-subunit complex containing the DNA translocase XPB, which uses ATP hydrolysis to unwind DNA and generate an open PIC (Egly & Coin, 2011).

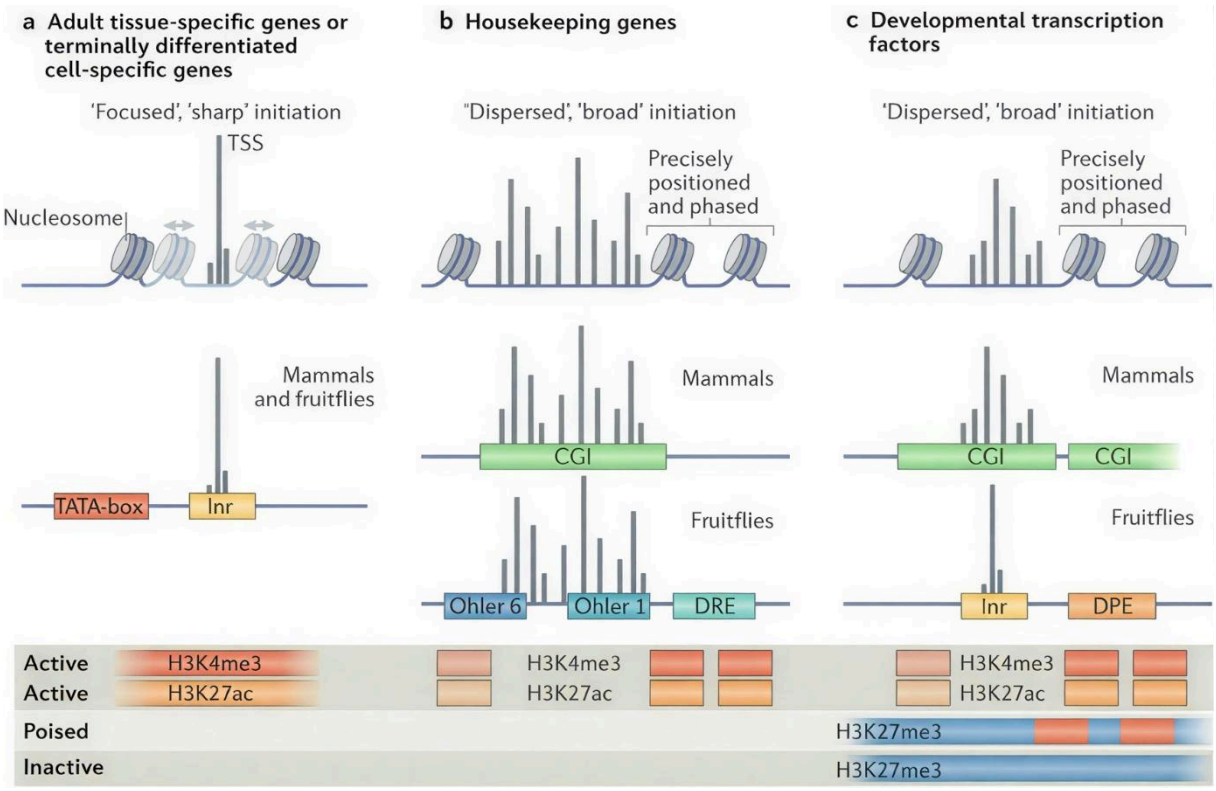

Figure 17. Distinct promoter architectures and transcription initiation patterns. Promoters display diverse sequence features and transcription initiation profiles. TATA-box-containing promoters are typically associated with focused transcription initiation and cell-type-specific gene expression, whereas CpG island promoters exhibit broad initiation patterns and are commonly linked to housekeeping and developmental genes. These promoter classes are associated with distinct chromatin states, including active marks such as H3K27ac and H3K4me3, and, in the case of developmental genes, bivalent chromatin marked by H3K4me3 and H3K27me3. Reproduced from *Haberle and Stark, Nat Rev Mol Cell Biol (2018)*.

RNAPII activation is then initiated by the Mediator complex, which interacts with TFIIH and stimulates its kinase subunit CDK7 to phosphorylate serine 5 (Ser5) of the RNAPII carboxy-terminal domain (CTD). This modification promotes promoter clearance and the transition into productive transcription initiation (Compe & Egly, 2012). While GTF assembly at core promoters is sufficient to drive basal transcription initiation, this activity is generally weak and requires enhancement by transcription factors and histone-modifying enzymes bound at distal enhancers. These factors recruit transcriptional cofactors that interact with and stabilize the PIC, thereby increasing transcriptional output. For instance, the histone acetyltransferase p300 can acetylate histones and transcriptional components, while the Mediator complex enhances RNAPII recruitment and activation at promoters (Eychenne *et al*, 2016; Boija *et al*, 2017).

Following initiation, RNAPII often transcribes only 30-50 nucleotides downstream of the TSS before entering a paused state (Cramer, 2019). Promoter-proximal pausing is a critical regulatory step that allows rapid and synchronous release of pre-engaged RNAPII into productive elongation, bypassing the slower processes of *de novo* recruitment and initiation, thereby enabling rapid transcriptional responses to regulatory signals (Henriques *et al*, 2013). Paused RNAPII is stabilized by the DRB sensitivity inducing factor (DSIF) and the negative elongation factor (NELF) complexes, which bind the exiting DNA-RNA hybrid and the surface of RNAPII, respectively, thereby restricting polymerase mobility (Aoi & Shilatifard, 2023).

Release from promoter-proximal pausing requires the kinase CDK9, which is the catalytic subunit of the positive transcription elongation factor b (P-TEFb) complex. P-TEFb can be recruited to promoters by transcriptional cofactors such as BRD4, which recognizes acetylated histone marks at enhancers (Jang *et al*, 2005). CDK9 phosphorylates DSIF, converting it into a positive elongation factor, induces dissociation of NELF, and phosphorylates serine 2 (Ser2) of the RNAPII CTD. These events collectively trigger pause release and promote productive transcription elongation (Figure 18) (Aoi & Shilatifard, 2023).

In addition to CDK9, other elongation-associated kinases, such as CDK12, contribute to efficient transcription elongation. CDK12 physically interacts with splicing factors to suppress premature usage of intronic polyadenylation sites and maintains Ser2 CTD phosphorylation along gene bodies (Liang *et al*, 2015). Depletion of CDK12 or other elongation factors slows RNAPII elongation and induces premature transcription termination, preferentially affecting the expression of long genes, including those involved in the DNA damage response (Krajewska *et al*, 2019), as will be discussed in later sections of this thesis.

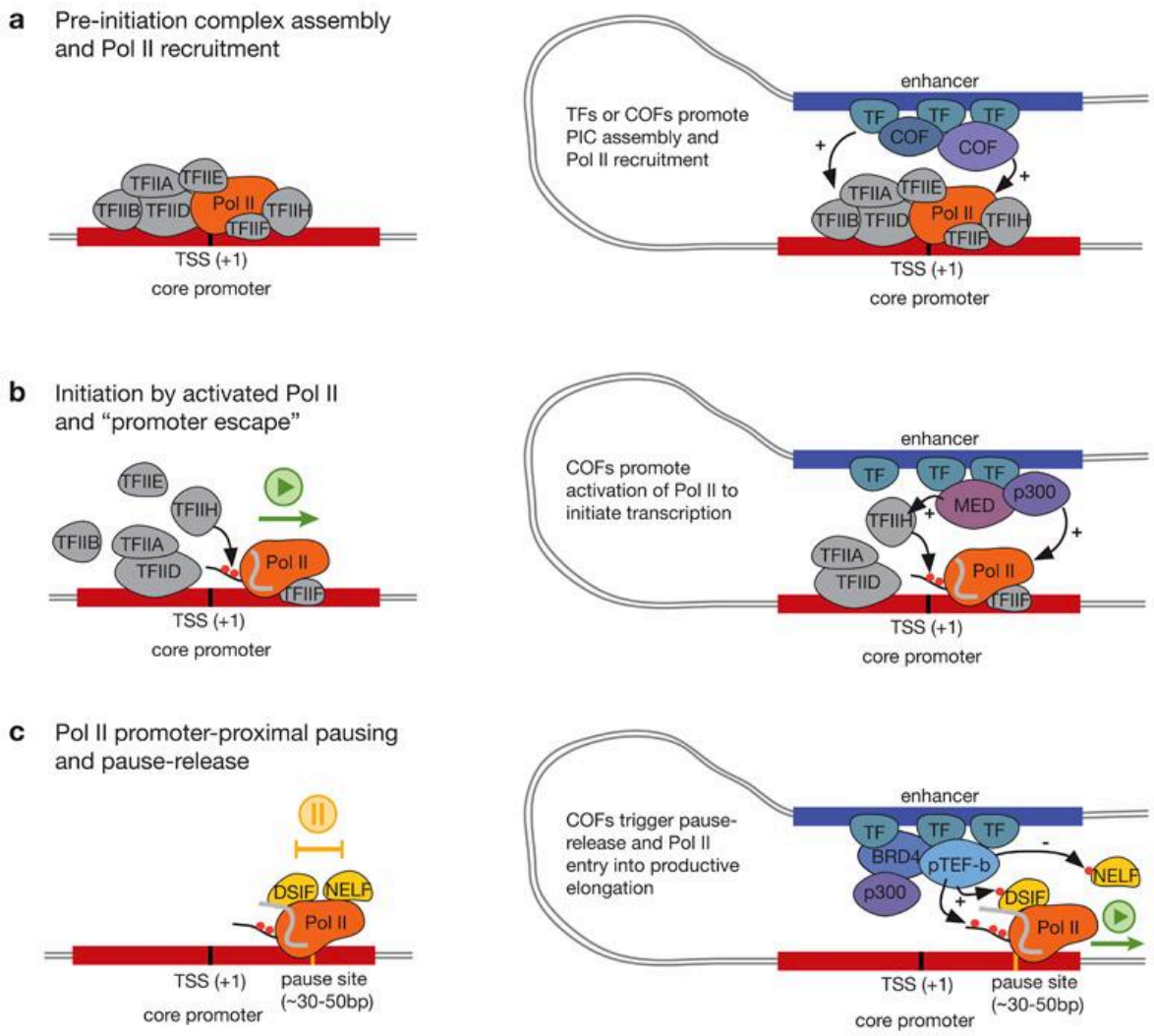

Figure 18. Regulation of RNA polymerase II initiation, pausing, and elongation. Transcription initiation involves assembly of the pre-initiation complex and recruitment of RNA polymerase II (RNAPII) at gene promoters, a process enhanced by transcription factors and co-activators such as Mediator and p300 bound at distal enhancers. Following initiation, RNAPII frequently enters a promoter-proximal paused state stabilized by DSIF and NELF. Release into productive elongation requires P-TEFb-mediated phosphorylation of RNAPII and pausing factors, often facilitated by BRD4, thereby promoting transcriptional elongation. Adapted from *Haberle and Stark, Nat Rev Mol Cell Biol (2018)*.

Finally, transcription termination occurs after RNAPII transcribes the full gene body and encounters the polyadenylation signal (PAS; AAUAAA) at the 3′ end of genes. Recognition of the PAS allows assembly of the 3′ end processing machinery, leading to cleavage of the nascent pre-mRNA and definition of the 3′ untranslated region (UTR), a critical step for transcription termination (Rodríguez-Molina *et al*, 2023). This cleavage and polyadenylation process promotes recruitment of termination factors, including the Glc7/PP1 phosphatase, which dephosphorylates RNAPII, resulting in transcriptional elongation slowing. This exposes the polymerase to 5′-3′ exonucleases, notably XRN2, which degrades the downstream RNA cleavage product until it reaches RNAPII, ultimately triggering its dissociation (Figure 19) (Eaton *et al*, 2020).

b. Gene expression dysregulation in cancer

The discovery of transcriptional control by Jacob and Monod in 1961 introduced the concept that genes are conditionally expressed and regulated by specific regulatory elements (Jacob & Monod, 1961), laying the foundation for subsequent decades of research demonstrating the central role of transcriptional regulation in maintaining cellular identity and homeostasis. The development of high-throughput sequencing and functional genomic screening technologies in early 2000s further revealed the extent to which transcriptional programs are profoundly altered in tumors. Thus, transcriptional dysregulation is now recognized as a pervasive feature of cancer, contributing to malignant progression, cellular plasticity, and therapeutic responsiveness (Bradner *et al*, 2017). Interestingly, a recent study has demonstrated that epigenetic and transcriptional alterations can be sufficient to drive tumorigenesis even in the absence of genetic mutations, underscoring the central role of gene expression dysregulation in cancer initiation and progression (Parreno *et al*, 2024).

Gene expression dysregulation in cancer can arise through alterations in trans-acting factors, primarily involving DNA-binding transcription factors and associated cofactors that regulate transcription, or through changes in cis-regulatory elements, which are DNA sequences located near or within the genes they regulate (Lee & Young, 2013). The latter includes the acquisition or remodeling of regulatory regions known as super-enhancers, which are densely occupied by transcriptional regulators and are increasingly recognized for their prominent role in sustaining oncogenic transcriptional programs. In the following sections, dysregulation in trans-acting and cis-regulatory factors and their contribution to tumorigenesis will be discussed, along with current strategies and their limitations in therapeutically targeting these transcriptional vulnerabilities.

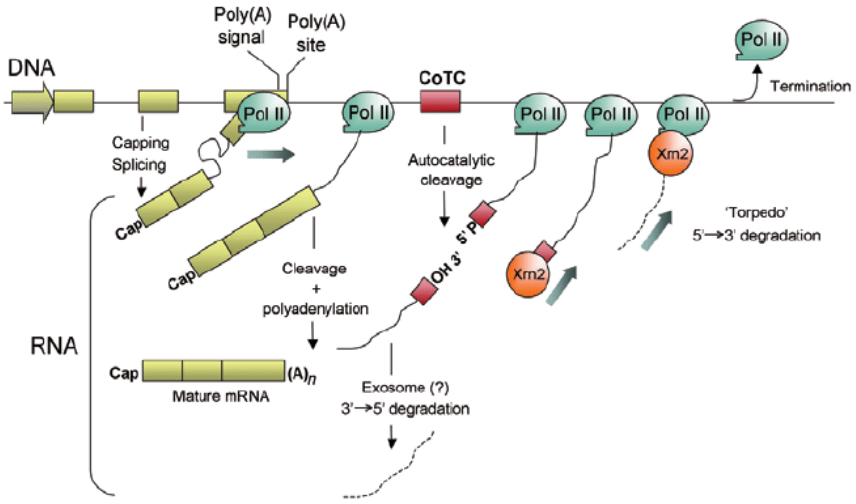

Figure 19. Transcription termination by exonuclease-mediated RNA degradation. Following cleavage at the polyadenylation site, the downstream RNA fragment is degraded by the 5′-3′ exonuclease XRN2, which progresses toward RNA polymerase II and promotes its dissociation from DNA. This mechanism ensures efficient transcription termination after completion of RNA processing. Adapted from *Kornblihtt, Nat Struct Mol Biol (2004)*.

i. Deregulation of trans-acting transcriptional regulators

Transcription factors (TFs) regulate gene expression by binding specific DNA elements, typically at enhancers or promoters, and recruiting co-activators or co-repressors to modulate transcriptional output (Lambert *et al*, 2018). While TFs were discovered decades ago, their direct implication in cancer became evident in 1997 with the identification of chromosomal translocations generating the oncogenic fusion TF PML-RARα in acute promyelocytic leukemia (Brown *et al*, 1997). Since then, numerous TFs have been shown to play central roles in tumorigenesis. Among the approximately 1,639 TFs encoded in the human genome (Xie *et al*, 2025), Lee and Young initially identified 33 TFs as recurrently dysregulated across cancer types (Lee & Young, 2013), with this number continuously expanding since. Dysregulated TFs in cancer can be broadly categorized into three functional groups: lineage-defining master TFs, proliferation-associated TFs, and signaling-responsive TFs (Bradner *et al*, 2017).

Master TFs are key regulators of cell identity and developmental gene expression programs, often operating within interconnected autoregulatory circuits that stabilize lineage specification (Figure 20) (Young, 2011). When aberrantly expressed, master TFs can reprogram transcriptional states and confer stem-like or plastic phenotypes. For example, SOX2, a regulator of stem cell identity, is frequently overexpressed in squamous cell carcinoma, where it drives transcriptional programs conferring stem cell properties and supporting tumor initiation and maintenance (Boumahdi *et al*, 2014). Similarly, the melanocyte lineage regulator MITF acts as a master TF in melanoma, where variations in its expression levels control the balance between proliferative and invasive cellular states (Ballotti *et al*, 2020). In another example, SNAIL1, normally activated during embryonic development and wound healing, becomes aberrantly expressed in breast cancer and promotes epithelial-mesenchymal transition (EMT) and tumor progression (Youssef *et al*, 2024).

Proliferation-associated TFs directly regulate genes controlling cell cycle progression and growth (Fischer *et al*, 2022). A prominent example is the MYC family of oncogenic TFs, among the most frequently deregulated drivers in cancer. For instance, c-MYC expression is commonly elevated in multiple tumor types through mutations, gene amplification, or translocations, where it enhances transcriptional output of growth-promoting genes in part by aberrantly recruiting the elongation factor P-TEFb to their promoters (Lin *et al*, 2012). Another paralogue, N-MYC, is frequently amplified in neuroblastoma, where it binds enhancers and cooperates with additional TFs to sustain aberrant gene expression programs required for tumor growth and survival (Durbin *et al*, 2018). In contrast, the tumor suppressor TF TP53 restrains

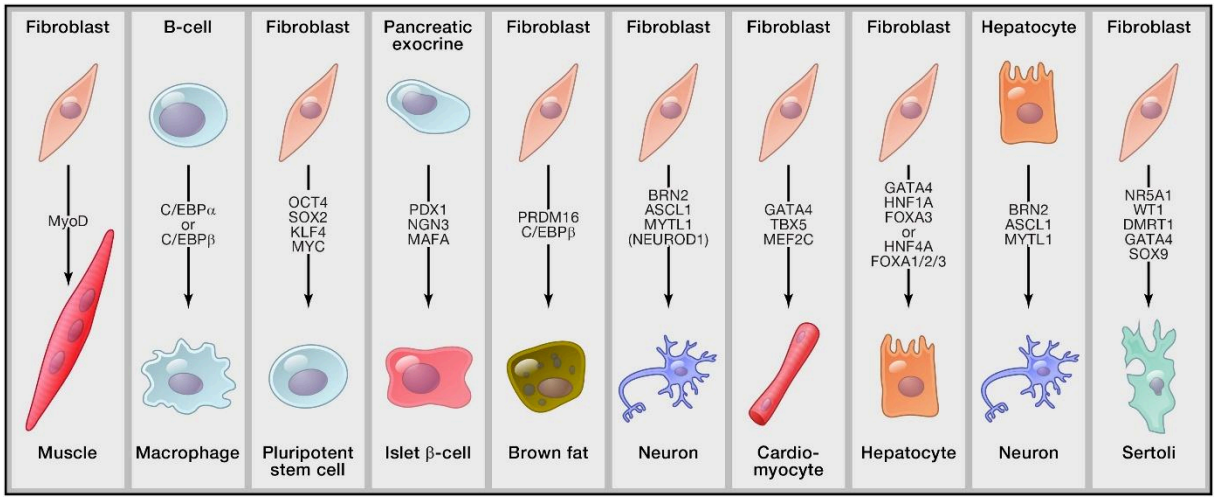

Figure 20. Master transcription factors control cell identity and lineage specification. Master transcription factors regulate cell identity by controlling lineage-specific gene expression programs and forming interconnected regulatory circuits. Their expression can reprogram cellular states, as illustrated by the conversion of differentiated cells into alternative lineages through defined combinations of transcription factors. Reproduced from *Lee and Young, Cell (2013)*.

proliferation by regulating genes involved in cell cycle arrest, DNA repair, and apoptosis. Loss-of-function mutations in TP53 occur in more than half of human cancers and are particularly prevalent in small-cell lung cancer (~90% of cases) (Chen *et al*, 2022).

Finally, signaling-responsive TFs are activated downstream of extracellular signaling pathways and translate environmental cues into transcriptional responses (Figure 21) (Sanchez-Vega *et al*, 2018). For example, STAT3 is activated downstream of the JAK signaling pathway in response to cytokines and is frequently hyperactivated in cancer. Elevated STAT3 activity in the tumor microenvironment contributes to immune evasion by repressing pro-immunogenic transcriptional programs and promoting exclusion of cytotoxic T cells, thereby limiting immunotherapy efficacy (Zhou *et al*, 2025). Similarly, aberrant activation of TGF-β signaling has been shown to cooperate with the RAS-associated TF RREB1 to induce EMT and tumor cell plasticity (Su *et al*, 2020). In parallel, TGF-β hyperactivation promotes SOX4 expression, which represses genes involved in anti-tumor immunity and fosters resistance to immunotherapy in triple-negative breast cancer (Bagati *et al*, 2021).

Besides classical sequence-specific TFs, cancer frequently involves deregulation of trans-acting co-regulators, including co-activator complexes, chromatin architectural proteins, and ATP-dependent chromatin remodelers. The Mediator is a conserved co-activator complex of ~26 subunits that integrates inputs from enhancer-bound transcription factors and couples them to RNA polymerase II, thereby regulating transcription initiation and pausing and contributing to enhancer-promoter communication, in part through functional interplay with the cohesin complex (Richter *et al*, 2022). In cancer, Mediator deregulation often involves its kinase module. For instance, amplification or overexpression of CDK8 has been shown to promote oncogenic transcriptional outputs, including pathway-dependent programs such as WNT/β-catenin signaling in colorectal cancer, as well as pro-tumorigenic transcriptional states in melanoma (Firestein *et al*, 2008; Kapoor *et al*, 2010). Moreover, MED12 is another Mediator subunit that regulates kinase-module function (Richter *et al*, 2022). Mutations in MED12 that induce global gene expression changes were identified by tumor exome sequencing in several cancers (Mäkinen *et al*, 2011; Barbieri *et al*, 2012; Lim *et al*, 2014), and have been extensively discussed as determinants of tumorigenesis and therapy responses (Zhang *et al*, 2020).

In addition, the cohesin complex is a major regulator of 3D genome organization. Cohesin uses ATP to extrude chromatin loops that are frequently positioned and constrained by CTCF, contributing to the establishment of loop domains and boundary insulation, and thereby shaping

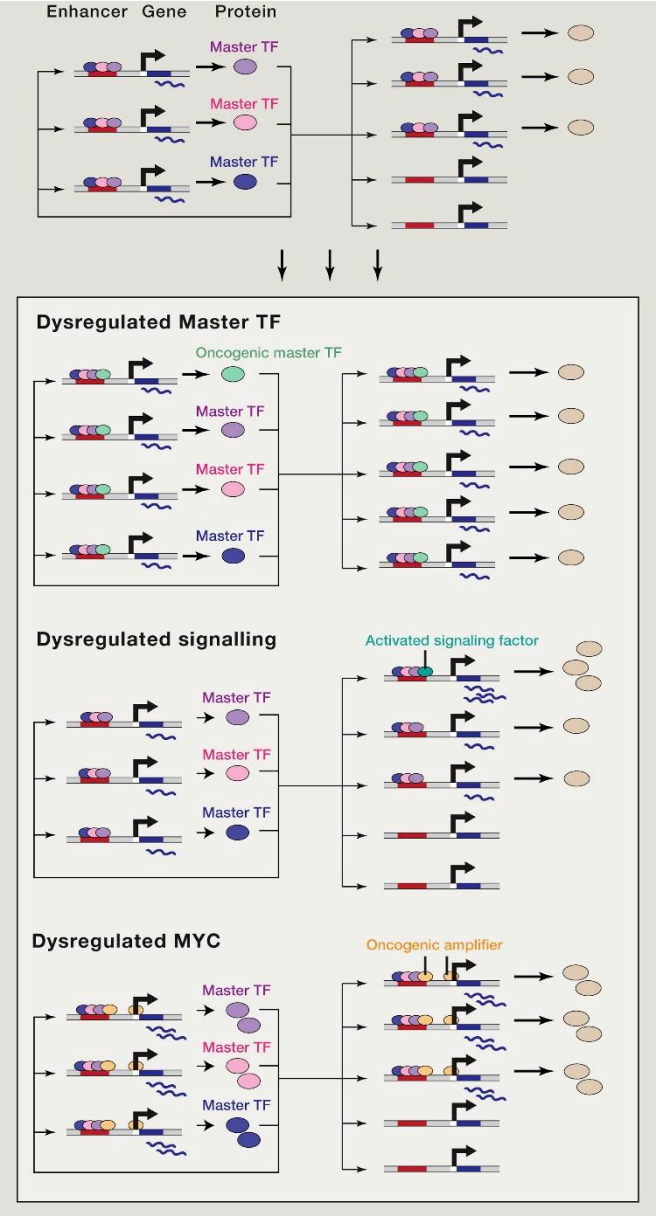

Figure 21. Mechanisms of transcription factor dysregulation in cancer. Transcriptional dysregulation in cancer arises through multiple mechanisms, including aberrant activity of master transcription factors, activation of signaling-responsive transcription factors, and amplification of oncogenic regulators such as MYC. These alterations lead to widespread changes in gene expression programs that promote tumor initiation, progression, and immune evasion. Adapted from *Bradner et al., Cell (2017)*.

enhancer-promoter communication and gene expression (Rittenhouse & Dowen, 2024; Nazarova & Sexton, 2026). Consistent with these functions, cohesin subunits and CTCF are recurrently altered in cancer (Figure 22). For example, loss-of-function mutations or deletions of the cohesin subunit STAG2 occur in multiple tumor types and have been linked to cohesin defects and aneuploidy, connecting cohesin disruption to chromosomal instability (Solomon *et al*, 2011). Beyond genome instability, leukemia-associated cohesin mutations can reinforce stem-like transcriptional programs and impair differentiation through altered chromatin accessibility and transcription factor occupancy (Viny *et al*, 2015; Mazumdar *et al*, 2015). More recently, functional genetic screens implicated cohesin components and CTCF as strong negative regulators of PD-L1, linking architectural deregulation to immune-relevant transcriptional states and potential immune-evasion phenotypes (Oreskovic *et al*, 2022). *In vivo* work also supports a tumor-suppressive role for CTCF dosage, demonstrating that CTCF hemizygosity predisposes to cancer and is associated with destabilized DNA methylation landscapes, and suggesting that partial loss of CTCF can erode epigenomic fidelity in ways that promote tumorigenesis (Kemp *et al*, 2014). Furthermore, CTCF genetic alterations have been characterized as pro-tumorigenic in endometrial carcinoma, with functional consequences that include altered epithelial organization and enhanced survival phenotypes (Marshall *et al*, 2017).

A further layer of trans-acting regulation involves ATP-dependent chromatin remodelers, most notably SWI/SNF (mSWI/SNF/BAF complexes), controlling developmental and cell-identity programs by regulating nucleosome positioning and chromatin accessibility (Centore *et al*, 2020). Large-scale analyses indicate that SWI/SNF subunits are among the most frequently altered chromatin regulators in cancer, with alterations reported in ~20% of human cancers (Kadoch *et al*, 2013). Importantly, SWI/SNF functions in cancer are context- and subcomplex-dependent, such that phenotypic outcomes depend on which module or subunit is affected (Figure 23) (Mittal & Roberts, 2020). For instance, recent work showed that the PBAF subcomplex can create accessibility within Polycomb-repressed chromatin to enable occupancy of the silencing transcription factor REST, and that ARID2/PBAF disruption impairs this repression program in melanoma-relevant contexts (Grossi *et al*, 2025). Conversely, other studies support pro-oncogenic roles for the SWI/SNF ATPases SMARCA4/SMARCA2 in sustaining proliferative and EMT-like programs and therapy resistance in EGFR-mutant lung cancer, highlighting that SWI/SNF deregulation is not monolithic but depends on the module or subunit that is perturbed (de Miguel *et al*, 2023).

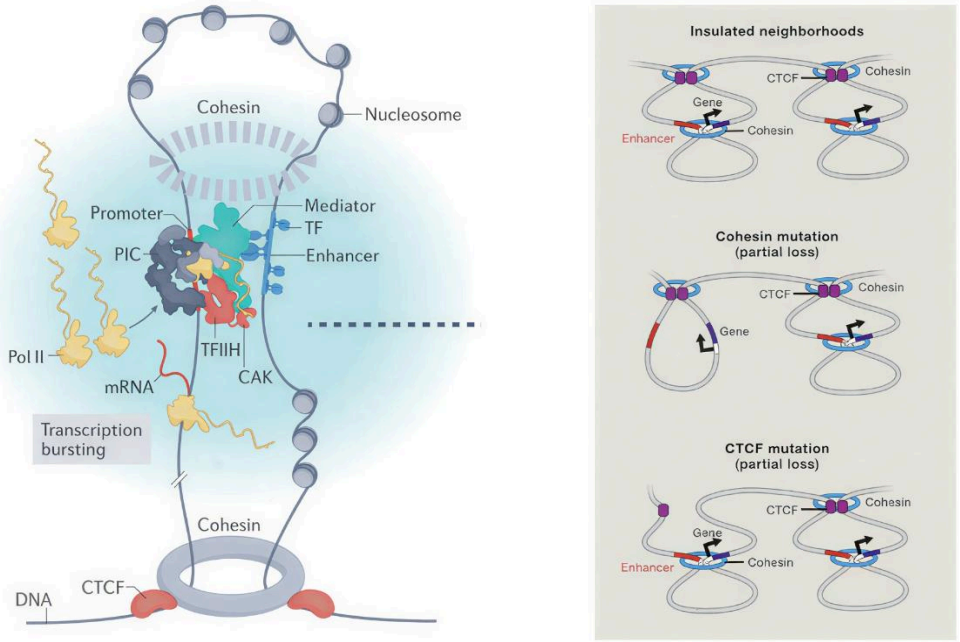

Figure 22. Cohesin- and CTCF-mediated chromatin organization and its alteration in cancer. Cohesin mediates ATP-dependent chromatin loop extrusion, which is constrained by CTCF to establish loop domains and facilitate enhancer-promoter interactions. Alterations in cohesin or CTCF disrupt chromatin architecture, leading to aberrant enhancer-promoter communication and dysregulated gene expression in cancer. Adapted from *Richter et al., Nat Rev Mol Cell Biol (2022)*; *Bradner et al., Cell (2017)*.

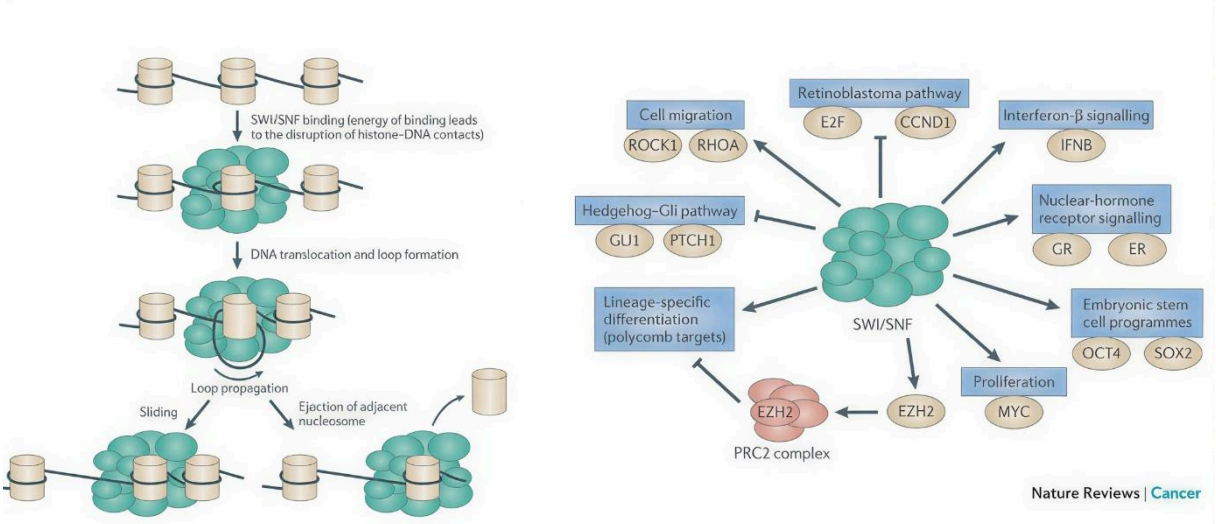

Figure 23. SWI/SNF chromatin remodeling and its role in regulating gene expression programs. SWI/SNF complexes use ATP-dependent chromatin remodeling to reposition or evict nucleosomes, thereby modulating chromatin accessibility. Through this activity, SWI/SNF regulates multiple gene expression programs, including proliferation, differentiation, and signaling pathways. Dysregulation of SWI/SNF components alters transcriptional networks and contributes to tumorigenesis. Adapted from *Wilson and Roberts, Nat Rev Cancer (2011)*.

Collectively, dysregulation of trans-acting TFs and co-regulators drives large-scale reprogramming of gene expression networks that promote tumor initiation, progression, plasticity, and immune evasion.

ii. Deregulation of cis-regulatory architecture: emergence of super-enhancers and transcriptional condensates

Early cancer research focused primarily on alterations within coding regions of the human genome. However, subsequent studies revealed that frequent alterations also occur within cis-regulatory elements located outside coding sequences, with the first cis-regulatory alteration directly linked to tumorigenesis identified in 1982, following the discovery of chromosomal translocations repositioning MYC regulatory elements in lymphoma (Taub *et al*, 1982). Since then, it has become clear that dysregulation of promoters, insulators, and enhancers represents a major mechanism driving oncogenic transcriptional programs.

Promoters can acquire mutations that directly alter the output of transcriptional programs. A prominent example is hotspot point mutations in the TERT promoter, identified in 2013 in approximately 71% of melanoma samples in two independent reports (Horn *et al*, 2013; Huang *et al*, 2013), and later detected in other cancer types (Killela *et al*, 2013; Kinde *et al*, 2013). These mutations create de novo binding sites for ETS transcription factors, leading to increased TERT expression, along with elevated DNA damage, telomerase activity and telomere stabilization (Figure 24) (Bell *et al*, 2015; Elliott *et al*, 2024).

Insulators, frequently bound by the architectural protein CTCF, prevent inappropriate enhancer-promoter interactions that could lead to undesirable gene activation (Gaszner & Felsenfeld, 2006). Disruption of CTCF binding sites has been frequently observed in colorectal cancer (Katainen *et al*, 2015). Beyond direct mutations, one study found that metabolic alterations, more specifically succinate dehydrogenase (SDH) deficiency, induce global DNA hypermethylation in gastrointestinal tumors, leading to loss of CTCF binding at insulator elements. This disrupts TAD boundaries and chromatin loops, enabling ectopic enhancer-promoter contacts and driving aberrant activation of oncogenic programs (Figure 25) (Flavahan *et al*, 2019).

Among cis-regulatory alterations, enhancer dysregulation has emerged as one of the most extensively studied mechanisms in cancer. Approximately one million enhancers have been identified in the human genome across multiple cell types (ENCODE Project Consortium, 2012). Among these, tumorigenesis frequently involves dysregulation of relatively small

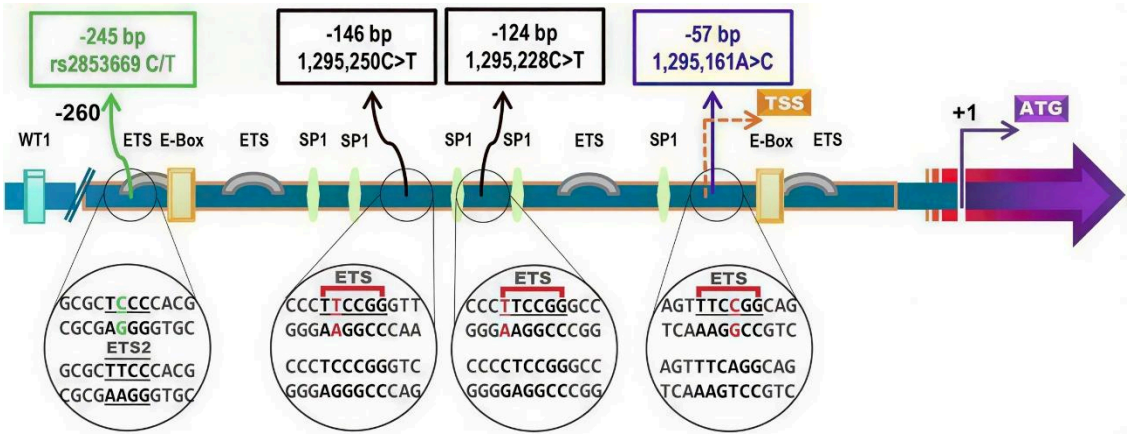

Figure 24. TERT promoter mutations create de novo transcription factor binding sites. Recurrent hotspot mutations in the TERT promoter generate consensus binding motifs for ETS transcription factors, leading to increased TERT expression and activation of telomerase. These mutations enhance transcriptional output by altering promoter sequence composition and transcription factor recruitment. Reproduced from Rachakonda et al., *Int J Cancer (2021)*.

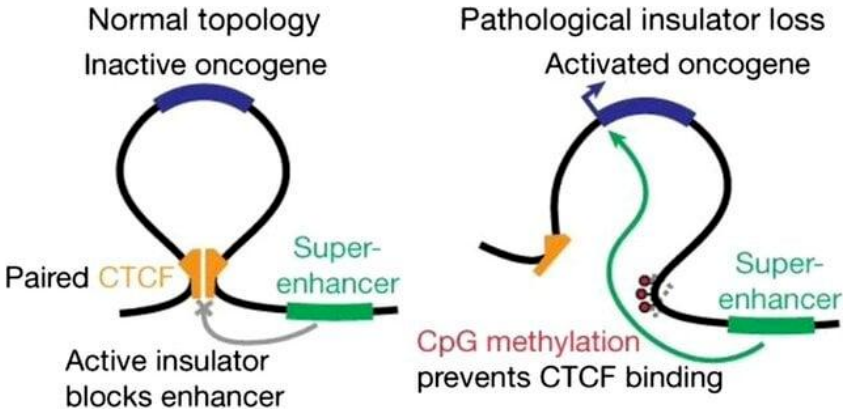

Figure 25. Disruption of CTCF-mediated insulation drives oncogene activation. In normal chromatin architecture, CTCF-bound insulators restrict enhancer-promoter interactions. In cancer, DNA hypermethylation can prevent CTCF binding, leading to loss of insulation, aberrant chromatin looping, and ectopic activation of oncogenes by distal enhancers. Adapted from *Flavahan et al., Nature (2019)*.

subsets of regulatory regions through the acquisition or remodeling of super-enhancers (SEs). SEs are defined as large clusters of enhancers in close genomic proximity that are densely occupied by transcription factors (TFs) and co-activators, and that drive exceptionally high and cell-type-specific expression of genes critical for cell identity or oncogenesis (Figure 26) (Pott & Lieb, 2015). Compared to normal cells, cancer cells often acquire SEs that are larger, display higher co-activator occupancy, drive aberrantly elevated expression of oncogenes, and often exhibit increased sensitivity to transcriptional perturbation (Hnisz *et al*, 2013).

The notion of SEs was first introduced in a study on mouse embryonic stem cells (mESCs) by Whyte and colleagues in 2013, who discovered that among 8,793 putative enhancers, approximately 40% of the total Mediator signal was concentrated within 231 enhancer domains, which they termed "super-enhancers." SEs were characterized mainly by (i) a substantially larger genomic span compared to typical enhancers (median size ~8,667 bp vs ~703 bp), and (ii) exceptionally high occupancy of Mediator, master transcription factors (e.g., KLF4 and Esrrb), and the active histone mark H3K27ac (Figure 27A). Gene ontology analyses revealed that SEs preferentially control key embryonic stem cell genes essential for pluripotency, such as Oct4, SOX2, and Nanog, without being associated with other highly expressed housekeeping genes. Importantly, knockdown of the Mediator subunit MED12 selectively reduced expression of SE-associated genes, with limited effects on genes associated with typical enhancers (Whyte *et al*, 2013).

Shortly thereafter, SEs were identified in multiple myeloma, where they were found to drive transcription of oncogenes controlling hematopoietic identity and proliferation (e.g., MYC, IRF4, XBP1), and were distinguished from typical enhancers by markedly higher MED1 and BRD4 occupancy (~16 to 18-fold enrichment) (Figure 27B). SE-associated oncogenes were expressed at substantially higher levels than genes linked to typical enhancers, and disruption of BRD4 preferentially suppressed SE-driven oncogenic transcription (Lovén *et al*, 2013). Subsequent studies identified SE-driven oncogenes across a broad range of tumor types, including neuroblastoma (Chipumuro *et al*, 2014), breast (Wang *et al*, 2015), and gastric cancers (Ooi *et al*, 2016).

In some cases, SEs can also participate in cell-fate transitions during cancer initiation. For example, in zebrafish models of melanoma, $BRAF^{V600E}$/p53 mutations promote the establishment of a SE at SOX10, a key gene involved in neural crest cell formation (Kaufman *et al*, 2016). Furthermore, comparative analyses of multiple tumors have shown that SEs controlling key oncogenes such as MYC are frequently unique to cancer cells and absent in

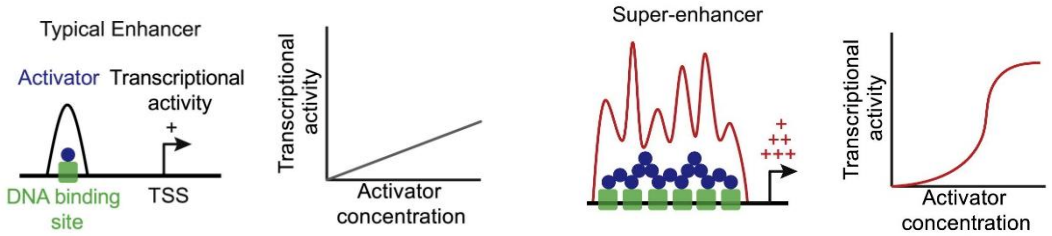

Figure 26. Super-enhancers drive high transcriptional output through clustered regulatory activity. Super-enhancers are clusters of enhancers densely occupied by transcription factors and co-activators that drive high levels of gene expression. Compared to typical enhancers, they exhibit increased transcriptional output and heightened sensitivity to transcription factor concentration, contributing to robust activation of key cell identity and oncogenic genes. Adapted from *Lovén et al., Cell (2013)*.

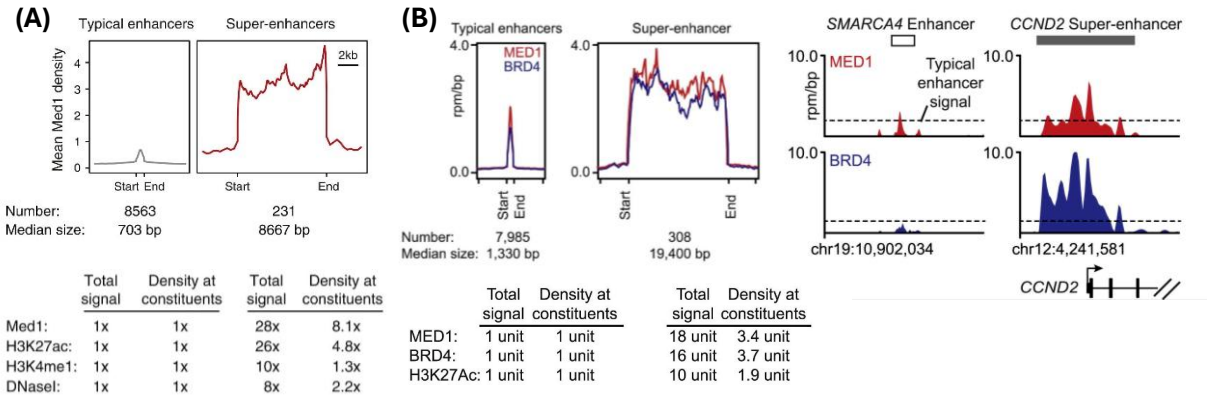

Figure 27. Super-enhancers are defined by large genomic domains and high co-activator occupancy. (A) Super-enhancers are larger than typical enhancers and display disproportionately high levels of Mediator and active chromatin marks such as H3K27ac **(B)** Super-enhancers exhibit markedly increased occupancy of co-activators including MED1 and BRD4 compared to typical enhancers, and are associated with elevated expression of key cell identity and oncogenic genes. Adapted from *Whyte et al., Cell (2013); Lovén et al., Cell (2013*).

their healthy counterparts (Hnisz *et al*, 2013), highlighting SE acquisition as a tumor-specific regulatory event. Following studies revealed that SE formation in cancer can arise through two major mechanisms: (i) local alterations in cis-regulatory elements and (ii) large-scale chromosomal rearrangements (Figure 28) (Sengupta & George, 2017).

Alterations in cis-regulatory elements leading to SE formation were first demonstrated in T-cell acute lymphoblastic leukemia, where insertions of short DNA sequences upstream of the TAL1 oncogene created de novo binding sites for the MYB transcription factor, leading to recruitment of CBP/p300 acetyltransferase, formation of a SE, and aberrant TAL1 overexpression (Mansour *et al*, 2014). Single-nucleotide mutations have similarly been shown to generate SEs in neuroblastoma (Oldridge *et al*, 2015). In diffuse large B-cell lymphoma, hypermutations within oncogene-associated SEs, found in ~92% of patients, disrupt transcriptional repressor binding, resulting in aberrant oncogenic activation (Bal *et al*, 2022). Chromosomal rearrangements represent a second mechanism of SE hijacking, first demonstrated in adenoid cystic carcinoma, where translocations repositioned a distal SE near the MYB gene, leading to its overexpression (Drier *et al*, 2016). Focal amplification of SE regions has also been observed, for example in neuroblastoma, further enhancing oncogenic transcriptional output (Chipumuro *et al*, 2014).

In addition to structural alterations, oncogenic signaling pathways contribute to SE acquisition and maintenance. One study revealed that SEs are enriched for terminal TFs downstream of major oncogenic pathways such as Wnt and TGF-β. Pharmacological inhibition of these pathways preferentially reduces expression of SE-associated genes, suggesting that signaling cascades act as upstream regulators of SE architecture (Hnisz *et al*, 2015). Although SEs are frequently associated with oncogene activation, they can also regulate tumor suppressor genes. For instance, in lung cancer, loss of the histone methyltransferase KMT2D impairs a SE controlling the tumor suppressor PER2, leading to its downregulation and promoting tumorigenesis in mouse models (Alam *et al*, 2020).

Despite these findings, conceptual limitations challenging the SE notion remain (Blobel *et al*, 2021). For a start, SEs lack a strict functional definition and clear rules separating them from typical or stitched enhancers. Currently, SE identification is based on ChIP-seq signal enrichment using the ROSE (Ranking Order of Super-Enhancers) algorithm, which stitches enhancer entities within 12.5 kb and ranks them according to normalized enrichment of MED1, BRD4, or H3K27ac. Plotting the distribution of intensity values generates an inflection point, above which regions are classified as SEs, while those below are considered typical enhancers (Figure 29) (Lovén *et al*, 2013). This operational definition has fueled debate regarding whether

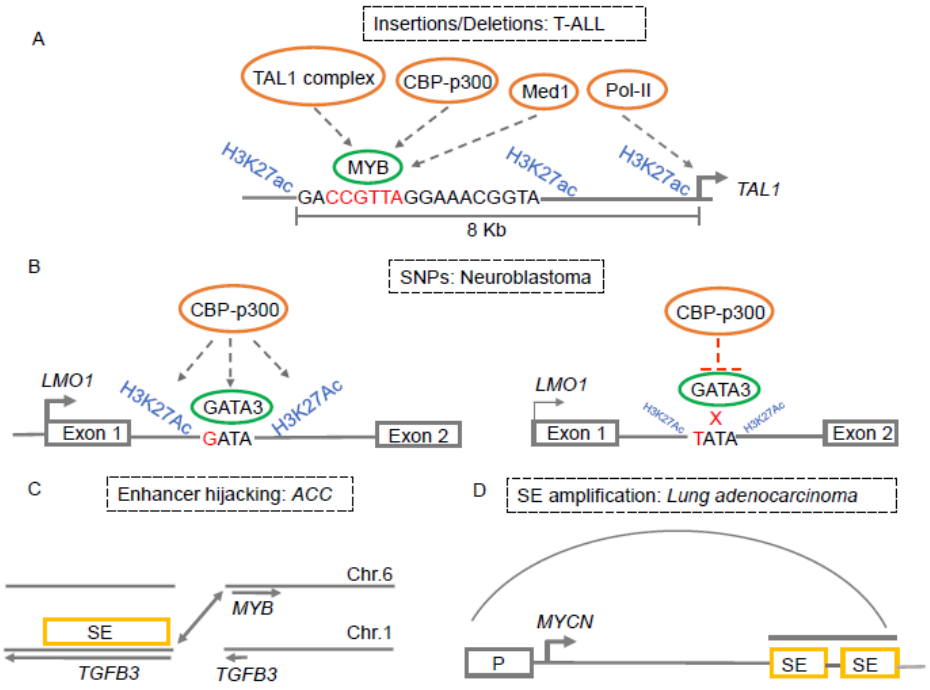

Figure 28. Mechanisms of super-enhancer formation and hijacking in cancer. Super-enhancers can arise through multiple genomic alterations, including insertions or point mutations that create de novo transcription factor binding sites, enhancer hijacking through chromosomal rearrangements, and focal amplification of regulatory regions. These events promote recruitment of transcriptional co-activators and establishment of super-enhancers, leading to aberrant activation of oncogenes. Reproduced from *Sengupta and George, Trends Cancer (2017)*.

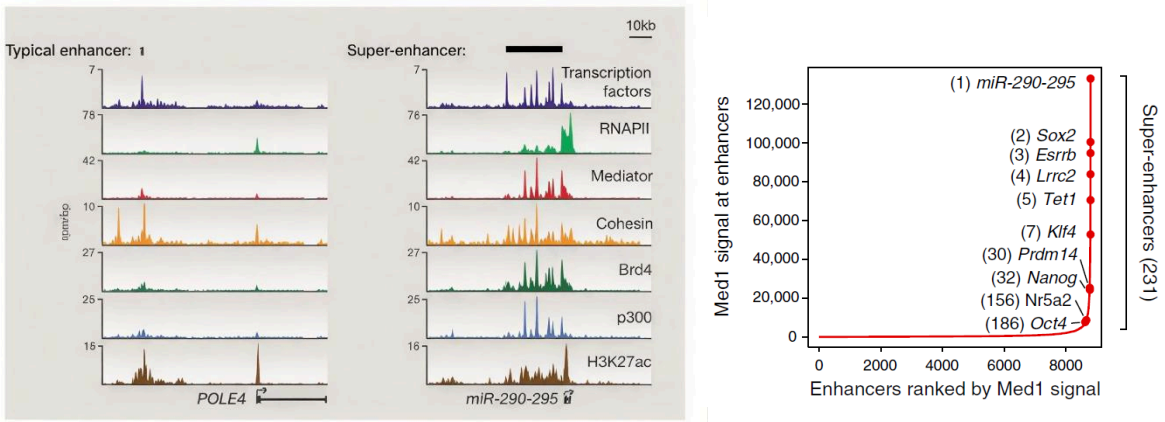

Figure 29. Identification of super-enhancers based on signal enrichment and ranking. Super-enhancers are defined by high levels of transcriptional regulators such as MED1, BRD4, and H3K27ac compared to typical enhancers. ROSE algorithm stitches enhancers within 12.5 kb and rank them according to normalized signal intensity, creating an inflection point that separates super-enhancers from typical enhancers. Adapted from *Hnisz et al., Mol Cell (2015); Cell (2017)*.

SEs represent a biologically distinct entity or the upper extreme of a continuum of enhancer activity.

At the functional level, constituent elements within SEs exhibit increased capacity to activate transcription compared to typical enhancers (Hnisz *et al*, 2015). However, the mechanism underlying this enhanced functionality was not fully understood. A recent study of the mouse α-globin SE demonstrated that among its five constituent elements, two functioned as classical enhancers (R1, R2), whereas three lacked intrinsic activity and were termed "facilitators" (R3, Rm, and R4). Strikingly, removal of these facilitator elements markedly impaired Mediator recruitment and promoter interaction, resulting in near-complete loss of SE activity (Blayney *et al*, 2023). These findings support a cooperative and modular model of SE architecture in gene activation.

For many years, traditional models of transcription based on stable "lock-and-key" interactions could not fully explain how enhancer clusters drive exceptionally high transcriptional activity (Liu *et al*, 2011). A mechanistic explanation for the amplified transcriptional output of SEs has emerged from studies of biomolecular condensates (Hnisz *et al*, 2017). Subsequent research revealed that transcription occurs within dynamic nuclear compartments or "transcription hubs", where transcription factors, Mediator, BRD4, and RNA polymerase II (RNAPII) accumulate transiently. Many of these proteins contain intrinsically disordered regions (IDRs) in their C-terminal domains, which lack stable three-dimensional structure and enable dynamic multivalent interactions that promote liquid-liquid phase separation (LLPS) and formation of transcriptional condensates (Figure 30) (Banani *et al*, 2017; Mehta & Zhang, 2022).

Other studies demonstrated that BRD4 and MED1 condensates are highly enriched at SEs relative to typical enhancers. Disruption of these condensates using 1,6-hexanediol (an aliphatic alcohol that dissolves liquid-like droplets), preferentially reduces BRD4, MED1 and RNAPII occupancy at SEs and selectively decreases expression of SE-associated genes (Figure 31). Importantly, forced IDR mutations in BRD4 and MED1 impair their ability to form condensates and diminish transcriptional activation (Sabari *et al*, 2018; Boija *et al*, 2018), supporting a model in which phase separation contributes to amplification of SE-driven transcription. In addition to TFs and co-activators, a recent study demonstrated accumulation of extrachromosomal DNA (ecDNA) at SEs to form transcriptional condensates with MED1 and drive aberrant oncogenic expression (Taghbalout *et al*, 2025), extending current models of SE-driven regulation beyond canonical TF-centered mechanisms.

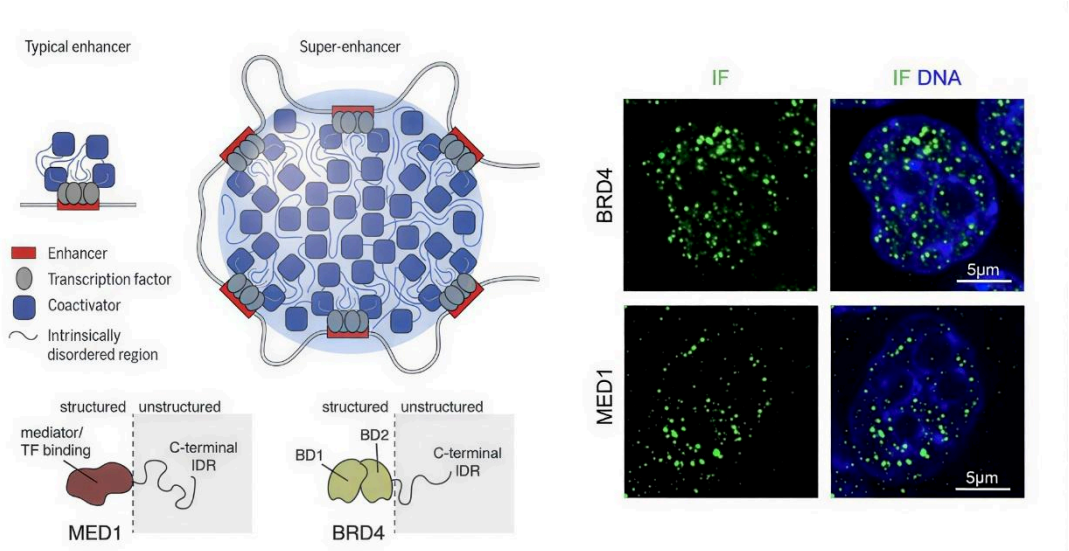

Figure 30. Transcriptional condensates at super-enhancers driven by phase separation. Super-enhancers promote the formation of transcriptional condensates through accumulation of transcription factors, co-activators such as MED1 and BRD4, and RNA polymerase II. Unstructured, intrinsically disordered regions (IDRs) within these proteins enable multivalent interactions that drive liquid-liquid phase separation, leading to the formation of dynamic transcriptional hubs with high local concentration of the transcriptional machinery. Adapted from *Sabari et al., Science (2017); Mehta and Zhang, Nat Rev Cancer (2022)*.

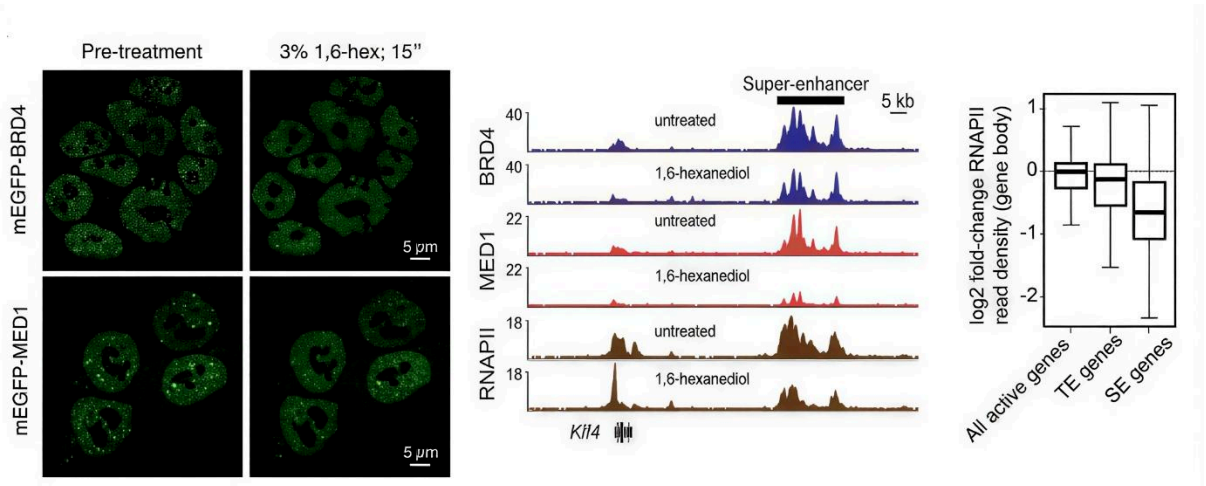

Figure 31. Disruption of transcriptional condensates preferentially affects super-enhancer activity. Chemical disruption of phase-separated condensates using 1,6-hexanediol reduces the occupancy of BRD4, MED1, and RNA polymerase II at super-enhancers. This leads to a preferential decrease in transcription of super-enhancer-associated genes compared to genes linked to typical enhancers, supporting a role for condensates in amplifying transcriptional output. Adapted from *Sabari et al., Science (2018)*.

Recently, a super-resolution imaging study proposed a “three-way kissing” model in which condensates formed at SEs dynamically interact with target gene promoters, enhancing transcriptional bursting. Increased proximity between condensates and promoters correlates with elevated burst frequency and amplitude (Figure 32) (Du *et al*, 2024). Together, these findings support a model in which cooperative enhancer architecture and condensate formation amplify transcription at SE-associated genes, providing a mechanistic basis for their disproportionate regulatory influence in cancer and representing an opportunity for therapeutic intervention in tumors characterized by SE-driven transcriptional programs that are not effectively targeted by conventional therapies.

c. Targeting transcriptional addiction in cancer: current strategies and limitations

The concept of oncogenic addiction was proposed in 2006 to describe the absolute dependence of cancer cells on oncogenes that were initially acquired during early steps of tumorigenesis and that remain critical for the ongoing proliferation and survival even after transformation into a neoplastic state (Weinstein & Joe, 2006). In 2017, Bradner et al. extended this notion to include dependence on transcriptional and epigenomic apparatus that regulates these oncogenes (e.g., cis-regulatory elements, transcription factors, chromatin machinery) (Figure 33) (Bradner *et al*, 2017), highlighting the importance of upstream transcriptional regulators required to sustain oncogene expression. Building on this conceptual framework, targeting transcriptional addiction in cancer has emerged as an attractive therapeutic strategy, consistent with the earlier proposal of James E. Darnell to therapeutically target overactive transcription factors (TFs) in cancer (Darnell, 2002).

Despite its appeal, for many years, TF targeting faced major challenges, leading to a view that TFs are “undruggable”. This perception arose from several structural and biochemical constraints. In particular, DNA-binding domains of TFs often present convex and highly positively charged surfaces that lack discrete binding cavities. In addition, many TFs interfaces are relatively flat and lack the deep pockets typically found in enzyme active sites, making it difficult for small molecules to achieve sufficient affinity and specificity (Bushweller, 2019). However, this view has shifted, as recent studies have demonstrated notable success in indirectly modulating TF activity through several approaches.

First, small molecules targeting nuclear receptors upstream of terminal TF outputs represent one of the most clinically successful TF-targeting paradigms to date. A prominent example is

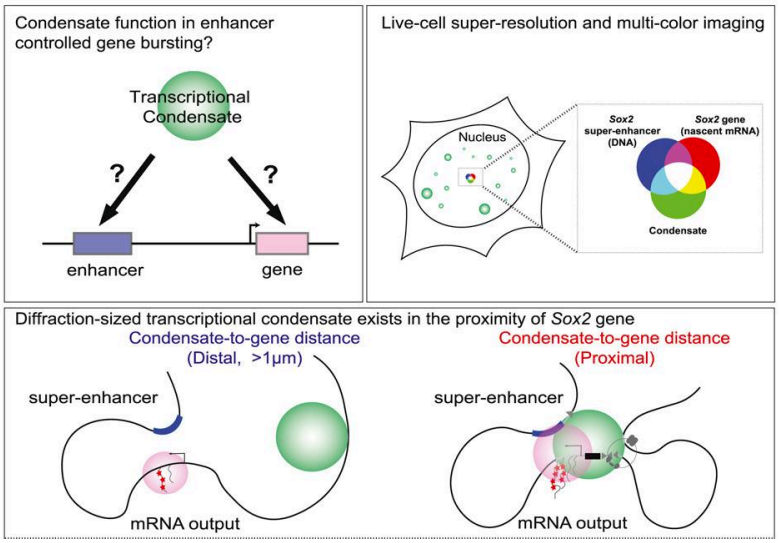

Figure 32. Spatial coupling between super-enhancer condensates and target genes regulates transcriptional bursting. Super-resolution imaging reveals that transcriptional condensates formed at super-enhancers dynamically interact with target gene promoters. Increased proximity between condensates and genes correlates with enhanced transcriptional bursting. Reproduced from *Du et al., Cell (2024)*.

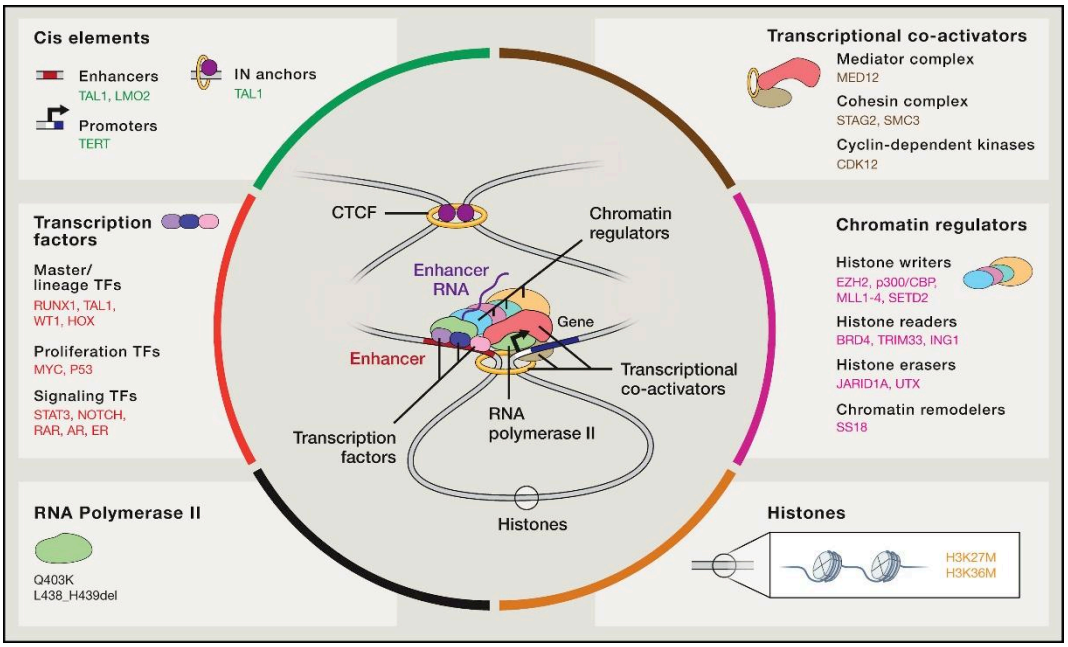

Figure 33. Integration of cis-regulatory elements and trans-acting factors in transcriptional control. Gene expression is regulated through the interplay between cis-regulatory elements, such as enhancers and promoters, and trans-acting factors including transcription factors, co-activators, chromatin regulators, and RNA polymerase II. In cancer, alterations in these elements drive aberrant oncogenic transcriptional programs. Reproduced from *Bradner et al., Cell (2017)*.

the use of selective hormone receptor modulators such as tamoxifen, which binds the ligand-binding domain (LBD) of estrogen receptors and blocks the conformational changes required for co-activators recruitment in breast cancer, thereby reducing oncogenic expression (Figure 34A) (Shiau *et al*, 1998). The main limitation of this approach is that it is primarily applicable to hormone-dependent cancers, which represent only a subset of cancer cases worldwide (~19%) (Bray *et al*, 2024).

Second, targeting protein-protein interactions involving TFs has emerged as an additional option, with increasing success over the last decade in developing small molecules that disrupt these interactions (Nada *et al*, 2024). A notable example is the development of inhibitors targeting the menin-MLL fusion TF, which arises from chromosomal translocations and drives therapeutic resistant in acute leukemias. Thus, compounds such as MI-463 and MI-503 inhibit the menin-MLL interaction, reducing occupancy at target loci and diminishing the expression of key genes that drive leukemia (Figure 34B) (Borkin *et al*, 2015). Nonetheless, small-molecule inhibitors of protein-protein interactions are often limited by high molecular weight and associated pharmacokinetic challenges, which can refrain their clinical translation (Bushweller, 2019).

Because TFs regulate large gene networks and play key roles in cellular function, their protein levels are often regulated by ubiquitination and proteasomal degradation (Mark & Rape, 2021). Accordingly, a more recent strategy is to modulate TF stability by targeting the ubiquitin-proteasome system. For instance, p53 is a major tumor suppressor TF that is frequently altered in human cancers, and its levels are controlled under normal conditions by the E3 ligase MDM2, which mediates ubiquitination and proteasomal degradation of p53. Overexpression of MDM2 occurs in multiple cancers and can substantially alter transcriptional networks and therapeutic response (Bevill *et al*, 2023). As a consequence, MDM2 inhibitors have been developed and shown to increase p53 protein levels and induce expression of tumor suppressive target genes such as p21 (Tovar *et al*, 2013). Several MDM2 inhibitors are currently in clinical trials, although clinical efficacy has so far been limited and has failed to demonstrate sufficient benefit (Wang *et al*, 2024).

More broadly, Bondeson et al. elegantly demonstrated that an E3 ligase can be recruited to a target protein via a bifunctional small molecule, thereby driving selective ubiquitination and proteasome-mediated degradation of the target (Figure 35). These molecules, termed PROTACs, provide an opportunity to target TFs by knocking down all of their functions rather than inhibiting a specific activity, with several PROTACs currently undergoing clinical trials

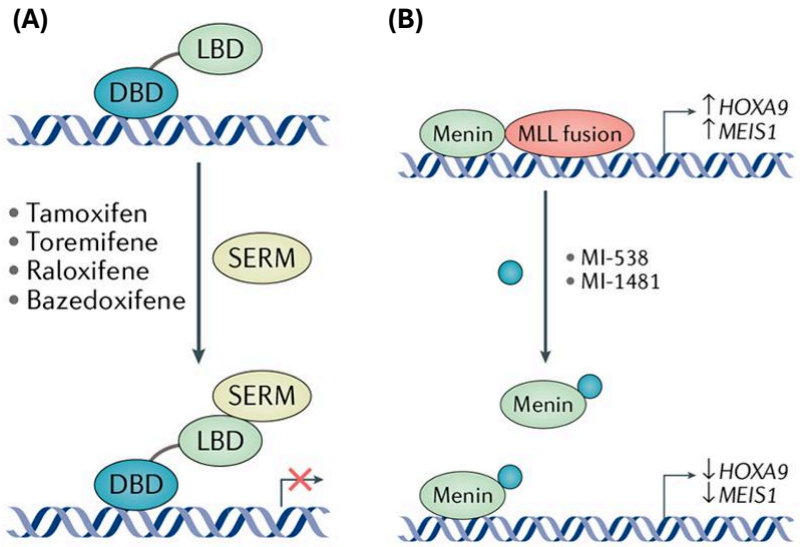

Figure 34. Targeting transcription factor activity through nuclear receptor modulation and disruption of protein-protein interactions. (A) Selective estrogen receptor modulators (SERMs), such as tamoxifen, bind the ligand-binding domain (LBD) of nuclear receptors and prevent co-activator recruitment, thereby inhibiting transcriptional activation. **(B)** Small-molecule inhibitors targeting protein-protein interactions, such as menin-MLL inhibitors, disrupt oncogenic transcription factor complexes and reduce expression of downstream target genes. Adapted from *Bushweller, Nat Rev Cancer (2019)*.

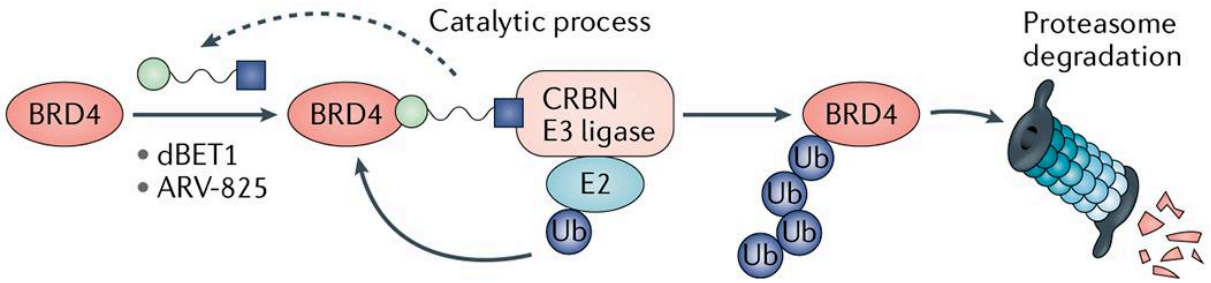

Figure 35. Targeted protein degradation using PROTACs. PROTACs are bifunctional molecules that simultaneously bind a target protein and an E3 ubiquitin ligase, promoting ubiquitination of the target and its subsequent degradation by the proteasome. This approach enables removal of transcription factors and associated proteins rather than inhibition of a single functional domain. Adapted from *Bushweller, Nat Rev Cancer (2019)*.

(Bondeson *et al*, 2015). Despite their promise, PROTACs present several limitations, including large molecular weight and off-target effects that may contribute to undesired toxicity (Gao et al, 2020).

Finally, targeting regulators of TF function provides another route to indirectly modulate TF-driven transcriptional programs. For instance, THZ1, a covalent inhibitor of the TFIIH component CDK7, inhibits phosphorylation of the RNA polymerase II (RNAPII) CTD and impairs transcription initiation and pause regulation (Kwiatkowski *et al*, 2014). Although none of these approaches has yet become broadly used as a standard-of-care strategy to directly target TFs, they represent important progress in overcoming the "undruggable" paradigm and have paved the way to therapeutically exploit super-enhancer (SE)-dependent transcription in cancer.

One of the most commonly used strategies to disrupt SE-driven transcription has been BET inhibition, exemplified by the chemical probe JQ1, which was first developed by the laboratory of James Bradner to target BRD4 and displace it from its chromatin targets (Filippakopoulos *et al*, 2010). BRD4 is a member of the bromodomain and extraterminal (BET) subfamily and contains twin acetyl-lysine recognition domains that enable binding to acetylated chromatin. BRD4 promotes transcription elongation in part through its interactions with the Mediator complex and recruitment of the elongation factor P-TEFb (Jang *et al*, 2005; Wu & Chiang, 2007). The initial attempt to target BRD4 stemmed from the discovery of chimeric BRD4-NUT fusion oncoproteins in aggressive carcinomas, which bind acetylated chromatin to block differentiation and activate proliferative transcriptional programs (French *et al*, 2003, 2008). JQ1 potently displaced BRD4-NUT from its target sites, inducing differentiation and anti-proliferative effects in murine models harboring primary human carcinoma xenografts (Filippakopoulos *et al*, 2010).

Subsequent studies demonstrated JQ1 activity in cancers lacking BRD4-NUT fusions, linking its effects to disruption of MYC regulation and anti-apoptotic transcriptional programs (Dawson *et al*, 2011; Puissant *et al*, 2013). This broader activity was clarified by the discovery that BRD4 is aberrantly recruited to SEs and regulates their function. Accordingly, JQ1 treatment induces a preferential loss of BRD4 and its associated cofactors at SEs, resulting in collapse of the SE-associated oncogenic transcriptional programs and improved survival in *in vivo* preclinical cancer models (Figure 36) (Lovén *et al*, 2013; Chapuy *et al*, 2013). These findings positioned BRD4 as a major target for attempts to disrupt SE activity.

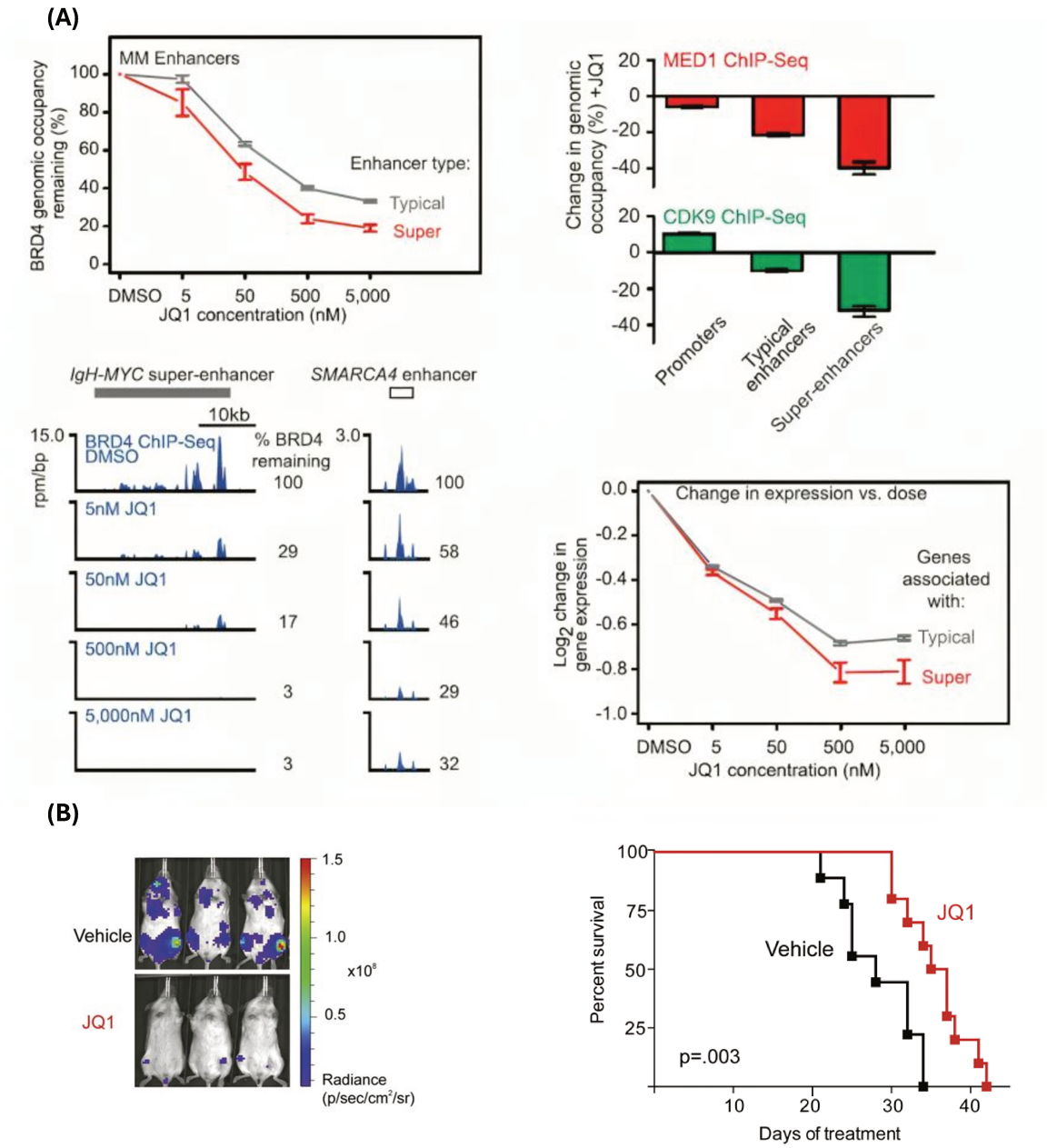

Figure 36. BET inhibition disrupts super-enhancer function and suppresses tumor growth. (A) Treatment with the BET inhibitor JQ1 reduces occupancy of BRD4 and associated co-activators such as MED1 and CDK9 at super-enhancers more strongly than at typical enhancers, leading to a preferential decrease in expression of super-enhancer-associated genes. **(B)** In preclinical cancer models, JQ1 treatment reduces tumor progression and improves survival, highlighting the therapeutic vulnerability of super-enhancer-driven transcriptional programs. Adapted from *Lovén et al., Cell (2013); Chapuy et al., Cancer Cell (2013)*.

In addition to BRD4, ChIP-seq analyses revealed that CDK7 is also enriched at oncogene-associated SEs in T-cell acute lymphoblastic leukemia (T-ALL), where it phosphorylates the RNAPII CTD and supports transcription initiation at SE-driven genes. Therefore, inhibition of CDK7 with THZ1 led to rapid loss of CDK7 at SEs and reduced RNAPII occupancy across promoters and gene bodies, resulting in preferential downregulation of SE-driven oncogenes (Figure 37) (Kwiatkowski *et al*, 2014). Subsequent studies reported potent THZ1 activity in additional cancers, including neuroblastoma (Chipumuro *et al*, 2014), triple-negative breast cancer (Wang *et al*, 2015), melanoma (Eliades *et al*, 2018), and prostate cancer (Rasool *et al*, 2019), highlighting CDK7 inhibition as additional powerful strategy to target SE-driven tumors.

Although the mechanistic basis of SE-selective sensitivity to transcriptional inhibitors is not fully resolved, several explanations have been proposed. One hypothesis is that many TFs and their mRNA have relatively short half-lives (Lam *et al*, 2001; Sharova *et al*, 2009), and that master TFs often bind and autoregulate their own genes (Crews & Pearson, 2009; Kwiatkowski *et al*, 2014). Thus, disruption of key transcriptional cofactors with JQ1 or THZ1 can rapidly reduce TF abundance and disproportionately impair TF recruitment at large oncogenic SEs where these factors are highly concentrated. Nonetheless, one report showed that JQ1 treatment induced eviction of Mediator at only half of the oncogenic SEs, concluding that disruption of transcriptional co-factors does not always correlate with pre-existing SE occupancy and implying that additional factors contribute to differential sensitivity (Bhagwat *et al*, 2016).

At the physicochemical level, heightened sensitivity of SE-associated oncogenes has been proposed to arise from co-operative binding of TFs, whereby binding of one TF to DNA influences binding of others (Hnisz *et al*, 2017). Compared to typical enhancers, SEs are occupied by highly co-operative assemblies with high local densities of TFs and co-activators, estimated at up to ~10-fold higher density than typical enhancers (Hnisz *et al*, 2013). As a result, perturbation of one TF or co-activator can compromise the binding and function of other components, leading to collapse of the SE as a regulatory unit and enhanced vulnerability to transcriptional inhibitors.

Furthermore, multivalent interactions between transcriptional components at SEs can drive formation of transcriptional condensates by phase separation (Sabari *et al*, 2018; Boija *et al*, 2018; Shrinivas *et al*, 2019), and recent work further suggests that several drugs, including JQ1 and THZ1, can concentrate in condensates, increasing local drug concentration independently of target engagement (Klein *et al*, 2020; Boija *et al*, 2021).

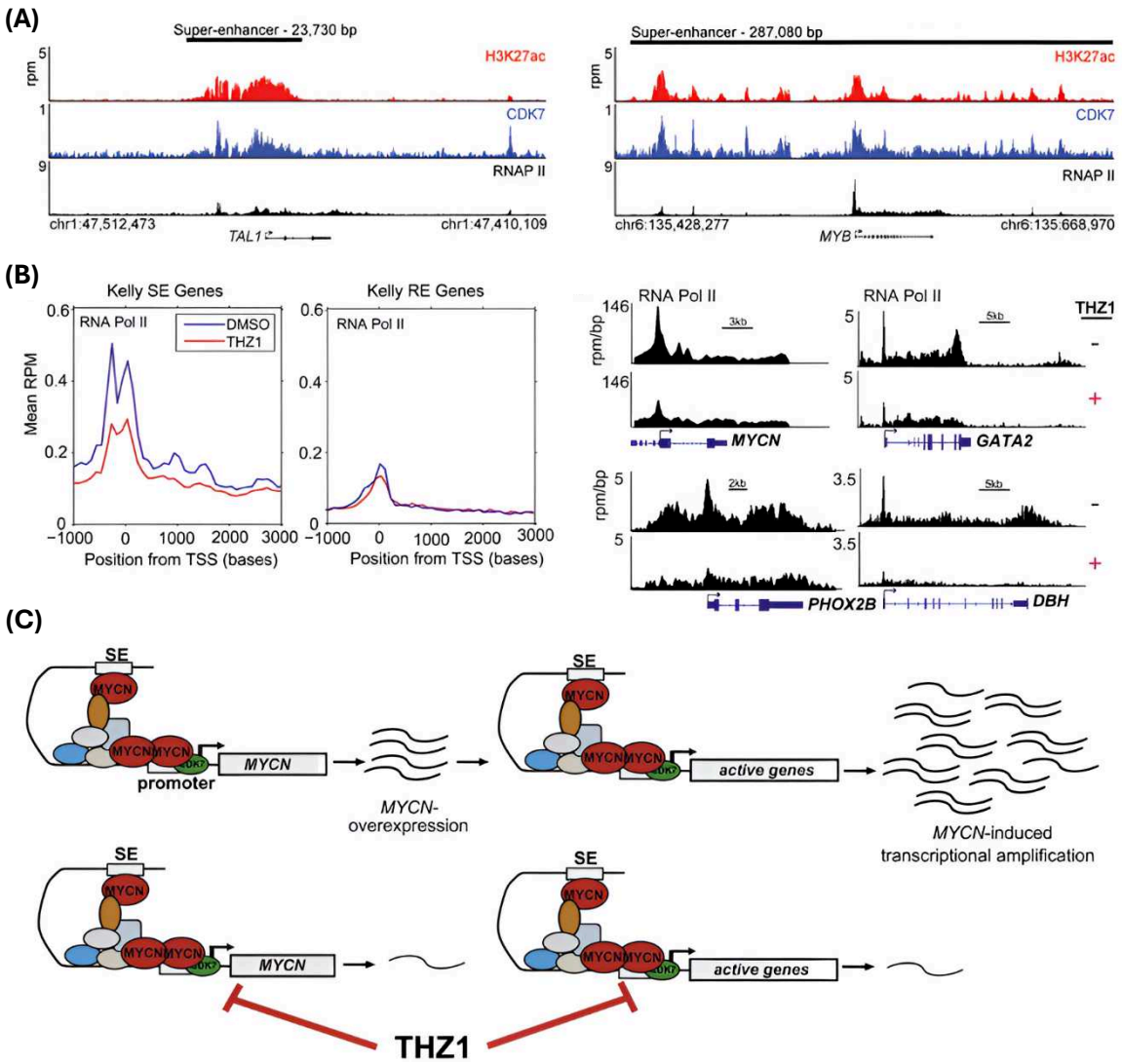

Figure 37. CDK7 inhibition selectively disrupts super-enhancer-driven transcription. (A) CDK7 is enriched at oncogene-associated super-enhancers, where it promotes transcription through phosphorylation of the RNA polymerase II (RNAPII) C-terminal domain. **(B)** Inhibition of CDK7 with THZ1 preferentially reduces RNAPII occupancy at promoters and gene bodies of super-enhancer-associated genes compared to typical enhancer-driven genes. **(C)** Proposed model in which CDK7 inhibition impairs transcription initiation and elongation at super-enhancers, leading to selective downregulation of oncogenic transcriptional programs. Adapted from *Kwiatkowski et al., Nature (2014); Chipumuro et al., Cell (2014)*.

Moreover, larger Mediator-associated condensates at SEs exhibit longer half-lives than smaller condensates at typical enhancers, potentially prolonging local drug residence and contributing to increased sensitivity of SE-associated transcription. Nonetheless, MED1 overexpression can also expand condensate volume, which dilutes the drug concentration and reduces its efficacy (Figure 38) (Klein *et al*, 2020).

Despite encouraging preclinical results, these transcriptional inhibitors have faced substantial clinical challenges. For example, BET inhibitors such as JQ1 exhibit short plasma half-life (~1 hour) and suboptimal pharmacokinetics (Trabucco *et al*, 2015; Li *et al*, 2020), limiting durable responses and necessitating dose escalation that can drive dose-limiting toxicities in clinical trials (Wang *et al*, 2023). Moreover, another study reported that although BET inhibition reduced tumor growth in prostate cancer mouse models, it also enhanced tumor invasion and metastasis by suppressing the expression of the negative-invasion regulator FOXA1, resulting in activation of multiple invasion-associated programs, including EMT (Wang *et al*, 2020b). Similarly, phase I clinical trials for CDK7 inhibitors have been rapidly discontinued due to insufficient activity and significant toxicity (Garralda *et al*, 2024). Such toxicity may be linked to a widespread loss of promoter-proximal paused RNAPII beyond SE-associated genes (Sampathi *et al*, 2019).

In addition, current inhibitors of SE-activity are susceptible to resistance, as demonstrated in several preclinical cancer models. Mechanisms of resistance to BET inhibition are well characterized and include reduced recruitment of BRD4 to target genes by activation of alternative pathways, such as Wnt/β-catenin signaling (Fong *et al*, 2015), hyperphosphorylation of BRD4 due to decreased PP2A phosphatase activity (Shu *et al*, 2016), upregulation of autophagy and anti-apoptotic pathways (Jang *et al*, 2017), and loss of the SWI/SNF subunit BRD7, which increases TEAD-YAP chromatin binding and reduces dependency on BRD4 regulation (Shu *et al*, 2020). Conversely, resistance mechanisms to THZ1 are less well defined but have mainly been associated with upregulation of drug efflux pumps (Gao *et al*, 2018; Sava *et al*, 2020). Previous work from our laboratory linked THZ1 resistance in melanoma to reduced levels of MITF, leading to induction of GATA6-driven drug-tolerance programs including upregulation of the efflux pump ABCG2 (Berico *et al*, 2021). These limitations have motivated development of additional approaches to disrupt SE-driven oncogenic transcription, with some already demonstrating promising success in preclinical cancer models. Those include selective degradation of BRD4 with PROTAC (Winter *et al*, 2015; Shi *et al*, 2023), inhibition of p300/CBP acetyltransferase activity using the selective inhibitor A-485 (Narita *et al*, 2021) or

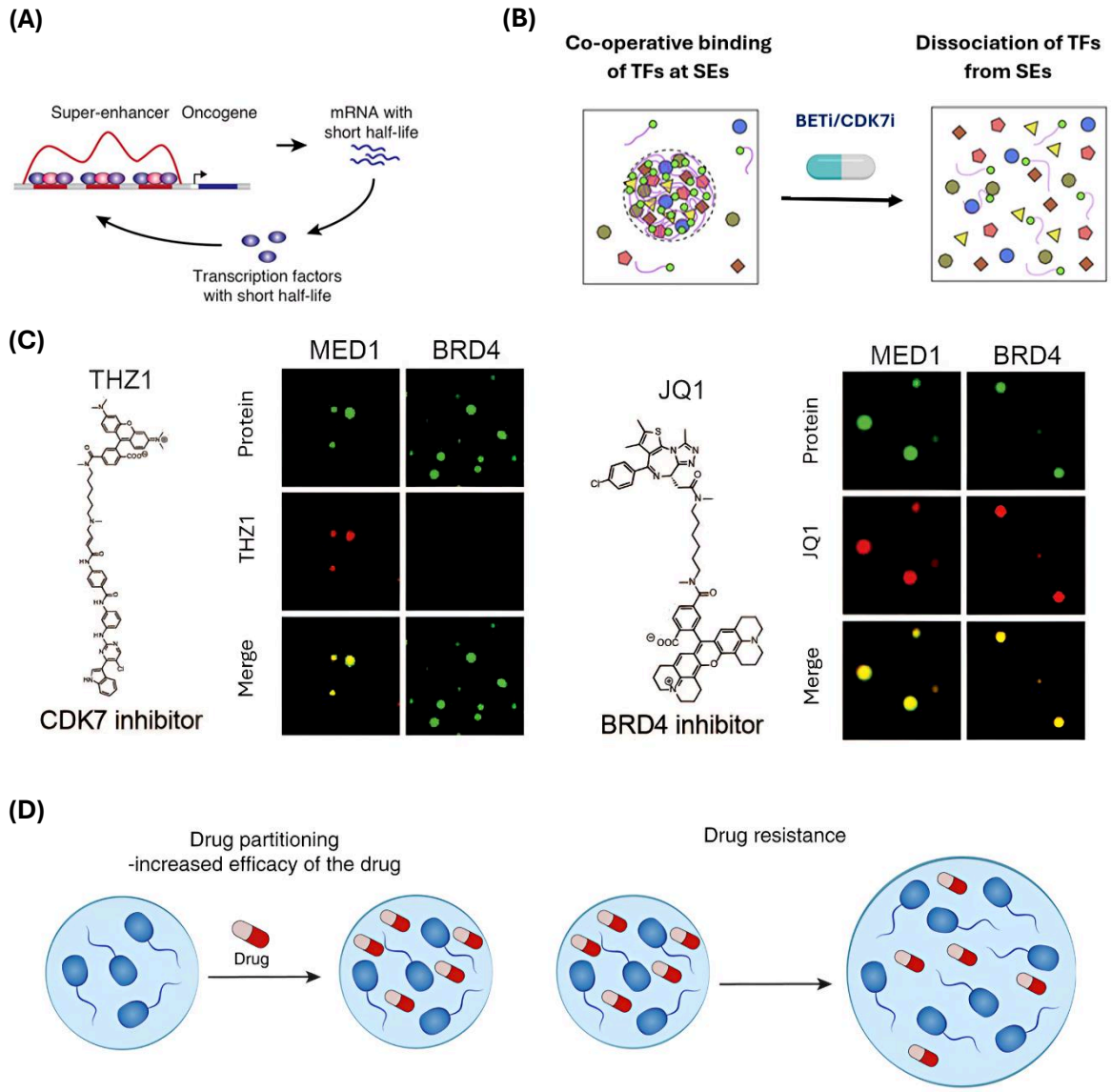

Figure 38. Proposed mechanisms underlying super-enhancer sensitivity to transcriptional inhibitors. (A) Short half-life of transcription factors and autoregulatory circuits render super-enhancer-driven genes highly sensitive to transcriptional perturbation. **(B)** Co-operative binding of transcription factors at super-enhancers creates interdependent regulatory assemblies, such that disruption of a single component destabilizes the entire complex. **(C)** Transcriptional condensates formed at super-enhancers concentrate transcriptional inhibitors such as JQ1 and THZ1, increasing their local activity. **(D)** Expansion of condensate volume, for example through MED1 overexpression, can dilute local drug concentration and reduce inhibitor efficacy. Adapted from *Bradner et al., Cell (2017); Hnisz et al., Cell (2017); Sabari et al., Science (2018); Klein et al., Science (2020); Boija et al., Cancer cell (2021).*

p300/CBP-directed PROTACs (Luo *et al*, 2025), CDK12 inhibition using compounds such as THZ531 (Zhang *et al*, 2016) or SR-4835 (Dai *et al*, 2022), chemical perturbation of extrachromosomal DNA (Taghbalout *et al*, 2025), and inhibition of the Mediator kinases CDK8 and CDK19. Notably, in acute myeloid leukemia (AML), CDK8/19 inhibition has been reported to enhance expression of SE-associated tumor suppressor programs, illustrating that distinct SE-centered interventions may yield context-dependent outcomes (Pelish *et al*, 2015). Furthermore, although intrinsically disordered regions (IDRs) were historically viewed as poor drug targets due to lack of stable structure, emerging work suggests that partner-bound conformations can reveal transient cavities that may eventually be exploited to disrupt condensate-mediated regulation (Bushweller, 2019). Despite their promise, these approaches remain to be clinically validated.

Beyond targeting enzymatic activities of SE-associated proteins, an alternative approach involves disrupting TF-DNA binding or inhibiting the expression of these factors using DNA-binding small molecules. Our laboratory has pursued this strategy using synthetic ecteinascidins, which constitute the central compounds studied in this thesis and will be developed in later chapters.

III- DNA damage and repair pathways in cancer:

DNA is constantly exposed to exogenous and endogenous agents that can threaten its integrity and lead to mutations that may be lethal for the organism. Indeed, it is estimated that human cells experience up to 70,000 DNA lesions or modifications per day (Tubbs & Nussenzweig, 2017). Consequently, during evolution, cells have developed multiple mechanisms to repair DNA damage and restore genome integrity depending on the type of lesion (Friedberg, 2008). Collectively, these mechanisms are referred to as the DNA damage response (DDR) pathways (Figure 39) (Huang & Zhou, 2021).

Alterations in DDR genes can lead to genome instability, which is considered a major hallmark of cancer, as an increased mutational burden raises the probability of activating oncogenes or inactivating tumor suppressor genes that drive tumorigenesis (Hanahan & Weinberg, 2011). On the other hand, genome instability in cancer cells also provides unique therapeutic opportunities, as targeting DDR pathways can selectively induce lethal levels of DNA damage in tumor cells. Accordingly, an increasing number of therapeutic strategies based on small-molecule inhibitors targeting DDR components are being developed (Groelly *et al*, 2023).

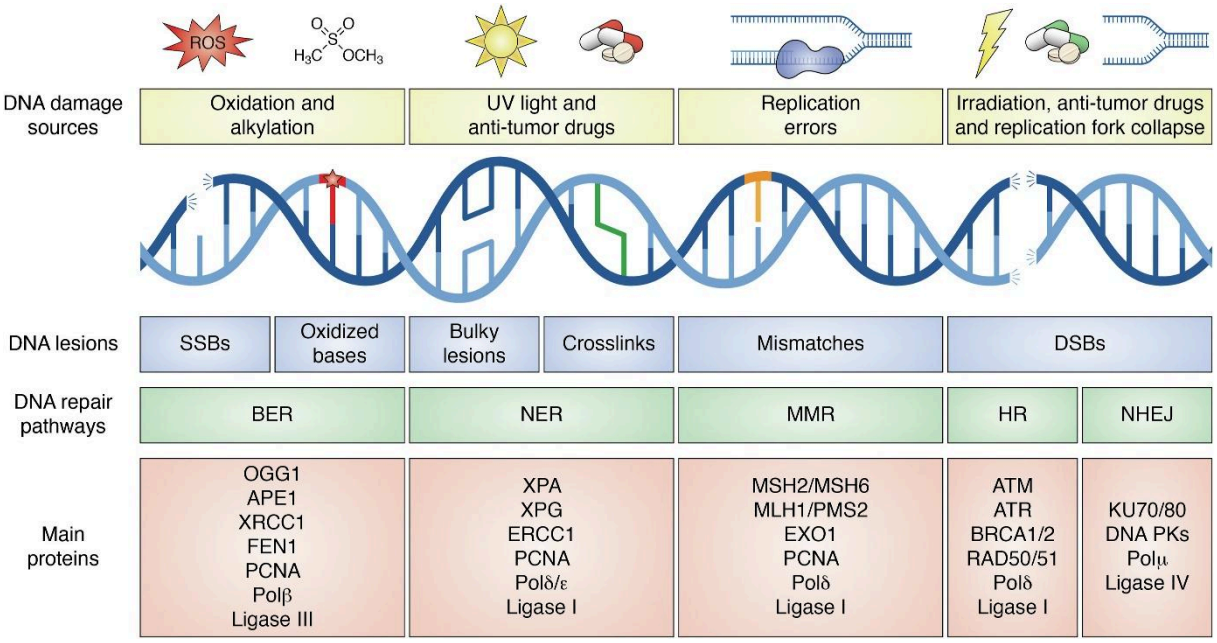

Figure 39. Overview of DNA damage sources, lesions, and repair pathways. DNA is continuously exposed to endogenous and exogenous insults, including reactive oxygen species (ROS), UV light, replication errors, and genotoxic stress from irradiation or anti-tumor drugs. These generate diverse DNA lesions such as single-strand breaks (SSBs), oxidized bases, bulky adducts, crosslinks, mismatches, and double-strand breaks (DSBs). To maintain genome integrity, cells rely on specialized repair pathways: base excision repair (BER), nucleotide excision repair (NER), mismatch repair (MMR), homologous recombination (HR), and non-homologous end joining (NHEJ). Key proteins involved in each pathway are indicated. Reproduced from *Dall'Agnese et al., JBC (2023)*.

The following sections will first describe the main sources of DNA damage and the major pathways responsible for their repair, before focusing on double-strand break repair through homologous recombination and the therapeutic exploitation of its deficiency in cancer.

a. Sources of DNA damage and major DNA repair pathways

Early evidence of damage to genetic material dates back to the 1930s, when UV radiation was found to cause bacterial death, while certain bacteria could survive sublethal doses and resume growth, providing the first hint that organisms might recover from damaging agents (Hollaender & Duggar, 1938). Shortly after the elucidation of DNA structure by Watson and Crick in 1953, the chemical mutagen benzene was shown to induce chromosome breakage, rearrangements, and increased mutation rates in erythroleukemia patients, providing one of the first links between DNA damage and human disease (Forni & Moreo, 1969).

In 1964, the concept of DNA repair was formally established with the discovery of photoreactivation in UV-irradiated *E. coli*, a light-dependent process that directly reverses cyclobutane pyrimidine dimers (CPDs) (Boyce & Howard-Flanders, 1964; Schuster, 1964). Shortly thereafter, nucleotide excision repair (NER) was identified as a light-independent pathway capable of removing UV-induced lesions through excision of damaged DNA fragments in bacteria (Setlow & Carrier, 1964), and was later shown to operate in human cells (Regan *et al*, 1968). Subsequent studies demonstrated that defects in NER underlie xeroderma pigmentosum, establishing a direct link between impaired DNA repair and increased cancer susceptibility (Cleaver, 1968; Setlow *et al*, 1969).

NER removes bulky DNA lesions that distort the DNA helix, including UV-induced pyrimidine dimers, benzo[a]pyrene adducts, and damages caused by anticancer chemotherapeutic drugs, such as cisplatin (Figure 40) (Chatterjee & Walker, 2017). Two NER subpathways operate in eukaryotic cells: global genome NER (GG-NER), which surveys the entire genome, and transcription-coupled NER (TC-NER), which specifically removes lesions from the transcribed strand of active genes. The two pathways differ mainly in the damage recognition step. In GG-NER, lesions are detected by the XPC/RAD23B/CETN2 complex, whereas in TC-NER damage is sensed through stalling of RNA polymerase II (RNAPII), leading to recruitment of the CSA and CSB proteins (Marteijn *et al*, 2014). Following damage recognition, both pathways converge on the recruitment of the TFIIH complex, whose helicase subunits XPB and XPD unwind the DNA around the lesion accompanied by dissociation of the CDK-activating kinase (CAK) subcomplex (Coin *et al*, 2008).

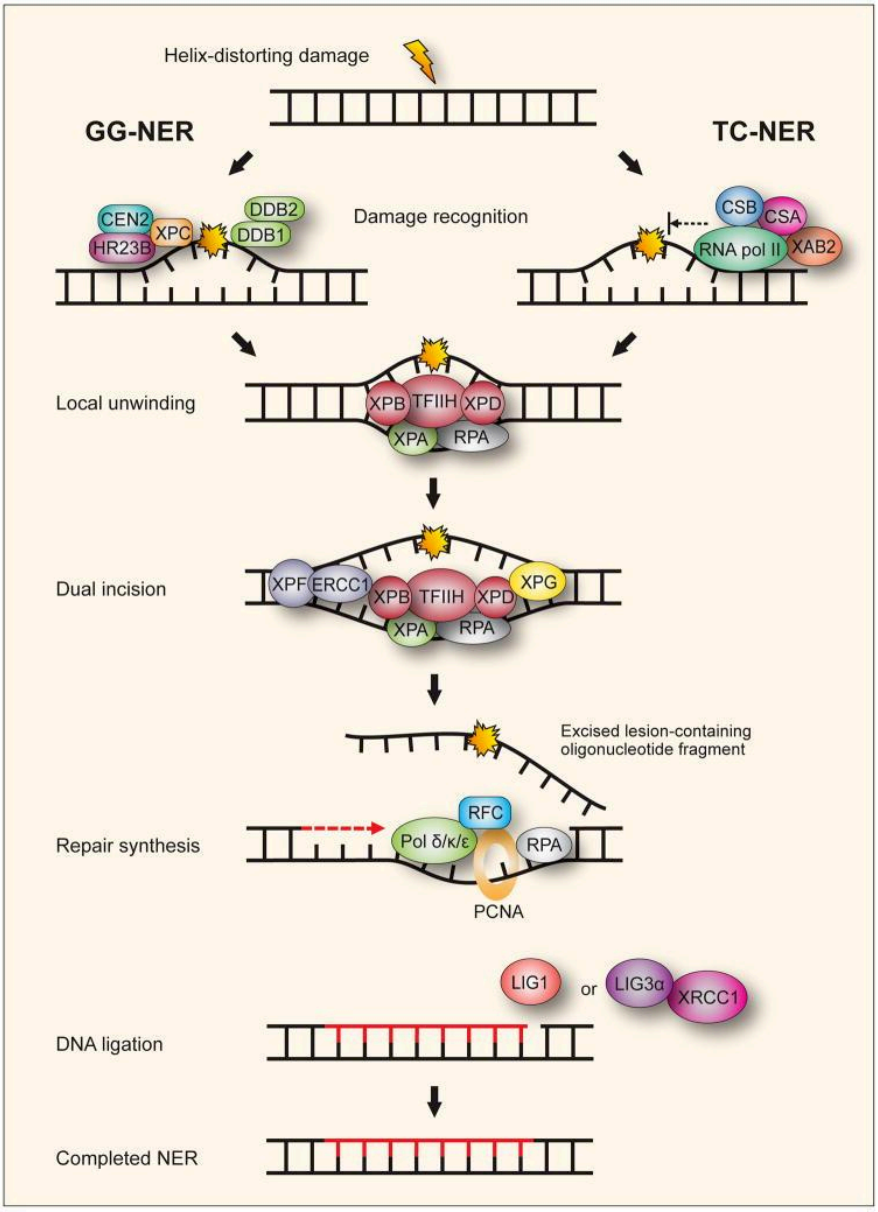

Figure 40. Mechanism of nucleotide excision repair (NER). NER removes bulky DNA lesions that distort the DNA helix, such as UV-induced pyrimidine dimers and bulky chemical adducts. Two subpathways operate in eukaryotic cells: global genome NER (GG-NER), in which lesions are recognized by the XPC complex, and transcription-coupled NER (TC-NER), initiated by RNA polymerase II stalling and recruitment of CSA and CSB. Both pathways converge on the recruitment of the TFIIH complex, whose helicase subunits XPB and XPD unwind DNA around the lesion. The damaged strand is then excised by the endonucleases XPF-ERCC1 and XPG, generating a short oligonucleotide gap that is subsequently filled by DNA polymerases δ/ε and sealed by DNA ligases I or III. Reproduced from *Jeppesen et al., Progress in Neurobiology (2011)*.

The damaged strand is then excised by the endonucleases XPF-ERCC1 and XPG, removing a short oligonucleotide of approximately 22-30 nucleotides (Compe & Egly, 2012). The resulting gap is subsequently filled by DNA polymerases δ/ε and ligated by DNA ligases I or III, restoring DNA integrity (Marteijn *et al*, 2014).

Later, Thomas Lindahl demonstrated that uracil from deamination can be excised from DNA as a free base, providing the first evidence of base excision repair (BER) as a repair mechanism distinct from NER (Lindahl, 1974). BER primarily repairs small base lesions generated by deamination, oxidation, or alkylation, which commonly arise from reactive oxygen species, radiation, or chemical agents (Hindi *et al*, 2021). The pathway is initiated by DNA glycosylases, which recognize damaged bases and remove them, generating an abasic (AP) site (Jacobs & Schär, 2012). The AP site is then cleaved by AP endonuclease 1 (APE1), producing a DNA break that is processed by DNA polymerase β, which inserts the correct nucleotide (Mol *et al*, 2000; Sobol *et al*, 2000). BER can proceed through short-patch repair, where a single nucleotide is replaced, or long-patch repair, involving synthesis of a short DNA tract with the participation of replication-associated factors such as PCNA. The choice between short- and long-patch repair depends on the lesion type, the specificity of initiating glycosylases, and the availability of BER factors (Krokan & Bjørås, 2013). Finally, the DNA strand is sealed by DNA ligases I or III, restoring DNA integrity (Hegde *et al*, 2008). Defects in BER components have been associated with genome instability and increased cancer risk, and mutations in BER genes have been reported in several tumor types, highlighting the importance of this pathway in maintaining genome integrity (Wallace *et al*, 2012; Grundy & Parsons, 2020).

The discovery of the mismatch repair (MMR) pathway revealed that incorrect nucleotide incorporation can occur during normal DNA replication (Wagner & Meselson, 1976). Indeed, DNA polymerases are estimated to introduce approximately one error per 10^5 nucleotides during replication (Bębenek & Ziuzia-Graczyk, 2018). Therefore, the role of MMR is to correct base-base mismatches and small insertion-deletion loops generated during DNA replication. The process is initiated by recognition of the mismatch mainly by the MSH2-MSH6 protein complex, which binds the lesion and forms a sliding clamp on DNA (Edelbrock *et al*, 2013). This is followed by recruitment of additional repair factors, including EXO1, which excises the error-containing DNA strand (Genschel *et al*, 2002), while RPA stabilizes the exposed single-stranded DNA and prevents further degradation (Lin *et al*, 1998). Following removal of the mismatched bases, the gap is filled by DNA polymerase and sealed by DNA ligase (Figure 41) (Kunkel & Erie, 2005).

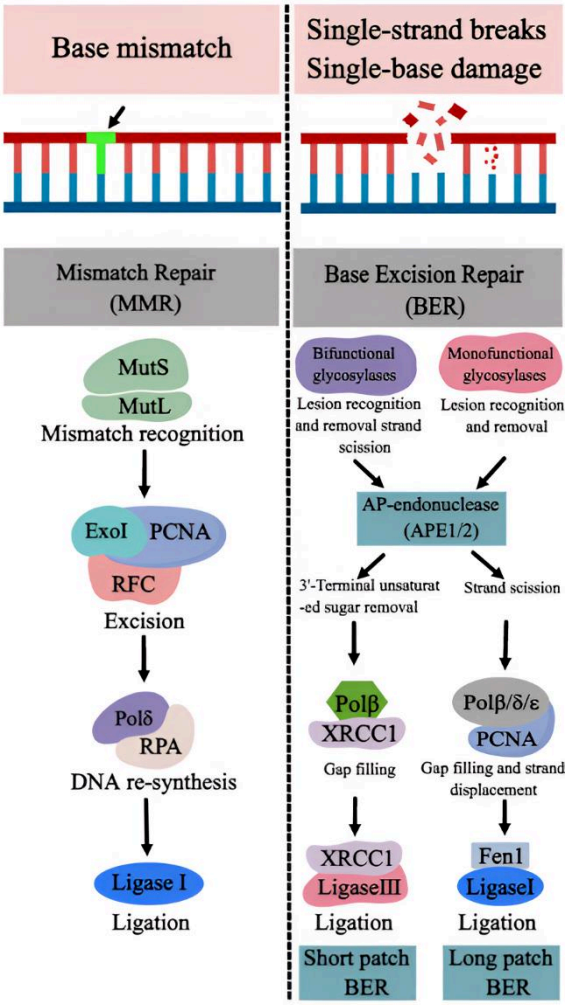

Figure 41. Mechanisms of base excision repair (BER) and mismatch repair (MMR). BER repairs small base lesions such as oxidized, deaminated, or alkylated bases. Damage is first recognized by DNA glycosylases, which excise the altered base to generate an abasic (AP) site. This is processed by APE1, followed by gap filling by DNA polymerases and ligation. BER can proceed via short-patch or long-patch repair. MMR corrects base-base mismatches and insertion-deletion loops generated during DNA replication. In eukaryotic cells, mismatches are recognized by the MSH2-MSH6 complex (homologs of bacterial MutS/MutL), followed by recruitment of additional repair factors, excision of the error-containing strand by EXO1, DNA resynthesis, and ligation. Adapted from *Wang et al., Int J Mol Sci (2023)*.

Due to its critical role in maintaining replication fidelity, defects in MMR lead to increased mutation rates and microsatellite instability (MSI), which is associated with several cancer types (Cortes-Ciriano *et al*, 2017; Pećina-Šlaus *et al*, 2020). Interestingly, tumors with MMR deficiency often show enhanced responses to immune checkpoint inhibitors (ICIs), likely due to their high mutational burden and increased neoantigen formation (Le *et al*, 2015a, 2017; Johannet *et al*, 2025).

In addition to chemical base modifications, DNA damage can also occur through breakage of the phosphodiester backbone. Among these lesions, single-strand breaks (SSBs) are the most frequent, occurring at rates of hundreds of thousands per cell per day (Caldecott, 2022). SSBs can arise directly from oxidative damage caused by reactive oxygen species, ionizing radiation, or abortive activity of DNA topoisomerases during replication and transcription, or indirectly as intermediates of other repair pathways such as BER (Caldecott, 2008). If left unrepaired, SSBs can block replication fork progression during S phase and lead to the formation of double-strand breaks (DSBs), which have more catastrophic consequences and are more difficult to repair (Kuzminov, 2001).

To counteract this, cells employ a single-strand break repair (SSBR) pathway. Repair is initiated by PARP1 and PARP2, which detect SSBs and catalyze poly(ADP-ribosyl)ation (PARylation) using NAD^+, thereby recruiting repair factors such as XRCC1, a scaffold protein that coordinates downstream repair steps (Durkacz *et al*, 1980; El-Khamisy *et al*, 2003; Schreiber *et al*, 2006; De Vos *et al*, 2012). Afterwards, PARP1/2 auto-PARylate and rapidly dissociate from DNA, and the PAR chains are degraded by poly(ADP-ribose) glycohydrolase (PARG) to promote subsequent rounds of SSB repair (Polo & Jackson, 2011). Following PARP dissociation, DNA ends are processed with the help of XRCC1, which directly stimulates the activity of end-processing enzymes such as PNKP (Whitehouse *et al*, 2001), APTX (Clements *et al*, 2004), and TDP1 (Plo *et al*, 2003). The resulting gap is then filled primarily by DNA polymerase β, and the strand is finally sealed by DNA ligases I or III, restoring DNA integrity (Figure 42) (Caldecott, 2003). Defects in SSBR are primarily associated with neurological disorders, and impaired repair of SSBs has not been directly associated with an increased risk of cancer (Caldecott, 2024). However, mutations in the DNA polymerase Pol β have been identified in approximately 30% of tumors, some of which may affect polymerase fidelity during SSBR (Sweasy *et al*, 2006).

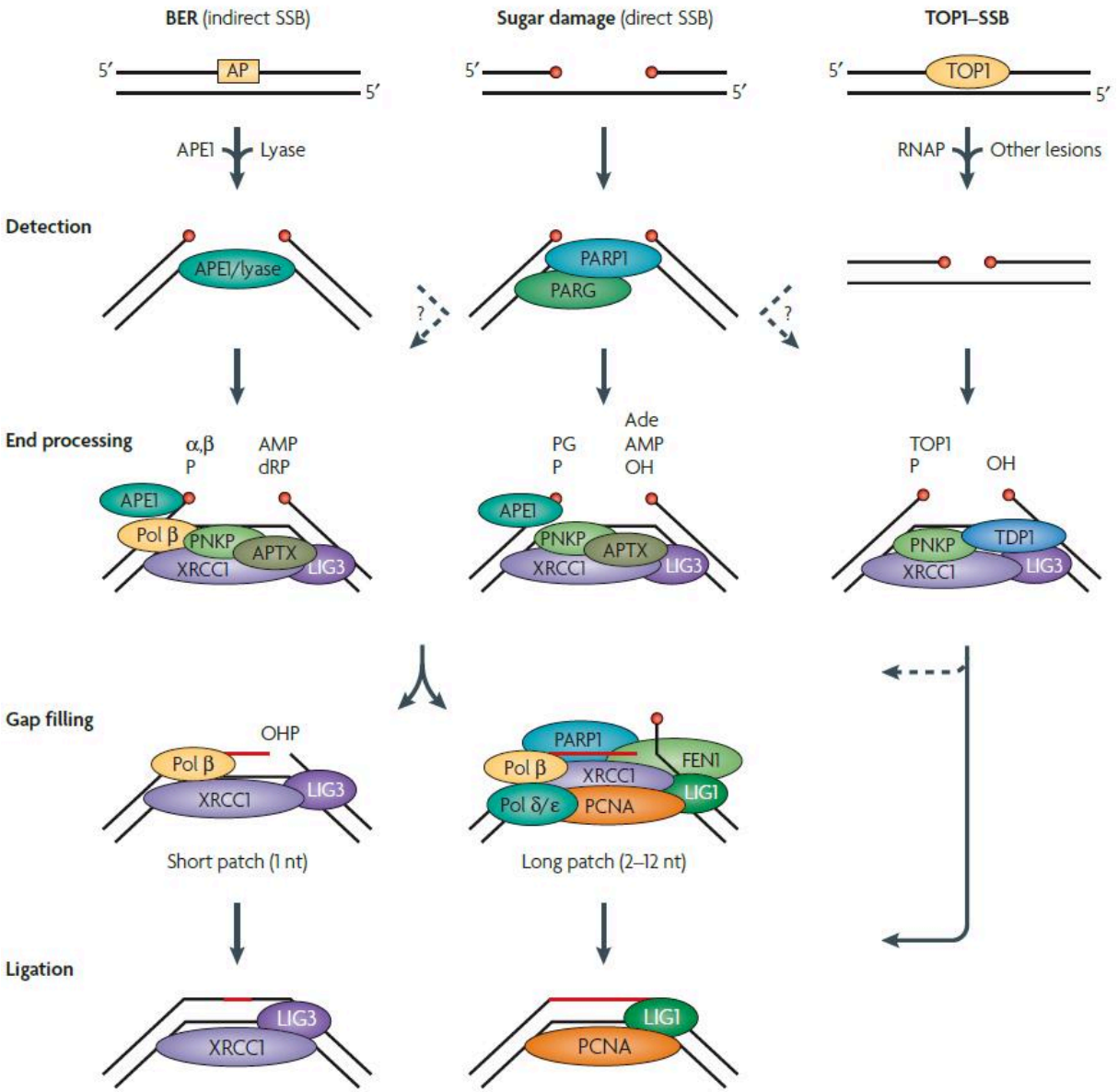

Figure 42. Mechanism of single-strand break repair (SSBR). SSBR repairs DNA single-strand breaks (SSBs), which can arise directly from oxidative damage, ionizing radiation, or topoisomerase activity, or indirectly as intermediates of base excision repair (BER). In direct SSBR, damage is detected by PARP1, which catalyzes poly(ADP-ribosyl)ation (PARylation) to recruit repair factors such as XRCC1. DNA ends are then processed by enzymes including PNKP, APTX, and TDP1 to restore ligatable termini. The resulting gap is filled primarily by DNA polymerase β, and the strand is sealed by DNA ligases I or III. Short- and long-patch repair synthesis can occur depending on the nature of the lesion. Reproduced from *Caldecott, Nat Rev Genet (2008)*.

On the other hand, double-strand breaks (DSBs) are rarer than SSBs, but they pose a greater threat to genome stability and are more difficult to repair due to the absence of an intact complementary strand that could serve as a template for accurate repair (Vilenchik & Knudson, 2003). DSBs can arise from exogenous sources such as ionizing radiation and chemotherapeutic agents, or from endogenous processes including metabolic reactions and replication of DNA containing unrepaired SSBs (Mehta & Haber, 2014). Two major pathways repair DSBs: non-homologous end joining (NHEJ) and homologous recombination (HR). NHEJ is a rapid repair pathway that operates throughout the cell cycle and ligates broken DNA ends without requiring a homologous template, often resulting in small insertions or deletions that can lead to chromosomal rearrangements (Chang *et al*, 2017). In contrast, homologous recombination is a highly accurate repair mechanism that uses a homologous template, typically the sister chromatid, allowing precise restoration of the DNA sequence. Consequently, HR is largely restricted to the S and G2 phases of the cell cycle, when the sister chromatid is available (Wright *et al*, 2018). Importantly, alterations in DSB repair pathways contribute to cancer development and influence responses to therapy, but also provide important therapeutic opportunities (Huang & Zhou, 2021). The following section will therefore focus on the molecular mechanisms of DSB repair, particularly homologous recombination, and on how deficiencies in these pathways can be therapeutically exploited in cancer.

b. Double-strand break repair and the role of homologous recombination in cancer

The repair of DNA double-strand breaks (DSBs) through non-homologous end joining (NHEJ) and homologous recombination (HR) involves distinct molecular mechanisms and protein complexes. NHEJ is initiated by the binding of the Ku70-Ku80 heterodimer to broken DNA ends, which promotes the recruitment of additional NHEJ factors, including the DNA-dependent protein kinase catalytic subunit (DNA-PKcs) (Gottlieb & Jackson, 1993). DNA-PKcs binds to DNA-bound Ku at each DNA end to form the DNA-PK holoenzyme, which stabilizes the broken ends and promotes their alignment into a synaptic complex. Subsequent autophosphorylation of DNA-PKcs induces conformational changes that allow access to end-processing enzymes, such as the nuclease Artemis, which processes DNA ends to generate ligatable termini. Following end processing, the scaffold protein XRCC4 recruits additional NHEJ factors, including XLF and PAXX, which stabilize the DNA ends, as well as DNA ligase IV (LIG4), which catalyzes the final ligation step to restore DNA continuity (Figure 43) (Nick McElhinny *et al*, 2000; Ahnesorg *et al*, 2006; Ochi *et al*, 2015).

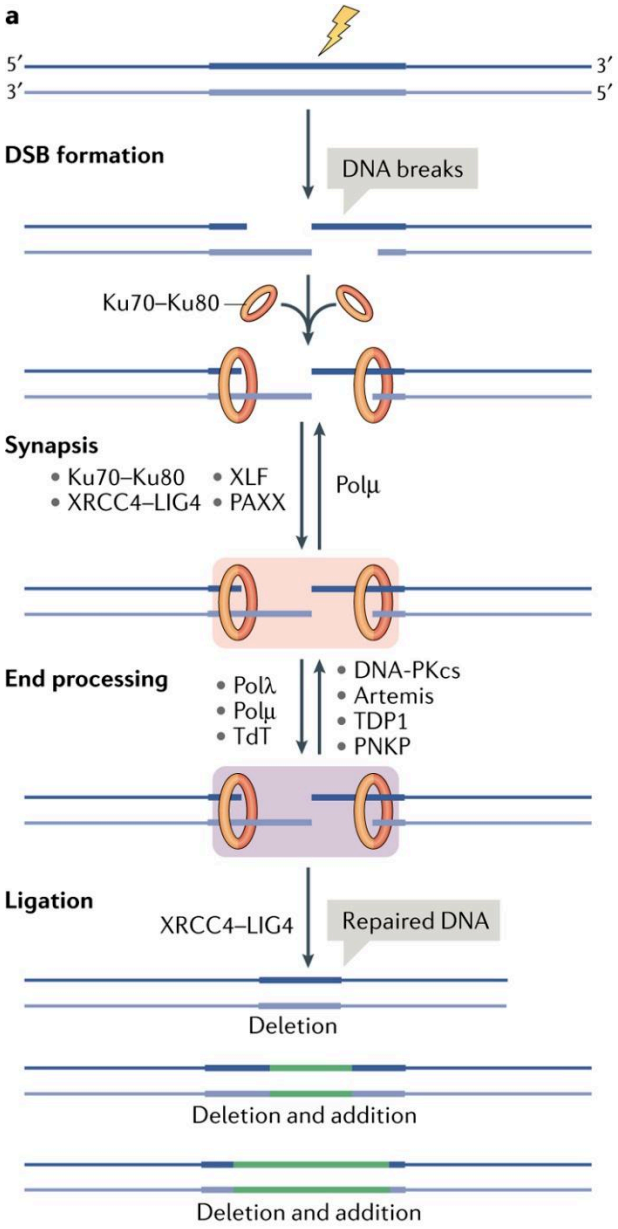

Figure 43. Mechanism of non-homologous end joining (NHEJ). NHEJ repairs DNA double-strand breaks (DSBs) through direct ligation of DNA ends. The pathway is initiated by binding of the Ku70-Ku80 heterodimer to broken DNA ends, followed by recruitment of DNA-PKcs to form the DNA-PK holoenzyme, which stabilizes and aligns the DNA ends. DNA-PKcs autophosphorylation promotes access to end-processing enzymes such as Artemis, which generate ligatable termini. The scaffold protein XRCC4 then recruits additional factors including XLF and PAXX to stabilize the synaptic complex, while DNA ligase IV catalyzes the final ligation step to restore DNA integrity. Adapted from Zhao et al., *Nat Rev Mol Cell Biol (2020)*.

In addition to classical NHEJ (c-NHEJ), cells can also repair DSBs through an alternative end-joining pathway, often referred to as alternative NHEJ (alt-NHEJ) or microhomology-mediated end joining (MMEJ). This pathway relies on short microhomologous DNA sequences exposed during limited DNA end resection to align broken DNA ends before ligation. Key factors involved in alt-NHEJ include PARP1, DNA polymerase θ (POLQ), and DNA ligase III. Because this mechanism frequently results in deletions or chromosomal rearrangements, alt-NHEJ is considered an error-prone repair pathway and is generally used as a backup mechanism when c-NHEJ or HR are compromised (Ceccaldi *et al*, 2016a; Sfeir *et al*, 2024). Notably, alt-NHEJ activity has been reported to increase in HR-deficient cancers, contributing to genomic instability (Ceccaldi *et al*, 2015).

In contrast to NHEJ, which directly ligates DNA ends without requiring sequence homology, HR uses a homologous DNA molecule from the sister chromatid as a template to repair DSBs, ensuring high-fidelity restoration of genome integrity. HR is initiated by recognition of DSBs by the MRE11-RAD50-NBN (MRN) complex, which together with CtIP (CtBP-interacting protein) promotes DNA end resection. This process involves the nuclease activity of MRE11 during the initial resection step, followed by long-range resection mediated by the BLM helicase and EXO1, generating extended 3′ single-stranded DNA (ssDNA) overhangs (Lisby *et al*, 2004; Sartori *et al*, 2007; Nimonkar *et al*, 2011; Shibata *et al*, 2014). The ssDNA is subsequently coated by the heterotrimeric complex replication protein A (RPA), which stabilizes the ssDNA and prevents secondary structure formation. RPA is later displaced to allow loading of the RAD51 recombinase, a step that requires BRCA1 and BRCA2 (Sung *et al*, 2003).

In this process, BRCA1 interacts with PALB2, which promotes recruitment of BRCA2 to DSB sites, where it facilitates loading of RAD51 onto ssDNA (Pellegrini *et al*, 2002; Xia *et al*, 2006; Sy *et al*, 2009). RAD51 then assembles into nucleoprotein filaments along ssDNA, mediating homology search and strand invasion into a homologous DNA duplex, typically located on the sister chromatid, forming a displacement loop (D-loop) (Jensen *et al*, 2010). DNA polymerases δ/ε subsequently extend the invading 3′ end using the homologous template, enabling DNA synthesis across the break site. Repair can then proceed through synthesis-dependent strand annealing (SDSA) or through the formation of double Holliday junctions following second-end capture. These recombination intermediates are ultimately dissolved by the BLM-TOPIIIα-RMI complex or resolved by structure-specific resolvases to restore two intact DNA molecules (Figure 44) (Mazón *et al*, 2010; Wright *et al*, 2018).

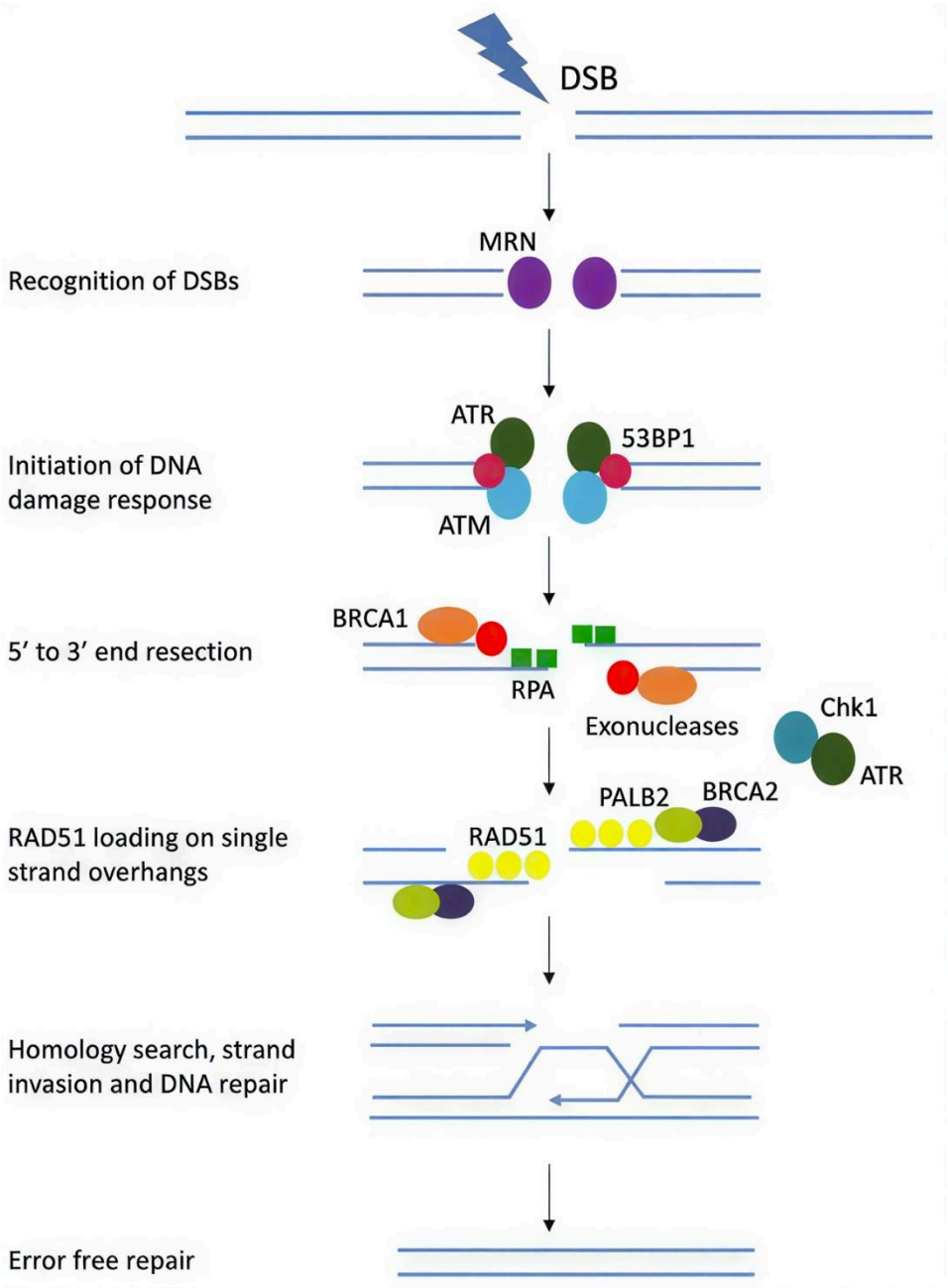

Figure 44. Mechanism of homologous recombination (HR). HR repairs DNA double-strand breaks (DSBs) using a homologous DNA template, typically the sister chromatid, ensuring high-fidelity repair. The pathway is initiated by recognition of DSBs by the MRN complex, followed by activation of ATM/ATR signaling and 5′ to 3′ DNA end resection to generate single-stranded DNA (ssDNA). The resulting ssDNA is coated by RPA and subsequently replaced by RAD51 with the assistance of BRCA1, PALB2, and BRCA2. RAD51 nucleoprotein filaments mediate homology search and strand invasion into a homologous DNA duplex, enabling DNA synthesis and repair of the damaged region. This process ultimately restores DNA integrity in an error-free manner. Adapted from *Hockings and Miller, Ther Adv Med Oncol (2023)*.

It should be emphasized that these steps represent the classical model of HR repair, although the regulatory landscape of this pathway continues to expand. For instance, recent studies have shown that cohesin can facilitate homology search through loop-extrusion-driven chromatin scanning around DNA double-strand breaks (Teloni *et al*, 2025; Marin-Gonzalez *et al*, 2025), while structural analyses revealed that RAD51 paralogs form higher-order complexes that coordinate RAD51 filament nucleation and stabilization (Koo *et al*, 2026).

Because NHEJ and HR act on the same DNA lesions, cells must tightly regulate pathway choice to maintain genome stability. In general, HR and NHEJ factors compete for access to DSB ends, with NHEJ occurring rapidly within seconds following radiation-induced DSBs, while HR factors show delayed recruitment, suggesting that NHEJ is often the default DSBR pathway (Shibata *et al*, 2011). Pathway choice is primarily governed by the cell-cycle stage, the extent of DNA end resection, and activation of DNA damage response signaling pathways (Scully *et al*, 2019). HR is largely restricted to the S and G2 phases of the cell cycle, when a sister chromatid is available as a repair template, while NHEJ operates throughout the cell cycle and predominates in G1 (Takata *et al*, 1998). Indeed, time-course analyses of DSBR have shown that HR activity, measured through RAD51 accumulation at break sites, peaks during the G2 phase (Aymard *et al*, 2014). However, this classical view has been challenged by recent work demonstrating that HR can also occur in G1 during repair of centromeric DNA (Yilmaz *et al*, 2021).

In addition to cell-cycle regulation, DNA end resection represents a key step controlling repair pathway choice. During S phase, cyclin-dependent kinase (CDK) activity promotes phosphorylation of CtIP, which stimulates DNA end resection and recruitment of BRCA1, thereby favoring HR (Aylon *et al*, 2004; Ira *et al*, 2004; Anand *et al*, 2016). Conversely, the DNA damage sensor 53BP1 promotes NHEJ in G1 by limiting BRCA1 accumulation and inhibiting end resection (Figure 45) (Zimmermann *et al*, 2013).

Repair pathway choice is also influenced by the surrounding chromatin environment. Genome-wide analyses of inducible DSBs revealed that HR-prone breaks occur preferentially within transcriptionally active chromatin enriched in histone marks such as H3K36me3 and H2BK120ub. During repair, HR-associated breaks display nucleosome loss and chromatin remodeling, whereas NHEJ-prone breaks are associated with histone modifications such as H4K20me2 that facilitate recruitment of repair factors including 53BP1 (Figure 46) (Fradet-Turcotte *et al*, 2013; Clouaire *et al*, 2018).

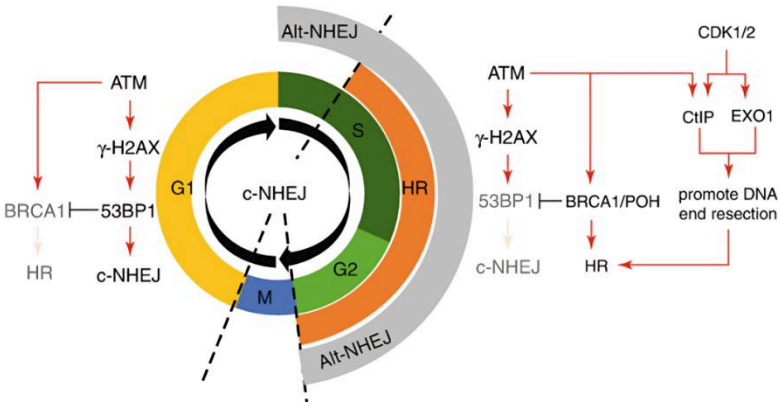

Figure 45. Cell-cycle and resection-dependent regulation of DSB repair pathway choice. Repair pathway choice is tightly linked to the cell cycle. In G1, 53BP1 limits DNA end resection and promotes canonical NHEJ. In S/G2, ATM and CDK activity promote CtIP- and EXO1-dependent resection together with BRCA1, thereby favoring homologous recombination (HR). Thus, cell-cycle-dependent control of DNA end resection is a major determinant of DSB repair pathway choice. Reproduced from *Gerelchuluun, Proton Beam Radiotherapy (2020)*.

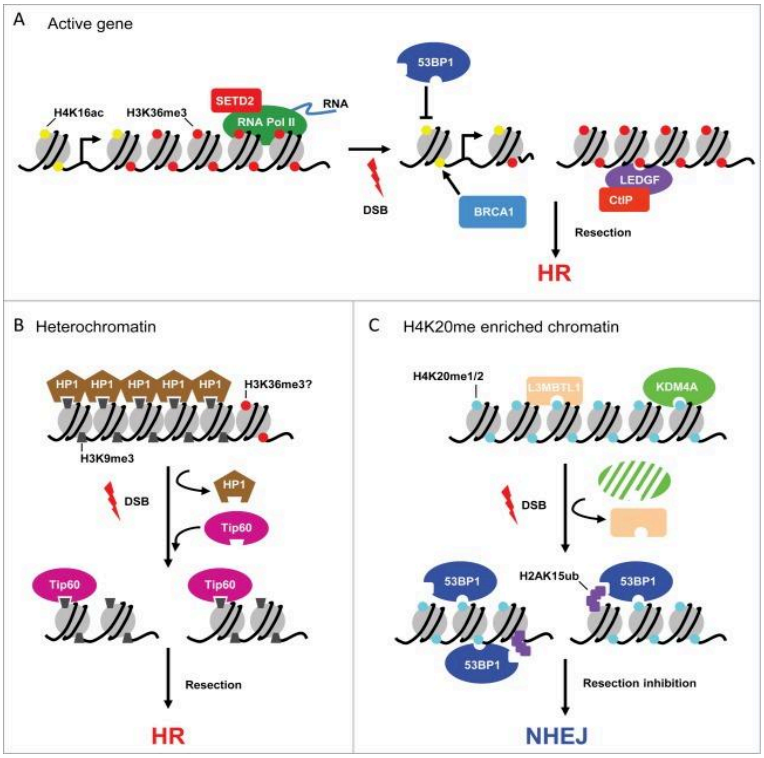

Figure 46. Chromatin context influences DSB repair pathway choice. The chromatin environment surrounding DNA double-strand breaks (DSBs) influences repair pathway selection. Breaks in transcriptionally active chromatin enriched in marks such as H3K36me3 preferentially undergo homologous recombination (HR), whereas breaks in chromatin enriched in H4K20 methylation favor 53BP1 recruitment and non-homologous end joining (NHEJ). Reproduced from *Clouaire and Legube, Nucleus (2015)*.

More recently, an implication of higher-order genome organization has been demonstrated in DSBR regulation, as large-scale chromatin compartmentalization and three-dimensional genome architecture influence repair pathway usage and the spatial distribution of repair events across the genome (Arnould *et al*, 2023).

In addition to local repair factors, DSB repair is coordinated by upstream signaling pathways collectively referred to as the DNA damage response (DDR). Central to this signaling network are the phosphatidylinositol-3-kinase-related kinases ATM, ATR, and DNA-PKcs, which coordinate distinct aspects of the DNA damage response, including double-strand break signaling, replication stress responses, and non-homologous end joining, respectively (Polo & Jackson, 2011). The DDR is initiated by lesion recognition, in which the MRN complex recruits and activates the DDR kinase ATM (ataxia telangiectasia mutated) at DSB sites (Lee & Paull, 2004). In parallel, ATR (ATM and Rad3-related) is recruited to resected DNA ends through its partner ATRIP, which recognizes RPA-coated single-stranded DNA generated during DNA end resection (Zou & Elledge, 2003). DNA-PKcs, in contrast, is recruited and activated through its interaction with the Ku70-Ku80 heterodimer bound to DNA ends (Blackford & Jackson, 2017).

A central function of these DDR kinases is the phosphorylation of serine 139 on the C-terminal tail of the histone variant H2AX, generating γH2AX chromatin domains that can spread over kilobase to megabase regions surrounding DNA damage sites. These chromatin modifications promote recruitment of additional DDR factors and chromatin-modifying complexes, facilitating the assembly and retention of DNA repair machinery at DSB sites (Prabhu *et al*, 2024). While DNA-PKcs primarily functions in the activation of NHEJ pathway, ATR and ATM play broader roles in coordinating DNA damage signaling and cell-cycle checkpoint activation. In particular, ATR and ATM phosphorylate the checkpoint kinases CHK1 and CHK2, respectively, leading to inhibition of cyclin-dependent kinase (CDK) activity and cell-cycle arrest to allow time for DNA repair (Figure 47) (Barnum & O'Connell, 2014; Panagopoulos & Altmeyer, 2021).

Besides checkpoint activation, ATM also regulates local chromatin and transcriptional responses to DNA damage. For example, ATM-mediated signaling promotes RNA polymerase II (RNAPII) eviction and transcriptional silencing in the vicinity of DNA breaks (Shanbhag *et al*, 2010). ATM also phosphorylates the adaptor protein MDC1 (mediator of DNA damage checkpoint 1), creating docking sites for the E3 ubiquitin ligase RNF8 and promoting recruitment of repair factors such as 53BP1 and BRCA1 (Stucki *et al*, 2005; Huen *et al*, 2007).

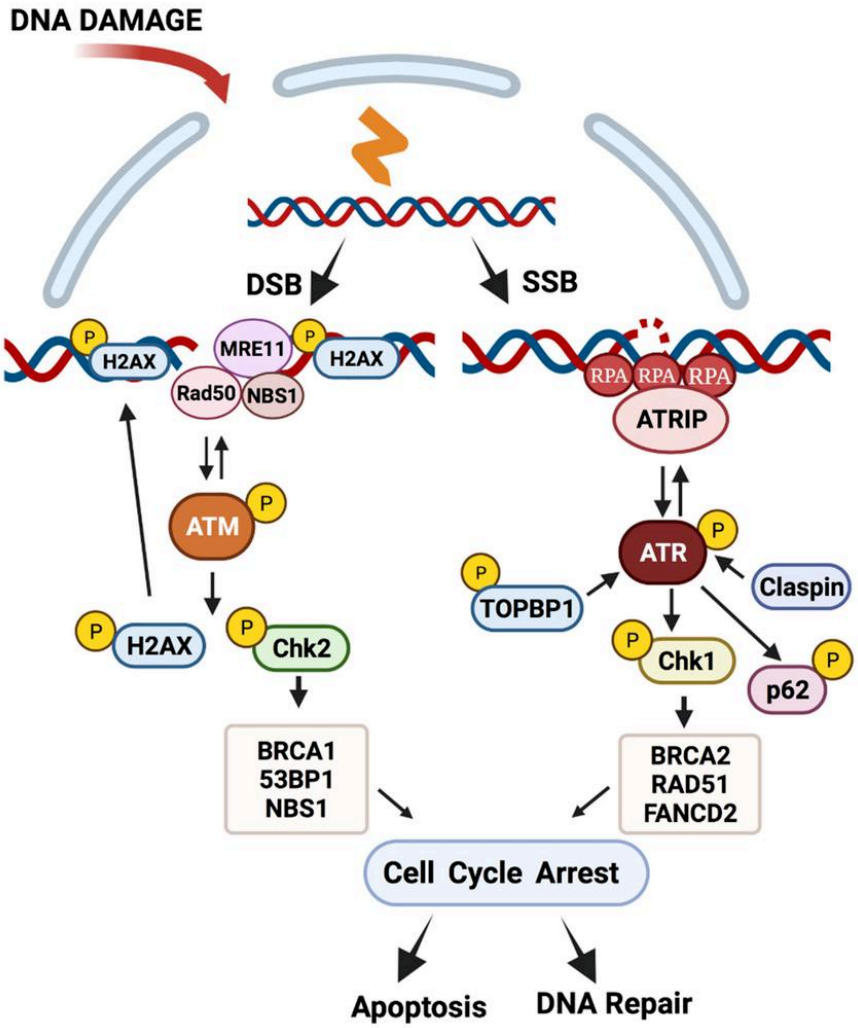

Figure 47. DNA damage response signaling pathways coordinating DNA repair and cell-cycle checkpoints. DNA damage activates the DDR kinases ATM and ATR through distinct sensing mechanisms involving the MRN complex at double-strand breaks (DSBs) and RPA-ATRIP at single-stranded DNA (ssDNA), respectively. These kinases phosphorylate histone H2AX (γH2AX) and downstream checkpoint kinases CHK2 and CHK1, leading to inhibition of cyclin-dependent kinase (CDK) activity and induction of cell-cycle arrest. This coordinated signaling network promotes recruitment of DNA repair factors and ensures proper resolution of DNA damage. Reproduced from *Gusho and Laimins, Viruses (2021)*.

Given the central role of DDR signaling in coordinating DNA repair, these pathways have become attractive therapeutic targets in cancer. Pharmacological inhibitors targeting DDR kinases have therefore been developed to enhance the efficacy of DNA-damaging therapies (Groelly *et al*, 2023). For example, ATM inhibitors have been shown to potentiate the cytotoxic effects of topoisomerase inhibitors (Hickson *et al*, 2004), whereas ATR inhibitors increase replication stress and sensitize tumor cells to ionizing radiation (Figure 48) (Reaper *et al*, 2011). Consequently, several inhibitors targeting ATM and ATR are currently undergoing clinical evaluation (Priya *et al*, 2023).

Alterations in DSBR pathways, particularly homologous recombination, are now well recognized as major determinants of cancer development and therapeutic response. Indeed, overexpression of HR components has been associated with resistance to chemotherapy and radiotherapy in multiple cancer types (Luo *et al*, 2016; Chen *et al*, 2018; Zhou *et al*, 2020; Hoppe *et al*, 2021). Moreover, intratumoral heterogeneity in DNA repair capacity has been reported, with cancer stem cells often displaying elevated HR activity that may influence treatment outcomes (Rouault *et al*, 2025b). For instance, the epithelial-to-mesenchymal transition transcription factor ZEB1 has been shown to regulate CHK1 stability and enhance HR activity, thereby promoting radioresistance in breast cancer stem cell populations (Zhang *et al*, 2014).

Conversely, deficiencies in HR caused by mutations in HR genes, most notably BRCA1 and BRCA2, are common in several cancers, and contribute to genomic instability that promotes tumorigenesis (Toh & Ngeow, 2021). On the other hand, HR-deficient cancer cells become highly dependent on single-strand break repair mediated by poly(ADP-ribose) polymerase (PARP), to prevent the conversion of unrepaired single-strand breaks into toxic double-strand breaks during DNA replication. This dependency renders such tumors particularly sensitive to PARP inhibitors, representing a paradigm of synthetic lethality that has been successfully exploited in cancer therapy (Farmer *et al*, 2005; McCabe *et al*, 2006). The following sections will therefore discuss the development and mechanisms of action of PARP inhibitors, as well as their clinical limitations and emerging strategies aimed at overcoming therapeutic resistance.

c. Synthetic lethality and therapeutic targeting of homologous recombination deficiency in cancer

i. PARP inhibitors: discovery and clinical development

Poly(ADP-ribosyl)ation (PARylation) was first described by Pierre Chambon and colleagues in the early 1960s during studies of nuclear enzymatic activities. While investigating RNA

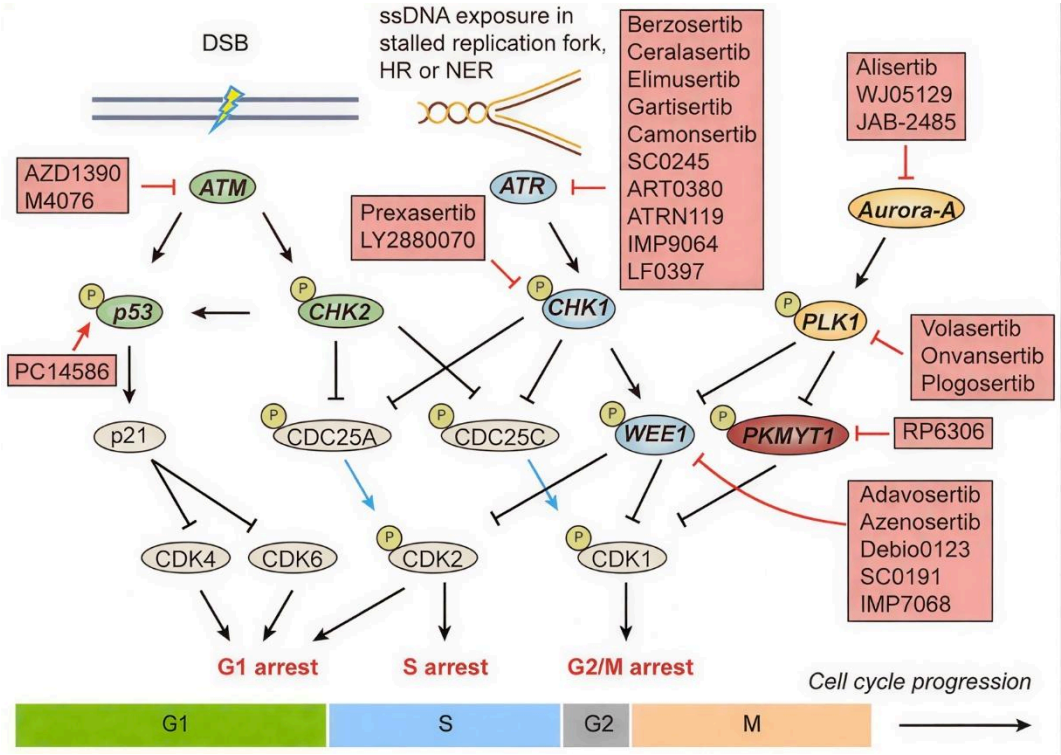

Figure 48. Therapeutic targeting of DNA damage response (DDR) signaling pathways. Pharmacological inhibition of DDR kinases disrupts DNA damage signaling and cell-cycle checkpoint control to enhance the efficacy of genotoxic therapies. Inhibitors targeting ATM and ATR impair activation of CHK2 and CHK1, respectively, leading to defective checkpoint signaling and increased replication stress. Downstream inhibition of regulators such as WEE1, PLK1, and CDKs further promotes cell-cycle progression in the presence of DNA damage, ultimately sensitizing cancer cells to DNA-damaging agents. Reproduced from *Li et al., Signal Transduct Target Ther (2023)*.

polymerase, they observed an unexpected NAD^+-dependent incorporation of ADP-ribose units, even in the absence of the nucleotides required for RNA synthesis. Although initially misinterpreted as poly(A) formation, subsequent biochemical analyses demonstrated that the product was in fact a polymer of ADP-ribose, leading to the identification of poly(ADP-ribose) polymerase (PARP) and the characterization of ADP-ribosylation as a novel post-translational modification (Chambon *et al*, 1963, 1966; Kraus, 2015).

Following this discovery, extensive research revealed that PARP enzymes play important roles in the cellular response to DNA damage. A major breakthrough occurred in 1980, when Durkacz and colleagues demonstrated that inhibition of PARP activity delays the repair of DNA strand breaks, providing the first direct evidence linking PARylation to DNA repair (Durkacz *et al*, 1980). Subsequent studies showed that PARP1 rapidly binds to DNA single-strand breaks (SSBs) through its N-terminal zinc finger domains, becomes activated, and catalyzes the synthesis of poly(ADP-ribose) chains on itself and target proteins. This auto-PARylation promotes its dissociation from DNA and facilitates the recruitment of DNA repair factors such as XRCC1 (Ménissier-de Murcia *et al*, 1989; Satoh & Lindahl, 1992; El-Khamisy *et al*, 2003; Pandey & Black, 2021).

Consistent with this role, PARP1-deficient mice display hypersensitivity to DNA-damaging agents and increased genomic instability (de Murcia *et al*, 1997). PARP1 is therefore recognized as a key regulator of single-strand break repair (SSBR) (Caldecott, 2008). PARP has also been implicated in base excision repair (BER), particularly in the processing of repair intermediates (Dantzer *et al*, 1999, 2000). However, its contribution appears to be context-dependent, as PARP deficiency or inhibition does not uniformly confer hypersensitivity to all base-damaging agents, suggesting that PARylation is not essential for all BER pathways (Vodenicharov *et al*, 2000; Ray Chaudhuri & Nussenzweig, 2017a).

The PARP family comprises approximately 17 members involved in diverse cellular processes, including transcriptional regulation, chromatin remodeling, and cell death (Figure 49) (Leung, 2017). The clinical relevance of PARP inhibition became apparent in the context of cancers harboring mutations in BRCA1 and BRCA2, which are essential for homologous recombination (HR) (Bhamidipati *et al*, 2023). Germline mutations in these genes are strongly associated with increased risks of breast and ovarian cancers, with lifetime risks reaching approximately 70% for breast cancer and 50% for ovarian cancer in mutation carriers, compared to approximately 12% and 2% in the general population (Petrucelli *et al*, 1993; Stoppa-Lyonnet, 2016).

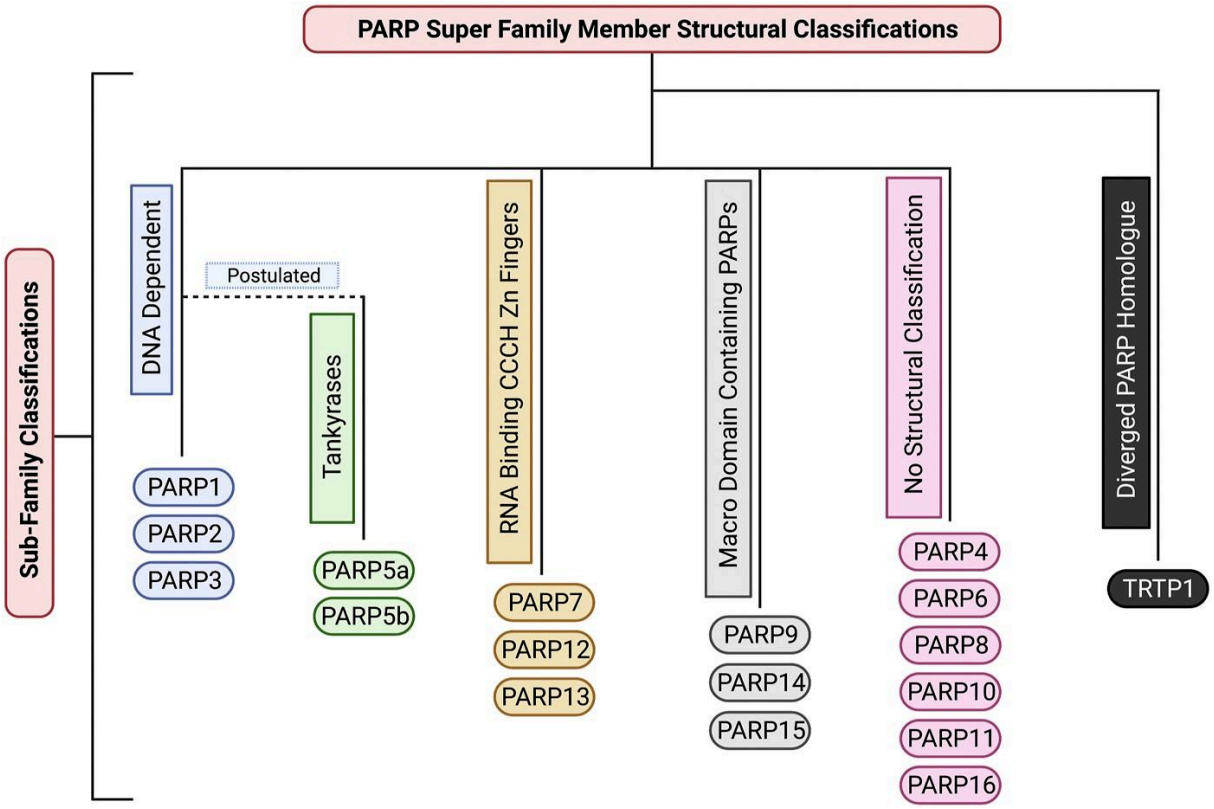

Figure 49. Structural and functional classification of the PARP protein family. The PARP family comprises multiple members grouped into distinct subfamilies based on domain organization and functional properties. These include DNA-dependent PARPs, tankyrases, and mono-ADP-ribosyltransferases, reflecting the diverse cellular roles of PARP proteins in DNA repair, transcriptional regulation, and chromatin organization. Reproduced from *Richard et al., Front Cell Dev Biol (2022)*.

A major conceptual breakthrough occurred in 2005, when two independent studies demonstrated that inhibition of PARP selectively induces cell death in BRCA1/2-deficient cells through synthetic lethality (Bryant *et al*, 2005; Farmer *et al*, 2005; Gonçalves *et al*, 2026). In this context, PARP inhibition leads to the accumulation of unrepaired SSBs, which are converted into double-strand breaks (DSBs) during DNA replication. These lesions require HR for repair; therefore, HR-deficient cells are unable to resolve them, resulting in genomic instability and cell death (Figure 50). This discovery established PARP inhibition as a targeted therapeutic strategy for HR-deficient tumors and paved the way for the clinical development of selective PARP inhibitors.

The inhibition of PARP activity was first described in the early 1970s using nicotinamide, a by-product of NAD^+ hydrolysis that functions as a product inhibitor of the PARP catalytic domain (Preiss *et al*, 1971). This observation laid the foundation for the development of current PARP inhibitors, which act as NAD^+ mimetics that competitively occupy the catalytic site of PARP enzymes, thereby blocking PARylation activity (Zeng *et al*, 2024). Following their development, numerous clinical trials evaluated the efficacy and safety of PARP inhibitors. Two phase II proof-of-concept studies demonstrated that olaparib, a selective PARP inhibitor, exhibited significant antitumor activity in patients with BRCA1/2-mutated advanced breast and ovarian cancers, with objective response rates of 41% and 33%, respectively, in the 400 mg twice-daily cohorts (Tutt *et al*, 2010; Audeh *et al*, 2010).

These findings were further supported by a subsequent maintenance study in patients with platinum-sensitive recurrent serous ovarian cancer, in which olaparib significantly prolonged progression-free survival compared with placebo (median PFS 8.4 months versus 4.8 months) following response to platinum-based chemotherapy (Ledermann *et al*, 2012). Together with additional clinical data, these studies led to the first FDA approval of olaparib in 2014 for patients with germline BRCA-mutated advanced ovarian cancer previously treated with multiple lines of chemotherapy (Kaufman *et al*, 2015), followed by its approval in 2018 for germline BRCA-mutated HER2-negative metastatic breast cancer (Robson *et al*, 2017).

Since then, several other PARP inhibitors have received regulatory approval. These include rucaparib, approved in 2016 for BRCA-mutated advanced ovarian cancer after prior chemotherapy (Swisher *et al*, 2017b), niraparib, approved in 2017 as maintenance therapy for recurrent ovarian, fallopian tube, or primary peritoneal cancer regardless of BRCA status (Mirza *et al*, 2016), and talazoparib, approved in 2018 for patients with germline BRCA-mutated HER2-negative locally advanced or metastatic breast cancer (Litton *et al*, 2018).

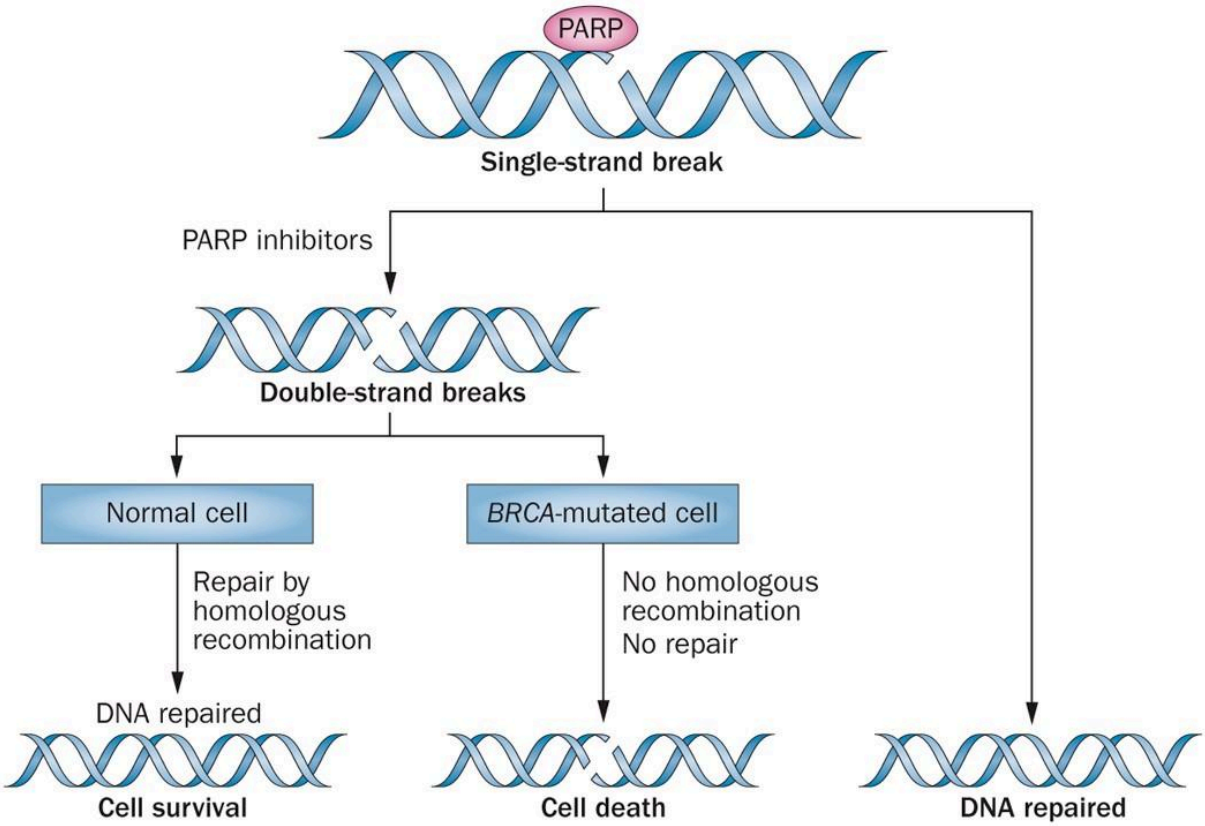

Figure 50. Synthetic lethality induced by PARP inhibition in homologous recombination-deficient cells. PARP inhibition leads to the accumulation of unrepaired single-strand breaks (SSBs), which are converted into double-strand breaks (DSBs) during DNA replication. In normal cells, these lesions are repaired by homologous recombination (HR), allowing cell survival. In contrast, BRCA1/2-deficient cells lack functional HR and are unable to repair DSBs, resulting in genomic instability and cell death. Reproduced from *Sonnenblick et al., Nat Rev Clin Oncol (2015)*.

In addition, a fifth PARP inhibitor, Veliparib, is currently undergoing clinical trials but has not yet been approved for routine clinical use (Coleman *et al*, 2019).

Importantly, the clinical efficacy of PARP inhibitors extends beyond breast and ovarian cancers, as they have demonstrated significant benefit in prostate and pancreatic cancers harboring BRCA1/2 mutations. These findings led to the FDA approval of olaparib and rucaparib for metastatic castration-resistant prostate cancer, and of olaparib for metastatic pancreatic cancer (Figure 51) (Golan *et al*, 2019; de Bono *et al*, 2020).

Despite their clinical success, important questions remain regarding the precise mechanisms underlying PARP inhibitor cytotoxicity and the emergence of resistance. The following sections will therefore focus on the molecular mechanisms of PARP inhibitor action, the major resistance pathways, and ongoing strategies to overcome these limitations.

ii. Molecular mechanisms of PARP inhibitor cytotoxicity

Despite their extensive clinical use, the precise mechanisms underlying the cytotoxic effects of PARP inhibitors (PARPi) in homologous recombination-deficient (HRD) cancer cells remain incompletely understood and continue to be actively investigated. The initial studies demonstrating the increased sensitivity of BRCA-deficient cells to PARP inhibition proposed a model based on synthetic lethality, in which PARPi impair the repair of DNA single-strand breaks (SSBs), leading to their accumulation and subsequent conversion into double-strand breaks (DSBs) during DNA replication. In HR-deficient cells, these replication-associated lesions cannot be efficiently repaired, ultimately resulting in overwhelming DNA damage and cell death (Bryant *et al*, 2005; Farmer *et al*, 2005). Nevertheless, this model was later challenged and refined by subsequent studies showing that genetic depletion of PARP1 interacting partner XRCC1 with small interfering RNA does not phenocopy pharmacological PARP inhibition, as it does not lead to comparable accumulation of SSBs or synthetic lethality in BRCA-deficient cells (Figure 52). These observations suggest that PARPi cytotoxicity cannot be solely explained by inhibition of SSB repair (Patel *et al*, 2011; Ström *et al*, 2011).

Among the alternative mechanisms proposed, PARP trapping has emerged as a major determinant of PARPi-induced cytotoxicity. In this model, PARPi bind to the NAD^+-binding site of PARP1 and prevent its auto-PARylation and release, thereby stabilizing PARP1 on DNA and generating persistent PARP1-DNA complexes that interfere with replication fork progression. This leads to replication fork stalling and collapse, resulting in the accumulation of DNA damage during S phase (Rose *et al*, 2020). Initial evidence supporting this model came

Table 1: Summary of PARP Inhibitor Approvals

	OLAPARIB[6]	RUCAPARIB[7]	NIRAPARIB[8]	TALAZOPARIB[9]
Advanced epithelial ovarian, fallopian tube, or primary peritoneal cancer	1. As monotherapy for germline BRCA-mutated (gBRCAm) advanced ovarian cancer after three or more prior lines of chemotherapy 2. In combination with bevacizumab as the first-line maintenance therapy in advanced HRR-mutant cancer for patients with complete or partial response to first-line platinum-based chemotherapy	Only approved for gBRCAm advanced ovarian cancer after two or more prior lines of chemotherapy	1. Maintenance therapy for patients with a complete or partial response to first-line platinum-based chemotherapy 2. HRR-mutated advanced ovarian cancer progressing more than six months after response to the last platinum-based chemotherapy.	Not approved
Recurrent epithelial ovarian, fallopian tube or primary peritoneal cancer	Maintenance therapy for patients with a complete or partial response to platinum-based chemotherapy	Maintenance therapy for patients with a complete or partial response to platinum-based chemotherapy	Maintenance therapy for patients with a complete or partial response to platinum-based chemotherapy	Not approved
Human epidermal growth factor receptor 2 (HER2)-negative metastatic breast cancer	After one or more lines of chemotherapy in the neoadjuvant, adjuvant or metastatic setting (and at least one endocrine therapy for hormone-receptor positive cancers)	Not approved	Not approved	deleterious or suspected deleterious germline BRCA-mutated (gBRCAm) HER2-negative locally advanced or metastatic breast cancer
Metastatic prostate adenocarcinoma	Only approved for gBRCAm cancer that has not progressed on at least 16 weeks of first-line platinum-based chemotherapy	Not approved	Not approved	Not approved
Metastatic castration-resistant prostate cancer (mCRPC)	As monotherapy for HRR-mutated mCRPC after progression on abiraterone or enzalutamide	As monotherapy for BRCA-mutated mCRPC after progression on abiraterone or enzalutamide, and a taxane chemotherapy	Not approved	Not approved

© 2020 Digital Science Press, Inc. and UroToday.com

Figure 51. Summary of FDA-approved PARP inhibitors and their clinical indications. Overview of the main PARP inhibitors (olaparib, rucaparib, niraparib, and talazoparib) and their approved indications across different cancer types, including ovarian, breast, and prostate cancers. These agents are primarily used in tumors with homologous recombination deficiency, particularly those harboring BRCA1/2 mutations. Reproduced from https://www.urotoday.com/library-resources/mcrpc-treatment/122336-parp-inhibitors-a-breakthrough-in-targeted-therapies-for-prostate-cancer.html

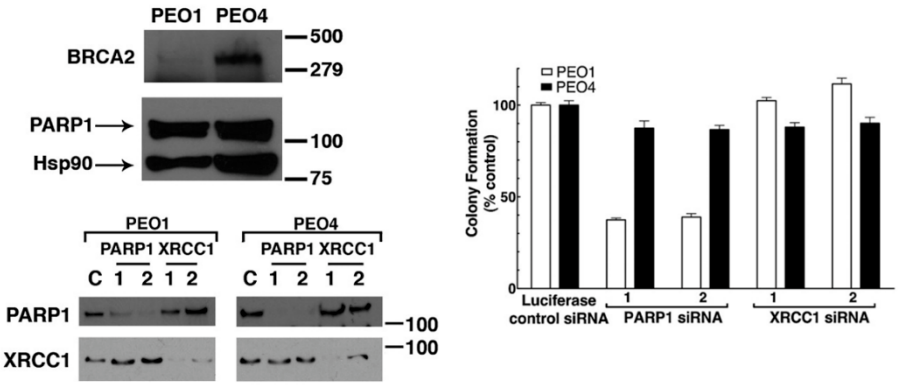

Figure 52. PARP inhibitor cytotoxicity is not solely due to inhibition of single-strand break repair. PARP1 inhibition selectively reduces survival of BRCA2-deficient (PEO1) cells, whereas XRCC1 depletion does not recapitulate this synthetic lethal effect. These results indicate that PARP inhibitor cytotoxicity cannot be explained solely by defective SSB repair. Adapted from *Patel et al., PNAS (2011)*.

from the observation that different PARP inhibitors exhibit markedly distinct trapping potencies despite having similar catalytic inhibitory activity. Notably, talazoparib displays substantially higher PARP-trapping capacity than niraparib, olaparib, and rucaparib, whereas veliparib shows relatively weak trapping activity. This hierarchy correlates with cytotoxic potency in tumor cell lines, providing a mechanistic explanation for why pharmacological PARP inhibition is more toxic than genetic depletion of PARP1 (Figure 53) (Murai *et al*, 2012).

Since its initial description, multiple studies have provided mechanistic and functional support for the PARP trapping model. For instance, factors involved in the resolution of PARP1-DNA complexes, such as the ATPase p97/VCP, the chromatin remodeler ALC1, and RNase H2, have been shown to promote the clearance of PARP1 from chromatin. Accordingly, their loss or inhibition enhances PARP trapping and potentiates PARPi-induced cytotoxicity in HR-deficient contexts (Zimmermann *et al*, 2018; Verma *et al*, 2021; Krastev *et al*, 2022).

At the molecular level, structural and biochemical studies have provided important insights into how PARP inhibitors promote trapping. In particular, Zandarashvili et al. demonstrated that different PARP inhibitors induce distinct allosteric conformations of PARP1, which differentially affect its ability to dissociate from DNA breaks sites. While some inhibitors stabilize PARP1 in a conformation that favors release from DNA (niraparib, rucaparib, and veliparib), others promote a more persistent PARP1-DNA interaction, thereby enhancing trapping (olaparib, talazoparib) (Figure 54) (Zandarashvili *et al*, 2020). Consistent with this, recent work identified a specific PARP1 mutation that selectively alters the trapping capacity of individual PARP inhibitors without affecting their ability to inhibit PARP catalytic activity. Notably, this mutation reduced the trapping efficiency of certain inhibitors (saruparib) while enhancing that of others (olaparib, veliparib), leading to corresponding changes in cytotoxicity in BRCA1-deficient models (Ribeiro *et al*, 2025). These results demonstrate that catalytic inhibition and trapping can be mechanistically uncoupled, and further support the notion that PARP trapping, rather than enzymatic inhibition alone, is a key determinant of PARP inhibitor efficacy.

Importantly, recent studies have also provided insight into how PARP trapping contributes to selective toxicity in HR-deficient cells. PARPi-induced PARP1 retention on DNA has been shown to interfere with RAD51 filament stability and strand exchange, thereby exacerbating HR defects. In BRCA-proficient cells, BRCA2 counteracts this effect by limiting PARP1 retention and promoting RAD51 function, providing a mechanistic basis for the selective vulnerability of BRCA-deficient tumors to PARP inhibition (Lahiri *et al*, 2025).

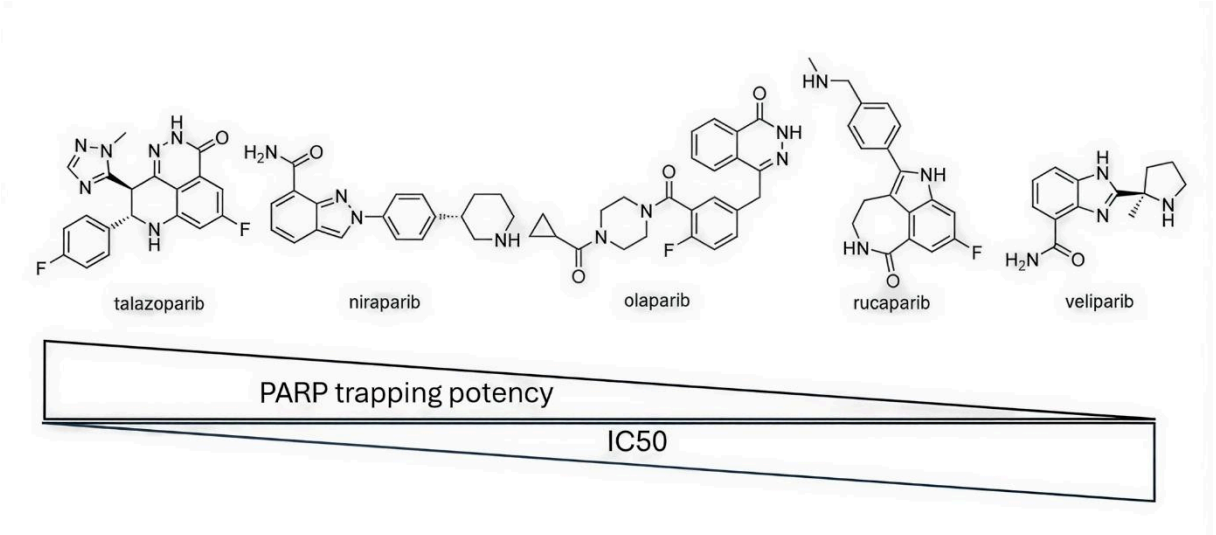

Figure 53. Differential PARP-trapping potency of PARP inhibitors. PARP inhibitors display varying abilities to trap PARP1 on DNA, with talazoparib showing the highest trapping potency, followed by niraparib, olaparib, rucaparib, and veliparib. This hierarchy correlates with cytotoxic activity (IC50). Adapted from *Murai et al., Cancer Research (2012); Rose et al., Front Cell Dev Biol (2020)*.

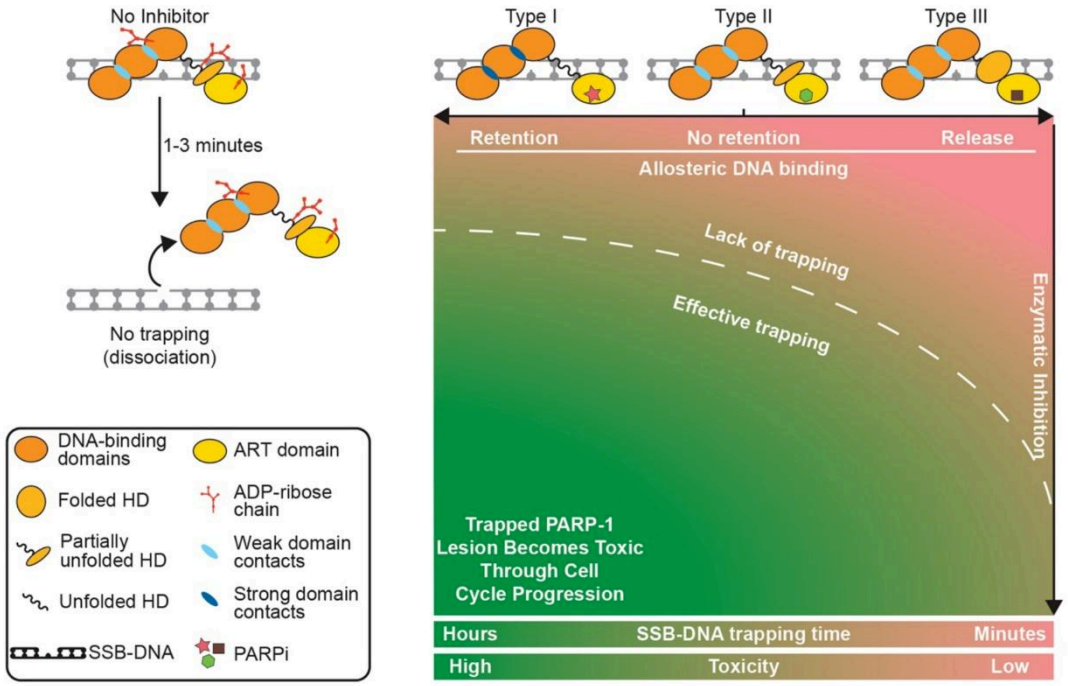

Figure 54. Differential PARP1 trapping induced by PARP inhibitors. PARP inhibitors induce distinct allosteric conformations of PARP1 that differentially affect its dissociation from DNA damage sites. While some inhibitors promote PARP1 release, others stabilize PARP1-DNA complexes, leading to prolonged trapping, impaired replication-fork progression, and increased DNA damage and cytotoxicity. Reproduced from *Zandarashvili et al., Science (2020)*.

Although PARP trapping is widely considered a major determinant of PARPi cytotoxicity, several observations suggest that it does not fully explain clinical responses. For example, PARP inhibitors with markedly different trapping potencies, including olaparib (Fong *et al*, 2010), niraparib (Sandhu *et al*, 2013), and talazoparib (de Bono *et al*, 2017), have shown broadly comparable response rates in clinical trials involving BRCA-mutated ovarian cancers. This indicates that additional mechanisms likely contribute to therapeutic efficacy.

Several complementary models have therefore been proposed. One emerging mechanism involves alterations in replication dynamics. PARPi treatment has been shown to increase replication fork speed, leading to replication stress and the accumulation of single-stranded DNA gaps that can be converted into DSBs (Figure 55) (Maya-Mendoza *et al*, 2018). More recent work from the same group demonstrated that this effect is dependent on DNA polymerase α-primase activity, which enables repriming and continued fork progression while limiting pathological gap accumulation. Accordingly, depletion of POLA1 leads to increased gap formation and enhanced sensitivity to PARPi, particularly in BRCA1-deficient cells (Machacova *et al*, 2024).

In addition, recent evidence highlights a role for PARP1 in coordinating transcription and replication. PARP1 has been shown to interact with fork protection factors such as TIMELESS and TIPIN, and its inhibition can lead to transcription-replication conflicts, resulting in DNA damage that requires homologous recombination for resolution. Interestingly, inhibition of transcription elongation has been reported to confer resistance to PARP inhibitors in BRCA-deficient cells, suggesting that enzymatic inhibition of PARP1 may contribute to cytotoxicity through transcription-associated mechanisms (Figure 56) (Petropoulos *et al*, 2024). While intriguing, further studies are required to define the relative contribution of this mechanism.

Consistent with this, PARP1 has also been shown to play direct roles in transcriptional regulation by promoting RNA polymerase II (RNAPII) pause release through ADP-ribosylation of the negative elongation factor (NELF), and its inhibition may therefore impair transcription elongation (Gibson *et al*, 2016). Conversely, PARP1-mediated PARylation has been shown to inhibit global transcription following DNA damage through disruption of P-TEFb function (Fu *et al*, 2022). Although the contribution of transcriptional perturbation to PARPi cytotoxicity in BRCA-deficient cancers remains less well defined, these findings suggest that transcriptional dysregulation may contribute, at least in part, to the cellular sensitivity to PARP inhibition in certain contexts.

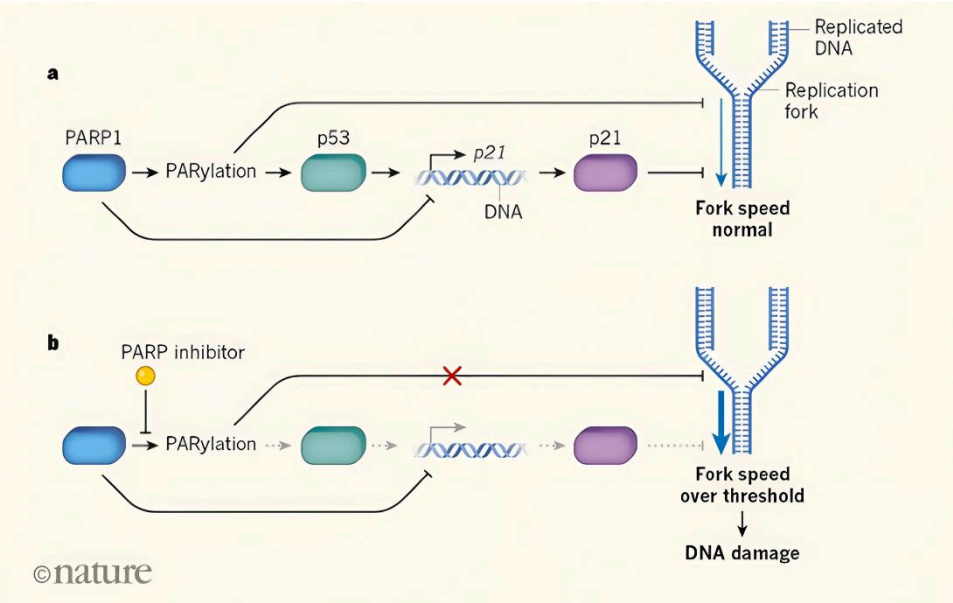

Figure 55. PARP inhibition alters replication fork dynamics. PARP inhibition disrupts PARylation-dependent regulation of replication, leading to increased replication fork speed and accumulation of DNA damage. This replication stress contributes to genomic instability, particularly in homologous recombination-deficient cells. Reproduced from *Quinet and Vindigni, Nature (2018)*.

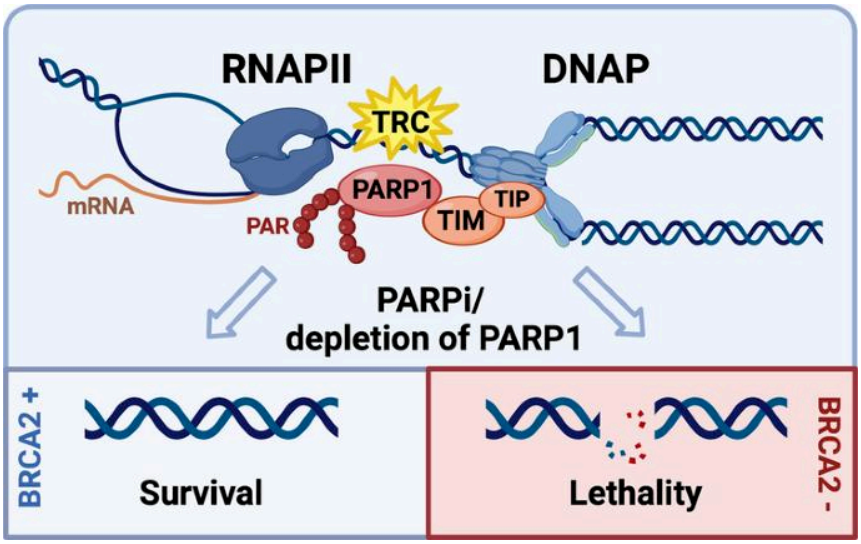

Figure 56. PARP1 regulates transcription-replication conflicts. PARP1 coordinates transcription and replication through interactions with fork protection factors such as TIMELESS and TIPIN. PARP inhibition disrupts this regulation, promoting transcription-replication conflicts and DNA damage that require homologous recombination for resolution, leading to selective lethality in BRCA-deficient cells. Reproduced from *Kolesnichenko and Scheidereit, Signal Transduct Target Ther (2025)*.

Finally, alternative models involving increased reliance on error-prone repair pathways such as NHEJ have been proposed. Early studies suggested that PARP inhibition promotes NHEJ activity, as evidenced by elevated phosphorylation of DNA-PK substrates, and that disruption of NHEJ can rescue PARPi-induced lethality (Patel *et al*, 2011). However, subsequent work demonstrating synergistic effects between PARP inhibitors and DNA-PK inhibitors argues against NHEJ activation as a universal mechanism (Fok *et al*, 2019).

While no single universal model fully explains PARPi cytotoxicity in BRCA-mutated cancer cells, ongoing research continues to refine our understanding of the mechanisms underlying synthetic lethality. In this regard, the study of acquired and intrinsic resistance to PARP inhibitors has emerged as a powerful approach to uncover the key determinants of PARPi sensitivity. The next section will therefore focus on the major resistance mechanisms identified to date, as well as emerging strategies being developed to overcome therapeutic resistance.

iii. Resistance mechanisms to PARP inhibitors

PARP inhibitors (PARPi) have revolutionized cancer therapy as the first successful clinical application of synthetic lethality. However, despite strong initial responses, most patients ultimately develop resistance, leading to disease relapse (Noordermeer & van Attikum, 2019). Mechanisms of resistance to PARPi largely converge on a limited number of functional outcomes, including restoration of homologous recombination (HR), stabilization of replication forks, and reduction of effective drug-target engagement, through decreased PARP trapping and increased drug efflux (Figure 57).

The most well-established mechanism of resistance involves restoration of HR capacity. This frequently occurs through secondary “reversion” mutations in BRCA1 or BRCA2, most often represented by short deletions that restore the open reading frame and reconstitute functional protein expression (Collet *et al*, 2024). These mutations were first identified in cancer cell lines, where they restore HR activity and confer cross-resistance to platinum agents and PARPi (Edwards *et al*, 2008; Sakai *et al*, 2008). Later, BRCA1/2 reversion mutations have been observed across multiple tumor types in patients’ samples with acquired PARPi-resistance, including ovarian, breast, prostate, and pancreatic cancers (Christie *et al*, 2017; Pettitt *et al*, 2020). Clinically, the presence of BRCA1/2 reversion mutations is associated with a marked reduction in progression-free survival (9 to 1.8 months) in ovarian cancer patients treated with rucaparib (Lin *et al*, 2019).

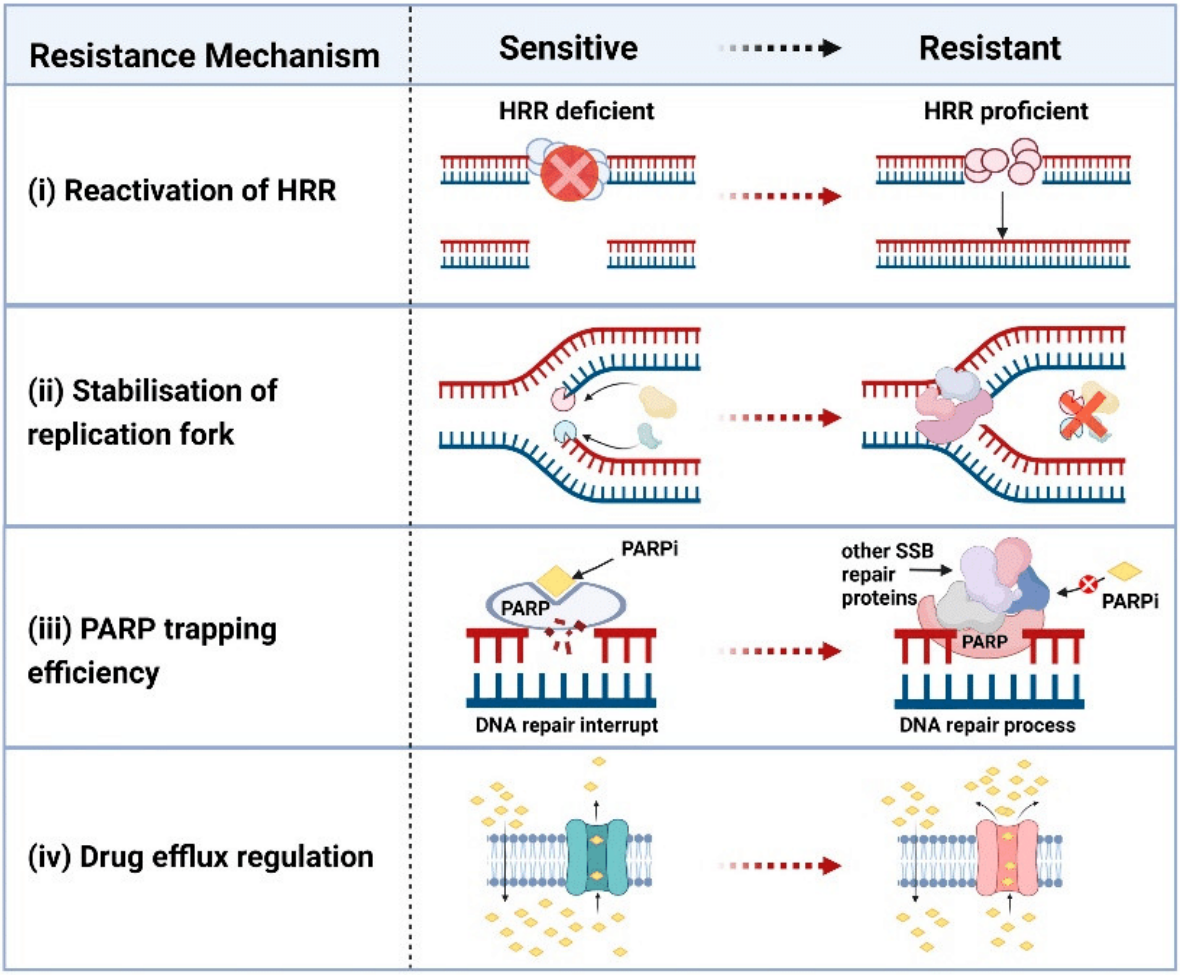

Figure 57. Major mechanisms of resistance to PARP inhibitors. PARP inhibitor resistance arises through multiple mechanisms that restore DNA repair capacity or reduce drug efficacy. These include reactivation of homologous recombination (HR), stabilization of replication forks, decreased PARP trapping, and increased drug efflux. These adaptations enable cancer cells to tolerate PARP inhibition and promote therapeutic resistance. Reproduced from *Rose et al., Front Cell Dev Biol (2020)*.

Importantly, similar reversion events have also been described in other HR-related genes such as RAD51, further highlighting restoration of HR as a central driver of resistance (Kondrashova *et al*, 2017). This phenomenon has been described as "tumor suppressor tolerance", in which loss of a tumor suppressor gene is required for tumor initiation, whereas restoration of its function increases tumor fitness under therapeutic pressure (Dias *et al*, 2021). In addition to genetic reversions, alternative mechanisms can restore BRCA function. For example, a recent study identified the molecular chaperone HSP90 as a stabilizer of mutant BRCA1 proteins, retaining their interaction with partner proteins and thereby conferring resistance to PARPi. Notably, low-level HSP90 inhibition restores PARPi sensitivity (Gracia *et al*, 2025).

HR restoration can also occur independently of BRCA1/2 through rewiring of DNA repair pathway choice. In particular, loss of 53BP1 or components of its effector pathway, including the Shieldin complex, restores DNA end resection in BRCA1-deficient cells, thereby rescuing HR activity and conferring resistance to PARPi (Figure 58) (Bunting *et al*, 2010; Bouwman *et al*, 2010; Jaspers *et al*, 2013; Noordermeer & van Attikum, 2019). Similarly, overexpression of the TRIP13 ATPase, observed in a large cohort of BRCA1-mutated carcinomas, promotes PARPi resistance by suppressing REV7-dependent NHEJ activity and enabling HR restoration (Clairmont *et al*, 2020). More recently, HR restoration has been shown to occur through non-canonical mechanisms involving replication-associated repair pathways that permit RAD51 loading and partial HR activity without full restoration of BRCA1/2 function. These intermediate "HR-like" states are sufficient to confer PARPi resistance (Peng *et al*, 2025).

Beyond HR restoration, stabilization of stalled replication forks represents another major mechanism of resistance. In BRCA-deficient cells, replication forks are normally unstable and prone to degradation by nucleases such as MRE11, leading to genomic instability. However, suppression of nucleolytic processing can restore fork stability and promote cell survival (Figure 59) (Ray Chaudhuri & Nussenzweig, 2017b). For example, depletion of the chromatin remodeler SMARCAL1 limits MRE11 recruitment to stalled forks, preventing nascent DNA degradation and conferring resistance to PARPi and DNA crosslinking agents in BRCA1/2-deficient cells (Taglialatela *et al*, 2017). Similarly, the histone methyltransferase EZH2 promotes fork degradation through histone methylation and recruitment of the MUS81 nuclease, and its depletion stabilizes replication forks and induces PARPi resistance (Rondinelli *et al*, 2017). Additional factors, such as the short isoform of the histone methyltransferase NSD3 (NSD3S), have recently been shown to contribute to fork protection by restricting PTIP-MRE11

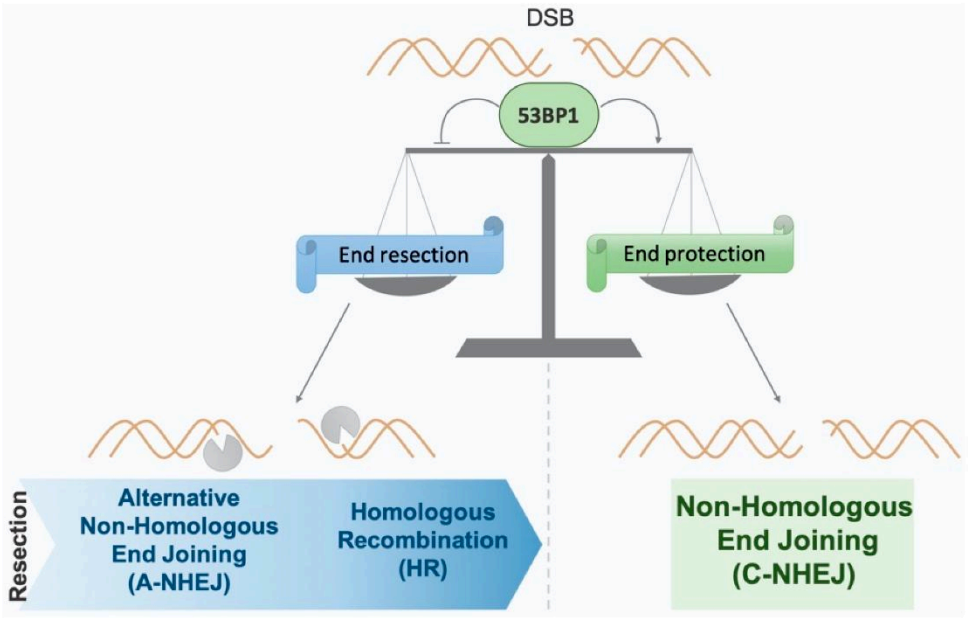

Figure 58. Regulation of DNA repair pathway choice by 53BP1. 53BP1 promotes non-homologous end joining (NHEJ) by limiting DNA end resection, thereby restricting homologous recombination (HR). Loss of 53BP1 or its downstream effectors restores DNA end resection in BRCA1-deficient cells, enabling HR reactivation and contributing to resistance to PARP inhibitors. Reproduced from *Rass et al., Genes (2022)*.

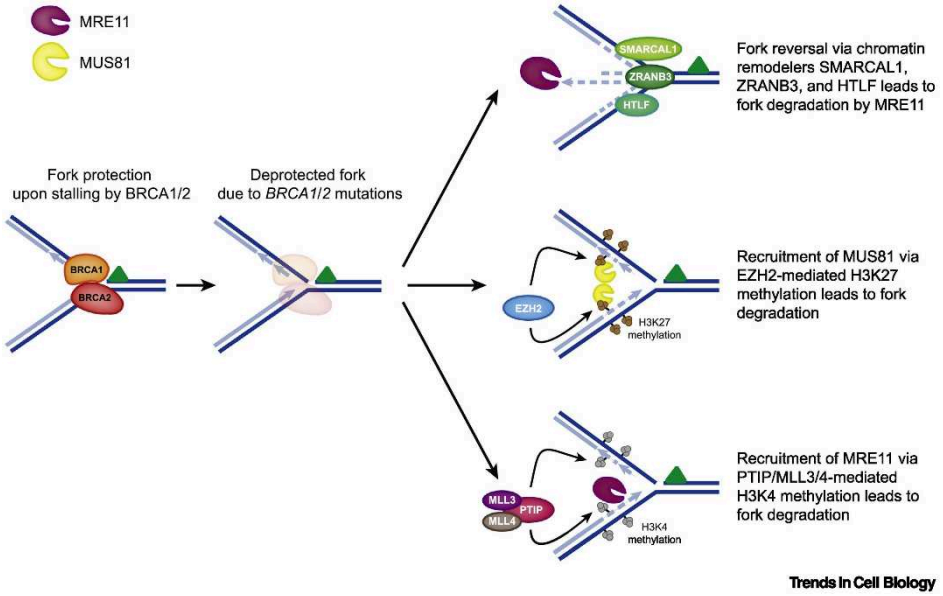

Figure 59. Replication fork stabilization as a mechanism of resistance to PARP inhibitors. In BRCA-deficient cells, stalled replication forks are normally degraded by nucleases such as MRE11, contributing to genomic instability. However, suppression of nucleolytic processing, through inhibition of fork reversal factors or chromatin-mediated recruitment of nucleases (e.g., MRE11), restores fork stability and confers resistance to PARP inhibitors. Reproduced from *Noordermeer and Haico van Attikum, Trends Cell Biol (2019)*.

activity, further underscoring replication fork stability as a key determinant of PARPi response independently of HR restoration (Zhu *et al*, 2025).

Resistance can also arise through alterations affecting drug-target interactions. For instance, overexpression of the drug efflux transporter ABCB1 reduces intracellular PARPi concentrations and confers resistance in BRCA-deficient models, an effect that can be reversed by pharmacological inhibition of ABCB1 (Jaspers *et al*, 2015; Vaidyanathan *et al*, 2016). In addition, point mutations in PARP1 that reduce inhibitor binding or impair PARP1 trapping on DNA have been identified as resistance mechanisms in preclinical models (Pettitt *et al*, 2018). Similarly, loss of the PAR-degrading enzyme PARG restores PARylation levels and reduces PARP trapping, thereby promoting PARPi resistance (Figure 60) (Gogola *et al*, 2018). Although these mechanisms are well established experimentally, their clinical relevance remains to be determined.

In addition to these canonical mechanisms, emerging evidence suggests that resistance can arise through dynamic cellular adaptation and chromatin-based processes. For instance, the histone chaperone NASP has been recently identified as a regulator of genome stability under PARPi treatment, promoting histone turnover and limiting accumulation of lethal DNA damage. Interestingly, loss of NASP reverses resistance and sensitizes tumor cells to PARPi both *in vitro* and *in vivo* (Moser *et al*, 2025). More broadly, resistance to PARPi can arise through gradual cellular adaptation rather than discrete genetic events. In this context, França and colleagues showed that BRCA-deficient cancer cells exposed to PARPi progressively transition through distinct transcriptional and phenotypic states, forming a continuum from initial drug tolerance to stable resistance (Figure 61). These findings indicate that PARPi resistance can emerge through phenotypic plasticity rather than solely through selection of pre-existing resistant clones (França *et al*, 2024).

These insights have prompted the development of strategies to overcome PARPi resistance. One approach involves preventing HR restoration by targeting upstream pathways that regulate HR activity, including PI3K-AKT, VEGF, and EGFR signaling, whose inhibition has been shown to impair HR and enhance PARPi sensitivity (Wang *et al*, 2016; Bizzaro *et al*, 2021; Xiao *et al*, 2026). Consistent with this, combining PARPi with VEGF inhibitors improves progression-free survival in ovarian cancer patients (Mirza *et al*, 2019).

Another strategy involves targeting cell-cycle checkpoint signaling. Replication fork stabilization has been shown to depend on ATR, which promotes RAD51 loading onto DSBs

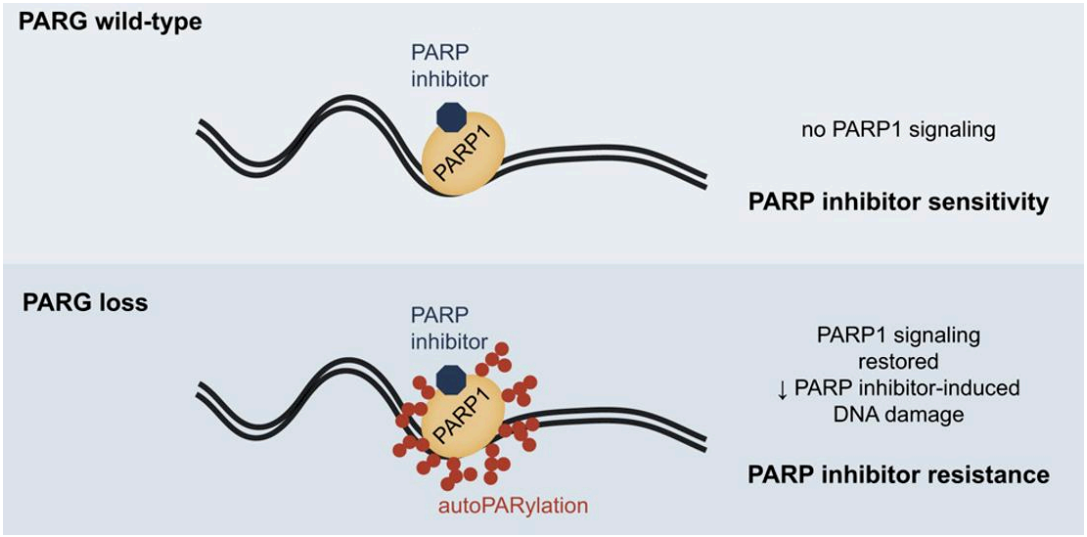

Figure 60. PARG loss promotes resistance to PARP inhibitors. Loss of the PAR-degrading enzyme PARG restores PARylation despite PARP inhibition, thereby reducing PARP1 trapping on DNA and limiting DNA damage. This restoration of PARP1 signaling promotes resistance to PARP inhibitors. Adapted from *Gogola et al., Cancer Cell (2018)*.

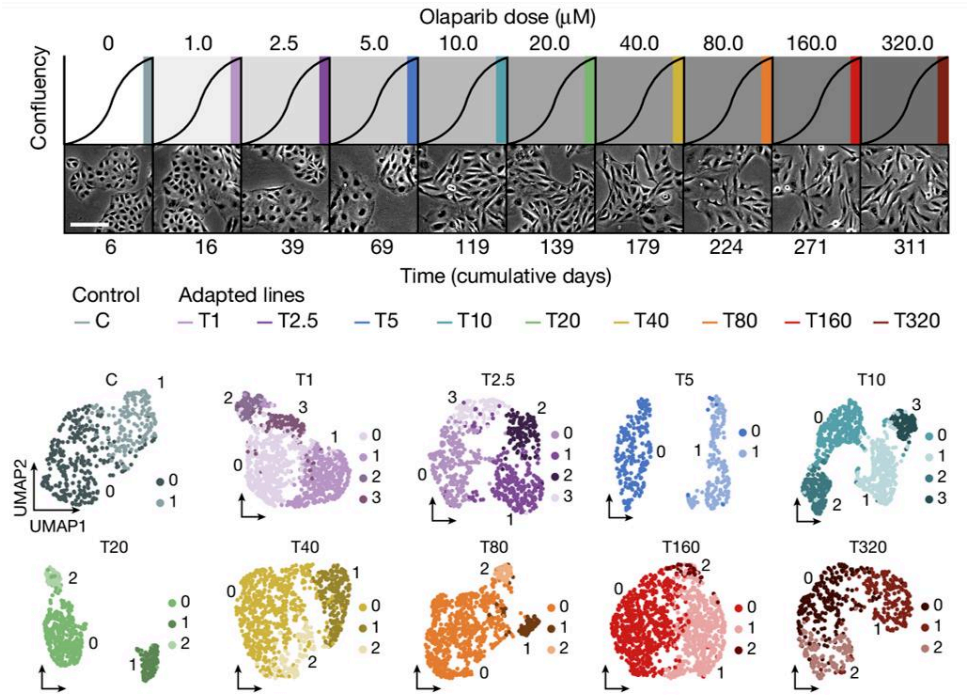

Figure 61. Gradual emergence of PARP inhibitor resistance through phenotypic adaptation. Stepwise dose escalation of PARP inhibitors drives progressive adaptation of BRCA-deficient cells, resulting in the emergence of resistant populations. Single-cell transcriptomic analysis reveals a continuum of transcriptional states from drug-tolerant to fully resistant cells, indicating that resistance to PARP inhibitors can also arise through phenotypic plasticity. Adapted from *França et al., Nature (2024)*.

and stalled forks. Accordingly, ATR inhibition disrupts RAD51 loading and replication fork protection, thereby overcoming PARPi resistance in BRCA-deficient cells (Yazinski *et al*, 2017).

In addition, PARPi-resistant cells can acquire specific vulnerabilities that may be therapeutically exploited. For example, resistance driven by loss of the 53BP1-Shieldin axis restores DNA end resection and HR-like repair, but at the cost of increased sensitivity to DNA nicks. In this context, nickase-based approaches selectively induce lethal DNA damage in PARPi-resistant BRCA1-deficient cells, highlighting a synthetic vulnerability associated with this resistance mechanism (Whalen *et al*, 2025).

Finally, modulation of the tumor immune microenvironment has emerged as a promising avenue to overcome resistance. Activation of the cGAS-STING-interferon pathway restores immune infiltration and enhances antitumor responses in PARPi-resistant models, suggesting that immune-based strategies may complement DNA repair-targeted therapies (Pedretti *et al*, 2025).

Despite these advances, a major limitation of PARPi therapy is that only a small subset of patients harbors BRCA mutations and may therefore benefit from the treatment. To expand the utility of PARPi, the concept of "BRCAness" has emerged, referring to tumors that exhibit HR deficiency in the absence of BRCA mutations. The following section will explore this concept and the strategies developed to extend PARPi sensitivity beyond BRCA-mutant cancers.

iv. BRCAness: expanding PARPi utility beyond BRCA mutations

PARP inhibitors (PARPi) have revolutionized the treatment of cancers harboring BRCA1/2 mutations. However, their clinical use remains limited by the relatively low frequency of BRCA1/2 alterations, restricting their applicability to only 5–10% of breast and ovarian cancers, and approximately 1–7% of pancreatic and prostate tumors (Armstrong *et al*, 2019; Zhang *et al*, 2011; Iqbal *et al*, 2012; Oh *et al*, 2019). To address this limitation, the concept of BRCAness emerged in 2004, describing a homologous recombination-deficient (HRD) state that phenocopies BRCA1/2-mutant tumors in the absence of germline BRCA1/2 mutations, and is likewise associated with increased sensitivity to platinum agents and PARP inhibitors (Figure 62) (Turner *et al*, 2004). Since then, major efforts have been made to identify the molecular determinants of BRCAness. These include genetic alterations affecting other HR genes, epigenetic deregulation of HR-related pathways, and more recently, the pharmacological induction of a functional HRD state (Lord & Ashworth, 2016; Abbotts *et al*, 2022).

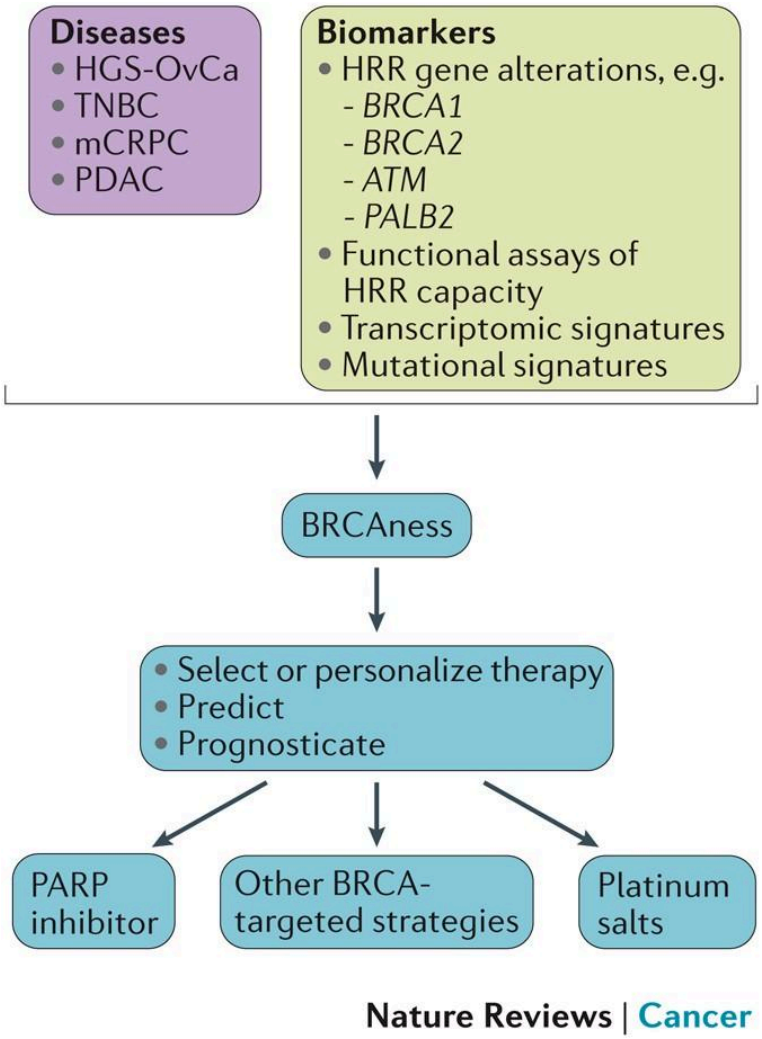

Figure 62. Concept of BRCAness and its clinical implications. The BRCAness phenotype describes tumors that lack functional homologous recombination (HR) despite the absence of BRCA1/2 mutations. This state can arise from genetic or epigenetic alterations in HR-related genes, as well as from specific transcriptomic and mutational signatures or functional deficiencies in HR activity. Identification of this phenotype has important clinical implications, enabling patient stratification, prediction of therapeutic response, and selection of treatments such as PARP inhibitors or platinum-based chemotherapy. Reproduced from *Lord and Ashworth, Nat Rev Cancer (2016)*.

Among genetic determinants of BRCAness, alterations in other DNA repair genes involved in homologous recombination have been extensively studied, including PALB2, RAD51, ATM, and ATR. Among these, PALB2 represents one of the most clinically relevant examples. PALB2 recruits BRCA2 to DNA double-strand breaks (DSBs) and facilitates RAD51 loading; accordingly, its depletion results in a profound defect in RAD51 foci formation and HR activity (Ducy *et al*, 2019). Germline loss-of-function mutations in PALB2 have been identified in up to 3.9% of breast cancer patients, depending on the population studied (Antoniou *et al*, 2014). Importantly, metastatic breast cancer patients carrying germline PALB2 mutations show high response rates to PARPi, with median progression-free survival even exceeding that observed in some patients with somatic BRCA1/2 mutations (13.3 vs 6.3 months) (Grellety *et al*, 2020; Tung *et al*, 2020). In parallel, RAD51 itself is a key HR effector and a functional biomarker of HR proficiency and PARPi response (Cruz *et al*, 2018, 201; Bonilla *et al*, 2020). Mutations in RAD51 paralogs have been identified in ovarian cancer patients' samples, and are associated with increased PARPi sensitivity, whereas secondary reversion mutations can restore HR and confer acquired resistance (Kondrashova *et al*, 2017).

Beyond these core HR components, the Fanconi anemia (FA) pathway plays a central role in coordinating the repair of DNA interstrand crosslinks and the maintenance of replication fork stability. The FA pathway promotes monoubiquitination of FANCD2 and FANCI, facilitating the recruitment of nucleases and HR factors required for lesion processing and repair (Kottemann & Smogorzewska, 2013; Ceccaldi *et al*, 2016b). Notably, several FA genes directly integrate HR machinery into this pathway (Figure 63A). Consequently, defects in FA components can induce a homologous recombination-deficient state and contribute to BRCAness, thereby sensitizing cancer cells to DNA-damaging agents and PARP inhibitors (McCabe *et al*, 2006; Kais *et al*, 2016; Rouault *et al*, 2025a).

Similarly, defects in DNA damage response signaling can also contribute to BRCAness. A frequently altered DDR factor is ATM, which is mutated in approximately 5% of tumors across several cancer types (Pitter *et al*, 2021). ATM loss delays DNA end resection and shifts repair toward NHEJ, thereby sensitizing cells to PARPi and, in some contexts, reversing resistance (Figure 63B) (Bakr *et al*, 2015; Xu *et al*, 2015; Wang *et al*, 2017). However, the predictive value of ATM deficiency for PARPi response remains less robust than that of BRCA1/2 or PALB2 loss, as clinical studies have shown only limited progression-free survival benefit in tumors compared with BRCA1/2- or PALB2-mutated cases (Tung *et al*, 2020; de Bono *et al*, 2020).

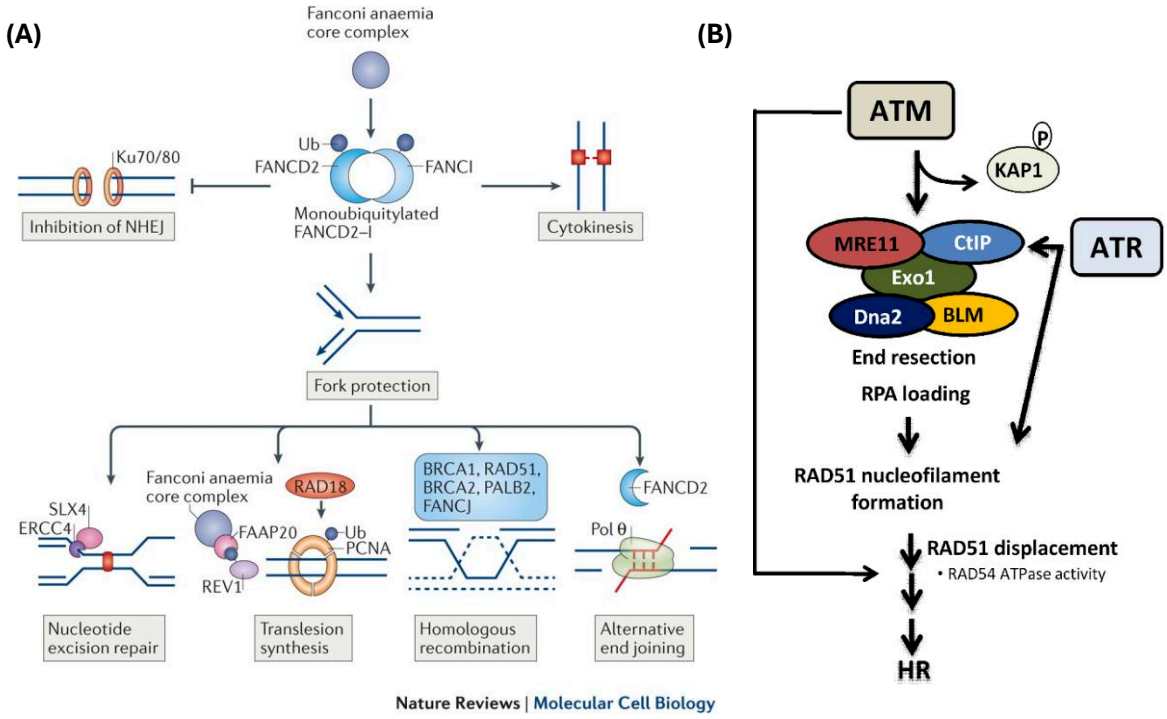

Figure 63. Regulation of homologous recombination through Fanconi anemia and ATM-dependent pathways. (A) The Fanconi anemia (FA) pathway coordinates the repair of DNA interstrand crosslinks and promotes replication fork stability through monoubiquitination of the FANCD2–FANCI complex. This activation facilitates the recruitment of nucleases, translesion synthesis factors, and homologous recombination (HR) proteins, including BRCA1, BRCA2, PALB2, and RAD51, thereby integrating multiple DNA repair pathways. **(B)** ATM-dependent signaling regulates DNA end resection, a critical step for HR initiation. ATM promotes the recruitment and activation of resection factors such as MRE11, CtIP, EXO1, BLM, and DNA2, leading to single-stranded DNA formation, RPA loading, and subsequent RAD51 nucleofilament assembly. Together, these pathways ensure efficient HR-mediated DNA repair, and their disruption can impair HR activity, contributing to homologous recombination deficiency and the emergence of a BRCAness phenotype. Adapted from *Ceccaldi et al., Nat Rev Mol Cell Biol (2016); Bakr et al., NAR (2015)*.

Furthermore, BRCAness can arise from alterations that do not directly affect HR genes but instead modulate HR activity through signaling or epigenetic mechanisms (Byrum *et al*, 2019). One classical example is PTEN, a tumor suppressor best known as a negative regulator of the PI3K-AKT pathway and one of the most frequently mutated tumor suppressors in human cancer (Lee *et al*, 2018). Interestingly, PTEN loss has been reported to impair HR and sensitize BRCA-proficient cancer cells to PARPi (Mendes-Pereira *et al*, 2009), possibly through its nuclear functions in maintaining chromosomal integrity (Shen *et al*, 2007), regulating DNA repair (Bassi *et al*, 2013), and controlling replication fork recovery (He *et al*, 2015). Likewise, epigenetic silencing of HR genes can induce a BRCAness phenotype. For example, hypermethylation of BRCA1 and RAD51C has been associated with PARPi sensitivity in ovarian cancer (Swisher *et al*, 2017a; Kondrashova *et al*, 2018), whereas loss of RAD51C promoter methylation has been linked to PARPi resistance (Nesic *et al*, 2021).

As it became increasingly clear that HRD is not restricted to BRCA1/2-mutant tumors, efforts were made to develop biomarkers capable of identifying BRCAness more broadly. One such biomarker is the HRD score, based on genomic scar features such as copy-number alterations and loss of heterozygosity, which has shown predictive value for response to platinum-based chemotherapy and, in some studies, to PARPi (Telli *et al*, 2016; Zhao *et al*, 2024). In parallel, several transcriptomic studies have identified and validated a list of gene expression signatures associated with BRCAness and improved response to DNA-damaging therapies, including PARPi (Konstantinopoulos *et al*, 2010; Peng *et al*, 2014; Lord & Ashworth, 2016; Zimmermann *et al*, 2018).

More recently, BRCAness has also been proposed as a pharmacologically inducible state, raising the possibility of extending PARPi sensitivity to BRCA-proficient tumors through drug combinations (Figure 64) (Abbotts *et al*, 2022). One early example comes from the observation that tumor hypoxia downregulates BRCA1 expression and thereby promotes HR deficiency (Bindra *et al*, 2005), providing a rationale for targeting angiogenic pathways. Accordingly, inhibition of VEGF signaling has been shown to sensitize BRCA-proficient models to PARPi (Bizzaro *et al*, 2021).

Another classical example is the PI3K signaling pathway, whose activity is required to maintain HR in cancer cells. Therefore, treatment with selective PI3K inhibitors downregulates BRCA1/2 expression and sensitizes BRCA-proficient breast cancer xenografts to PARPi (Yh *et al*, 2012). In yet another example, a recent study demonstrated that the antibiotic nifuroxazide

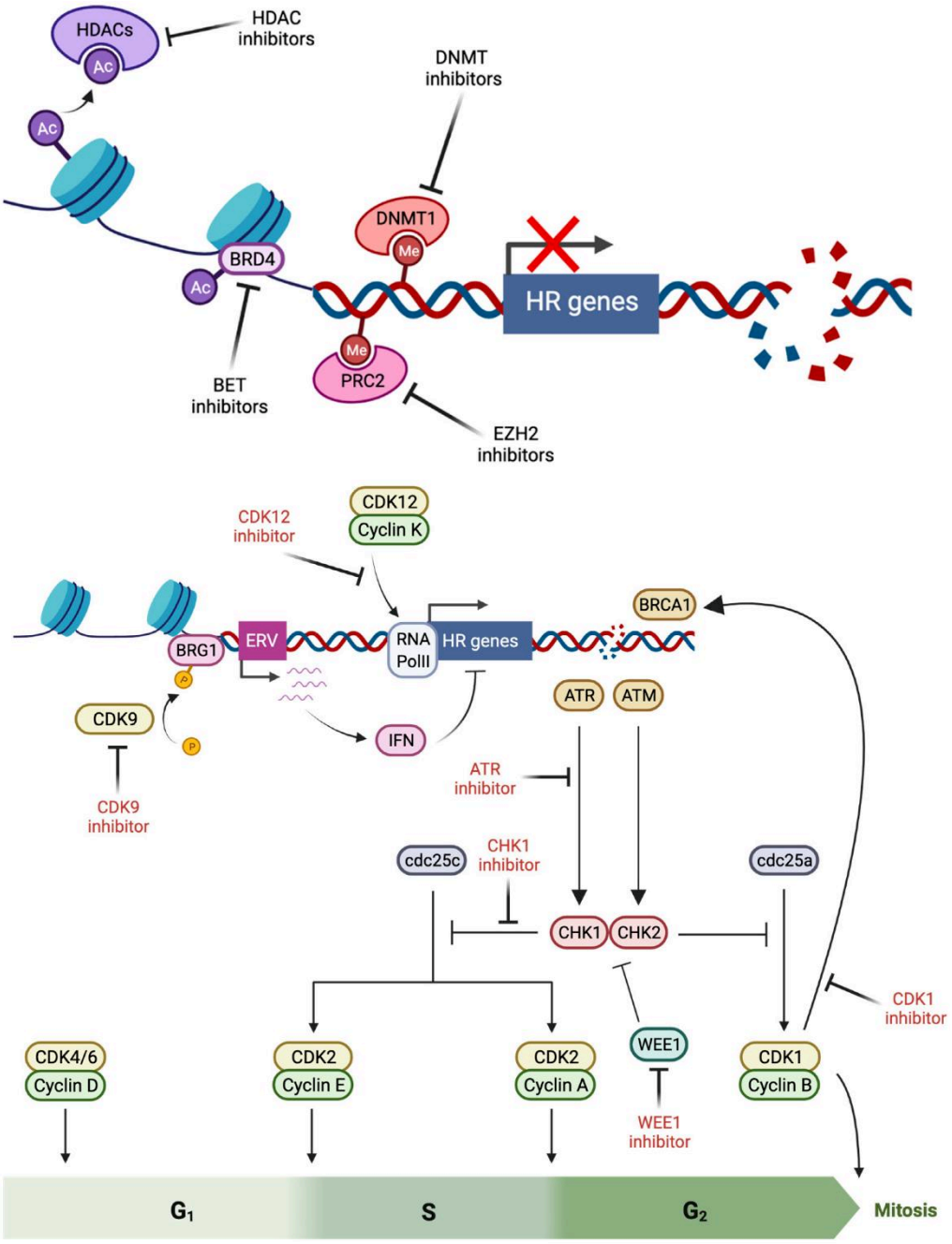

Figure 64. Examples of pharmacological induction of BRCAness through targeting transcription, chromatin regulation, and DNA damage response pathways. Pharmacological inhibition of transcriptional regulators (e.g., CDK12, CDK9), chromatin modifiers (e.g., BET, DNMT, and EZH2 inhibitors), and DNA damage response kinases (e.g., ATR, CHK1, and WEE1) can downregulate homologous recombination (HR) gene expression or impair HR function. These interventions induce a functional homologous recombination-deficient (HRD) state, thereby promoting BRCAness and sensitizing BRCA-proficient tumors to PARP inhibitors. Adapted from *Abbotts et al., Cancers (2022)*.

inhibits the STAT3/Fanconi anemia axis in breast cancer stem cells, thereby inducing a chemical HRD state and restoring PARPi sensitivity in a cell-state-specific manner (Rouault *et al*, 2025a). This is particularly relevant given that cancer stem cells are often resistant to conventional therapies and display a strong dependence on HR, creating vulnerabilities that may be therapeutically exploitable (Rouault *et al*, 2025b).

Among pharmacological strategies to induce BRCAness, transcriptional inhibition has emerged as a particularly attractive approach. Indeed, transcriptional addiction in cancer cells can be exploited to induce HR deficiency by repressing the expression of HR genes. A central mechanism, and one that will be developed throughout this thesis, is the inhibition of transcriptional elongation, which has been shown in several studies to selectively affect the expression of HR-related genes. The best-characterized example is cyclin-dependent kinase 12 (CDK12), which phosphorylates Ser2 within the C-terminal domain of RNA polymerase II (RNAPII) to promote productive transcriptional elongation (Bartkowiak *et al*, 2010). CDK12 also phosphorylates pre-mRNA processing factors such as components of the U1 snRNP complex, thereby suppressing the use of intronic polyadenylation (IPA) sites.

As a result, inhibition of CDK12 with agents such as THZ531 induces premature cleavage and polyadenylation, leading to truncated transcripts and early transcription termination. This effect is particularly pronounced in long genes (>45 kb) enriched in cryptic polyadenylation sites, a category that includes many DNA damage response and HR genes such as BRCA1, BRCA2, RAD51, ATR, FANCI, and FANCD2 (Figure 65) (Blazek *et al*, 2011; Dubbury *et al*, 2018; Krajewska *et al*, 2019). Accordingly, CDK12 inhibition induces a BRCAness-like state, sensitizes BRCA-proficient cancer cells to PARPi, and can even reverse acquired PARPi resistance (Johnson *et al*, 2016; Quereda *et al*, 2019). In addition, truncating and missense mutations in CDK12 have been associated with improved response to PARPi, further reinforcing the link between CDK12 loss and HR deficiency (Bajrami *et al*, 2014).

Other transcription-associated cyclin-dependent kinases, including CDK7 and CDK9, have also been implicated in this process. Their inhibition, either alone or in combination with CDK12 targeting, has been shown to destabilize transcriptional elongation, repress HR gene expression, induce a functional BRCAness state, and sensitize HR-proficient cancer cells to PARPi across several tumor types (Shan *et al*, 2020; Chu *et al*, 2022; Gui *et al*, 2025).

Similarly, the BET family protein BRD4, which promotes transcriptional elongation in part through recruitment of P-TEFb, has also been shown to regulate HR. BRD4 controls the

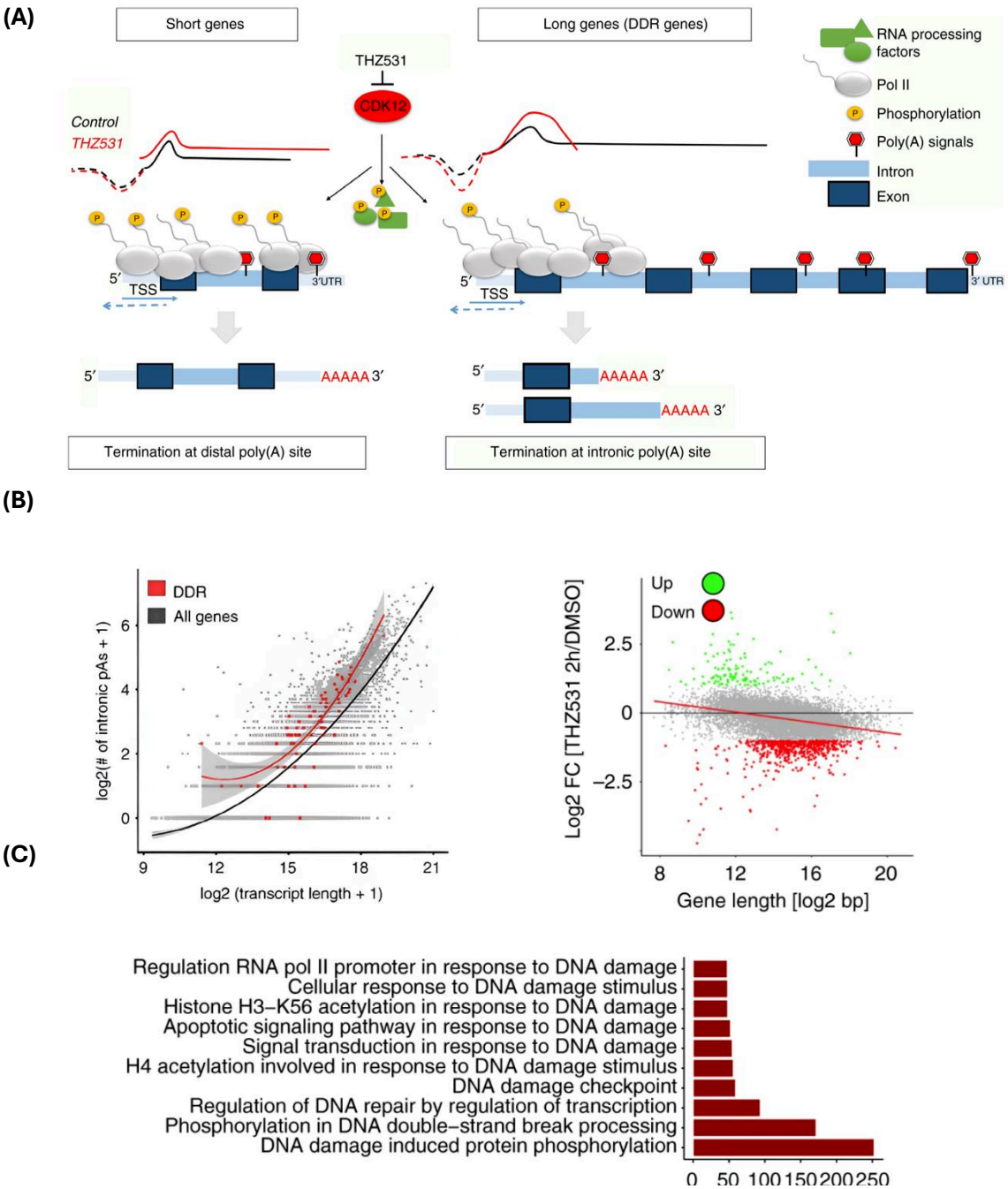

Figure 65. CDK12 inhibition induces preferential downregulation of long DNA damage response genes through premature transcriptional termination. (A) CDK12 promotes transcriptional elongation and suppresses intronic polyadenylation (IPA). Its inhibition induces premature cleavage and early transcription termination, particularly in long, DNA damage response (DDR) genes. **(B)** IPA usage increases with gene length and is particularly enriched in DDR genes, and long genes are preferentially downregulated upon CDK12 inhibition with THZ531. **(C)** Downregulated genes upon CDK12 inhibition are enriched for DNA repair and DNA damage response pathways, consistent with induction of a functional homologous recombination-deficient (HRD) state. Adapted from *Krajewska et al., Nat Commun (2019)*.

expression of HR genes, including the end resection factor CtIP, by binding to their enhancers and promoters. Therefore, BET inhibition represses the transcription of key HR factors, induces a BRCAness-like phenotype in HR-proficient cancer cells and enhances PARPi-induced DNA damage independently of PARP trapping (Figure 66) (Yang *et al*, 2017; Sun *et al*, 2018).

More broadly, epigenetic regulators have also emerged as potential pharmacological inducers of BRCAness. Several studies have shown that inhibition of chromatin modifiers such as EZH2, DNMTs, and HDACs can induce transcriptional changes associated with HR deficiency and sensitize cancer cells to PARPi independently of BRCA1/2 mutation status, further supporting transcriptional and epigenetic targeting as promising strategies to expand PARPi efficacy (Ha *et al*, 2014; Abbotts *et al*, 2022; Karakashev *et al*, 2020).

Altogether, these studies demonstrate that BRCAness is not restricted to inherited BRCA1/2 defects, but can arise through a wide range of genetic, epigenetic, and pharmacologically induced alterations that converge on impaired homologous recombination. However, despite extensive preclinical evidence, most of these strategies have not yet translated into clinically validated approaches, highlighting a critical gap between experimental findings and therapeutic application. Therefore, identifying clinically relevant compounds capable of inducing a robust and reproducible BRCAness-like state remains an important challenge. In particular, the possibility of inducing BRCAness through transcriptional repression of HR genes provides a strong conceptual framework to expand the therapeutic use of PARP inhibitors beyond BRCA-mutant tumors.

In this context, the clinically approved transcriptional inhibitors of the ecteinascidin family have been shown to induce DNA damage in cancer cells, although the extent to which this effect is linked to their impact on transcription remains unclear. Based on this rationale, one of the objectives of this thesis is to investigate whether synthetic ecteinascidins can induce transcriptional reprogramming that preferentially affects the expression of HR genes, thereby promoting a BRCAness-like state and sensitizing BRCA-proficient cancer cells to PARP inhibition.

The next section will therefore introduce the family of synthetic ecteinascidins, including their structural and pharmacological properties, as well as the current, limited understanding of their mechanism of action, before outlining the rationale for their use to target super-enhancer-driven oncogenic transcription and DNA repair programs in cancer.

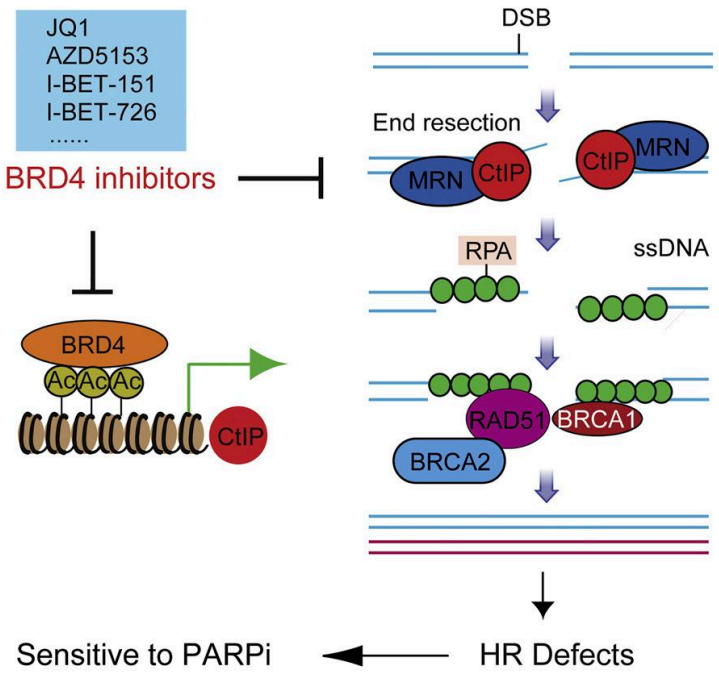

Figure 66. BET inhibition impairs homologous recombination through repression of end resection factors. BRD4 promotes transcription of homologous recombination (HR) genes, including the end resection factor CtIP, through binding at regulatory elements. BET inhibition reduces CtIP expression, thereby impairing DNA end resection and RAD51 loading, leading to HR defects. This induces a BRCAness-like phenotype and enhances sensitivity to PARP inhibitors independently of PARP trapping. Reproduced from *Sun et al., Cancer Cell (2018)*.

IV- Synthetic ecteinascidins: DNA-binding transcriptional inhibitors as promising anti-cancer agents:

While most current strategies to target transcriptional dysregulation in cancer rely on the enzymatic inhibition of transcriptional regulators (e.g., CDKs, bromodomain proteins), an alternative approach consists in directly targeting DNA to interfere with transcriptional processes. Ecteinascidins represent a class of DNA-binding agents with demonstrated clinical relevance, including trabectedin and its synthetic derivative lurbinectedin, the latter being approved for the treatment of small cell lung cancer. These compounds have been shown to inhibit transcription through sequence-selective DNA binding and interference with RNA polymerase II activity. In the following sections, the origin, structure, synthesis, and clinical applications of ecteinascidins will be presented, followed by a discussion of their known mechanisms of action, before introducing the rationale and objectives of their use in this work.

a. Ecteinascidins: from natural compounds to clinically relevant synthetic derivatives

Ecteinascidins are a group of marine-derived natural products that constitute a class of anti-cancer agents originally isolated from the tunicate *Ecteinascidia turbinata*, which primarily inhabits the Caribbean Sea and the Gulf of Mexico (Le *et al*, 2015b). Marine organisms are a rich source of bioactive compounds, producing thousands of structurally diverse molecules with potential therapeutic applications (Conte *et al*, 2020). In this context, the National Cancer Institute initiated screening programs in the 1950s to identify promising marine-derived anti-cancer agents, leading to the discovery of anti-tumor activity in extracts from Ecteinascidia turbinata in 1969 (Rinehart, 2000).

Later studies revealed that ecteinascidins are not directly produced by the tunicate itself, but rather by a bacterial symbiont, *Candidatus Endoecteinascidia frumentensis*, where they likely serve antimicrobial functions (Wang *et al*, 2020a). However, the extremely low abundance of these compounds in natural extracts, combined with the inability to culture the producing symbiont, significantly limited their early development. It was not until 1990 that the first clinically relevant compound, ecteinascidin-743 (Et-743), later known as trabectedin, was successfully isolated (Rinehart *et al*, 1990).

Due to these limitations, trabectedin and its analogues are now produced through semi-synthetic approaches by the Spanish pharmaceutical company and our collaborator, PharmaMar (Figure 67). In particular, large-scale production relies on chemical modification of the structurally

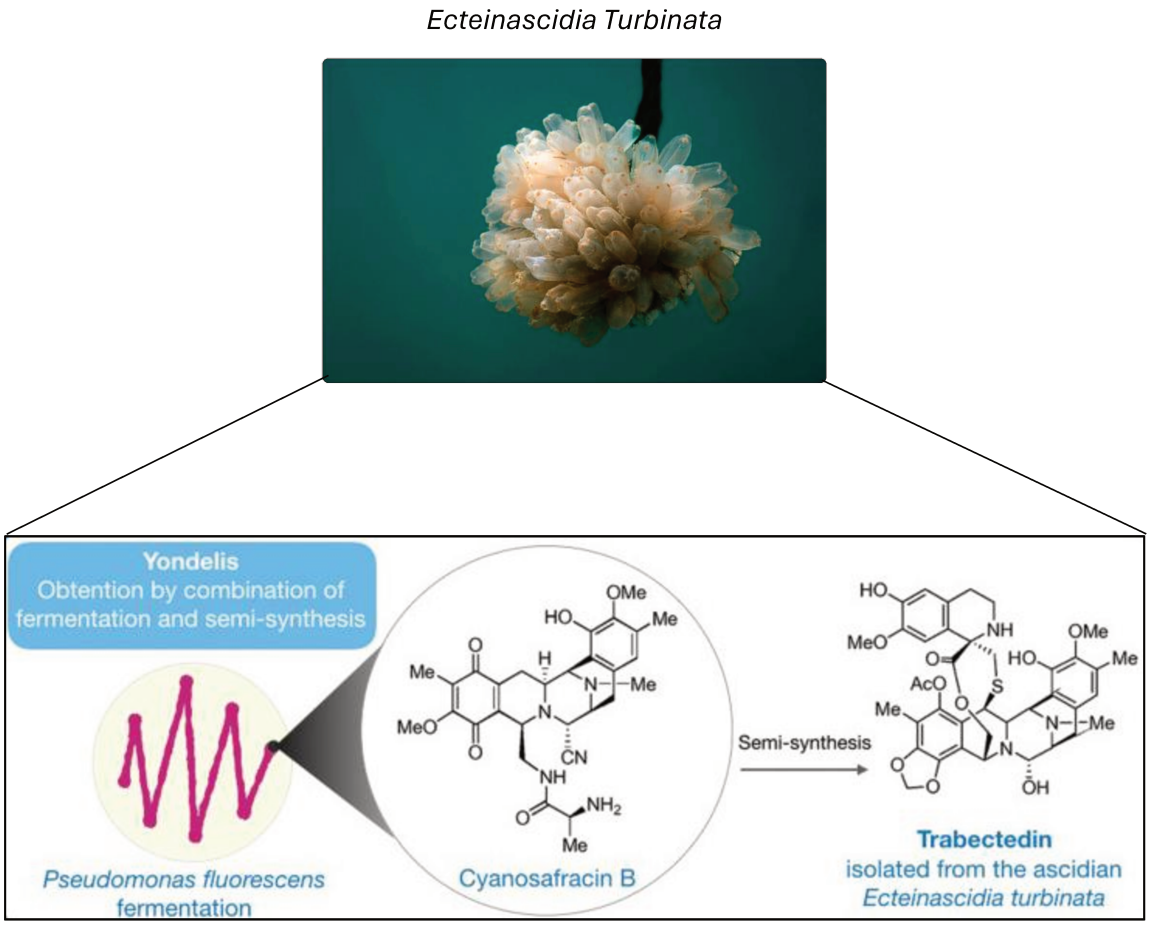

Figure 67. Natural origin and semi-synthetic production of ecteinascidins. Ecteinascidins were initially isolated from the marine tunicate Ecteinascidia turbinata, but are in fact produced by the symbiotic bacterium Candidatus Endoecteinascidia frumentensis. Due to their extremely low natural abundance and the inability to culture the producing microorganism, large-scale production of trabectedin (Et-743) relies on semi-synthesis from the bacterial metabolite cyanosafracin B. Adapted from *Christine Jimenez et al., Clinics (2018)*.

close bacterial metabolite cyanosafracin B, as established by pioneering synthetic work (Martinez & Corey, 2000). Accordingly, throughout this thesis, these compounds will be referred to as synthetic ecteinascidins.

The structure of trabectedin was resolved in 1992 and revealed a highly complex architecture composed of three fused tetrahydroisoquinoline subunits (A, B, and C). The A and B subunits are responsible for DNA binding through covalent interactions, notably via alkylation of guanine residues in the minor groove, while the C subunit is thought to mediate interactions with DNA-associated proteins, contributing to its biological activity (Sakai *et al*, 1992).

The potent anti-tumor activity of trabectedin across multiple cancer types, both *in vitro* and *in vivo* (Hendriks *et al*, 1999, 100; Mabuchi *et al*, 2011), led to the initiation of clinical trials in Europe and the United States. These studies demonstrated a reduction in tumor progression and a measurable benefit in patient outcomes, ultimately resulting in its approval by the FDA in 2015 for the treatment of patients with advanced soft tissue sarcoma after prior anthracycline-based therapy (Barone *et al*, 2017). However, trabectedin treatment is associated with significant hematological toxicities, including anemia and neutropenia, as well as fatigue, and provides limited improvement in overall survival in some contexts (Le *et al*, 2015b).

To improve therapeutic efficacy and tolerability, second-generation derivatives of trabectedin were developed. Among them, lurbinectedin has emerged as a key compound and represents one of the central molecules investigated in this thesis (Leal *et al*, 2010). Lurbinectedin differs from trabectedin at the level of the C subunit, where the tetrahydroisoquinoline moiety is replaced by a tetrahydro-β-carboline (Figure 68). Although structurally subtle, this modification results in significant pharmacokinetic and pharmacodynamic differences. Notably, lurbinectedin exhibits a lower volume of distribution (1460 L/m2 vs 438 L/m2) and a higher maximum tolerated dose (1.2 mg/m2 vs 5 mg/m2) compared to trabectedin (Ryan *et al*, 2001; Benton *et al*, 2019; Povo-Retana *et al*, 2024).

Consistent with these improvements, lurbinectedin demonstrated robust anti-tumor activity in multiple preclinical cancer models (Leal *et al*, 2010), and was subsequently granted accelerated approval by the FDA in 2020 for the treatment of patients with metastatic small cell lung cancer who progressed after platinum-based chemotherapy (Singh *et al*, 2021). This approval was based on a phase II open-label, multi-cohort clinical trial reporting an overall response rate of 35.2% and a median duration of response of 5.3 months in 105 patients treated with intravenous lurbinectedin (3.2 mg/m2, 1-hour infusion every 3 weeks) (Trigo *et al*, 2020). The treatment

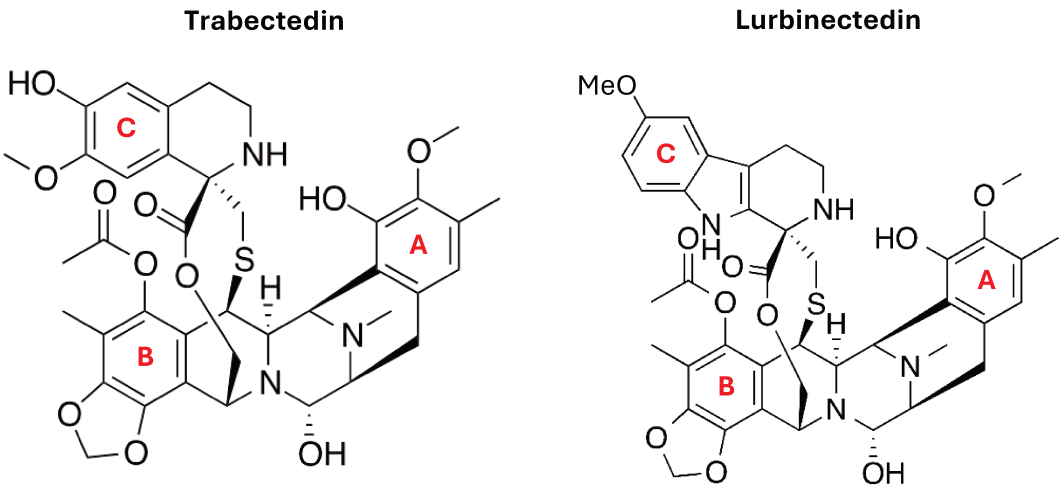

Figure 68. Structural comparison of trabectedin and lurbinectedin. Trabectedin is composed of three fused tetrahydroisoquinoline subunits (A, B, and C). The A and B subunits mediate DNA binding through covalent interactions with guanine residues in the minor groove, whereas the C subunit contributes to interactions with DNA-associated proteins. Lurbinectedin is a second-generation derivative that differs from trabectedin at the level of the C subunit, where the tetrahydroisoquinoline moiety is replaced by a tetrahydro-β-carboline. This structural modification underlies distinct pharmacokinetic and pharmacodynamic properties. Adapted from *Leal et al., Br J Pharmacol (2010); Le et al., Nat Prod Rep (2015); Povo-Retana et al., Molecules (2024)*.

exhibited a manageable safety profile, with predominantly hematological adverse events observed in a subset of patients.

Despite their clinical success, the precise mechanism of action underlying the anti-tumor activity of synthetic ecteinascidins remain incompletely understood. Current models converge on their ability to bind DNA, interfere with transcriptional processes, and induce DNA damage, ultimately leading to cancer cell death (Gadducci & Cosio, 2022; Calles *et al*, 2025). However, the detailed molecular basis of these effects, particularly at the transcriptional level, remains insufficiently characterized, which may limit the rational development of new therapeutic applications and combinatorial strategies. In the next section, the current understanding of the mechanisms of action of synthetic ecteinascidins will be discussed in greater detail.

b. Transcription-dependent mechanisms of action of synthetic ecteinascidins

Despite differences in pharmacokinetic and pharmacodynamic properties, trabectedin and lurbinectedin share highly similar mechanisms of action (Romano *et al*, 2013; Lima *et al*, 2016; Gadducci & Cosio, 2022). At the molecular level, synthetic ecteinascidins function as DNA-binding agents that interfere with transcriptional processes.

Biochemical studies, including electrophoretic mobility shift assays and DNase I footprinting, have shown that these compounds covalently bind to one DNA strand while establishing non-covalent interactions with the opposite strand, thereby preventing strand separation. More specifically, synthetic ecteinascidins bind to guanine residues in the DNA minor groove, preferentially within CG-rich triplets such as CGG, TGG, GGC, and AGC, where they alkylate the N2 position of the central guanine and form stable DNA adducts. This interaction induces a widening of the minor groove and a bending of the DNA helix toward the major groove, while the adduct is further stabilized through van der Waals interactions and hydrogen bonding involving the A and B subunits of the molecule (Seaman & Hurley, 1998; Zewail-Foote & Hurley, 1999; Santamaría Nuñez *et al*, 2016).

Early mechanistic insights into their transcriptional effects came from gel shift assays showing that trabectedin binding prevents the access of several transcription factors to GC-rich DNA regions *in vitro*, including NF-Y, TBP, E2F, and SRF/TCF (Bonfanti *et al*, 1999). These findings provided the first evidence linking ecteinascidin activity to transcriptional inhibition. More recently, genome-wide approaches such as Chem-seq have refined this model by demonstrating that lurbinectedin preferentially binds to the CpG islands at promoters of actively transcribed genes (Figure 69).

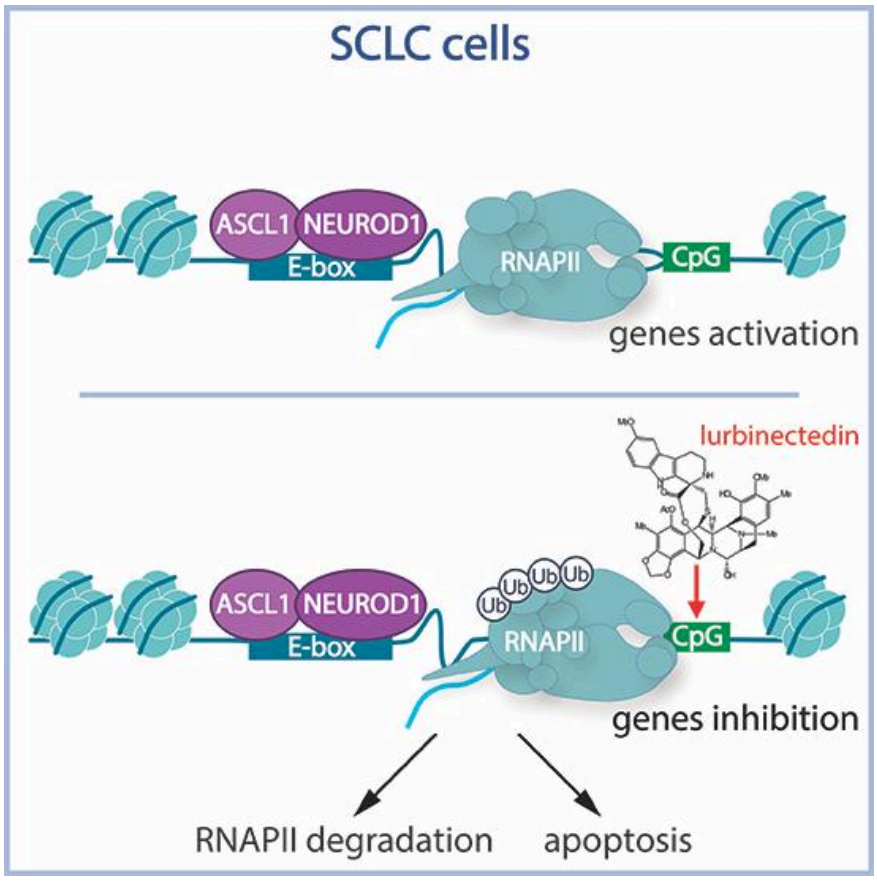

Figure 69. Lurbinectedin targets active promoters and induces RNAPII degradation. In small cell lung cancer (SCLC) cells, ASCL1- and NEUROD1-driven transcriptional programs promote gene activation through recruitment of RNA polymerase II (RNAPII) at CpG-rich promoters. Lurbinectedin preferentially binds to CpG islands at promoters of actively transcribed genes, leading to RNAPII stalling at transcription start sites, followed by its ubiquitination and proteasomal degradation. This results in transcriptional repression of ASCL1- and NEUROD1-responsive genes and ultimately induces apoptosis. Reproduced from *Costanzo et al., EMBO Mol Med (2022)*.

In small cell lung cancer (SCLC) models, lurbinectedin was shown to target promoters of ASCL1- and NEUROD1-driven transcriptional programs, leading to stalling of RNA polymerase II (RNAPII) at transcription start sites, followed by its ubiquitination and proteasomal degradation. This results in the downregulation of a large fraction of ASCL1- and NEUROD1-responsive genes and ultimately induces apoptosis in SCLC cells (Costanzo *et al*, 2022).

In addition to transcriptional interference, synthetic ecteinascidins induce DNA damage that contributes to their cytotoxic activity. Treatment with these compounds activates key DNA damage response kinases, including ATR and ATM, and increases H2AX phosphorylation, consistent with the formation of DNA double-strand breaks (DSBs) (Tavecchio *et al*, 2007; Lima *et al*, 2016). Accordingly, cells deficient in homologous recombination (HR) exhibit markedly increased sensitivity to ecteinascidins, and pharmacological inhibition of ATR further enhances their cytotoxic effects (Soares *et al*, 2007; Schultz *et al*, 2023).

Importantly, the formation of DNA breaks is not a direct consequence of DNA alkylation per se, but rather results from transcription-coupled nucleotide excision repair (TC-NER) processing of ecteinascidin-induced DNA adducts. In contrast to classical DNA-damaging agents such as cisplatin, which are more effective in NER-deficient contexts, ecteinascidins require a functional TC-NER pathway for maximal cytotoxicity. Cells deficient in TC-NER components display reduced sensitivity and decreased DNA break formation following trabectedin treatment, whereas defects in global genome NER (e.g., XPC loss) do not significantly affect drug sensitivity (Takebayashi *et al*, 2001). Mechanistically, the stalled RNAPII activates TC-NER, which attempts to remove the ecteinascidin-induced DNA adducts through dual incision by XPF and XPG endonucleases. While the 5′ incision by XPF proceeds normally, the 3′ incision by XPG is impaired by the drug-DNA adduct, resulting in persistent single-strand breaks that are converted into double-strand breaks during transcription (Figure 70) (Son *et al*, 2024). Thus, DNA damage induced by ecteinascidins arises from abortive repair of transcription-blocking lesions.

In addition to their direct effects on tumor cells, synthetic ecteinascidins have been shown to modulate the tumor microenvironment. Both trabectedin and lurbinectedin reduce tumor-associated macrophages and monocytes, which are key drivers of inflammation and angiogenesis, partly through transcriptional repression of pro-inflammatory mediators such as CCL2, IL-6, and VEGF, and through activation of caspase-8-dependent apoptosis in leukocytes (Germano *et al*, 2010, 2013; Belgiovine *et al*, 2017). More recently, lurbinectedin has been

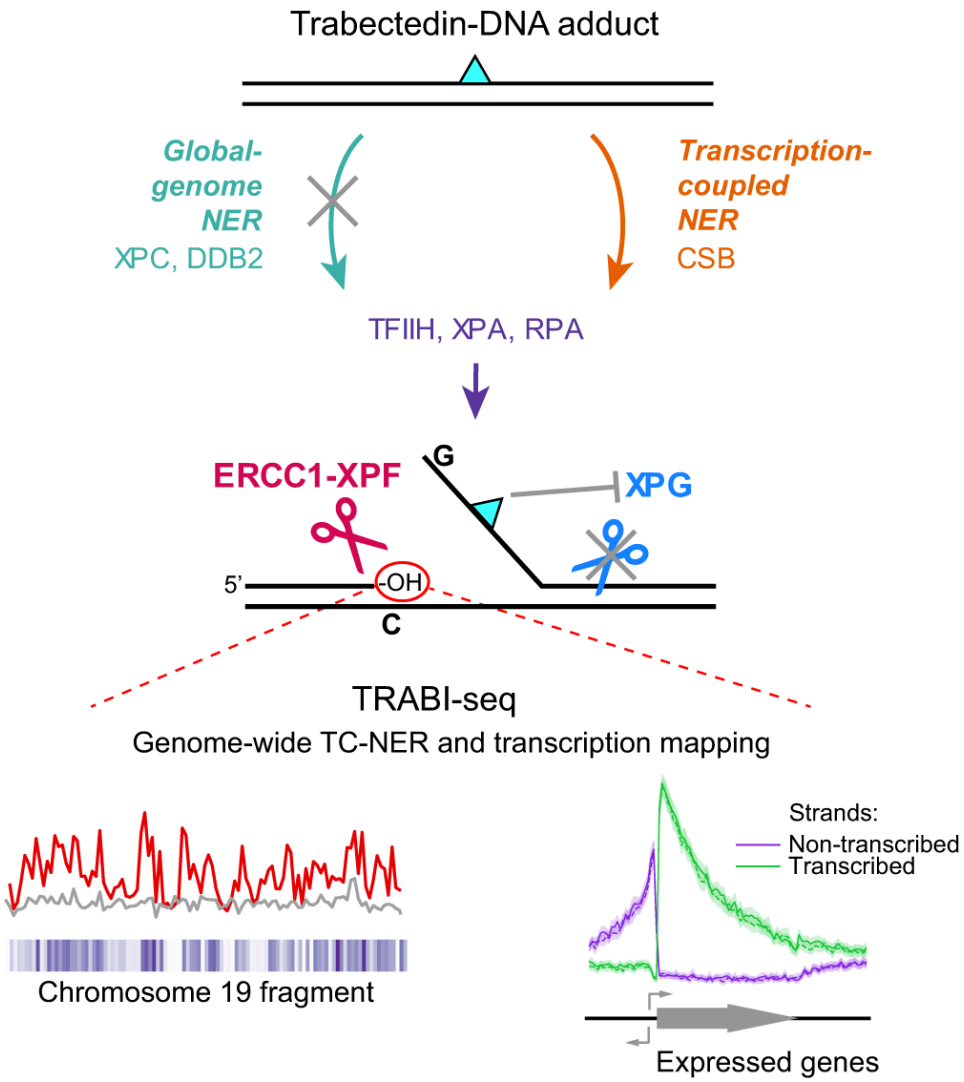

Figure 70. Transcription-coupled NER mediates ecteinascidin-induced DNA damage. Trabectedin forms covalent DNA adducts that stall RNA polymerase II (RNAPII) and are selectively recognized by transcription-coupled nucleotide excision repair (TC-NER), rather than global genome NER. This process involves recruitment of TC-NER factors such as CSB and the core NER machinery (TFIIH, XPA, RPA), followed by dual incision by the endonucleases ERCC1-XPF (5′) and XPG (3′). While the 5′ incision proceeds efficiently, the 3′ incision is impaired by the drug-DNA adduct, leading to persistent single-strand breaks. These lesions can be converted into double-strand breaks during ongoing transcription. Genome-wide mapping of these breaks reveals their enrichment at promoters and within highly transcribed genes, consistent with a transcription-dependent mechanism. Reproduced from *Son et al., Nat Commun (2024)*.

reported to enhance anti-tumor immune responses by activating the cGAS-STING pathway in response to DNA damage, thereby promoting type I interferon signaling and increasing $CD8^+$ T-cell infiltration (Figure 71) (Chakraborty *et al*, 2024). In line with these findings, clinical studies such as the IMforte trial have shown improved outcomes when lurbinectedin is combined with immune checkpoint inhibitors (Paz-Ares *et al*, 2025).

Despite these advances, the molecular mechanisms underlying the transcriptional effects of synthetic ecteinascidins remain incompletely understood. In particular, the identity of the transcriptional programs most susceptible to these compounds, as well as the precise relationship between transcriptional inhibition and DNA damage induction, remain unclear. Furthermore, a significant proportion of mechanistic studies have been performed at suprapharmacological micromolar concentrations, despite the nanomolar potency of these agents, raising the possibility that some reported effects may not fully reflect their physiological mode of action.

c. Objective: Dual targeting of transcriptional addiction and DNA repair in cancer with synthetic ecteinascidins

Given their ability to covalently bind DNA and interfere with transcriptional processes, synthetic ecteinascidins represent a unique class of anti-cancer agents that may exploit transcriptional vulnerabilities in tumor cells through mechanisms distinct from classical transcriptional inhibitors such as JQ1 or THZ1, which act by enzymatically targeting transcriptional regulators. While these approaches have provided important mechanistic insights, their clinical efficacy has remained limited, in part due to pharmacokinetic and therapeutic constraints. In this context, DNA-binding transcriptional inhibitors may offer an alternative and potentially more effective strategy to target transcriptional addiction.

Accordingly, the first objective of this work is to evaluate the therapeutic potential of three synthetic ecteinascidins in targeting oncogenic transcriptional programs: the clinically approved lurbinectedin, as well as two next-generation derivatives developed by PharmaMar, Ecubectedin (PM14) and PM54. These novel compounds were designed to improve the pharmacological properties of ecteinascidins and may exhibit enhanced efficacy or distinct activity profiles. At the mechanistic level, this objective seeks to characterize the transcriptional programs affected by these compounds across diverse cancer cellular states, including those with therapy resistance. A particular attention will be given to the impact of ecteinascidins on enhancer landscapes, notably super-enhancers that drive oncogenic transcription.

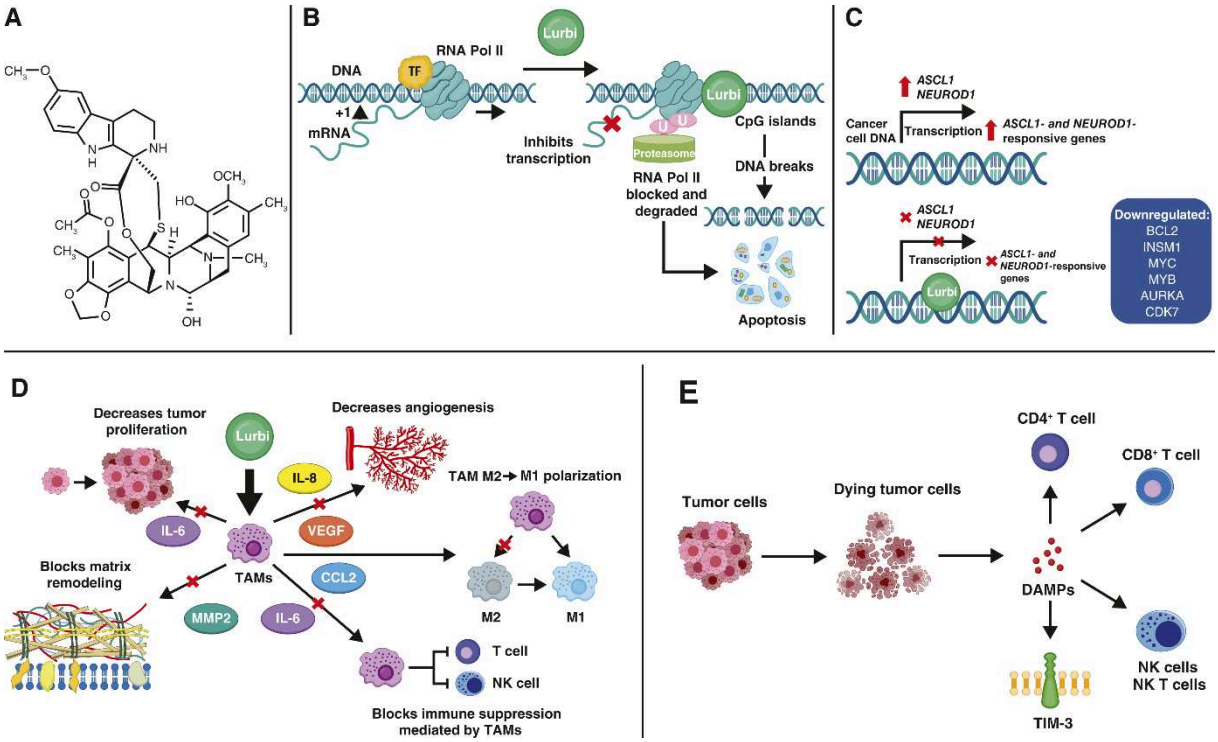

Figure 71. Integrated mechanism of action of synthetic ecteinascidins. Synthetic ecteinascidins exert anti-tumor activity through multiple complementary mechanisms. At the tumor cell level, they bind DNA and inhibit transcription by inducing RNA polymerase II stalling, ubiquitination, and degradation, leading to DNA damage and apoptosis. In parallel, these compounds modulate the tumor microenvironment by reducing tumor-associated macrophages and monocytes, and by repressing the expression of pro-inflammatory and pro-angiogenic factors such as CCL2, IL-6, and VEGF. Finally, ecteinascidin-induced DNA damage promotes the release of damage-associated molecular patterns (DAMPs) and activation of innate immune pathways, including cGAS-STING signaling, thereby enhancing $CD8^+$ T cell-mediated anti-tumor immunity. Reproduced from *Calles et al., Mol Cancer Ther (2025)*.

The second objective of this thesis aims to elucidate the interplay between transcriptional inhibition and DNA repair following ecteinascidin treatment. Building on evidence that these compounds induce DNA damage in a transcription-dependent manner, we will test whether ecteinascidin-mediated transcriptional reprogramming leads to downregulation of homologous recombination pathways and induces a state of BRCAness in cancer cells. This may sensitize otherwise HR-proficient tumors to PARP inhibitors, thereby providing a rationale for combination strategies based on synthetic lethality.

To address the first objective in a biologically relevant context, this work focuses in part on cutaneous melanoma as a model to study the transcriptional effects of ecteinascidins, as it is characterized by high tumor heterogeneity driven by transcriptional plasticity and a strong dependence on oncogenic transcriptional programs, which contribute to resistance to multiple therapies, including classical chemotherapies, targeted therapies, and immunotherapy. The following section will therefore introduce melanoma as a model system to study the effects of ecteinascidins on transcriptional reprogramming in cancer.

Altogether, this thesis seeks to establish synthetic ecteinascidins as dual-function therapeutic agents that simultaneously disrupt transcriptional addiction and impair DNA repair capacity in cancer cells, thereby offering new opportunities for targeting transcriptionally driven and therapy-resistant malignancies.

V- Cutaneous melanoma: a powerful model of transcriptional addiction and plasticity:

To investigate the impact of transcription-targeting strategies on cancer cell states, it is essential to rely on a model in which transcriptional regulation and cellular plasticity are prominent and mechanistically tractable. In this context, cutaneous melanoma represents a particularly relevant system and has been extensively studied in our laboratory. Melanoma is characterized by a high degree of intratumoral heterogeneity, with cells adopting distinct and reversible transcriptional states governed by lineage-specific master regulators, most notably MITF. These states are not fixed but can dynamically interconvert in response to microenvironmental cues, including therapeutic pressure, through a process known as phenotype switching (Figure 72) (Rambow *et al*, 2019). Importantly, the transcriptional programs underlying these cellular states have been shown to rely on super-enhancer (SE)-associated genes (Kaufman *et al*, 2016; Zhou *et al*, 2016; Fontanals-Cirera *et al*, 2017; Eliades *et al*, 2018; Berico *et al*, 2023a), supporting the notion that melanoma is highly dependent on enhancer-driven transcriptional regulation and therefore represents a suitable model to study compounds targeting SE function.

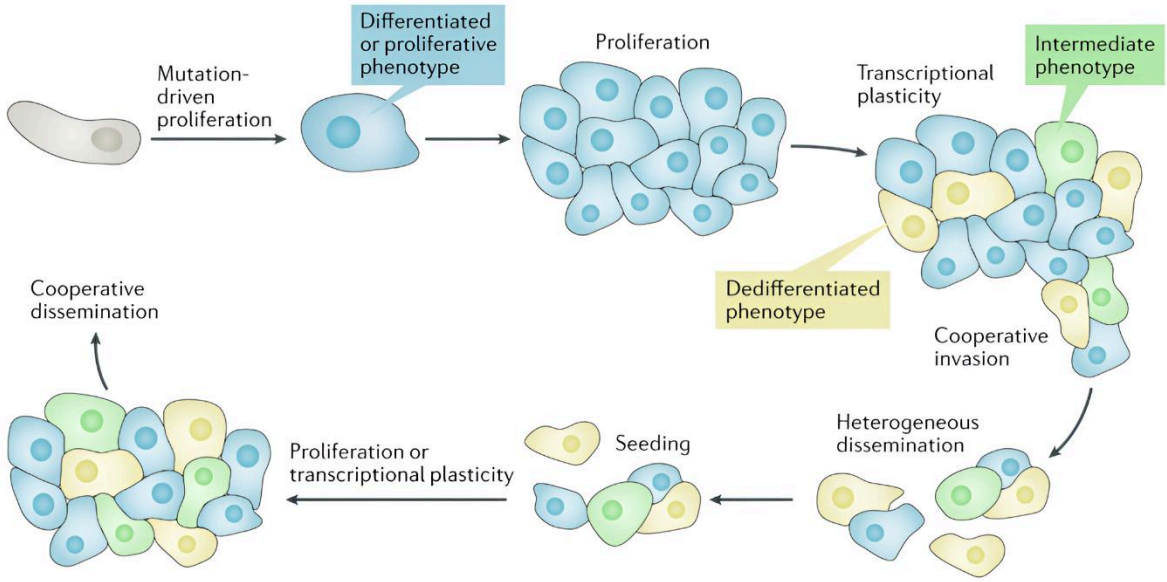

Figure 72. Transcriptional plasticity and phenotypic heterogeneity in melanoma. Following oncogenic transformation, melanoma cells adopt proliferative or differentiated states driven by lineage-specific transcriptional programs. Under microenvironmental cues and therapeutic pressure, cells undergo transcriptional reprogramming toward dedifferentiated and intermediate states, generating heterogeneous tumor populations. This plasticity enables cooperative invasion, dissemination, and metastatic seeding, with distinct cellular states contributing different functional properties. Adapted from *Arozarena et al., Nat Rev Cancer (2019)*.

Consistent with this, despite major therapeutic advances, including targeted therapies and immune checkpoint inhibitors, the majority of patients ultimately develop resistance (Robertson *et al*, 2024). This resistance is frequently driven by non-genetic mechanisms, including transcriptional reprogramming and cellular plasticity, rather than by the acquisition of new mutations alone.

Altogether, these features establish melanoma as a powerful model to investigate how transcriptional programs and enhancer-dependent regulatory networks shape tumor behavior, cellular heterogeneity, and therapeutic response. The following sections will therefore present the biological and clinical characteristics of cutaneous melanoma, including its epidemiology and classification, current therapeutic strategies, and the mechanisms of therapeutic resistance, with particular emphasis on transcriptional plasticity and phenotype switching.

a. Epidemiology, risk factors, and clinical classification of cutaneous melanoma

Cutaneous melanoma is a malignant tumor arising from melanocytes, which are specialized pigment-producing cells located in the basal layer of the epidermis. These cells synthesize melanin, which provides pigmentation to the skin, hair, and eyes, and plays a protective role against DNA damage induced by ultraviolet (UV) radiation (Cichorek *et al*, 2013). This process, known as melanogenesis, is tightly regulated by signals originating from keratinocytes in response to UV-induced DNA damage (Yardman-Frank & Fisher, 2021).

Upon UV exposure, keratinocytes activate TP53 and secrete proopiomelanocortin (POMC)-derived peptides, which are processed into adrenocorticotropic hormone (ACTH) and subsequently into α-melanocyte stimulating hormone (αMSH). These ligands activate melanocytes through the melanocortin 1 receptor (MC1R), leading to increased melanin synthesis. This response is largely coordinated by the transcription factor MITF, which regulates the expression of key melanogenic enzymes (Cui *et al*, 2007; D'Mello *et al*, 2016). Newly synthesized melanin is subsequently packaged into melanosomes and transferred to neighboring keratinocytes, where it forms suprcanuclear caps that act as physical barriers protecting genomic DNA from UV-induced damage (Figure 73) (Benito-Martínez *et al*, 2021; Centeno *et al*, 2023).

Despite representing only ~1% of all skin cancers, melanoma accounts for approximately 80% of skin cancer-related deaths, reflecting its high metastatic potential and marked clinical aggressiveness (Saginala *et al*, 2021). The incidence of melanoma has steadily increased over

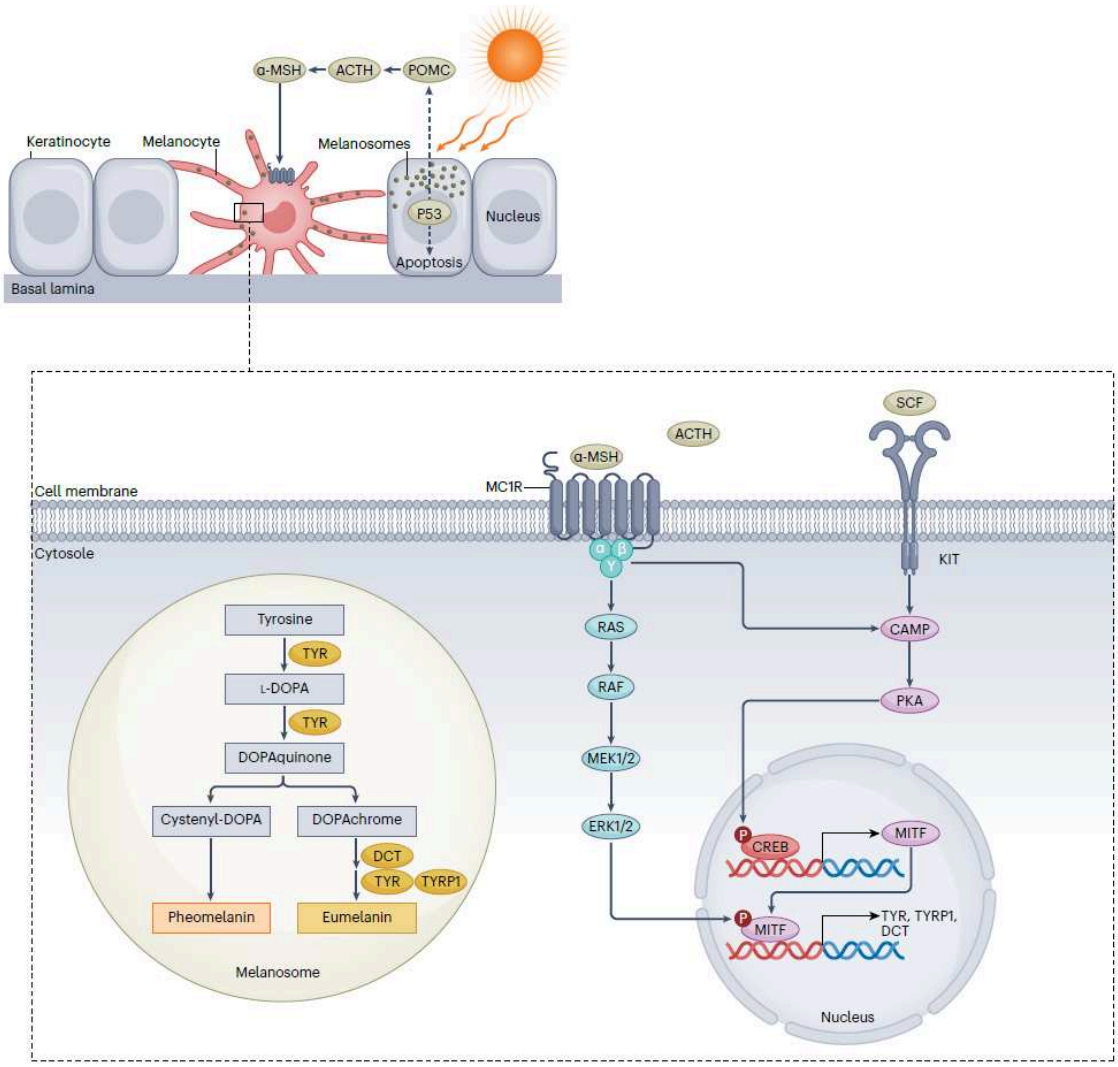

Figure 73. UV-induced melanogenesis and MITF-dependent transcriptional regulation in melanocytes. UV-induced DNA damage in keratinocytes activates TP53, leading to the production of proopiomelanocortin (POMC)-derived peptides, including α-melanocyte-stimulating hormone (α-MSH) and adrenocorticotropic hormone (ACTH). These ligands bind to the melanocortin 1 receptor (MC1R) on melanocytes, triggering cAMP/PKA and MAPK signaling pathways that converge on the activation of the lineage-specific transcription factor MITF. MITF drives the expression of key melanogenic enzymes, including tyrosinase (TYR), TYRP1, and DCT, thereby promoting melanin synthesis within melanosomes. Newly synthesized melanin is transferred to neighboring keratinocytes, where it forms supranuclear caps that protect genomic DNA from UV-induced damage. Reproduced from *Centeno et al., Nat Rev Cancer (2023)*.

recent decades, particularly in Western populations. Indeed, between 1982 and 2011, incidence rates rose by more than 3% annually (Whiteman *et al*, 2016), and global projections estimate up to 510,000 new cases and 96,000 deaths per year by 2040, compared with 325,000 cases and 57,000 deaths in 2020 (Arnold *et al*, 2022). Although early-stage melanomas can often be effectively treated by surgical excision, metastatic disease remains associated with poor prognosis, with a 5-year survival rate of approximately 35% (data from the American Cancer Society).

The primary environmental risk factor for melanoma is exposure to UV radiation, which is estimated to contribute to more than 75% of cases (Arnold *et al*, 2018). UV radiation induces the formation of cyclobutane pyrimidine dimers (CPDs) and 6-4 photoproducts (6-4PPs) between adjacent pyrimidine bases, notably thymine and cytosine residues, thereby generating helix-distorting DNA lesions (Figure 74). If left unrepaired, these lesions give rise to characteristic UV-signature mutations during replication, particularly C→T transitions at dipyrimidine sites (Pfeifer, 2020). As a result, melanoma exhibits one of the highest mutational burdens among solid tumors (Hodis *et al*, 2012). The UV-induced lesions are primarily repaired by the nucleotide excision repair (NER) pathway. Accordingly, inherited NER-deficiency syndromes such as xeroderma pigmentosum are associated with 2000-fold increased risk of melanoma due to the excessive accumulation of UV-induced mutations (Bradford *et al*, 2011; Yurchenko *et al*, 2023).

The efficiency of UV protection is strongly influenced by skin pigmentation, with eumelanin-rich darker skin providing greater protection than pheomelanin-rich lighter skin, thereby contributing to differences in melanoma incidence across populations (Nasti & Timares, 2015; Hennessy *et al*, 2005). Therefore, countries characterized by intense sun exposure and predominantly fair-skinned populations, notably Australia and New Zealand, display the highest melanoma incidence rates worldwide, reaching approximately 60 cases per 100,000 population per year (Long *et al*, 2023).

In addition to environmental exposure, host and genetic factors contribute to melanoma susceptibility. Individuals with a high number of melanocytic naevi or dysplastic naevi are at increased risk, and germline mutations in genes such as CDKN2A are detected in 20-40% of familial melanoma cases (Rossi *et al*, 2019). Beyond environmental factors, biological sex may also influence melanoma risk. In general, women display a lower overall incidence and a better prognosis than men (Schwartz *et al*, 2019).

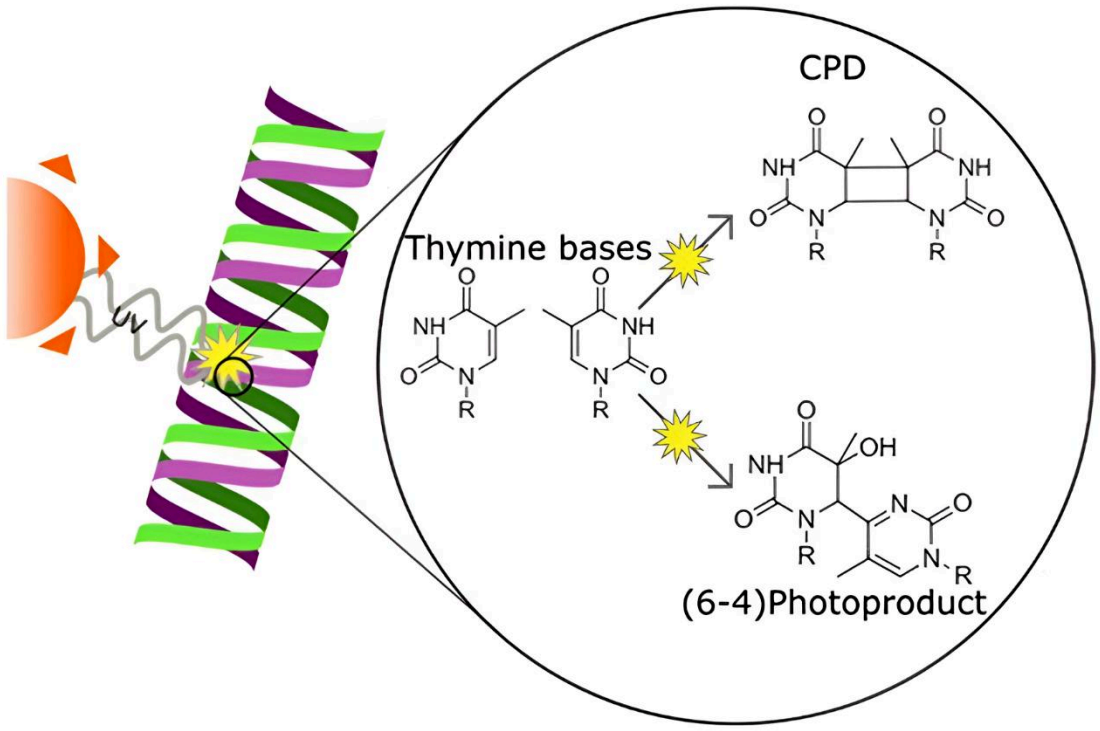

Figure 74. UV-induced DNA photolesions and mutagenic consequences. Ultraviolet (UV) radiation induces covalent bonding between adjacent pyrimidine bases, primarily thymine and cytosine, resulting in the formation of cyclobutane pyrimidine dimers (CPDs) and 6-4 photoproducts (6-4PPs). These lesions distort the DNA helix and interfere with replication and transcription. If not properly repaired, they lead to characteristic UV-signature mutations, notably C→T transitions at dipyrimidine sites, thereby contributing to the high mutational burden observed in melanoma. Reproduced from https://encyclopedia.pub/entry/20845.

This may be partially explained by the fact that women possess two copies of the X-linked RNA helicase DDX3X, a melanoma tumor suppressor, whereas mutations in this gene appear to occur exclusively in men (Alkallas *et al*, 2020). Nonetheless, recent work suggests an important exception, as women under the age of 50 show a higher incidence of melanoma than age-matched men. This vulnerability has been linked to loss of E-cadherin and hyperactivation of a sex-specific signaling axis involving estrogen receptor-α and GRPR, which in the premenopausal hormonal context may promote tumor aggressiveness and metastasis (Raymond *et al*, 2025).

At the genomic level, cutaneous melanoma can be broadly classified into four subtypes based on recurrent mutational patterns, most of which converge on aberrant activation of the mitogen-activated protein kinase (MAPK) pathway. The most frequent subtype is defined by BRAF mutations (~50% of melanomas), most commonly $BRAF^{V600E}$, which results in constitutive activation of the BRAF kinase. The remaining major genomic subtypes include RAS-mutant melanomas (~25%), NF1-mutant melanomas (~15%), and triple wild-type melanomas (~10%), which lack alterations in these three major groups (Cancer Genome Atlas Network, 2015). Although UV radiation is the principal mutagenic driver in melanoma, $BRAF^{V600E}$ does not correspond to a classical UV-signature mutation. Whereas direct UV damage most commonly causes C→T transitions, $BRAF^{V600E}$ results from a T→A transversion. Such transversions may arise indirectly through UV-associated recruitment of error-prone DNA polymerases (Thomas *et al*, 2006) or through atypical UV-induced photoproducts that preferentially facilitate this type of substitution (Laughery *et al*, 2020).

From a clinical perspective, the World Health Organization (WHO) categorizes melanoma into nine distinct subtypes defined by their evolutionary pathways. More broadly, however, cutaneous melanomas can be divided according to cumulative sun exposure into chronically sun-damaged (CSD) and non-CSD melanomas (Elder *et al*, 2020). CSD melanomas arise in skin exposed to long-term UV radiation, typically on the head, neck, and dorsal extremities. They usually occur in older individuals (>55 years) and display a high mutational burden associated with NF1, NRAS, and non-V600E BRAF mutations. In contrast, non-CSD melanomas affect sites with low to intermediate sun exposure, such as the trunk and proximal extremities. These generally arise in younger individuals (<55 years), exhibit a lower mutational burden, and are more strongly associated with $BRAF^{V600E}$ mutations (Figure 75) (Curtin *et al*, 2005; Bastian, 2014; Shain & Bastian, 2016). This classification further highlights

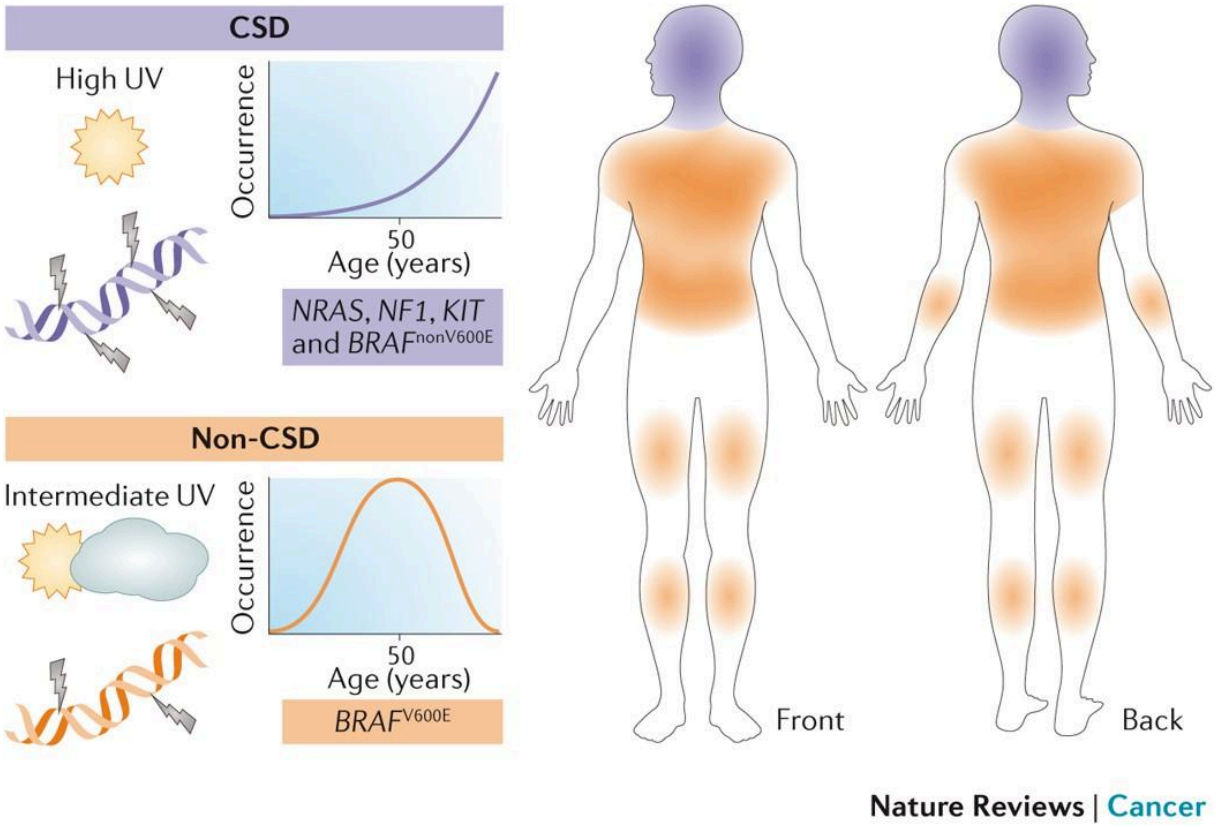

Figure 75. Clinical and molecular distinction between CSD and non-CSD melanomas. Cutaneous melanomas can be classified based on cumulative sun exposure into chronically sun-damaged (CSD) and non-CSD subtypes. CSD melanomas arise in highly UV-exposed areas, occur in older individuals, and display a high mutational burden with frequent NF1, NRAS, KIT, and non-V600E BRAF alterations. In contrast, non-CSD melanomas develop in intermittently exposed sites, arise in younger patients, and are predominantly driven by $BRAF^{V600E}$. Reproduced from *Shain and Bastian, Nat Rev Cancer (2016)*.

the heterogeneity of melanoma and underscores the impact of environmental exposure on its molecular landscape.

Melanoma can also be described according to its histopathological progression, classically evolving from melanocytic naevus to dysplastic naevus, melanoma *in situ*, invasive melanoma, and ultimately metastatic melanoma (Shain *et al*, 2015; Shain & Bastian, 2016; Long *et al*, 2023). Whereas normal melanocytes divide fewer than twice a year, genomic alterations such as $BRAF^{V600E}$ can trigger increased proliferation and formation of a pre-neoplastic melanocytic naevus (Centeno *et al*, 2023). Most melanocytic naevus do not change in size for many years and enter a "senescence-like" state of irreversible cell cycle arrest (Michaloglou *et al*, 2005), likely reinforced in part by immune surveillance (Kuilman *et al*, 2008). Additional driver alterations, including in genes such as TERT and CDKN2A, can promote progression toward dysplastic naevi, which exhibit greater mutational complexity and occasional mitotic activity (Glatz *et al*, 2010; Shain *et al*, 2015). Although individuals with dysplastic naevi have an increased lifetime risk of melanoma (Shors *et al*, 2006), the absolute risk associated with any single lesion remains relatively low (Tucker *et al*, 2002).

Further mutational accumulation, much of it driven by UV radiation, can cooperate with MAPK pathway activation to promote the emergence of melanoma *in situ*, a malignant lesion characterized by an irregular proliferation of melanocytes confined to the epidermis (Shain *et al*, 2015; Shain & Bastian, 2016; Karponis *et al*, 2025). Melanoma *in situ* may remain localized for years before progressing to invasive melanoma, a transition that appears to require both additional genetic alterations and escape from immune surveillance (Long *et al*, 2023).

The transition to invasive melanoma is marked by penetration of malignant cells into the dermis, which is strongly associated with increased metastatic risk. Bi-allelic inactivation of CDKN2A is considered a key genetic event at this stage (Ackermann *et al*, 2005; Shain *et al*, 2015). In addition, invasive melanomas frequently harbor alterations in subunits of the SWI/SNF chromatin remodeling complex, most notably ARID2 (mutated in 20% of melanoma cases), supporting the idea that chromatin regulators contribute to melanoma progression. Recent studies further support a tumor suppressor role for ARID2 in melanoma, showing that its loss promotes activation of melanoma-specific transcriptional programs and enhances metastatic colonization *in vivo* (Figure 76) (Carcamo *et al*, 2022; Grossi *et al*, 2025). As the tumor deepens, the direct influence of UV radiation diminishes, and the mutational profile shifts from point mutations toward copy number alterations (Bauer & Bastian, 2006; Shain & Bastian, 2016).

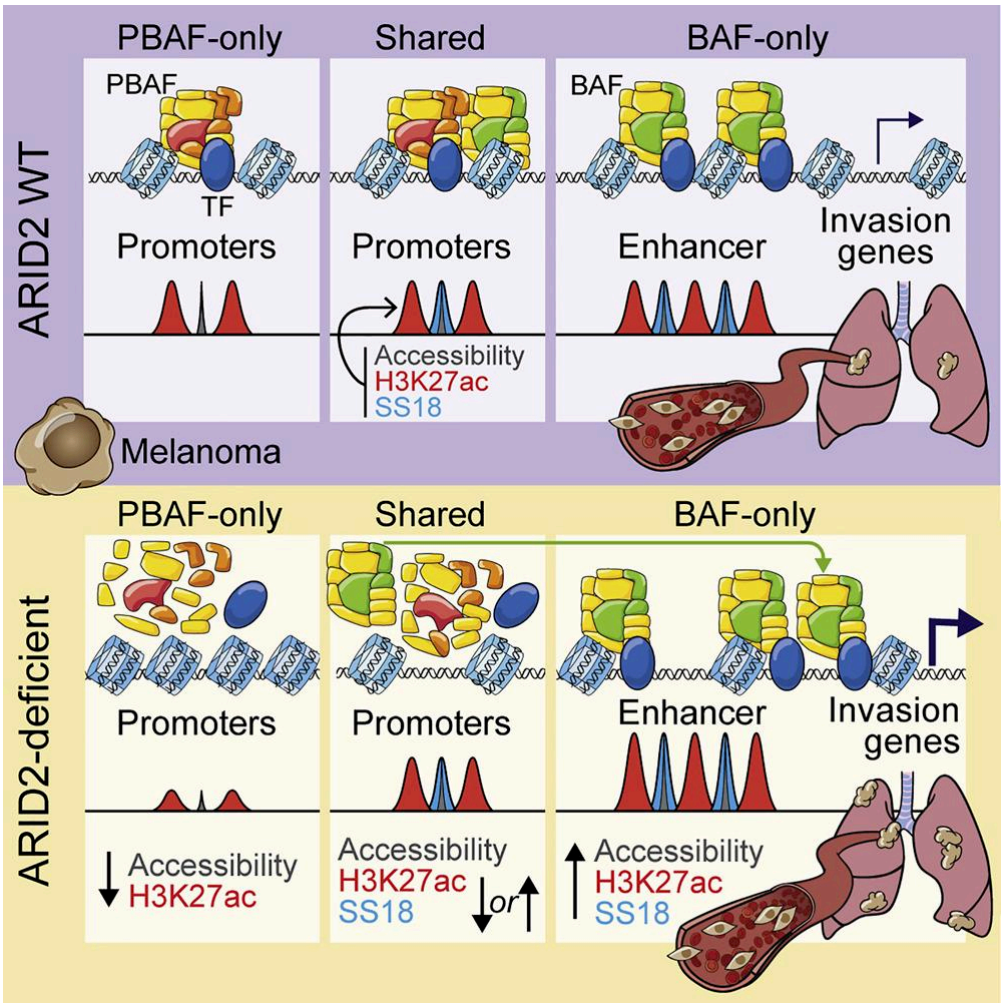

Figure 76. ARID2 loss promotes enhancer activation and metastatic transcriptional programs in melanoma. In ARID2-proficient cells, the PBAF SWI/SNF complex regulates chromatin accessibility at promoters and enhancers, maintaining controlled transcriptional programs. In contrast, ARID2 deficiency alters SWI/SNF composition and redistributes chromatin accessibility, leading to increased H3K27ac deposition and enhancer activation that promotes the expression of invasion-associated gene networks and enhances metastatic potential, highlighting the contribution of chromatin remodeling to melanoma progression. Reproduced from *Carcamo et al., Cell Reports (2022)*.

Later stages of progression also frequently involve loss of PTEN and TP53 (Dankort *et al*, 2009; Viros *et al*, 2014)

Finally, melanoma is considered metastatic once tumor cells disseminate beyond the primary site and colonize distant organs, most commonly the lymph nodes, lungs, liver, and brain, resulting in a marked worsening of prognosis (Sundararajan *et al*, 2026). Metastatic melanoma also displays the highest proliferative index among the major stages of disease progression (Figure 77) (Straume *et al*, 2000). Although genomic analyses have not identified recurrent driver mutations that uniquely distinguish metastatic lesions from earlier disease stages (Turajlic *et al*, 2012; Ding *et al*, 2014), experimental studies suggest that activation of WNT/β-catenin signaling can promote metastasis in melanoma models (Damsky *et al*, 2011; Sanborn *et al*, 2015), and more recent evidence implicates NF-κB pathway activation in the development of melanoma brain metastases (Rodriguez-Baena *et al*, 2025).

It is important to note, however, that this linear model represents an oversimplification of melanoma evolution, as in many cases, melanomas arise *de novo* without a detectable precursor lesion, and approximately 4% of patients present with metastatic disease without an identifiable primary tumor (Shain & Bastian, 2016), indicating that melanoma progression cannot be fully explained by the stepwise accumulation of genetic alterations alone.

Altogether, these observations highlight the complexity and heterogeneity of melanoma, which cannot be fully captured by genetic or histopathological classifications alone. Nevertheless, extensive characterization of melanoma biology has led to major therapeutic advances over the past decade, markedly improving patient management, particularly in advanced disease. The following sections will therefore present the currently approved therapeutic strategies for metastatic melanoma, followed by an analysis of therapeutic resistance and its underlying mechanisms.

b. Currently approved treatments for cutaneous melanoma

The majority of melanoma patients are diagnosed at an early stage of the disease, when the tumor is still localized in the epidermis and has not yet spread to distant organs. In this context, local excision of the tumor by surgery represents the first line of treatment, and the 5-year survival rate is close to 100% (Melanoma of the Skin - Cancer Stat Facts). Nonetheless, for some patients with high-risk resectable melanoma, adjuvant therapy can be administered after surgery to prevent postsurgical recurrence (Long *et al*, 2023).

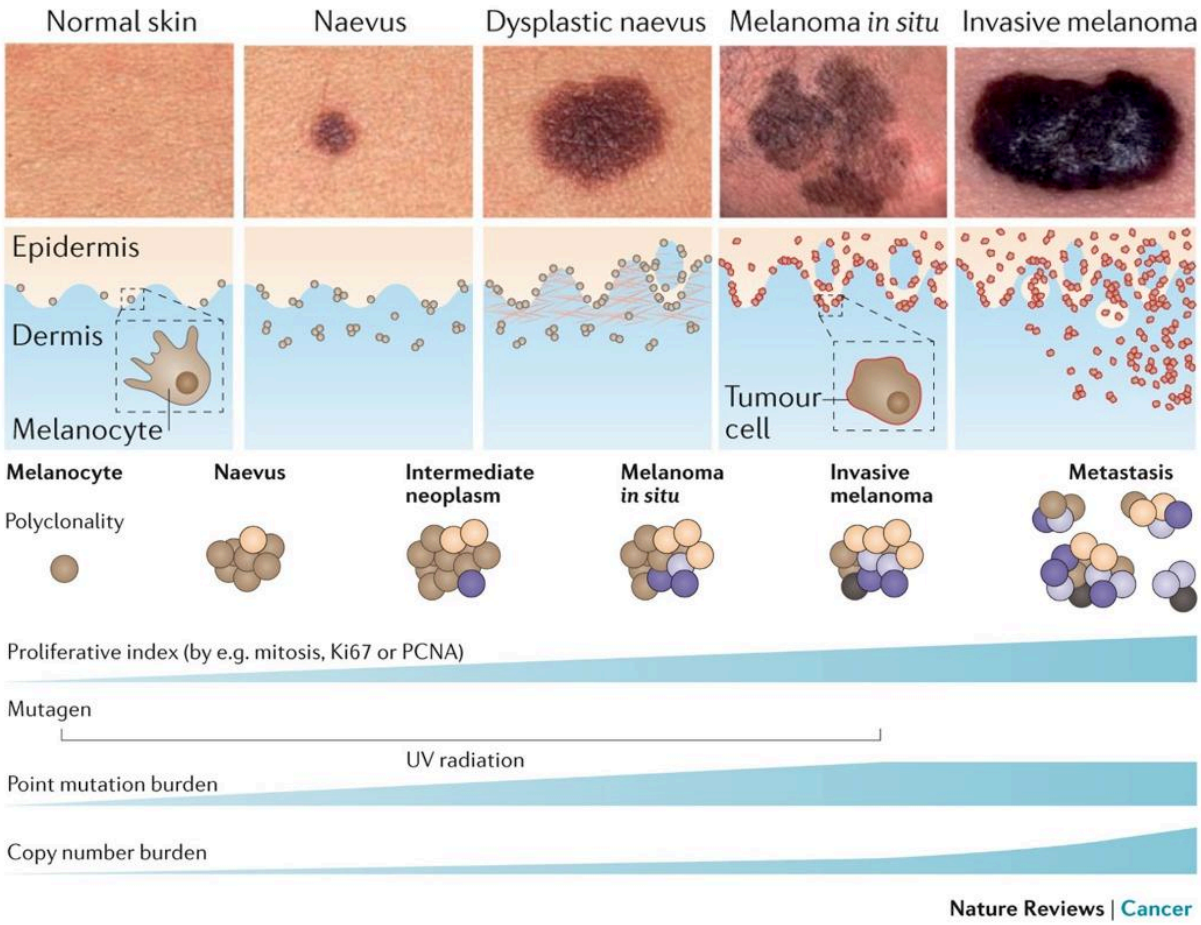

Figure 77. Histopathological progression of melanoma. Activating mutations, commonly $BRAF^{V600E}$, drive the formation of benign melanocytic naevi, which typically undergo oncogene-induced senescence. Additional genetic alterations promote progression to dysplastic naevi and melanoma in situ, characterized by malignant melanocyte proliferation confined to the epidermis. Subsequent acquisition of invasive properties enables dermal penetration and dissemination, culminating in metastatic disease. This progression is accompanied by increasing proliferative capacity, mutational burden, and genomic instability. Adapted from *Shain and Bastian, Nat Rev Cancer (2016)*.

In contrast, patients with advanced melanoma, in which the tumor has metastasized to lymph nodes and distant organs, require systemic therapeutic interventions. Historically, these patients had very limited treatment options, with chemotherapeutic agents such as dacarbazine and interleukin-2 therapy showing limited efficacy, and median survival not exceeding a few months (Falkson *et al*, 1998; Keilholz *et al*, 1998). The introduction of targeted therapies and immunotherapies, notably MAPK inhibitors (MAPKi) and immune checkpoint inhibitors (ICI), approved in 2011, has revolutionized the treatment of metastatic melanoma and dramatically improved outcomes, with durable disease control and long-term survival now occurring in approximately 50% of cases (Boutros *et al*, 2024).

The MAPK pathway is conventionally activated upon binding of extracellular ligands to receptor tyrosine kinases, leading to activation of the downstream GTPase RAS. Activated RAS promotes the recruitment and activation of RAF, a serine/threonine kinase that phosphorylates MEK, which in turn activates ERK1/2. Phosphorylated ERK1/2 translocates to the nucleus, where it regulates the activity of multiple transcription factors, including c-Fos, c-Jun, and c-Myc (Guo *et al*, 2020). Activating mutations in NRAS and BRAF, observed in approximately 28% and 52% of melanoma patients, respectively, as well as inactivating mutations in NF1, a negative regulator of RAS (~14% of cases), result in constitutive activation of the MAPK pathway and uncontrolled melanoma cell proliferation (Cancer Genome Atlas Network, 2015).

Based on these alterations, selective inhibitors of the MAPK pathway are widely used in the treatment of advanced melanoma and show high initial response rates. These include selective $BRAF^{V600E}$ inhibitors (BRAFi), such as vemurafenib and dabrafenib, as well as MEK inhibitors (MEKi) including trametinib and cobimetinib (Figure 78) (Caksa *et al*, 2022). Early clinical trials demonstrated that BRAFi significantly improved progression-free survival compared with dacarbazine (Chapman *et al*, 2011; Hauschild *et al*, 2012). However, responses were often not durable. To overcome this limitation, BRAFi were combined with MEKi, which act downstream of BRAF, resulting in improved progression-free survival and delayed resistance compared with BRAFi monotherapy (Long *et al*, 2014; Larkin *et al*, 2014). As a result, combined BRAF and MEK inhibition (e.g., dabrafenib plus trametinib or vemurafenib plus cobimetinib) has become the standard of care for patients with BRAF-mutant melanoma, achieving long-term survival rates of approximately 35% at 5 years (Long *et al*, 2017; Ascierto *et al*, 2021).

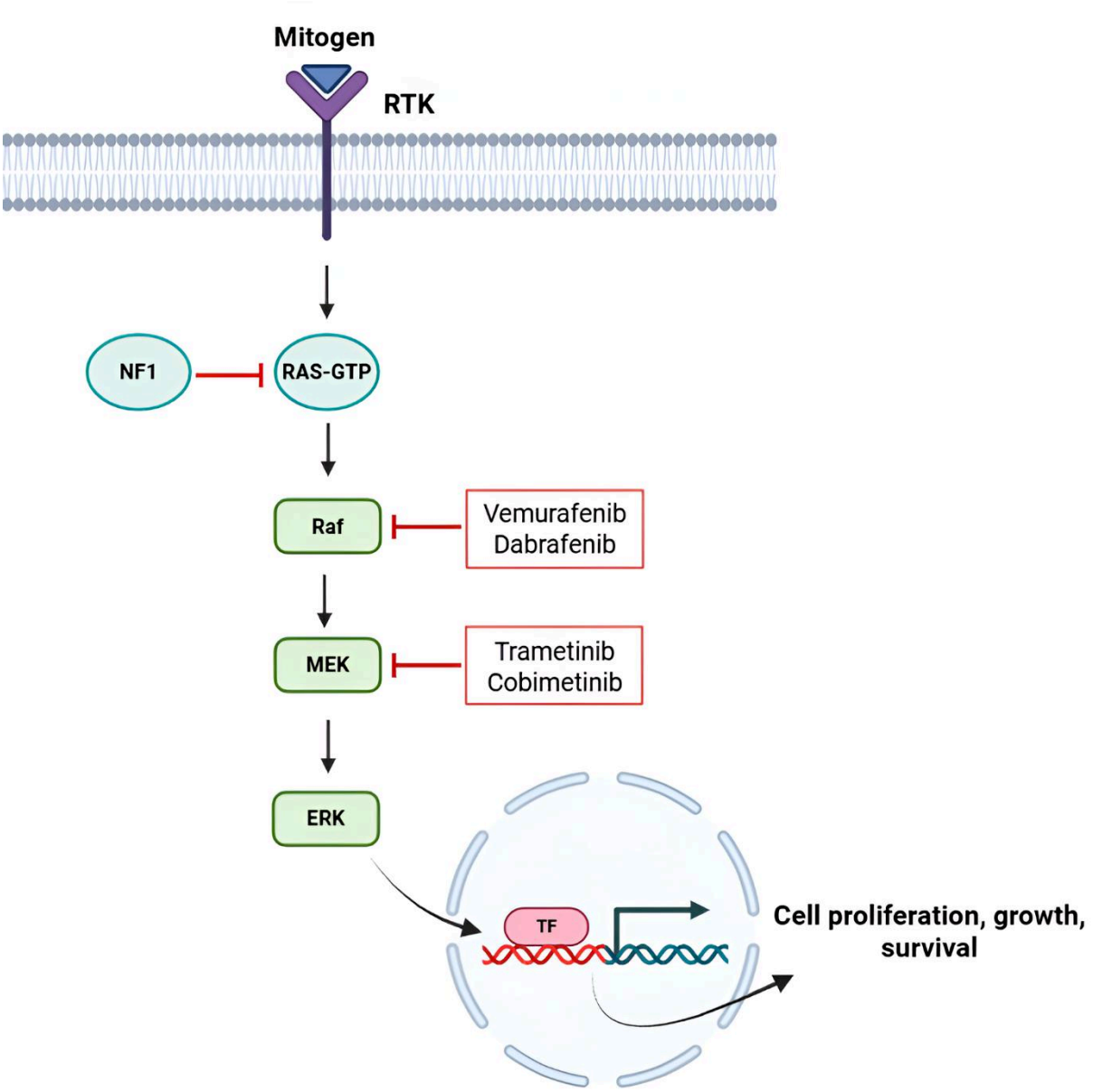

Figure 78. MAPK pathway activation and targeted inhibition in melanoma. Ligand binding to receptor tyrosine kinases (RTKs) activates RAS, which promotes RAF kinase activation, leading to sequential phosphorylation of MEK and ERK. Activated ERK translocates to the nucleus and regulates transcription factors that drive cell proliferation, growth, and survival. In melanoma, activating mutations in BRAF and NRAS, or loss of NF1, result in constitutive pathway activation. Targeted therapies inhibit this signaling axis at multiple levels, including $BRAF^{V600E}$ inhibitors (vemurafenib, dabrafenib) and MEK inhibitors (trametinib, cobimetinib), which suppress downstream transcriptional programs and tumor growth. Created with *BioRender.com*.

In parallel, the development of immune checkpoint inhibitors has profoundly transformed melanoma treatment and contributed to a marked reduction in mortality, with an approximately 18% decrease in overall mortality observed between 2013 and 2016 (Berk-Krauss *et al*, 2020). The strong response of melanoma to immunotherapy is thought to be linked to its high mutational burden (Alexandrov *et al*, 2013), which is believed to increase the generation of tumor neoantigens and enhance immune recognition (Verdegaal *et al*, 2016). Consistent with this, several studies have shown that melanoma patients with higher mutational loads tend to respond better to immunotherapy, with the caveat that mutational load is not always a definitive indicator of therapy response (Samstein *et al*, 2019; Mao *et al*, 2026).

Immune checkpoint inhibitors function by blocking inhibitory signaling pathways that tumors exploit to suppress T-cell activity, thereby restoring anti-tumor immune responses (Sharma *et al*, 2023). Ipilimumab, a monoclonal antibody targeting cytotoxic T-lymphocyte antigen 4 (CTLA-4), was the first agent approved for metastatic melanoma. Although it provided a survival benefit, its efficacy was limited, with median progression-free survival of approximately 3 months and overall survival of around 10 months (Hodi *et al*, 2010). Shortly after, the introduction of the Programmed cell Death-1 (PD-1) inhibitors pembrolizumab and nivolumab significantly improved median overall survival and progression-free survival by two- to threefold compared to ipilimumab, leading to their FDA approval for the treatment of metastatic melanoma (Figure 79) (Robert *et al*, 2015a, 2015b).

Importantly, combination strategies have further enhanced therapeutic efficacy. The CheckMate trial, which randomized 945 patients and followed them for 5 years, demonstrated that combined nivolumab and ipilimumab therapy resulted in an overall response rate of approximately 60%, compared with 45% for nivolumab monotherapy and 20% for ipilimumab alone (Larkin *et al*, 2019). A more recent 10-year follow-up of the same trial reported a median overall survival of approximately 72 months for combination therapy, compared with approximately 37 months for nivolumab alone and 20 months for ipilimumab, with 37% of patients remaining alive at the end of the study (Wolchok *et al*, 2025). These results have established the combination of ipilimumab and nivolumab as a standard treatment option for metastatic melanoma, irrespective of BRAF mutational status (Long *et al*, 2023).

Despite the variety of treatment options currently available for metastatic melanoma, therapy selection remains challenging. MAPK inhibitors typically induce rapid tumor regression, which is beneficial for patients requiring immediate symptom control. However, rapid resistance frequently develops, occurring in approximately 50% of patients within one year and up to 80%

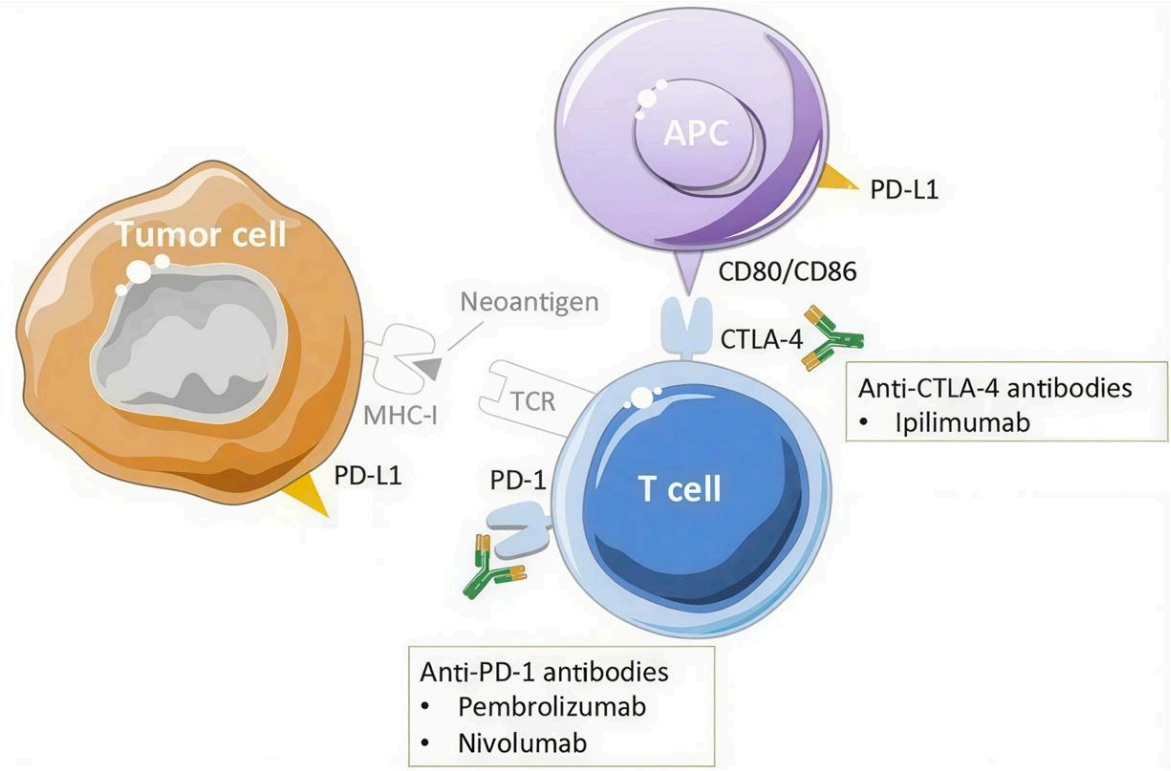

Figure 79. Immune checkpoint inhibition in melanoma. Tumor-derived neoantigens are presented on major histocompatibility complex class I (MHC-I) molecules and recognized by T-cell receptors (TCRs), initiating anti-tumor immune responses. Tumors evade immune surveillance by engaging inhibitory pathways, notably through PD-L1 expression, which binds PD-1 on T cells and suppresses their activity. In parallel, CTLA-4 competes with CD80/CD86 on antigen-presenting cells (APCs) to limit T-cell activation. Immune checkpoint inhibitors block these inhibitory signals, restoring T-cell function, including anti-CTLA-4 antibodies (ipilimumab) and anti-PD-1 antibodies (pembrolizumab, nivolumab), thereby enhancing anti-tumor immunity. Adapted from *Rouanne et al., World Journal of Urology (2018)*.

within five years (Robert *et al*, 2019; Kozar *et al*, 2019). Moreover, patients without BRAF mutations, such as those with NRAS-driven melanoma, are intrinsically resistant to BRAFi and MEKi (Van Allen *et al*, 2014). On the other hand, immune checkpoint inhibitors can be used regardless of BRAF status and often induce more durable responses, but they have slower onset of action and can cause significant immune-related adverse events, affecting up to 98% of patients (Wolchok *et al*, 2025). Consequently, ongoing efforts aim to optimize treatment strategies, including determining the best sequencing of targeted therapy and immunotherapy. For instance, a recent phase III DREAMseq trial demonstrated that initiating treatment with combined ipilimumab and nivolumab followed by dabrafenib and trametinib resulted in a ~20% improvement in overall survival compared with the reverse sequence (Atkins *et al*, 2023).

Recent advances in immunotherapy have also renewed interest in therapeutic vaccination strategies for melanoma, particularly personalized neoantigen-based approaches. Unlike earlier vaccines targeting shared antigens, these platforms exploit tumor-specific mutations to induce highly specific T-cell responses, with early studies demonstrating their feasibility, safety, and ability to generate durable antitumor immunity (Figure 80) (Sahin *et al*, 2020; Kjeldsen *et al*, 2021). More recently, mRNA-based vaccines such as mRNA-4157 (V940), combined with pembrolizumab, have shown promising clinical benefit in high-risk melanoma, significantly improving recurrence-free survival in the KEYNOTE-942 trial (Weber *et al*, 2024). Although these approaches are not yet part of standard care for metastatic disease, they represent a rapidly evolving strategy that may enhance the durability of responses to checkpoint blockade.

Despite these major therapeutic advances, a substantial proportion of patients still fail to achieve durable responses, with resistance occurring in at least half of patients treated with immunotherapy and even more frequently in those receiving targeted therapies (Gide *et al*, 2018; Kozar *et al*, 2019). Understanding the molecular and cellular basis of this resistance therefore remains a critical challenge, and the following sections will examine current knowledge of the mechanisms involved in therapeutic resistance.

c. Therapeutic resistance to targeted therapy and immune checkpoint inhibitors

The development of targeted therapies and immunotherapies has transformed melanoma from a largely incurable disease into a cancer that can be effectively controlled over the long term, significantly improving survival outcomes for patients with advanced disease (Long *et al*, 2023). Nonetheless, these advances remain limited by the frequent emergence of therapeutic

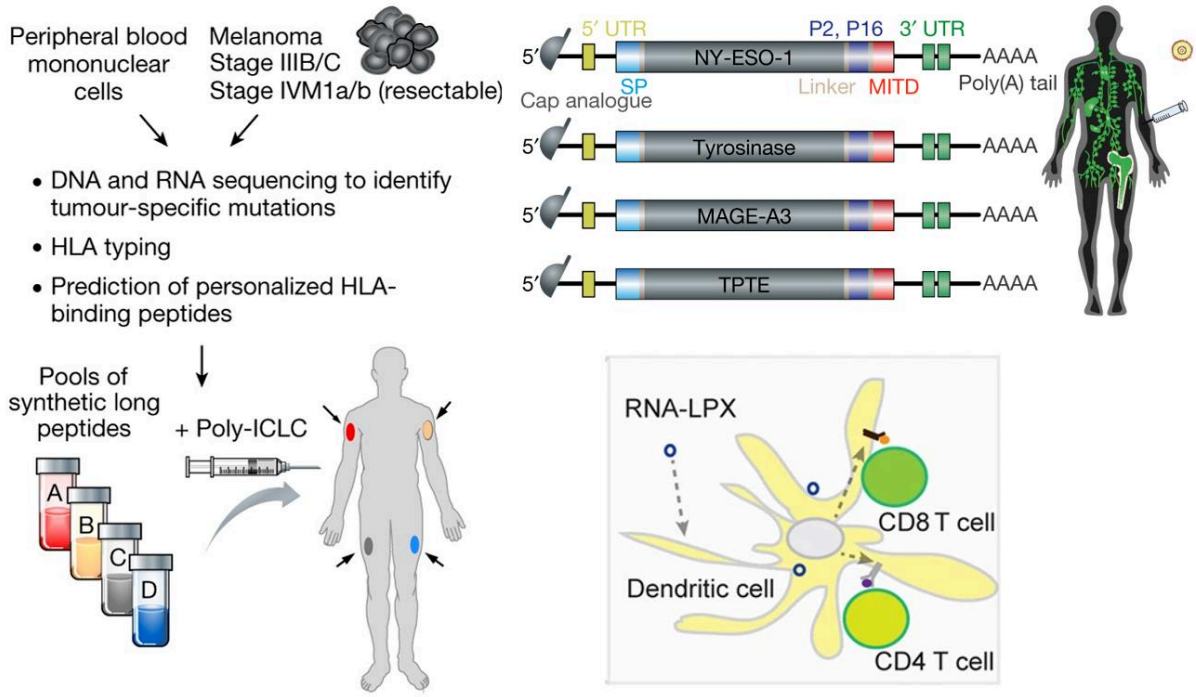

Figure 80. Personalized neoantigen-based vaccination and mRNA-induced anti-tumor immunity in melanoma. Tumor and matched normal samples are sequenced to identify patient-specific mutations, enabling prediction of neoantigens presented on HLA molecules. These antigens are incorporated into vaccine platforms, including synthetic peptides or mRNA constructs, and administered with adjuvants. Following delivery, vaccines are taken up by dendritic cells, leading to antigen processing and presentation, and activation of $CD4^+$ and $CD8^+$ T cells. This induces tumor-specific immune responses capable of recognizing and eliminating melanoma cells. Adapted from *Ott et al., Nature (2017); Sahin et al., Nature (2020); Li et al., Signal Transduct Target Ther (2020)*.

resistance. Over the past years, extensive efforts have been dedicated to understanding the underlying mechanisms of resistance, leading to the identification of multiple processes involved in resistance to both MAPK-targeted therapies and immune checkpoint inhibitors (Gide *et al*, 2018; Kozar *et al*, 2019). In melanoma, drug resistance can arise either through a "Darwinian-type" selection of pre-existing resistant clones (Shaffer *et al*, 2017), or through a "Lamarckian-type" process, in which tumor cells acquire genetic and non-genetic adaptations in response to therapeutic pressure (Su *et al*, 2017).

In the majority of cases, resistance to MAPK inhibitors is driven by reactivation of the MAPK pathway or activation of compensatory signaling pathways (Kozar *et al*, 2019). Indeed, MAPK pathway reactivation is observed in approximately 80% of tumors resistant to BRAF inhibitors (Moriceau *et al*, 2015), highlighting the strong dependency of melanoma cells on this signaling axis. Several mechanisms contribute to this reactivation. For instance, the expression of alternative RAF isoforms, such as CRAF, can sustain MEK activation despite BRAF inhibition (Villanueva *et al*, 2010; Doudican & Orlow, 2017). Similarly, overexpression of the kinase COT (MAP3K8), frequently detected in biopsies from relapsing patients, enables RAF-independent activation of MEK/ERK signaling (Johannessen *et al*, 2010; Guo *et al*, 2021). In addition, amplification of the BRAF allele or the expression of BRAF splice variants, observed in a substantial subset of resistant tumors, promotes RAF dimerization and sustained downstream signaling despite inhibitor treatment (Vido *et al*, 2018).

In parallel, melanoma cells can bypass MAPK inhibition by activating alternative signaling pathways that support proliferation and survival. Among these, activation of the PI3K/AKT/mTOR pathway represents one of the most frequent mechanisms. This can occur through loss of function of PTEN, a negative regulator of PI3K signaling, which is observed in a subset of melanoma patients and contributes to resistance to BRAF inhibitors (Figure 81) (Xing *et al*, 2012; Shi *et al*, 2014a, 2014b; Irvine *et al*, 2018).

In addition to tumor-intrinsic alterations, the tumor microenvironment also plays an important role in mediating resistance. Stromal cells can secrete growth factors such as hepatocyte growth factor (HGF), leading to activation of both MAPK and PI3K signaling pathways and thereby promoting intrinsic resistance to MAPK inhibitors. Importantly, inhibition of HGF signaling was shown to restore drug sensitivity in preclinical models (Straussman *et al*, 2012).

Beyond these established mechanisms, more recent studies have identified additional pathways contributing to resistance. Notably, loss of the autophagy regulator AMBRA1 has been

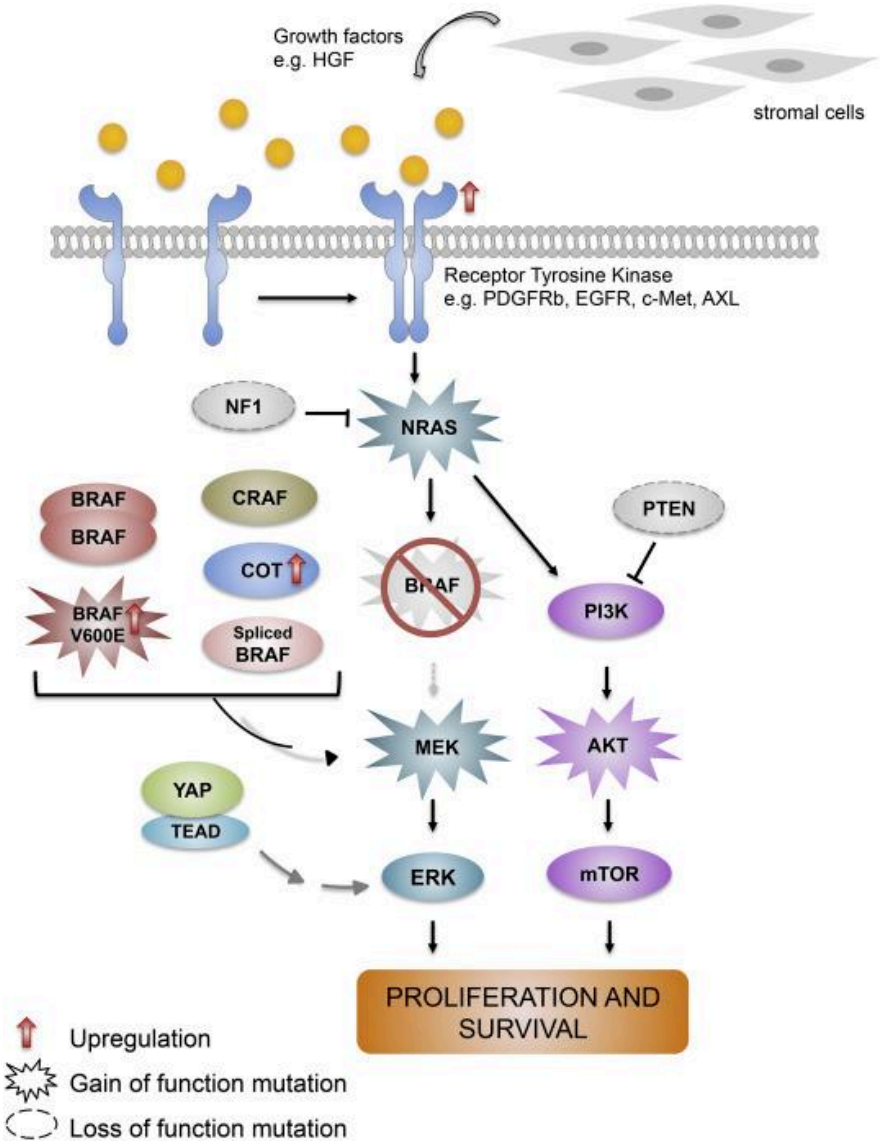

Figure 81. Major mechanisms of resistance to MAPK pathway inhibition in melanoma. Multiple mechanisms contribute to resistance to MAPK inhibitors in melanoma through reactivation of ERK signaling or activation of compensatory pathways. Reactivation of the MAPK cascade can occur via upregulation of receptor tyrosine kinases, activating mutations in NRAS, expression of alternative RAF isoforms such as CRAF, overexpression of COT (MAP3K8), or amplification and alternative splicing of BRAF, all of which sustain MEK/ERK signaling despite BRAF inhibition. In parallel, activation of the PI3K/AKT/mTOR pathway, frequently driven by loss of PTEN, provides an alternative route to maintain cell proliferation and survival. Reproduced from *Kozar et al., Biochim Biophys Acta Rev Cancer (2019).*

associated with poor response to MAPK inhibitors in melanoma patients, through activation of focal adhesion kinase 1 (FAK1) signaling (Di Leo *et al*, 2024). Consistent with this, transcriptomic analyses have revealed frequent upregulation of focal adhesion pathways in resistant tumors. As a result, pharmacological inhibition of FAK was able to overcome resistance not only in MAPK inhibitor-resistant melanoma models, but also in immunotherapy-resistant syngeneic mouse models, suggesting a broader role for this pathway in therapeutic resistance (Lubrano *et al*, 2025).

Similarly to targeted therapies, a substantial proportion of melanoma patients fail to respond to immune checkpoint inhibitors due to either primary or acquired resistance. While these mechanisms remained less understood for a long time, advances in high-throughput and single-cell transcriptomic approaches have enabled the identification of key resistance pathways. Overall, resistance to immune checkpoint blockade can arise through defects in antigen presentation, immune exclusion, T-cell dysfunction, and transcriptional reprogramming toward dedifferentiated states (Gide *et al*, 2018). The latter will be discussed in detail in the next section in the context of phenotype switching.

Initial transcriptomic studies of melanoma patients treated with PD-1 blockade revealed that tumors responding to therapy are characterized by a high mutational burden and enrichment in specific genetic alterations such as BRCA2 mutations. In contrast, non-responding tumors display a distinct transcriptional profile termed the innate anti-PD-1 resistance (IPRES) signature, characterized by increased expression of genes associated with cell adhesion, angiogenesis, wound healing, and epithelial-to-mesenchymal transition (Figure 82A) (Hugo *et al*, 2016). Nonetheless, subsequent large-scale multiomic analyses failed to identify a unifying genetic mechanism underlying resistance to PD-1 and CTLA-4 inhibitors, highlighting the heterogeneity of resistance pathways across patients (Newell *et al*, 2022).

Among acquired resistance mechanisms, defects in antigen presentation and interferon signaling represent some of the most well-characterized processes. Loss-of-function mutations in components of the major histocompatibility complex class I (MHC-I) machinery, such as β2-microglobulin (B2M), impair antigen presentation to CD8+ T cells and prevent immune recognition (Zaretsky *et al*, 2016). In addition, mutations affecting SEC24C and SEC24D have recently been identified in melanoma patients with acquired resistance, leading to impaired STING-dependent innate immune signaling and reduced antigen presentation (Figure 82B) (Schiantarelli *et al*, 2025).

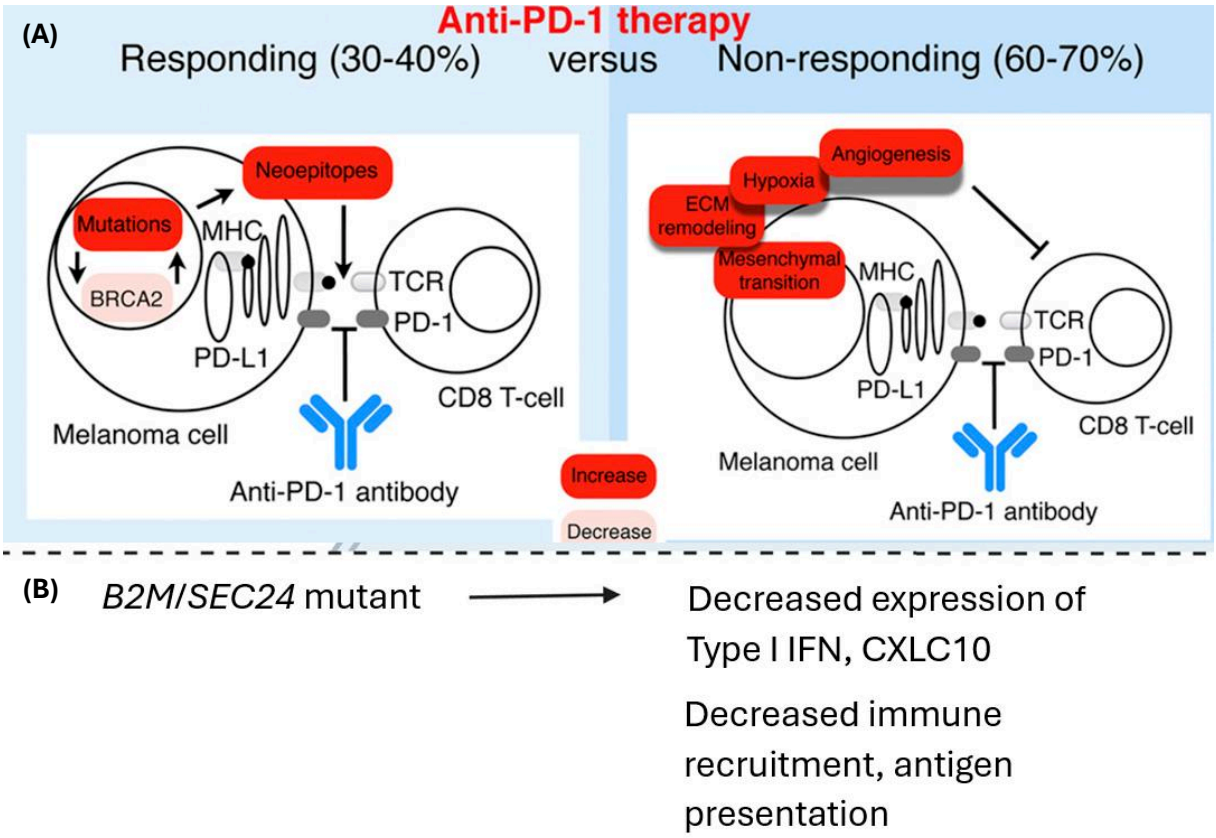

Figure 82. Selected mechanisms of resistance to immune checkpoint blockade in melanoma. (A) Responding tumors are characterized by a high mutational burden and increased neoantigen presentation, promoting effective $CD8^+$ T-cell activation. In contrast, non-responding tumors display the innate anti-PD-1 resistance (IPRES) transcriptional signature, marked by enrichment of pathways related to angiogenesis, hypoxia, extracellular matrix remodeling, and mesenchymal transition, which contribute to immune exclusion and impaired T-cell function. **(B)** Acquired resistance can arise through defects in antigen presentation and interferon signaling. Loss-of-function mutations in components of the MHC class I machinery, such as B2M, impair antigen presentation, while alterations affecting SEC24-dependent trafficking pathways disrupt STING-mediated type I interferon signaling, reducing immune cell recruitment and anti-tumor immunity. Adapted from *Hugo et al., Cell (2016); Zaretsky et al., NEJM (2016); Schiantarelli et al., Cancer Cell (2025).*

Beyond genetic alterations, epigenetic repression also contributes to immune evasion, as the Polycomb repressive complex 2 (PRC2) can silence genes involved in MHC-I antigen processing and presentation through deposition of the H3K27me3 repressive mark, thereby limiting tumor immunogenicity (Burr *et al*, 2019).

In addition to impairing immune recognition, melanoma cells can actively prevent immune infiltration by establishing an immune-excluded tumor microenvironment. Activation of β-catenin and TGFβ signaling pathways suppresses the recruitment of CD103+ dendritic cells (cDC1s), thereby limiting T-cell priming and infiltration into the tumor (Figure 83). Restoring dendritic cell recruitment or inhibiting TGFβ signaling has been shown to enhance T-cell infiltration and improve response to immunotherapy (Spranger *et al*, 2015; Mariathasan *et al*, 2018). In parallel, CDK4/6-dependent transcriptional programs have also been implicated in T-cell exclusion, with CDK4/6 inhibition restoring sensitivity to immune checkpoint blockade in resistant melanoma models (Figure 84) (Jerby-Arnon *et al*, 2018).

Furthermore, resistance to ICIs can arise from dysfunction within the immune compartment itself. Single-cell transcriptomic analyses of melanoma tumors have revealed distinct CD8+ T-cell states associated with either response or resistance to checkpoint blockade. In particular, the presence of TCF7-positive progenitor-like T cells correlates with favorable clinical outcomes, whereas terminally exhausted T cells lacking proliferative capacity are enriched in non-responders (Sade-Feldman *et al*, 2018). Consistent with this, long-term responders to immunotherapy harbor persistent memory T-cell populations in both the skin and blood circulation, further emphasizing the importance of sustained T-cell functionality (Han *et al*, 2021).

Beyond these mechanisms, transcriptional reprogramming toward dedifferentiated or mesenchymal-like states has emerged as a major contributor to immune escape. These states are associated with downregulation of melanocytic lineage antigens such as MART1 and PMEL, reducing tumor visibility to antigen-specific T cells (Lim *et al*, 2023;). A recent study has identified the transcription factor TCF4 as a key regulator of these programs, promoting a mesenchymal-like phenotype while repressing both melanocytic differentiation and antigen presentation pathways (Pozniak *et al*, 2024).

Recent work has further uncovered additional mechanisms of immune evasion, including the release of extracellular vesicles or melanosome-like structures containing MHC-I molecules that interact with CD8+ T cells and induce their dysfunction or apoptosis, thereby acting as

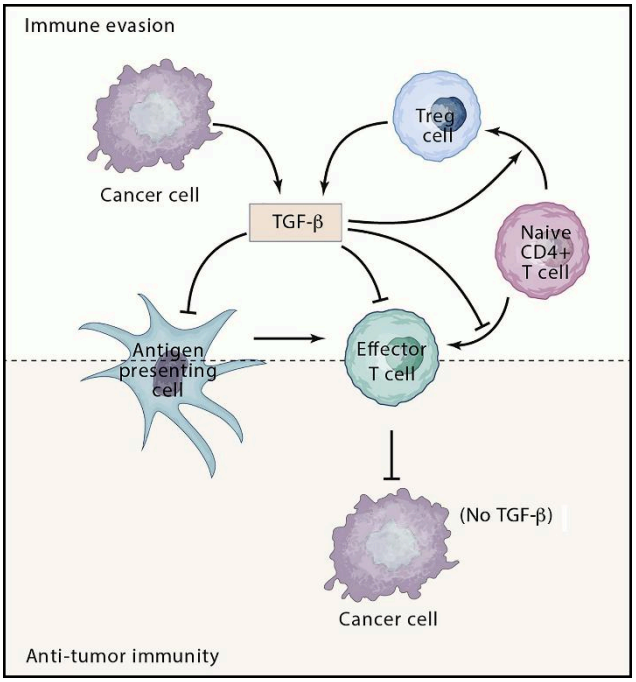

Figure 83. TGF-β-mediated immune evasion in melanoma. TGF-β signaling promotes immune evasion by suppressing anti-tumor immunity within the tumor microenvironment. Tumor cells and regulatory T cells (Tregs) produce TGF-β, which inhibits antigen-presenting cell function and limits the activation of effector T cells. Reproduced from *Batlle and Massagué, Immunity (2019)*.

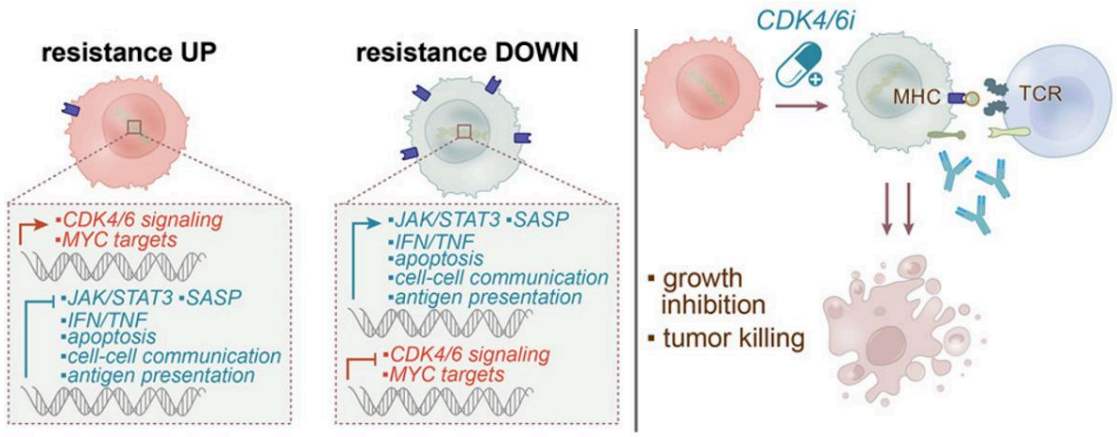

Figure 84. Tumor-intrinsic transcriptional programs contribute to resistance to immune checkpoint blockade in melanoma. Single-cell and bulk transcriptomic analyses identify a resistance-associated state characterized by increased CDK4/6 signaling and MYC-driven transcriptional programs, alongside reduced expression of genes involved in interferon signaling, antigen presentation, and cell-cell communication. Pharmacological inhibition of CDK4/6 restores antigen presentation and enhances T-cell–mediated tumor killing, highlighting the role of CDK4/6-dependent pathways in shaping tumor-immune interactions and therapeutic response. Adapted from *Jerby-Arnon et al., Cell (2018)*.

decoys that divert immune responses away from tumor cells. Blocking melanosome release reduces immune evasion, enhances $CD8^+$ T-cell infiltration, and limits tumor growth in vivo (Figure 85) (Chemla *et al*, 2026). These findings highlight the increasing complexity of tumor-immune interactions and suggest that immune evasion extends beyond classical cell-intrinsic or microenvironmental mechanisms.

It is worth noting that resistance mechanisms to targeted therapies and immunotherapies are not entirely independent, as resistance to MAPK inhibitors has been shown to confer cross-resistance to immune checkpoint blockade, despite their distinct modes of action. This phenomenon has been linked to MAPK pathway reactivation-driven alterations in the tumor microenvironment, notably a reduction in mature dendritic cells, which impairs immune priming and promotes immune evasion (Haas *et al*, 2021). These observations indicate that resistance to different therapeutic modalities can converge on shared tumor-intrinsic and microenvironmental adaptations.

Altogether, while the mechanisms described above highlight specific genetic and signaling alterations driving therapeutic resistance, increasing evidence suggests that non-genetic mechanisms play a central role in melanoma. In particular, melanoma cells can reversibly transition between distinct transcriptional and phenotypic states in response to environmental cues and therapeutic pressure. This process, referred to as phenotype switching, enables dynamic adaptation, promoting both metastatic potential and therapy resistance (Arozarena & Wellbrock, 2019; Karras *et al*, 2024). The next section will therefore explore the molecular mechanisms underlying phenotype plasticity and its role in melanoma progression and therapeutic resistance.

d. Phenotype switching as a transcription-driven mechanism of resistance and invasion

Melanoma is one of the most heterogeneous tumors, making it a particularly challenging disease to treat. Importantly, this intratumoral heterogeneity cannot be solely explained by genetic diversity. Instead, accumulating evidence indicates that melanoma cells adopt distinct, dynamic, and reversible transcriptional states that define their phenotypic behavior independently of specific mutations and are strongly influenced by the tumor microenvironment (Arozarena & Wellbrock, 2019). At the core of these transcriptional states lies the melanocytic lineage transcription factor MITF, which functions as a master regulator of melanocyte identity by controlling differentiation, proliferation, and survival programs. This lineage program is

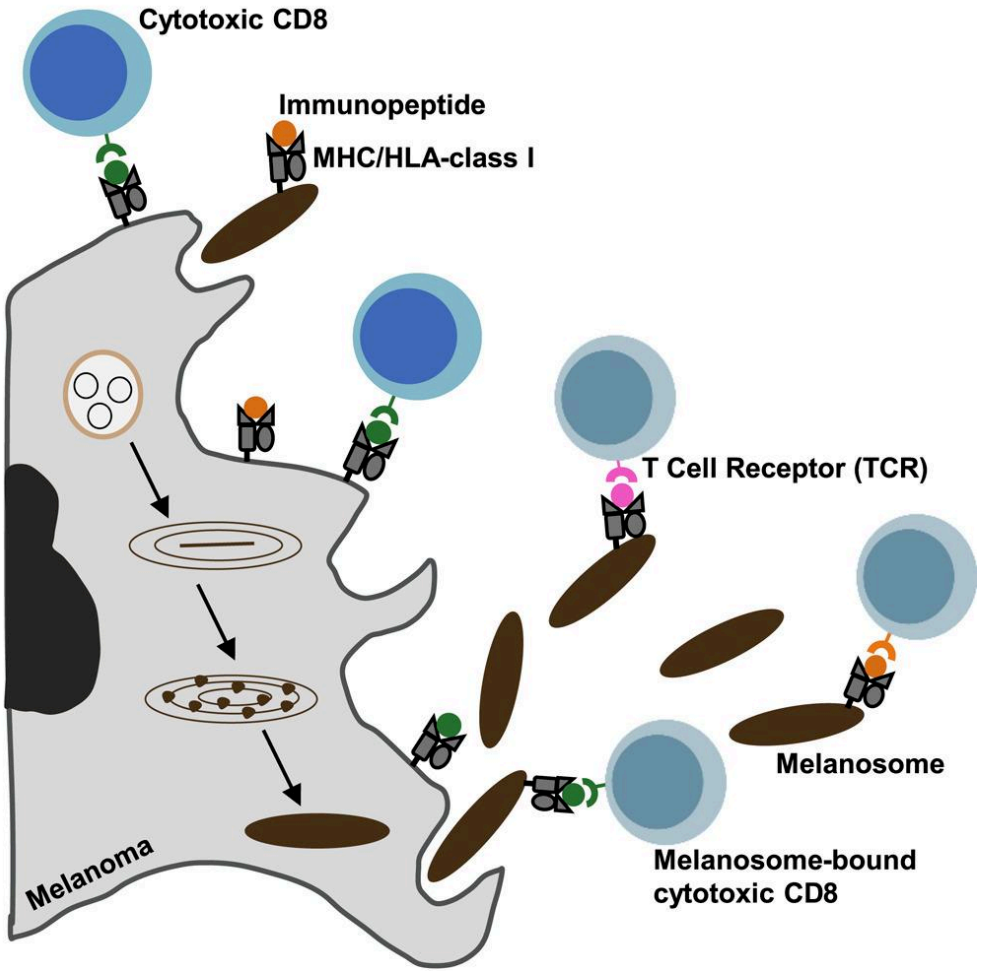

Figure 85. Melanosome-mediated immune evasion through decoy MHC-I presentation. Melanoma cells release melanosome-like extracellular vesicles containing MHC class I-bound immunopeptides that can interact with CD8+ T cells. These vesicles act as decoys by engaging T-cell receptors independently of tumor cells, leading to T-cell dysfunction or apoptosis and diverting cytotoxic activity away from malignant cells. Inhibition of melanosome release restores effective T-cell-mediated tumor recognition, enhances immune infiltration, and limits tumor growth. Reproduced from *Chemla et al., Cell (2026)*.

supported by additional neural-crest transcription factors such as SOX10 and PAX3, which together define the melanocytic state and its associated gene expression profile (Shain *et al*, 2015; Shain & Bastian, 2016; Centeno *et al*, 2023).

Early evidence supporting this concept dates back to gene expression profiling studies showing that melanoma cells can adopt distinct phenotypic behaviors associated with specific transcriptional programs. For instance, cells expressing high levels of motility-associated genes such as integrin β and WNT5A were found to display increased invasive capacities in vitro (Bittner *et al*, 2000). Building on this, Hoek and colleagues defined two major melanoma phenotypes: a "proliferative" state driven by MITF and SOX10, and an "invasive" state associated with TGFβ signaling and extracellular matrix remodeling factors (Hoek *et al*, 2006). These findings were later validated *in vivo*, where melanoma cells were shown to switch between MITF-positive proliferative states and MITF-negative invasive states within the same tumor (Hoek *et al*, 2008), establishing the foundation of the phenotype-switching model.

Building on this, high-throughput studies revealed that variations in MITF activity define transitions between differentiated and dedifferentiated melanoma cell states. In particular, an inverse relationship between MITF and the tyrosine kinase receptor AXL was observed in melanoma biopsies, with AXL-high cells displaying loss of differentiation markers such as MART-1 and gp100 and increased invasive potential (Sensi *et al*, 2011).

At the chromatin level, these phenotypic states are associated with distinct regulatory landscapes. Proliferative cells exhibit open chromatin-associated enhancer profiles similar to melanocytes, whereas invasive cells display enhancer activation patterns resembling mesenchymal or fibroblast-like states. Furthermore, the regulatory landscape of invasive melanoma genes was found to be driven in part by AP-1 and TEAD transcription factors, which are key regulators of invasive and stress-responsive transcriptional programs (Figure 86) (Verfaillie *et al*, 2015).

Moreover, the application of single-cell analyses has confirmed tumor heterogeneity in melanoma patient biopsies, demonstrating that major transcriptional states coexist within the same tumor. Specifically, $MITF^{high}$ populations, characterized by melanocytic markers such as MLANA, often coexist with AXL^{high} dedifferentiated populations, which express stem cell markers such as NGFR and are associated with therapy resistance (Tirosh *et al*, 2016). Building on this, Tsoi and colleagues expanded the classical binary view into a four-state hierarchical model identified in PDX models and patient biopsies. This model includes the two primary

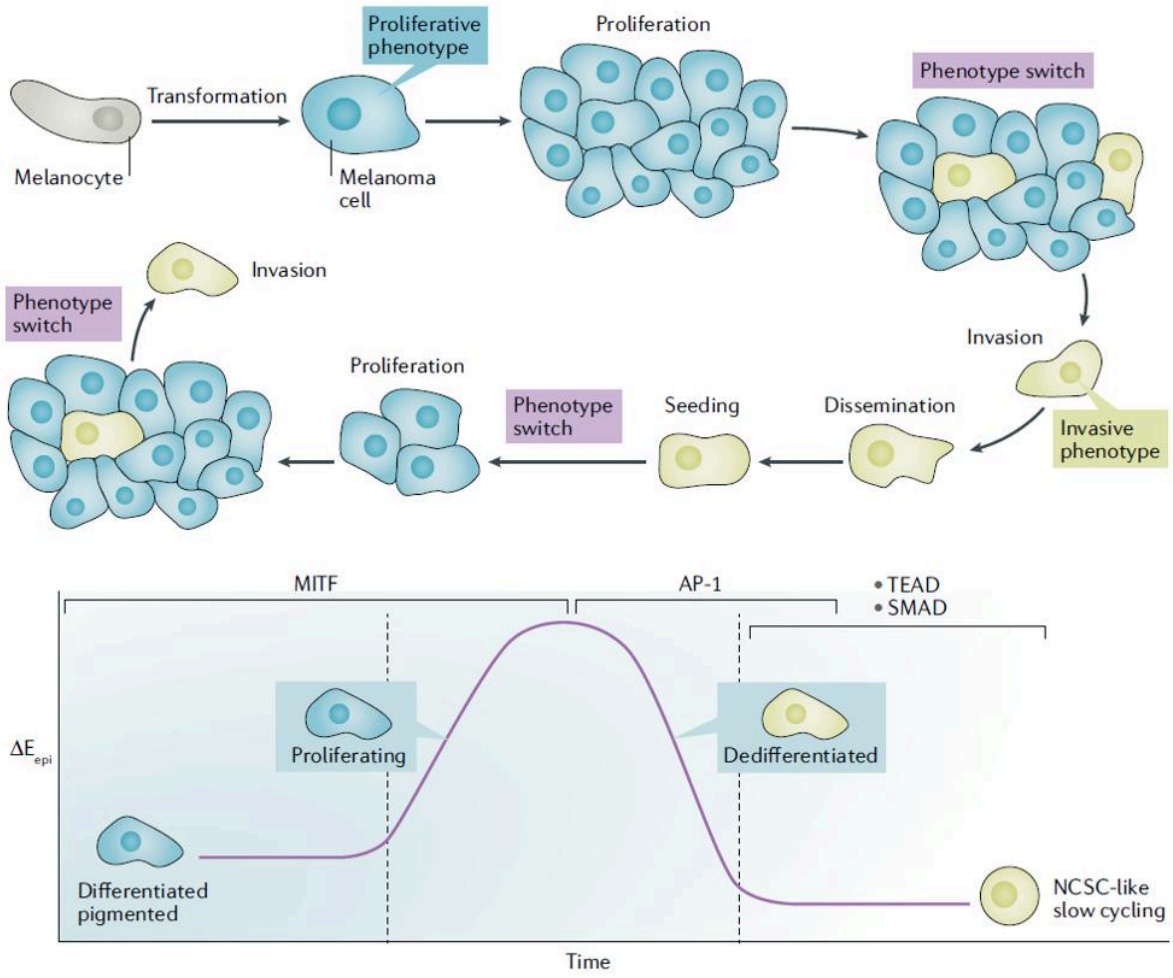

Figure 86. Transcriptional plasticity and phenotype switching in melanoma. Melanoma cells exhibit dynamic and reversible transitions between distinct transcriptional states that drive tumor heterogeneity and progression. Proliferative melanoma cells can switch to invasive phenotypes, enabling local invasion, dissemination, and metastatic seeding, followed by reversion to proliferative states at secondary sites. These phenotypic transitions are governed by variations in MITF activity, where intermediate to high MITF levels support proliferation, while reduced MITF activity is associated with dedifferentiated and invasive states. This continuum is accompanied by epigenetic and transcriptional reprogramming, with AP-1, TEAD transcription factors contributing to the activation of invasive gene expression programs. Adapted from *Arozarena and Wellbrock, Nat Rev Cancer (2019)*.

melanocytic and invasive states, as well as two transitory states, including an $MITF^{medium}$ starvation-like state, and a dedifferentiated $MITF^{low}/NGFR^{high}/SOX10^{high}$ neural-crest-like state. Notably, these phenotypes exist prior to treatment (Tsoi *et al*, 2018), suggesting that phenotype switching is a continuous and structured process that can be triggered by external stress cues, such as MAPK-targeted therapy or immunotherapy, to confer therapeutic resistance (Figure 87).

Accordingly, a growing body of evidence indicates that this transcriptional plasticity is a central driver of therapeutic resistance. In the context of MAPK-targeted therapies, early studies demonstrated that MAPK inhibitor-resistant cells from relapsed patient biopsies displayed a significant reduction in MITF expression, accompanied by increased AXL expression. This shift activates survival signaling independently of the MAPK pathway, directly linking AXL expression to therapy resistance (Figure 88) (Konieczkowski *et al*, 2014; Müller *et al*, 2014). Consequently, treatment with an AXL-specific antibody has been shown to reverse this resistance, cooperating with MAPK inhibitors to eradicate resistant populations and inhibit tumor growth *in vivo* (Boshuizen *et al*, 2018).

Further research using single-cell RNA sequencing in BRAF-mutant melanoma cohorts exposed to MAPKi identified several drug-tolerant transcriptional states co-occurring within minimal residual disease (MRD). Beyond the classical AXL/AP-1/TEAD-driven invasive state, a dedifferentiated neural crest stem cell-like (NCSC) state driven by the nuclear receptor RXRG was shown to confer resistance. As a result, treatment with an RXR antagonist limited the accumulation of the NCSC population and delayed resistance development (Rambow *et al*, 2018). Surprisingly, the same study also identified an $MITF^{high}$ population distinct from the classical melanocytic state, termed “pigmented” cells, which were enriched in MRD and contributed to resistance (Rambow *et al*, 2018).

This complexity is further illustrated by additional studies showing that, although MITF expression generally correlates with therapy sensitivity, its overexpression, mediated by PAX3, can enhance survival signaling and counteract MAPK inhibitor-induced cell death, thereby promoting resistance (Smith *et al*, 2013, 2016). These observations indicate that therapeutic resistance is not linked to a single cellular state, but rather that melanoma cells can transition between distinct phenotypes to sustain drug resistance.

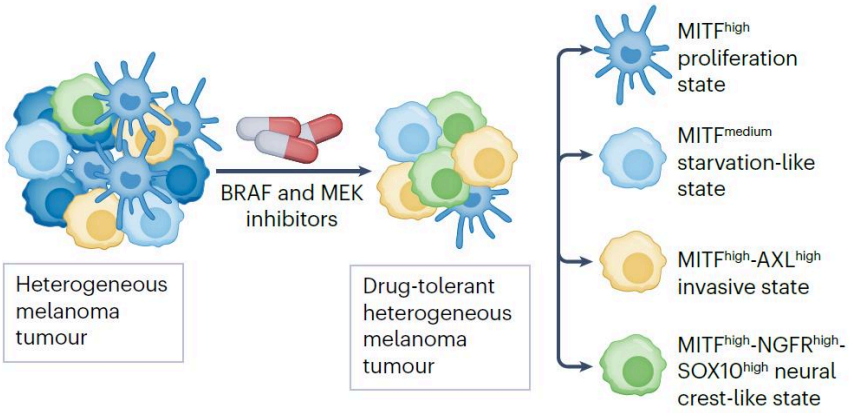

Figure 87. Transcriptional states and hierarchical organization of melanoma cell plasticity. Single-cell analyses reveal that multiple transcriptional states coexist within melanoma tumors, reflecting extensive intratumoral heterogeneity. These states include a proliferative MITF^{high} melanocytic population, a dedifferentiated AXL^{high} invasive population, and intermediate states such as a MITF^{medium} starvation-like state and a neural crest-like NGFR^{high}/SOX10^{high} state. These phenotypes are organized along a continuum and are present prior to treatment. Reproduced from *Centeno et al., Nat Rev Cancer (2023)*.

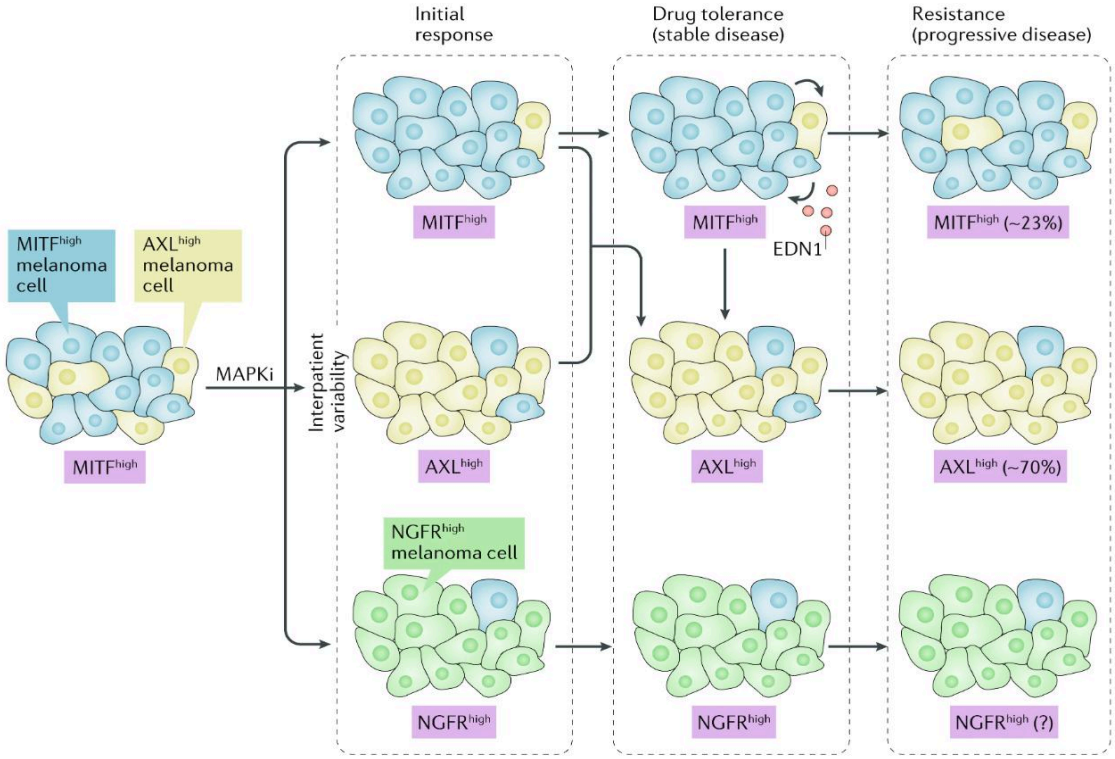

Figure 88. Therapy-induced transcriptional reprogramming and selection of resistant melanoma cell states. MAPK-targeted therapies shift melanoma cell populations from MITF^{high} melanocytic states toward dedifferentiated AXL^{high} and NGFR^{high} states associated with drug tolerance and resistance. Reproduced from *Arozarena and Wellbrock, Nat Rev Cancer (2019)*.

Phenotype switching also plays a major role in resistance to immunotherapy. For instance, mutational heterogeneity induced by UVB can increase tumor aggressiveness and reduce antitumor immunity, regardless of the overall mutational burden, suggesting that high intratumoral heterogeneity impairs immune control (Wolf *et al*, 2019). Furthermore, tumors with innate resistance to anti-PD-1 therapy are enriched in dedifferentiated, mesenchymal-like transcriptional programs, including high AXL expression (Hugo *et al*, 2016).

Similarly, immune-mediated pressures can actively induce dedifferentiation, as demonstrated by T cell-driven phenotype switching leading to loss of melanoma differentiation antigens and immune escape (Landsberg *et al*, 2012). More recently, spatial multi-omics analyses confirmed that dedifferentiated mesenchymal-like populations are significantly enriched in non-responders to immune checkpoint inhibitors. This study identified the transcription factor TCF4 as a master regulator of this mesenchymal signature, repressing melanocytic differentiation and antigen presentation programs. Notably, inhibition of TCF4 using bromodomain inhibitors increased the immunogenicity of the mesenchymal cells and restored sensitivity to both immunotherapy and targeted therapy (Figure 89) (Pozniak *et al*, 2024).

Before being implicated in therapeutic resistance, phenotype switching was primarily described as a driver of metastatic progression. In this model, melanoma cells transiently adopt a dedifferentiated, invasive phenotype to disseminate and subsequently revert to a proliferative melanocytic state upon colonization of distant sites (Pinner *et al*, 2009; Kim *et al*, 2017).

More recently, this model has been refined by single-cell transcriptomic analyses revealing a hierarchical organization of melanoma cell states. In particular, Karras and colleagues identified a pre-epithelial-to-mesenchymal neural crest stem cell-like (pre-EMT NC-stem cell like) population positioned at the apex of this hierarchy, capable of generating multiple downstream progenitor-like states. Importantly, this stem-like compartment was localized within perivascular niches and maintained by microenvironmental cues such as NOTCH3 signaling. In contrast, a distinct mesenchymal-like population expressing PRRX1 exhibited strong invasive properties but contributed minimally to tumor growth, instead acting as a reservoir of metastasis-initiating cells (Karras *et al*, 2022). These findings indicate that phenotype switching is not purely stochastic but can be constrained by spatial organization and niche-specific signals.

Of note, the different melanoma signatures do not correlate with the presence of canonical melanoma driver mutations (Verfaillie *et al*, 2015), as the transcriptional reprogramming during phenotype switching is disconnected from mutations and is mainly driven by

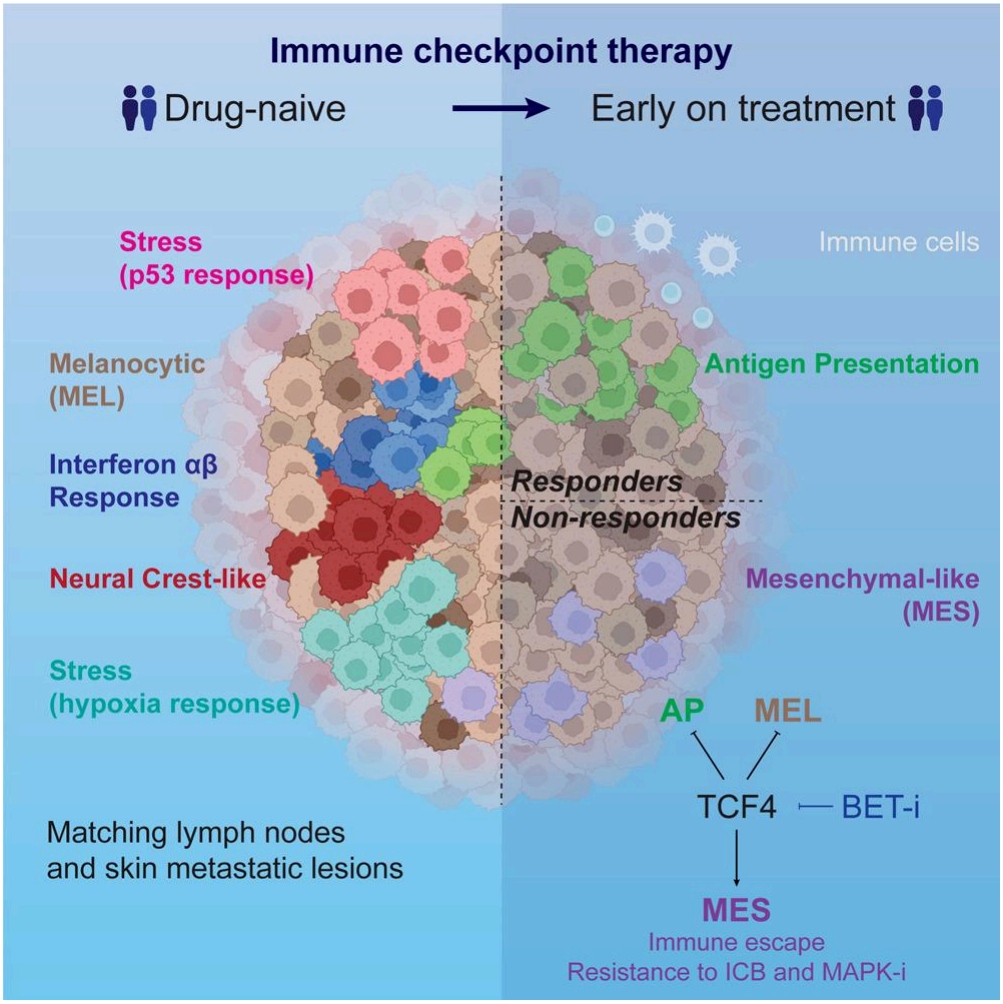

Figure 89. TCF4-driven dedifferentiation and resistance to immune checkpoint blockade in melanoma. Spatial multi-omics analysis reveals that mesenchymal-like (MES) melanoma cell populations are enriched in non-responders to immune checkpoint therapy, whereas responders display higher antigen presentation and interferon-response programs. The transcription factor TCF4 acts as a central regulator of this MES state by repressing melanocytic differentiation and antigen presentation, thereby promoting immune escape and resistance to both immunotherapy and MAPK-targeted therapies. Pharmacological inhibition of TCF4 (e.g., BET inhibition) restores immunogenicity and therapeutic sensitivity. Reproduced from *Pozniak et al., Cell (2024)*.

microenvironmental cues (Kim *et al*, 2017). In this context, the tumor microenvironment acts as a central regulator of melanoma cell identity by providing extracellular signals that dynamically modulate transcriptional programs (Figure 90). For instance, stromal components such as cancer-associated fibroblasts (CAFs) have been shown to promote a switch toward an invasive $MITF^{low}/AXL^{high}$ phenotype, as demonstrated by both single-cell analyses of patient biopsies and co-culture experiments, which revealed a strong association between CAF abundance and dedifferentiated transcriptional states (Tirosh *et al*, 2016; Seip *et al*, 2016).

In parallel, inflammatory signals constitute a major driver of phenotype plasticity. Pro-inflammatory cytokines such as TNF can suppress MITF expression while inducing AP-1 activity through JUN, thereby promoting a dedifferentiated $MITF^{low}/JUN^{high}$ state associated with immune evasion. Notably, this process is functionally linked to resistance to immune-mediated killing, as TNF-driven transcriptional reprogramming enables melanoma cells to escape cytotoxic T cell responses (Landsberg *et al*, 2012; Riesenberg *et al*, 2015).

Metabolic constraints within the tumor microenvironment further contribute to phenotype switching. For instance, hypoxic conditions, frequently encountered in poorly vascularized tumor regions, promote dedifferentiation through activation of HIF-1α, which induces the expression of the transcriptional repressor BHLHE40 and the tyrosine kinase receptors ROR1 and ROR2, leading to suppression of MITF expression (Feige *et al*, 2011; O'Connell *et al*, 2013).

Adding a further layer of complexity, recent work has demonstrated that phenotype plasticity can also be directly regulated by physical constraints within the tumor microenvironment. More particularly, this study showed that mechanical confinement is sufficient to induce transcriptional reprogramming toward a dedifferentiated, invasive-like state. This process was associated with alterations in chromatin organization and transcription factor activity, mainly mediated by the high mobility group protein HMGB2, indicating that biomechanical forces can directly shape melanoma cell identity independently of genetic alterations (Hunter *et al*, 2025).

At the regulatory level, these lineage-specific transcriptional states are supported by enhancer-rich regulatory architectures, including super-enhancers (SEs), which drive high expression of key identity and survival genes. In melanoma, master regulators such as MITF and SOX10, as well as invasive transcriptional programs driven by factors such as AP-1 and TEAD, are controlled by SE-associated networks. As such, transitions between phenotypic states are accompanied by extensive remodeling of the enhancer landscape, reflecting a dynamic

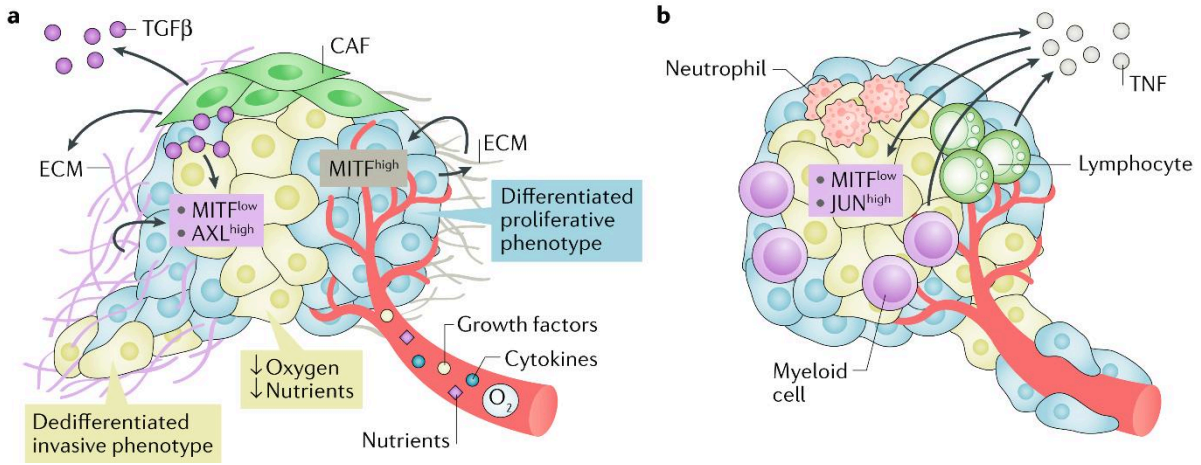

Figure 90. Microenvironmental control of melanoma phenotype switching. Tumor microenvironmental signals dynamically regulate melanoma cell states by modulating MITF activity. Stromal-derived factors, including cancer-associated fibroblasts (CAFs), TGFβ, extracellular matrix (ECM) components, and metabolic constraints such as hypoxia and nutrient deprivation, promote a switch toward a dedifferentiated $MITF^{low}/AXL^{high}$ invasive phenotype. These stresses further reinforce this transition through pathways such as HIF-1α and are associated with resistance to MAPK-targeted therapies. In parallel, inflammatory cues from immune cells, particularly TNF produced by neutrophils, T cells, and myeloid cells, drive an $MITF^{low}/JUN^{high}$ state characterized by enhanced cytokine responsiveness, loss of melanocytic differentiation antigens, and reduced T-cell recognition. Together, these microenvironmental inputs drive reversible phenotype switching independently of genetic alterations, contributing to tumor heterogeneity, immune evasion, and therapeutic resistance. Reproduced from *Arozarena and Wellbrock, Nat Rev Cancer (2019)*.

reorganization of transcriptional control (Kaufman *et al*, 2016; Zhou *et al*, 2016; Fontanals-Cirera *et al*, 2017; Eliades *et al*, 2018; Berico *et al*, 2023b). This strong dependence on enhancer-driven transcription establishes melanoma as a paradigm of transcriptional addiction and a relevant model to study transcription-targeting strategies.

While phenotype switching promotes metastasis and therapeutic resistance, it also exposes a potential vulnerability. Although targeting individual regulators of transcriptional states, such as AXL, RXR, KDM1A, or TCF4 (Boshuizen *et al*, 2018; Rambow *et al*, 2018; Khaliq *et al*, 2021; Pozniak *et al*, 2024), has shown promise in reversing resistant phenotypes, these approaches remain limited by the redundancy and adaptability of transcriptional networks, which enable melanoma cells to dynamically rewire their regulatory programs. These observations suggest that targeting upstream transcriptional dependencies, rather than individual downstream effectors, may provide a more effective strategy to overcome tumor heterogeneity and adaptive resistance.

Based on this rationale, the first objective of this thesis is to investigate the therapeutic potential of synthetic ecteinascidins, a class of DNA-binding transcriptional inhibitors, to interfere with oncogenic transcriptional programs in heterogenous types of cancer such as melanoma. The following section presents the results obtained using these compounds, focusing on their impact on transcriptional regulation and genome stability in cancer cells.

Results

Part I: Targeting super-enhancer-driven transcriptional addiction in melanoma

Preface to Article 1:

This work originated from a collaboration between the laboratory and the Spanish pharmaceutical company PharmaMar, aimed at investigating the molecular mechanisms of two novel synthetic ecteinascidins: Ecubectedin (previously PM14) and PM54, which are next-generation analogues of trabectedin and lurbinectedin, two DNA-binding agents known to interfere with transcriptional processes in cancer cells. Since the early 2010s, PharmaMar has collaborated extensively with the former head of our laboratory, Jean-Marc Egly, to study the impact of ecteinascidins on transcription and DNA repair, leading to the demonstration that lurbinectedin binds DNA, inhibits the transcription of actively transcribed oncogenes, and induces DNA breaks (Santamaría Núñez et al., *Molecular Cancer Therapeutics*, 2016).

When I joined the laboratory during my Master 1 internship in 2020, a new phase of this collaboration had just begun, with the objective of characterizing the transcriptional effects of Ecubectedin and PM54 and comparing them to Lurbinectedin using high-throughput sequencing approaches. To investigate the impact of these compounds across heterogeneous transcriptional states, we selected cutaneous melanoma as a model system due to its pronounced transcriptional plasticity and highly divergent melanocytic and mesenchymal phenotypes.

During my Master 1 and Master 2 internships, under the supervision of Max Cigrang, who was a PhD student, I participated in the initial characterization of the compounds through cell viability assays, phenotypic analyses, and RNA-sequencing experiments. At the beginning of my PhD, the project evolved toward the identification of genome-wide drug-binding sites using biotinylated derivatives. My principal contribution to this study was the implementation and optimization of the Chem-map approach, performed during the first year of my PhD. This technique enabled genome-wide mapping of the drug-binding sites through immunoprecipitation of biotinylated compounds followed by high-throughput sequencing.

In parallel, CUT&Tag profiling of histone modifications and chromatin-associated factors was performed, allowing integration of chromatin landscapes with Chem-map datasets. These analyses demonstrated that synthetic ecteinascidins preferentially affect active oncogenes associated with super-enhancer-driven transcriptional programs. In addition to the experimental work, I performed the majority of the bioinformatic analyses associated with the Chem-map and CUT&Tag datasets, largely through self-training in computational biology during my PhD.

This work resulted in a co-first author publication with Max Cigrang in *Nature Communications*, published in January 2025 after extensive 8 months of peer-review revisions.

The successful completion of this study also relied heavily on the technical expertise and support provided by the laboratory engineer, Maguelone Nogaret.

nature communications

Article

https://doi.org/10.1038/s41467-024-55667-z

Pan-inhibition of super-enhancer-driven oncogenic transcription by next-generation synthetic ecteinascidins yields potent anti-cancer activity

Received: 25 April 2024

Accepted: 19 December 2024

Published online: 08 January 2025

Check for updates

Max Cigrang[1,2,3,4,10], Julian Obid[1,2,3,4,10], Maguelone Nogaret[1,2,3,4], Léane Seno[1,2,3,4], Tao Ye[1,2,3,4], Guillaume Davidson[1,2,3,4], Philippe Catez[1,2,3,4], Pietro Berico[1,2,3,4,5,6], Clara Capelli[1,2,3,4], Clara Marechal[1,2,3,4], Amélie Zachayus[1,2,3,4], Clémence Elly[1,2,3,4], Marie Jose Guillen Navarro[7], Marta Martinez Diez[7], Gema Santamaria Nunez[7], Tsai-Kun Li[8,9], Emmanuel Compe[1,2,3,4], Pablo Avilés[7], Irwin Davidson[1,2,3,4], Jean-Marc Egly[1,2,3,4,9], Carmen Cuevas[7] & Frédéric Coin[1,2,3,4]

The plasticity of cancer cells facilitates their ability to adopt heterogeneous differentiation states, posing a significant challenge to therapeutic interventions. Specific gene expression programs, driven in part by super-enhancers (SEs), underlie cancer cell states. Here we successfully inhibit SE-driven transcription in phenotypically distinct metastatic melanoma cells using next-generation synthetic ecteinascidins. Through functional genomic methodologies, we demonstrate that these compounds inhibit the expression of genes encoding lineage-specific or ubiquitous transcription factors/coactivators by selectively targeting the CpG-rich sequences within their promoters and/or enhancers. This prevents the formation of transcription factor/coactivator condensates necessary for SE-dependent gene expression. Consequently, these compounds exhibit cytotoxic activity across distinct subpopulations of metastatic melanoma cells and inhibit tumor proliferation, including those resistant to current therapies. These findings extend to other cancers, like small cell lung cancer, recently approved for ecteinascidin-based treatment. Overall, our study provides preclinical proof that pan-inhibition of SE-dependent genes with synthetic ecteinascidins is a promising therapeutic approach for tumors with heterogeneous transcriptional landscapes.

In recent years, the concept of 'transcriptional addiction' has emerged as a hallmark of cancer cells. Indeed, dysregulated gene expression programs and their associated transcriptional regulatory machinery play crucial roles in sustaining cancer cell phenotypes, thereby rendering them susceptible to transcriptional inhibitors[1–5]. One of the primary mechanisms contributing to gene expression dysregulation in cancer cells involves the aberrant acquisition of large clusters of enhancers known as "super-enhancers" (SEs), which drive and maintain the robust expression of oncogenes. SEs are characterized by the aggregated histone modifications H3K27ac and H3K4me1, over longer genomic distances compared to typical enhancers[6,7]. Moreover, SE-dependent oncogene transcription requires the activity of ubiquitous

A full list of affiliations appears at the end of the paper. e-mail: fredr@igbmc.fr

transcription factors (e.g., the Cyclin Dependent Kinase 7 (CDK7) of TFIIH) and transcriptional coactivators (e.g., Bromodomain-containing protein 4 (BRD4)), and is maintained by core autoregulatory feedback loops involving master transcription factors and the Mediator complex[8]. Recent evidence has demonstrated that SEs form phase-separated biomolecular condensates, concentrating the transcription apparatus in nuclear puncta to drive the high expression of their regulated oncogenes[9]. Targeting these oncogenic SEs and their spatial organization has emerged as a potential therapeutic strategy[10]. Therefore, several compounds aiming to disrupt factors involved in oncogenic SE-driven gene expression, including CDK7 and BRD4 inhibitors, have entered clinical trials[11,12]. However, they have had limited success due to poor pharmacokinetics and short half-lives[13–16].

Cutaneous melanoma is often cited as a prime example of transcriptional addiction due to its frequent dysregulation of specific transcription factors and signaling pathways that drive its aggressive behavior and resistance to treatment[17–20]. Despite significant advances in developing inhibitors targeting the mutated MAPK signaling pathway (BRAFi and MEKi), along with the introduction of immune checkpoint inhibitors targeting programmed cell death protein 1 (PD-1) and cytotoxic T-lymphocyte-associated antigen 4 (CTLA-4), this cancer remains the most lethal form of skin cancer. Indeed, more than 50% of metastatic melanoma patients either do not initially respond or eventually acquire resistance to these therapies[21–23]. Melanoma cells evade conventional therapeutic strategies by transitioning between melanocytic/differentiated states, governed by SE-dependent genes essential for cell proliferation, such as the *lineage-specific master transcription factors Microphthalmia-associated transcription factor* (*MITF*) and the *SRY-box transcription factor 10* (*SOX10*), and mesenchymal-like/undifferentiated states, governed by key regulator genes such as the *AXL Receptor Tyrosine Kinase* (*AXL*) and the *Activator Protein* (*AP-1*)/TEAD genes implicated in targeted therapy/immunotherapy resistance and invasion[18,24–30]. This phenotypic adaptation/switch, facilitated by dynamic transcriptional and epigenetic reprogramming mechanisms in response to microenvironmental cues, complicates treatment outcomes[19,31] and underscores the need for therapeutics that can uniformly target divergent transcription programs governing different tumor cell states[32].

Ecteinascidins, a group of natural compounds derived from marine organisms, particularly tunicates, have garnered significant attention due to their anticancer properties[33]. Synthetic ecteinascidins refer to compounds that are chemically synthesized to mimic the structure and biological activity of natural ecteinascidins. These synthetic compounds are designed to retain the anticancer properties of natural ecteinascidins while potentially offering advantages such as improved potency, selectivity, and pharmacokinetic properties. A notable member of this class is lurbinectedin, derived from the natural compound trabectedin. Lurbinectedin acts as a DNA binder and transcriptional inhibitor[34,35] It is the first molecule approved by the FDA for the treatment of relapsed small-cell lung cancer (SCLC) in the last decade, showcasing the considerable potential of synthetic ecteinascidins as anticancer compounds[36].

In this work, in an effort to potentially enhance the benefits of these DNA binders, we develop next-generation synthetic ecteinascidins and test these compounds on melanoma cells due to their well-established transcriptional addiction and propensity for treatment resistance. Our study demonstrates potent anti-proliferative and apoptotic effects of these next-generation DNA binders on differentiated and undifferentiated *BRAF*, *NRAS*, and triple-wild type mutated melanoma cells in various in vitro 2-D and 3-D models and in cell-derived xenograft (CDX) mouse models. We further observe that these compounds potently inhibit a set of genes encoding ubiquitous transcription factors/coactivators through binding to the CpG islands located in their promoters and/or enhancers. These factors are highly enriched at cell-specific SEs, regulating the expression of cancer-promoting genes. Consequently, synthetic ecteinascidins disorganize the phase-separated condensates of transcription factors/coactivators, inducing a pan-inactivation of SEs in melanoma cells irrespective of their cell state and driver mutations. This mechanism of action is not observed with BRAFi, MEKi, or DNA-damaging agents such as dacarbazine. Intriguingly, we demonstrate that this uncovered mechanism is also operative in clinically relevant scenarios, such as the treatment of SCLC cells with lurbinectedin, thereby explaining the clinical efficiency of this compound.

Results

Lurbinectedin shows notable efficacy against distinct melanoma cell types

To ascertain the cytotoxic effects of the first-in-class synthetic ecteinascidin lurbinectedin (Fig. 1a) on melanoma cells, we first conducted a dose-response analysis across ten metastatic melanoma cell cultures representing the two primary phenotypes and encompassing the most prevalent driver mutations. We evaluated primary differentiated melanocytic-type cultures derived from patient biopsies, including MM011 ($NRAS^{Q61K}$), MM074 ($BRAF^{V600E}$), MM117 (Triple-wt), alongside commonly used metastatic melanoma cell lines 501mel ($BRAF^{V600E}$), IGR37 ($BRAF^{V600E}$) and SkMel-28 ($BRAF^{V600E}$) (Table 1). These cells demonstrated moderate to high expression levels of the lineage-specific master transcription factors MITF and SOX10, while showing low to undetectable expression levels of the pro-metastatic factors EGFR and AXL[14,18,37] (Fig. 1b). Additionally, we examined primary undifferentiated metastatic mesenchymal-like melanoma cell cultures derived from patient biopsies, including MM029 ($BRAF^{V600K}$), MM047 ($NRAS^{Q61R}$) and MM099 ($BRAF^{V600E}$), along with the undifferentiated metastatic mesenchymal-like melanoma cell line IGR39 ($BRAF^{V600E}$). These cells exhibited low to undetectable levels of MITF and SOX10, but elevated expression levels of EGFR and/or AXL[14].

We observed varying sensitivities of these metastatic melanoma cells to clinically utilized targeted therapy agents, such as the BRAF inhibitors (BRAFi) vemurafenib and dabrafenib, as well as the MEK inhibitor (MEKi) trametinib (Fig. 1c–e and Table 1). Differentiated $BRAF^{V600E}$ melanoma cells were the most responsive to these compounds, whereas undifferentiated cells displayed high resistance. In stark contrast, all melanoma cells showed high sensitivity to lurbinectedin, with IC50 values in the low nanomolar range, from 0.44 to 2.07 nM (Fig. 1f and Table 1). Furthermore, we generated vemurafenib-resistant cells $501mel^{VemuR}$ and $MM074^{VemuR}$ by exposing initially sensitive cells to increasing drug concentrations in vitro (Fig. 1c and Table 1)[14]. These cells acquired a hyperpigmentation phenotype and exhibited cross-resistance to dabrafenib (in the case of $MM074^{VemuR}$) and trametinib (Fig. 1d, e and Table 1), yet remained highly sensitive to lurbinectedin (Fig. 1f and Table 1).

Collectively, these findings underscore the heightened sensitivity of melanoma cells to lurbinectedin, regardless of cellular phenotypes or driver mutations.

Next-generation ecteinascidins show high cytotoxic effects on melanoma cells

In our pursuit of enhancing the anti-cancer efficacy of synthetic ecteinascidins, we synthesized and assessed next-generation compounds. These molecules, named ecubectedin and PM54, exhibit distinct chemical structures in the non-DNA-binding moieties[38]. Ecubectedin features a substituted spiro-β-carboline, while PM54 contains a spiro-benzofuropyridine (Fig. 2a, b). Spiro compounds often exhibit enhanced biological activities due to their rigid and three-dimensional structures, which can lead to improved interactions with biological targets. The introduction of a spiro-benzofuropyridine in PM54 is particularly relevant because this moiety was not previously identified in natural ecteinascidins. These unique three-dimensional shapes can contribute to increased selectivity for specific biological

https://doi.org/10.1038/s41467-024-55667-z

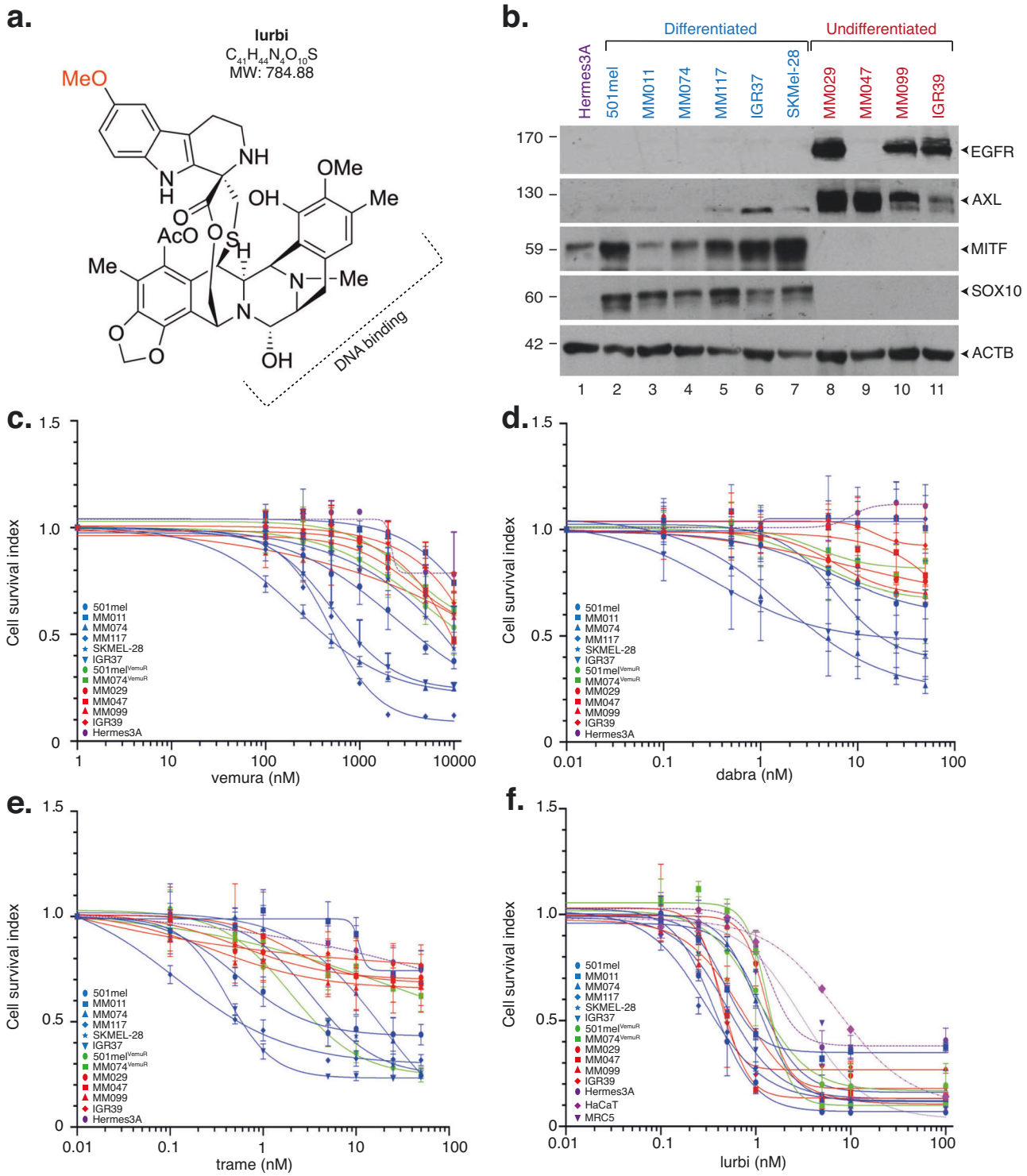

Fig. 1 | Metastatic melanoma cells show high sensitivity to lurbinectedin. **a** Chemical structure of lurbinectedin, the first-in-class synthetic ecteinascidin containing tetrahydroisoquinoline subunits. The moiety of the molecule interacting with DNA is indicated. Molecular Weight (MW) is indicated. **b** Protein lysates from either the immortalized Hermes3A melanocytes, differentiated melanoma cells 501mel, MM011, MM074, MM117, IGR37 and SKMel-28 or undifferentiated melanoma cells MM029, MM047, MM099 and IGR39 were immuno-blotted for proteins as indicated. Molecular mass of the proteins is indicated (kDa). Source data are provided as a Source Data file. This experiment was repeated independently three times with similar results. **c**–**f** Indicated melanoma cells were treated with increasing concentrations of vemurafenib **c**, dabrafenib **d**, trametinib **e**, or lurbinectedin **f** for 72 h. Mean growth is shown relative to vehicle (DMSO)-treated cells. Error bars indicate mean values +/− Standard Deviation (SD) for three biological triplicates. Differentiated (MITF-High, proliferative) melanoma cells are shown in blue, while undifferentiated (MITF-low, invasive) melanoma cells are shown in red. Hyperpigmented melanoma cells with acquired resistance to vemurafenib are shown in green. Immortalized Hermes3A melanocytes, skin keratinocyte HaCaT and embryonic fibroblastic MRC5 cells are shown in violet. Source data are provided as a Source Data file.

https://doi.org/10.1038/s41467-024-55667-z

Table 1 | Melanoma cell sensitivity against MAPKi and synthetic ecteinascidins

Cells	G	S/T	P	G	vemu	dabra	tram	lurb	ecub	PM54	B-lurb	B-PM54
HaCat	M	WT	Kera	WT	nd	nd	nd	3.2 nM	5.2 nM	10.3 nM	nd	nd
MRC5	M	WT	Fibro	WT	nd	nd	nd	7.5 nM	2.9 nM	12.5 nM	nd	nd
Hermes3A	M	WT	Mel	WT	>10μM	>50 nM	>50 nM	2.7 nM	2.9 nM	4.9 nM	nd	nd
501mel	F	MNS/NS	Diff	$BRAF^{V600E}$	2.4μM	>50 nM	3.0 nM	0.4 nM	1.2 nM	1.7 nM	1.4 nM	5.0 nM
MM011	F	LNM/ALM	Diff	$NRAS^{Q61R}$	>10μM	>50 nM	>50 nM	0.5 nM	1.0 nM	1.4 nM	nd	nd
MM074	F	LNM/SSM	Diff	$BRAF^{V600E}$	225 nM	4.7 nM	0.5 nM	1.1 nM	1.1 nM	3.8 nM	nd	nd
MM117	NS	NS/NS	Diff	Triple-WT	490 nM	>50 nM	10.2 nM	0.3 nM	0.7 nM	1.2 nM	nd	nd
SKMEL-28	M	ALN/NS	Diff	$BRAF^{V600E}$	>10μM	1.0 nM	5.1 nM	1.2 nM	1.3 nM	1.7 nM	nd	nd
IGR37	M	GLN/NS	Diff	$BRAF^{V600E}$	520 nM	25.3 nM	0.5 nM	0.5 nM	1.0 nM	1.5 nM	nd	nd
$501mel^{VemuR}$	F	MNS/NS	Pigmented	$BRAF^{V600E}$	>10μM	>50 nM	>50 nM	1.1 nM	1.0 nM	2.1 nM	nd	nd
$MM074^{VemuR}$	F	LNM/SSM	Pigmented	$BRAF^{V600E}$	>10μM	>50 nM	4.6 nM	1.3 nM	1.6 nM	3.1 nM	nd	nd
MM029	F	LNM/SSM	Undiff	$BRAF^{V600K}$	>10μM	>50 nM	>50 nM	1.3 nM	1.4 nM	4.7 nM	1.4 nM	6.0 nM
MM047	M	NS/NS	Undiff	$NRAS^{Q61R}$	>10μM	>50 nM	>50 nM	0.4 nM	0.9 nM	1.4 nM	nd	nd
MM099	M	LT/NS	Undiff	$BRAF^{V600E}$	>10μM	>50 nM	>50 nM	0.7 nM	1.4 nM	1.8 nM	nd	nd
IGR39	M	LT/SSM	Undiff	$BRAF^{V600E}$	>10μM	>50 nM	>50 nM	0.4 nM	0.8 nM	0.8 nM	nd	nd
MM074 + INFγ	F	LNM/SSM	Pseudo-Inter	$BRAF^{V600E}$	8μM	ns	ns	0.9 nM	1.0 nM	1.0 nM	nd	nd

IC50 of vemurafenib (vemu), dabrafenib (dabra), trametinib (tram), lurbinectedin (lurb), ecubectedin (ecub) and PM54 against various melanoma cells. The gender (G) of the patient, site and tumor type (S/T), phenotype (P) and genotype (G) of these cells are indicated. Hermes3A are transformed melanocytes. WT= Wild-type, NS= Not Specified, MNS= Metastatic, Not Specified, LNM= Lymph Node Metastasis, SSM= Superficial Spreading Melanoma, ALM= Acral Lentiginous Melanoma, ALN= Axillary Lymph Node, LT= Left Thigh, GLN= Groin Lymph Node, nd= Not Determined. IC50 of Bio-lurbi (B-lurbi) and Bio-PM54 (B-PM54) are also indicated.

targets, reducing off-target effects and warranting further investigation. We observed that all melanoma cells displayed high sensitivity to these next-generation synthetic ecteinascidins, with IC50 values in the low nanomolar range, spanning from 0.7 to 5 nM (Fig. 2c, d and Table 1). Notably, the non-cancerous Hermes3A immortalized melanocytes, the skin keratinocyte HaCaT cells, and the embryonic fibroblastic MRC5 cells were consistently 3- to 7-times less sensitive to synthetic ecteinascidins compared to melanoma cells.

These findings demonstrate that the next-generation synthetic ecteinascidins exhibit high cytotoxic effects on a range of melanoma cells containing distinct driver mutations and cellular phenotypes.

Synthetic ecteinascidins induce melanoma cell apoptotic death

We next compared the efficacy of synthetic ecteinascidins on cell proliferation and survival. Clonogenic assays demonstrated a significant impact of these molecules on all tested metastatic melanoma cell cultures or cell lines (Fig. 3a), accompanied by a significant inhibition of melanoma cell proliferation (Fig. 3b). Concurrently, there was a notable blockade of cell cycle progression in the G2/M phase (Fig. 3c) and induction of apoptosis (Fig. 3d). The compounds also significantly inhibited the invasion capacities of undifferentiated metastatic melanoma cell cultures (Fig. 3e). Lurbinectedin is known to trigger a DNA damage response characterized by the activation of γH2AX due to drug-induced DNA breaks[34]. Using immunofluorescence, we observed γH2AX accumulation in differentiated 501mel or undifferentiated MM029 cells upon treatment with the three synthetic ecteinascidins (Supplementary Fig. 1a–d), which was confirmed by immunoblotting (Supplementary Fig. 1e). In parallel, phosphorylation of the protein kinase ataxia telangiectasia mutated (ATM), the master damage response protein, was observed in these cells (Supplementary Fig. 1e). Of note, MAPKi did not induce activation of γH2AX in sensitive 501mel cells.

We further employed 3-D melanosphere culture assays to assess the response of melanospheres derived from the melanocytic-like MM074 cells to BRAFi and MEKi. In sharp contrast to the response observed in 2-D cultures, BRAFi and MEKi failed to reduce cell viability in the 3-D cultures, even at doses equivalent to 5x of the IC50 concentrations determined in 2-D (Supplementary Fig. 2a). Conversely, synthetic ecteinascidins demonstrated significant cytotoxic effects on MM074 melanospheres (Supplementary Fig. 2b), inducing apoptosis at nanomolar concentrations (Supplementary Fig. 2c). These findings elucidate the pro-apoptotic impacts of synthetic ecteinascidins on both differentiated and undifferentiated melanoma cells cultured in 2- or 3-D settings.

Synthetic ecteinascidins exhibit robust anti-tumor activities

The above data prompted us to examine the impact of synthetic ecteinascidins on melanoma cell-derived xenograft (CDX) mouse models. We first monitored the tumor volumes following intravenous (IV) administration of synthetic ecteinascidins once per week for three consecutive weeks at a concentration of 1.2 mg/kg. Treatments commenced (d.0) when the tumors reached 150 mm^3 in athymic nude female mice aged 4 to 6 weeks ($n = 10$/group) and finished fourteen days later (d.14). We tested CDXs obtained from two highly proliferative melanoma cell lines widely used for drug screening (LOX-IMVI$^{BRAF\text{-}V600E}$ and WM-266-4$^{BRAF\text{-}V600D}$)[39]. For both CDXs, we observed significant tumor growth regression upon treatment with synthetic ecteinascidins, starting d.5 (Fig. 4a, b). The tumor growth delay was persistent even after d.14 when treatment was withdrawn, and lasted until d.25, emphasizing a period of latency of 10 days following the end of the treatment. Simultaneously, a marked augmentation in overall survival was observed, predominantly evident during the latency phase (Fig. 4c, d).

https://doi.org/10.1038/s41467-024-55667-z

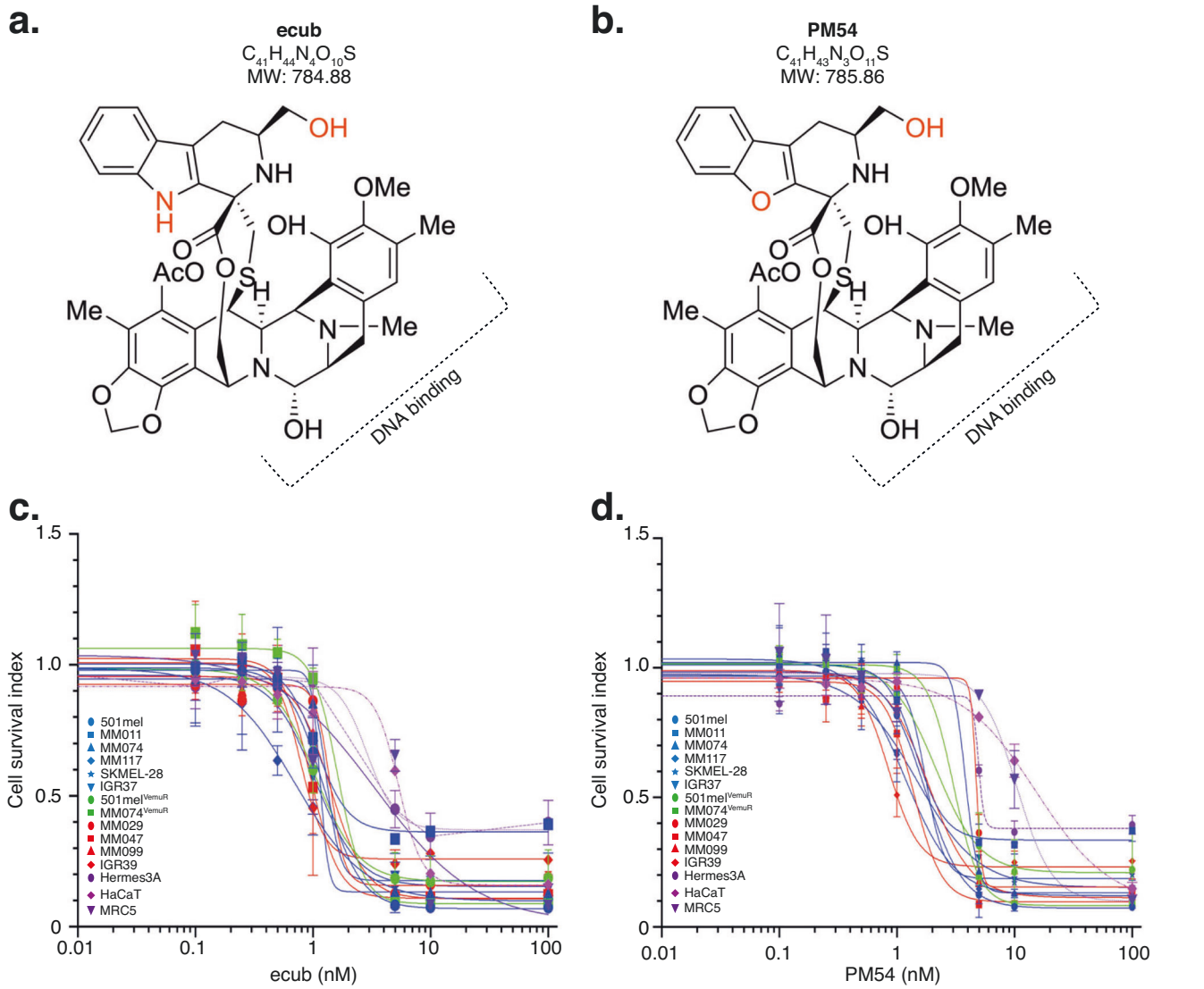

Fig. 2 | Metastatic melanoma cells show high sensitivity to next-generation synthetic ecteinascidins. a, **b** Chemical structure of ecubectedin **a** and PM54 **b**, two next-generation synthetic ecteinascidins analogs of lurbinectedin. The modifications are highlighted in red. The moiety of the molecule interacting with DNA is indicated. Molecular Weight (MW) is indicated. **c**, **d** Indicated melanoma cells were treated with increasing concentrations of ecubectedin **c** or PM54 **d**, for 72 h. Mean growth is shown relative to vehicle (DMSO)-treated cells. Error bars indicate mean values ± Standard Deviation (SD) for three biological triplicates. Differentiated (MITF-High, proliferative) melanoma cells are shown in blue, while undifferentiated (MITF-low, invasive) melanoma cells are shown in red. Hyperpigmented melanoma cells with acquired resistance to vemurafenib are shown in green. Immortalized Hermes3A melanocytes, skin keratinocyte HaCaT and embryonic fibroblastic MRC5 cells are shown in violet. Source data are provided as a Source Data file.

We next analyzed the effect of the drugs on MAPKi-resistant cells using the 501mel and 501mel^{VemuR} cells. Once the tumors reached a size of 150 mm^3 in female NSG mice, a single IV dose of either ecubectedin or PM54 at a concentration of 1.2 mg/kg was administrated to the animals (n = 8/group). Twenty-four hours after this single IV dose, we assessed the mitotic or apoptotic indexes on tumor sections using immunostaining of phospho-histone H3 (pHH3) or caspase-3 cleavage, respectively[40]. We observed a significantly decreased mitotic index and increased apoptosis upon treatment with synthetic ecteinascidins, for CDXs derived from both 501mel and 501mel^{VemuR} (Supplementary Fig. 3a–d). Consequently, we observed that treatments with synthetic ecteinascidins significantly impacted the tumor growth of CDXs derived from 501mel and 501mel^{VemuR} melanoma cells (Figs. 4e and 2f) and increased the overall survival of the mice (Fig. 4g, h). Altogether, these studies suggest that synthetic ecteinascidins are highly active at inhibiting the growth and inducing apoptosis in melanoma tumors in vivo, even in those presenting resistance to clinically relevant treatments.

Synthetic ecteinascidins affect the expression of cancer-promoting genes

Given the proposed impact of lurbinectedin on transcription[35], we conducted gene expression profiling (RNA-Seq) in 2-D cultures of differentiated and undifferentiated melanoma cells. Following the treatment with synthetic ecteinascidins, major transcriptional effects were observed, with a large number of genes being downregulated for both cell types, and a lesser number of genes being upregulated (Supplementary Fig. 4a–c and Supplementary Data 1). However, significant differences in the types of genes being affected in either differentiated or undifferentiated cells were observed. Among the downregulated genes, we noted the presence of several cancer-promoting genes such as *MITF*, *Paired Box 3 (PAX3)* or *SOX10* specifically in differentiated melanoma cells or *AXL*, *Epidermal Growth Factor Receptor (EGFR)*, SRY-Box Transcription Factor 9 (SOX9), *FOS Like 2 (FOSL2)* and *TEAD4* specifically in undifferentiated cells. These data were confirmed in 2-D models by RT-qPCR and/or immunoblotting (Supplementary

https://doi.org/10.1038/s41467-024-55667-z

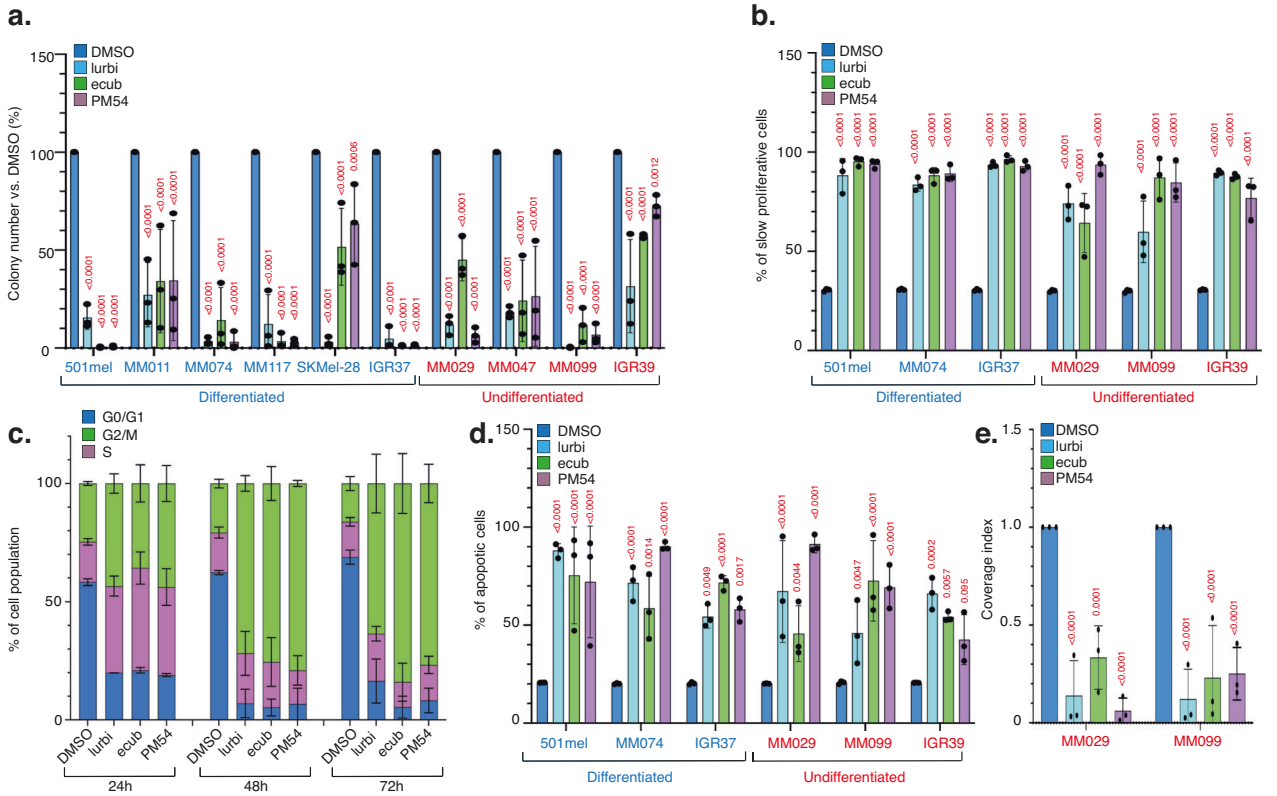

Fig. 3 | Synthetic ecteinascidins induce cell cycle arrest and apoptosis. **a** Metastatic melanoma cells were treated with either vehicle (DMSO), lurbinectedin, ecubectedin or PM54 (1xIC50 concentration, 48 h) and allowed to grow for additional 10 days in the absence of drugs. Results are shown as the mean colony numbers ± SD for three biological triplicates. Ordinary one-way ANOVA using Dunnett's multiple comparisons test was used to determine the *p*-values (vs. DMSO). Source data are provided as a Source Data file. **b** Metastatic melanoma cells were incubated with CellTrace and subsequently treated with either vehicle (DMSO), lurbinectedin, ecubectedin or PM54 (1xIC50 concentration, 72 h). Quantifications of populations with high CellTrace signal in DMSO or drug-treated cells are shown as mean values ± SD for three biological triplicates. Proliferative cells show low CellTrace signal while non proliferative cells show high CellTrace signal. Ordinary one-way ANOVA using Dunnett's multiple comparisons test was used to determine the *p*-values (vs. DMSO). Source data are provided as a Source Data file. **c** 501mel cells were treated with either vehicle (DMSO), lurbinectedin, ecubectedin or PM54 (1xIC50 concentration, 72 h). Cell cycle was studied by propidium iodide staining and flow cytometry, and results are shown as mean values ± SD for three biological triplicates. Source data are provided as a Source Data file. **d** Metastatic melanoma cells were treated with either vehicle (DMSO), lurbinectedin, ecubectedin or PM54 (1xIC50 concentration, 72 h). Apoptosis was studied by flow cytometry using annexin V-APC staining. Results are shown as mean values ± SD for three biological triplicates. Ordinary one-way ANOVA using Dunnett's multiple comparisons test was used to determine the *p*-values (vs. DMSO). Source data are provided as a Source Data file. **e** MM029 and MM099 metastatic melanoma cells were treated with either vehicle (DMSO), lurbinectedin, ecubectedin or PM54 (1xIC50 concentration, 48 h). Invasion was determined using Boyden chamber assays. Results are shown as mean values of coverage index +/- SD for three biological triplicates. Ordinary one-way ANOVA using Dunnett's multiple comparisons test was used to determine the *p*-values (vs. DMSO). Source data are provided as a Source Data file.

Fig. 5a–d) and in 3-D models by RT-qPCR (Supplementary Fig. 5e,f). Collectively, our findings underscore the significant and partially cell-type-specific inhibition of expression of cancer-promoting genes in metastatic melanoma cells upon treatment with synthetic ecteinascidins.

We next undertook a comparative analysis of gene expression profiles in response to treatment with synthetic ecteinascidins. Notably, the three molecules commonly down-regulated 1365 and 1104 genes in differentiated and undifferentiated cells, respectively (Supplementary Fig. 6a). It is worth mentioning that among these genes, 757 displayed consistent down-regulation (and only 110 displayed up-regulation) across both differentiated and undifferentiated cells in response to all the three compounds (Supplementary Fig. 6b,c,d and Supplementary Data 2). Gene ontology (GO) analysis revealed that a substantial proportion of these 757 genes were intricately involved in transcriptional processes (Supplementary Fig. 6e and Supplementary Data 2 and 8).

We subsequently compared each next-generation synthetic ecteinascidin with lurbinectedin. We observed that ecubectedin exhibited strikingly similar effects, with no genes exhibiting statistically significant differential expression upon a comparative analysis in either differentiated or undifferentiated cells (Supplementary Fig. 7a,b). In stark contrast, PM54 distinctly induced specific transcriptional effects compared to lurbinectedin, revealing a more focused alteration in gene expression, as a smaller subset of genes exhibited deregulation in both differentiated and undifferentiated melanoma cells, (Supplementary Fig. 7a,c). This distinction was further substantiated by GO analysis, which elucidated that PM54 exerts weaker effects on genes involved in diverse cellular processes such as interferon response or oxidative phosphorylation but exerts a more direct influence on genes involved in transcriptional regulation (Supplementary Fig. 7d and Supplementary Data 2 and 8). Globally, our analysis demonstrates that PM54 distinguishes itself by exerting the least influence on the transcriptional program of melanoma cells, while presenting virtually the same cytotoxic effects, emphasizing a unique and potentially advantageous pharmacological profile.

Synthetic ecteinascidins suppress the expression of SE-dependent genes

To decipher the molecular mechanism underlying the cytotoxicity of synthetic ecteinascidins, we conducted an extensive analysis of RNA-Seq datasets derived from three distinct cancer cell types treated with

https://doi.org/10.1038/s41467-024-55667-z

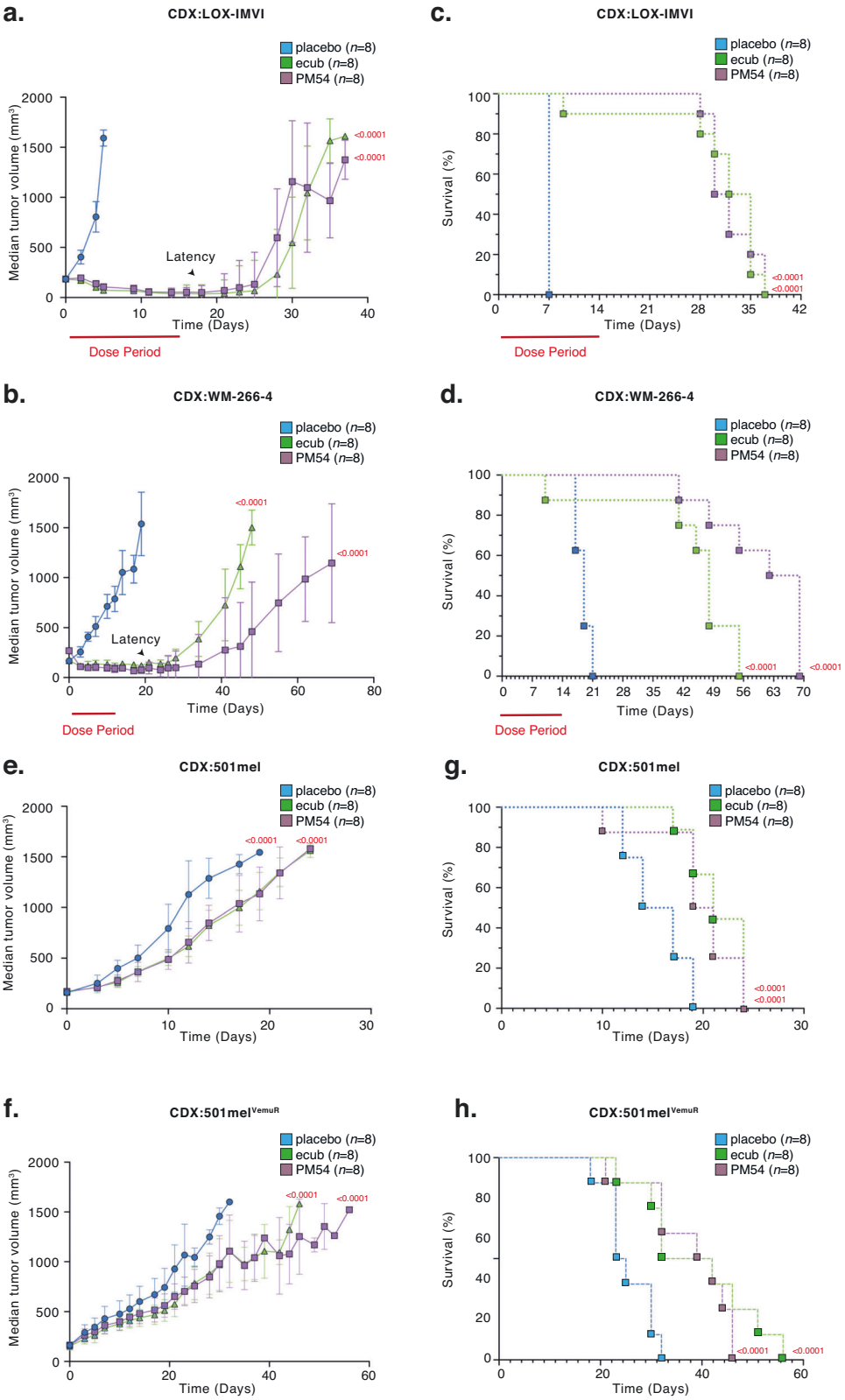

lurbinectedin. These cells were derived from metastatic melanoma (501mel), metastatic non-SCLC (A549) (GSE179074[35]) and metastatic SCLC (DMS53) (GSE179074[35]), the latter being a cancer type for which lurbinectedin has recently gained clinical approval. This analysis revealed that a common set of 642 genes underwent significant downregulation upon drug exposure (Fig. 5a and Supplementary Data 3). GO analysis revealed once again a strong enrichment of genes involved in transcriptional regulation (Supplementary Fig. 8a and Supplementary Data 2 and 8), with notable downregulated genes including ubiquitous transcription factors/coactivators (such as *CDK7*, *CDK12*, *CDK13*, *E1A-associated cellular p300 (EP300)*, *CREB-binding protein* (*CBP*)) and genes coding for Mediator complex subunits (such as *CDK8* and *MED13*). These results were confirmed in differentiated and undifferentiated melanoma cells by immunoblotting (Fig. 5b). Notably, in vivo

Fig. 4 | Potent in vivo effects of synthetic ecteinascidins. a,**b** Indicated CDX models ($n = 10$ at the beginning of the experiment) from LOX-IMVI **a** or WM-266-4 **b** melanoma cells were treated with placebo, ecubectedin or PM54 at 1.2 mg/kg once a week for 3 consecutive weeks (on days 0, 7 and 14) and tumor volumes were measured. Results are shown as mean values ± SD for "*n*" mice. The red bar indicates the dose period. The latency phase is indicated by an arrow. Logrank (Mantel–Cox) test was used to determine the *p*-values. Source data are provided as a Source Data file. **c**, **d** Indicated CDX models ($n = 10$ at the beginning of the experiment) from LOX-IMVI **c** or WM-266-4 **d** melanoma cells were treated weekly with Placebo, ecubectedin or PM54 at 1.2 mg/kg and survival was assessed. Results are shown as mean values ± SD for "*n*" mice. The red bar indicates the dose period. The latency phase is indicated by an arrow. Logrank (Mantel–Cox) test was used to determine the *p*-values. Source data are provided as a Source Data file. **e**, **f** Indicated CDX models ($n = 8$ at the beginning of the experiment) from 501mel **e** or 501mel^{VemuR} **f** melanoma cells were treated once with Placebo, ecubectedin or PM54 at 1.2 mg/kg and tumor volumes were measured. Results are shown as mean values ± SD for "*n*" mice. Logrank (Mantel–Cox) test was used to determine the *p*-values. Source data are provided as a Source Data file. **g**, **h** Indicated CDX models ($n = 8$ at the beginning of the experiment) from 501mel **g** or 501mel^{VemuR} **h** melanoma cells were treated once with Placebo, ecubectedin or PM54 at 1.2 mg/kg and survival was assessed. Results are shown as mean values ± SD for "*n*" mice. Logrank (Mantel–Cox) test was used to determine the *p*-values. Source data are provided as a Source Data file.

experiments utilizing melanoma CDXs also demonstrated a rapid down-regulation of these genes, together with lineage-specific master transcription factors such as *MITF*, *SOX10* or *PAX3* following short-term treatments with synthetic ecteinascidins (Fig. 5c).

Ubiquitous transcription factors/coactivators and the mediator complex are pivotal in driving oncogenic expression in cancer cells by activating genes dependent on SEs. Therefore, in an effort to identify SEs in our melanoma cell models, we performed Cut&Tag assays targeting H3K27ac and BRD4 in differentiated and undifferentiated cells (501mel and MM029, respectively). Using the Rank Ordering of Super-Enhancers (ROSE) algorithm and cross-referencing the list of SEs identified from the Cut&Tag on H3K27ac and that on BRD4, we identified 533 and 347 bona fide SEs in differentiated and undifferentiated metastatic melanoma cells, respectively (Supplementary Fig. 8b,c and Supplementary Data 4). Subsequently, we identified by ROSE 1,255 and 951 genes putatively regulated by these bona fide SEs, in differentiated and undifferentiated melanoma cells, respectively (Supplementary Fig. 8d and Supplementary Data 4). Although 261 SE-dependent genes were shared between differentiated and undifferentiated cells, most SE-dependent genes seemed to be cell-state-specific. We next crossed these data with the list of downregulated genes in both differentiated and undifferentiated metastatic melanoma cells following treatments with synthetic ecteinascidins and observed a significant enrichment of SE-dependent genes among those down-regulated genes (Fig. 5d). This was also observed in vivo, where SE-dependent oncogenes such as *MITF*, *SOX10*, *SAMMSON* or *MYC* were strongly downregulated upon treatment with synthetic ecteinascidins (Fig. 5c).

Synthetic ecteinascidins target transcriptionally active, CpG-rich genomic regions

We next sought to map the genome-wide binding sites of synthetic ecteinascidins in melanoma cells. Using bioactive biotinylated versions of lurbinectedin and PM54 (Bio-lurbi and Bio-PM54) (Table 1), we conducted an in situ mapping of our compounds to genomic DNA using Chem-map[41]. We performed three biological replicates per compound, using both differentiated or undifferentiated melanoma cells (501mel and MM029, respectively), observing a high reproducibility with Spearman correlations exceeding 0.7 (Supplementary Fig. 9a) Our analysis revealed approximately 30,000 drug-binding sites in differentiated and 15,000 in undifferentiated cells (Fig. 6a and Supplementary Data 5). Notably, approximately 75 % of the identified drug-binding sites were found to be located in gene regions, with promoter (~25–34 %) and intronic (~32–35%) binding frequencies being consistent for both Bio-lurbi and Bio-PM54, in both cell types (Fig. 6b and Supplementary Fig. 9b). Overall, we observed a highly significant correlation between drug-bound gene promoters and genes down-regulated by the drugs (Fig. 6c and Supplementary Fig. 9c). Genome-wide, peaks of synthetic ecteinascidins predominantly co-localized with the transcriptionally active H3K27ac chromatin mark, RNAPII, BRD4 and positive ATAC-seq signals, and not with the repressive H3K27me3 chromatin mark (GSE205463[42]) (Fig. 6d and Supplementary Fig. 9d). Indeed, between 80 and 90 % of the synthetic ecteinascidins binding sites in 501mel and MM029 cells exhibited substantial overlaps with ATAC-seq signals (Fig. 6e and Supplementary Fig. 9e–g). Furthermore, our genome-wide analysis indicated that over 35% of synthetic ecteinascidins binding sites in 501mel cells and over 45 % in MM029 cells exhibited substantial overlaps with CpG islands (Fig. 6f and Supplementary Fig. 9h). Most of the CpG islands bound by the drugs were located in open chromatin regions, positive for ATAC-seq signal (Fig. 6g and Supplementary Fig. 9i). These data underscore the preferential binding of synthetic ecteinascidins to transcriptionally active genomic sites such as promoter regions, and suggest that they target the CpG islands located within these sites.

Synthetic ecteinascidins exhibit distinct patterns of chromatin binding associated with cell phenotypes

We subsequently integrated the chem-map data and observed a robust overlap (~80%) between the promoter regions bound by Bio-lurbi and those bound by Bio-PM54 in a given cell type (Fig. 7a, left panel). Notably, among the promoters bound by synthetic ecteinascidins, a significant fraction demonstrated concurrent binding by the two drugs in both cell types (Fig. 7a, right panel). This included promoters that regulate the expression of ubiquitous transcription factors/coactivators or Mediator subunits (Supplementary Data 6). In these promoters, such as those regulating expression of *EP300* or *CDK7*, a pronounced overlap was observed between the binding sites of synthetic ecteinascidins and CpG islands, H3K27ac, RNAPII and ATAC-seq signal (Fig. 7b).

Apart from the commonality in drug-bound promoters depicted above, each melanoma cell type also exhibited a subset of distinct and unique binding sites associated with its specific cellular phenotype. We observed a strong overlap between cell-state-exclusive binding sites and cell-state-specific H3K27ac sites at the corresponding genomic loci, once again suggesting a connection between drug binding and open chromatin (Fig. 7c and Supplementary Fig. 10a–d). In these specific binding sites, we identified sets of promoters which indeed demonstrated exclusive activity in either differentiated or undifferentiated cells. For instance, synthetic ecteinascidins bound to the promoter of the lineage-specific master transcription factor *MITF* gene only in differentiated cells, where it is highly expressed (Fig. 7d). Conversely, the promoter regulating the *Baculoviral IAP repeat-containing protein 3* gene (*BIRC3*), an inhibitor of apoptosis expressed only in undifferentiated melanoma cells, was occupied by synthetic ecteinascidins in undifferentiated but not in differentiated cells (Fig. 7e).

When examining the deposition of synthetic ecteinascidins along the *MITF* gene, drug-binding to its SE was also observed (Fig. 7d). In agreement, almost all (~95 %) of the bona fide SEs identified by ROSE in differentiated and undifferentiated cells were directly bound by the compounds (Fig. 7f). To gain a global understanding of the interplay between synthetic ecteinascidins and enhancer activity, we used the Active-By-Contact (ABC) model[43] to integrate our ATAC-seq, Cut&Tag, and RNAseq data with publicly available HiC data obtained in

https://doi.org/10.1038/s41467-024-55667-z

differentiated melanoma cells (GSE105491[44]). We generated a genome-wide annotation of all active cis-candidate regulatory regions (cCRE) directly implicated in activating gene expression in 501mel cells (Supplementary Fig. 11a). Based on differential gene expression data, this model thus allowed the prediction of interactions between active enhancers and genes that were either positively or negatively

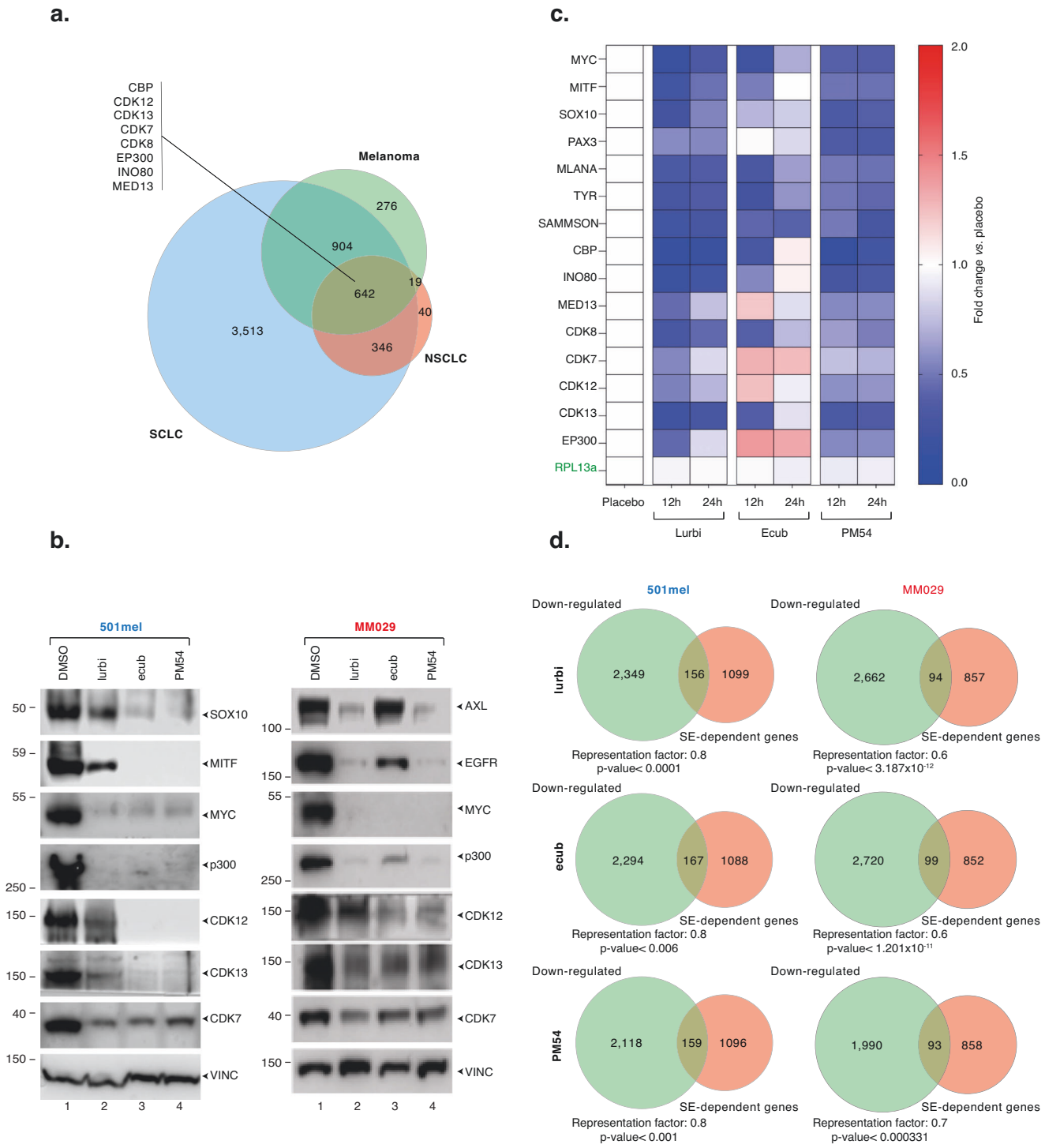

Fig. 5 | Synthetic ecteinascidins inhibit the expression of SE-dependent genes. **a** Venn diagram showing the overlap of genes down-regulated in melanoma (GSE256100), SCLC (GSE179074) and NSCLC (GSE179074), following treatment with lurbinectedin. **b** Differentiated 501mel (left) or undifferentiated MM029 (right) melanoma cells were treated with synthetic ecteinascidins as indicated (5xIC50 concentration, 24 h) and protein lysates were immuno-blotted for proteins as indicated. Molecular mass of the proteins is indicated (kDa). Source data are provided as a Source Data file. This experiment was repeated independently three times with similar results. **c** CDXs from 501mel cells ($n = 3$) were treated with a single dose of lurbinectedin, ecubectedin or PM54 at 1.2 mg/kg and tumors were collected 12 or 24 h later. Heatmap shows average placebo-normalized expression of the indicated genes obtained by qRT-PCR analysis. RPL13a is a housekeeping gene. **d** Venn diagram showing the overlap of genes downregulated by synthetic ecteinascidins, as indicated, in 501mel (left) or MM029 cells (right) (10xIC50 concentration, 8 h) ($n = 3$) and SE-dependent genes identified in these cells using H3K27ac- and BRD4-profiling by Cut&Tag and the ROSE algorythm[42]. Representation factor and hypergeometric p-value are indicated and were determined using Graeber lab software. Hypergeometric distribution test was used to determine the p-values.

https://doi.org/10.1038/s41467-024-55667-z

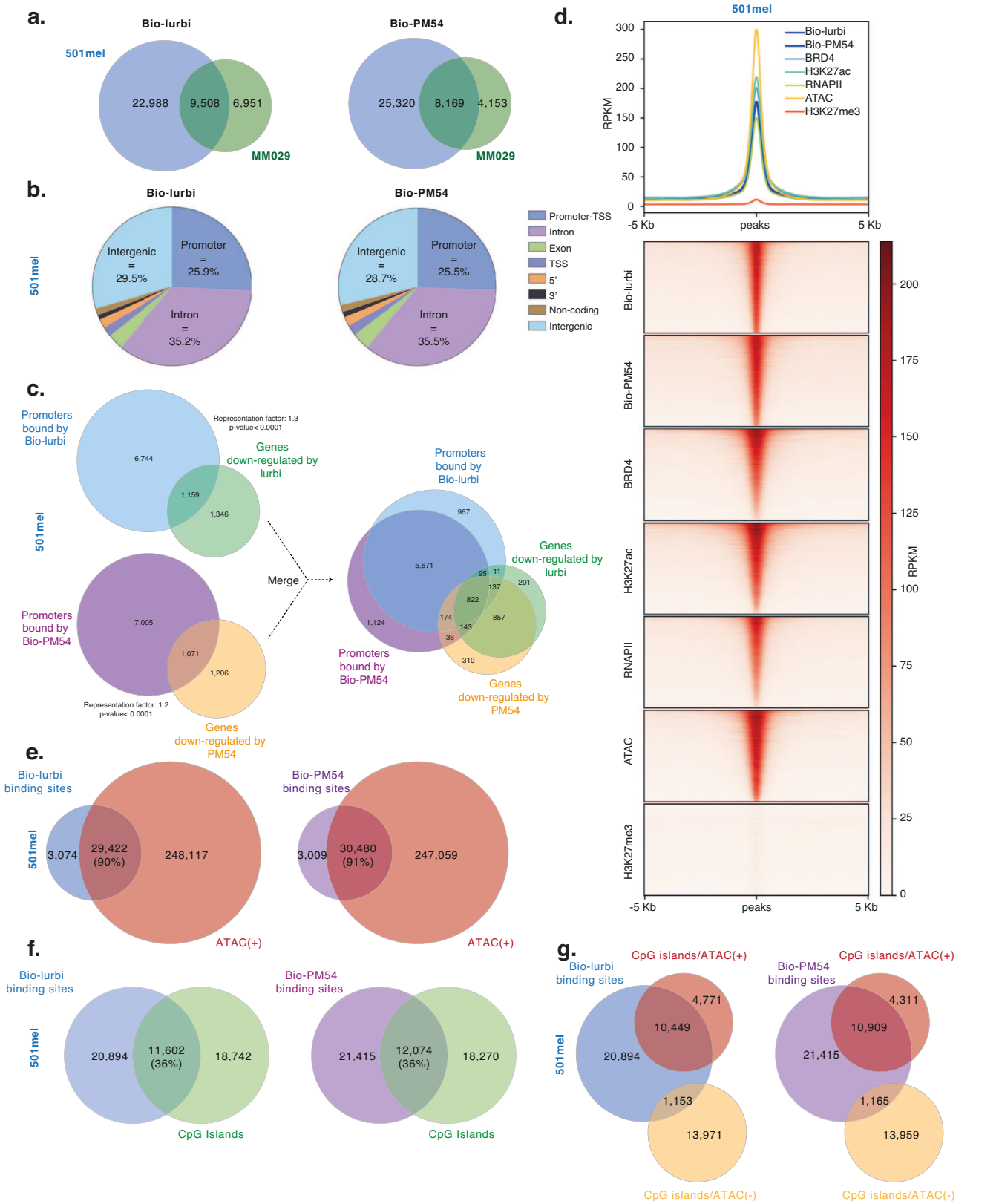

impacted by treatment with synthetic ecteinascidins. Notably, 4436 enhancers were inferred to be in contact with the promoters of genes down-regulated by treatment with synthetic ecteinascidins, such as the SE controlling SOX10 expression (Supplementary Fig. 11b), while only 736 enhancers were inferred to be in contact with promoters of genes up-regulated by the same treatments (Supplementary Data 6). Enhancers controlling the expression of down-regulated genes tended to be characterized by a higher ABC-score (higher enhancer activity) and contacted more genes than enhancers controlling expression of up-regulated genes (Supplementary Fig. 11c). In conclusion, the ABC model indicates that genes under the dependence of strong enhancers, such as SEs, might be particularly vulnerable to synthetic ecteinascidins, and that active enhancer-promoter interactions might be weakened by drug binding.

Fig. 6 | Synthetic ecteinascidins bind to CpG-rich sequences located in open chromatin regions. a Venn diagram of drug-binding sites (Bio-lurbi in the left and Bio-PM54 in the right) in 501mel vs. MM029 cells ($n = 3$). **b** Pie chart showing the distribution of annotated peaks (in percentages) for Bio-lurbi (top) and Bio-PM54 (bottom) all over the genome (hg19) in 501mel cells ($n = 3$). **c** Left panel**:** Venn diagram ($n = 3$) between promoters bound by Bio-lurbi or Bio-PM54 and genes down-regulated by lurbinectedin or PM54 in 501mel cells. Right panel: the two Venn diagrams ($n = 3$) were merged. Representation factor and hypergeometric *p*-value are indicated and were determined using Graeber lab software. Hypergeometric distribution test was used to determine the *p*-values. **d** Upper panel**:** Metaplot distribution ($n = 3$) of Bio-lurbi, Bio-PM54, BRD4, RNAPII, H3K27ac, H3K27me3 enrichment and ATAC-Seq signals in a ± 5 kb window around the occupied DNA binding sites of Bio-lurbi in differentiated 501mel cells. Lower panel: Heatmap profiles representing the read density clusterings obtained with seqMINER for the DNA-occupied sites of Bio-lurbi in differentiated 501mel cells relative to Bio-PM54, BRD4, RNAPII, H3K27ac, H3K27me3 enrichments and ATAC-Seq signals. Peak order is determined by Bio-lurbi and identical for all clusterings. **e** Venn diagram ($n = 3$) between Bio-lurbi (left) or Bio-PM54 (right) binding sites and positive ATAC-seq peaks (indicative of chromatin open regions) in differentiated 501mel cells. **f** Venn diagram ($n = 3$) between Bio-lurbi (left) or Bio-PM54 (right) binding sites and human CpG islands in differentiated 501mel cells. **g** Venn diagram ($n = 3$) between Bio-lurbi (left) and Bio-PM54 (right) binding sites in differentiated 501mel cells and human CpG islands. Human CpG islands are divided into those found in open chromatin regions (CpG islands/ATAC(+)) and those found in closed chromatin regions (CpG islands/ATAC(−)).

Collectively, these findings suggest that synthetic ecteinascidins impact SE-mediated oncogenic transcription by binding to and inhibiting the activity of the promoters of ubiquitous transcription factors/coactivators enriched at SEs, and potentially by directly targeting the enhancer/SEs driving oncogenic expression.

Synthetic ecteinascidins disrupt coactivator condensation at SEs

It was demonstrated that SE-enriched transcriptional coactivators such as BRD4 or the MED1 subunit of the Mediator complex form discrete nuclear puncta at SEs ex vivo to ensure robust expression of SE-dependent genes[9]. Based on the above data, we hypothesized that synthetic ecteinascidins could disrupt these condensates. Immunofluoresence revealed nuclear puncta for BRD4 that co-localized with the SE-specific histone mark H3K27ac in differentiated or undifferentiated melanoma cells (Supplementary Fig. 12a). Synthetic ecteinascidins disrupted BRD4 and MED1 puncta in both types of cells, similar to what was observed with 1,6-hexanediol, widely used to disorganize liquid-like condensates[9] (Fig. 8a, b and Supplementary Fig. 12b). In contrast, treatment with dacarbazine, an alkylating compound that causes DNA damage and that is clinically used in the treatment of melanoma, did not affect BRD4 and MED1 puncta (Fig. 8a, b and Supplementary Fig. 12b). Treatment with the MEKi trametinib even resulted in a significant increase in BRD4 and MED1 puncta, likely due to the reprograming of enhancer/SE formation observed in melanoma cells following MEKi treatment, leading to hyperdifferentiation[45]. In agreement with these observations, trametinib and dacarbazine did not decrease the expression of SE-dependent genes such as *MITF* and *SOX10* in differentiated cells (MEKi even increased their expression) or *AXL* and *EGFR* in undifferentiated cells (Supplementary Fig. 12c,d). ChIP-qPCR was used to further reveal that together with the inhibition of expression observed above, the level of H3K27ac and BRD4 was significantly reduced at the SEs regulating the expression of *MITF*, *SOX10*, *EGFR* or *AXL*, upon short-term treatment with synthetic ecteinascidins (Fig. 8c, d and Supplementary Fig. 12e,f). Note also that the level of H3K27ac was unaffected at the promoter of the 60S Ribosomal Protein L13a (RPL13a) housekeeping gene in these conditions (Supplementary Fig. 12g,h). Collectively, these results indicate that synthetic ecteinascidins disrupt the integrity of transcriptional condensates, consequently leading to the inactivation of SEs. They also highlight the specific mechanism of action of these drugs compared to current clinical treatments.

Synthetic ecteinascidins induce waves of transcriptional inhibition in melanoma and SCLC cells

The data above imply a model in which the inhibition of ubiquitous transcription factors/coactivators induces the inhibition of SE-dependent oncogenes. To test this model, we conducted kinetic analyzes, revealing that transcription factors/coactivators were down-regulated before SE-dependent genes in melanoma cells (Fig. 9a, b and Supplementary Fig. 13a,b). We explored whether a similar mechanism could occur in SCLC following treatment with synthetic ecteinascidins. We observed that transcription factors/coactivators were down-regulated very early in SCLC DMS53 cells upon treatments with synthetic ecteinascidins, followed by the inhibition of SCLC-specific SE-dependent genes such as *Achaete-scute homolog 1* (*ASCL1*), *B-Cell Leukemia/Lymphoma 2* (*BCL2*), *MYC*, *Neurogenic Differentiation Factor 1* (*NEUROD1*) or *TEAD1* genes (Fig. 9c). In agreement, a significant enrichment of SE-dependent genes was observed among those down-regulated upon treatment with synthetic ecteinascidins in these cells (Supplementary Fig. 13c). While the ChIP-qPCR data in Fig. 8 cannot be generalized to all dysregulated genes in melanoma, we extended this analysis to SCLC using published data (GSE179074[35]). We re-analyzed these data by focusing on three groups of genes with H3K27ac peaks at their TSS: those commonly down-regulated in melanoma, SCLC, and NCLC (348 genes); SCLC-specific SE-dependent genes (424 genes); and genes that were commonly unaffected (1434 genes) (Supplementary Data 7). ChIP-seq for H3K27ac, performed before and after treatment with lurbinectedin (GSE195663[35]), revealed a loss of this active transcriptional mark at the promoters of commonly down-regulated genes (e.g., *CDK8*) and SCLC-specific super-enhancer-dependent genes (e.g., *MYC*) (Fig. 9d, e). Notably, H3K27ac was significantly less affected at the promoters of genes whose expression was unaffected by lurbinectedin, such as the housekeeping gene *RPL13a*. Overall, these data suggest that synthetic ecteinascidins induce an initial inactivation of promoters regulating the expression of transcription factors and coactivators, which triggers a secondary inactivation of the promoters of SE-dependent oncogenes.

Discussion

Metastatic melanoma cells exhibit significantly higher mutational burdens compared to other cancer types, potentially leading to proportional dysregulation of gene expression patterns. Furthermore, the well-documented cell-state plasticity of melanoma cells underscores their robust reliance on tightly regulated oncogenic gene expression programs. This cancer type, therefore, serves as an ideal model for investigating the clinical relevance and therapeutic potential of targeting oncogenic transcriptional addiction. Comparative analyzes were conducted to evaluate the impact of three synthetic ecteinascidins relative to clinically utilized MAPKi agents. Notably, metastatic undifferentiated melanoma cells displaying inherent resistance to MAPKi/immunotherapy, as well as in vitro engineered hyperpigmented cells with acquired MAPKi resistance[14], exhibited comparable sensitivity to the three synthetic ecteinascidins at low nanomolar concentrations. Single-cell sequencing has unveiled additional cell states within melanoma tumors, such as interferon-active melanoma cells that emerge during the minimal residual disease phase, post-treatment with MAPKi[19,30]. The significance of these cells in the context of resistance to treatment has been significantly underestimated. In an attempt to mimic these cell subpopulations in vitro, we have generated pseudo-interferon-active melanoma cells by treatment with interferon-γ. Intriguingly, these pseudo-interferon-active melanoma

https://doi.org/10.1038/s41467-024-55667-z



cells exhibited sustained sensitivity to synthetic ecteinascidins while acquiring resistance to MAPKi (Supplementary Fig. 14 and Table 1). In vivo, we observed significant decreases in mitotic indexes and increases in cell death and overall survival in four different melanoma CDX models, including MAPKi-resistant CDXs. Our data demonstrate that synthetic ecteinascidins exhibit high cytotoxic impact both in vitro and in vivo on the most common melanoma cell phenotypes, as well as on drug-tolerant cell populations emerging during the minimal residual disease phase.

Our results elucidate the mechanisms of action of synthetic ecteinascidins, highlighting their common features and revealing some notable differential molecular effects. Low nanomolar doses of synthetic ecteinascidins consistently reduced the proliferation and invasive capacities of metastatic melanoma cells while inducing

Fig. 7 | Synthetic ecteinascidins exhibit distinct patterns of chromatin binding associated with cell phenotypes. a Left panel: Venn diagrams ($n = 3$) between promoters bound by Bio-lurbi and Bio-PM54 in 501mel (top) and MM029 (bottom) cells. Right panel: the two Venn diagrams were merged. **b** Gene tracks of Bio-lurbi, Bio-PM54, RNAPII, H3K27ac occupancy, ATAC-seq and RNA-Seq signals at CDK7 (left) or EP300 (right) loci in 501mel or MM029 cells. RNA-Seq signals show that these genes are expressed in both 501mel and MM029 melanoma cells. In blue, drug binding at promoters is highlighted. Localization of CpG islands is shown. **c** Left panel: Venn diagrams ($n = 3$) comparing genomic bindings sites uniquely bound by Bio-lurbi in either 501mel or MM029 cells with H3K27ac peaks found exclusively in either 501mel or MM029 cells. Right panel: Venn diagrams comparing genomic bindings sites uniquely bound by Bio-PM54 in either 501mel or MM029 cells with H3K27ac peaks found exclusively in either 501mel or MM029 cells. We considered different peaks as overlapping if there was at least 1 bp of overlap. **d** Gene tracks of Bio-lurbi, Bio-PM54, RNAPII, H3K27ac occupancy, ATAC-seq and RNA-Seq signals at the MITF locus in 501mel or MM029 cells. RNA-Seq signals show that this gene is only expressed in differentiated 501mel cells. The red square indicates the SE regulating the expression of MITF. In blue, drug binding at the promoter is highlighted. In red, drug binding at the SE is highlighted. Localization of CpG islands is shown. Note that MITF-M isoform is expressed in melanoma. **e** Gene tracks of Bio-lurbi, Bio-PM54, RNAPII, H3K27ac occupancy, ATAC-Seq and RNA-Seq signals at the BIRC3 locus in 501mel or MM029 cells. RNA-Seq signals show that this gene is only expressed in undifferentiated MM029 melanoma cells. In blue, drug binding at the promoter is highlighted. Localization of CpG islands is shown. **f** Upper panel: Venn diagrams ($n = 3$) comparing all genomic bindings sites commonly bound by Bio-lurbi and Bio-PM54 and bona fide super-enhancers identified in 501mel cells. Lower panel: Venn diagrams comparing all genomic bindings sites commonly bound by Bio-lurbi and Bio-PM54 and bona fide super-enhancers identified in MM029 cells.

apoptosis and blocking the cell cycle in the G2/M phase. Drug treatments also led to the significant disruption of oncogene expression. Importantly, the transcriptional effects of the compounds appeared to exhibit a high degree of specificity for distinctly overexpressed oncogenes depending on the melanoma cell state. For instance, while the expression of housekeeping genes was unaffected in 2- or 3-D conditions by short-term drug treatments, lineage-specific drivers of proliferation such as MITF, SOX10 or PAX3 were strongly inhibited specifically in differentiated cells. In undifferentiated cells, different genes were affected, such as the key regulators AXL or EGFR, the anti-apoptotic protein BIRC3 or the cell-type master transcription factors FOSL2 and TEAD4. These observations arguably reveal the most interesting feature of these next-generation compounds: synthetic ecteinascidins appear to specifically inhibit the distinct oncogenic transcription programs on which a given cancer cell subpopulation depends. Thus, this unique mechanism of action differentiates synthetic ecteinascidins from conventional chemotherapeutic DNA-binders/DNA-modifiers, such as platinum derivatives or dacarbazine, which induce DNA damage uniformly across the genome. Moreover, the efficacy of synthetic ecteinascidins does not depend on the phenotypic nature of the melanoma cell, a feature that differentiates these drugs from conventional MAPKi therapies and immunotherapies[20].

Mechanistically, our results highlight a multifaceted mechanism of action by which synthetic ecteinascidins impede oncogenic transcription. Synthetic ecteinascidins bind to promoter/enhancer regions of genes encoding ubiquitous transcription factors/coactivators, usually strongly enriched at SEs, leading to their rapid inhibition. This effect is likely potentiated by the fact that promoters/enhancers of genes encoding lineage-specific master transcription factors such as MITF or SOX10 are also heavily bound by synthetic ecteinascidins in melanoma cells. These master regulators are known to bind SEs to form autoregulatory loops that constitute the core transcriptional regulatory circuitries of cancer cells. The disruption of these oncogenic expression loops, coupled with the strong binding of synthetic ecteinascidins to SEs themselves, albeit with uncertain biological consequences, potentially ensures the robust inhibition of SE-driven oncogenic transcription. Importantly, these observations extend beyond melanoma cells, as SE-driven transcription was also inhibited in SCLC cells exposed to synthetic ecteinascidins, establishing these molecules as potential universal pan-disruptors of SEs. Overall, the inhibition of SE-driven oncogenic transcription has a potent cytostatic/cytotoxic impact on cancer cells, as demonstrated in vivo by the inhibition of cell proliferation and induction of apoptosis. In a second line of attack, synthetic ecteinascidins induce DNA breaks that persist over time and that synergize with transcription inhibition to trigger cell death.

Delving deeper into the transcriptional effects elicited by the three compounds, we observed that while the gene expression changes elicited by lurbinectedin and ecubectedin greatly overlapped, the transcriptional effects of PM54 significantly diverged. Notably, PM54 treatments deregulated fewer genes than lurbinectedin or ecubectedin while eliciting the same cytostatic and cytotoxic effects, potentially representing a clinical benefit. Although the exact mechanism explaining this difference is yet to be determined, it may be related to the fact that the moiety modified in PM54 vs. lurbinectedin is located in the area of the molecule described as interacting with DNA binding proteins/transcription factors[46]. Such a differential interaction between the drug and transcription factors might result in fewer systemic gene expression disruptions and, thus, fewer unwanted secondary effects, while still potently targeting oncogenic SE-dependent gene expression, leading to cancer cell death. Consequently, Phase I clinical trials for PM54 in advanced solid tumors, including melanoma, were initiated (ClinicalTrials.gov Identifier: NCT05841563, EudraCT Number 2022-002031-65).

Collectively, our data provide a comprehensive overview of the cellular and molecular effects of a potential therapeutic approach to melanoma and other transcriptionally-addicted cancers based on SE-dependent oncogenic inhibition. The current study further illuminates the intricacies of gene expression dependencies of different melanoma cell subpopulations and their molecular responses to transcriptional disruptions. This preclinical work might justify the clinical testing of synthetic ecteinascidins as a second-line melanoma treatment following MAPKi/immunotherapy relapse, but it also highlights the potential benefits of further exploring the effects of additional structural analogs. Finally, recent observations demonstrated that synthetic ecteinascidins, such as lurbinectedin, synergize with immune checkpoint blockade and stimulates proliferation of CD4+ and CD8 + T cells. These immune-modulatory functions make synthetic ecteinascidins a potential platform for immunotherapy combination in melanoma[47,48].

Methods

All animal experimental procedures were reviewed and approved by an Internal Ethical Committee and by "O.H. Universidad Miguel Hernandez de Elche" and "O.H. Hospital General Universitario Gregorio Marañón", and, finally, authorized by "Comunidad Autónoma de Madrid, CAM" (regional Institutional Animal Care and Use Committee), reference PROEX 042/16 and PROEX 285.7/23. All experimental procedures were performed in accordance with national and international laws and policies: Spanish directive RD 53/2013 and EU Directive 2010/63/EU. Animals were euthanized through the administration of an overdose of a general anesthetic when their tumors reached ca. 1500 mm3 and/or severe necrosis was seen. Treatments which produced >20 % lethality and/or 20 % net body weight loss were considered toxic and stopped.

Cell culture and treatment

When registered, cells used in this work are identified by a research resource identification number (RRID number (https://rrid.site)). Cell

https://doi.org/10.1038/s41467-024-55667-z

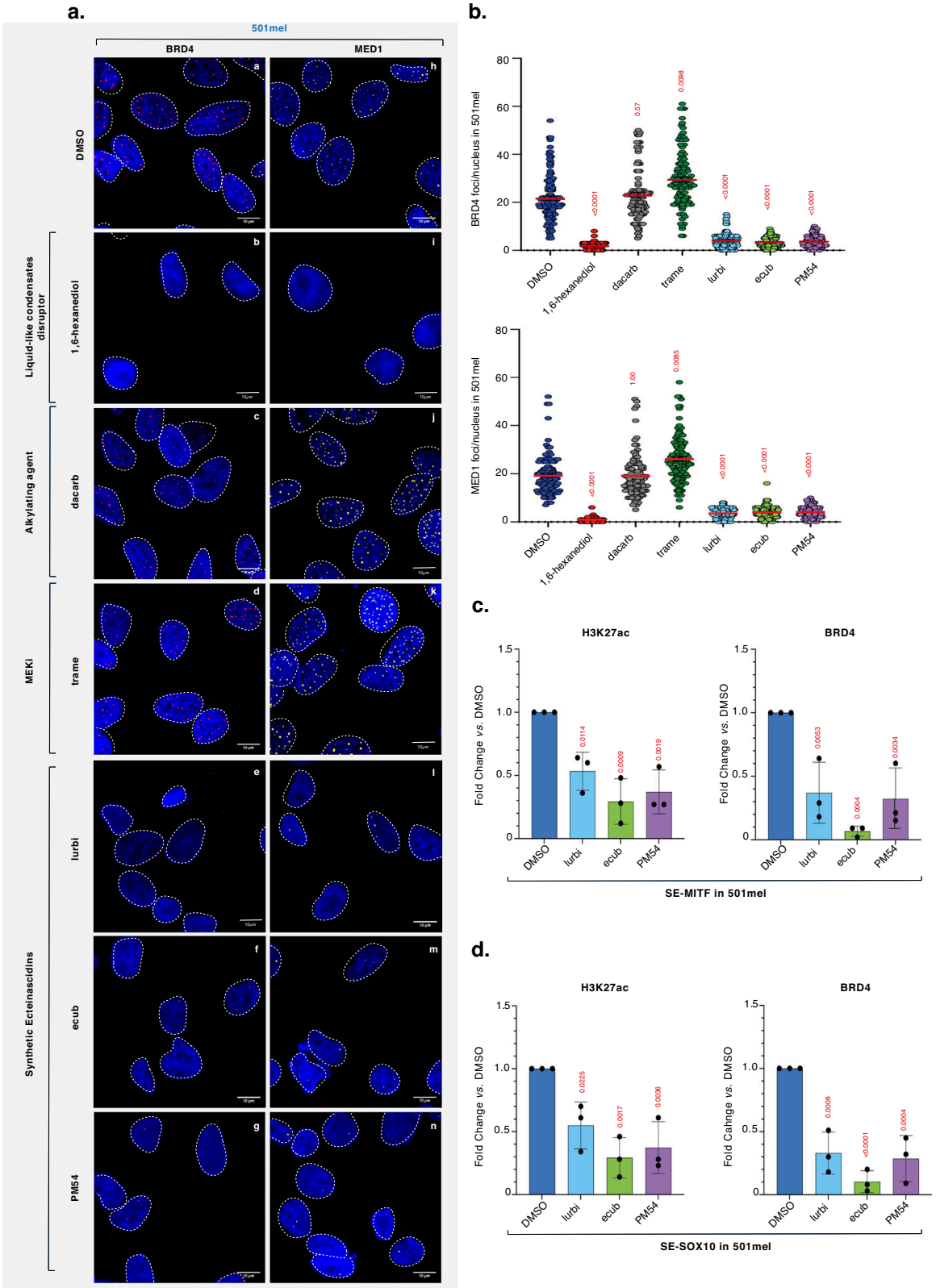

line identity, when applicable, was confirmed annually through STR profiling provided by ATCC's cell authentication service. Hermes3A, RRID:CVCL_VS10; DMS53, RRID:CVCL_1177; 501mel, RRID:CVCL_4633; SKMEL-28, RRID:CVCL_0526; IGR37, RRID:CVCL_2075; IGR39, RRID:CVCL_2076; WM266-4, RRID:CVCL_2765; LOX-IMVI, RRID:CVCL_1381; A549, RRID:CVCL_0023; HaCaT, RRID:CVCL_0038; MRC5, RRID:CVCL_0440. All cells were obtained from ATCC or collaborators, as indicated in Supplementary Data 8. Cells were grown at 37 °C in 5% CO_2 (10 % for Hermes 3A) and were regularly checked for mycoplasma contamination by the PluriCell East Platform (https://www.igbmc.fr/en/plateforms-and-services/services/pluricell-east). MM patient-derived short-term melanoma cultures (MM011, MM074, MM117, MM029, MM047, MM099) are derived from patient biopsies and were grown in HAM-F10 (Gibco, Invitrogen) supplemented with 10

Fig. 8 | Synthetic ecteinascidins disrupt transcription factor/coactivator condensates at SEs. a Representative confocal microscopy images ($n = 3$) of 501mel melanoma cells treated with either DMSO, the condensate disruptor 1,6-hexanediol (3% vol, 20 min), the MEKi trametinib (15 nM, 10 h), the DNA damaging agent dacarbazine (50 µM, 10 h) or the synthetic ecteinascidins (5xIC50, 10 h). Cells were immunostained with anti-BRD4 (red) or anti-MED1 (white) antibodies. Images of the cells were obtained with the same microscopy system and constant acquisition parameters for a given staining. Source data are provided as a Source Data file. Scale bar: 10 µm. **b** The numbers of MED1 and BRD4 foci per nucleus observed in 501mel cells following treatment with the drugs described above are shown ± SD for three biological triplicates. Red bars indicate mean integrated density. One-way ANOVA with post-hoc Tukey adjustment comparisons were used to determine the *p*-values (vs. DMSO). **c**, **d** ChIP-qPCR monitoring the fold change of H3K27ac mark or BRD4 protein at the SEs regulating MITF (left) or SOX10 (right) in mock- or synthetic ecteinascidin-treated (5xIC50, 10 h) differentiated 501mel cells. Error bars indicate mean values ± SD for three biological triplicates. One-way ANOVA with post-hoc Tukey adjustment comparisons were used to determine the *p*-values (vs. DMSO). Source data are provided as a Source Data file.

% Fetal Calf Serum (FCS), 25 mM HEPES, 5.2 mM GLUTAMAX and penicillin–streptomycin. Melanoma cell lines 501mel and SKmel28 were grown in RPMI w/o HEPES (Gibco, Invitrogen) supplemented with 10 % FCS and gentamycin. Vemurafenib-resistant cells (501mel^{VemuR} and MM074^{VemuR}) were additionally supplemented with 1.5 mM of vemurafenib. Melanoma IGR cell lines (IGR37 and IGR39) were grown in RPMI w/o HEPES (Gibco, Invitrogen) supplemented with 15 % FCS and gentamycin. Immortalized melanocytes Hermes-3A were grown in RPMI w/o HEPES supplemented with 10 % FCS, penicillin-streptomycin, 200 nM TPA (Sigma Aldrich), 200 p.m. Cholera Toxin (Sigma Aldrich), 10 ng/mL hSCF (Life Technologies), 10 nM EDN-1 (Sigma Aldrich) and 2 mM Glutamine (Invitrogen). HaCaT and MRC5 were grown in DMEM (1 g/L glucose) +10% FCS + Gentamycin 40 mg/ml. SCLC cell line DMS53 was grown in Waymouth's MB medium (Gibco, Invitrogen), supplemented with 10% FCS and gentamycin. 501mel, SKmel28, IGR and DMS53 cells were purchased from ATCC, MM and Hermes-3A cells were obtained from collaborators. Vemurafenib (PLX4032), trametinib (GSK1120212), dabrafenib (GSK2118436) and dacarbazine (S1221) were purchased from Selleckchem. 1,6-Hexanediol was obtained from Sigma Aldrich (88571). Lurbinectedin (PM1183), ecubectedin (PM14), and PM54 were obtained from PharmaMar S.A. Recombinant Human IFN-γ was obtained from Peprotech (300-02).

Different in vitro drug incubation periods were chosen depending on the nature of the experiments, considering that cell viability is reduced by 50% after 72 h of treatment with 1xIC50 concentrations. For assays studying the impact of the treatments on cancer cell phenotypes related to cancer cell death, such as the inhibition of cell proliferation, the induction of apoptosis and cell cycle blockage, we opted to refer to these same conditions (1xIC50, 72 h). To assess effects preceding cell death, such as impacts on clonogenicity and invasive capacities, a shorter incubation period was chosen (1xIC50, 48 h). For effects relating to gene expression, shorter incubation periods with higher drug concentrations (5xIC50, 12 h for RT-qPCRs; 10xIC50, 8 h for RNA-Seq and Chem-Map, 5xIC50, 24 h for Western Blotting and 5xIC50, 10 h for immunofluorescence and ChIP-qPCR) allowed us to study more closely the immediate and direct effects of the drugs on cancer cell transcriptomes and epigenomes. The used drug concentrations and treatment durations are stated in the respective figure legends.

Protein extraction and western blotting

For whole cell extracts, cells were rinsed once with cold PBS, before pelleting and resuspension in LSDB 0.5 M buffer (500 mM KCl, 50 mM Tris pH 7.9, 20% glycerol, 1% NP-40, 1 mM DTT, phosphatase inhibitor and protease inhibitor cocktail). Afterwards, cells were fully disrupted with 3 cycles of heat shock (liquid nitrogen followed by 37 °C water bath). Then, samples were centrifugated for 15 min at 11,000 g to remove cell debris. Lysates were subjected to SDS–polyacrylamide gel electrophoresis (SDS-PAGE) and proteins were transferred onto a nitrocellulose membrane. Membranes were incubated overnight 4 °C with primary antibodies in PBS + 5% milk powder + 0.01 % Tween-20. The membranes were then incubated with HRP-conjugated secondary antibody (Jackson ImmunoResearch) for 1 h at room temperature and visualized using the ECL detection system (GE Healthcare).

IC50 estimation

Cells were seeded at 5×10^3 cells/well in 96-well plates and treated with increasing concentrations of vemurafenib, dabrafenib, trametinib, lurbinectedin, ecubectedin, or PM54. After 72 h of incubation, cells were treated with PrestoBlue reagent (ThermoFisher) according to the manufacturer's instructions. The absorbance per well was measured with a CellInsight CX5 microplate reader (ThermoFisher). Determination of IC50 values was performed by nonlinear curve fitting using the Prism9 statistical software (GraphPad). To assess the effect of IFNγ on drug sensitivities, cells were pre-treated with IFNγ (20 ng/mL) for 24 h, before being treated as mentioned above, while maintaining IFNγ (20 ng/mL) in the medium.

Clonogenicity assay

Cells were drug-treated at IC50 concentrations during 48 h before seeding 1×10^3 or 2×10^3 cells in 6-well plates without drugs, where they grew for 10 days to allow for colony formation. Afterwards, cells were washed once with PBS, then fixed for 10 min with 4% Paraformaldehyde solution, and stained with Crystal Violet solution 0.2% for 15 min. The wells were finally washed twice with deionized water, air dried, scanned and analyzed with Fiji software to count the number of colonies.

Cell proliferation, apoptosis, and cell cycle analysis by flow cytometry

2×10^5 cells were seeded in 6-well plates and were incubated 24 h later with 1 µM of CellTrace Violet reagent (ThermoFisher) according to the manufacturer's instructions, immediately before rinsing and drug treatment at IC50 concentrations. After 72 h of incubation, cells were rinsed and incubated with AnnexinV-APC (BD Biosciences). Cell proliferation and apoptosis were detected on a BD LSRFortessaTM Flow Cytometer. Data were analyzed with FlowJo software. To define slow proliferating or apoptotic cells, we proceeded as follows: We considered that slow proliferating cells represented the 30 % of cells with the highest concentration of CellTrace Violet signal in the DMSO control. We then calculated the % of cells that had a signal greater than or equal to this value with drug treatment. For apoptotic cells, we considered the 20% of cells with the highest signal of AnnexinV-APC in the DMSO control.

For cell cycle analysis, 2×10^5 cells were seeded in 6 well plates. After 72 h of drug treatments at IC50 concentrations, cells were pelleted and fixed with 70% ethanol for 1 h at 4 °C. After 2 washes with cold PBS, cells were incubated with RNAseA and Propidium Iodide (PI, Biolegend) for 1 h in the dark, before being analyzed on a BD LSRFortessaTM Flow Cytometer. Data were analyzed with FlowJo software.

For apoptosis assays with 3D-grown melanoma cells, TrypLe Select 10x reagent (Gibco) was used to dissociate melanospheres to obtain single-cell suspensions. These cells were incubated with AnnexinV-APC (Biolegend) and PI. With bivariant dot plots, we distinguished between viable (AnnexinV− / PI −), early apoptotic (AnnexinV+ /PI −), late apoptotic (AnnexinV+ / PI +) and necrotic cells (AnnexinV− / PI +).

Boyden chamber invasion assay

2×10^5 cells were seeded inside Boyden Chamber inserts (Fisher Scientific) with 4% Matrigel (Corning) and covered with serum-free media.

https://doi.org/10.1038/s41467-024-55667-z

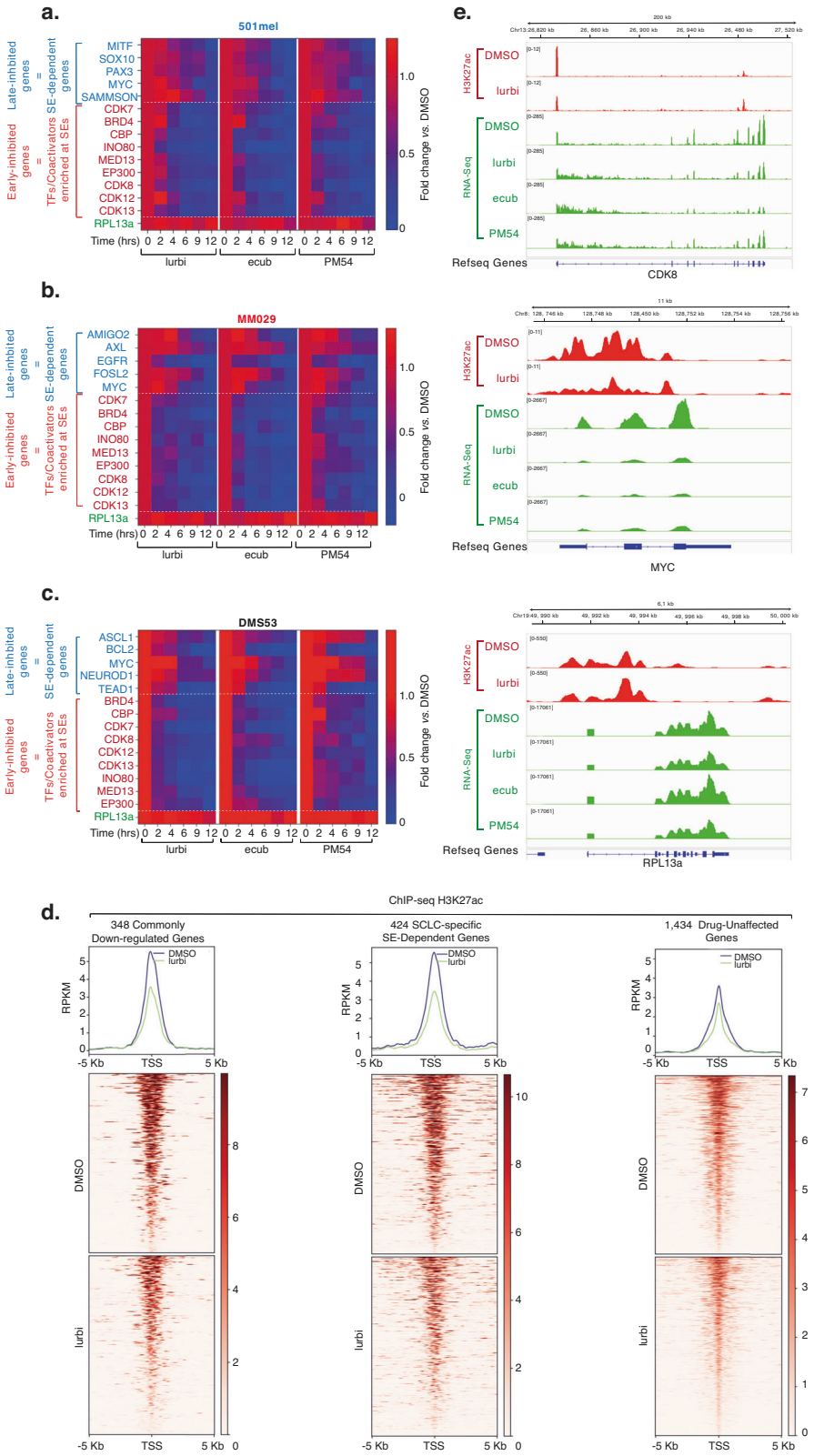

The inserts were placed in 24 well plates filled with complete medium. After 24 h, the inserts were washed once with PBS, fixed for 10 min with 4% paraformaldehyde solution, and stained with Crystal Violet solution 0.2% for 15 min. The wells were finally washed twice with deionized water, air dried, and photos were collected using an EVOS xl Core microscope. The pictures were analyzed with Fiji to assess the area of occupancy of the cells.

Melanosphere formation and viability assay

5×10^4 cells were seeded in ultra-low attachment hydrogel-layered 96 well plates (Corning 7007) in KO DMEM medium supplemented with 20 % KSR, AANE, 2 mM Glutamax, Penicillin/Streptomycin and 100 µM Beta-mercaptoethanol. To allow for melanosphere formation, cells were left to grow for 4 days before drug treatment.

Fig. 9 | Transcriptional inhibition waves induced by synthetic ecteinascidins in melanoma and SCLC cells. a, **b** Heatmap showing average 18S-normalized expression ($n = 3$) of the indicated genes in 501mel **a** and MM029 **b** cells treated with either lurbinectedin, ecubectedin or PM54 (5xIC50 concentration) for the indicated period of time. Results were obtained by RT-qPCR and are shown as relative expression compared to DMSO-treated cells. RPL13a is a housekeeping gene. **c** Heatmap showing average 18S-normalized expression ($n = 3$) of the indicated genes in DMS53 cells (SCLC) treated with synthetic ecteinascidins (5xIC50 concentration (IC50 = 0.11 nM for lurbinectedin, 0.16 nM for ecubectedin and 0.15 nM for PM54)) for the indicated period of time. Results were obtained by RT-qPCR and are shown as relative expression compared to DMSO-treated cells. RPL13a is a housekeeping gene. **d** Upper panel**:** This analysis ($n = 3$) focuses on three gene sets: (1) genes commonly downregulated after treatment in melanoma, SCLC, and NSCLC cells, (2) putative super-enhancer-dependent genes in DMS53 SCLC cells, and (3) genes whose expression exhibited a fold change between 0.9 and 1.1 relative to DMSO, which we considered unaffected by the treatment (GSE195663). These sets comprised 648, 424, and 8435 genes, respectively. From these genes, we selected only the genes presenting H3K27ac peaks located at their transcription start sites (TSS), yielding 348 genes for the commonly downregulated genes across the three cancers, 424 for the SCLC super-enhancer-dependent genes, and 1434 for the unaffected genes (see Supplementary Data 7). Metaplot distribution shows H3K27ac signal in a ± 5 kb window around the TSS of these three groups of genes in mock- or lurbinectedin-treated DMS53 cells (GSE179074). Lower panel: Heatmap profiles representing the read density clusters obtained with seqMINER for the H3K27ac signal. **e** Gene tracks showing H3K27ac occupancy and RNA-Seq signals ($n = 3$) at the CDK8 (top), MYC (middle) and RPL13a (bottom) loci in mock- or lurbinectedin-treated DMS53 cells.

To analyze melanosphere viability after drug treatment, cells were treated with CellTiterGlo reagent (Promega) according to the manufacturer's instructions. Luminescence signals were measured with a Centro XS LB 960 microplate reader (Berthold).

Immunofluorescence assays

After PBS-rinsing, cells grown on coverslips were fixed with 4% paraformaldehyde for 15 min. Cells were then permeabilized with PBS and 0.1% Triton X-100. Blocking was done with 10% BSA. Primary antibodies were incubated overnight at 4 °C, after which cells were stained for 1 h at room temperature with AlexaFluor-conjugated secondary antibodies diluted in PBS + 10% FCS (Life technologies) and stained with DAPI. For BRD4 and MED1 foci quantifications, image acquisition was performed on a TCS SP5 inverted confocal microscope (Leica), and foci were counted using the Cell Counter plugin of the Fiji software.

For immunohistology, tumors were grown as mentioned above and were extracted after 24 h following a single dose of placebo treatment or 1.2 mg/kg of ecubectedin or PM54. In parallel, untreated tumors were extracted. The tumors were fixed in 10% formalin and embedded in paraffin for histology. Slides prepared from 5 µm-thick paraffin sections were processed for antigen retrieval in 10 mM sodium citrate buffer (PH = 6.0) for 45 min at 95 °C in a water bath. The slides were cooled down at room temperature (RT) for 15 min. They were rinsed in PBS and then incubated in a humidified chamber for 16 h at 4 °C, with the primary antibodies diluted in PBS containing 0.1% (v/v) Tween 20 (PBST) to detect mitotic (pHH3-positive) and apoptotic (cleaved caspase 3-positive) cells. After rinsing in PBST, detection of the bound primary antibodies was performed for 1 h at room temperature in a humidified chamber using 555-conjugated secondary rabbit IgG antibody. The sections were then counterstained with DAPI to label nuclei. Stained sections were digitalized using a slide scanner (Nanozoomer 2.0-HT, Hamamatsu) and analyzed with the corresponding ND.View2 software.

Large 8-Bits digital scanned images of tumors stained for nuclei (10,000 to 30,000 nuclei per section) and pHH3 or cleaved caspase 3 were processed through an inhouse python (v3.8) algorithm to quantify positive cells. Basically, blue channels were proposed to a Cellpose2 model (deep learning model backboned by pytorch process) to segment nuclei. Subsequently, nuclei were analyzed for specific signals. For pHH3, a nucleus was considered positive if total pixels above 50 in intensity value exceeds 20% of nuclei surface (in 8 Bits image values range from 0 [no signal] to 255). Hence, we ensured that we did not consider unspecific background signals or insignificantly bright signals. The same procedure was applied to Caspase3 with pixel value set to 50 and minimal covered surface set to 30%. For each image, a ratio of positive cells/total nuclei was returned as the experimental variable. Statistics were produced using python's pingouin library (v0.5.3) with two-way ANOVA and post hoc tests being built-in functions.

High throughput sequencing

Supplementary Data 9 provides additional information about high throughput sequencing data, including among others, sequences quality controls, preprocessing, mapping, quantification and normalization methods, as well as size-number matched shuffled regions controls for Chem-Map data.

a. Bulk RNA-Seq and analysis. Library preparation was performed at the GenomEast platform at the Institute of Genetics and Molecular and Cellular Biology using TruSeq Stranded Total RNA Reference Guide - PN 1000000040499. Total RNA-Seq libraries were generated from 700 ng of total RNA using TruSeq Stranded Total RNA Library Prep Gold kit and TruSeq RNA Single Indexes kit A and B (Illumina, San Diego, USA), according to manufacturer's instructions. Briefly, cytoplasmic and mitochondrial ribosomal RNA (rRNA) was removed using biotinylated, target-specific oligos combined with Ribo-Zero rRNA removal beads. Following purification, the depleted RNA was fragmented into small pieces using divalent cations at 94 °C for 8 min. Cleaved RNA fragments were then copied into first strand cDNA using reverse transcriptase and random primers followed by second strand cDNA synthesis using DNA Polymerase I and RNase H. Strand specificity was achieved by replacing dTTP with dUTP during second strand synthesis. The double stranded cDNA fragments were blunted using T4 DNA polymerase, Klenow DNA polymerase and T4 PNK. A single 'A' nucleotide was added to the 3' ends of the blunt DNA fragments using a Klenow fragment (3' to 5'exo minus) enzyme. The cDNA fragments were ligated to double stranded adapters using T4 DNA Ligase. The ligated products were enriched by PCR amplification. Surplus PCR primers were further removed by purification using AMPure XP beads (Beckman-Coulter, Villepinte, France) and the final cDNA libraries were checked for quality and quantified using capillary electrophoresis. Libraries were sequenced on an Illumina HiSeq 4000 sequencer as single read 50 base reads. Image analysis and base calling were performed using RTA version 2.7.7 and bcl2fastq version 2.20.0.422.

Reads were preprocessed to remove adapter and low-quality sequences (Phred quality score below 20). After this preprocessing, reads shorter than 40 bases were discarded for further analysis. These preprocessing steps were performed using cutadapt version 1.10. Reads were mapped to rRNA sequences using bowtie version 2.2.8 and reads mapping to rRNA sequences were removed for further analysis. Reads were mapped onto the hg19 assembly of Homo sapiens genome using STAR version 2.5.3a. Gene expression quantification was performed from uniquely aligned reads using htseq-count version 0.6.1p1, with annotations from Ensembl version 75 and "union" mode. Only non-ambiguously assigned reads have been retained for further analyzes. Read counts have been normalized across samples with the median-of-ratios method proposed by Anders and Huber[12] to make these counts comparable between samples. Comparisons of interest were performed using the Wald test for differential expression[49] and implemented in the Bioconductor package DESeq2 version 1.16.1.

Genes with high Cook's distance were filtered out and independent filtering based on the mean of normalized counts was performed. *P*-values were adjusted for multiple testing using the Benjamini and Hochberg method[50]. Deregulated genes were defined as genes with log2(Fold change) > 1 or < −1 and adjusted *P*-value < 0.05.

Volcano plots were generated using the Prism9 statistical software (GraphPad). Heatmaps were generated using Morpheus (https://software.broadinstitute.org/morpheus). Venn diagrams were generated using DeepVenn (http://www.deepvenn.com/) and representation factors and hypergeometric *P*-values were determined using Graeber lab software (https://systems.crump.ucla.edu/hypergeometric/). GO Analysis was performed using ShinyGO. Metascape and enrichr analyzes can be found in Supplementary Data 9[51]. The number of assigned reads for each sample exceeds 15.10^6 (Supplementary Data 9), ensuring adequate coverage of the majority of expressed genes, with the exception of very low-expressed ones.

b. Chem-map and Cut&Tag. 501mel and MM029 cells were seeded and grown to sub-confluency in 15-cm plates before treatment for 8 h with DMSO, biotinylated lurbinectedin (Bio-lurbi) or biotinylated PM54 (Bio-PM54) at a concentration equivalent to 10xIC50 **(see** Table 1**)**. Chem-map (Biological triplicates) and CUT&TAG (Biological duplicates) were then performed using the Active Motif CUT&Tag-IT assay kit (53160, 53165), following the manufacturer's instructions. Briefly, 5×10^5 cells per condition were collected and washed twice before being bound to Concanavalin A beads and then incubated overnight at 4 °C with primary antibodies (1:50 dilutions). The following day, the corresponding guinea pig Anti-rabbit or rabbit Anti-mouse secondary antibodies were used at a 1:100 dilution in digitonin buffer and incubated at room temperature for 1 h. Subsequently, the CUT&Tag-IT Assembled pA-Tn5 Transposomes were incubated at room temperature for 1 h, and cells were resuspended in Tagmentation buffer and incubated at 37 °C for 1 h. The Tagmentation process was then stopped by adding EDTA and SDS. Protein digestion was performed by adding Proteinase K (10 mg/mL) and incubating at 55 °C for 1 h. The DNA was retrieved with DNA purification columns provided by the manufacturer and was then subjected to library preparation and PCR amplification and purified by 2 successive washes with SPRI beads. Libraries were sequenced on an Illumina NextSeq 2000 sequencer as paired-end 50 base reads. Image analysis and base calling were performed using RTA version 2.7.7 and BCL Convert version 3.8.4. The adapter sequence: CTGTCTCTTATA has been trimmed with cutadapt 1.18 with option: -a CTGTCTCTTATA -A CTGTCTCTTATA -m 5 -e 0.1 and Bowtie2[52] parameter: -N 1 -X 1000, was used for mapping to the human genome (hg19). After the mapping, reads overlapping with ENCODE blacklist V2 were filtered. Each de-duplicated read was extended to its fragment size. Tracks were normalized with RPKM method. Peak calling was performed using Macs2 2.2.7.1[53] in BEDPE and narrow mode. narrowPeaks from biological triplicate samples were then merged to a single master peak set. BEDtools[54] was used to calculate the read coverage for each peak and for each sample. Peaks were annotated using Homer[55] software with ucsc 6.4 gene annotation. Promoters were defined as regions extending from 1 kb upstream to 100 bp downstream of the TSS and the "Annotate peaks" Homer tool was then employed to identify the promoters bound by the drugs. Bigwig tracks were generated using bamCoverage from deepTools 3.5.4[56] and normalized with RPKM method. The differential analysis was performed using DESeq2[57]. Peak correlation analysis was performed using DiffBind[58] r package. Heatmap and average profile analyzes were performed using seqMINER[59] and deepTools. For Super-Enhancer calling, ROSE algorithm version 0.1 (http://younglab.wi.mit.edu/super_enhancer_code.html) was applied with default parameters (stitch distance = 12500[8,60]) using the BRD4 or H3K27ac peaks identified by MACS2 with the Cut&Tag experiments. TSS regions (Refseq TSS ± 1000 bp) were excluded. We defined SEs as 'bona fide' if they were positive for both H3K27ac and BRD4 signals. ROSE-gene mapper (Default parameters, hg19) was used to link super enhancers to targeted genes based on proximity and regulation potential. We considered Bio-lurbi or Bio-PM54 binding peaks to be overlapping with bona fide SEs if there was at least 1 bp of overlap. Similarly, all other overlapping analyzes considered different peaks as overlapping if there was at least 1 bp of overlap.

c. ATAC-Seq. 501mel and MM029 cells were seeded and grown to sub-confluency in 15-cm plates, and ATAC-Seq was then performed using the Active Motif ATAC-Seq Kit (53150), following the manufacturer's instructions. Briefly, 1×10^5 nuclei were isolated by adding 100 µL ice cold ATAC-lysis buffer to the cell pellet. After centrifugation (500 g, 10 min at 4 °C), cells were washed and incubated with the tagmentation master mix in a shaking heat block at 37 °C/200 g for 30 min. Obtained DNA was taken up in DNA purification buffer, purified using the contained DNA purification columns, amplified for 10 cycles using indexed primers, and size-selected using SPRI beads. Libraries were sequenced on an Illumina NextSeq 2000 sequencer as paired-end 50 base reads. Image analysis and base calling were performed using RTA version 2.7.7 and BCL Convert version 3.8.4. Samples were analyzed using the ENCODE ATACseq pipeline release v2.0.2 with hg19 assembly. All the experiments were performed in biological duplicates.

d. Shuffled analysis. To assess the specificity of signal enrichment, a control dataset was generated by using shuffled genomic regions for Bio-Ecteinascidins, ATAC-seq, CpG islands and super-enhancer peaks. The shuffling process was implemented using "bedtools shuffle" tool, which randomly redistributed the control regions across the genome while ensuring they did not overlap with the experimental regions. These shuffled regions were subjected to the same analysis pipeline as the targeted regions to serve as a negative control in downstream enrichment analysis.

Identification of active enhancers using ABC-scoring

The Active-By-Contact (ABC) model[43] was used to integrate ATAC-Seq, Cut&Tag and RNA-Seq data to generate a genome-wide annotation of all active cis-candidate regulatory regions (cCRE) directly implicated in activating gene expression in 501mel cells. First, candidate cCREs were identified using the makeCandidateRegions function which integrated ATAC-Seq narrow peaks and ATAC-Seq bam alignments. Settings were changed to 250 bp extension from the summit and peak strength equal to 1.5×10^5. cCRE activity was then measured using the run.neighborhoods function where candidate cCREs were integrated with H3K27ac bam alignments, followed by an additional removal of cCREs linked to housekeeping genes whose activity may interfere with ones linked to cell-state/identity genes. Next, we estimated the ABC power law score using the predict function. Here, the obtained cCREs were assessed for their predicted physical contacts with nearby genes based on HiC data. HiC parameters were obtained using the juicebox_dump and compute_powerlaw_fit_from_hic functions and a publicly available SKMEL-5 (differentiated melanoma cells) HiC h5 matrix (GSE105491[44]), used to train the model. This HiC matrix was converted into juicer format using hic-converter (https://github.com/4DGB/hic-converter). HiC parameters were set as follows: --hic_gamma 0.9456060921860431, --hic_scale 5.081208553261949, --hic_gamma_reference 0.87, --hic_pseudocount_distance 5000. All putative cCREs were filtered using the filter_prediction script, and setting an ABC-score threshold of 0.02 we removed self-promoter contacts and retained only cCREs linked to expressed genes. Using R, cCREs were ranked based on their final ABC-scores measured as the sum of the ABC-score values of their related genes. Differentially expressed genes determined by RNA-Seq were used to identify their associated promoter-cCRE interactions. Plots were generated using R and GraphPad Prism.

RNA extraction and RT-qPCR

Total RNA isolation was performed according to the manufacture protocol with NucleoSpin RNA Plus kit (Macherey-Nagel). RNA was retrotranscribed with Reverse Transcriptase Superscript IV (Invitrogen), qPCR was performed with SYBR Green (Roche) and on a LightCycler 480 (Roche). Target gene expression was normalized using 18S as reference gene.

ChIP-qPCR

501mel and MM029 cells were seeded and grown to sub-confluency in 15-cm plates. After drug treatments, cells were fixed with 0.4 % PFA for 10 min and quenched with 2 M Glycin pH 8. Cells pellets were lysed in 25 mM HEPES pH 7.8, 10 mM NaCl, 1.5 mM $MgCl_2$, 0.5 % NP-40, 1 mM DTT. Nuclei were resuspended in in 50 mM Hepes-KOH pH 7.8, 140 mM NaCl, 1 mM EDTA, 1% Triton X-100, 0.1 mM Na-deoxycholate, 0.1 % SDS and sonicated at 4 °C with a Q500 sonicator (Qsonica) to get DNA fragments between 100-500 bp. 50 μg of the sonicated chromatin was then diluted in Dilution buffer (1 % Triton X-100, 2 mM EDTA, 20 mM Tris HCl pH 7.5, 150 mM NaCl) and incubated overnight at 4 °C with 5 μg of respective antibodies. The antibody-chromatin complex was then captured with a mix of protein A and G Dynabeads (Invitrogen) for 2 h at 4 °C, and beads were then washed twice in Low Salt Washing Buffer (1 % Triton, 2 mM EDTA, 20 mM Tris HCl pH 7.5, 150 mM NaCl, 0.1 % SDS), High salt Washing Buffer (1 % Triton, 2 mM EDTA, 20 mM Tris HCl pH 7.5, 500 mM NaCl, 0.1 % SDS), and TE buffer (100 mM Tris HCl pH 7.5, 10 mM EDTA). Immunoprecipitated chromatin was subsequently eluted from beads in 1 % SDS and 100 mM $NaHCO_3$ at 65 °C for 30 min, and crosslinks were reversed by overnight incubation with Proteinase K (50 μg/ml) at 65 °C. The DNA was finally purified with the QIAquick PCR Purification kit (QIAGEN), resuspended in 200 μL of water, and analyzed by qPCR. Quantification of ChIP DNA concentrations with qPCR was performed by calculating the percent of input for each ChIP sample, calculated as 2^(Ct_input - Ct_IP) × 100. Subsequently, the obtained percentage was normalized to the negative control IgG. Finally, the fold enrichment of the drug-treated samples over the DMSO-treated samples was calculated.

Animal studies. Animal studies were carried out at PharmaMar, which complies with ethical standards and principles governing the use of animal models. 4- to 6-week-old NSG (Charles River laboratory) or athymic nude female (Inotiv laboratory) mice were subcutaneously implanted into their right flank with human melanoma cell suspensions (LOX-IMVI, WM-266-4, 501mel, or 501mel^{VemuR}). Athymic nude mice were used for their lack of T-cell mediated immunity, which is suitable for studies requiring longer-term tumor growth observations (LOX-IMVI and WM-266-4). NSG mice were chosen for their more severely compromised immune systems, which allow for robust engraftment and growth of human melanoma cells, including those resistant to therapies (501mel and 501mel^{VemuR}). The experiments performed in this study is not affected by sex of the animal, consequently only females were used. When tumors began to develop, these were measured 2-3 times per week. Tumor volume was calculated with the equation (a x b^2)/2, where “a” and “b” referred to the longest and shortest diameters, respectively. When tumors reached a size of 150 mm3, tumor bearing animals (N = 8/group) were treated with placebo (saline solution) or ecubectedin or PM54 at 1.2 mg/kg weekly. Tumor volume and animal body weights were measured 2–3 times per week, starting from the first day of treatment. The median was determined for tumor volume/size on each measurement day. Treatment tolerability was assessed by monitoring body weight evolution, clinical signs of systemic toxicity, as well as evidences of local damage in the injection site. Differences on antitumor effect were evaluated by comparing tumor volume data as well as median survival time from the placebo-treated group with Ecubectedin or PM54 treated groups. For this, a two-tailed Mann-Whitney U test was used. According to animal care and enforcement, the maximum allowable diameter for subcutaneous tumors in mice is 20 mm. This limit was not exceeded at any point. All animals used in this research were housed in a specific pathogen-free (SPF) environment with a 12 h dark/light cycle, constant and appropriate room temperature (22–25 °C), with relative humidity between 55 ± 10% and had free access to food and water.

Antibodies dilutions. ACTb, WB Dilution 1/1000, Cat# 558623, RRID:AB_1645341; ATM, WB Dilution 1/1000, Cat# 2873S, RRID:AB_2062659; AXL, WB Dilution 1/1000, Cat# 13196-1-AP RRID:AB_10642006; Biotin, 2.5μg/ ChIP-CUT&Tag assay, Cat# 5597S, RRID:AB_10828011; BRD4, 2.5μg/ ChIP-CUT&Tag assay, Cat# 39909, RRID:AB_2615059; CDK12, WB Dilution 1/1000, Cat# ABE1861; CDK13, WB Dilution 1/1000, Cat# ABE1860; CDK7, WB Dilution 1/2000, Cat# 556345, RRID:AB_396374; Cleaved Caspase-3 (Asp175), WB Dilution 1/2000, Cat# 9661S RRID:AB_2341188; EGFR, WB Dilution 1/2000 Cat# sc-373746, RRID:AB_10920395; EP300, WB Dilution 1/1000 Cat# 61401, RRID:AB_2716754; H3K27ac, 1μg/ChIP-CUT&Tag assay, Cat# 91193, RRID:AB_2793797; H3K27me3, 1 μg/ChIP-CUT&Tag assay, 9733, RRID:AB_2616029; IRF1, WB Dilution 1/2000, Cat# 8478S RRID:AB_10949108; MED1, WB Dilution 1/1000, Cat# ab64965, AB_1142301; MITF, WB Dilution 1/2000, Cat# 12590S, RRID:AB_2616024; MYC, WB Dilution 1/1000, Cat# sc-764, RRID:AB_631276; PD-L1, WB Dilution 1/2000 Cat# 13684S, RRID:AB_2687655; Phospho-ATM (Ser1981), WB Dilution 1/2000, Cat# 13050S, RRID:AB_2798100; Phospho-Histone H3 (Ser10), WB Dilution 1/2000, Cat# 06-570, RRID:AB_310177; Phospho-Stat1 (Tyr701), WB Dilution 1/1000, Cat# 9167S, RRID:AB_561284; γH2AX, WB and IF Dilution 1/1000, Cat# AB22551, RRID:AB_447150; RPB1, 2.5μg/ ChIP-CUT&Tag assay, Cat# AF6851, RRID:AB_2847574; RPB1, 2.5μg/ ChIP-CUT&Tag assay, Cat# AF6851, RRID:AB_2847574; SOX10, WB Dilution 1/1000, Cat# sc-365692, RRID:AB_10844002; SOX9, WB Dilution 1/1000 Cat# 82630S, RRID:AB_2665492; STAT1, WB Dilution 1/1000, Cat# 14994S, RRID: AB_2737027; Vinculin, WB Dilution 1/1000, Cat# V4505-100UL, RRID:AB_477617

Statistics and reproducibility

Experimental data was plotted and analyzed using either Excel (Microsoft) or GraphPad Prism (GraphPad Software Inc.). The tests used included ordinary one-way ANOVA using Dunnett’s multiple comparisons test, Logrank (Mantel-Cox) test, Hypergeometric distribution test, One-way ANOVA with post-hoc Tukey adjustment comparisons, the Benjamini and Hochberg test method, the ‘Fisher’s Exact Test, and the Wald test. Differences were considered significant at $P < 0.05$. Each in vitro experiment was repeated independently at least three times unless indicated differently. The number of samples and replicates are indicated in the respective figure legends. No data were excluded from the analyzes. These experiments do not require blinding of the investigator.

Resource availability

Lead contact. Further information and requests for resources and reagents should be directed to and will be fulfilled by the Lead Contact, Frédéric Coin (fredr@igbmc.fr). All data are available in the Source Data File.

Extended resource table. An extended resource table with antibodies, oligonucleotide sequences, chemicals and reagents used in this work is provided in Supplementary Data 8.

Reporting summary

Further information on research design is available in the Nature Portfolio Reporting Summary linked to this article.

Data availability

The publicly available data used in this study are available in the GEO database under the following accession codes: the RNA-seq, ChIP-seq and ATAC-seq data from SCLC cell lines; GSE179074[35] and

GSE195663[35], the RNA-seq data from the MM047 cell line; GSE205463[42], the ATAC-seq and CUT&Tag data from the ECC4, A99 and DMS53 cell lines; GSE190618[61], and the SKMEL-5 (differentiated melanoma cells) HiC h5 matrix GSE105491[44]. The raw RNA-seq, ATAC-seq, and Cut&Tag data generated in this study have been deposited at GEO under accession numbers GSE256100 and GSE256094. The remaining data are available within the Article, Supplementary Information or Source Data file. Source data are provided with this paper.

References

1. Bradner, J. E., Hnisz, D. & Young, R. A. Transcriptional Addiction in Cancer. *Cell* **168**, 629–643 (2017).
2. Sengupta, S. & George, R. E. Super-Enhancer-Driven Transcriptional Dependencies in Cancer. *Trends Cancer* **3**, 269–281 (2017).
3. Zanconato, F. et al. Transcriptional addiction in cancer cells is mediated by YAP/TAZ through BRD4. *Nat. Med* **24**, 1599–1610 (2018).
4. Hogg, S. J., Beavis, P. A., Dawson, M. A. & Johnstone, R. W. Targeting the epigenetic regulation of antitumour immunity. *Nat. Rev. Drug Discov.* **19**, 776–800 (2020).
5. Vervoort, S. J. et al. Targeting transcription cycles in cancer. *Nat. Rev. Cancer* **22**, 5–24 (2022).
6. Pott, S. & Lieb, J. D. What are super-enhancers? *Nat. Genet* **47**, 8–12 (2015).
7. Hnisz, D. et al. Super-enhancers in the control of cell identity and disease. *Cell* **155**, 934–947 (2013).
8. Whyte, W. A. et al. Master transcription factors and mediator establish super-enhancers at key cell identity genes. *Cell* **153**, 307–319 (2013).
9. Sabari, B. R. et al. Coactivator condensation at super-enhancers links phase separation and gene control. *Science* **361**, eaar3958 (2018).
10. Boija, A., Klein, I. A. & Young, R. A. Biomolecular Condensates and Cancer. *Cancer Cell* **39**, 174–192 (2021).
11. Laham-Karam, N., Pinto, G. P., Poso, A. & Kokkonen, P. Transcription and Translation Inhibitors in Cancer Treatment. *Front. Chem.* **8**, 276 (2020).
12. Bushweller, J. H. Targeting transcription factors in cancer — from undruggable to reality. *Nat. Rev. Cancer* **19**, 611–624 (2019).
13. Kwiatkowski, N. et al. Targeting transcription regulation in cancer with a covalent CDK7 inhibitor. *Nature* **511**, 616–620 (2014).
14. Berico, P. et al. CDK7 and MITF repress a transcription program involved in survival and drug tolerance in melanoma. *EMBO Rep.* https://doi.org/10.15252/embr.202051683 (2021).
15. Fontanals-Cirera, B. et al. Harnessing BET Inhibitor Sensitivity Reveals AMIGO2 as a Melanoma Survival Gene. *Mol. Cell* **68**, 731–744.e9 (2017).
16. Donati, B., Lorenzini, E. & Ciarrocchi, A. BRD4 and Cancer: going beyond transcriptional regulation. *Mol. Cancer* **17**, 164 (2018).
17. Hoek, K. S. et al. In vivo switching of human melanoma cells between proliferative and invasive states. *Cancer Res.* **68**, 650–656 (2008).
18. Verfaillie, A. et al. Decoding the regulatory landscape of melanoma reveals TEADS as regulators of the invasive cell state. *Nat. Commun.* **6**, 6683 (2015).
19. Wouters, J. et al. Robust gene expression programs underlie recurrent cell states and phenotype switching in melanoma. *Nat. Cell Biol.* **22**, 986–998 (2020).
20. Pozniak, J. et al. A TCF4-dependent gene regulatory network confers resistance to immunotherapy in melanoma. *Cell* **187**, 166–183.e25 (2024).
21. Gide, T. N., Wilmott, J. S., Scolyer, R. A. & Long, G. V. Primary and Acquired Resistance to Immune Checkpoint Inhibitors in Metastatic Melanoma. *Clin. Cancer Res.* **24**, 1260–1270 (2018).
22. Weiss, S. A., Wolchok, J. D. & Sznol, M. Immunotherapy of Melanoma: Facts and Hopes. *Clin. Cancer Res.* **25**, 5191–5201 (2019).
23. Schadendorf, D. et al. Melanoma. *Lancet* **392**, 971–984 (2018).
24. Jerby-Amon, L. et al. A Cancer Cell Program Promotes T Cell Exclusion and Resistance to Checkpoint Blockade. *Cell* **175**, 984-+ (2018).
25. Tsoi, J. et al. Multi-stage Differentiation Defines Melanoma Subtypes with Differential Vulnerability to Drug-Induced Iron-Dependent Oxidative Stress. *Cancer Cell* **33**, 890–904.e5 (2018).
26. Arozarena, I. & Wellbrock, C. Phenotype plasticity as enabler of melanoma progression and therapy resistance. *Nat. Rev. Cancer* **19**, 377–391 (2019).
27. Benboubker, V., Boivin, F., Dalle, S. & Caramel, J. Cancer Cell Phenotype Plasticity as a Driver of Immune Escape in Melanoma. *Front. Immunol.* **13**, 873116 (2022).
28. Chauhan, J. S., Hölzel, M., Lambert, J., Buffa, F. M. & Goding, C. R. The MITF regulatory network in melanoma. *Pigment Cell Melanoma Res* **35**, 517–533 (2022).
29. Comandante-Lou, N., Baumann, D. G. & Fallahi-Sichani, M. AP-1 transcription factor network explains diverse patterns of cellular plasticity in melanoma cells. *Cell Rep.* **40**, 111147 (2022).
30. Karras, P. et al. A cellular hierarchy in melanoma uncouples growth and metastasis. *Nature* **610**, 190–198 (2022).
31. Hoek, K. S. & Goding, C. R. Cancer stem cells versus phenotype-switching in melanoma. *Pigment Cell Melanoma Res* **23**, 746–759 (2010).
32. Rambow, F., Marine, J. C. & Goding, C. R. Melanoma plasticity and phenotypic diversity: therapeutic barriers and opportunities. *Genes Dev.* **33**, 1295–1318 (2019).
33. Molinski, T. F., Dalisay, D. S., Lievens, S. L. & Saludes, J. P. Drug development from marine natural products. *Nat. Rev. Drug Discov.* **8**, 69–85 (2009).
34. Santamaria Nunez, G. et al. Lurbinectedin Specifically Triggers the Degradation of Phosphorylated RNA Polymerase II and the Formation of DNA Breaks in Cancer Cells. *Mol. Cancer Ther.* **15**, 2399–2412 (2016).
35. Costanzo, F. et al. Promoters of ASCL1- and NEUROD1-dependent genes are specific targets of lurbinectedin in SCLC cells. *EMBO Mol. Med* https://doi.org/10.15252/emmm.202114841 (2022).
36. Trigo, J. et al. Lurbinectedin as second-line treatment for patients with small-cell lung cancer: a single-arm, open-label, phase 2 basket trial. *Lancet Oncol.* **21**, 645–654 (2020).
37. Widmer, D. S. et al. Systematic classification of melanoma cells by phenotype-specific gene expression mapping. *Pigment Cell Melanoma Res* **25**, 343–353 (2012).
38. David-Cordonnier, M.-H. et al. DNA and Non-DNA Targets in the Mechanism of Action of the Antitumor Drug Trabectedin. *Chem. Biol.* **12**, 1201–1210 (2005).
39. Couto, G. K. et al. The Melding of Drug Screening Platforms for Melanoma. *Front. Oncol.* **9**, 512 (2019).
40. Casper, D. J. et al. Use of Anti-phosphohistone H3 Immunohistochemistry to Determine Mitotic Rate in Thin Melanoma. *Am. J. Dermatopathol.* **32**, 650–654 (2010).
41. Yu, Z. et al. Chem-map profiles drug binding to chromatin in cells. *Nat. Biotechnol.* **41**, 1265–1271 (2023).
42. Berico, P. et al. Super-enhancer-driven expression of BAHCC1 promotes melanoma cell proliferation and genome stability. *Cell Rep.* **42**, 113363 (2023).
43. Fulco, C. P. et al. Activity-by-contact model of enhancer–promoter regulation from thousands of CRISPR perturbations. *Nat. Genet* **51**, 1664–1669 (2019).
44. The ENCODE Project Consortium. An integrated encyclopedia of DNA elements in the human genome. *Nature* **489**, 57–74 (2012).
45. Zawistowski, J. S. et al. Enhancer Remodeling during Adaptive Bypass to MEK Inhibition Is Attenuated by Pharmacologic Targeting of the P-TEFb Complex. *Cancer Discov.* **7**, 302–321 (2017).
46. Le, V. H., Inai, M., Williams, R. M. & Kan, T. Ecteinascidins. A review of the chemistry, biology and clinical utility of potent tetrahydroisoquinoline antitumor antibiotics. *Nat. Prod. Rep.* **32**, 328–347 (2015).

47. Xie, W. et al. Lurbinectedin synergizes with immune checkpoint blockade to generate anticancer immunity. *OncoImmunology* **8**, e1656502 (2019).
48. Dumoulin, D. W. et al. Lurbinectedin shows clinical activity and immune-modulatory functions in patients with pre-treated small cell lung cancer and malignant pleural mesothelioma. *Eur. J. Cancer* **172**, 357–366 (2022).
49. Love, M. I., Huber, W. & Anders, S. Moderated estimation of fold change and dispersion for RNA-seq data with DESeq2. *Genome Biol.* **15**, 1–21 (2014).
50. Benjamini, Y. & Hochberg, Y. Controlling the False Discovery Rate: A Practical and Powerful Approach to Multiple Testing. *J. R. Stat. Soc.: Ser. B (Methodol.)* **57**, 289–300 (1995).
51. Ge, S. X., Jung, D. & Yao, R. ShinyGO: a graphical gene-set enrichment tool for animals and plants. *Bioinformatics* **36**, 2628–2629 (2020).
52. Langmead, B. & Salzberg, S. L. Fast gapped-read alignment with Bowtie 2. *Nat. Methods* **9**, 357–359 (2012).
53. Zhang, Y. et al. Model-based analysis of ChIP-Seq (MACS). *Genome Biol.* **9**, R137 (2008).
54. Quinlan, A. R. & Hall, I. M. BEDTools: a flexible suite of utilities for comparing genomic features. *Bioinformatics* **26**, 841–842 (2010).
55. Heinz, S. et al. Simple Combinations of Lineage-Determining Transcription Factors Prime cis-Regulatory Elements Required for Macrophage and B Cell Identities. *Mol. Cell* **38**, 576–589 (2010).
56. Ramírez, F. et al. deepTools2: a next generation web server for deep-sequencing data analysis. *Nucleic Acids Res* **44**, W160–W165 (2016).
57. Love, M. I., Huber, W. & Anders, S. Moderated estimation of fold change and dispersion for RNA-seq data with DESeq2. *Genome Biol.* **15**, 550 (2014).
58. Ross-Innes, C. S. et al. Differential oestrogen receptor binding is associated with clinical outcome in breast cancer. *Nature* **481**, 389–393 (2012).
59. Ye, T. et al. seqMINER: an integrated ChIP-seq data interpretation platform. *Nucleic Acids Res.* **39**, e35–e35 (2011).
60. Loven, J. et al. Selective inhibition of tumor oncogenes by disruption of super-enhancers. *Cell* **153**, 320–334 (2013).
61. Horie, M. et al. An integrative epigenomic approach identifies *ELF3* as an oncogenic regulator in *ASCL1* -positive neuroendocrine carcinoma. *Cancer Sci.* **114**, 2596–2608 (2023).

Acknowledgements

This study was supported by the Ligue contre le cancer (Equipe Labélisée 2022-2024), the Institut National du Cancer (INCa) (INCa_18353), the grant ANR-10-LABX-0030-INRT, a French State fund managed by the Agence Nationale de la Recherche under the frame program Investissements d'Avenir ANR-10-IDEX-0002-02. This work of the Interdisciplinary Thematic Institute IMCBio+, as part of the ITI 2021-2028 program of the University of Strasbourg, CNRS and Inserm, was supported by IdEx Unistra (ANR-10-IDEX-0002), and by SFRI-STRAT'US project (ANR-20-SFRI-0012) and EUR IMCBio (ANR-17-EURE-0023) under the framework of the France 2030 Program. Sequencing was performed by the IGBMC GenomEast platform, a member of the "France Génomique" consortium (ANR-10-INBS-0009). Histology and subsequent image analysis were performed by the pathology facility of the mouse clinic institute (ICS), a member of the Celphedia/Phenomin infrastructures (ANR-10-INBS-0007). We also thank the IGBMC PluriCell East facility, Flow cytometry and Photonic microscopy services. P.B is supported by the Ligue contre le Cancer. JME was sponsored by a Mount Jade Scholar Fellow from the MOST of Taiwan and a Yonglin Chair Professor grant of National Taiwan University. We thank Dr Hsiang-Hung Huang for having initiated the work on SCLC cells.

Author contributions

Conceptualization: FC. Methodology: MC, JO, ID, C-Cuevas, FC. Investigation: MC, JO, MN, LS, PC, PB, C-Capelli, CM, AZ, CE, MJGN, TKL, EC, PA, MMD and GSN. Analysis of data: TY, GD, JME. Funding acquisition: FC. Supervision: FC. Writing – original draft: FC. Writing – review & editing: ID, EC, CC, MC, JO.

Competing interests

PA and C-Cuevas are PharmaMar S.A employees and shareholders. MJGN, MMD, GSM are PharmaMar employees. The remaining authors declare no competing interests.

Additional information

Supplementary information The online version contains supplementary material available at https://doi.org/10.1038/s41467-024-55667-z.

Correspondence and requests for materials should be addressed to Frédéric Coin.

Peer review information *Nature Communications* thanks the anonymous reviewers for their contribution to the peer review of this work. A peer review file is available.

Reprints and permissions information is available at http://www.nature.com/reprints

Publisher's note Springer Nature remains neutral with regard to jurisdictional claims in published maps and institutional affiliations.

Open Access This article is licensed under a Creative Commons Attribution-NonCommercial-NoDerivatives 4.0 International License, which permits any non-commercial use, sharing, distribution and reproduction in any medium or format, as long as you give appropriate credit to the original author(s) and the source, provide a link to the Creative Commons licence, and indicate if you modified the licensed material. You do not have permission under this licence to share adapted material derived from this article or parts of it. The images or other third party material in this article are included in the article's Creative Commons licence, unless indicated otherwise in a credit line to the material. If material is not included in the article's Creative Commons licence and your intended use is not permitted by statutory regulation or exceeds the permitted use, you will need to obtain permission directly from the copyright holder. To view a copy of this licence, visit http://creativecommons.org/licenses/by-nc-nd/4.0/.

© The Author(s) 2025

[1]IGBMC, Institut de Génétique et de Biologie Moléculaire et Cellulaire Illkirch Cedex, C.U. Equipe Labélisée Ligue contre le Cancer, Strasbourg, France. [2]UMR7104, Illkirch, France. [3]U1258, Illkirch, France. [4]Université de Strasbourg, Illkirch, France. [5]Department of Pathology, New York University Grossman School of Medicine, New York, USA. [6]Interdisciplinary Melanoma Cooperative Group, Perlmutter Cancer Center, NYU Langone Health, New York, USA. [7]Cell Biology Department, Research and Development, PharmaMar SA, Colmenar Vejo, Spain. [8]Graduate Institute of Microbiology, College of Medicine, National Taiwan University, Taipei, Taiwan. [9]College of Medicine, National Taiwan University, Taipei city, Taiwan. [10]These authors contributed equally: Max Cigrang, Julian Obid. ✉e-mail: fredr@igbmc.fr

Supplemental Figure 1

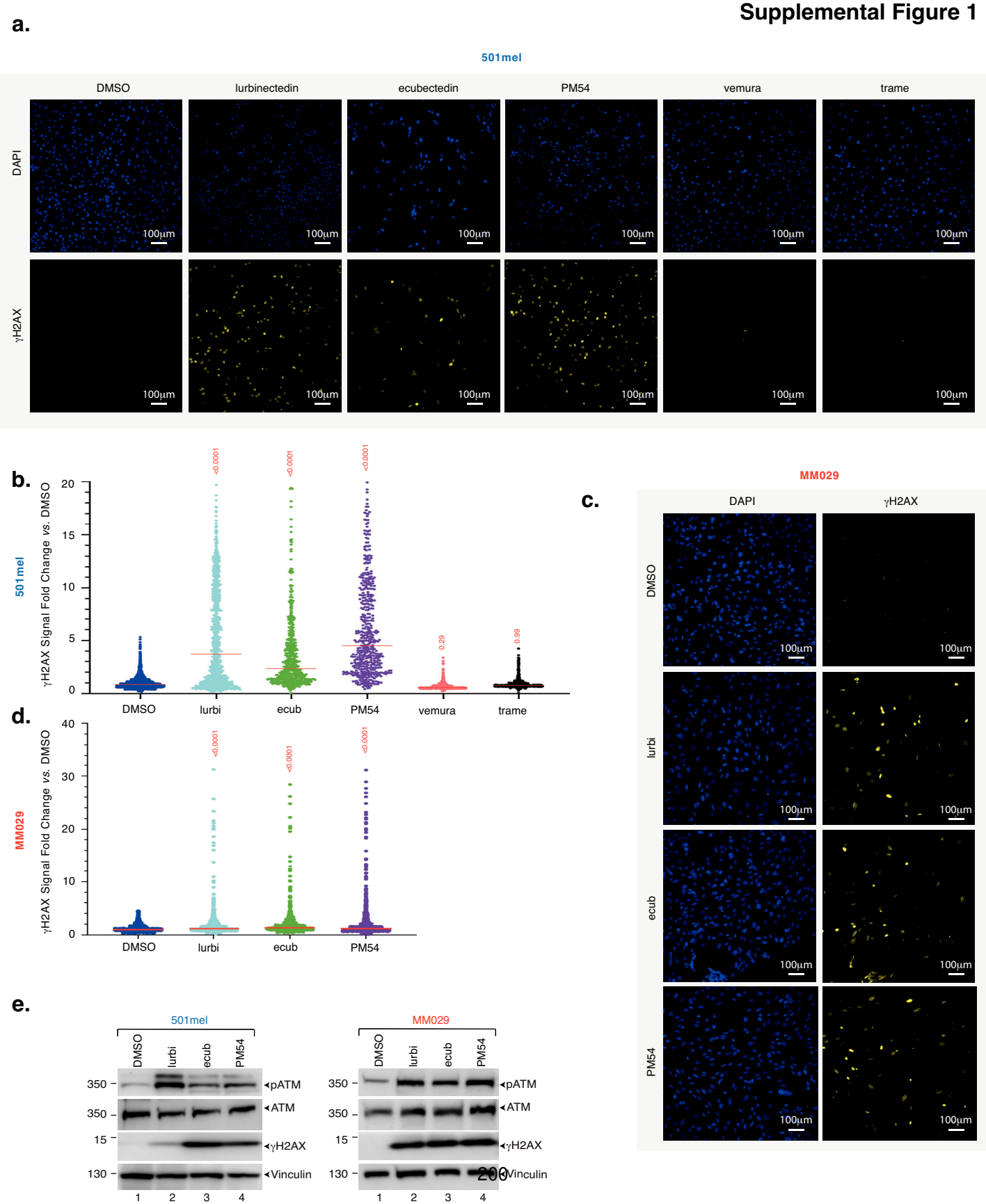

Supplemental Figure 1: Synthetic ecteinascidins potently induce DSBs

a-d. Differentiated 501mel (**a, b**) or undifferentiated MM029 (**c, d**) cells were treated with the indicated drugs (5xIC50 concentration, 24 hours) and γH2AX induction was assessed by immunofluorescence. Representative images are shown (**a, c**) as well as γH2AX signal quantification (n= at least 500 nuclei in three independent experiments). Bars indicate mean values (**b, d**). Source data are provided in the source data file. Scale bars are indicated in **(a)** and **(c)**.

e. Protein lysates from differentiated 501mel or undifferentiated MM029 treated with either lurbinectedin, ecubectedin or PM54 (5xIC50 concentration, 24 hours), were immuno-blotted for proteins as indicated. Molecular mass of the proteins is indicated (kDa). Source data are provided in the source data file. This experiment was repeated independently three times with similar results.

Supplemental Figure 2

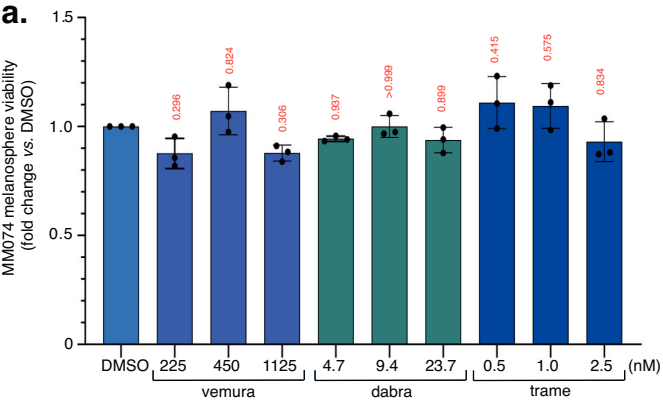

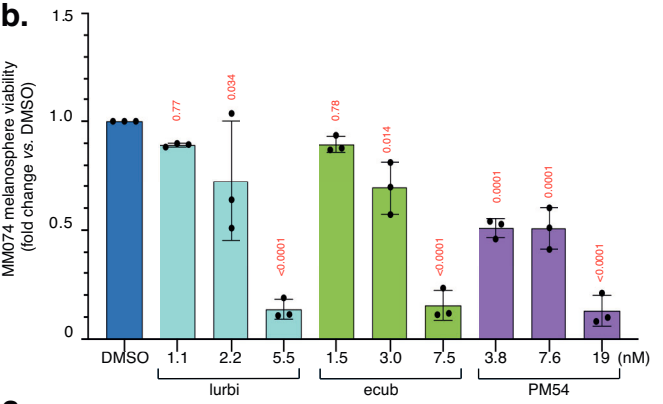

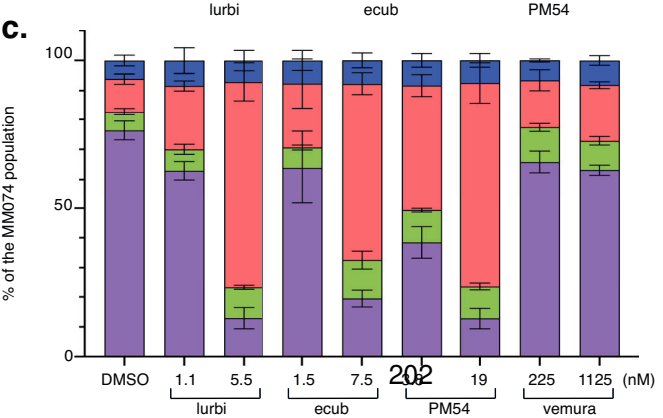

Supplemental Figure 2: Melanospheres display high sensitivity to synthetic ecteinascidins

a-b. MM074 melanospheres were treated with drugs as indicated for 72 hours, and cell viability was measured with CellTiter-Glo assay. Results are shown as mean values of viability *vs.* DMSO +/- SD for three biological triplicates. Ordinary one-way ANOVA using Dunnett's multiple comparisons test was used to determine the p-values. Source data are provided in the source data file.

c. MM074 melanospheres were treated with either vehicle (DMSO), lurbinectedin, ecubectedin, PM54 or vemurafenib as indicated for 72 hours. Apoptosis was studied by flow cytometry with Annexin V-APC and propidium iodide staining. Results are shown as mean values +/- SD for three biological triplicates. Source data are provided in the source data file.

Supplemental Figure 3

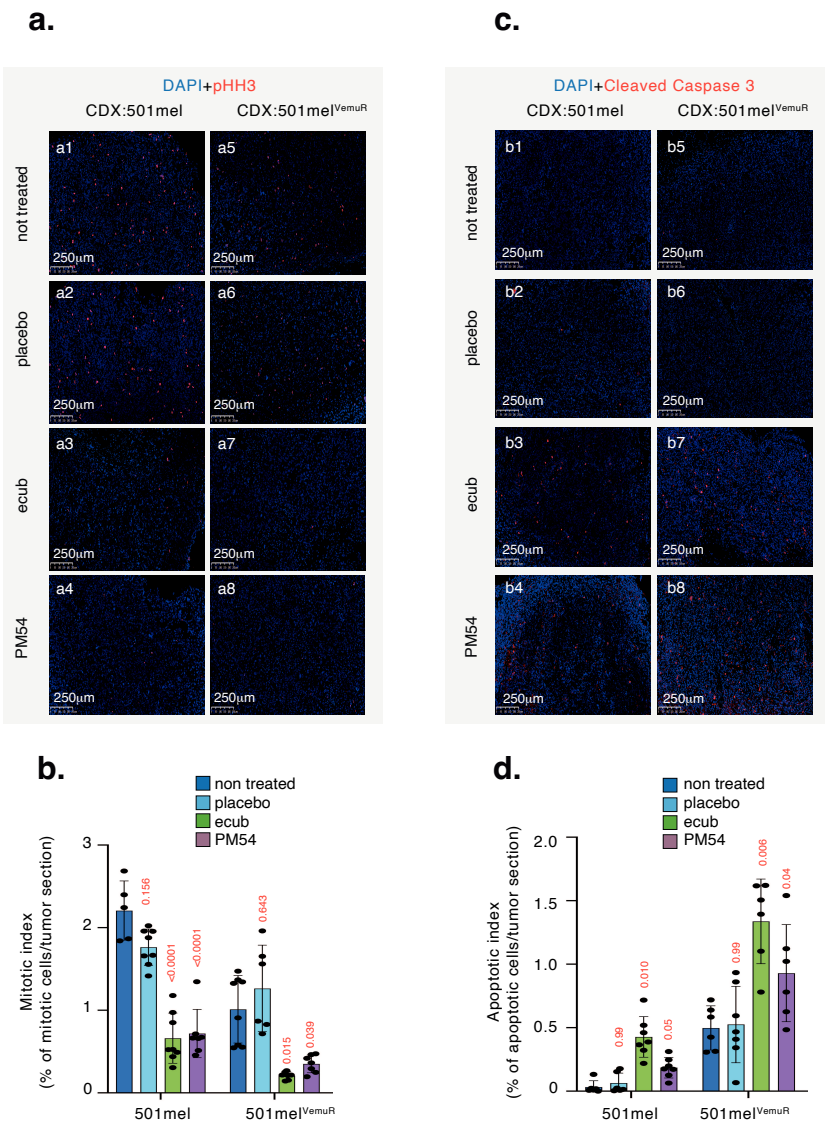

Supplemental Figure 3: Synthetic ecteinascidins inhibit cell proliferation and induce apoptosis of melanoma cells in CDX models

a. Representative fluorescence microscopy images (n=3) of pHH3-positive cells in tumor sections of 501mel or 501mel^{VemuR} CDX models after a 24-hour treatment with a one-time dose of Placebo, ecubectedin or PM54 at 1.2mg/kg. Scale bars are indicated.

b. Quantification of the mitotic index (n=3) (% of pHH3-positive cells/tumour section(n>3)) is shown as mean values +/- SD for tumour sections. Ordinary one-way ANOVA using Dunnett's multiple comparisons test was used to determine the p-values (*vs.* non treated).

c. Representative fluorescence microscopy images (n=3) of cleaved caspase-3-positive cells in tumor sections of 501mel or 501mel^{VemuR} CDX models after a 24-hour treatment with a one-time dose of Placebo, ecubectedin or PM54 at 1.2mg/kg. Scale bars are indicated.

d. Quantification of the apoptotic index (n=3) (% of cleaved caspase-3-positive cells/tumor section(n>3)) is shown as mean values +/- SD for tumour sections. Ordinary one-way ANOVA using Dunnett's multiple comparisons test was used to determine the p-values (*vs.* non treated).

Supplemental Figure 4

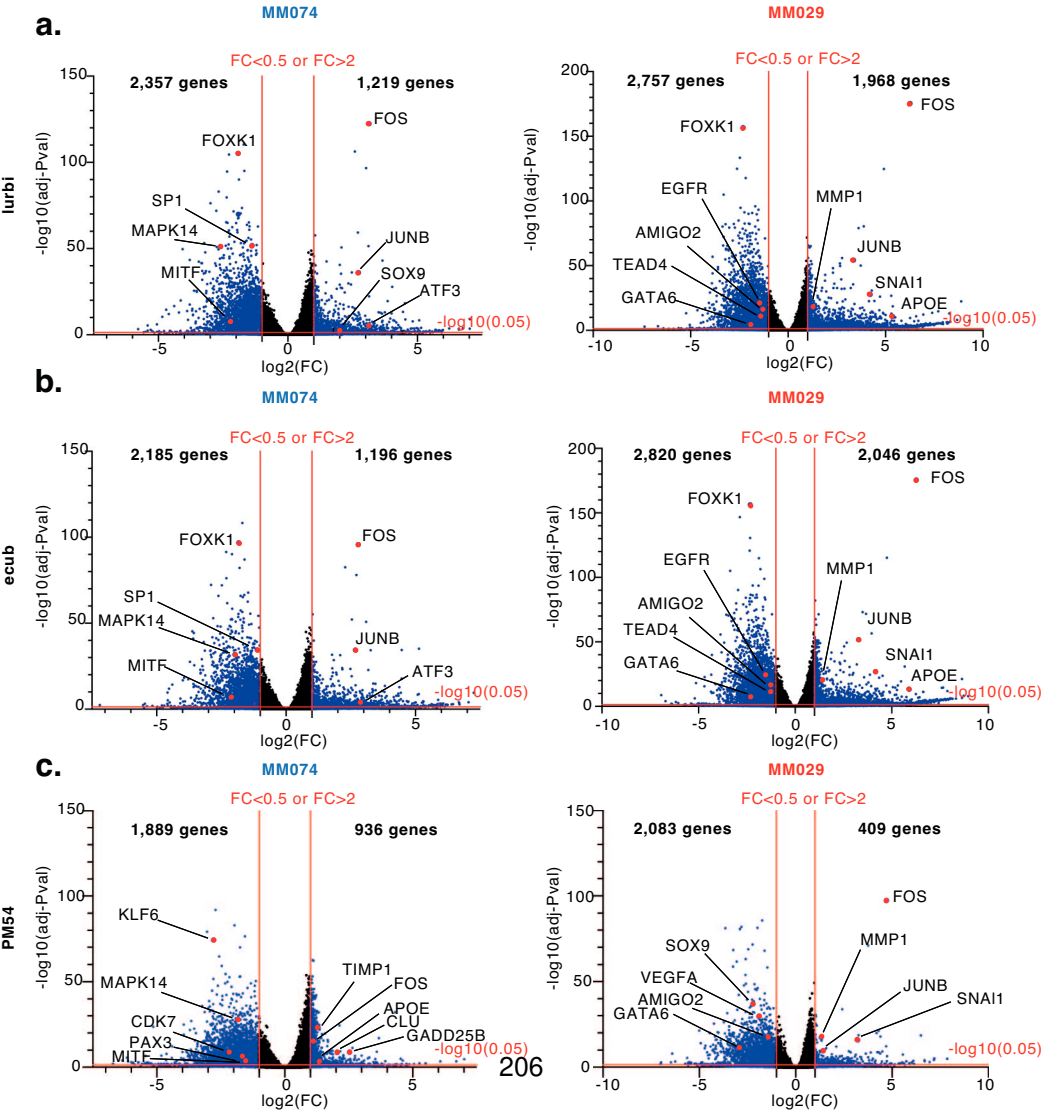

Supplemental Figure 4: Synthetic ecteinascidins affect the transcription program of melanoma cells

a-c. Volcano plots (n=3) showing differentially expressed genes between DMSO-treated *vs.* **(a)** Lurbi-, **(b)** Ecubectedin-, or **(c)** PM54- treated MM074 (left) or MM029 (right) cells, determined by RNA-Seq (10xIC50 concentration, 8 hours). Examples of significantly deregulated genes are shown, which were defined as genes with log2(Fold change) > 1 or < -1 and adjusted P-value < 0.05.

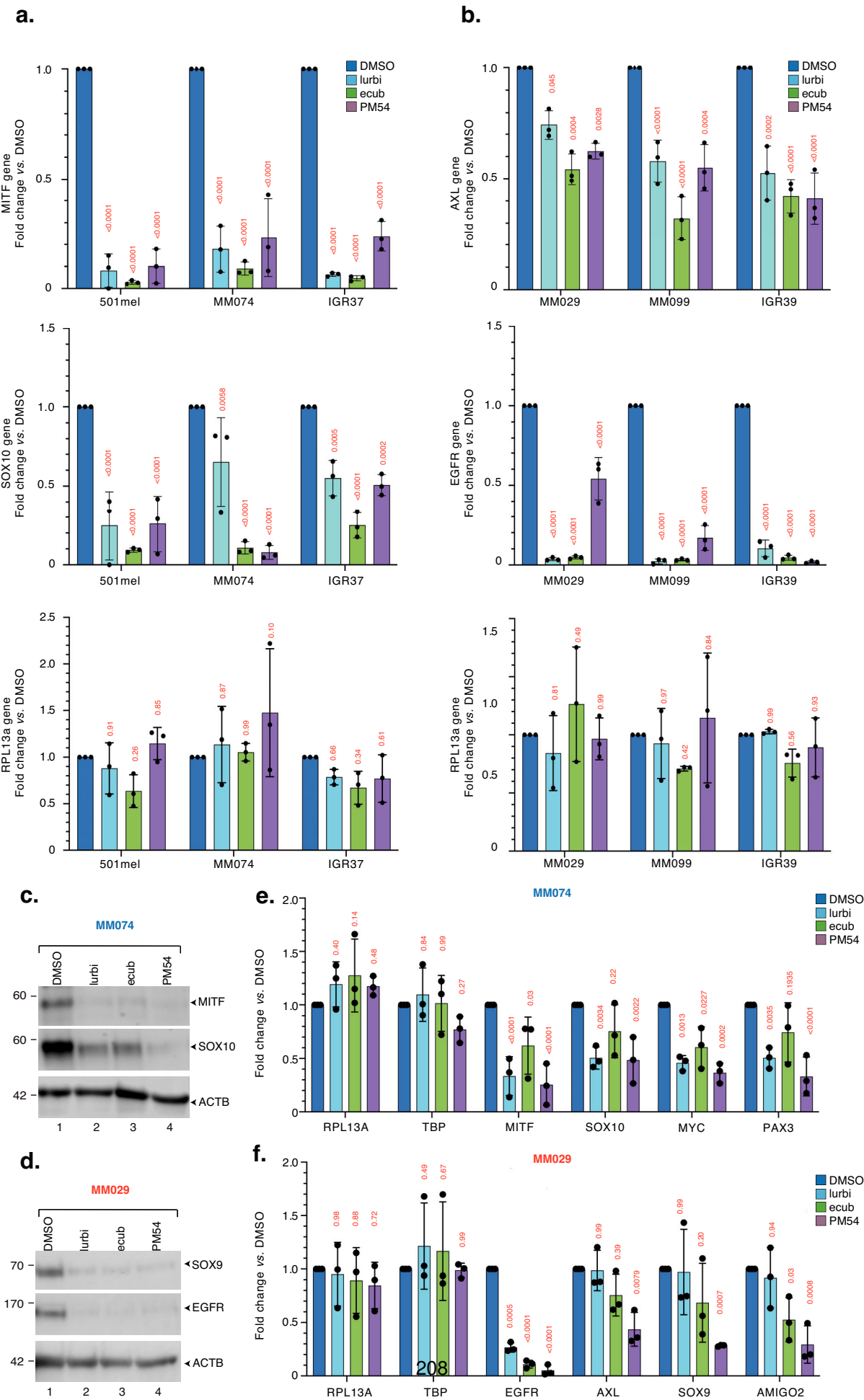
a.
b.
DMSO
lurbi
ecub
PM54
MITF gene
Fold change vs. DMSO
501mel
MM074
IGR37
AXL gene
MM029
MM099
IGR39
SOX10 gene
EGFR gene
RPL13a gene
c.
MM074
MITF
SOX10
ACTB
d.
MM029
SOX9
EGFR
e.
RPL13A
TBP
MITF
SOX10
MYC
PAX3
f.
AMIGO2
208

Supplemental Figure 5: Synthetic ecteinascidins impair crucial cancer-promoting genes in melanoma

a. qRT-PCR analysis showing average 18S-normalized expression of MITF, SOX10 and RPL13a in the differentiated 501mel, MM074 and IGR37 cells treated with either vehicle (DMSO), lurbinectedin, ecubectedin or PM54 (5xIC50 concentration, 12 hours). Error bars indicate mean values + SD for three biological triplicates. Ordinary one-way ANOVA using Dunnett's multiple comparisons test was used to determine the p-values (*vs.* DMSO). Source data are provided in the source data file.

b. qRT-PCR analysis showing average 18S-normalized expression of AXL, EGFR and RPL13a in the undifferentiated MM029, MM099 and IGR39 treated with either vehicle (DMSO), lurbinectedin, ecubectedin or PM54 (5xIC50 concentration, 12 hours). Error bars indicate the mean values +/- SD for three biological triplicates. Ordinary one-way ANOVA using Dunnett's multiple comparisons test was used to determine the p-values (*vs.* DMSO). Source data are provided in the source data file.

c-d. The differentiated MM074 **(c)** or undifferentiated MM099 **(d)** cells were treated with either vehicle (DMSO), lurbinectedin, ecubectedin or PM54 (5xIC50 concentration, 24 hours). Protein lysates were immuno-blotted for proteins as indicated. Molecular mass of the proteins is indicated (kDa). Source data are provided in the source data file. This experiment was repeated independently three times with similar results.

e-f. qRT-PCR analysis showing average 18S-normalized gene expression in the differentiated MM074 **(e)** and undifferentiated MM029 **(f)** melanospheres treated with either vehicle (DMSO), lurbinectedin, ecubectedin or PM54 (5xIC50 concentration, 24 hours). Error bars indicate mean values + SD for three biological triplicates. Ordinary one-way ANOVA using Dunnett's multiple comparisons test was used to determine the p-values (*vs.* DMSO). Source data are provided in the source data file. This experiment was repeated independently three times with similar results.

Supplemental Figure 6

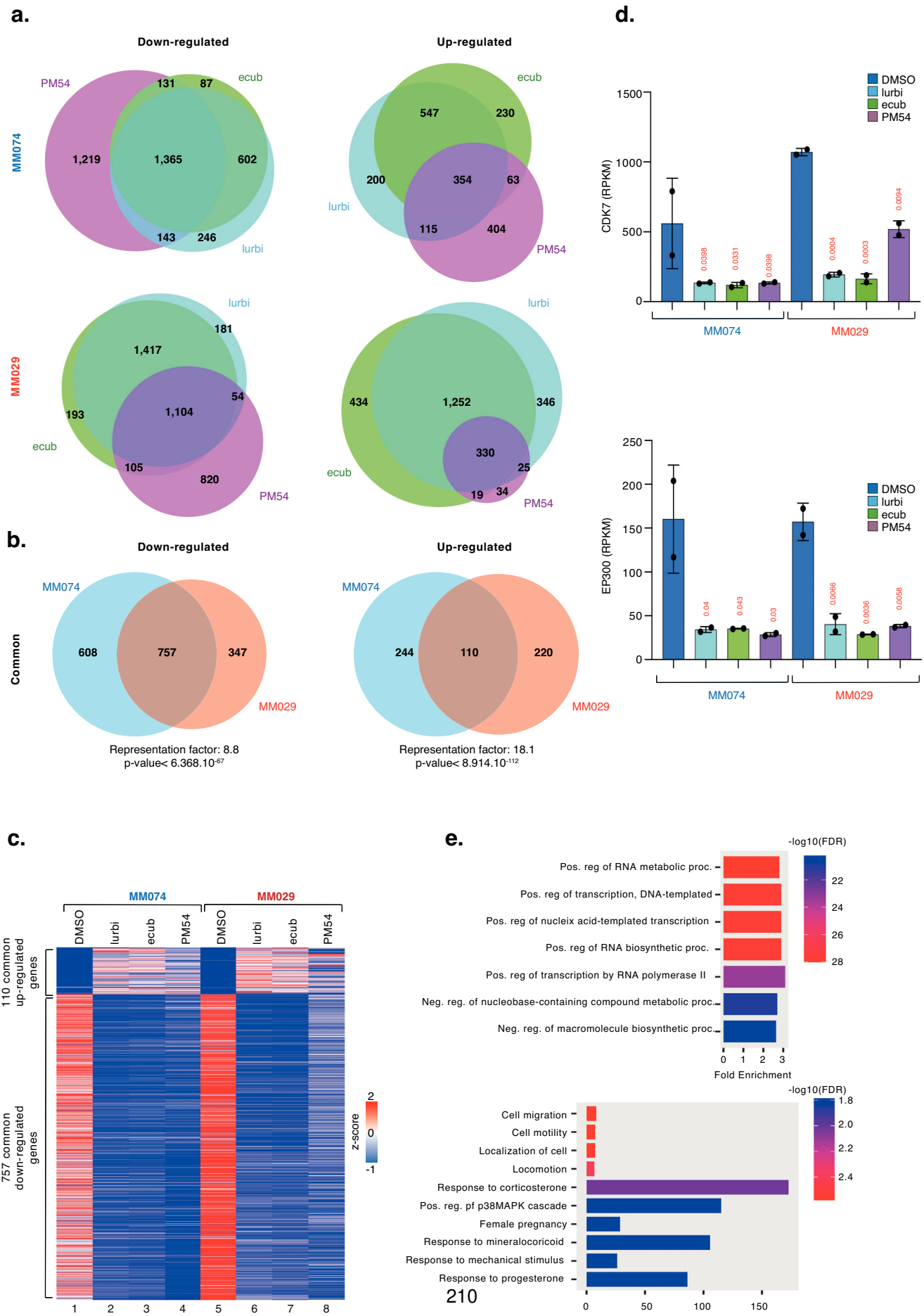

Supplemental Figure 6: Comparison of down-and up-regulated genes in melanoma cell subtypes following treatment with synthetic ecteinascidins

a. Venn diagram (n=3) comparing significantly down-regulated (left) and up-regulated (right) genes identified by RNA-Seq in differentiated MM074 (top) and undifferentiated MM029 (bottom) upon treatment with either lurbinectedin, ecubectedin or PM54 (10xIC50 concentration, 8 hours).

b. Venn diagram (n=3) comparing genes identified by RNA-Seq as being commonly down-regulated (left) or up-regulated (right) in both differentiated MM074 and undifferentiated MM029 by the three synthetic ecteinascidins. Representation factor and hypergeometric p-values are represented.

c. Heatmap (n=3) depicting common up- and down-regulated genes from either DMSO, lurbinectedin, ecubectedin or PM54 treatments (10xIC50 concentration, 8 hours), in MM074 cells and MM029 cells. RPKM values are represented as z-score.

d. Graphs (n=3) showing the expression of CDK7 and EP300 following treatment with drugs (IC50x10 for 8h) in both MM074 and MM029 cells. Results are shown as normalized RPKM values divided by median of transcripts length in kb, as mean values for two biological RNA-Seq duplicates. Ordinary one-way ANOVA using Dunnett's multiple comparisons test was used to determine the p-values.

e. GO (Biological process) analysis (n=3) of the 757 genes significantly down-regulated (Top) and 110 genes significantly up-regulated (Bottom) in both MM074 and MM029 by the three synthetic ecteinascidins, as identified in **(b)**. The histogram shows the top deregulated biological pathways according to the FDR and fold enrichment.

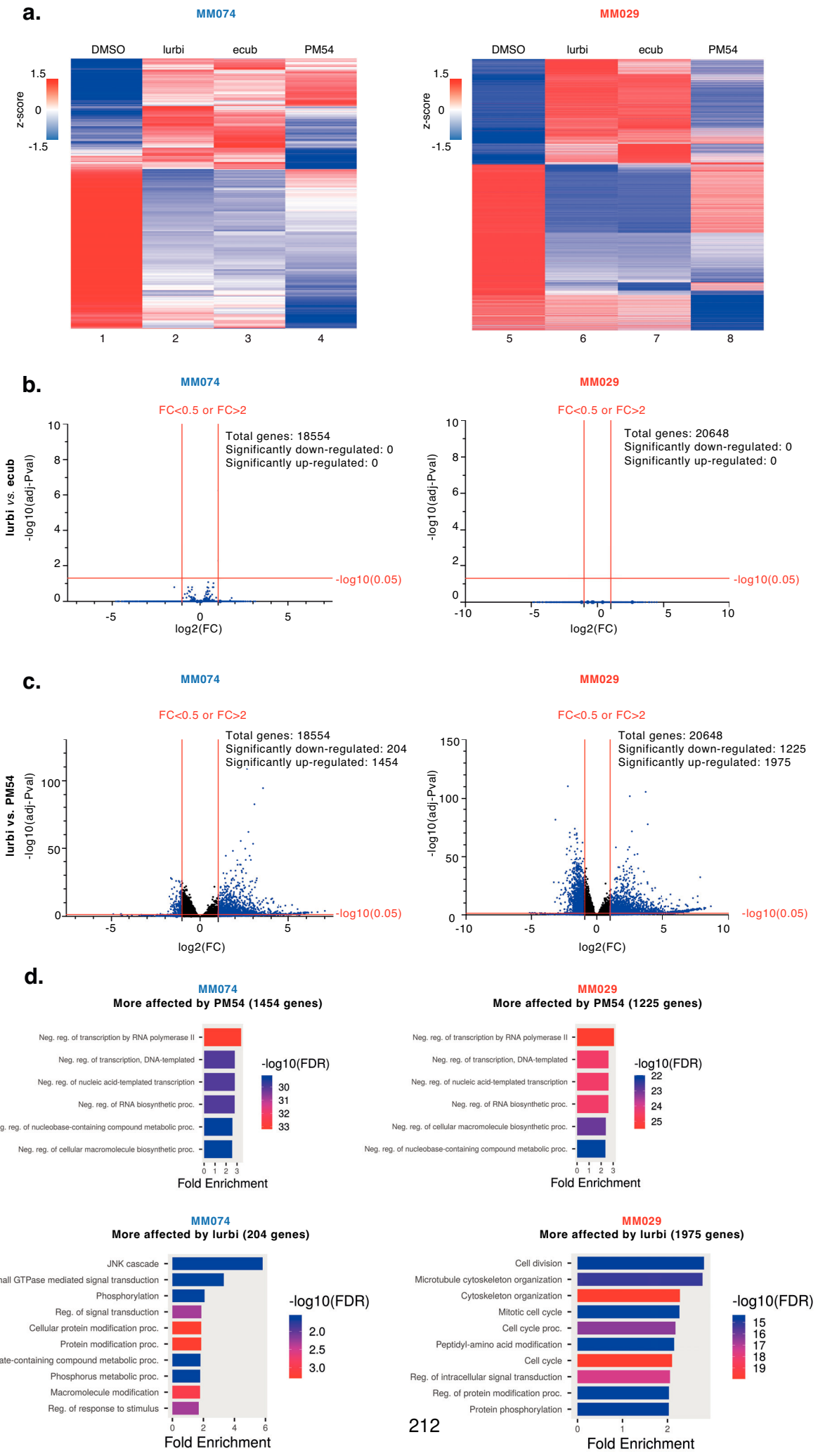
a.
MM074
MM029
DMSO
lurbi
ecub
PM54
z-score
1.5
0
-1.5
1
2
3
4
5
6
7
8
b.
MM074
MM029
FC<0.5 or FC>2
Total genes: 18554
Significantly down-regulated: 0
Significantly up-regulated: 0
Total genes: 20648
Significantly down-regulated: 0
Significantly up-regulated: 0
lurbi vs. ecub
-log10(adj-Pval)
-log10(0.05)
log2(FC)
c.
MM074
MM029
FC<0.5 or FC>2
Total genes: 18554
Significantly down-regulated: 204
Significantly up-regulated: 1454
Total genes: 20648
Significantly down-regulated: 1225
Significantly up-regulated: 1975
lurbi vs. PM54
-log10(adj-Pval)
-log10(0.05)
log2(FC)
d.
MM074
More affected by PM54 (1454 genes)
Neg. reg. of transcription by RNA polymerase II
Neg. reg. of transcription, DNA-templated
Neg. reg. of nucleic acid-templated transcription
Neg. reg. of RNA biosynthetic proc.
Neg. reg. of nucleobase-containing compound metabolic proc.
Neg. reg. of cellular macromolecule biosynthetic proc.
-log10(FDR)
Fold Enrichment
MM029
More affected by PM54 (1225 genes)
Neg. reg. of transcription by RNA polymerase II
Neg. reg. of transcription, DNA-templated
Neg. reg. of nucleic acid-templated transcription
Neg. reg. of RNA biosynthetic proc.
Neg. reg. of cellular macromolecule biosynthetic proc.
Neg. reg. of nucleobase-containing compound metabolic proc.
-log10(FDR)
Fold Enrichment
MM074
More affected by lurbi (204 genes)
JNK cascade
Small GTPase mediated signal transduction
Phosphorylation
Reg. of signal transduction
Cellular protein modification proc.
Protein modification proc.
Phosphate-containing compound metabolic proc.
Phosphorus metabolic proc.
Macromolecule modification
Reg. of response to stimulus
-log10(FDR)
Fold Enrichment
MM029
More affected by lurbi (1975 genes)
Cell division
Microtubule cytoskeleton organization
Cytoskeleton organization
Mitotic cell cycle
Cell cycle proc.
Peptidyl-amino acid modification
Cell cycle
Reg. of intracellular signal transduction
Reg. of protein modification proc.
Protein phosphorylation
-log10(FDR)
Fold Enrichment

Supplemental Figure 7: PM54 differentially affects gene expression compared to lurbinectedin and ecubectedin

a. Heatmap (n=3) depicting all deregulated genes from either lurbinectedin, ecubectedin or PM54 treatments (10xIC50 concentration, 8 hours), in MM074 cells (left) or MM029 cells (right). RPKM values are represented as z-score.

b-c. Volcano plots (n=3) showing differentially expressed genes between lurbinectedin and either ecubectedin **(b)** or PM54 **(c)** treatment in MM074 (left) and MM029 (right) as determined by RNA-Seq. Deregulated genes were defined as genes with log2(Fold change) > 1 or < -1 and adjusted P-value < 0.05.

d. GO (Biological process) analysis (n=3) of the genes significantly down-regulated (up) or up-regulated (bottom) in MM074 (left) and MM029 (right) cells treated with lurbinectedin *vs.* PM54. The histogram shows the top deregulated biological pathways according to the FDR and fold enrichment.

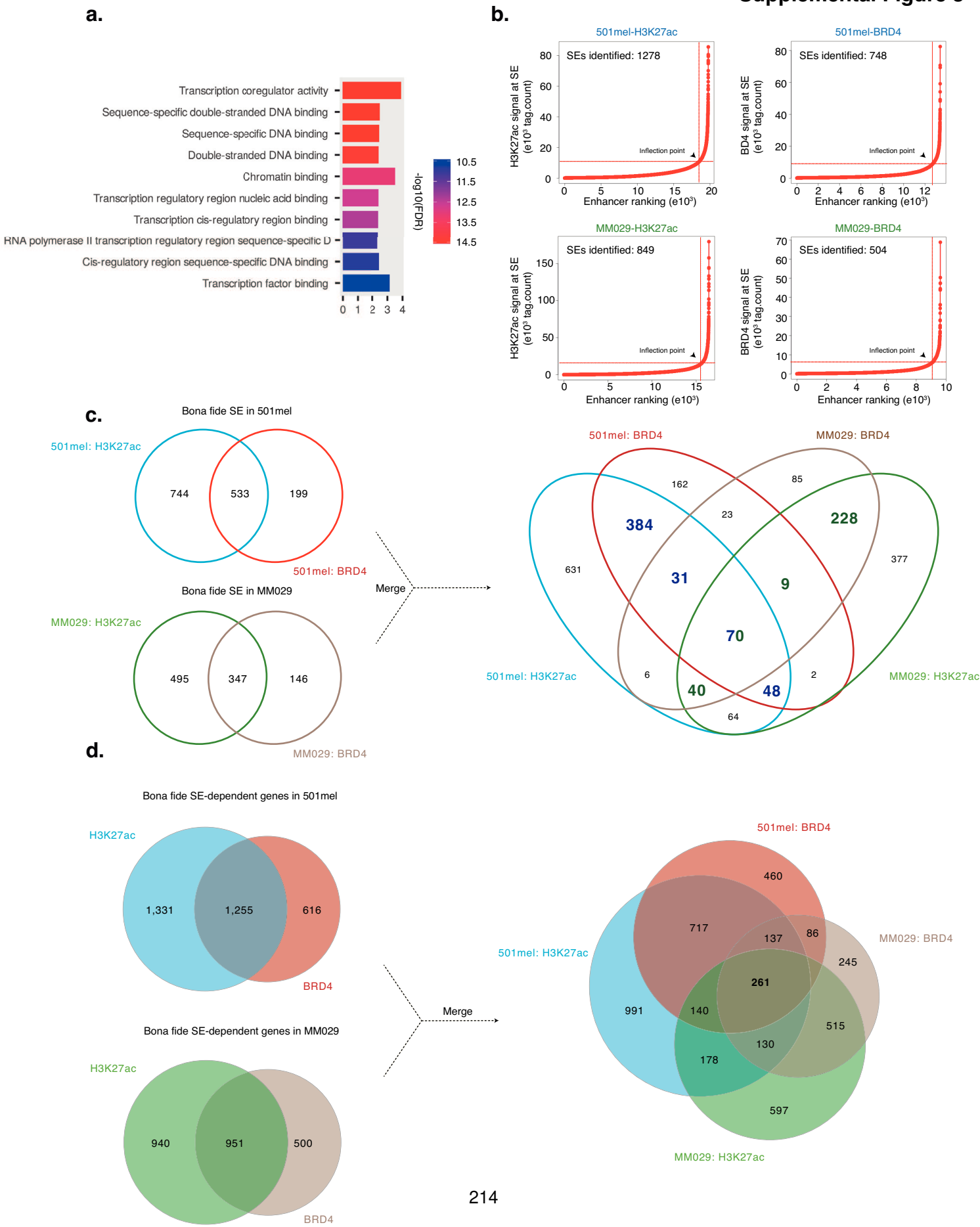
a.
Transcription coregulator activity
Sequence-specific double-stranded DNA binding
Sequence-specific DNA binding
Double-stranded DNA binding
Chromatin binding
Transcription regulatory region nucleic acid binding
Transcription cis-regulatory region binding
RNA polymerase II transcription regulatory region sequence-specific D
Cis-regulatory region sequence-specific DNA binding
Transcription factor binding
0 1 2 3 4
-log10(FDR)
10.5
11.5
12.5
13.5
14.5
b.
501mel-H3K27ac
SEs identified: 1278
H3K27ac signal at SE (e10³ tag.count)
Inflection point
Enhancer ranking (e10³)
501mel-BRD4
SEs identified: 748
BD4 signal at SE (e10³ tag.count)
MM029-H3K27ac
SEs identified: 849
MM029-BRD4
SEs identified: 504
BRD4 signal at SE (e10³ tag.count)
c.
Bona fide SE in 501mel
501mel: H3K27ac
744
533
199
501mel: BRD4
Bona fide SE in MM029
MM029: H3K27ac
495
347
146
MM029: BRD4
Merge
501mel: BRD4
MM029: BRD4
162
85
384
23
228
631
377
31
9
70
501mel: H3K27ac
6
2
MM029: H3K27ac
40
48
64
d.
Bona fide SE-dependent genes in 501mel
H3K27ac
1,331
1,255
616
BRD4
Bona fide SE-dependent genes in MM029
H3K27ac
940
951
500
BRD4
Merge
501mel: BRD4
460
717
137
86
MM029: BRD4
501mel: H3K27ac
245
261
991
140
515
130
178
597
MM029: H3K27ac

Supplemental Figure 8: Identification of SEs in differentiated and undifferentiated melanoma cells

a. GO (Molecular Function) analysis (n=3) of the common set of 642 genes that underwent significant down-regulation upon lurbinectedin exposure of melanoma, SCLC and Non-SCLC cells. The histogram shows the top deregulated biological pathways according to the FDR and fold enrichment.

b. H3K27ac and BRD4 signal (n=3) across enhancer regions for all enhancers in differentiated 501mel and undifferentiated MM029 cells. SEs were defined as enhancers surpassing the respective inflection point signal threshold.

c. Left panel; Venn diagram (n=3) comparing SEs identified by ROSE using either the H3K27ac- or BRD4-occupied sites in differentiated 501mel or undifferentiated MM029 cells. We defined as 'bona fide' SEs bound by both H3K27ac and BRD4. **Right panel**; the two Venn diagrams were merged.

d. Left panel; Venn diagram (n=3) comparing SE-dependent genes identified by ROSE using either the H3K27ac- or BRD4-occupied sites in differentiated 501mel or undifferentiated MM029 cells. We defined as 'bona fide' SE-dependent genes if their SEs are bound by both H3K27ac and BRD4. **Right panel**; the two Venn diagrams were merged.

Supplemental Figure 9

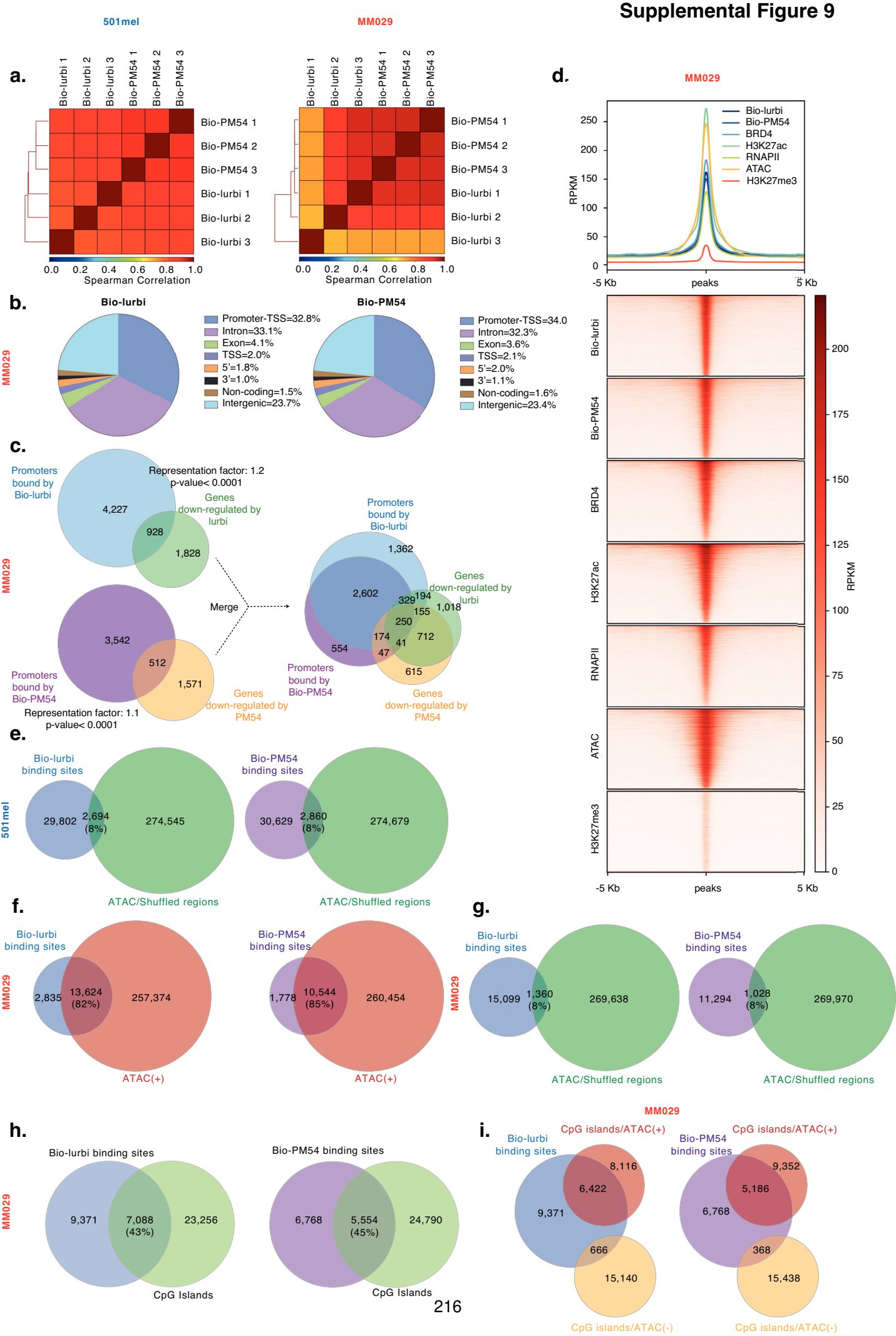

Supplemental Figure 9: Synthetic ecteinascidins engage with transcriptionally active genomic regions in melanoma cells

a. Spearman correlation between triplicates of Chem-map analysis (n=3) of Bio-lurbi and Bio-PM54 in 501mel (left) or MM029 (right) cells.

b. Pie chart showing the distribution of Bio-lurbi- (top) and Bio-PM54-(bottom) annotated peaks (in percentage) all over the genome (hg19) in undifferentiated MM029 cells.

c. Left panel; Venn diagram (n=3) comparing promoters bound by Bio-lurbi or Bio-PM54 and genes down-regulated by Lurbinectedin or PM54 in MM029 cells. **Right panel**; the two Venn diagrams were merged. Representation factor and hypergeometric p-value are indicated.

d. **Upper panel;** Metaplot distribution of Bio-lurbi, Bio-PM54, BRD4, RNAPII, H3K27ac enrichment and ATAC-Seq signals in a +/-5kb window around the occupied DNA binding sites of Bio-lurbi in undifferentiated MM029 cells. **Lower panel**; Heatmap profiles representing the read density clusterings obtained with seqMINER for the DNA-occupied sites of Bio-lurbi in undifferentiated MM029 cells relative to Bio-PM54, BRD4, RNAPII, H3K27ac enrichments and ATAC-Seq signals. Peak order is determined by Bio-lurbi and identical for all clusterings.

e. Venn diagram (n=3) comparing Bio-lurbi (left) and Bio-PM54 (right) binding sites in differentiated 501mel cells and ATAC-seq/ Shuffled regions peaks.

f. Venn diagram (n=3) comparing Bio-lurbi (left) and Bio-PM54 (right) binding sites in differentiated MM029 cells and positive ATAC-seq peaks, indicative of chromatin open region.

g. Venn diagram (n=3) comparing Bio-lurbi (left) and Bio-PM54 (right) binding sites in differentiated MM029 cells and ATAC-seq/ Shuffled regions peaks.

h. Venn diagram (n=3) comparing Bio-lurbi (top) and Bio-PM54 (bottom) binding sites identified in MM029 cells and human CpG Islands.

i. Venn diagram (n=3) comparing Bio-lurbi (left) and Bio-PM54 (right) binding sites in undifferentiated MM029 cells and human CpG islands. Human CpG islands are divided into those found in open chromatin regions (CpG islands/ATAC(+)) and those found in closed chromatin regions (CpG islands/ATAC(-)).

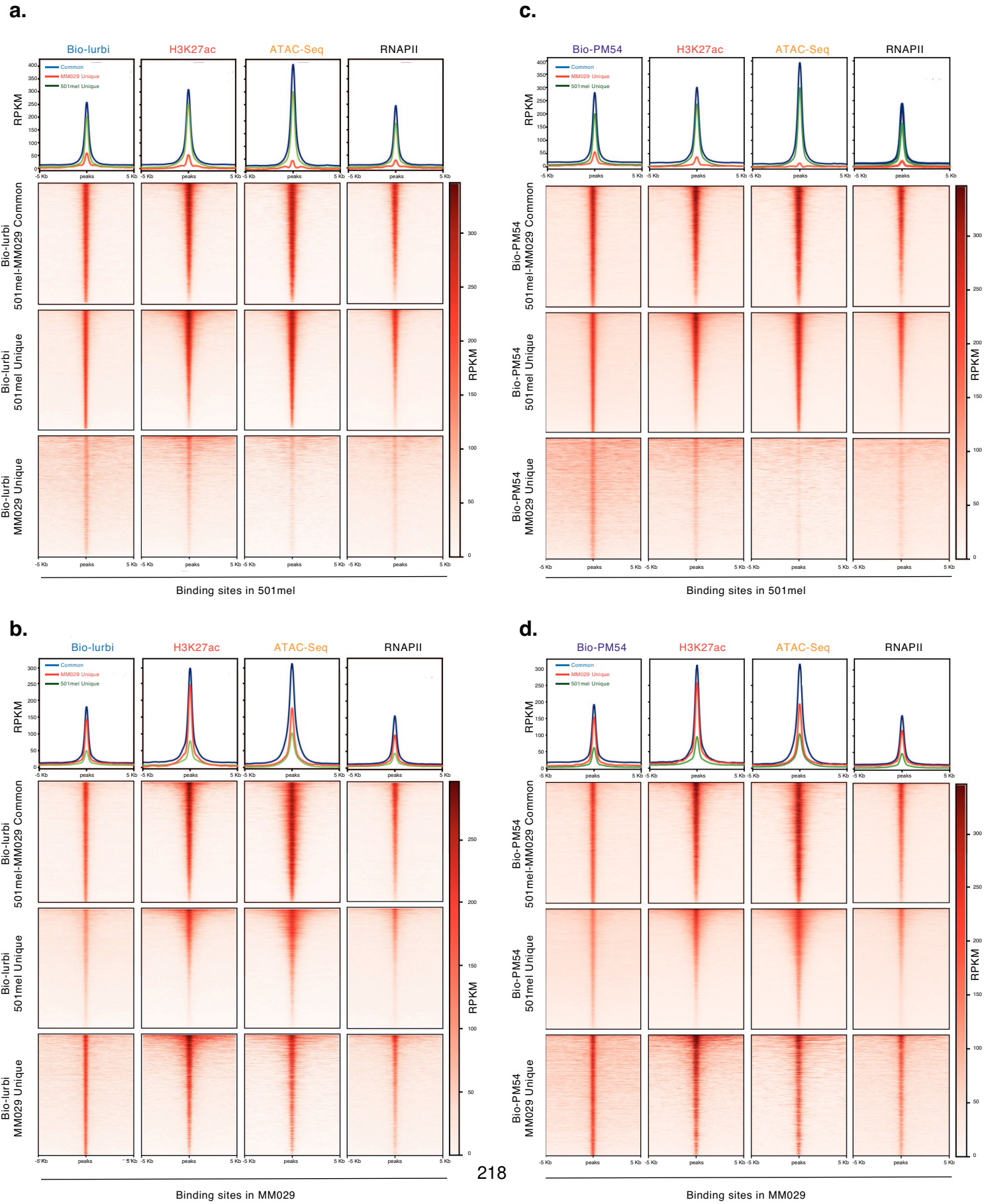
a.
Bio-lurbi
H3K27ac
ATAC-Seq
RNAPII
Common
MM029 Unique
501mel Unique
RPKM
Bio-lurbi 501mel-MM029 Common
Bio-lurbi 501mel Unique
Bio-lurbi MM029 Unique
-5 Kb
peaks
5 Kb
Binding sites in 501mel
c.
Bio-PM54
H3K27ac
ATAC-Seq
RNAPII
Common
MM029 Unique
501mel Unique
RPKM
Bio-PM54 501mel-MM029 Common
Bio-PM54 501mel Unique
Bio-PM54 MM029 Unique
-5 Kb
peaks
5 Kb
Binding sites in 501mel
b.
Bio-lurbi
H3K27ac
ATAC-Seq
RNAPII
Common
MM029 Unique
501mel Unique
RPKM
Bio-lurbi 501mel-MM029 Common
Bio-lurbi 501mel Unique
Bio-lurbi MM029 Unique
-5 Kb
peaks
5 Kb
Binding sites in MM029
d.
Bio-PM54
H3K27ac
ATAC-Seq
RNAPII
Common
MM029 Unique
501mel Unique
RPKM
Bio-PM54 501mel-MM029 Common
Bio-PM54 501mel Unique
Bio-PM54 MM029 Unique
-5 Kb
peaks
5 Kb
Binding sites in MM029

Supplemental Figure 10. Synthetic Ecteinascidins bind to open chromatin

a-b. Top; Metaplot showing the distribution of Bio-lurbi binding sites, exclusively in either 501mel (a) or MM029 (b) cells, or commonly in both, within a ±5 kb window around the total occupied DNA binding sites of Bio-lurbi, H3K27ac, ATAC-Seq, and RNAPII. The data represent enrichment signals. **Bottom**; Heatmap profiles displaying read density clusters generated using seqMINER for DNA-occupied sites where Bio-lurbi is bound exclusively in either 501mel or MM029, or commonly in both. The heatmaps are relative to the total occupied DNA binding sites of Bio-lurbi, H3K27ac, ATAC-Seq, and RNAPII.

c-d. Top; Metaplot showing the distribution of Bio-PM54 binding sites, exclusively in either 501mel (a) or MM029 (b) cells, or commonly in both, within a ±5 kb window around the total occupied DNA binding sites of Bio-PM54, H3K27ac, ATAC-Seq, and RNAPII. The data represent enrichment signals. **Bottom**; Heatmap profiles displaying read density clusters generated using seqMINER for DNA-occupied sites where Bio-PM54 is bound exclusively in either 501mel or MM029, or commonly in both. The heatmaps are relative to the total occupied DNA binding sites of Bio-PM54, H3K27ac, ATAC-Seq, and RNAPII.

Supplemental Figure 11

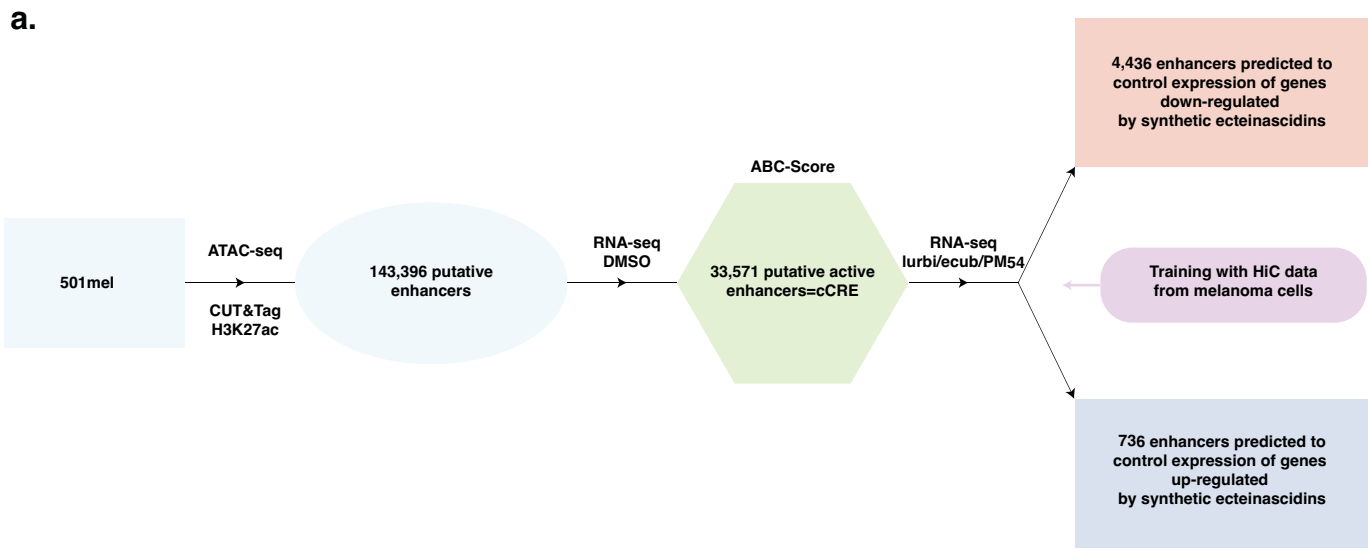

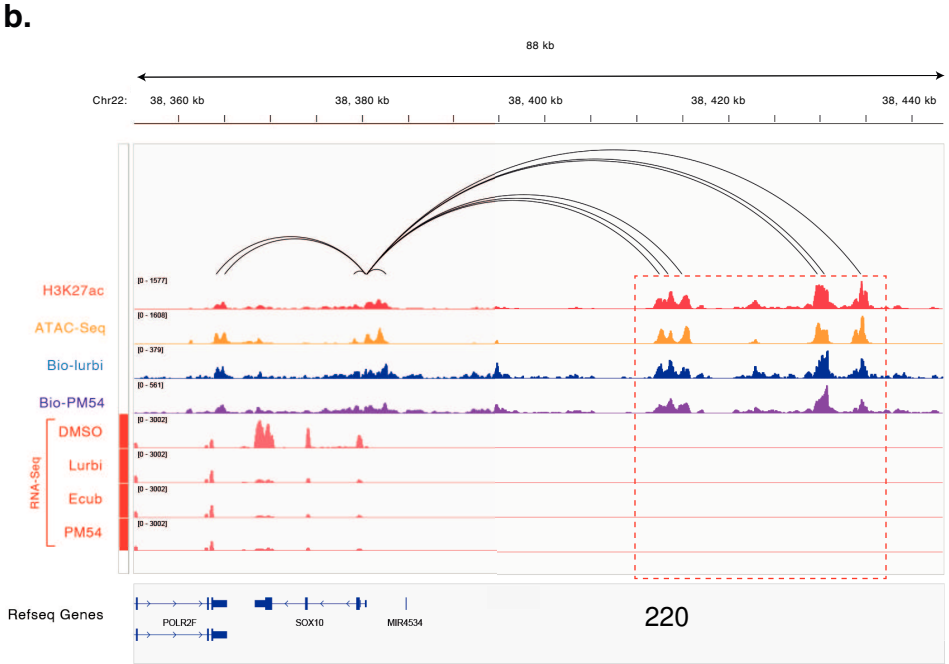

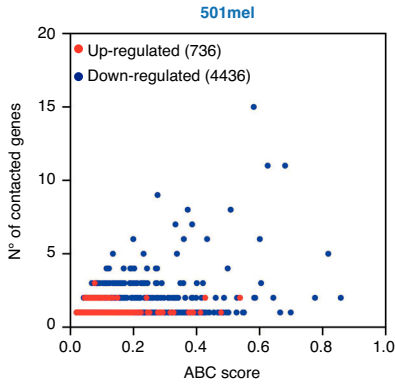

Supplemental Figure 11: Identification of active enhancers in 501mel cells and prediction of their regulated genes

a. Schematic representation of the workflow for ABC-scoring and inferring of enhancer status in 501mel cells.

b. H3K27ac, ATAC-seq, Bio-lurbi, Bio-PM54, and RNA-Seq signal tracks at the SOX10 locus in 501mel cells. Enhancer-promoter interactions predicted by ABC scoring to be negatively affected by synthetic ecteinascidins are shown with black arcs. In red square, the SE putatively regulating SOX10 is shown.

c. Enhancers predicted to be contacting genes either downregulated (blue dots) or upregulated (red dots) in 501mel cells were plotted in regards to their ABC score (relative enhancer strength) and the number of their putatively regulated genes.

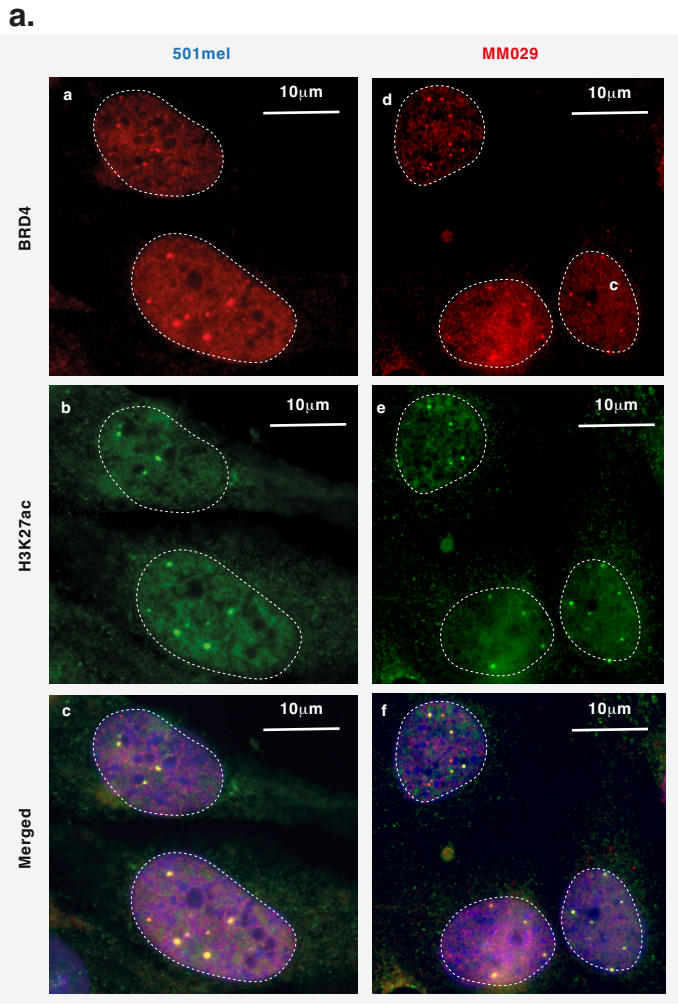
a.
501mel
MM029
BRD4
H3K27ac
Merged
10μm

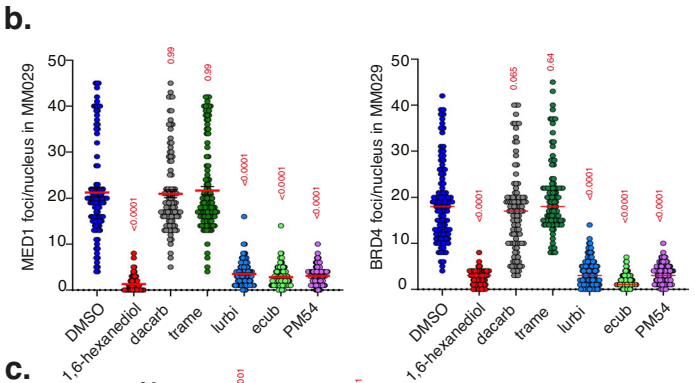
b.
MED1 foci/nucleus in MM029
BRD4 foci/nucleus in MM029
DMSO
1,6-hexanediol
dacarb
trame
lurbi
ecub
PM54

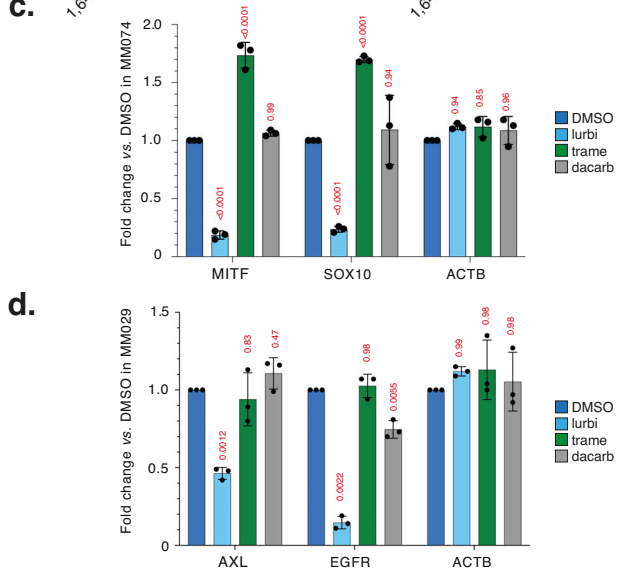
c.
Fold change vs. DMSO in MM074
MITF
SOX10
ACTB
DMSO
lurbi
trame
dacarb
d.
Fold change vs. DMSO in MM029
AXL
EGFR
ACTB

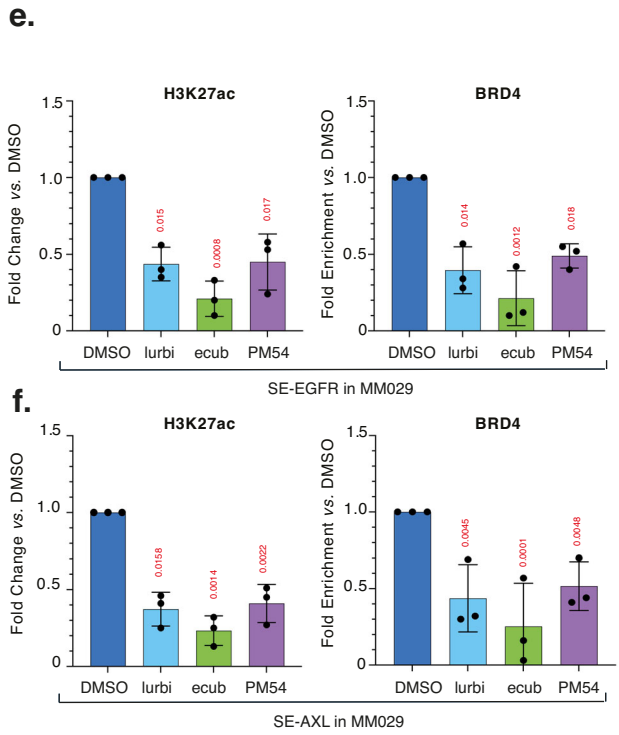
e.
H3K27ac
BRD4
Fold Change vs. DMSO
Fold Enrichment vs. DMSO
DMSO
lurbi
ecub
PM54
SE-EGFR in MM029

f.
H3K27ac
BRD4
Fold Change vs. DMSO
Fold Enrichment vs. DMSO
DMSO
lurbi
ecub
PM54
SE-AXL in MM029

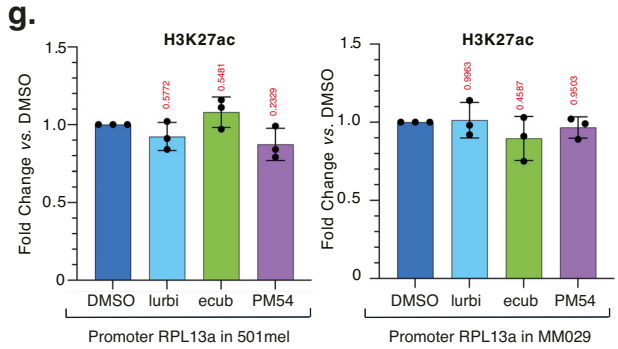
g.
H3K27ac
H3K27ac
Fold Change vs. DMSO
DMSO
lurbi
ecub
PM54
Promoter RPL13a in 501mel
Promoter RPL13a in MM029

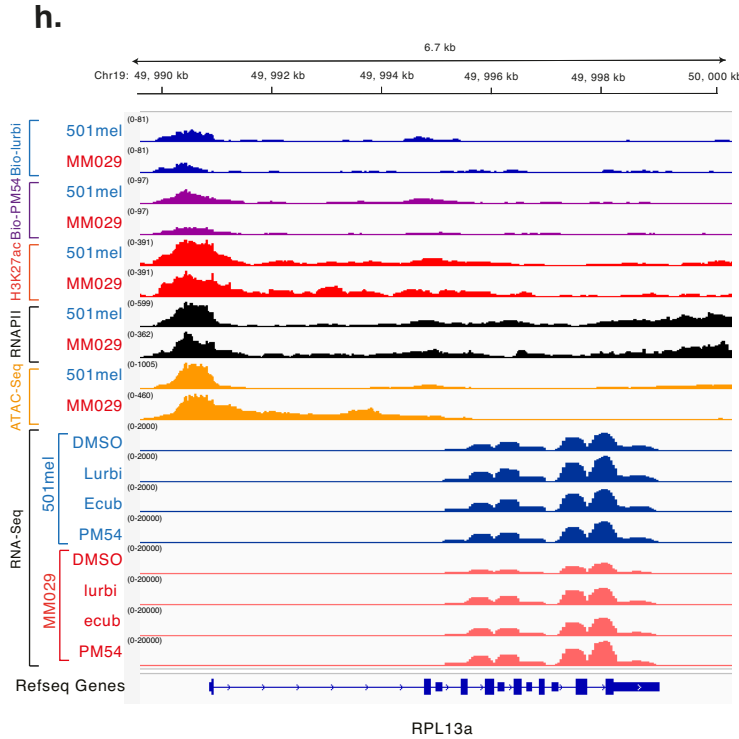
h.
6.7 kb
Chr19: 49, 990 kb
49, 992 kb
49, 994 kb
49, 996 kb
49, 998 kb
50, 000 kb
Bio-lurbi
Bio-PM54
H3K27ac
RNAPII
ATAC-Seq
RNA-Seq
501mel
MM029
DMSO
Lurbi
Ecub
PM54
lurbi
ecub
Refseq Genes
RPL13a

Supplemental Figure 12: Synthetic ecteinascidins inactivate SEs in melanoma cells

a. Representative fluorescence microscopy images (n=3) of 501mel or MM029 melanoma cells co-immunostained with anti-BRD4 (red) and anti-H3K27ac (green) antibodies. Images of the cells were obtained with the same microscopy system and constant acquisition parameters for a given staining. Source data are provided in the source data file. Scale bars are indicated.

b. The numbers of MED1 and BRD4 foci per nucleus (n=100) observed in MM029 cells following treatment with either DMSO, the liquid-phase condensate disruptor 1,6-hexanediol (3% vol, 20 minutes), the MEKi Trametinib (50nM, 10 hours), the DNA damaging agent Dacarbazine (50μM, 10 hours) or the synthetic ecteinascidins (5xIC50, 10 hours) are shown +/- SD. Red bars indicate mean integrated density. One-way ANOVA with post-hoc Tukey adjustment comparisons were used to determine the p-values (*vs.* DMSO).

c-d. qRT-PCR analysis (n=3) showing average 18S-normalized expression of MITF, SOX10 and ACTB in the differentiated MM074 cells **(c)** or AXL, EGFR and ACTB in the undifferentiated MM029 cells **(d)** treated with either vehicle (DMSO), lurbinectedin (5xIC50 concentration, 10 hours), the MEKi Trametinib (2.5nM for MM074 and 50nM for MM029, 10 hours) or the DNA damaging agent Dacarbazine (50μM, 10 hours). Error bars indicate mean values + SD for three biological triplicates. Ordinary one-way ANOVA using Dunnett's multiple comparisons test was used to determine the p-values (*vs.* DMSO). Source data are provided in the source data file.

e-f. ChIP-qPCR (n=3) monitoring the fold change of H3K27ac mark or BRD4 protein at the SEs regulating EGFR (e) or AXL (f) (+/- SD) in mock- or synthetic ecteinascidin-treated undifferentiated MM029 cells (5xIC50, 10 hours). One-way ANOVA with post-hoc Tukey adjustment comparisons were used to determine the p-values (*vs.* DMSO). Source data are provided in the source data file.

g. ChIP-qPCR (n=3) monitoring the fold change of H3K27ac mark at the promoter regulating RPL13a (+/- SD) in mock- or synthetic ecteinascidin-treated undifferentiated 501mel or MM029 cells (5xIC50, 10 hours). One-way ANOVA with post-hoc Tukey adjustment comparisons were used to determine the p-values (*vs.* DMSO). Source data are provided in the source data file.

h. Gene tracks of Bio-lurbi, Bio-PM54, RNAPII, H3K27ac occupancy, ATAC-seq and RNA-Seq signals at *RPL13a* loci in 501mel or MM029 cells. RNA-Seq signals show that this gene is expressed in both 501mel and MM029 melanoma cells and unaffected by drug-treatment.

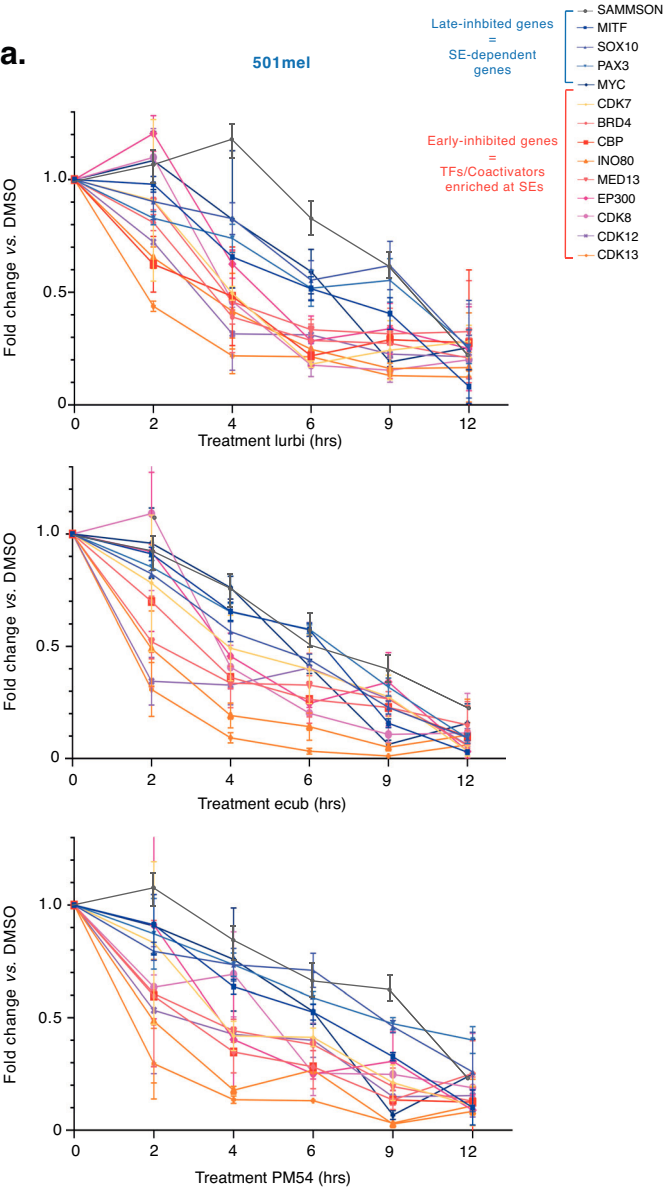
a.
501mel
Late-inhbited genes = SE-dependent genes
SAMMSON
MITF
SOX10
PAX3
MYC
Early-inhibited genes = TFs/Coactivators enriched at SEs
CDK7
BRD4
CBP
INO80
MED13
EP300
CDK8
CDK12
CDK13
Fold change vs. DMSO
Treatment lurbi (hrs)
Treatment ecub (hrs)
Treatment PM54 (hrs)

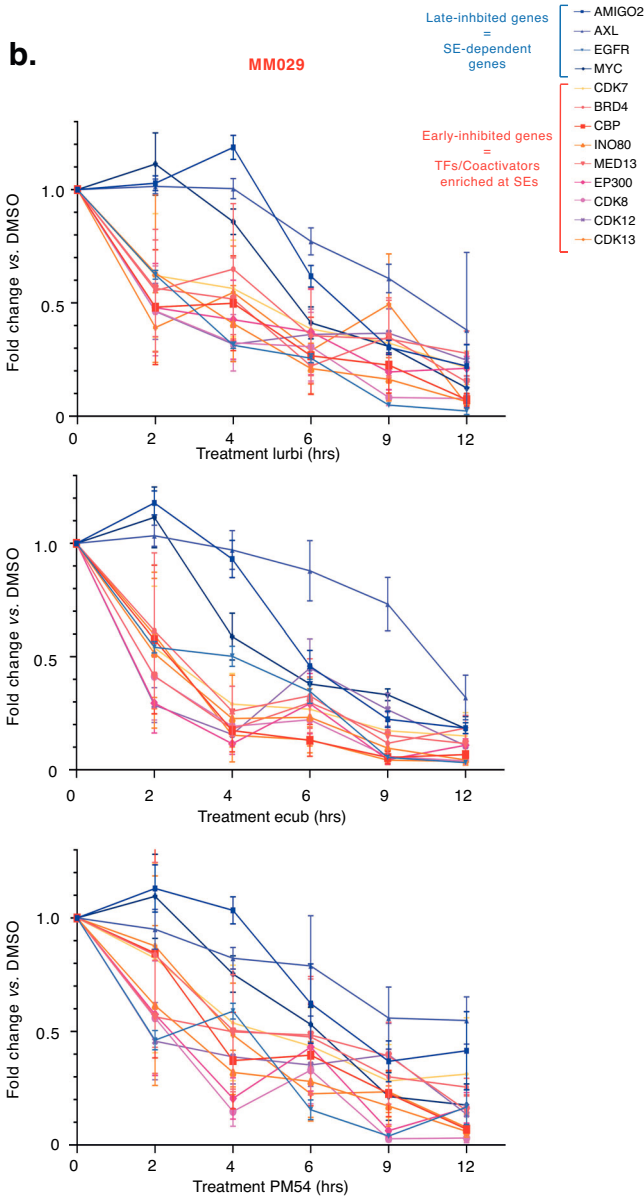
b.
MM029
Late-inhbited genes = SE-dependent genes
AMIGO2
AXL
EGFR
MYC
Early-inhibited genes = TFs/Coactivators enriched at SEs
CDK7
BRD4
CBP
INO80
MED13
EP300
CDK8
CDK12
CDK13
Fold change vs. DMSO
Treatment lurbi (hrs)
Treatment ecub (hrs)
Treatment PM54 (hrs)

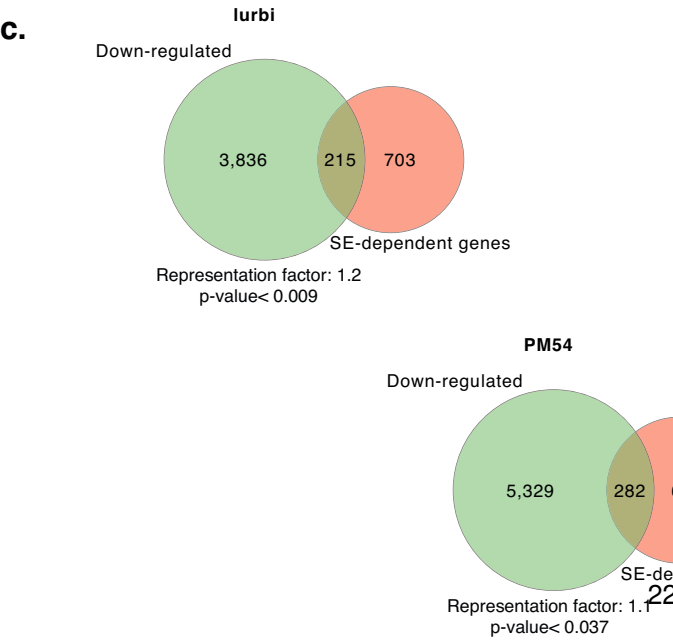
c.
lurbi
Down-regulated
3,836
215
703
SE-dependent genes
Representation factor: 1.2
p-value< 0.009
ecub
Down-regulated
4,083
242
676
SE-dependent genes
Representation factor: 1.2
p-value< 0.000275
PM54
Down-regulated
5,329
282
636
SE-dependent genes
Representation factor: 1.1
p-value< 0.037

Supplemental Figure 13: Synthetic ecteinascidins affect transcription factors/coactivators and specific SE-dependent genes in melanoma cells

a-b. qRT-PCR (n=3) analysis showing average 18S-normalized expression of the indicated genes in the differentiated 501mel **(a)** or undifferentiated MM029 melanoma cells **(b)** following treatment with Lurbinectedin, Ecubectedin or PM54 (5xIC50 concentration) for the indicated period of time. Error bars indicate the mean values +/- SD for three biological triplicates. Results are shown as relative expression compared to mock-treated cells. Source data are provided in the source data file.

c. Venn diagram (n=3) comparing the genes downregulated by ecteinascidins, as indicated, in DMS53 cells (SCLC) (10xIC50 concentration, 8 hours) and SE-dependent genes identified in these cells (GSE190618 [1]). Representation factor and hypergeometric p-value are indicated.

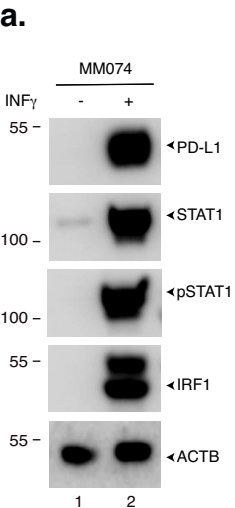
a.
MM074
INFγ
-
+
55
PD-L1
100
STAT1
100
pSTAT1
55
IRF1
55
ACTB
1
2

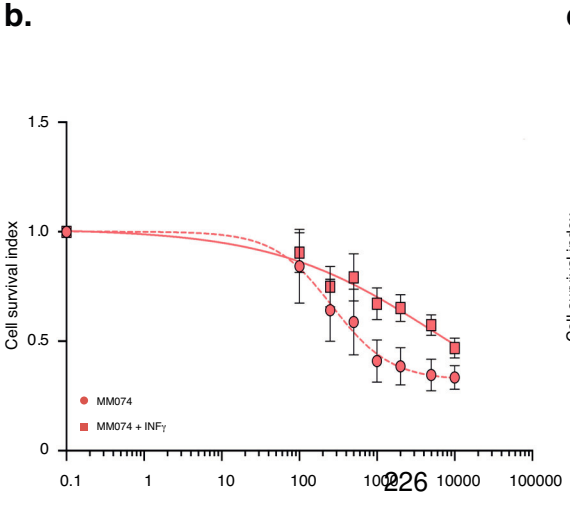
b.
Cell survival index
1.5
1.0
0.5
0
MM074
MM074 + INFγ
0.1
1
10
100
1000
10000
100000
Concentration of Vemurafenib (nM)

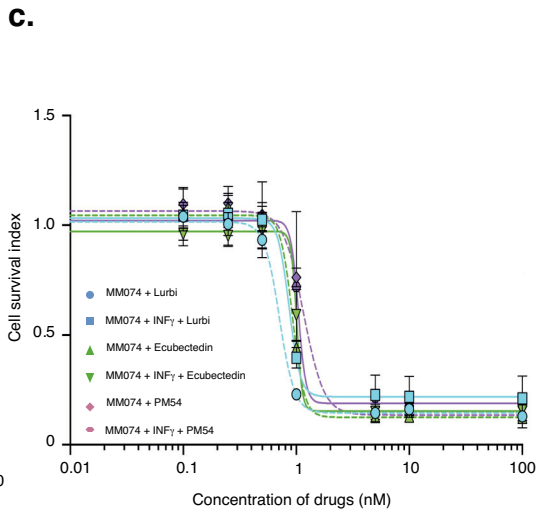
c.
Cell survival index
1.5
1.0
0.5
0
MM074 + Lurbi
MM074 + INFγ + Lurbi
MM074 + Ecubectedin
MM074 + INFγ + Ecubectedin
MM074 + PM54
MM074 + INFγ + PM54
0.01
0.1
1
10
100
Concentration of drugs (nM)

Supplemental Figure 14: Pseudo-interferon-active melanoma cells are resistant to MAPKi but sensitive to synthetic ecteinascidins

a. Protein lysates from differentiated MM074 melanoma cells treated or not with INFγ (20ng/ml, 24 hours), were immuno-blotted for proteins as indicated. Molecular mass of the proteins is indicated (kDa). Source data are provided in the source data file. This experiment was repeated independently three times with similar results.

b. MM074 cells were pre-treated with INFγ (20ng/ml, 24 hours) and then with increasing doses of vemurafenib, in the presence of INFγ. Mean growth is shown relative to vehicle (H2O)-treated cells. Error bars indicate mean values +/- Standard Deviation (SD) for three biological triplicates. Source data are provided in the source data file.

c. MM074 cells were treated with INFγ for (20ng/ml, 24 hours), and then with increasing concentrations of lurbinectedin, ecubectedin or PM54, in the presence of INFγ. Mean growth is shown relative to mock-treated cells. Error bars indicate mean values +/- Standard Deviation (SD) for three biological triplicates. Source data are provided in the source data file.

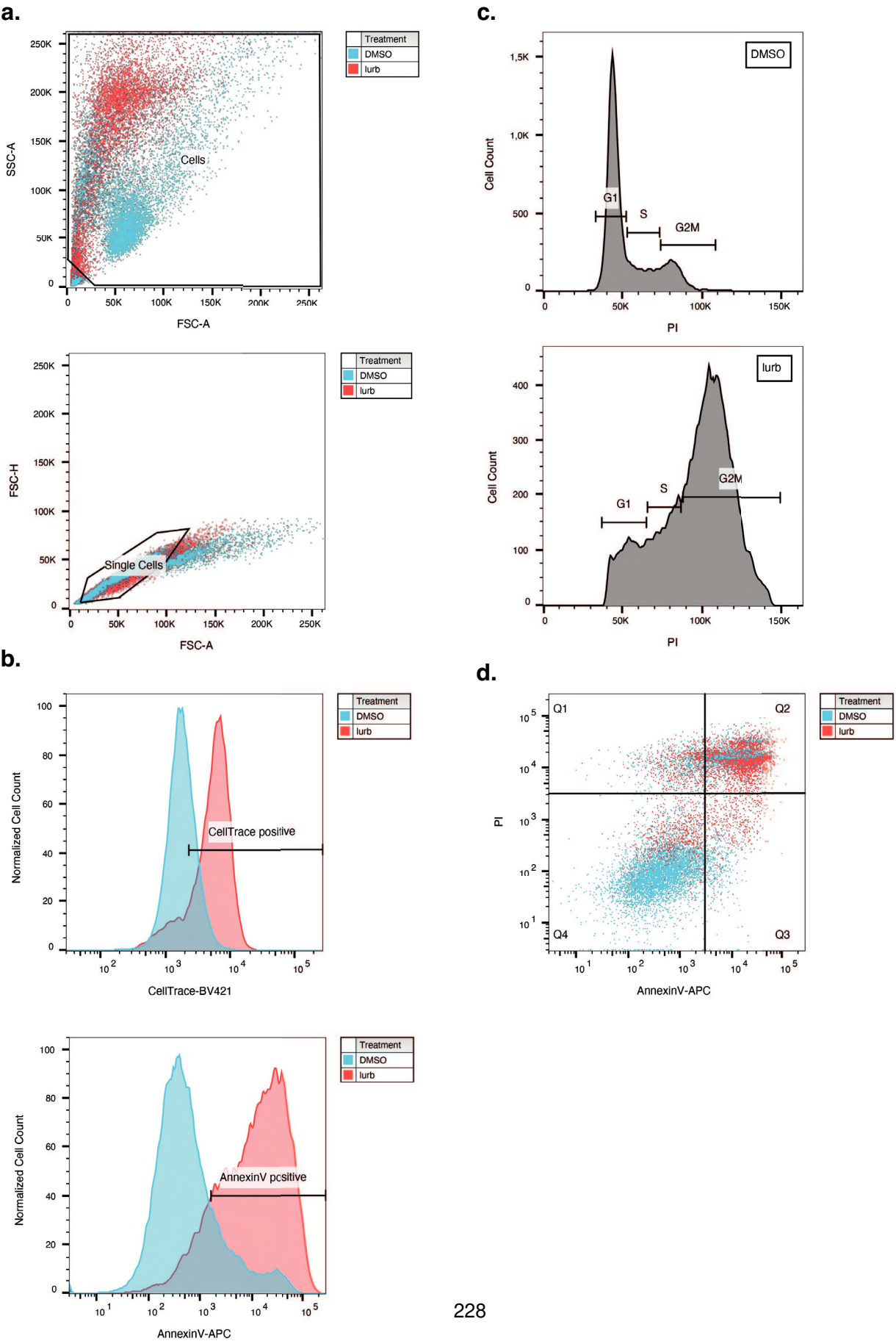
a.
Treatment
DMSO
lurb
SSC-A
FSC-A
Cells
FSC-H
Single Cells
b.
Normalized Cell Count
CellTrace-BV421
CellTrace positive
AnnexinV-APC
AnnexinV positive
c.
DMSO
lurb
Cell Count
PI
G1
S
G2M
d.
Q1
Q2
Q3
Q4
PI
AnnexinV-APC

Supplemental Figure 15: Gating strategies for flow cytometry data analysis

a. Representative gating strategies. Upper panel shows the exclusion of debris, and the lower panel illustrates the isolation of single cells. These strategies were consistently applied across all flow cytometry assays, analyzing a minimum of 20,000 single cells per sample.

b. Representative gating strategies for CellTrace and Annexin V assays. Slow-proliferating cells were defined as the 30% of cells with the highest CellTrace Violet signal in the DMSO control. Drug-treated samples were then assessed for the percentage of cells exceeding this threshold (upper panel). Apoptotic cells were identified as the 20% of cells with the highest Annexin V-APC signal in the DMSO control (lower panel).

c. Propidium iodide (PI) intensity was used to determine cell cycle phases.

d. Representative example of a bivariant dot plot distinguishing cell populations: viable (Q4, Annexin V− / PI−), early apoptotic (Q3, Annexin V+ / PI−), late apoptotic (Q2, Annexin V+ / PI+), and necrotic (Q1, Annexin V− / PI+).

Part II: Induction of BRCAness-like state through transcription elongation inhibition

Preface to Article 2:

Following the publication of our first study in *Nature Communications*, our next objective was to identify therapeutic strategies capable of enhancing the anti-cancer activity of synthetic ecteinascidins. To this end, we expanded our transcriptional analyses beyond cutaneous melanoma to include five distinct cancer models, with the aim of identifying transcriptional programs commonly affected by the compounds. Interestingly, these analyses revealed a consistent downregulation of DNA repair pathways, particularly genes involved in homologous recombination (HR) and the Fanconi anemia pathway, independently of cancer type.

These findings initiated a new project that I started during the second year of my PhD and continued throughout the remainder of my doctoral work, which I co-led together with Max Cigrang. The primary objective of this study was to understand the molecular basis underlying the preferential repression of DNA repair genes by synthetic ecteinascidins, and to determine whether this transcriptional repression could induce a functional HR-deficient state resembling BRCA1/2-mutated tumors, thereby sensitizing HR-proficient cancers to PARP inhibitors and potentially extending the clinical utility of these therapies beyond the limited subset of patients harboring BRCA1/2 mutations.

During the last three years of my PhD, I was primarily responsible for experimental design, high-throughput sequencing analyses, and the characterization of drug combinations between ecteinascidins and PARP inhibitors, with valuable support from Max Cigrang. The central finding of this work is that synthetic ecteinascidins impair RNA polymerase II elongation and induce premature transcription termination, preferentially affecting long DNA repair genes, including BRCA1/2 and multiple homologous recombination and Fanconi anemia factors. This transcriptional vulnerability results in a BRCAness-like state associated with homologous recombination deficiency and sensitization of multiple HR-proficient cancer models to PARP inhibition.

At the time of writing this manuscript, the *in vitro* component of the project is nearly completed, with additional RNA polymerase II Ser2 phosphorylation ChIP-sequencing datasets currently being finalized. In parallel, we are collaborating with PharmaMar to evaluate these findings *in vivo* using patient-derived xenograft models. The manuscript presented below, on which I am listed as co-first author, contains the *in vitro* findings generated during this project and will be submitted upon completion of the ongoing *in vivo* validation studies. This project also greatly benefited from the technical and scientific contributions of Maguelone Nogaret, as well as Clara Capelli, a PhD student in the laboratory whom I supervised during her Master internship.

Ecteinascidin-induced transcription elongation defects trigger a BRCAness-like state and sensitize HR-proficient tumors to PARP inhibitors

Julian Obid [1, 2, 3, 4*], Max Cigrang [1, 2, 3, 4*], Maguelone Nogaret [1, 2, 3, 4], Clara Capelli [1, 2, 3, 4], Anthony Hannus [1,2, 3, 4], Tao Ye [1,2, 3, 4], Matthieu Jung [1,2, 3, 4], Guillaume Davidson [1,2, 3, 4], Frédéric Coin [1, 2, 3, 4, 5]

1 IGBMC, Institut de Génétique et de Biologie Moléculaire et Cellulaire Illkirch Cedex, C.U., Strasbourg, France

2 Centre National de la Recherche Scientifique, UMR7104, 67404 Illkirch, France

3 Institut National de la Santé et de la Recherche Médicale, U1258, 67404 Illkirch, France

4 Université de Strasbourg, 67404 Illkirch, France

5 Corresponding author, fredr@igbmc.fr

* Co-first authors

Tel: +33 3 88 65 34 49

Subtitle*:* Clinically approved ecteinascidins extend PARP inhibitor sensitivity to HR-proficient and PARPi-resistant cancers through transcriptional repression of homologous recombination

Key words: PARP inhibitors, BRCAness, homologous recombination, transcription elongation, ecteinascidins, lurbinectedin, synthetic lethality, DNA damage response

Abstract:

PARP inhibitors (PARPi) exploit synthetic lethality with homologous recombination (HR) deficiency (HRD) to treat BRCA1/2-mutated cancers, but their clinical utility is limited by the rarity of BRCA mutations and the frequent emergence of resistance. Here, we show that sublethal doses of the clinically approved synthetic ecteinascidin lurbinectedin or its analog PM54 pharmacologically reprogram the transcriptional landscape of cancer cells toward a BRCAness phenotype. Using functional genomics, we find that synthetic ecteinascidin treatment impairs RNA polymerase II elongation and promotes premature transcription termination, disproportionately downregulating long DNA repair genes, including BRCA1, BRCA2, ATM, and ATR. This transcriptional rewiring generates a HRD state that strongly synergizes with PARPi to induce synthetic lethality in multiple HR-proficient cancer models. The combination triggers extensive DNA damage in actively transcribed genomic regions, leading to apoptosis. Remarkably, it also restores PARPi sensitivity in acquired resistant BRCA1-mutant tumors. These findings identify synthetic ecteinascidins as mechanistically distinct, broad-spectrum inducers of BRCAness and potentially provide an immediately translatable strategy to expand and prolong the efficacy of PARP inhibitors in cancer therapy.

Introduction:

Poly (ADP-ribose) polymerase inhibitors (PARPi) have transformed the treatment of BRCA-mutated cancers, yet their clinical impact remains limited by two major challenges: the relatively low frequency of BRCA1/2 mutations and the frequent emergence of intrinsic or acquired resistance[1–4]. Extending the efficacy of PARPi to homologous recombination (HR)-proficient tumors therefore represents a major unmet therapeutic need.

The rationale for PARPi therapy is based on the principle of synthetic lethality, whereby the simultaneous impairment of two complementary DNA repair pathways results in cell death, while disruption of either pathway alone is tolerated[5–7]. In this context, HR represents a critical pathway for the accurate repair of DNA double-strand breaks (DSBs). HR is an error-free repair mechanism that uses the sister chromatid as a template, thereby preserving genomic integrity[8,9]. Accordingly, in HR-deficient (HRD) cells, such as those harboring BRCA1/2 alterations, cells become increasingly reliant on PARP-mediated single-strand breaks (SSBs) repair pathway for survival. As a consequence, inhibition of PARP in BRCA-deficient tumors leads to the accumulation of unrepaired DNA lesions, replication fork collapse, and ultimately cell death[10–12]. Clinically, four PARPi (olaparib, rucaparib, niraparib, and talazoparib) have been approved for the treatment of BRCA-mutated breast, ovarian, prostate, pancreatic, and peritoneal cancers[13–18]. These agents act by inhibiting PARP catalytic activity and by trapping PARP-DNA complexes, which interfere with DNA replication and generate cytotoxic DSBs in HRD contexts [19–22]. Nevertheless, BRCA1/2 mutations are rare, occurring in only ~5-15% of breast and ovarian cancers, and even at lower frequencies in other malignancies[1,2,23–25]. Moreover, up to half of BRCA-mutated tumors fail to respond to PARPi or acquire resistance during treatment [3,26–28], thereby limiting the broader applicability of PARPi-based therapies.

One strategy to overcome these limitations is to induce a BRCAness-like state, defined as a functional deficiency in HR mimicking BRCA1/2 loss, in otherwise BRCA-proficient tumors[29,30]. Such states can arise from alterations affecting additional HR or DNA interstrand crosslink (ICL) repair genes, including PALB2, ATM, ATR, or components of the Fanconi anemia (FA) pathway[29,31–34], but these events remain relatively infrequent in patients. Pharmacological

approaches to induce BRCAness have therefore been explored[35], notably using inhibitors of transcriptional regulators (e.g., BRD4, CDK7, CDK12)[36–42], DNA damage response kinases (ATM, ATR)[43–46], or oncogenic signaling pathways [47–49]. While these strategies have shown promise in preclinical settings, no clinically approved agent has yet been demonstrated to reliably induce a BRCAness-like state in HR-proficient tumors, highlighting a critical gap in current therapeutic strategies.

Ecteinascidins are marine-derived alkaloids with potent antitumor activity. Lurbinectedin, a synthetic ecteinascidin, binds covalently to CpG-rich DNA sequences and preferentially targets open chromatin regions at active promoters and enhancers. This interaction disrupts transcriptional programs and induces DNA damage at nanomolar concentrations [50–52]. Lurbinectedin is approved for the treatment of relapsed small-cell lung cancer, and multiple clinical trials are currently evaluating its combination with DNA-damaging agents or DNA damage response inhibitors [53–55]. In addition, we previously developed PM54, a synthetic analog of lurbinectedin with optimized structural features that may enhance selectivity and pharmacological properties while retaining similar DNA-binding and transcriptional inhibitory activity, and which is currently under clinical evaluation in advanced solid tumors[56].

Here, we identify a previously unrecognized property of ecteinascidins: their ability to induce a transcription-dependent BRCAness-like state in HR-proficient cancers. Using integrated functional genomics approaches, we show that lurbinectedin and PM54 rapidly suppress the expression of BRCA1, BRCA2, and other key double-strand break repair genes, including PALB2, ATM, and ATR. Mechanistically, ecteinascidins impair transcription elongation, reduce RNA polymerase II processivity, and promote premature transcription termination, effects that disproportionately affect long genes, notably those involved in HR. This induced HR-deficient state results in strong synergy between ecteinascidins and PARPi, leading to synthetic lethality across multiple HR-proficient cancer models. The combination enhances DNA damage within actively transcribed regions and promotes apoptotic cell death. Notably, this approach is also effective in PARPi-resistant models.

Together, our findings identify ecteinascidins as clinically approved or advanced agents capable of inducing a transcription-dependent BRCAness-like state, providing a mechanistically distinct strategy to extend PARP inhibitor sensitivity to HR-proficient cancers.

Results:

Ecteinascidins induce a BRCAness-like state and HR deficiency

We previously demonstrated that synthetic ecteinascidins (hereinafter just referred as 'ecteinascidins') exert potent cytotoxic effects across phenotypically distinct cancers such as melanoma and small cell lung cancer by selectively binding to CG-rich regions of transcriptionally active chromatin, thereby inducing highly cell type-specific transcriptional inhibition[56].

To identify a potential common signature of transcription inhibition induced by ecteinascidin treatment, we performed RNA sequencing (RNA-seq) on five HR-proficient cancer cell lines derived from distinct tissue types: 501mel (melanoma), DMS53 (small cell lung cancer), A549 (non-small cell lung cancer), MCF7 (breast cancer), and SKOV3 (ovarian cancer). Cells were treated with either lurbinectedin or PM54 for 12 hours at 5×IC50 concentrations. Ecteinascidin treatments induced substantial transcriptional reprogramming across the five cancer cell lines (Figure 1a,b), with 449 genes consistently downregulated by both compounds (adjusted $P < 0.001$) (Figure 1c). Notably, gene ontology analysis revealed homologous recombination (HR) and Fanconi anemia (FA) pathways among the most significantly enriched categories within the downregulated gene set (Supplementary Figure 1a). Commonly repressed genes included key HR/FA effectors such as BRCA2, TOPBP1, BLM, MCM9, and MMS22L, as well as transcriptional regulators including CDK7, CDK12, CDK13, and BRD4 (Supplementary Figure 1b).

To further assess pathway-specific effects, we analyzed curated DNA repair gene sets. Genes involved in double-strand break repair (DSBR) and interstrand crosslink repair (ICLR), particularly those mediating HR and FA pathways, were consistently more significantly downregulated than genes associated with other repair processes such as single-strand break repair (SSBR) (Figure 1d). Across models, 45-70% of DSBR and ICLR genes were significantly

repressed, compared to 25-45% of genes in other DNA repair pathways (Supplementary Figure 1c).

To evaluate the broader impact of ecteinascidin treatment on BRCAness-associated transcriptional programs, we next interrogated the expression of curated BRCAness and PARP inhibitor sensitivity signatures, integrating gene sets from Lord & Ashworth and Zimmermann et al.[29,33] (hereafter referred to as the 'BRCAness signature'). Across all five models, ecteinascidins treatment resulted in a consistent and significant repression of BRCAness-associated genes (Supplementary Figure 1d,e). Downregulation of key HR components was confirmed at the protein level by western blot analysis, demonstrating reduced expression of BRCA1, BRCA2, BLM, WRN, and RAD51, as well as transcriptional regulators CDK7, CDK9, CDK12, BRD4, and EP300 (Figure 1e). In contrast, protein levels of canonical non-homologous end joining (NHEJ) factors (LIG4, XRCC4) and the SSBR enzyme PARP1 remained largely unchanged. Ecteinascidin treatment also induced apoptosis, as evidenced by cleaved caspase-3, and triggered DNA double-strand break formation, as indicated by γH2AX accumulation (Figure 1e).

In parallel, we analysed the impact of our compounds on validated gene expression signatures shown to predict functional HR deficiency (HRD) and clinical response to PARP inhibitors or platinum-based chemotherapy, integrating the Peng et al. and Beinse et al. datasets[57,58] (referred to as the 'HRD signature'). Ecteinascidin-treated cells showed coordinated downregulation of genes typically repressed in HRD tumors and upregulation of genes commonly induced under HRD conditions (Supplementary Figures 1f-h). Functionally, both lurbinectedin and PM54 markedly impaired HR efficiency across all models, as measured by HR reporter assays, with effects even exceeding those observed upon BRCA1 or BRCA2 siRNA-mediated knockdown (Figure 1f and Supplementary Figures 1j,k).

To determine whether this transcriptional reprogramming toward a BRCAness-like state was specific to ecteinascidins rather than a general response to DNA damage or DNA-binding agents, we treated cells with cisplatin under comparable conditions. Unlike ecteinascidins, cisplatin did not elicit consistent downregulation of BRCAness-associated genes, as assessed

by RT-qPCR (Supplementary Figure 1d), western blot analysis (Supplementary Figure 1i), or HR reporter assay (Figure 1f). On the contrary, cisplatin treatment led to marked increases in protein levels of the HR effectors BRCA1, BRCA2, BLM, and RAD51, as well as transcriptional regulators CDK9 and CDK12, and HR activity.

Together, these findings demonstrate that ecteinascidins selectively suppress key components of HR and FA pathways across diverse cancer models, resulting in both transcriptional and functional hallmarks of a BRCAness-like state. This mechanistically distinguishes ecteinascidins from classical DNA-damaging agents and supports their potential to induce HR deficiency through targeted transcriptional repression.

Ecteinascidins bind broadly to active genes but preferentially repress long ones

To investigate the mechanistic basis underlying the preferential downregulation of homologous recombination (HR) and Fanconi anemia (FA) genes, we first assessed whether ecteinascidins exhibit selective binding to these loci. Given their established function as DNA-binding transcriptional inhibitors, we hypothesized that preferential targeting of DSBR- and ICLR-associated genes could account for their selective repression.

To test this, we performed Chem-Map profiling by combining biotinylated ecteinascidins with CUT&Tag to map genome-wide binding sites. Across cell lines, we identified between 35,000 and 70,000 high-confidence binding sites per model. Approximately 70% of binding events were located within gene bodies, with a strong enrichment at promoter regions (Supplementary Figure 2a). Binding profiles varied substantially between cancer types, with only 10-20% of sites shared across all models and 20-40% being cell-type specific (Supplementary Figure 2b), consistent with differential transcriptional programs. In agreement with these observations, ecteinascidin binding strongly correlated with chromatin accessibility, as evidenced by a robust positive correlation between Bio-Lurbi or Bio-PM54 signal and ATAC-seq promoter signal (Figure 2a), indicating preferential association with open chromatin.

Visualization of Chem-map signal confirmed substantial ecteinascidin binding at promoters of DNA repair genes across all models (Supplementary Figure 2c). However, this binding was not restricted to DSBR-associated genes, as comparable or higher signal was observed at

SSBR promoters. Consistently, neither ecteinascidin binding intensity nor promoter accessibility correlated with transcriptional changes after treatment, as measured by RNA-seq log2 fold change (Figures 2b,c). Direct comparison of DSBR and SSBR gene sets further revealed no significant differences in drug binding or promoter accessibility (Figure 2d), indicating that selective repression of HR and FA pathways cannot be explained by preferential ecteinascidin recruitment.

We therefore sought alternative determinants underlying this specificity. We first examined intrinsic gene features that could influence transcriptional sensitivity. No significant differences were observed in basal expression levels (Figure 2e) or GC content (Figure 2f) between DSBR and SSBR genes. In contrast, gene architecture analysis revealed that DSBR-associated genes are significantly longer than SSBR genes across all models (Figures 2g,h). Consistently, genes downregulated upon ecteinascidin treatment were significantly enriched for long genes (Figure 2i), and transcriptome-wide analysis revealed a robust negative correlation between gene length and expression fold change following treatment (Figure 2j).

Together, these findings demonstrate that while ecteinascidins bind broadly to transcriptionally active chromatin, transcriptional repression is strongly dependent on gene length, providing a potential mechanistic explanation for the selective vulnerability of long DSBR and ICLR genes to ecteinascidin treatment.

Rapid downregulation of transcription elongation regulators underlies BRCAness induction

The observed gene length-dependent transcriptional repression suggested that defects in transcription elongation may underlie the effects of ecteinascidins. Notably, key regulators of productive transcription elongation, including CDK7, CDK9, CDK12, and BRD4, are known to control the expression of homologous recombination (HR) genes and have been previously linked to HR deficiency-like states upon depletion [37–42,59–61]. Consistent with this, these elongation regulators were among the most strongly and consistently downregulated genes across all cancer models following ecteinascidin treatment (Figure 1e; Supplementary Figures 1b,d).

Based on these findings, we hypothesized that ecteinascidins initiate a two-step mechanism: an early wave of transcriptional inhibition targeting transcription elongation regulators, followed by secondary downregulation of BRCAness genes. Time-course qPCR and Western blot analyses supported this model. In the early phase (2-6 hours), expression of BRD4, CDK7, CDK9, and CDK12 was rapidly reduced (Figures 3a-c), coinciding with an early decreased phosphorylation of RNA polymerase II at serine 2 compared to serine 5, consistent with defective transcriptional elongation. In a subsequent wave (8-20 hours), we observed coordinated downregulation of core BRCAness factors including BRCA2, BRCA1, ATM, BLM, and RAD51, alongside increased DNA damage and apoptosis markers. Importantly, the expression status of PARP1, a canonical SSBR regulator, the NHEJ factor XRCC4 and housekeeping gene ACTB remained unaffected (Figure 3c).

These results indicate a temporal separation between the early loss of transcription elongation regulators and the subsequent repression of HR genes, supporting a model in which ecteinascidins indirectly suppress BRCAness-associated transcriptional programs through disruption of elongation. To functionally validate this mechanism, we performed siRNA-mediated knockdowns of CDK7, CDK9, CDK12, and BRD4. Depletion of these factors resulted in marked downregulation of HR genes, including BRCA1, BRCA2, ATM, and BLM, while having limited effects on genes associated with other DNA repair pathways (Figures 3d,e). To extend these observations, we analyzed RNA-seq data from 501mel cells treated with the pharmacological inhibitor of CDK7, THZ1. Consistent with our previous results, genes involved in HR and FA pathways were strongly downregulated, while SSBR-associated genes were less affected (Figure 3f).

Together, these findings support a model in which ecteinascidins induce rapid suppression of transcription elongation regulators, leading to secondary downregulation of long HR and FA genes, thereby contributing to the establishment of a BRCAness-like state.

Ecteinascidins induce BRCAness through defective transcription elongation and premature transcriptional termination

Given the rapid downregulation of transcription elongation regulators, we next investigated whether ecteinascidins directly impair RNA polymerase II (RNAPII) dynamics and transcriptional elongation. To address this, we performed RNAPII CUT&Tag and nascent RNA sequencing (TT-seq) analyses. To evaluate the impact of ecteinascidins on transcription as a function of gene architecture, genes were stratified according to their genomic length into three categories: short (7-20 kb), medium (20-60 kb), and long (>60 kb).

Genome-wide profiling of RNAPII occupancy revealed a marked redistribution of RNAPII signal following ecteinascidin treatment, characterized by increased signal at promoter-proximal regions and a concomitant decrease across gene bodies (Figure 4a). This effect was strongly dependent on gene length, with long genes exhibiting the most pronounced reduction in gene body occupancy, consistent with a defect in transcriptional elongation. To quantitatively assess RNAPII distribution, we calculated the traveling ratio (TR), defined as the ratio of RNAPII signal at promoter-proximal regions to that within gene bodies[62] (Figure 4b). An increased TR reflects enhanced promoter-proximal accumulation of RNAPII and impaired transition into productive elongation. Consistent with this, ecteinascidin treatment led to a significant increase in TR values across all gene categories, with the strongest effects observed in long genes (Figure 4c).

Because homologous recombination (HR) and Fanconi anemia (FA) genes are significantly longer than housekeeping genes (Figure 4d), we next examined whether this elongation defect disproportionately affected these gene classes. Indeed, HR+FA genes displayed significantly higher Δlog2TR values compared to housekeeping genes (Figure 4e), indicating increased promoter-proximal RNAPII accumulation and reduced elongation efficiency at these loci.

To directly assess transcriptional output, we next analyzed nascent transcription using TT-seq[63]. Metagene analysis revealed a pronounced reduction in transcriptional signal across gene bodies following ecteinascidin treatment, with minimal effects at promoter-proximal regions (Figure 4f). This effect was again strongly dependent on gene length, with long genes

showing the most severe loss of transcriptional output, whereas short genes were comparatively preserved. To further quantify transcriptional elongation efficiency, we defined an elongation index (EI) as the ratio of gene body signal to promoter-proximal signal (Figure 4g). In contrast to TR, a decrease in EI reflects reduced productive transcription elongation. Consistent with impaired elongation, EI values were significantly decreased following ecteinascidin treatment, with the strongest reductions observed in long genes (Figure 4h).

Absolute quantification of nascent transcription using spike-in normalized TT-seq confirmed that longer genes were preferentially downregulated following ecteinascidin treatment (Supplementary Figure 3a). Accordingly, HR+FA genes were significantly more strongly repressed than housekeeping genes (Figure 4i), with a greater proportion of HR+FA genes transcriptionally downregulated upon treatment (Figure 4j). Furthermore, 3,650 genes were found to be commonly downregulated between the two ecteinascidins (Supplementary Figure 3b). Importantly, gene ontology analysis of these genes revealed enrichment for DNA damage response and DNA repair pathways (Supplementary Figure 3c).

These effects were also evident at the single-gene level. At the BRCA2 locus, a representative long HR gene (~84 kb), ecteinascidin treatment induced accumulation of RNAPII at the promoter accompanied by reduced occupancy across the gene body, together with a marked decrease in nascent transcription (Supplementary Figure 3d). In contrast, the short housekeeping gene ACTB (~3.3 kb) displayed increased RNAPII signal across both promoter and gene body, along with maintained or increased transcriptional output (Supplementary Figure 3d), consistent with its relative insensitivity to elongation defects.

Mechanistically, elongation regulators such as CDK12 have been shown to maintain full-length transcription of HR/FA genes by sustaining RNAPII processivity and suppressing intronic polyadenylation (IPA). Their loss diminishes RNAPII processivity, resulting in premature cleavage and polyadenylation within introns, a vulnerability particularly pronounced in long, IPA site-rich genes such as ATM, BRCA2, and BLM[38,40,59]. Consistently, genes involved in HR and FA exhibit a significantly higher density of IPA sites compared to SSBR genes (Supplementary Figure 4a).

Strikingly, ecteinascidin treatment preferentially downregulated genes harboring IPA sites, consistent with a transcriptional elongation defect involving premature mRNA cleavage (Supplementary Figure 4b). To directly test this model, we performed quantitative PCR assays targeting regions upstream and downstream of annotated intronic polyadenylation sites in key BRCAness-associated genes (ATM, ATR, BLM, and BRCA2)[59]. In all cases, downstream regions exhibited markedly greater reductions in transcript abundance than upstream regions following ecteinascidin exposure, consistent with premature cleavage and transcriptional termination. Notably, this effect was not observed following cisplatin treatment (Supplementary Figures 4c-e).

Together, these findings demonstrate that ecteinascidins impair transcription elongation by disrupting RNAPII processivity, leading to promoter-proximal accumulation of RNAPII and reduced transcriptional output across gene bodies. This elongation defect is further coupled to increased usage of intronic polyadenylation sites, resulting in premature transcriptional termination. Because long genes, particularly those involved in HR and FA pathways, harbor a higher density of intronic polyadenylation sites, they are disproportionately sensitive to this mechanism, providing a mechanistic basis for the selective induction of BRCAness and homologous recombination deficiency by ecteinascidins.

Ecteinescidins synergize with PARP inhibition in multiple cancer models

Given the induction of HR deficiency following ecteinascidin treatment, we next investigated whether the loss of HR and FA pathway components sensitizes BRCA-proficient cancer cells to PARP inhibition. To this end, we assessed cell viability using PrestoBlue assays following 72h treatment with increasing concentrations of ecteinascidins in combination with the PARP inhibitor olaparib. Synergy between treatments was evaluated using the Highest Single Agent (HSA) model[64,65]. The combination of ecteinascidins with olaparib resulted in robust and reproducible synergy across all tested cancer cell lines, with maximal HSA scores ranging from 21 to 44.5 for lurbinectedin and from 25.1 to 49.9 for PM54 (Figure 5a). In contrast, the combination of cisplatin with olaparib showed markedly lower synergy, with maximal HSA scores ranging from 4.87 to 17.67 (Supplementary Figure 5a). Notably, ecteinascidins

markedly increased cancer cell sensitivity to olaparib at doses where monotherapy had minimal effect, while cisplatin failed to elicit similar degree of sensitization (Supplementary Figure 5b).

To further characterize these interactions, we performed dose-response analyses and calculated Combination Index (CI) values using the Chou-Talalay method[66]. Consistent with the HSA analysis, ecteinascidin-olaparib combinations displayed strong synergistic interactions across all models, with mean CI values <1, whereas the cisplatin-olaparib combination showed minimal or no synergy (Figure 5b; Supplementary Figure 5c). We next evaluated the therapeutic benefit of these combinations using Dose Reduction Index (DRI) analysis[67]. Ecteinascidin-olaparib combinations yielded favorable DRI values (>1), indicating that effective doses of both agents could be reduced when used in combination. Conversely, DRI values for cisplatin-olaparib combinations were ≤1, suggesting no dose-reduction advantage (Supplementary Figure 5d).

To experimentally validate these findings under sublethal conditions, cells were treated with ecteinascidins at 50% of their IC50, alone or in combination with olaparib, for 72 h. At these doses, ecteinascidins induced downregulation of key HR genes, including BRCA1 and BRCA2, as well as transcriptional regulators such as BRD4, CDK7, and CDK12, at both mRNA and protein levels, without affecting PARP1 or housekeeping gene expression (Supplementary Figures 6a,b). Cell survival was then assessed at the same concentrations using crystal violet staining. Combination treatment with ecteinascidins and olaparib resulted in a marked reduction in cell viability compared to either monotherapy across all tested models (Figures 5c, d). In contrast, this effect was less pronounced with the combination of cisplatin and olaparib, which resulted in only modest effects (Supplementary Figure 5e).

Together, these results demonstrate that ecteinascidins strongly sensitize BRCA-proficient cancer cells to PARP inhibition, resulting in robust and reproducible synergistic anti-proliferative effects across multiple cancer models. This synergy is consistent with the induction of a transcription-dependent HR-deficient state, and distinguishes ecteinascidins

from conventional DNA-damaging agents such as cisplatin, which fail to elicit comparable combinatorial efficacy with PARP inhibitors.

Ecteinascidins and PARP inhibition combination enhances DNA damage in actively transcribed regions and induces apoptosis

Having observed strong synergy between ecteinascidins and olaparib, we next sought to investigate the functional mechanisms underlying this interaction. Given that ecteinascidins induce DNA double-strand breaks (DSBs)[51,56,68], and, as shown above, impair homologous recombination repair (HRR), we hypothesized that their combination with PARP inhibitors, would lead to an accumulation of unrepaired DNA lesions through simultaneous disruption of complementary repair pathways.

To test this, we assessed DNA damage using γH2AX immunofluorescence following 72h treatment with ecteinascidins and olaparib at sublethal concentrations (50% IC50). Across multiple cancer models, combination treatment resulted in a marked increase in γH2AX signal compared to either agent alone, whereas single treatments induced only modest effects (Figures 6a, b). This was further supported by immunoblot analyses showing increased levels of γH2AX, phosphorylated ATR (pATR), and phosphorylated ATM (pATM), together with induction of apoptosis markers including cleaved caspase-3 and cleaved PARP (Supplementary Figure 6b), as well as increased Annexin V staining (Supplementary Figure 6c). The combination of cisplatin and olaparib, in contrast, showed minimal or no increase in apoptosis and γH2AX levels compared to single-agent treatments (Supplementary Figures 6c, 7a). Consistent with these observations, comet assays revealed a substantial increase in DNA double-strand breaks following ecteinascidin-olaparib co-treatment in melanoma (501mel) and ovarian cancer (SKOV3) cells, whereas the cisplatin-olaparib combination failed to induce comparable levels of DNA damage (Supplementary Figures 7b, c).

To determine the genomic localization of DNA damage, we performed γH2AX CUT&Tag in SKOV3 cells following 72h of treatment at sublethal concentrations. Combination treatment led to a strong increase in γH2AX signal compared to single-agent conditions (Figure 6c). Notably, DNA damage sites were highly enriched at ecteinascidin binding sites identified by Chem-Map

(Bio-Lurbi and Bio-PM54), indicating that olaparib enhances the persistence of DNA lesions generated at these loci rather than inducing new damage sites. Since we previously showed that ecteinascidins preferentially bind to open chromatin at actively transcribed genes[56], we next examined whether DNA damage overlapped with transcriptionally active or inactive chromatin states. Indeed, the γH2AX-enriched regions strongly overlapped with active chromatin marked by H3K27ac, but not with repressive H3K27me3-marked regions (Figure 6d), and were particularly prominent at key regulatory genes such as JUN (Supplementary Figure 7d).

Together, these findings demonstrate that ecteinascidins induce DNA damage at actively transcribed genomic regions corresponding to their chromatin binding sites, and that PARP inhibition enhances this effect by preventing repair of these lesions. This results in the accumulation of unrepaired DNA damage and increased apoptosis, providing a mechanistic basis for the synergistic cytotoxicity observed in BRCA-proficient cancer cells.

Ecteinascidins resensitize cancer cells with acquired PARP inhibitor resistance

A major mechanism of acquired resistance to PARP inhibitors (PARPi) involves restoration of homologous recombination (HR), most commonly through BRCA1/2 reversion mutations or upregulation of alternative HR pathway[3,69,70]. We therefore hypothesized that the broad transcriptional repression of HR-related genes induced by ecteinascidins could overcome PARPi resistance and restore drug sensitivity in BRCA-mutated cancer cells. To test this, we used the triple-negative breast cancer (TNBC) cell line MDA-MB-436, which harbors a BRCA1 mutation and is intrinsically sensitive to PARPi (referred to as MDA-MB-436 WT). We generated two PARPi-resistant derivatives, MDA-MB-436 OlapR and MDA-MB-436 TalaR, through stepwise dose escalation with olaparib or talazoparib, respectively, until cells tolerated concentrations at least 10-fold higher than the original IC50 (Supplementary Figures 8a, b).

Functional HR assays revealed that both resistant lines exhibited increased baseline HR activity compared to parental cells, consistent with HR restoration as a resistance mechanism (Figure 7c). We next treated all three models with ecteinascidins (5×IC50) and performed RNA-seq after 12 h. Ecteinascidin treatment resulted in robust downregulation of BRCAness-

associated genes, as well as HR and Fanconi anemia pathway components, across all models (Figures 7a,b, Supplementary Figure 8c). These transcriptional changes were confirmed at the protein level by immunoblotting (Figure 7d). Consistently, HR efficiency was significantly reduced following treatment in both parental and resistant cell lines (Figure 7c).

We next assessed the impact of ecteinascidins on PARPi sensitivity. Drug combination assays revealed strong synergy between ecteinascidins and either olaparib or talazoparib in resistant models, with maximal HSA scores ranging from 26.24 to 41.42 in OlapR cells and from 22.7 to 34.3 in TalaR cells (Figure 7e, f; Supplementary Figure 8h, i). Synergistic interactions were also observed in parental MDA-MB-436 cells, although to a lesser extent (Supplementary Figures 8d-g). At sublethal ecteinascidin concentrations (0.5×IC50), combination treatment with PARPi significantly reduced cell viability in both resistant models (Figure 7g), accompanied by increased DNA damage as measured by γH2AX signal (Figure 7h), and enhanced apoptosis (Supplementary Figure 8j).

Taken together, these results demonstrate that ecteinascidins overcome acquired PARP inhibitor resistance by repressing transcriptional programs required for homologous recombination, thereby reducing HR activity and restoring sensitivity to PARP inhibition. This effect extends the therapeutic potential of ecteinascidins to both BRCA-proficient tumors and PARPi-resistant BRCA-mutated cancers.

Discussion:

The clinical success of PARP inhibitors (PARPi) in BRCA-mutated cancers has firmly established synthetic lethality as a powerful therapeutic paradigm. However, their clinical application remains limited to a relatively small subset of patients, as large-scale genomic analyses indicate that BRCA1/2 and other homologous recombination (HR)-related alterations are infrequent across most solid tumors[71–73]. This constraint has driven extensive efforts to pharmacologically induce “BRCAness,” a functional HR-deficient (HRD) state, in HR-proficient cancers. Approaches targeting transcriptional regulators (e.g., BRD4), cyclin-dependent kinases (e.g., CDK7, CDK12), and DNA damage response (DDR) kinases (e.g., ATM, ATR)

have shown promising preclinical activity[39,46,59,74,75]. Yet, none has led to clinically approved agents capable of reliably inducing BRCAness in HR-proficient tumors.

In this study, we identify the clinically approved ecteinascidin lurbinectedin and its synthetic analog PM54 as potent and broadly active inducers of a transcription-dependent BRCAness state in HR-proficient cancer models. Mechanistically, ecteinascidins suppress the expression of key HR and Fanconi anemia (FA) genes through a transcriptional elongation defect. This is accompanied by rapid downregulation of core transcription elongation regulators, including CDK7, CDK9, CDK12, and BRD4. As a consequence, RNA polymerase II (RNAPII) processivity is impaired, leading to promoter-proximal accumulation of RNAPII, reduced transcriptional output across gene bodies, and premature transcriptional termination.

Notably, our findings indicate that ecteinascidins, as DNA-binding transcriptional inhibitors, act predominantly at the level of elongation rather than transcriptional initiation, providing novel mechanistic insight into how transcriptional stress induced by these molecules can selectively compromise DNA repair gene expression. While the precise basis for the rapid and coordinated depletion of elongation regulators remains to be fully elucidated, we speculate that it reflects the convergence of a constitutively open chromatin environment, elevated transcriptional activity, and the intrinsically high turnover of these factors in cancer cells. These proteins are continuously required to sustain oncogene-driven transcriptional programs, creating a state of transcriptional addiction that may render cancer cells particularly vulnerable to elongation-targeted perturbations induced by ecteinascidins[76–79].

Importantly, this elongation defect disproportionately affects long genes, particularly those involved in HR and FA pathways, which are enriched in intronic polyadenylation (IPA) sites and therefore highly dependent on efficient elongation for full-length transcription. While inhibition of CDK12/13 has previously been shown to induce similar length-dependent transcriptional defects and IPA-driven repression of DNA repair genes[38–42,59,80], our findings extend this paradigm by demonstrating that a DNA-binding transcriptional inhibitor can recapitulate this phenotype through a distinct upstream mechanism. These results establish a direct link between chromatin binding, RNAPII processivity, and premature transcriptional

termination, providing a unified mechanistic framework for transcription-dependent induction of BRCAness.

Functionally, we demonstrate that ecteinascidins strongly synergize with PARPi across multiple BRCA-proficient cancer models, including tumor types in which PARPi are not currently used, such as melanoma and non-small cell lung cancer. This broad activity highlights the potential of ecteinascidins to expand the clinical applicability of PARPi beyond their current indications. Mechanistically, this synergy is driven by the accumulation of DNA damage at transcriptionally active genomic regions. Ecteinascidins induce DNA lesions at their chromatin binding sites, and PARP inhibition enhances this effect by preventing repair of these lesions rather than generating new damage foci. This results in persistent DNA damage, increased replication stress, and enhanced apoptotic cell death. The spatial coupling between ecteinascidin binding, active chromatin marks (H3K27ac), and γH2AX accumulation further supports a model in which transcriptionally active regions represent key vulnerability nodes for combinatorial targeting.

A major limitation of PARPi therapy is the frequent emergence of resistance, particularly in BRCA-mutated tumors, where restoration of HR through secondary BRCA1/2 mutations or activation of compensatory repair pathways is commonly observed[3]. To investigate whether ecteinascidins could overcome this resistance, we employed two triple-negative breast cancer models generated with the MDA-MB-436 cell line, which is BRCA-1 mutant and was rendered resistant to Olaparib and Talazoparib through stepwise dose escalation. Previous reports have shown that resistance in this model involves RAD51 loading by splice variant of the mutant BRCA1 to restore HR[81]. Accordingly, our results demonstrate an increased HR capacity of these resistant cell lines compared to the original one, as measured by HR-assay. Interestingly, we found that ecteinascidinss reversed resistance in this context by transcriptionally repressing reactivated HR components, thereby re-establishing HRD. These findings indicate that ecteinascidins not only extend PARPi efficacy to HR-proficient tumors but also restore sensitivity in resistant BRCA-mutated cancers, addressing a major clinical challenge.

Importantly, clinical studies have already begun to explore combinations of Lurbinectedin and PARPi. Phase I/II trials in ovarian cancer patients have demonstrated a significant improvement in disease control and progression-free survival, with an acceptable safety profile[82,83]. Our work provides a mechanistic rationale for these observations by demonstrating that ecteinascidins suppress HR and FA transcriptional programs, thereby amplifying the vulnerabilities targeted by PARP inhibition.

Beyond PARP inhibition, our findings raise the possibility that ecteinascidins could be combined with other DNA damage response (DDR)-targeting agents. In particular, ATR inhibitors, which target replication stress signaling, may further enhance DNA damage accumulation when combined with transcriptional elongation defects. Consistent with this rationale, recent preclinical studies have reported enhanced efficacy of lurbinectedin in combination with ATR inhibitors in small cell lung cancer[84]. Notably, such combinations are currently being evaluated in clinical trials (e.g., NCT04802174). Exploring these therapeutic strategies may provide additional opportunities to exploit transcription-dependent vulnerabilities in cancer cells.

Despite these promising results, several limitations should be considered. Although ecteinascidins induce BRCAness across diverse cancer models, tumor-specific transcriptional dependencies may influence therapeutic response, and the potential emergence of resistance to ecteinascidins should also be taken into account. In addition, the molecular basis underlying the rapid depletion of transcription elongation regulators remains to be fully elucidated. Finally, as transcriptional inhibition affects fundamental cellular processes, careful evaluation of therapeutic windows and potential toxicities will be essential for clinical translation.

In summary, our study uncovers a transcription-based mechanism by which ecteinascidins induce BRCAness by inhibiting the transcription elongation, selectively affecting long HR and Fanconi anemia genes, resulting in synthetic lethality in HR-proficient cancer cells. These compounds also restore PARPi sensitivity in resistant BRCA-mutated models by repressing compensatory HR repair pathways. Together, these findings establish a compelling mechanistic foundation for the clinical development of ecteinascidins-PARPi combinations as

a strategy to broaden the reach of synthetic lethality-based therapies across cancer types currently excluded from or resistant to PARPi monotherapy.

Materials and methods:

Cell culture and treatments

All cell lines were obtained from ATCC and are referenced with Research Resource Identifiers (RRID; https://rrid.site): 501mel (RRID:CVCL_4633), DMS53 (RRID:CVCL_1177), A549 (RRID:CVCL_0023), MCF7 (RRID:CVCL_0031), SKOV3 (RRID:CVCL_0532), MDA-MB-436 (RRID:CVCL_0623), and HCC1937 (RRID:CVCL_0290). Cell line identity was verified annually by STR profiling (ATCC authentication service), and cultures were routinely tested for mycoplasma contamination. Cells were maintained at 37°C in 5% CO_2. 501mel, MDA-MB-436, and HCC1937 cells were cultured in RPMI (without HEPES; Gibco) supplemented with 10% FBS and gentamycin. DMS53 cells were grown in Waymouth's MB medium (Gibco) supplemented with 10% FBS. A549 cells were cultured in DMEM/HAM-F12 (1:1; Gibco) supplemented with 10% FBS. MCF7 cells were maintained in DMEM supplemented with 10% FBS, 0.6 µg/mL insulin (Thermo Fisher), and gentamycin. SKOV3 cells were grown in McCoy's 5A medium (Gibco) supplemented with 10% FBS and gentamycin. Lurbinectedin (PM1183) and PM54 were provided by PharmaMar. Olaparib and talazoparib were purchased from Selleckchem. Treatment durations were selected according to the experimental design, with IC50 values defined based on 72-hour viability assays.

RNA Extraction and RT-qPCR

Total RNA was extracted using the NucleoSpin RNA Plus kit (Macherey-Nagel) according to the manufacturer's instructions. Reverse transcription was performed using SuperScript IV Reverse Transcriptase (Invitrogen). Quantitative PCR was carried out using SYBR Green Master Mix (Roche) on a LightCycler 480 system (Roche). Gene expression levels were normalized to 18S rRNA.

Bulk RNA-Sequencing and analysis

Library preparation was performed at the GenomEast platform (IGBMC) using the Illumina Stranded Total RNA Prep Ligation with Ribo-Zero Plus kit (Illumina), following the

manufacturer's protocol. Libraries were generated from 100 ng of total RNA using IDT for Illumina RNA UD Indexes. DNA libraries were amplified by 13 PCR cycles and purified using two successive SPRIselect bead clean-ups (Beckman Coulter). Library quality and concentration were assessed using a Bioanalyzer 2100 system (Agilent Technologies). Sequencing was performed on an Illumina NextSeq 2000 platform in paired-end mode (50 bp reads). Image analysis and base calling were performed using RTA v2.7.7 and BCL Convert v3.8.4. Adapter sequences and low-quality bases (Phred score < 20) were removed using cutadapt v1.10. Reads shorter than 40 nucleotides after trimming were discarded. Ribosomal RNA reads were removed using Bowtie2 v2.2.8. Remaining reads were aligned to the human genome (hg19) using STAR v2.5.3a. Gene-level quantification was performed using HTSeq-count v0.6.1p1 (union mode) with Ensembl gene annotations (release 75). Only uniquely mapped and unambiguously assigned reads were retained. Normalization across samples was performed using the median-of-ratios method implemented in DESeq2 (v1.16.1). Differential gene expression analysis was conducted using Wald tests. Genes with high Cook's distance were excluded, and independent filtering based on mean normalized counts was applied. P-values were adjusted using the Benjamini–Hochberg method, with a significance threshold of adjusted $P < 0.001$. Heatmaps and violin plots were generated using Prism 10 (GraphPad). Venn diagrams were generated using DeepVenn. Gene enrichment analyses were performed using Enrichr and Metascape.

Chem-map and CUT&Tag

Cells were seeded in 15-cm dishes and grown to sub-confluency prior to treatment. For Chem-map experiments, cells were treated for 8 hours with DMSO, biotinylated lurbinectedin (Bio-Lurbi), or biotinylated PM54 (Bio-PM54) at 10×IC50. For CUT&Tag experiments, cells were treated for 8 hours with lurbinectedin or PM54 (0.5×IC50), olaparib (5 μM), or combinations. H3K27ac CUT&Tag was performed on DMSO-treated control cells. Chem-map (biological triplicates) and CUT&Tag (biological duplicates) were performed using the CUT&Tag-IT™ Assay Kit (Active Motif, #53160 and #53165). Briefly, 1×10^5 cells were bound to Concanavalin A-coated beads and incubated overnight at 4°C with primary antibodies. Secondary antibodies

were added for 1 hour at room temperature, followed by incubation with pA-Tn5 transposomes. Tagmentation was performed at 37°C for 1 hour. DNA was purified following protein digestion and used for library preparation. Libraries were amplified and purified using double SPRI bead clean-up. Sequencing was performed on an Illumina NextSeq 2000 platform (paired-end, 50 bp). Adapter trimming was performed using cutadapt v1.18. Reads were aligned to hg19 using Bowtie2 (parameters: -N 1 -X 1000). ENCODE blacklist regions were removed, and duplicate reads were filtered. Reads were extended to the estimated fragment length. Coverage tracks were generated using deepTools (bamCoverage) with RPKM normalization. For γH2AX CUT&Tag experiments, normalization was performed using spike-in-derived scaling factors. Peak calling was performed using MACS2 v2.2.7.1 in narrowPeak and BEDPE modes. Biological replicates were merged to define consensus peak sets. Read counts over peaks were quantified using BEDtools, and peak annotation was performed using HOMER. Heatmaps and average profiles were generated using deepTools and seqMINER. For RNA polymerase II CUT&Tag analyses, promoter-proximal regions (−30 bp to +300 bp from the TSS) and gene bodies (+300 bp to TES) were defined. The traveling ratio (TR) was calculated as the ratio of promoter-proximal signal to gene body signal. Statistical comparisons between groups were performed using two-sided Mann-Whitney tests or Kruskal-Wallis tests followed by Dunn's multiple comparisons tests, as appropriate.

Transient transcriptome sequencing (TT-seq)

501mel cells were treated with DMSO or 10×IC_{50} concentrations of either lurbinectedin or PM54 for 2, 4, or 6 hours. The nucleoside analog 4-thiouridine (4sU; Glentham Life Sciences, GN6085) was then added to a final concentration of 500 μM for a 10-minute pulse at 37°C in 5% CO_2. Following labeling, cells were washed with ice-cold 1× PBS and immediately lysed using TRI Reagent (Molecular Research Center Inc., TR 188). Newly synthesized RNAs were purified as previously described (Rabani et al., 2011; Rädle et al., 2013; Schwalb et al., 2016). Briefly, 4sU-labeled total RNA from Drosophila melanogaster spike-in cells was added to 250 μg of labeled total RNA from 501mel cells at a ratio of 1:10 prior to purification. RNA was precipitated and resuspended in 130 μL of RNase-free water (Sigma-Aldrich, 95284), and

fragmented using a Covaris E220 Focused-ultrasonicator with the following settings: 1% duty factor, 100 W peak incident power, 200 cycles per burst, for 80 seconds, yielding fragments ranging from ~10 kb to 200 bp. For purification, fragmented RNA was incubated at 60°C for 10 minutes and immediately chilled on ice for 2 minutes to disrupt secondary structures. Biotinylation was performed in labeling buffer (10 mM HEPES-KOH pH 7.5, 1 mM EDTA) with biotin-HPDP (0.2 mg/mL; Thermo Fisher Scientific, 21341) for 3 hours at room temperature (24°C) in the dark with gentle agitation. Unbound biotin-HPDP was removed by addition of an equal volume of chloroform/isoamyl alcohol (24:1), followed by centrifugation at 16,000 × g for 5 minutes at 4°C. RNA was precipitated at 20,000 × g for 20 minutes using 1/10 volume of 5 M NaCl and an equal volume of 100% isopropanol. The pellet was washed with 75% ethanol and centrifuged again at 20,000 × g for 10 minutes. The RNA pellet was then resuspended in 100 µL of RNase-free water. Biotinylation and purification of 4sU-labeled RNA were performed as previously described (Dölken et al., 2008; Wachutka et al., 2019). Biotinylated RNA was captured using 100 µL of streptavidin-coated µMACS magnetic beads (Miltenyi Biotec, 130-074-101) for 90 minutes at 24°C under gentle agitation. µMACS columns (Miltenyi Biotec) were placed on a MACS MultiStand and equilibrated twice with washing buffer (100 mM Tris-HCl pH 7.5, 10 mM EDTA, 1 M NaCl, 0.1% Tween-20) prior to sample loading. Columns were subsequently washed sequentially with increasing volumes (600 µL, 700 µL, 800 µL, 900 µL, and 1 mL) of washing buffer. 4sU-labeled RNA was eluted using two successive washes of 100 µL freshly prepared 100 mM DTT.

TT-seq data processing and analysis

Sequencing libraries were generated and sequenced at the GenomEast platform (IGBMC) on an Illumina platform in paired-end mode (50 bp reads). Adapter sequences, poly(A) stretches, and low-quality bases (Phred score < 20) were removed using cutadapt v4.2, and reads shorter than 40 nucleotides after trimming were discarded. Reads mapping to ribosomal RNA sequences (RefSeq and GenBank annotations) were filtered using Bowtie2 v2.3.5. Quality control was performed using FastQC v0.11.9 and RSeQC v5.0.1, including assessment of read quality, gene body coverage, transcript integrity number (TIN), genomic feature distribution,

and strand specificity. Reads were first aligned to Drosophila melanogaster rRNA references using Bowtie2, and unmapped reads were subsequently aligned to a composite reference genome comprising Homo sapiens (hg19, Ensembl release 75) and Drosophila melanogaster (BDGP6, Ensembl release 93) using STAR v2.7.10b. Only uniquely mapped reads were retained for downstream analyses. Spike-in normalization factors were calculated from Drosophila reads using the median-of-ratios method and applied to human read counts to allow quantitative comparison across conditions independently of global transcriptional changes. Gene-level quantification was performed using Ensembl gene annotations (release 75), retaining only non-ambiguously assigned reads. Differential expression analysis was conducted using DESeq2 v1.34.0 with Wald tests, using size factors derived from *Drosophila* spike-in reads for normalization. P-values were adjusted using the Benjamini-Hochberg method. Log2 fold-change shrinkage was applied using the apeglm method, and genes with high Cook's distance or removed by independent filtering were excluded from downstream analyses. Coverage tracks were generated using deepTools (bamCoverage) from aligned reads, using either RPKM normalization for signal distribution and metagene analyses or spike-in-derived scaling factors for absolute quantification of nascent transcription. For elongation analyses, promoter-proximal regions (−30 bp to +300 bp relative to the transcription start site) and gene bodies (+300 bp downstream of the TSS to the transcription end site) were defined, and read densities over these regions were quantified using deepTools (computeMatrix, scale-regions mode). The elongation index (EI) was calculated as the ratio of gene body signal to promoter-proximal signal. Gene enrichment analyses were performed using Enrichr with a significance threshold of adjusted $P < 0.001$, consistent with bulk RNA-seq analyses. Statistical comparisons between groups were performed using two-sided Mann-Whitney tests or Kruskal-Wallis tests followed by Dunn's multiple comparisons tests, as appropriate. Correlation analyses were performed using Pearson or Spearman coefficients, as indicated.

Protein extraction and Western Blotting

For whole cell extracts, cells were rinsed once with cold PBS, before pelleting and resuspension in LSDB 0.5M buffer (500mM KCl, 50mMTris pH 7.9, 20% glycerol, 1% NP-40, 1mM DTT, phosphatase inhibitor and protease inhibitor cocktail). Afterwards, cells were fully disrupted with 3 cycles of heat shock (liquid nitrogen followed by 37°C water bath). Then, samples were centrifugated for 15min at 11,000g to remove cell debris. Lysates were subjected to SDS–polyacrylamide gel electrophoresis (SDS-PAGE) and proteins were transferred onto a nitrocellulose membrane. Membranes were incubated overnight 4°C with primary antibodies in PBS+5% milk powder + 0.01 % Tween-20. The membranes were then incubated with HRP-conjugated secondary antibody (Jackson ImmunoResearch) for 1h at room temperature and visualized using the ECL detection system (GE Healthcare).

Homologous Recombination Activity Assay

HR activity was assessed with the HR Assay Kit (Norgen Biotek, SKU 35600) following the manufacturer's instructions. Briefly, cells were treated with Lurbi or PM54 for 12h and then transfected with 500 ng of two plasmids containing deletion mutants (dl-1 and dl-2) in the presence of FuGENE HD (Promega). Twelve hours after transfection, DNA was isolated with QIAamp DNA Mini Kit (Qiagen). HR efficiency was assessed by qPCR, using primer mixtures provided with the kit to amplify the HR product (assay primers) and the dl plasmids backbone (universal primers), used as normalisation method.

Generation of PARP Inhibitor-resistant Cell Lines

To generate acquired resistance to PARP inhibitors, BRCA1-mutated MDA-MB-436 cells were continuously exposed to gradually increasing concentrations of olaparib or talazoparib. This stepwise selection was carried out until the cells were able to proliferate in the presence of concentrations at least 10-fold higher than their respective initial IC50 values. To avoid confounding effects related to ongoing drug exposure, resistant cells were cultured in drug-free medium for a minimum of two weeks prior to their use in transcriptional and cell viability assays.

Cell viability and drug treatment assays

Cells were seeded in 96-well plates at a density of 5 000 to 10 000 cels/well, depending on the cell line, and treated for 72h with increasing concentrations of Lurbi (0.005–5 nM), PM54 (0.005–5 nM), Olaparib (1–100 µM) or Talazoparib (1 – 10 µM), either as single agents or in combination. Cell viability was then assessed using PrestoBlue Cell Viability Reagent (Thermo Fisher Scientific) according to the manufacturer's instructions. The absorbance per well was measured with a CellInsight CX5 High Content Screening platform (Thermo Fisher Scientific), and viability was expressed as percentage relative to DMSO-treated controls. For low-dose viability assays, 100 000 to 200 000 cells were seeded into 6-well plates, depending on the cell line, and then treated for 72h with Lurbi or PM54 (0.5×IC50) and olaparib (1–10 µM, depending on the cell line) or talazoparib (1 µM), either alone or in combination. Following treatment, cells were washed once with PBS, then fixed for 10 min with 4% Paraformaldehyde solution, and stained with Crystal Violet solution 0.2% for 15min. The wells were finally washed twice with deionized water, airdried, scanned. Cell staining intensity was quantified by measuring integrated density using Fiji (ImageJ).

Drug combination and synergy analysis

Synergistic interactions between Lurbi or PM54 and the PARP inhibitors olaparib or talazoparib were assessed using the Highest Single Agent (HSA) model[64,65] via the SynergyFinder+ web tool[85] (https://synergyfinderplus.org). According to this model, drug combinations with synergy scores > 0 are considered synergistic, < 0 antagonistic, and = 0 additive, with higher positive or negative values indicating stronger synergy or antagonism, respectively. Dose–response curves were generated from cell viability assays, and Combination Index (CI) and Dose-Reduction index (DRI) values were calculated using the Chou-Talalay method[66] with CompuSyn software (http://www.combosyn.com). CI values < 1 were interpreted as synergistic, CI = 1 as additive, and CI > 1 as antagonistic. DRI values > 1 were interpreted as favorable for dose-reduction, DRI = 1 as no dose-reduction, and CI < 1 as unfavorable dose-reduction.

γH2AX detection by immunofluorescence

Cells were seeded on coverslips in 24-well plates and treated for 72 hours with low concentrations of Lurbi or PM54 (0.5×IC50) and olaparib (1–10 µM, depending on the cell line), either alone or in combination. After treatment, cells were fixed in 4% paraformaldehyde for 10 minutes, permeabilized with 0.1% Triton X-100, and blocked in PBS containing 5% BSA. Cells were then incubated overnight at 4 °C with an anti-γH2AX primary antibody (anti-γ-H2AX (Ser139) clone JBW301 Millipore Corp, 1:500 dilution). The next day, cells were incubated with Alexa Fluor-conjugated secondary antibodies (diluted in PBS + 5% BSA) for 1 hour at room temperature. Nuclei were counterstained with DAPI. Images were acquired using a Leica TCS SP5 inverted confocal microscope, and γH2AX foci intensity was quantified using Fiji (ImageJ) software.

Neutral comet assays

Neutral comet assays were performed with CometAssay® Single Cell Gel Electrophoresis Assay (Bio-Techne, #4250-050-K) according to the manufacturer's instructions. Briefly, cells were seeded into 6-well plates and treated with low-dose concentrations of Lurbi, PM54 and olaparib as indicated in the cell viability assays. 72h later, cells were harvested and rinsed twice with ice-cold PBS. Afterwards, 5 000 cells were resuspended in low melting point agarose (LMAgarose) and embedded onto comet assay slides. Slides chilled at 4°C for 30 minutes to solidify the gel and then incubated in neutral lysis buffer overnight at 4°C. The following day, the slides were subjected to electrophoresis at 21 V for 45 minutes. Slides were subsequently immersed in DNA precipitation solution, followed by 70% ethanol for 30 minutes, then dried at 37°C for 15 minutes. DNA was stained using SYBR Gold Nucleic Acid Gel Stain (Invitrogen, #S11494) for 30 minutes in the dark. Images were captured using a TCS SP5 inverted confocal microscope (Leica). Comet tail moments were quantified using CometScore 2.0 software. For each condition, at least 50 cells per replicate were analyzed across three biological replicates.

Apoptosis analyses by flow cytometry

Between 100,000 and 200,000 cells were seeded per well in 6-well plates and treated for 72h with Lurbi or PM54 (0.5×IC50) and olaparib (1–10 µM, cell line–dependent), either individually

or in combination. For apoptosis analysis, cells were harvested, washed, and stained with Annexin V-APC (BD Biosciences) following the manufacturer's instructions. Apoptosis was measured using a BD LSRFortessa™ flow cytometer, and data were analyzed with FlowJo software. To determine the apoptotic population, we first established the Annexin V-APC intensity threshold by selecting the top 20% of Annexin V-positive cells in the DMSO-treated control.

Author contributions:

Conceptualization: JO, MC, FC

Methodology: JO, MC

Investigation: JO, MC, MN, CC, AH

Analysis of data: JO, MC, TY, MJ, GD

Funding acquisition: FC

Supervision: FC

Writing – original draft: JO, MC

Writing – review & editing: JO, MC, FC

References:

1. Alsop, K. *et al.* BRCA Mutation Frequency and Patterns of Treatment Response in BRCA Mutation–Positive Women With Ovarian Cancer: A Report From the Australian Ovarian Cancer Study Group. *J Clin Oncol* **30**, 2654–2663 (2012).
2. Maxwell, K. N., Domchek, S. M., Nathanson, K. L. & Robson, M. E. Population Frequency of Germline BRCA1/2 Mutations. *J Clin Oncol* **34**, 4183–4185 (2016).
3. Dias, M. P., Moser, S. C., Ganesan, S. & Jonkers, J. Understanding and overcoming resistance to PARP inhibitors in cancer therapy. *Nat Rev Clin Oncol* **18**, 773–791 (2021).
4. Kim, D. & Nam, H. J. PARP Inhibitors: Clinical Limitations and Recent Attempts to Overcome Them. *Int J Mol Sci* **23**, 8412 (2022).
5. McLornan, D. P. & Mufti, G. J. Applying Synthetic Lethality for the Selective Targeting of Cancer. *The new england journal of medicine* (2014).

6. O'Neil, N. J., Bailey, M. L. & Hieter, P. Synthetic lethality and cancer. *Nat Rev Genet* **18**, 613–623 (2017).
7. Gonçalves, E., Ryan, C. J. & Adams, D. J. Synthetic lethality in cancer drug discovery: challenges and opportunities. *Nat Rev Drug Discov* **25**, 22–38 (2026).
8. Scully, R., Panday, A., Elango, R. & Willis, N. A. DNA double-strand break repair-pathway choice in somatic mammalian cells. *Nat Rev Mol Cell Biol* **20**, 698–714 (2019).
9. Wright, W. D., Shah, S. S. & Heyer, W.-D. Homologous recombination and the repair of DNA double-strand breaks. *Journal of Biological Chemistry* **293**, 10524–10535 (2018).
10. Farmer, H. *et al.* Targeting the DNA repair defect in BRCA mutant cells as a therapeutic strategy. *Nature* **434**, 917–921 (2005).
11. Bryant, H. E. *et al.* Specific killing of BRCA2-deficient tumours with inhibitors of poly(ADP-ribose) polymerase. *Nature* **434**, 913–917 (2005).
12. McCabe, N. *et al.* Deficiency in the Repair of DNA Damage by Homologous Recombination and Sensitivity to Poly(ADP-Ribose) Polymerase Inhibition. *Cancer Research* **66**, 8109–8115 (2006).
13. Kaufman, B. *et al.* Olaparib monotherapy in patients with advanced cancer and a germline BRCA1/2 mutation. *J Clin Oncol* **33**, 244–250 (2015).
14. Mirza, M. R. *et al.* Niraparib Maintenance Therapy in Platinum-Sensitive, Recurrent Ovarian Cancer. *New England Journal of Medicine* **375**, 2154–2164 (2016).
15. Swisher, E. M. *et al.* Rucaparib in relapsed, platinum-sensitive high-grade ovarian carcinoma (ARIEL2 Part 1): an international, multicentre, open-label, phase 2 trial. *Lancet Oncol* **18**, 75–87 (2017).
16. Litton, J. K. *et al.* Talazoparib in Patients with Advanced Breast Cancer and a Germline BRCA Mutation. *N Engl J Med* **379**, 753–763 (2018).
17. Golan, T. *et al.* Maintenance Olaparib for Germline BRCA-Mutated Metastatic Pancreatic Cancer. *N Engl J Med* **381**, 317–327 (2019).
18. de Bono, J. *et al.* Olaparib for Metastatic Castration-Resistant Prostate Cancer. *N Engl J Med* **382**, 2091–2102 (2020).
19. Murai, J. *et al.* Trapping of PARP1 and PARP2 by Clinical PARP Inhibitors. *Cancer Res* **72**, 5588–5599 (2012).

20. Zandarashvili, L. *et al.* Structural basis for allosteric PARP-1 retention on DNA breaks. *Science* **368**, eaax6367 (2020).
21. Ribeiro, J. *et al.* Genetic evidence for PARP1 trapping as a driver of PARP inhibitor efficacy in BRCA mutant cancer cells. *Nucleic Acids Res* **53**, gkaf1398 (2025).
22. Lahiri, S. *et al.* BRCA2 prevents PARPi-mediated PARP1 retention to protect RAD51 filaments. *Nature* **640**, 1103–1111 (2025).
23. Armstrong, N., Ryder, S., Forbes, C., Ross, J. & Quek, R. G. A systematic review of the international prevalence of BRCA mutation in breast cancer. *CLEP* **Volume 11**, 543–561 (2019).
24. Oh, M. *et al.* The association of BRCA1 and BRCA2 mutations with prostate cancer risk, frequency, and mortality: A meta-analysis. *Prostate* **79**, 880–895 (2019).
25. Iqbal, J. *et al.* The incidence of pancreatic cancer in BRCA1 and BRCA2 mutation carriers. *Br J Cancer* **107**, 2005–2009 (2012).
26. Fong, P. C. *et al.* Inhibition of Poly(ADP-Ribose) Polymerase in Tumors from *BRCA* Mutation Carriers. *N Engl J Med* **361**, 123–134 (2009).
27. Noordermeer, S. M. & van Attikum, H. PARP Inhibitor Resistance: A Tug-of-War in BRCA-Mutated Cells. *Trends Cell Biol* **29**, 820–834 (2019).
28. Li, H. *et al.* PARP inhibitor resistance: the underlying mechanisms and clinical implications. *Molecular Cancer* **19**, 107 (2020).
29. Lord, C. J. & Ashworth, A. BRCAness revisited. *Nat Rev Cancer* **16**, 110–120 (2016).
30. Byrum, A. K., Vindigni, A. & Mosammaparast, N. Defining and Modulating 'BRCAness'. *Trends in Cell Biology* **29**, 740–751 (2019).
31. Wang, C., Jette, N., Moussienko, D., Bebb, D. G. & Lees-Miller, S. P. ATM-Deficient Colorectal Cancer Cells Are Sensitive to the PARP Inhibitor Olaparib. *Transl Oncol* **10**, 190–196 (2017).
32. Kondrashova, O. *et al.* Secondary Somatic Mutations Restoring RAD51C and RAD51D Associated with Acquired Resistance to the PARP Inhibitor Rucaparib in High-Grade Ovarian Carcinoma. *Cancer Discov* **7**, 984–998 (2017).
33. Zimmermann, M. *et al.* CRISPR screens identify genomic ribonucleotides as a source of PARP-trapping lesions. *Nature* **559**, 285–289 (2018).
34. Grellety, T. *et al.* Dramatic response to PARP inhibition in a PALB2-mutated breast cancer: moving beyond BRCA. *Ann Oncol* **31**, 822–823 (2020).

35. Abbotts, R., Dellomo, A. J. & Rassool, F. V. Pharmacologic Induction of BRCAness in BRCA-Proficient Cancers: Expanding PARP Inhibitor Use. *Cancers (Basel)* **14**, 2640 (2022).
36. Johnson, S. F. *et al.* CDK12 Inhibition Reverses De Novo and Acquired PARP Inhibitor Resistance in BRCA Wild-Type and Mutated Models of Triple-Negative Breast Cancer. *Cell Reports* **17**, 2367–2381 (2016).
37. Yang, L. *et al.* Repression of BET activity sensitizes homologous recombination–proficient cancers to PARP inhibition. *Science Translational Medicine* **9**, eaal1645 (2017).
38. Dubbury, S. J., Boutz, P. L. & Sharp, P. A. CDK12 regulates DNA repair genes by suppressing intronic polyadenylation. *Nature* **564**, 141–145 (2018).
39. Sun, C. *et al.* BRD4 Inhibition Is Synthetic Lethal with PARP Inhibitors through the Induction of Homologous Recombination Deficiency. *Cancer Cell* **33**, 401-416.e8 (2018).
40. Krajewska, M. *et al.* CDK12 loss in cancer cells affects DNA damage response genes through premature cleavage and polyadenylation. *Nat Commun* **10**, 1757 (2019).
41. Chu, Y.-Y. *et al.* Targeting the ALK–CDK9-Tyr19 kinase cascade sensitizes ovarian and breast tumors to PARP inhibition via destabilization of the P-TEFb complex. *Nat Cancer* **3**, 1211–1227 (2022).
42. Gui, F. *et al.* Acute BRCAness induction and AR pathway blockage through CDK12/7/9 degradation enhances PARP inhibitor sensitivity in prostate cancer. *Science Advances* **11**, eadu0847 (2025).
43. Bryant, H. E. & Helleday, T. Inhibition of poly (ADP-ribose) polymerase activates ATM which is required for subsequent homologous recombination repair. *Nucleic Acids Res* **34**, 1685–1691 (2006).
44. Mak, J. P. Y., Ma, H. T. & Poon, R. Y. C. Synergism between ATM and PARP1 Inhibition Involves DNA Damage and Abrogating the G2 DNA Damage Checkpoint. *Mol Cancer Ther* **19**, 123–134 (2020).
45. Kim, H. *et al.* Combining PARP with ATR inhibition overcomes PARP inhibitor and platinum resistance in ovarian cancer models. *Nat Commun* **11**, 3726 (2020).
46. Yazinski, S. A. *et al.* ATR inhibition disrupts rewired homologous recombination and fork protection pathways in PARP inhibitor-resistant BRCA-deficient cancer cells. *Genes Dev.* **31**, 318–332 (2017).
47. Li, L. *et al.* Androgen receptor inhibitor–induced “BRCAness” and PARP inhibition are synthetically lethal for castration-resistant prostate cancer. *Science Signaling* **10**, eaam7479 (2017).

48. Bizzaro, F. *et al.* VEGF pathway inhibition potentiates PARP inhibitor efficacy in ovarian cancer independent of BRCA status. *J Hematol Oncol* **14**, 186 (2021).
49. Rouault, C. D. *et al.* Inhibition of the STAT3/Fanconi anemia axis is synthetic lethal with PARP inhibition in breast cancer. *Nat Commun* **16**, 2159 (2025).
50. Leal, J. F. M. *et al.* PM01183, a new DNA minor groove covalent binder with potent in vitro and in vivo anti-tumour activity. *Br J Pharmacol* **161**, 1099–1110 (2010).
51. Santamaría Nuñez, G. *et al.* Lurbinectedin Specifically Triggers the Degradation of Phosphorylated RNA Polymerase II and the Formation of DNA Breaks in Cancer Cells. *Molecular Cancer Therapeutics* **15**, 2399–2412 (2016).
52. Costanzo, F. *et al.* Promoters of ASCL1- and NEUROD1-dependent genes are specific targets of lurbinectedin in SCLC cells. *EMBO Molecular Medicine* **14**, e14841 (2022).
53. Singh, S. *et al.* FDA Approval Summary: Lurbinectedin for the Treatment of Metastatic Small Cell Lung Cancer. *Clin Cancer Res* **27**, 2378–2382 (2021).
54. Schultz, C. W. *et al.* ATR inhibition augments the efficacy of lurbinectedin in small-cell lung cancer. *EMBO Mol Med* **15**, e17313 (2023).
55. Calles, A. *et al.* Unveiling the Mechanism of Lurbinectedin's Action and Its Potential in Combination Therapies in Small Cell Lung Cancer. *Mol Cancer Ther* **24**, 828–839 (2025).
56. Cigrang, M. *et al.* Pan-inhibition of super-enhancer-driven oncogenic transcription by next-generation synthetic ecteinascidins yields potent anti-cancer activity. *Nat Commun* **16**, 512 (2025).
57. Peng, G. *et al.* Genome-wide transcriptome profiling of homologous recombination DNA repair. *Nat Commun* **5**, 3361 (2014).
58. Beinse, G. *et al.* Discovery and validation of a transcriptional signature identifying homologous recombination-deficient breast, endometrial and ovarian cancers. *Br J Cancer* **127**, 1123–1132 (2022).
59. Quereda, V. *et al.* Therapeutic Targeting of CDK12/CDK13 in Triple-Negative Breast Cancer. *Cancer Cell* **36**, 545-558.e7 (2019).
60. Shan, W. *et al.* Systematic Characterization of Recurrent Genomic Alterations in Cyclin-Dependent Kinases Reveals Potential Therapeutic Strategies for Cancer Treatment. *Cell Reports* **32**, 107884 (2020).

61. Orhan, E. *et al.* CDK inhibition results in pharmacologic BRCAness increasing sensitivity to olaparib in BRCA1-WT and olaparib resistant in Triple Negative Breast Cancer. *Cancer Letters* **589**, 216820 (2024).
62. Rahl, P. B. *et al.* c-Myc regulates transcriptional pause release. *Cell* **141**, 432–445 (2010).
63. Schwalb, B. *et al.* TT-seq maps the human transient transcriptome. *Science* **352**, 1225–1228 (2016).
64. Berenbaum, M. C. What is synergy? *Pharmacological Reviews* **41**, 93–141 (1989).
65. Duarte, D. & Vale, N. Evaluation of synergism in drug combinations and reference models for future orientations in oncology. *Current Research in Pharmacology and Drug Discovery* **3**, 100110 (2022).
66. Chou, T.-C. Drug combination studies and their synergy quantification using the Chou-Talalay method. *Cancer Res* **70**, 440–446 (2010).
67. Zhang, N., Fu, J.-N. & Chou, T.-C. Synergistic combination of microtubule targeting anticancer fludelone with cytoprotective panaxytriol derived from panax ginseng against MX-1 cells in vitro: experimental design and data analysis using the combination index method. *Am J Cancer Res* **6**, 97–104 (2015).
68. Takebayashi, Y. *et al.* Antiproliferative activity of ecteinascidin 743 is dependent upon transcription-coupled nucleotide-excision repair. *Nat Med* **7**, 961–966 (2001).
69. Christie, E. L. *et al.* Reversion of BRCA1/2 Germline Mutations Detected in Circulating Tumor DNA From Patients With High-Grade Serous Ovarian Cancer. *J Clin Oncol* **35**, 1274–1280 (2017).
70. Rose, M., Burgess, J. T., O'Byrne, K., Richard, D. J. & Bolderson, E. PARP Inhibitors: Clinical Relevance, Mechanisms of Action and Tumor Resistance. *Front Cell Dev Biol* **8**, 564601 (2020).
71. Heeke, A. L. *et al.* Prevalence of Homologous Recombination-Related Gene Mutations Across Multiple Cancer Types. *JCO Precis Oncol* **2018**, PO.17.00286 (2018).
72. Knijnenburg, T. A. *et al.* Genomic and Molecular Landscape of DNA Damage Repair Deficiency across The Cancer Genome Atlas. *Cell Reports* **23**, 239-254.e6 (2018).
73. Xiao, Y. *et al.* Comprehensive analysis of DNA damage repair deficiency in 10,284 pan-cancer study. *Annals of Translational Medicine* **9**, 1661–1661 (2021).
74. Trigo, J. *et al.* Lurbinectedin as second-line treatment for patients with small-cell lung cancer: a single-arm, open-label, phase 2 basket trial. *The Lancet Oncology* **21**, 645–654 (2020).

75. Veo, B. *et al.* Transcriptional control of DNA repair networks by CDK7 regulates sensitivity to radiation in MYC-driven medulloblastoma. *Cell Reports* **35**, 109013 (2021).
76. Sharova, L. V. *et al.* Database for mRNA half-life of 19 977 genes obtained by DNA microarray analysis of pluripotent and differentiating mouse embryonic stem cells. *DNA Res* **16**, 45–58 (2009).
77. Miller, T. E. *et al.* Transcription elongation factors represent in vivo cancer dependencies in glioblastoma. *Nature* **547**, 355–359 (2017).
78. Liang, K. *et al.* Targeting Processive Transcription Elongation via SEC Disruption for MYC-Induced Cancer Therapy. *Cell* **175**, 766-779.e17 (2018).
79. Aoi, Y. & Shilatifard, A. Transcriptional elongation control in developmental gene expression, aging, and disease. *Mol Cell* **83**, 3972–3999 (2023).
80. Johnson, S. F. *et al.* CDK12 Inhibition Reverses De Novo and Acquired PARP Inhibitor Resistance in BRCA Wild-Type and Mutated Models of Triple-Negative Breast Cancer. *Cell Reports* **17**, 2367–2381 (2016).
81. Johnson, N. *et al.* Stabilization of mutant BRCA1 protein confers PARP inhibitor and platinum resistance. *Proceedings of the National Academy of Sciences* **110**, 17041–17046 (2013).
82. Poveda, A. *et al.* A phase I dose-finding, pharmacokinetics and genotyping study of olaparib and lurbinectedin in patients with advanced solid tumors. *Sci Rep* **11**, 4433 (2021).
83. Poveda, A. *et al.* Phase 2 Trial (POLA Study) of Lurbinectedin plus Olaparib in Patients with Advanced Solid Tumors: Results of Efficacy, Tolerability, and the Translational Study. *Cancers* **14**, 915 (2022).
84. Schultz, C. W. *et al.* ATR inhibition augments the efficacy of lurbinectedin in small-cell lung cancer. *EMBO Mol Med* **15**, e17313 (2023).
85. Zheng, S. *et al.* SynergyFinder Plus: Toward Better Interpretation and Annotation of Drug Combination Screening Datasets. *Genomics, Proteomics & Bioinformatics* **20**, 587–596 (2022).

Figures & Legends:

Starting from next page.

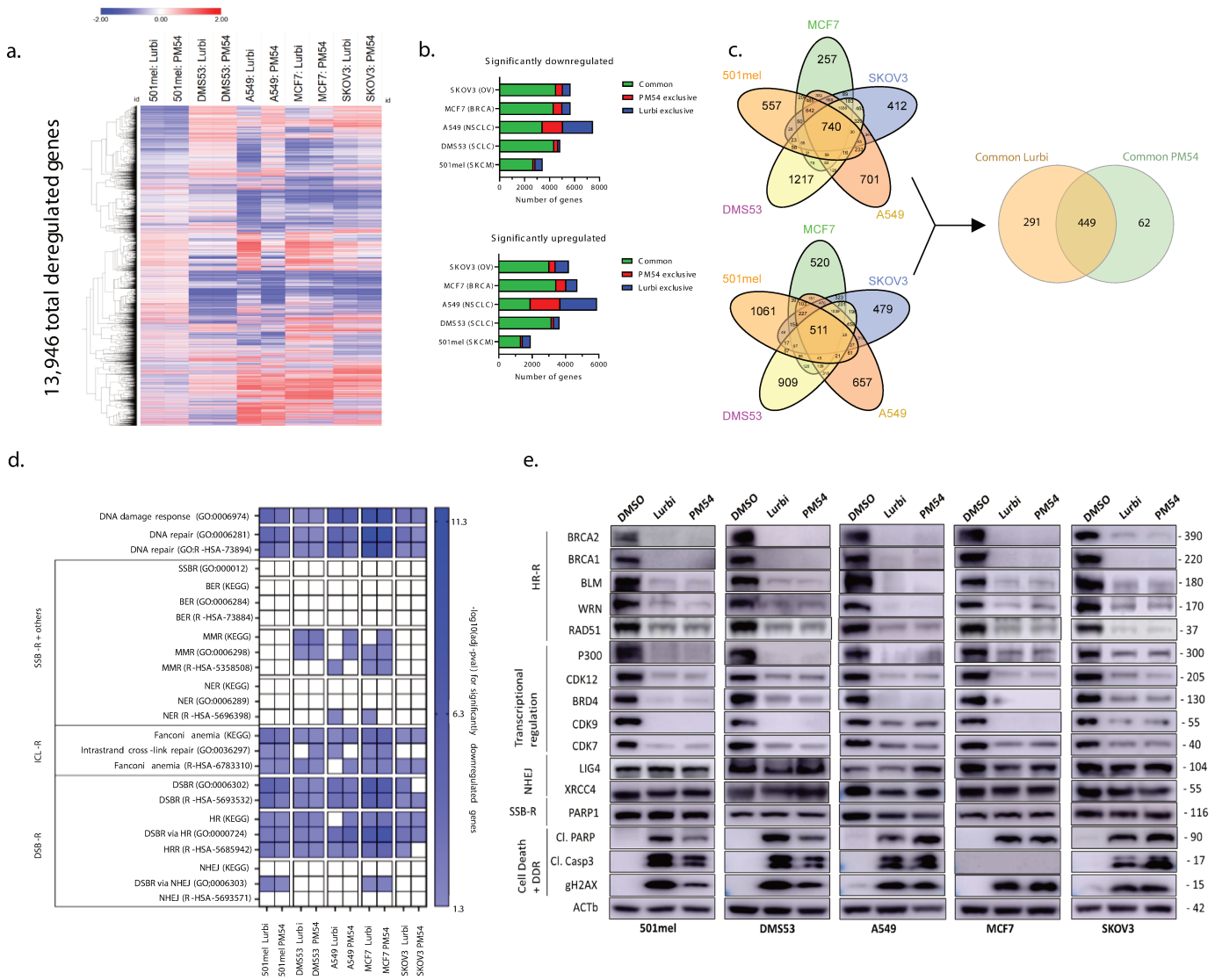
a.
13,946 total deregulated genes
501mel: Lurbi
501mel: PM54
DMS53: Lurbi
DMS53: PM54
A549: Lurbi
A549: PM54
MCF7: Lurbi
MCF7: PM54
SKOV3: Lurbi
SKOV3: PM54
b.
Significantly downregulated
Significantly upregulated
Common
PM54 exclusive
Lurbi exclusive
Number of genes
c.
MCF7
501mel
SKOV3
DMS53
A549
Common Lurbi
Common PM54
d.
DNA damage response (GO:0006974)
DNA repair (GO:0006281)
DNA repair (GO:R -HSA-73894)
SSBR (GO:000012)
BER (KEGG)
BER (GO:0006284)
BER (R -HSA-73884)
MMR (KEGG)
MMR (GO:0006298)
MMR (R-HSA-5358508)
NER (KEGG)
NER (GO:0006289)
NER (R -HSA-5696398)
Fanconi anemia (KEGG)
Intrastrand cross -link repair (GO:0036297)
Fanconi anemia (R-HSA-6783310)
DSBR (GO:0006302)
DSBR (R -HSA-5693532)
HR (KEGG)
DSBR via HR (GO:0000724)
HRR (R -HSA-5685942)
NHEJ (KEGG)
DSBR via NHEJ (GO;0006303)
NHEJ (R -HSA-5693571)
SSB -R + others
ICL -R
DSB -R
-log10(adj-pval) for significantly downregulated genes
e.
DMSO
Lurbi
PM54
HR-R
BRCA2
BRCA1
BLM
WRN
RAD51
Transcriptional regulation
P300
CDK12
BRD4
CDK9
CDK7
NHEJ
LIG4
XRCC4
SSB-R
PARP1
Cell Death + DDR
Cl. PARP
Cl. Casp3
gH2AX
ACTb
501mel
DMS53
A549
MCF7
SKOV3
f.
501mel (SKCM)
DMS53 (SCLC)
A549 (NSCLC)
MCF7 (BRCA)
SKOV3 (OV)
Relative HR Efficiency
DMSO
Lurbi
PM54
Cisplatin
siSCR
siBRCA1
siBRCA2

Figure 1. Ecteinascidins induce a BRCAness-like transcriptional program and impair homologous recombination across diverse cancer models.

a. Heatmap of differentially expressed genes across five HR-proficient cancer cell lines (501mel, DMS53, A549, MCF7, SKOV3) treated with lurbinectedin or PM54 for 12 h at 5×IC50 concentrations, relative to DMSO-treated controls.

b. Bar plots showing the number of significantly upregulated and downregulated genes in each cell line following treatment (adjusted $P < 0.001$).

c. Venn diagrams illustrating the overlap of commonly deregulated genes across cell lines and between lurbinectedin and PM54 treatments, identifying 449 commonly downregulated genes (adjusted $P < 0.001$).

d. Heatmap of -log10(adjusted P-values) for downregulated genes within curated DNA repair pathways across treated cell lines.

e. Western blot analysis of HR factors (BRCA1, BRCA2, BLM, WRN, RAD51), transcriptional regulators (CDK7, CDK9, CDK12, BRD4, EP300), and markers of DNA damage (γH2AX) and apoptosis (cleaved caspase-3/PARP) in cells treated for 12 h at 5×IC50. Protein levels were compared to DMSO-treated controls.

f. Quantification of homologous recombination (HR) efficiency in the indicated cell lines following treatment with lurbinectedin, PM54, cisplatin, or siRNA-mediated depletion of BRCA1/2. HR efficiency was normalized to control conditions (DMSO or siSCR). Data represent mean ± SD from three independent experiments. Statistical significance was determined using ordinary one-way ANOVA with Dunnett's multiple comparisons test.

Statistics: *$P < 0.05$, **$P < 0.01$, ***$P < 0.001$, ****$P < 0.0001$; ns, not significant.

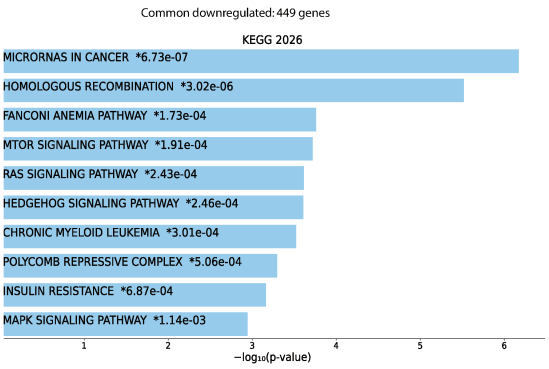
a.
Common downregulated: 449 genes
KEGG 2026
MICRORNAS IN CANCER *6.73e-07
HOMOLOGOUS RECOMBINATION *3.02e-06
FANCONI ANEMIA PATHWAY *1.73e-04
MTOR SIGNALING PATHWAY *1.91e-04
RAS SIGNALING PATHWAY *2.43e-04
HEDGEHOG SIGNALING PATHWAY *2.46e-04
CHRONIC MYELOID LEUKEMIA *3.01e-04
POLYCOMB REPRESSIVE COMPLEX *5.06e-04
INSULIN RESISTANCE *6.87e-04
MAPK SIGNALING PATHWAY *1.14e-03
1
2
3
4
5
6
−log10(p-value)

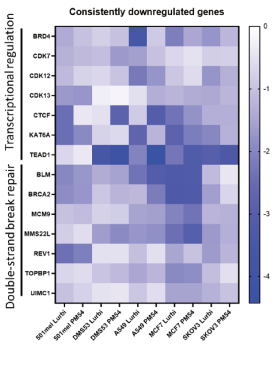
b.
Consistently downregulated genes
Transcriptional regulation
Double-strand break repair
BRD4
CDK7
CDK12
CDK13
CTCF
KAT6A
TEAD1
BLM
BRCA2
MCM9
MMS22L
REV1
TOPBP1
UIMC1
501mel Lurbi
501mel PM54
DMS53 Lurbi
DMS53 PM54
A549 Lurbi
A549 PM54
MCF7 Lurbi
MCF7 PM54
SKOV3 Lurbi
SKOV3 PM54
0
-1
-2
-3
-4

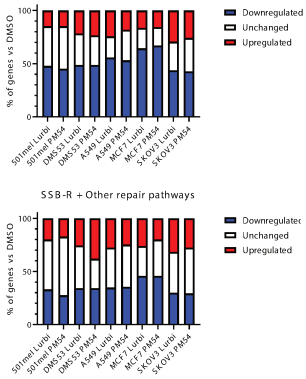
c.
DSB-R + ICL-R
% of genes vs DMSO
Downregulated
Unchanged
Upregulated
SSB-R + Other repair pathways
% of genes vs DMSO
Downregulated
Unchanged
Upregulated

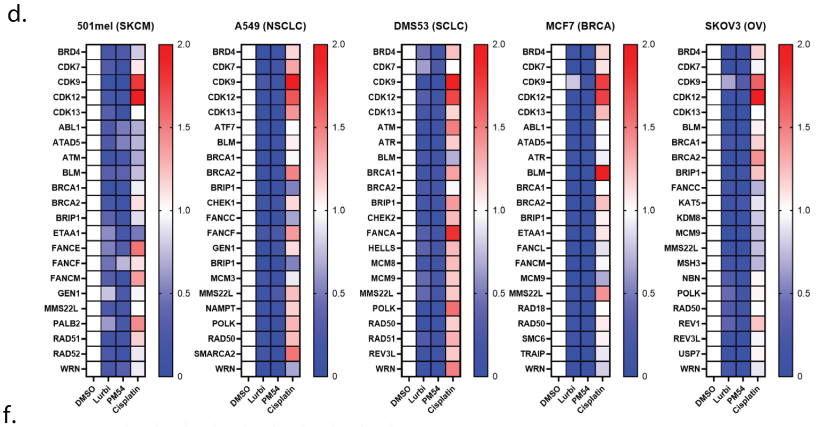
d.
501mel (SKCM)
A549 (NSCLC)
DMS53 (SCLC)
MCF7 (BRCA)
SKOV3 (OV)
DMSO
Lurbi
PM54
Cisplatin

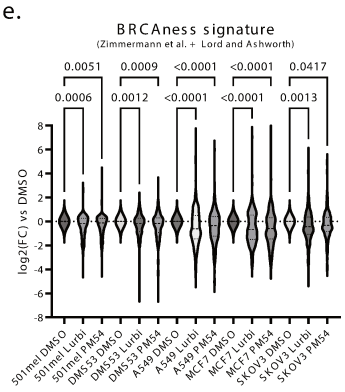
e.
BRCAness signature
(Zimmermann et al. + Lord and Ashworth)
0.0051
0.0009
<0.0001
<0.0001
0.0417
0.0006
0.0012
<0.0001
<0.0001
0.0013
log2(FC) vs DMSO

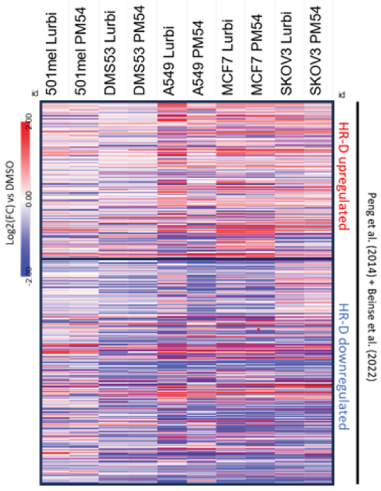
f.
501mel Lurbi
501mel PM54
DMS53 Lurbi
DMS53 PM54
A549 Lurbi
A549 PM54
MCF7 Lurbi
MCF7 PM54
SKOV3 Lurbi
SKOV3 PM54
Log2(FC) vs DMSO
HR-D upregulated
HR-D downregulated
Peng et al. (2014) + Beinse et al. (2022)

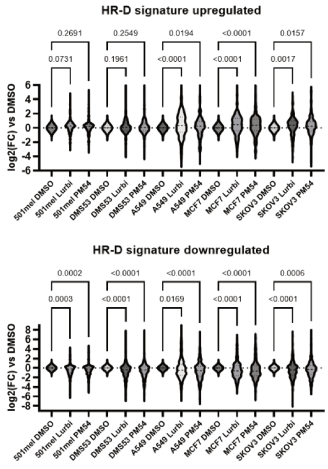
g.
HR-D signature upregulated
0.2691
0.2549
0.0194
<0.0001
0.0157
0.0731
0.1961
<0.0001
<0.0001
0.0017
log2(FC) vs DMSO
HR-D signature downregulated
0.0002
<0.0001
<0.0001
<0.0001
0.0006
0.0003
<0.0001
0.0169
<0.0001
<0.0001

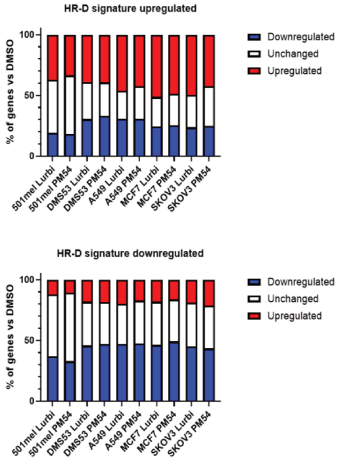
h.
HR-D signature upregulated
% of genes vs DMSO
Downregulated
Unchanged
Upregulated
HR-D signature downregulated
% of genes vs DMSO
Downregulated
Unchanged
Upregulated

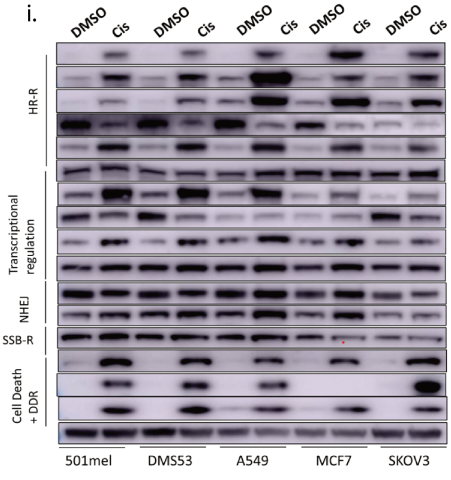
i.
DMSO
Cis
HR-R
Transcriptional regulation
NHEJ
SSB-R
Cell Death + DDR
BRCA2
BRCA1
BLM
WRN
RAD51
P300
CDK12
BRD4
CDK9
CDK7
XRCC4
LIG4
PARP1
Cl. PARP
Cl. CASP3
gH2AX
TUB
501mel
DMS53
A549
MCF7
SKOV3

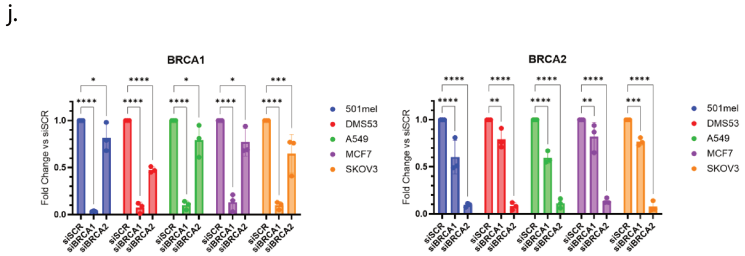
j.
BRCA1
BRCA2
Fold Change vs siSCR
501mel
DMS53
A549
MCF7
SKOV3
siSCR
siBRCA1
siBRCA2

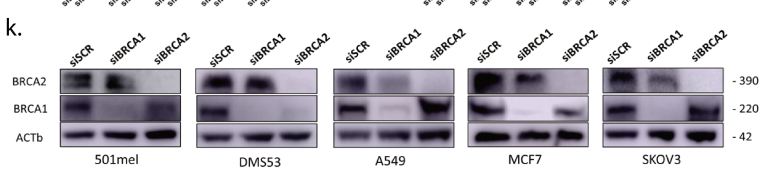
k.
siSCR
siBRCA1
siBRCA2
BRCA2
BRCA1
ACTb
- 390
- 220
- 42
501mel
DMS53
A549
MCF7
SKOV3

Supplementary Figure 1. Ecteinascidins repress HR-associated transcriptional programs and induce HR deficiency signatures.

a. Gene ontology enrichment analysis of commonly downregulated genes across five cancer cell lines following ecteinascidin treatment (12 h, 5×IC50). Adjusted P-values are shown.

b. Heatmap of consistently downregulated HR- and transcription-related genes across all models following ecteinascidin treatment.

c. Quantification of differential regulation of DNA repair pathways, comparing DSBR/ICLR versus SSBR and other repair-associated genes. The percentage of downregulated, unchanged, and upregulated genes relative to DMSO is shown**.**

d. RT-qPCR validation of selected BRCAness-associated and transcription-related genes following treatment with ecteinascidins or cisplatin (12 h, 5×IC50). Gene expression was normalized to 18s. Data represent mean ± SD from three biological replicates. Statistical significance was determined using ordinary one-way ANOVA with Dunnett's multiple comparisons test.

e. Violin plots showing log2 fold change (vs DMSO) of curated BRCAness-associated gene signatures across all cell lines. Statistical significance was assessed using two-sided Wilcoxon tests.

f-h. Analysis of homologous recombination deficiency (HRD) gene expression signatures across cell lines treated with ecteinascidins (12 h, 5×IC50). Log2 fold changes and the percentage of downregulated, unchanged, and upregulated genes relative to DMSO are shown. Statistical significance was assessed using two-sided Wilcoxon tests.

i. Western blot analysis of HR factors and transcriptional regulators following cisplatin treatment (12 h, 5×IC50).

j-k. HR efficiency assays and validation of BRCA1/2 knockdown controls. Data represent mean ± SD from at least three independent experiments. Statistical significance was determined using ordinary one-way ANOVA with Dunnett's multiple comparisons test.

Statistics: Exact P-values are indicated on the graphs; otherwise *P < 0.05, **P < 0.01, ***P < 0.001, ****P < 0.0001; ns, not significant.

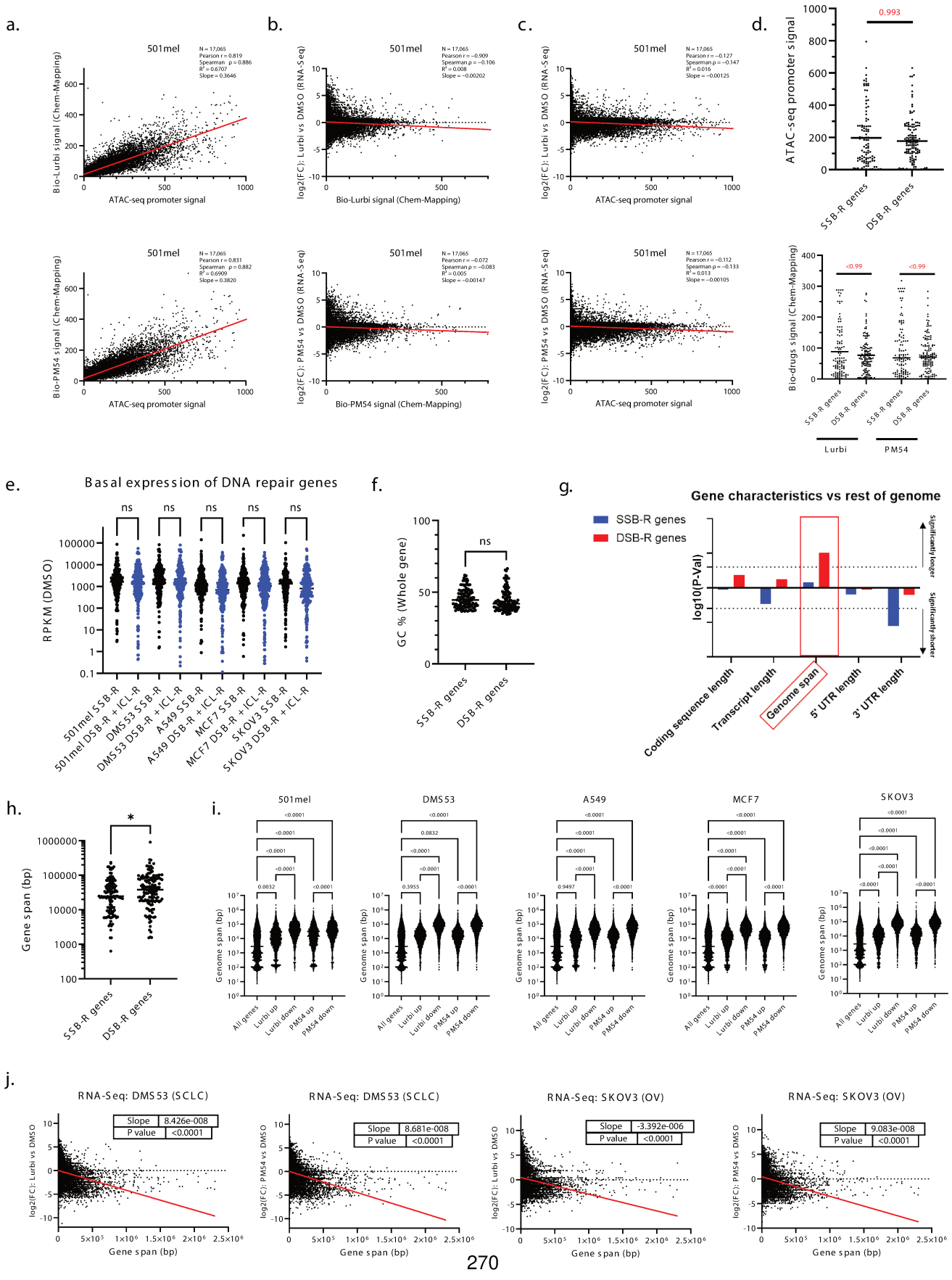
a.
501mel
N = 17,065
Pearson r = 0.819
Spearman ρ = 0.886
R² = 0.6707
Slope = 0.3646
Bio-Lurbi signal (Chem-Mapping)
ATAC-seq promoter signal
Bio-PM54 signal (Chem-Mapping)
b.
N = 17,065
Pearson r = −0.909
Spearman ρ = −0.106
R² = 0.008
Slope = −0.00202
log2(FC): Lurbi vs DMSO (RNA-Seq)
Bio-Lurbi signal (Chem-Mapping)
N = 17,065
Pearson r = −0.831
Spearman ρ = −0.882
R² = 0.6909
Slope = 0.3820
log2(FC): PM54 vs DMSO (RNA-Seq)
Bio-PM54 signal (Chem-Mapping)
c.
N = 17,065
Pearson r = −0.127
Spearman ρ = −0.147
R² = 0.016
Slope = −0.00125
N = 17,065
Pearson r = −0.072
Spearman ρ = −0.083
R² = 0.005
Slope = −0.00147
d.
ATAC-seq promoter signal
0.993
SSB-R genes
DSB-R genes
Bio-drugs signal (Chem-Mapping)
<0.99
<0.99
Lurbi
PM54
e.
Basal expression of DNA repair genes
RPKM (DMSO)
ns
501mel SSB-R
501mel DSB-R + ICL-R
DMS53 SSB-R
DMS53 DSB-R + ICL-R
A549 SSB-R
A549 DSB-R + ICL-R
MCF7 SSB-R
MCF7 DSB-R + ICL-R
SKOV3 SSB-R
SKOV3 DSB-R + ICL-R
f.
GC % (Whole gene)
SSB-R genes
DSB-R genes
g.
Gene characteristics vs rest of genome
SSB-R genes
DSB-R genes
log10(P-Val)
Significantly longer
Significantly shorter
Coding sequence length
Transcript length
Genome span
5' UTR length
3' UTR length
h.
Gene span (bp)
i.
501mel
DMS53
A549
MCF7
SKOV3
Genome span (bp)
All genes
Lurbi up
Lurbi down
PM54 up
PM54 down
j.
RNA-Seq: DMS53 (SCLC)
Slope 8.426e-008
P value <0.0001
RNA-Seq: DMS53 (SCLC)
Slope 8.681e-008
P value <0.0001
RNA-Seq: SKOV3 (OV)
Slope -3.392e-006
P value <0.0001
RNA-Seq: SKOV3 (OV)
Slope 9.083e-008
P value <0.0001
log2(FC): Lurbi vs DMSO
log2(FC): PM54 vs DMSO
Gene span (bp)

Figure 2. Ecteinascidins bind broadly to active chromatin but preferentially repress long genes.

a-c. Scatter plots showing correlations between ecteinascidin binding (Chem-Map signal using biotinylated lurbinectedin or PM54), chromatin accessibility (ATAC-seq promoter signal), and transcriptional response (RNA-seq log2 fold change vs DMSO) in 501mel cells. Each point represents a gene. Pearson and Spearman correlation coefficients are indicated.

d. Comparison of ecteinascidin binding intensity (Chem-Map signal) and promoter chromatin accessibility (ATAC-seq signal) between genes involved in single-strand break repair (SSBR) and double-strand break/interstrand crosslink repair (DSBR/ICLR). Comparisons between two groups were performed using two-sided Mann-Whitney test.

e. Basal expression levels of SSBR and DSBR/ICLR genes in DMSO-treated cells across models (RNA-seq, RPKM). Comparisons between two groups were performed using two-sided Mann-Whitney test.

f. GC content (%) of SSBR and DSBR/ICLR genes. Comparisons between two groups were performed using two-sided Mann-Whitney test.

g. Comparison of gene span (genomic length) across gene categories.

h. Distribution of gene span (bp) for SSBR and DSBR gene sets. Comparisons between two groups were performed using two-sided Mann-Whitney test.

i. Distribution of gene span across all genes stratified by transcriptional response (upregulated, downregulated, unchanged) following ecteinascidin treatment. Comparisons across multiple groups (i) were performed using Kruskal-Wallis test with Dunn’s multiple comparisons test.

j. Correlation between gene span (bp) and transcriptional changes (RNA-seq log2 fold change vs DMSO) following ecteinascidin treatment in representative cell lines. Linear regression slope and P-values are indicated.

Statistics: Exact P-values are indicated on the graphs; ns, not significant.

a.

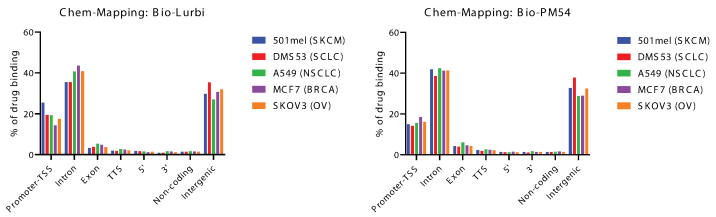
Chem-Mapping: Bio-Lurbi
Chem-Mapping: Bio-PM54
% of drug binding
501mel (SKCM)
DMS53 (SCLC)
A549 (NSCLC)
MCF7 (BRCA)
SKOV3 (OV)
Promoter-TSS
Intron
Exon
TTS
5'
3'
Non-coding
Intergenic

b.

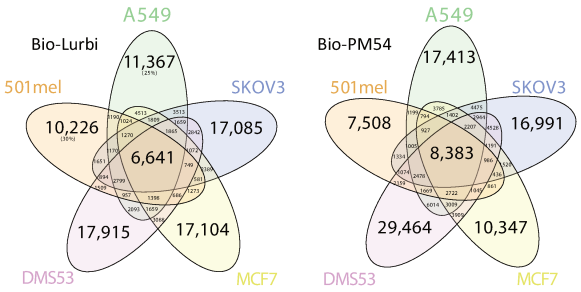
Bio-Lurbi
A549
501mel
SKOV3
DMS53
MCF7
11,367
10,226
17,085
6,641
17,915
17,104
Bio-PM54
17,413
7,508
16,991
8,383
29,464
10,347

c.

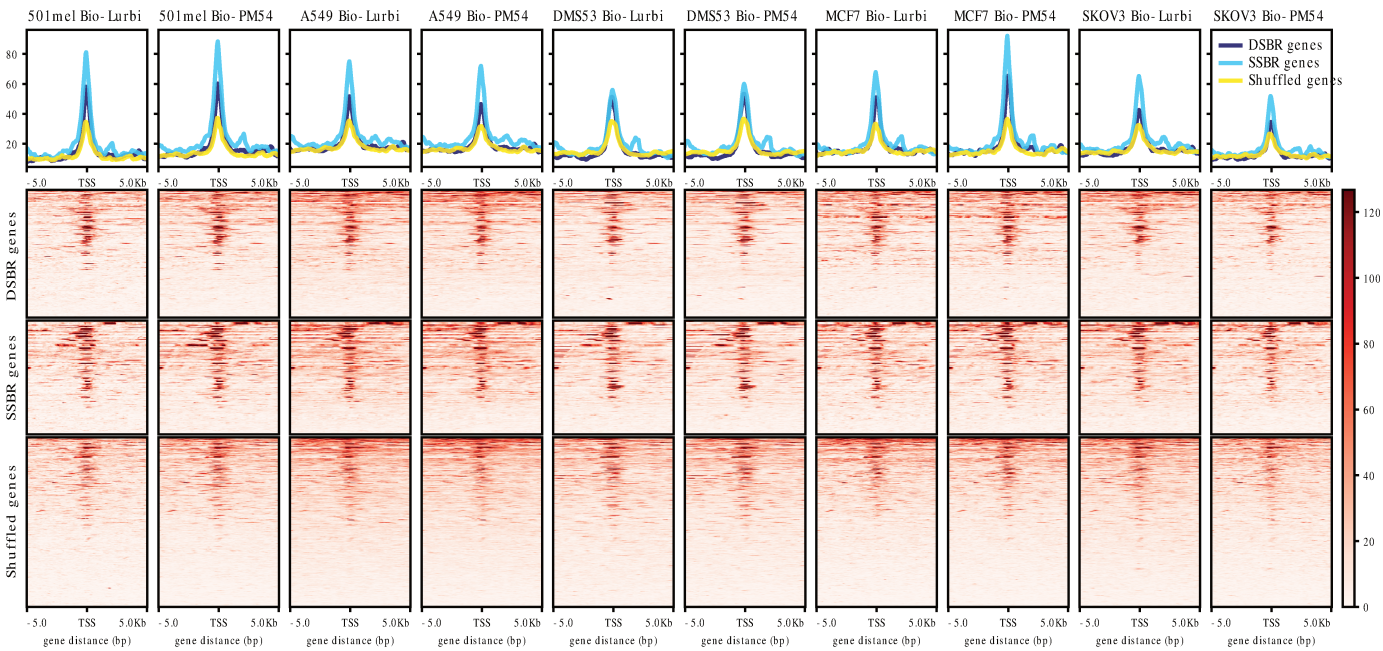
501mel Bio-Lurbi
501mel Bio-PM54
A549 Bio-Lurbi
A549 Bio-PM54
DMS53 Bio-Lurbi
DMS53 Bio-PM54
MCF7 Bio-Lurbi
MCF7 Bio-PM54
SKOV3 Bio-Lurbi
SKOV3 Bio-PM54
DSBR genes
SSBR genes
Shuffled genes
-5.0
TSS
5.0Kb
gene distance (bp)

Supplementary Figure 2. Genome-wide binding distribution of ecteinascidins across cancer models.

a. Genomic distribution of ecteinascidin binding sites identified by Chem-Map (biotinylated lurbinectedin or PM54) across genomic features, including promoters, gene bodies (introns/exons), transcription start sites (TSS), non-coding regions, and intergenic regions.

b. Overlap of ecteinascidin binding sites across five cancer cell lines for Bio-Lurbi and Bio-PM54.

c. Heatmaps and metagene profiles of ecteinascidin binding across five cancer cell lines at the transcription start sites (TSS) of DSBR genes, SSBR genes, and randomly shuffled genomic regions.

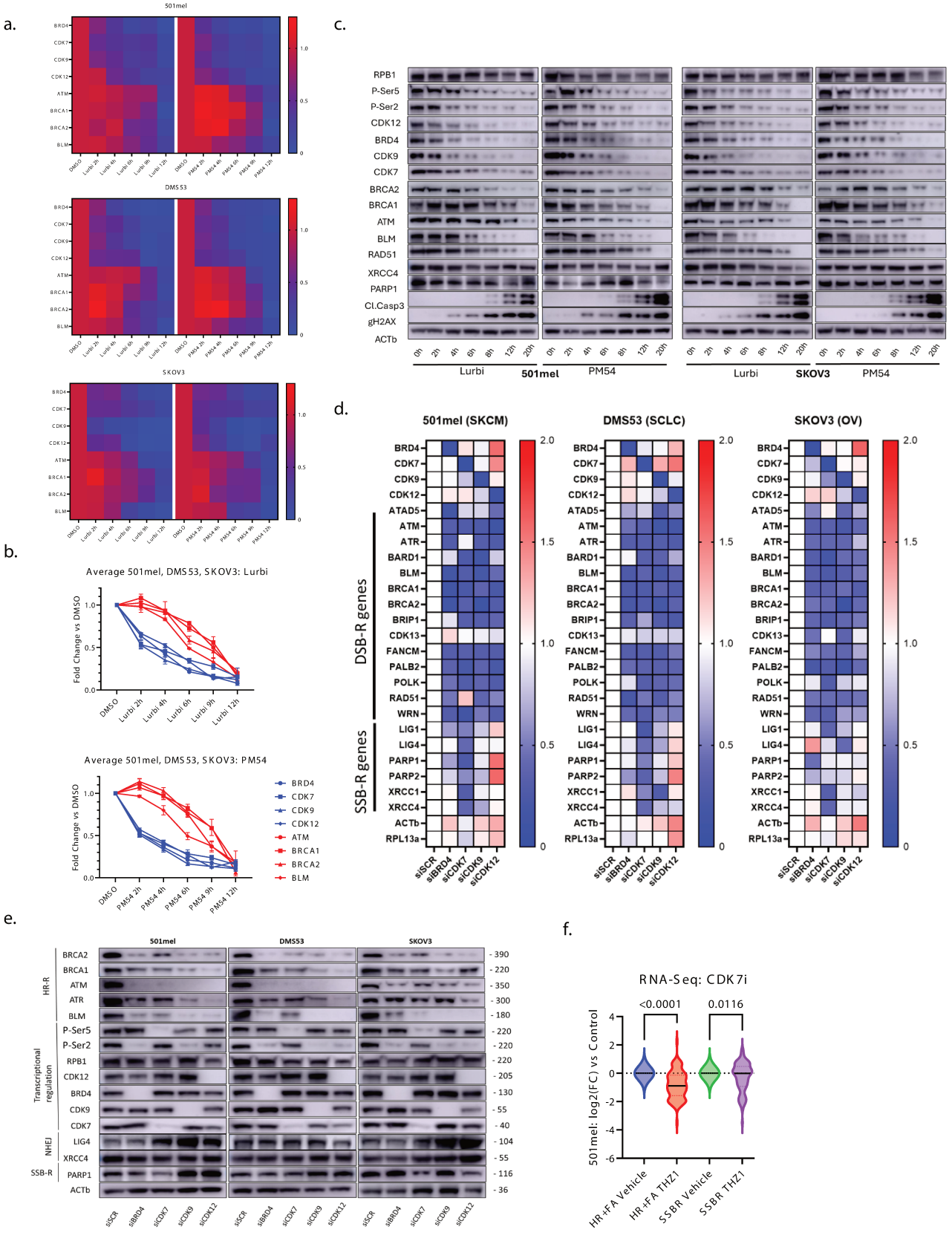
a.
501mel
DMS53
SKOV3
BRD4
CDK7
CDK9
CDK12
ATM
BRCA1
BRCA2
BLM
b.
Average 501mel, DMS53, SKOV3: Lurbi
Fold Change vs DMSO
Average 501mel, DMS53, SKOV3: PM54
c.
RPB1
P-Ser5
P-Ser2
CDK12
BRD4
CDK9
CDK7
BRCA2
BRCA1
ATM
BLM
RAD51
XRCC4
PARP1
Cl.Casp3
gH2AX
ACTb
Lurbi
501mel
PM54
SKOV3
d.
501mel (SKCM)
DMS53 (SCLC)
SKOV3 (OV)
DSB-R genes
SSB-R genes
ATAD5
BARD1
BRIP1
CDK13
FANCM
PALB2
POLK
RAD51
WRN
LIG1
LIG4
PARP1
PARP2
XRCC1
XRCC4
RPL13a
siSCR
siBRD4
siCDK7
siCDK9
siCDK12
e.
501mel
DMS53
SKOV3
HR-R
NHEJ
SSB-R
Transcriptional regulation
f.
RNA-Seq: CDK7i
<0.0001
0.0116
501mel: log2(FC) vs Control
HR-FA Vehicle
HR-FA THZ1
SSBR Vehicle
SSBR THZ1

Figure 3. Rapid suppression of transcription elongation regulators precedes downregulation of homologous recombination genes.

a. Heatmaps showing time-dependent changes in expression of transcription elongation regulators and HR-related genes in 501mel, DMS53, and SKOV3 cells treated with lurbinectedin or PM54 (2–12 h, 5×IC50).

b. Quantification of time-course expression changes (log2 fold change vs DMSO) for elongation regulators and HR genes, averaged across cell lines. Data represent mean ± SD from three independent experiments.

c. Western blot analysis of RNA polymerase II phosphorylation (Ser5 and Ser2), elongation regulators (CDK7, CDK9, CDK12, BRD4), HR factors (BRCA1, BRCA2, ATM, BLM, RAD51), and control proteins following time-course ecteinascidin treatment.

d. Heatmaps showing gene expression changes following siRNA-mediated knockdown of transcription elongation regulators (CDK7, CDK9, CDK12, BRD4) in indicated cell lines.

e. Western blot validation of HR gene expression following siRNA-mediated depletion of elongation regulators.

f. RNA-seq analysis of gene expression changes (log2 fold change vs control) following pharmacological inhibition of CDK7 (THZ1) in 501mel cells. Statistical analyses were performed using two-sided Wilcoxon tests.

Statistics: Exact P-values are indicated on the graphs.

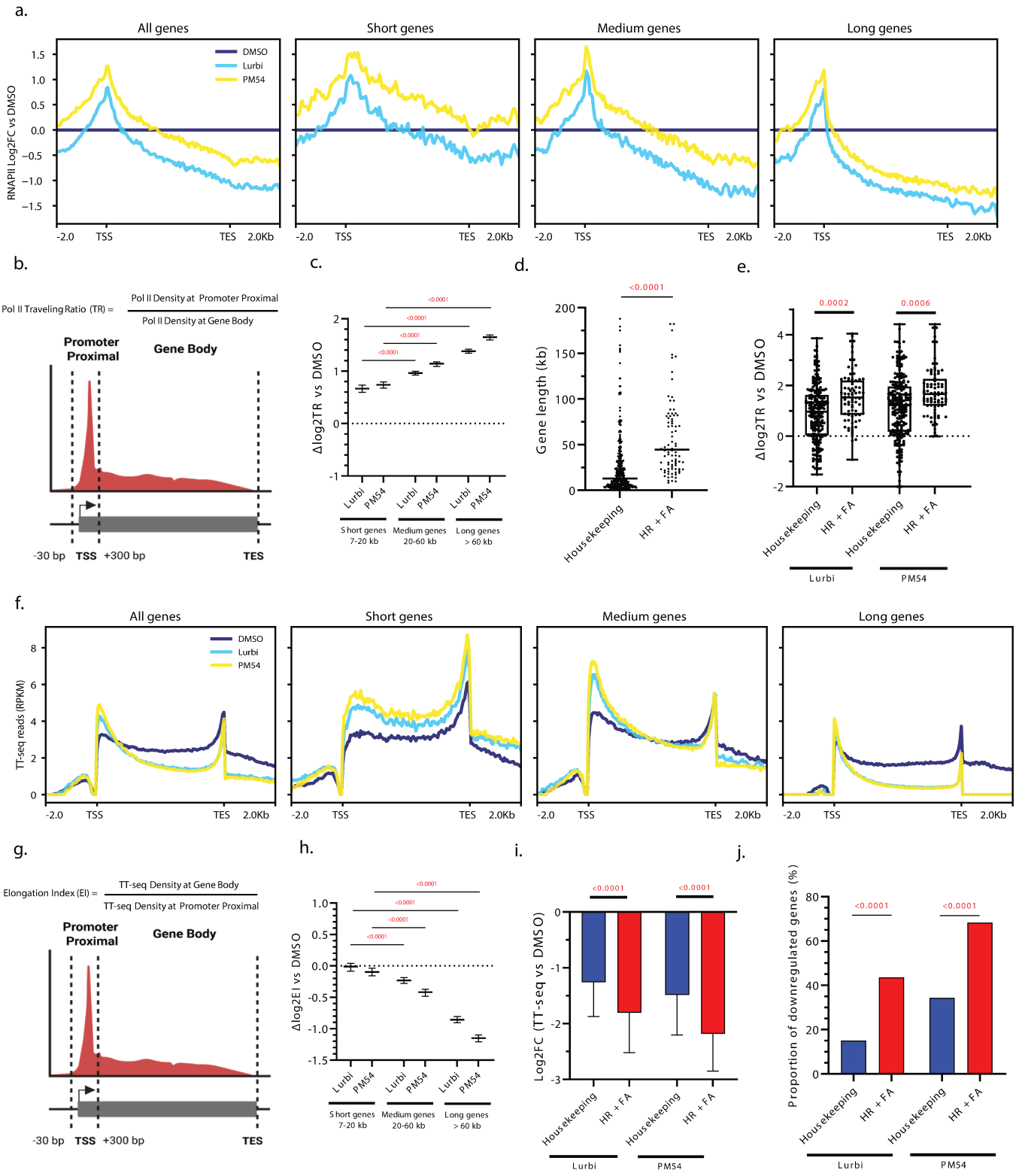
a.
All genes
Short genes
Medium genes
Long genes
DMSO
Lurbi
PM54
RNAPII Log2FC vs DMSO
-2.0
TSS
TES
2.0Kb
b.
Pol II Traveling Ratio (TR) =
Pol II Density at Promoter Proximal
Pol II Density at Gene Body
Promoter Proximal
Gene Body
-30 bp
TSS
+300 bp
TES
c.
Δlog2TR vs DMSO
<0.0001
Short genes 7-20 kb
Medium genes 20-60 kb
Long genes > 60 kb
d.
Gene length (kb)
Housekeeping
HR + FA
e.
Δlog2TR vs DMSO
0.0002
0.0006
Housekeeping
HR + FA
Lurbi
PM54
f.
All genes
Short genes
Medium genes
Long genes
DMSO
Lurbi
PM54
TT-seq reads (RPKM)
g.
Elongation Index (EI) =
TT-seq Density at Gene Body
TT-seq Density at Promoter Proximal
Promoter Proximal
Gene Body
-30 bp
TSS
+300 bp
TES
h.
Δlog2EI vs DMSO
Short genes 7-20 kb
Medium genes 20-60 kb
Long genes > 60 kb
i.
Log2FC (TT-seq vs DMSO)
<0.0001
Housekeeping
HR + FA
Lurbi
PM54
j.
Proportion of downregulated genes (%)
<0.0001
Housekeeping
HR + FA
Lurbi
PM54

Figure 4. Ecteinascidins impair transcription elongation and RNAPII processivity in a gene length-dependent manner.

a. Metagene profiles of RNAPII occupancy (CUT&Tag) across gene bodies in cells treated with ecteinascidins (12 h, 5×IC50) relative to DMSO. Genes are stratified by length (short: 7-20 kb, medium: 20-60 kb, long: >60 kb).

b. Schematic representation of the traveling ratio (TR), defined as the ratio of RNAPII signal at promoter-proximal regions to gene body signal.

c. Quantification of Δlog2TR (vs DMSO) across gene length categories. Data are represented as median ± 95% confidence interval. Comparisons across multiple groups were performed using Kruskal-Wallis test with Dunn's multiple comparisons test.

d. Comparison of gene length between HR+FA genes and housekeeping genes. Comparisons between two groups were performed using two-sided Mann-Whitney test.

e. Quantification of Δlog2TR (vs DMSO) for HR+FA genes versus housekeeping genes. Comparisons between two groups were performed using two-sided Mann-Whitney test.

f. Metagene profiles of nascent transcription (TT-seq, RPKM-normalized) across gene bodies following ecteinascidin treatment, stratified by gene length.

g. Schematic representation of the elongation index (EI), defined as the ratio of gene body signal to promoter-proximal signal.

h. Quantification of Δlog2EI (vs DMSO) across gene length categories. Data are represented as median ± 95% confidence interval. Comparisons across multiple groups were performed using Kruskal-Wallis test with Dunn's multiple comparisons test.

i. Spike-in normalized TT-seq analysis showing nascent transcription levels of HR+FA genes versus housekeeping genes following ecteinascidin treatment. Comparisons between two groups were performed using two-sided Mann-Whitney test.

j. Proportion of genes significantly downregulated (adjusted $P < 0.01$, $log2FC < 0$) among HR+FA and housekeeping gene sets following ecteinascidin treatment. Comparisons between groups were performed using Fisher's exact test.

Statistics: Exact P-values are indicated on the graphs.

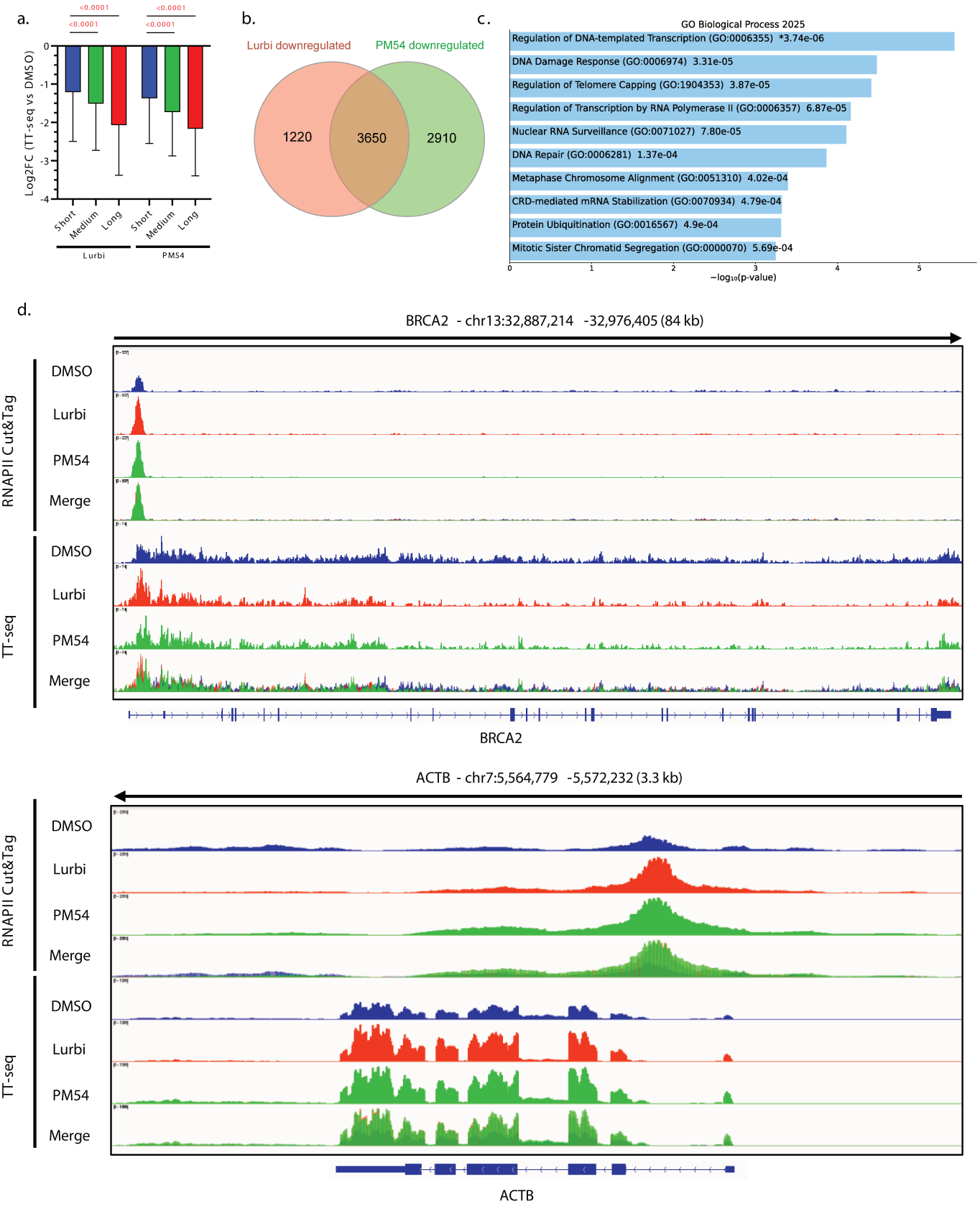
a.
<0.0001
<0.0001
<0.0001
<0.0001
Log2FC (TT-seq vs DMSO)
0
-1
-2
-3
-4
Short
Medium
Long
Short
Medium
Long
Lurbi
PM54
b.
Lurbi downregulated
PM54 downregulated
1220
3650
2910
c.
GO Biological Process 2025
Regulation of DNA-templated Transcription (GO:0006355) *3.74e-06
DNA Damage Response (GO:0006974) 3.31e-05
Regulation of Telomere Capping (GO:1904353) 3.87e-05
Regulation of Transcription by RNA Polymerase II (GO:0006357) 6.87e-05
Nuclear RNA Surveillance (GO:0071027) 7.80e-05
DNA Repair (GO:0006281) 1.37e-04
Metaphase Chromosome Alignment (GO:0051310) 4.02e-04
CRD-mediated mRNA Stabilization (GO:0070934) 4.79e-04
Protein Ubiquitination (GO:0016567) 4.9e-04
Mitotic Sister Chromatid Segregation (GO:0000070) 5.69e-04
0
1
2
3
4
5
−log₁₀(p-value)
d.
BRCA2 - chr13:32,887,214 -32,976,405 (84 kb)
RNAPII Cut&Tag
DMSO
Lurbi
PM54
Merge
TT-seq
DMSO
Lurbi
PM54
Merge
BRCA2
ACTB - chr7:5,564,779 -5,572,232 (3.3 kb)
RNAPII Cut&Tag
DMSO
Lurbi
PM54
Merge
TT-seq
DMSO
Lurbi
PM54
Merge
ACTB

Supplementary Figure 3. Transcriptional consequences of ecteinascidin treatment across gene length and DNA repair pathways.

a. Spike-in normalized TT-seq analysis showing nascent transcription levels across genes stratified by length categories following ecteinascidin treatment. Comparisons across multiple groups were performed using Kruskal-Wallis test with Dunn's multiple comparisons test

b. Venn diagram showing overlap of commonly downregulated genes between lurbinectedin and PM54 treatments.

c. Gene ontology (GO biological process) enrichment analysis of commonly downregulated genes.

d. Genome browser tracks showing RNAPII CUT&Tag and TT-seq signal at representative loci (BRCA2 and ACTB) following ecteinascidin treatment.

Statistics: Exact P-values are indicated on the graphs.

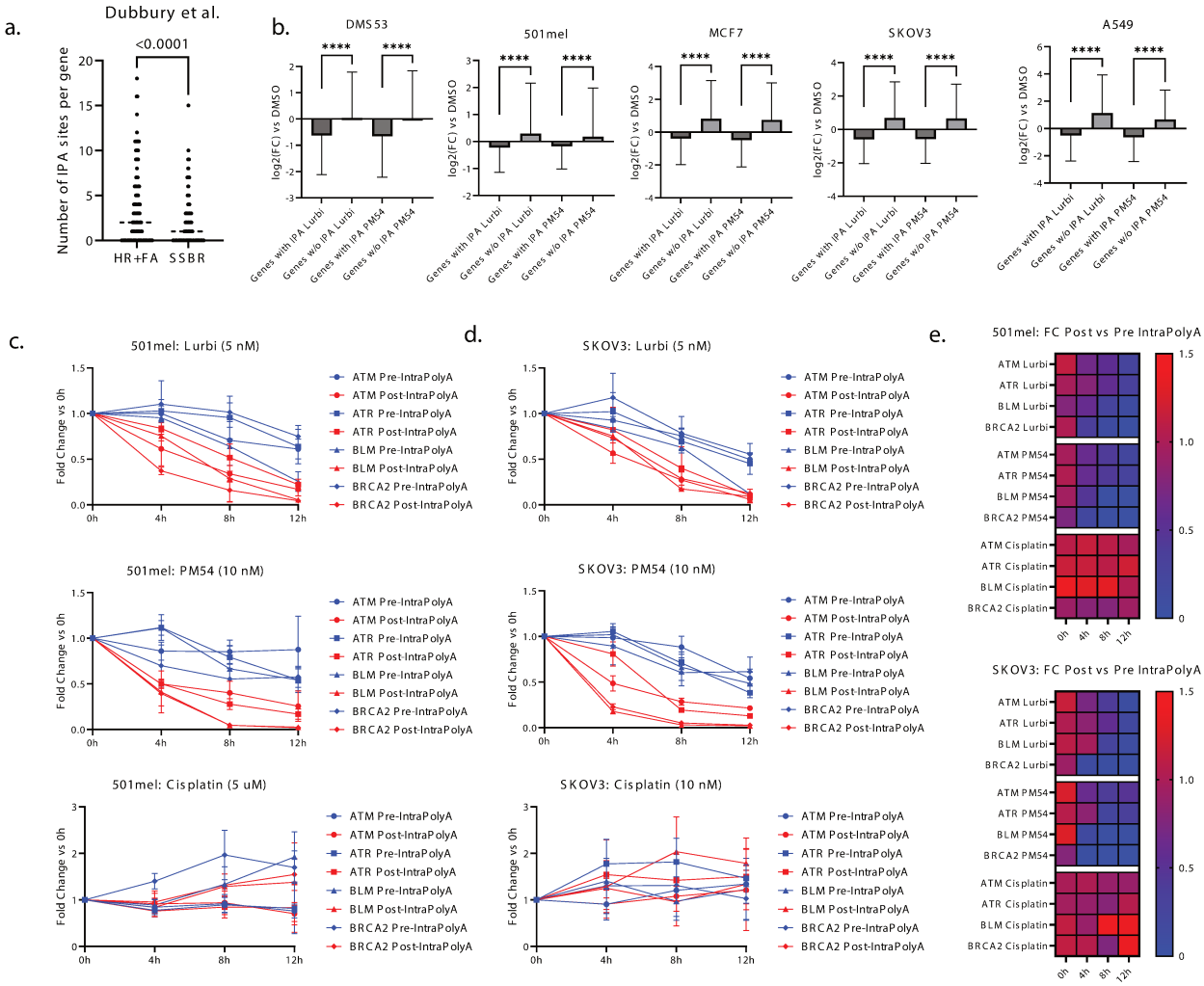
a.
Dubbury et al.
<0.0001
Number of IPA sites per gene
HR+FA
SSBR
b.
DMS53
501mel
MCF7
SKOV3
A549
log2(FC) vs DMSO
****
Genes with IPA Lurbi
Genes w/o IPA Lurbi
Genes with IPA PM54
Genes w/o IPA PM54
c.
501mel: Lurbi (5 nM)
501mel: PM54 (10 nM)
501mel: Cisplatin (5 uM)
d.
SKOV3: Lurbi (5 nM)
SKOV3: PM54 (10 nM)
SKOV3: Cisplatin (10 nM)
Fold Change vs 0h
0h
4h
8h
12h
ATM Pre-IntraPolyA
ATM Post-IntraPolyA
ATR Pre-IntraPolyA
ATR Post-IntraPolyA
BLM Pre-IntraPolyA
BLM Post-IntraPolyA
BRCA2 Pre-IntraPolyA
BRCA2 Post-IntraPolyA
e.
501mel: FC Post vs Pre IntraPolyA
SKOV3: FC Post vs Pre IntraPolyA
ATM Lurbi
ATR Lurbi
BLM Lurbi
BRCA2 Lurbi
ATM PM54
ATR PM54
BLM PM54
BRCA2 PM54
ATM Cisplatin
ATR Cisplatin
BLM Cisplatin
BRCA2 Cisplatin

Supplementary Figure 4. Ecteinascidins induce premature transcriptional termination through intronic polyadenylation.

a. Number of intronic polyadenylation (IPA) sites per gene in HR+FA versus SSBR gene sets, based on published datasets. Comparisons between two groups were performed using two-sided Mann-Whitney test.

b. Distribution of RNA-seq log2 fold change (vs DMSO) for genes with or without annotated IPA sites across multiple cancer cell lines following ecteinascidin treatment. Comparisons between groups were performed using two-sided Mann-Whitney test.

c-d. RT-qPCR analysis of transcript abundance upstream (pre-IPA) and downstream (post-IPA) of annotated intronic polyadenylation sites in HR genes (ATM, ATR, BLM, BRCA2) in 501mel and SKOV3 cells treated with ecteinascidins or cisplatin over time. Data are represented as mean ± SD from three biological replicates. Statistical significance was determined using ordinary one-way ANOVA with Dunnett's multiple comparisons test.

e. Ratio of post-IPA to pre-IPA transcript abundance across conditions and time points, shown as fold change relative to untreated cells.

Statistics: Exact P-values are indicated on the graphs; otherwise *P < 0.05, **P < 0.01, ***P < 0.001, ****P < 0.0001; ns, not significant.

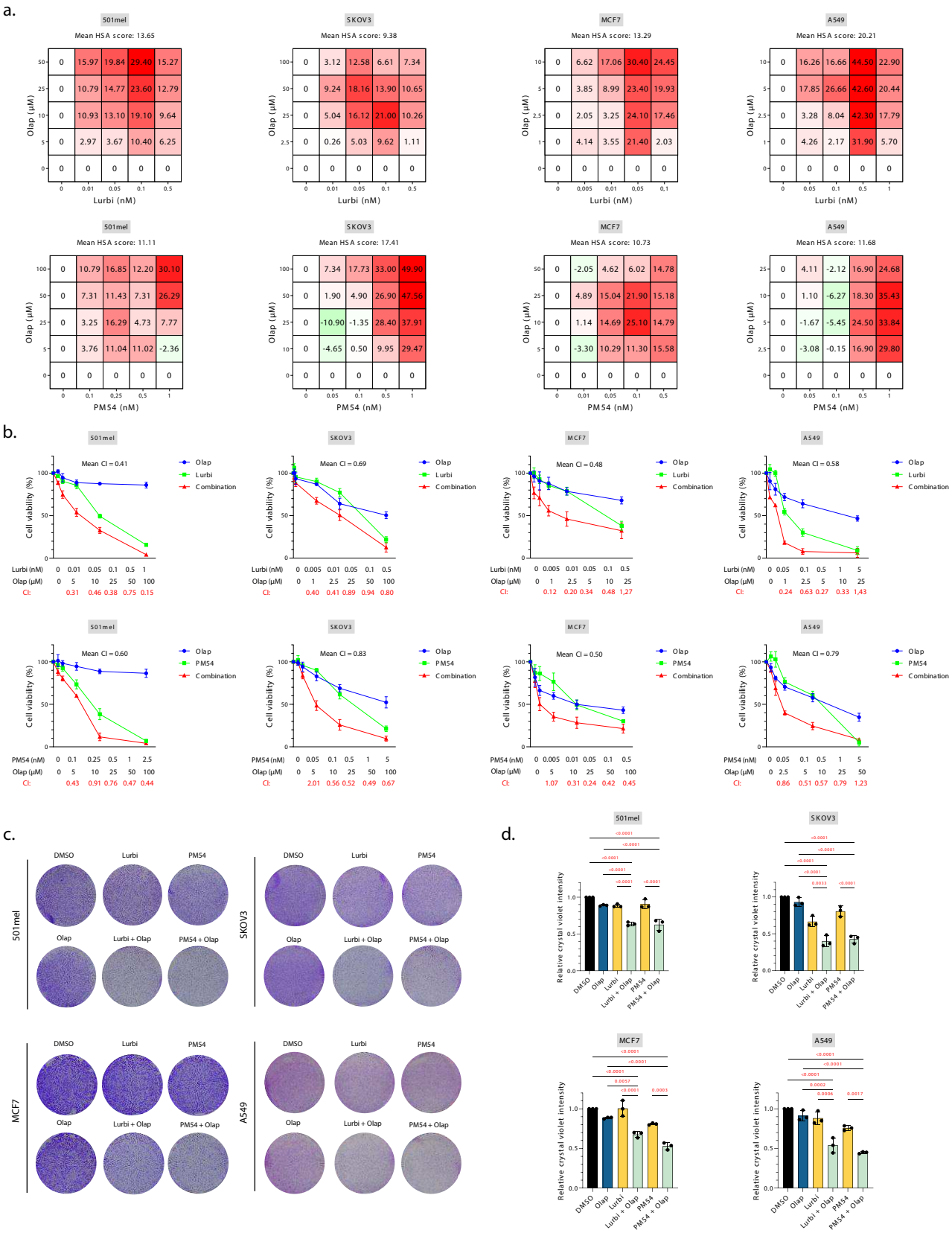
a.
501mel
Mean HSA score: 13.65
Olap (μM)
Lurbi (nM)
SKOV3
Mean HSA score: 9.38
MCF7
Mean HSA score: 13.29
A549
Mean HSA score: 20.21
501mel
Mean HSA score: 11.11
PM54 (nM)
SKOV3
Mean HSA score: 17.41
MCF7
Mean HSA score: 10.73
A549
Mean HSA score: 11.68
b.
501mel
Mean CI = 0.41
SKOV3
Mean CI = 0.69
MCF7
Mean CI = 0.48
A549
Mean CI = 0.58
Olap
Lurbi
Combination
Cell viability (%)
Lurbi (nM)
Olap (μM)
CI:
501mel
Mean CI = 0.60
SKOV3
Mean CI = 0.83
MCF7
Mean CI = 0.50
A549
Mean CI = 0.79
PM54
PM54 (nM)
c.
501mel
SKOV3
MCF7
A549
DMSO
Lurbi
PM54
Olap
Lurbi + Olap
PM54 + Olap
d.
501mel
SKOV3
MCF7
A549
Relative crystal violet intensity

Figure 5. Ecteinascidins synergize with PARP inhibition across multiple cancer models.

a. Heatmaps showing synergy scores calculated using the Highest Single Agent (HSA) model for combinations of lurbinectedin or PM54 with olaparib across indicated cancer cell lines after 72 h treatment. Red indicates synergistic interactions and green antagonistic interactions. Mean HSA scores are indicated for each condition.

b. Dose-response curves showing cell viability following treatment with olaparib, ecteinascidins, or their combinations across cancer cell lines. Combination Index (CI) values were calculated using the Chou-Talalay method at multiple dose combinations. Mean CI values are indicated for each condition.

c. Representative crystal violet staining of cancer cell lines treated with DMSO, ecteinascidins (lurbinectedin or PM54) at subthlethal doses (0.5 x IC50), olaparib, or their combinations for 72 h.

d. Quantification of crystal violet staining shown in panel c. Data are normalized to DMSO-treated controls and represent mean ± SD from three independent experiments. Statistical significance was determined using ordinary one-way ANOVA with Dunnett's multiple comparisons test.

Statistics: HSA scores > 0 indicate synergy. CI values < 1 indicate synergistic interactions. Exact P-values are indicated on the graphs.

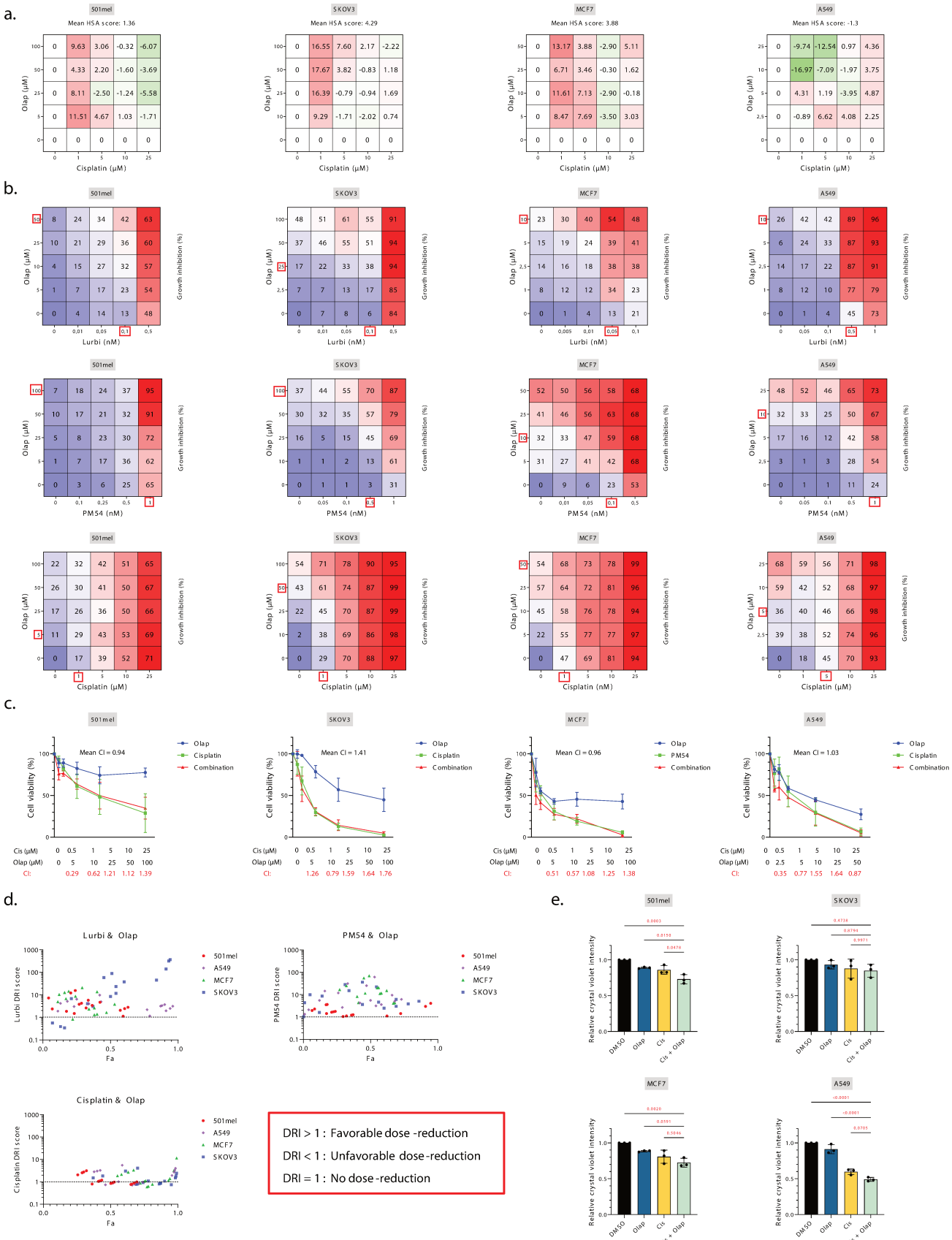
a.
501mel
Mean HSA score: 1.36
SKOV3
Mean HSA score: 4.29
MCF7
Mean HSA score: 3.88
A549
Mean HSA score: -1.3
Olap (µM)
Cisplatin (µM)
b.
Lurbi (nM)
PM54 (nM)
Growth inhibition (%)
c.
Mean CI = 0.94
Mean CI = 1.41
Mean CI = 0.96
Mean CI = 1.03
Cell viability (%)
Olap
Cisplatin
Combination
PM54
d.
Lurbi & Olap
PM54 & Olap
Cisplatin & Olap
Lurbi DRI score
PM54 DRI score
Cisplatin DRI score
Fa
501mel
A549
MCF7
SKOV3
DRI > 1 : Favorable dose -reduction
DRI < 1 : Unfavorable dose-reduction
DRI = 1 : No dose-reduction
e.
Relative crystal violet intensity
DMSO
Olap
Cis
Cis + Olap

Supplementary Figure 5. Comparative analysis of ecteinascidin and cisplatin combinations with olaparib.

a. Heatmaps showing HSA synergy scores for combinations of cisplatin and olaparib across cancer cell lines after 72 h treatment. Mean HSA scores are indicated.

b. Cell viability measurements following treatment with olaparib, ecteinascidins, cisplatin, or their combinations across cancer cell lines. Doses with the highest synergy scores are surrounded by a red rectangle.

c. Dose-response curves and Combination Index (CI) values for cisplatin-olaparib combinations across cancer cell lines. Mean CI values are indicated.

d. Dose Reduction Index (DRI) analysis for ecteinascidin-olaparib and cisplatin-olaparib combinations. DRI > 1 indicates favorable dose reduction, DRI = 1 no effect, and DRI < 1 unfavorable dose reduction.

e. Quantification of crystal violet staining following treatment with cisplatin at sublethal doses (0.5 x IC50), olaparib, or their combination.

Statistics: Exact P-values are indicated on the graphs.

a.

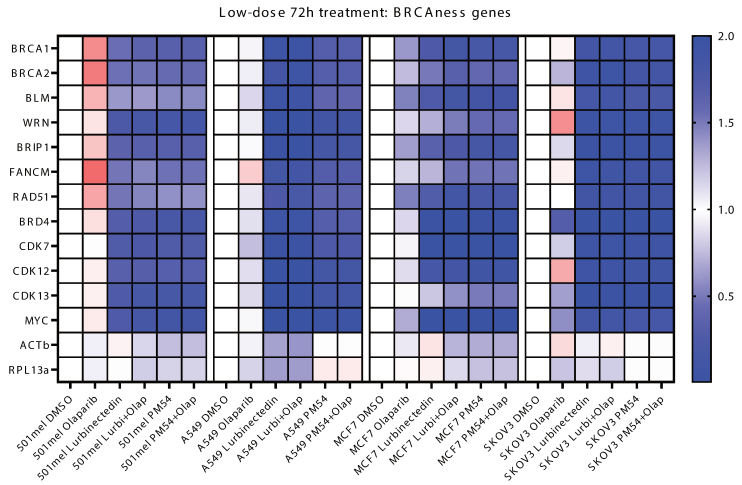
Low-dose 72h treatment: BRCAness genes
BRCA1
BRCA2
BLM
WRN
BRIP1
FANCM
RAD51
BRD4
CDK7
CDK12
CDK13
MYC
ACTb
RPL13a
2.0
1.5
1.0
0.5
501mel DMSO
501mel Olaparib
501mel Lurbinectedin
501mel Lurbi+Olap
501mel PM54
501mel PM54+Olap
A549 DMSO
A549 Olaparib
A549 Lurbinectedin
A549 Lurbi+Olap
A549 PM54
A549 PM54+Olap
MCF7 DMSO
MCF7 Olaparib
MCF7 Lurbinectedin
MCF7 Lurbi+Olap
MCF7 PM54
MCF7 PM54+Olap
SKOV3 DMSO
SKOV3 Olaparib
SKOV3 Lurbinectedin
SKOV3 Lurbi+Olap
SKOV3 PM54
SKOV3 PM54+Olap

b.

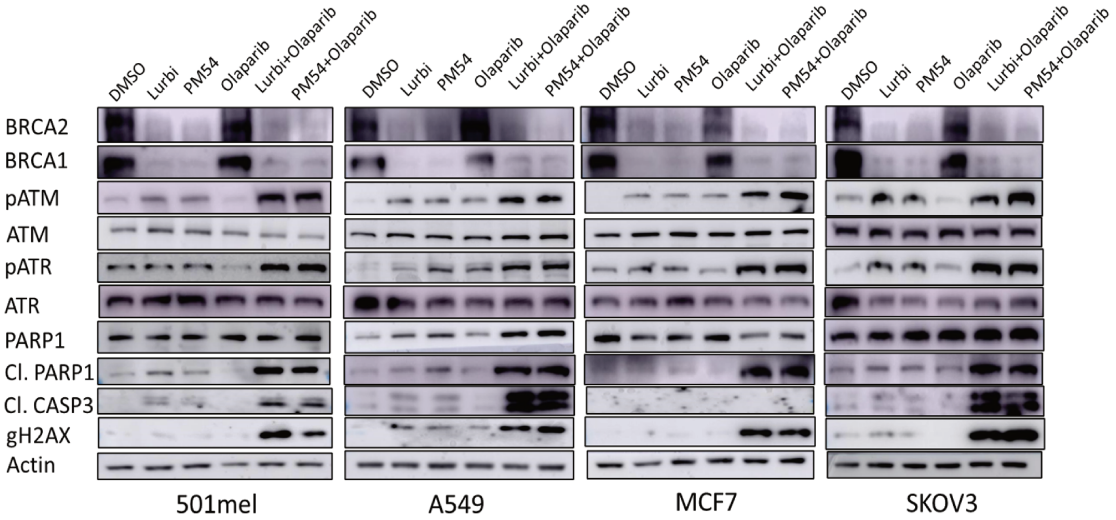
DMSO
Lurbi
PM54
Olaparib
Lurbi+Olaparib
PM54+Olaparib
BRCA2
BRCA1
pATM
ATM
pATR
ATR
PARP1
Cl. PARP1
Cl. CASP3
gH2AX
Actin
501mel
A549
MCF7
SKOV3

c.

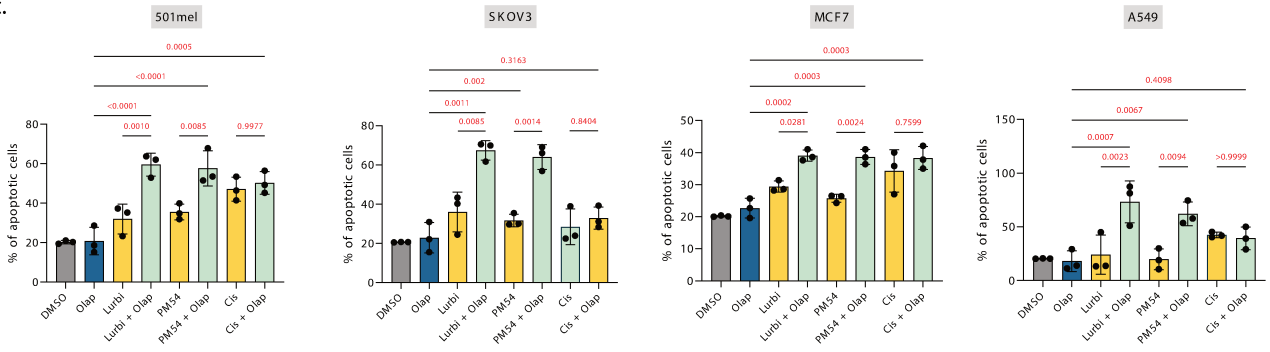
501mel
SKOV3
MCF7
A549
% of apoptotic cells
DMSO
Olap
Lurbi
Lurbi + Olap
PM54
PM54 + Olap
Cis
Cis + Olap
0.0005
<0.0001
<0.0001
0.0010
0.0085
0.9977
0.3163
0.002
0.0011
0.0085
0.0014
0.8404
0.0003
0.0003
0.0002
0.0281
0.0024
0.7599
0.4098
0.0067
0.0007
0.0023
0.0094
>0.9999

Supplementary Figure 6. Ecteinascidins downregulate HR genes and induce apoptosis in combination with PARP inhibition at sublethal doses.

a. Heatmap showing relative expression of HR-related genes and transcriptional regulators following 72h treatment with ecteinascidins, olaparib, cisplatin, or their combinations at sublethal doses (50% IC50) across cancer cell lines.

b. Western blot analysis of HR factors (BRCA1, BRCA2, BLM, WRN, RAD51), transcriptional regulators (BRD4, CDK7, CDK12, CDK13), and DNA damage/apoptosis markers (γH2AX, cleaved PARP1, cleaved caspase-3) following treatment conditions described in panel a. Representative blots from at least two independent experiments are shown.

c. Quantification of apoptotic cells measured by Annexin V staining and flow cytometry in indicated cancer cell lines following 72 h treatment with ecteinascidins, olaparib, cisplatin, or their combinations at sublethal doses (50% IC50). Data represent mean ± SD from three independent experiments. Statistical significance was determined using ordinary one-way ANOVA with Dunnett's multiple comparisons test.

Statistics: Exact P-values are indicated on the graphs.

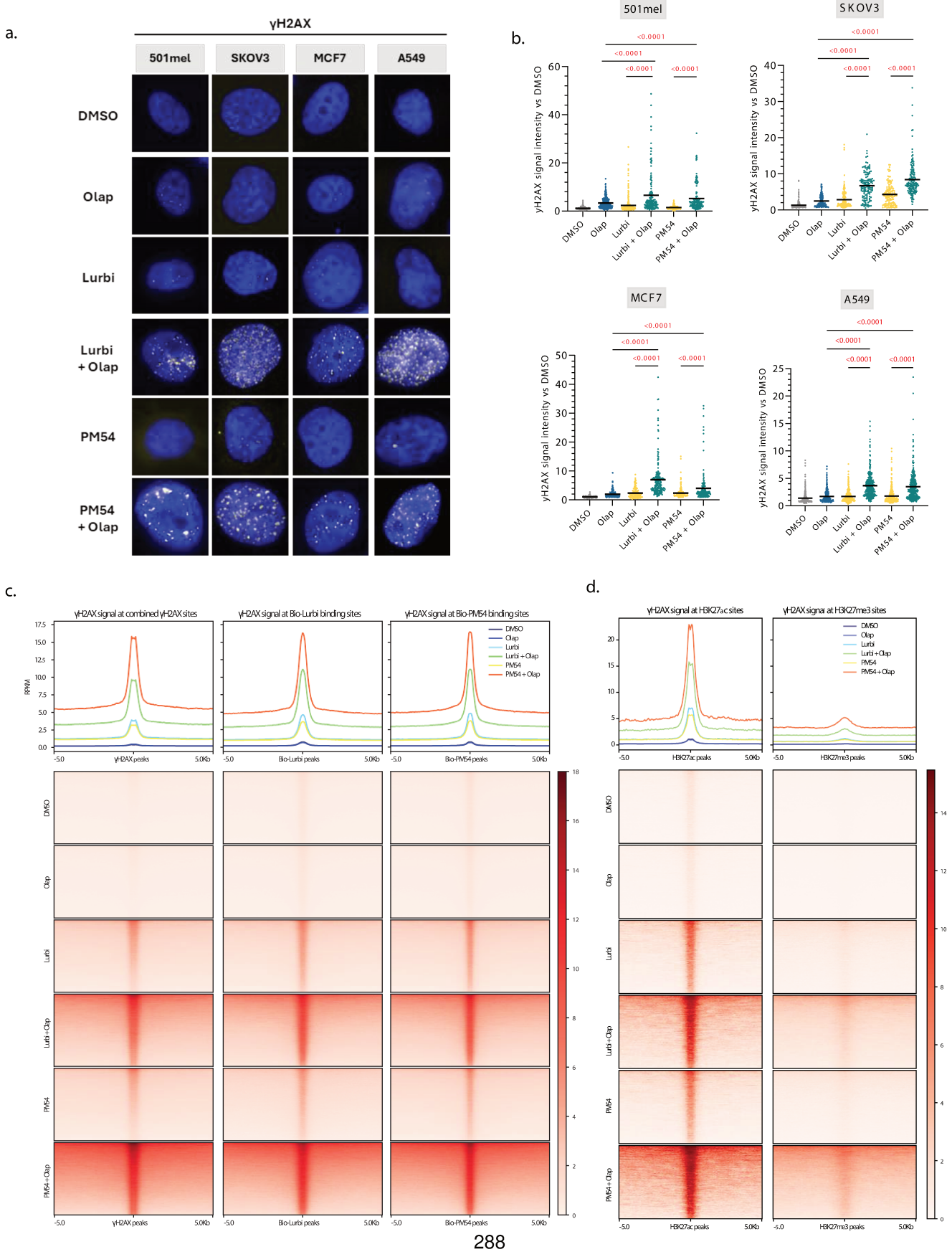
a.
γH2AX
501mel
SKOV3
MCF7
A549
DMSO
Olap
Lurbi
Lurbi + Olap
PM54
PM54 + Olap
b.
501mel
SKOV3
MCF7
A549
γH2AX signal intensity vs DMSO
<0.0001
DMSO
Olap
Lurbi
Lurbi + Olap
PM54
PM54 + Olap
c.
γH2AX signal at combined γH2AX sites
γH2AX signal at Bio-Lurbi binding sites
γH2AX signal at Bio-PM54 binding sites
RPKM
γH2AX peaks
Bio-Lurbi peaks
Bio-PM54 peaks
5.0Kb
d.
γH2AX signal at H3K27ac sites
γH2AX signal at H3K27me3 sites
H3K27ac peaks
H3K27me3 peaks

Figure 6. Ecteinascidin-PARP inhibitor combination enhances DNA damage in actively transcribed regions.

a. Representative immunofluorescence images of γH2AX staining in indicated cancer cell lines (501mel, SKOV3, MCF7, A549) following 72h treatment with DMSO, olaparib, ecteinascidins (lurbinectedin or PM54), or their combinations at sublethal concentrations (50% IC50).

b. Quantification of γH2AX signal intensity (normalized to DMSO) across treatment conditions shown in panel a. Data represent mean ± SD from three independent experiments. Statistical significance was determined using ordinary one-way ANOVA with Dunnett's multiple comparisons test.

c. Metagene profiles and heatmaps of γH2AX CUT&Tag signal centered on combined γH2AX peaks and ecteinascidin binding sites (Bio-Lurbi and Bio-PM54) in SKOV3 cells following 72h treatment (50% IC50). Normalized signal intensity (using Drosophile spike-in controls) is shown.

d. Metagene profiles and heatmaps of γH2AX CUT&Tag signal centered on H3K27ac and H3K27me3 peaks, showing distribution of DNA damage relative to active and repressive chromatin states. Normalized signal intensity (using Drosophile spike-in controls) is shown.

Statistics: Exact P-values are indicated on the graphs.

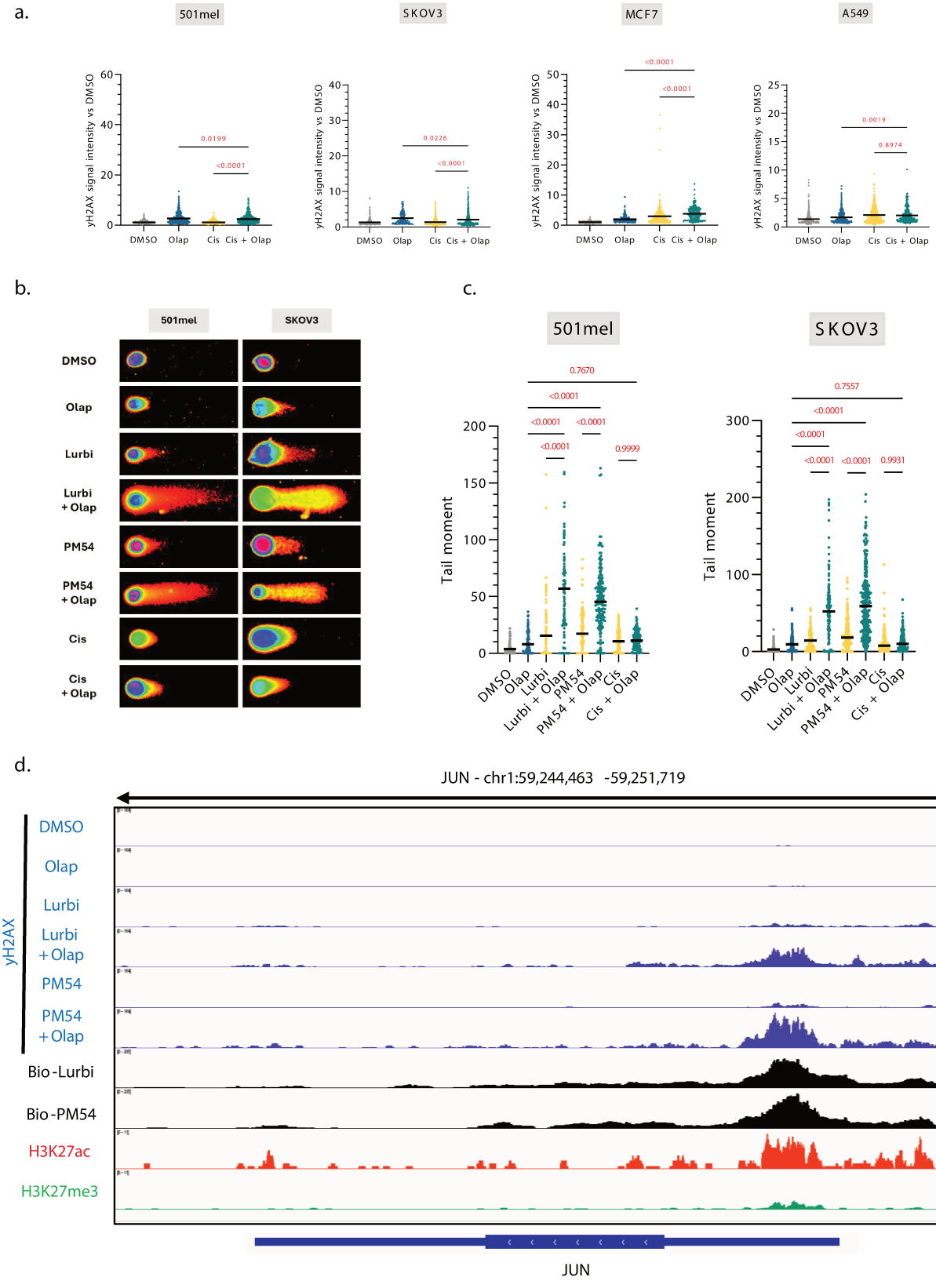
a.
501mel
SKOV3
MCF7
A549
γH2AX signal intensity vs DMSO
DMSO
Olap
Cis
Cis + Olap
0.0199
<0.0001
0.0226
<0.0001
<0.0001
<0.0001
0.0019
0.8974
b.
501mel
SKOV3
DMSO
Olap
Lurbi
Lurbi + Olap
PM54
PM54 + Olap
Cis
Cis + Olap
c.
501mel
SKOV3
Tail moment
0.7670
<0.0001
<0.0001
<0.0001
<0.0001
0.9999
0.7557
<0.0001
<0.0001
<0.0001
<0.0001
0.9931
Lurbi + Olap
PM54 + Olap
d.
JUN - chr1:59,244,463 -59,251,719
yH2AX
DMSO
Olap
Lurbi
Lurbi + Olap
PM54
PM54 + Olap
Bio-Lurbi
Bio-PM54
H3K27ac
H3K27me3
JUN

Supplementary Figure 7. DNA damage accumulation and genomic localization following combination treatment.

a. Quantification of γH2AX signal intensity (normalized to DMSO) following treatment with cisplatin, olaparib, or their combination across cancer cell lines (72h, 50% IC50). Data represent mean ± SD from three independent experiments. Statistical significance was determined using ordinary one-way ANOVA with Dunnett's multiple comparisons test.

b. Representative comet assay images in 501mel and SKOV3 cells following treatment with DMSO, olaparib, ecteinascidins, cisplatin, or their combinations (72h, 50% IC50).

c. Quantification of comet assay tail moment in 501mel and SKOV3 cells under the conditions described in panel b. Data represent mean ± SD from three independent experiments. Statistical significance was determined using ordinary one-way ANOVA with Dunnett's multiple comparisons test.

d. Genome browser tracks showing γH2AX signal, ecteinascidin binding (Bio-Lurbi, Bio-PM54), and chromatin marks (H3K27ac, H3K27me3) at the JUN locus following treatment conditions (72h, 50% IC50).

Statistics: Exact P-values are indicated on the graphs.

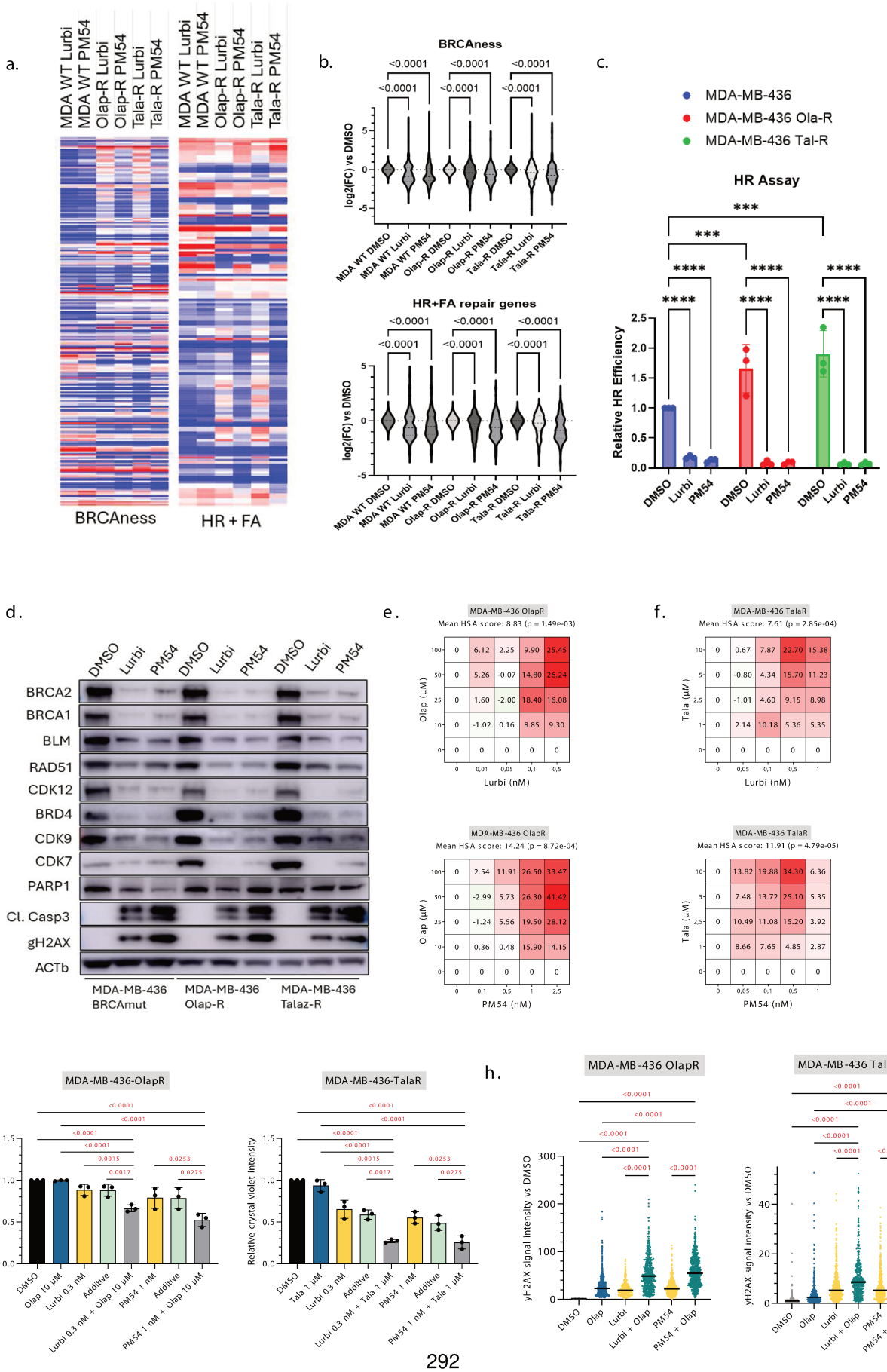
a.
MDA WT Lurbi
MDA WT PM54
Olap-R Lurbi
Olap-R PM54
Tala-R Lurbi
Tala-R PM54
BRCAness
HR + FA
b.
BRCAness
HR+FA repair genes
log2(FC) vs DMSO
MDA WT DMSO
MDA WT Lurbi
MDA WT PM54
Olap-R DMSO
Olap-R Lurbi
Olap-R PM54
Tala-R DMSO
Tala-R Lurbi
Tala-R PM54
<0.0001
c.
MDA-MB-436
MDA-MB-436 Ola-R
MDA-MB-436 Tal-R
HR Assay
Relative HR Efficiency
DMSO
Lurbi
PM54
d.
BRCA2
BRCA1
BLM
RAD51
CDK12
BRD4
CDK9
CDK7
PARP1
Cl. Casp3
gH2AX
ACTb
MDA-MB-436 BRCAmut
MDA-MB-436 Olap-R
MDA-MB-436 Talaz-R
e.
MDA-MB-436 OlapR
Mean HSA score: 8.83 (p = 1.49e-03)
Olap (µM)
Lurbi (nM)
Mean HSA score: 14.24 (p = 8.72e-04)
PM54 (nM)
f.
MDA-MB-436 TalaR
Mean HSA score: 7.61 (p = 2.85e-04)
Tala (µM)
Mean HSA score: 11.91 (p = 4.79e-05)
g.
MDA-MB-436-OlapR
MDA-MB-436-TalaR
Relative crystal violet intensity
DMSO
Olap 10 µM
Lurbi 0.3 nM
Additive
Lurbi 0.3 nM + Olap 10 µM
PM54 1 nM
Additive
PM54 1 nM + Olap 10 µM
Tala 1 µM
Lurbi 0.3 nM + Tala 1 µM
PM54 1 nM + Tala 1 µM
h.
MDA-MB-436 OlapR
MDA-MB-436 TalaR
γH2AX signal intensity vs DMSO
Olap
Lurbi
Lurbi + Olap
PM54
PM54 + Olap

Figure 7. Ecteinascidins restore PARP inhibitor sensitivity in resistant BRCA1-mutated cancer cells.

a. Heatmap of differentially expressed BRCAness, homologous recombination (HR) & Fanconi anemia (FA) genes in parental (WT), olaparib-resistant (OlapR), and talazoparib-resistant (TalaR) MDA-MB-436 cells following treatment with ecteinascidins (12h, 5×IC50).

b. Violin plots showing log2 fold change (vs DMSO) of BRCAness-associated gene signatures and HR and Fanconi anemia pathway genes across conditions. Statistical significance was assessed using two-sided Wilcoxon tests.

c. Quantification of homologous recombination (HR) efficiency across parental and resistant cell lines following ecteinascidin treatment. Data represent mean ± SD from three independent experiments. Statistical significance was determined using ordinary one-way ANOVA with Dunnett's multiple comparisons test.

d. Western blot analysis of HR factors (BRCA1, BRCA2, BLM, RAD51), transcriptional regulators (CDK7, CDK12, BRD4), and control proteins across parental and resistant cell lines following ecteinascidin treatment.

e-f. Heatmaps showing synergy scores (HSA model) for combinations of ecteinascdins and olaparib in OlapR cells, as well as ecteinascidins and talazoparib in TalaR cells.

g. Quantification of cell viability (crystal violet staining) following treatment with ecteinascidins, PARPi, or their combinations at sublethal concentrations (0.5×IC50). Data represent mean ± SD from three independent experiments. Statistical significance was determined using ordinary one-way ANOVA with Dunnett's multiple comparisons test.

h. Quantification of γH2AX signal intensity (normalized to DMSO) following treatment conditions described in panel j. Data represent mean ± SD from three independent experiments. Statistical significance was determined using ordinary one-way ANOVA with Dunnett's multiple comparisons test.

Statistics: Exact P-values are indicated on the graphs; otherwise *P < 0.05, **P < 0.01, ***P < 0.001, ****P < 0.0001; ns, not significant. HSA scores > 0 indicate synergy.

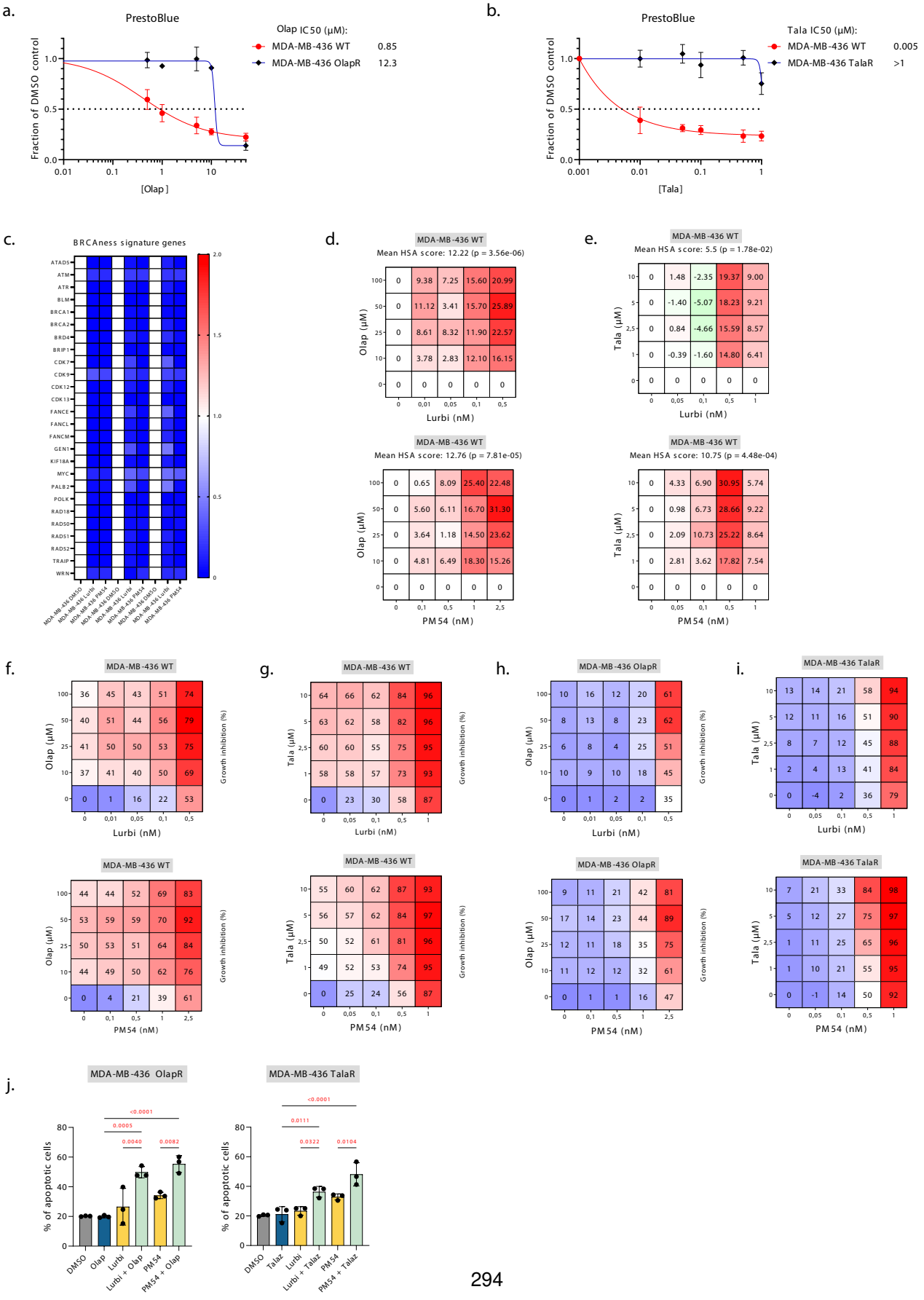
a.
PrestoBlue
Olap IC50 (μM):
MDA-MB-436 WT 0.85
MDA-MB-436 OlapR 12.3
Fraction of DMSO control
[Olap]
b.
PrestoBlue
Tala IC50 (μM):
MDA-MB-436 WT 0.005
MDA-MB-436 TalaR >1
Fraction of DMSO control
[Tala]
c.
BRCAness signature genes
ATADS
ATM
ATR
BLM
BRCA1
BRCA2
BRD4
BRIP1
CDK7
CDK9
CDK12
CDK13
FANCE
FANCL
FANCM
GEN1
KIF18A
MYC
PALB2
POLK
RAD18
RAD50
RAD51
RAD52
TRAIP
WRN
MDA-MB-436 DMSO
MDA-MB-436 Lurbi
MDA-MB-436 PM54
MDA-MB-436 DMSO
MDA-MB-436 Lurbi
MDA-MB-436 PM54
MDA-MB-436 DMSO
MDA-MB-436 Lurbi
MDA-MB-436 PM54
d.
MDA-MB-436 WT
Mean HSA score: 12.22 (p = 3.56e-06)
Olap (μM)
Lurbi (nM)
MDA-MB-436 WT
Mean HSA score: 12.76 (p = 7.81e-05)
Olap (μM)
PM54 (nM)
e.
MDA-MB-436 WT
Mean HSA score: 5.5 (p = 1.78e-02)
Tala (μM)
Lurbi (nM)
MDA-MB-436 WT
Mean HSA score: 10.75 (p = 4.48e-04)
Tala (μM)
PM54 (nM)
f.
MDA-MB-436 WT
Olap (μM)
Lurbi (nM)
Growth inhibition (%)
MDA-MB-436 WT
Olap (μM)
PM54 (nM)
Growth inhibition (%)
g.
MDA-MB-436 WT
Tala (μM)
Lurbi (nM)
Growth inhibition (%)
MDA-MB-436 WT
Tala (μM)
PM54 (nM)
Growth inhibition (%)
h.
MDA-MB-436 OlapR
Olap (μM)
Lurbi (nM)
Growth inhibition (%)
MDA-MB-436 OlapR
Olap (μM)
PM54 (nM)
Growth inhibition (%)
i.
MDA-MB-436 TalaR
Tala (μM)
Lurbi (nM)
Growth inhibition (%)
MDA-MB-436 TalaR
Tala (μM)
PM54 (nM)
Growth inhibition (%)
j.
MDA-MB-436 OlapR
% of apoptotic cells
DMSO
Olap
Lurbi
Lurbi + Olap
PM54
PM54 + Olap
MDA-MB-436 TalaR
% of apoptotic cells
DMSO
Talaz
Lurbi
Lurbi + Talaz
PM54
PM54 + Talaz

Supplementary Figure 8. Generation and characterization of PARP inhibitor-resistant models and response to ecteinascidins.

a. Dose-response curves (PrestoBlue) showing sensitivity of parental and OlapR MDA-MB-436 cells to olaparib.

b. Dose-response curves showing sensitivity of parental and TalaR cells to talazoparib.

c. Heatmap showing expression of BRCAness-associated genes following ecteinascidin treatment across parental and resistant models.

d-e. Heatmaps showing synergy scores (HSA model) for ecteinascidin-PARPi combinations in parental MDA-MB-436 cells.

h-i. Cell viability measurements following treatment with olaparib, ecteinascidins, cisplatin, or their combinations across parental or PARP inhibitor-resistant MDA-MB-436 cells.

j. Quantification of apoptotic cells measured by Annexin V staining following treatment with ecteinascidins, PARPi, or their combinations at sublethal concentrations (0.5×IC50). Data represent mean ± SD from three independent experiments. Statistical significance was determined using ordinary one-way ANOVA with Dunnett's multiple comparisons test.

Statistics: Exact P-values are indicated on the graphs.

General discussion

Over the last decades, the extensive characterization of transcriptional regulation has highlighted the central importance of oncogenic gene expression programs in cancer biology, thereby opening new therapeutic opportunities. In particular, the discovery of super-enhancers (SEs) and transcriptional condensates by the laboratory of Richard Young provided a mechanistic framework explaining how cancer cells sustain exceptionally high levels of oncogenic transcription, sometimes independently of classical driver mutations (Whyte *et al*, 2013). These findings established SE-associated oncogenic programs as central vulnerabilities of transcriptional addiction, a concept further emphasized by Bradner and colleagues in 2017 (Bradner *et al*, 2017). Consequently, considerable efforts have been devoted to developing molecules targeting factors that control SE activity, most notably inhibitors of BRD4 and CDK7, such as JQ1 and THZ1, which demonstrated strong preclinical efficacy in multiple cancer models (Lovén *et al*, 2013; Kwiatkowski *et al*, 2014). Despite these promising results, the clinical efficacy of such approaches has so far remained limited, in part because of suboptimal pharmacokinetic properties, toxicity, and therapeutic constraints. This highlights the need for alternative clinically active compounds capable of targeting SE-driven oncogenic transcription through mechanisms distinct from the classical enzymatic inhibition of transcriptional regulators.

In this context, disrupting transcription using DNA-binding molecules represents a comparatively understudied therapeutic strategy. This approach was pursued in our laboratory using synthetic ecteinascidins, a family of DNA-binding compounds that includes the clinically approved molecule lurbinectedin and the next-generation analogs PM14 and PM54. Although ecteinascidins have been studied for more than two decades and are known to inhibit transcription through DNA binding, interference with transcription factor accessibility, and perturbation of RNA polymerase II (RNAPII) (Calles *et al*, 2025), the precise molecular mechanisms by which they reshape transcriptional programs in cancer cells remained incompletely understood.

The first part of this thesis addressed this question in cutaneous melanoma, a cancer type characterized by strong cellular plasticity. This plasticity is mainly represented by the coexistence of melanocytic-like differentiated and mesenchymal-like undifferentiated states, the latter being associated with resistance to MAPK inhibitors and immunotherapies currently used as first-line treatments for patients with metastatic melanoma. The ability of melanoma cells to switch between these states relies on tightly regulated transcriptional programs, many of which are controlled by SE activity (Centeno *et al*, 2023). Melanoma therefore represents a

highly relevant model to investigate whether synthetic ecteinascidins can target transcriptional dependencies in heterogeneous and therapy-resistant tumors.

Using high-throughput transcriptional and genomic approaches, we demonstrated that lurbinectedin and its analogs can target distinct SE-driven transcriptional programs in melanoma cells with different phenotypic states, including mesenchymal-like cells resistant to MAPK inhibition. In contrast to classical SE disruptors, which generally act through enzymatic inhibition of transcriptional regulators and co-activators, we showed that ecteinascidins bind preferentially to highly active, CpG-rich promoters associated with open chromatin. This binding leads to rapid downregulation of key transcription factors and co-activators, resulting in their decreased recruitment to SEs and the subsequent inhibition of lineage-specific SE-dependent oncogenes. These include MITF and SOX10 in differentiated melanoma cells, and AXL and EGFR in undifferentiated melanoma states. Functionally, this transcriptional collapse induces melanoma cell apoptosis and leads to tumor regression and improved survival in mouse melanoma models.

Overall, this first part of the thesis provided preclinical evidence that synthetic ecteinascidins can act as DNA-binding disruptors of SE-driven oncogenic transcription. These findings suggest that this class of molecules may represent a promising therapeutic strategy for tumors with heterogeneous transcriptional landscapes, particularly those that fail to respond durably to conventional targeted therapies. Importantly, this work also contributed to the initiation of a phase I clinical trial evaluating PM54 in patients with advanced solid tumors, including melanoma (NCT05841563).

Beyond transcriptional addiction, targeting DNA repair has emerged as one of the most successful examples of exploiting cancer-specific vulnerabilities. In particular, PARP inhibitors have demonstrated the clinical relevance of synthetic lethality in tumors deficient in homologous recombination. This concept was established by two landmark studies published in 2005 by Farmer and colleagues and Bryant and colleagues, which showed that BRCA1/2-deficient cells are highly sensitive to PARP inhibition (Farmer *et al*, 2005; Bryant *et al*, 2005). Since then, several PARP inhibitors have entered clinical practice and have become major therapeutic agents in BRCA1/2-mutated breast, ovarian, pancreatic, and prostate cancers (Rose *et al*, 2020).

However, the clinical application of PARP inhibitors remains limited by the relatively low frequency of BRCA1/2 mutations across cancer patients. The concept of BRCAness, first introduced by Turner and colleagues in 2004, was proposed to describe genetic, epigenetic, or functional alterations in sporadic cancers that phenocopy BRCA1/2 deficiency and induce

homologous recombination deficiency (Turner *et al*, 2004). Since then, extensive efforts have been made to identify molecular determinants of BRCAness, both to predict response to PARP inhibitors and to pharmacologically induce HR deficiency in BRCA-proficient tumors. Several molecules have been shown in preclinical models to induce BRCAness-like states and synergize with PARP inhibition (Abbotts *et al*, 2022). However, most of these approaches have remained confined to preclinical studies and have not yet been translated into approved therapeutic combinations.

In the second part of this thesis, we demonstrated that synthetic ecteinascidins induce a functional BRCAness state by preferentially downregulating genes involved in homologous recombination and the Fanconi anemia pathway in multiple BRCA-proficient cancer models. Importantly, this effect was observed not only in breast and ovarian cancer models, where PARP inhibitors are already clinically used, but also in melanoma, small-cell lung cancer, and non-small-cell lung cancer models, where PARP inhibitors are not routinely used because these tumors are generally not characterized by canonical HR deficiency. These findings suggest that ecteinascidins may broaden the therapeutic relevance of BRCAness beyond classical BRCA-mutated or HRD-positive tumor contexts.

Mechanistically, we found that this HRD-like state is associated with the early downregulation of transcription elongation factors, including CDK9, CDK12, and BRD4. This leads to impaired transcription elongation and preferential repression of long genes. Notably, homologous recombination and Fanconi anemia genes are significantly longer than most genes in the genome, including housekeeping genes and genes involved in single-strand break repair. They are also enriched in intronic polyadenylation (IPA) sites, which may increase their vulnerability to elongation defects and premature transcription termination. Therefore, the sensitivity of HR and FA genes to ecteinascidins appears to be explained, at least in part, by their genomic architecture and dependence on efficient transcription elongation.

Beyond its relevance to BRCAness, this work also provides new mechanistic insight into how synthetic ecteinascidins inhibit transcription. Historically, the transcriptional effects of these compounds have been largely attributed to local DNA binding, blockade of transcription factor accessibility, and RNAPII stalling or degradation (Santamaría Nuñez *et al*, 2016). Our results suggest that transcription elongation defects and premature transcription termination are major contributors to the global transcriptional consequences of ecteinascidin treatment. Importantly, the absence of a direct correlation between binding intensity of biotinylated ecteinascidins and gene expression changes indicates that DNA binding alone is not sufficient to explain transcriptional repression. Instead, our findings support a model in which ecteinascidin binding

preferentially occurs at accessible regulatory regions, while downstream transcriptional repression depends on the disruption of elongation programs and gene-specific vulnerabilities. This mechanism is consistent with previous studies showing that transcription elongation defects can induce BRCAness-like states (Dubbury *et al*, 2018). In particular, selective inhibitors of transcription elongation regulators, such as THZ531 targeting CDK12 and JQ1 targeting BRD4, have been shown to repress HR gene expression and sensitize cancer cells to PARP inhibition (Johnson *et al*, 2016; Sun *et al*, 2018; Krajewska *et al*, 2019). Compared with these approaches, our work identifies clinically approved or clinically advanced DNA-binding agents, namely lurbinectedin and PM54, as compounds capable of inducing a similar transcription elongation-dependent BRCAness state. This supports the idea that DNA-binding transcriptional inhibitors may represent a clinically advantageous alternative to classical enzymatic inhibitors of transcriptional regulators.

At the functional level, synthetic ecteinascidins synergize with PARP inhibition to promote the accumulation of DNA damage at transcriptionally active genomic regions, including sites bound by the drugs. These results suggest that PARP inhibition exacerbates ecteinascidin-induced DNA damage, leading to persistent DNA lesions, increased replication stress, and enhanced apoptosis compared with either treatment alone. Importantly, these effects were not reproduced to the same extent with cisplatin, which did not induce HR gene repression and showed only minimal synergy with PARP inhibition. This comparison supports the idea that DNA binding and DNA damage induction alone are not sufficient to drive strong PARP inhibitor sensitization. Instead, the transcriptional impact of ecteinascidins, particularly their ability to induce a functional HRD-like state, appears to be a key determinant of their synergy with PARP inhibitors.

This distinction is important therapeutically because it suggests that ecteinascidins should not be considered only as DNA-damaging agents. Rather, their ability to simultaneously generate DNA lesions and impair the transcriptional maintenance of homologous recombination may create a particularly favorable context for PARP inhibitor sensitization. This dual mechanism may help explain why ecteinascidins cooperate with PARP inhibitors more efficiently than other DNA-damaging agents that do not induce a comparable HRD-like transcriptional state.

In addition to the limited frequency of BRCA1/2 mutations in cancer patients, the emergence of therapeutic resistance represents another major challenge for the long-term efficacy of PARP inhibitors. Clinical evidence from patients who initially responded to PARP inhibitors but later relapsed has shown that resistance is frequently associated with restoration of HR activity, either through reversion mutations or through activation of compensatory repair pathways (Dias *et al*,

2021). In this context, we generated olaparib- and talazoparib-resistant BRCA1-mutated cell lines and observed increased HR activity compared with parental cells, consistent with restoration of HR proficiency. Interestingly, ecteinascidin treatment re-induced HR deficiency in these resistant cells and restored sensitivity to olaparib and talazoparib. These findings suggest that ecteinascidins may not only expand the use of PARP inhibitors to BRCA-proficient tumors, but could also represent a strategy to overcome PARP inhibitor resistance driven by HR restoration.

Despite these promising findings, several important limitations and unresolved questions remain. First, although ecteinascidin-induced HR gene repression and PARP inhibitor synergy were demonstrated in multiple cancer cell models, additional validation in more physiological *in vivo* systems is necessary. Cell culture models are powerful for mechanistic dissection, but they do not fully recapitulate tumor architecture, drug pharmacokinetics, stromal interactions, immune components, or normal tissue toxicity. Ongoing work in collaboration with PharmaMar therefore aims to evaluate these findings in ovarian cancer patient-derived xenograft models. These experiments will determine whether ecteinascidin treatment can induce HR repression *in vivo* and whether the combination with PARP inhibition improves therapeutic response.

Second, the relative contribution of direct DNA damage, transcription elongation defects, and HR repression to the observed synergy with PARP inhibitors remains to be fully dissected. Our data support a model in which DNA damage induction alone is not sufficient to explain the synergy, as illustrated by the comparison with cisplatin. However, ecteinascidins simultaneously induce DNA lesions, perturb transcription, and repress DNA repair gene expression. These mechanisms are likely interconnected rather than fully separable. Future experiments will therefore be needed to determine the extent to which HR gene repression is required for PARP inhibitor sensitization, and whether this effect can be uncoupled from ecteinascidin-induced DNA damage.

Third, biomarkers capable of predicting response to ecteinascidin-PARP inhibitor combinations remain to be defined. Several possibilities emerge from this work, including basal transcriptional state, SE activity, chromatin accessibility, expression of elongation factors, HR/FA gene repression, or functional HRD markers such as RAD51 foci formation. However, it remains unclear which of these parameters would be most predictive in a clinical setting. Future studies should therefore aim to identify robust biomarkers that can stratify patients most likely to benefit from these combinations.

Fourth, the optimal treatment schedule and therapeutic window remain open questions. Because ecteinascidins can affect transcription and DNA repair in proliferating cells, combination with

PARP inhibitors may increase toxicity in normal tissues. Determining whether sequential or concomitant treatment provides the best balance between efficacy and toxicity will be essential. In this regard, the kinetics of HR gene repression, DNA damage accumulation, and recovery after drug withdrawal will be important parameters to define. These preclinical validations may ultimately support the development of clinical trials combining ecteinascidins with PARP inhibitors. Early-phase clinical studies in ovarian cancer patients have already suggested that the combination of lurbinectedin and olaparib can improve progression-free survival (Poveda *et al*, 2021, 2022). However, these studies were performed in relatively small patient cohorts and were not necessarily stratified according to HR status. Therefore, future clinical trials will need to incorporate appropriate biomarkers to evaluate whether HR gene repression, transcription elongation defects, or other indicators of functional BRCAness can predict response to the combination. In parallel, careful assessment of toxicity in normal tissues will be essential, particularly because both ecteinascidins and PARP inhibitors can potentially affect proliferative and DNA repair-proficient cells.

Fifth, the molecular determinants of ecteinascidin binding specificity remain incompletely understood. Our data indicates that these compounds preferentially bind active, accessible, CpG-rich regulatory regions, but the precise DNA or chromatin features that drive this selectivity remain to be clarified. One hypothesis currently being explored in the laboratory is that ecteinascidins may preferentially bind specific secondary DNA structures, such as G-quadruplexes. These structures are enriched at promoter regions and have been implicated in the regulation of oncogenic transcription in cancer cells. Determining whether G-quadruplexes contribute to ecteinascidin recruitment could provide an additional mechanistic explanation for their preferential activity at transcriptionally active regulatory elements.

Finaly, beyond PARP inhibitor combinations, another important direction concerns the potential interaction between ecteinascidins and anti-tumor immunity. Several studies have shown that lurbinectedin can modulate the tumor microenvironment and enhance the activity of immune checkpoint inhibitors in preclinical models (Belgiovine *et al*, 2017; Chakraborty *et al*, 2024). In addition, lurbinectedin has recently shown promising clinical activity in combination with immune checkpoint blockade in small-cell lung cancer (Paz-Ares *et al*, 2025). In our laboratory, we are currently investigating whether ecteinascidins can also improve the response to immune checkpoint inhibitors in melanoma. These studies use immunocompetent mouse melanoma models, together with single-cell and spatial transcriptomic approaches, to dissect how ecteinascidin treatment reshapes tumor and immune cell states. This work may help determine

whether transcriptional reprogramming induced by ecteinascidins can increase tumor immunogenicity or improve sensitivity to immunotherapy.

Overall, this thesis identifies synthetic ecteinascidins as potent DNA-binding transcriptional inhibitors capable of targeting SE-driven oncogenic programs and inducing a functional BRCAness state through perturbation of transcription elongation. This dual mechanism opens new perspectives for targeting tumors with heterogeneous transcriptional landscapes, expanding the use of PARP inhibitors beyond canonical HRD-positive cancers, and overcoming resistance driven by restoration of homologous recombination. More broadly, this work highlights DNA-binding transcriptional inhibitors as promising tools to simultaneously target oncogenic transcription and genome maintenance in cancer.

Annexes

Preface to annexed Articles 3, 4, and 5:

In addition to my co-first author studies, I contributed to several collaborative projects within the laboratory that resulted in additional co-author publications. Shortly after publication of our *Nature Communications* article on synthetic ecteinascidins and super-enhancers, the editorial team of médecine/sciences invited us to write a short review article in French highlighting the major findings of this work. This publication constitutes the only article in this thesis written entirely in French. My contribution mainly involved figure preparation and revision of the manuscript text.

In another melanoma-focused study led by Pietro Berico, a former PhD student in our laboratory currently pursuing a postdoctoral fellowship at New York University, our group identified BAHCC1 as a super-enhancer-associated regulator overexpressed in metastatic melanoma that plays an important role in cell proliferation and DNA repair. Inhibition of BAHCC1 impaired melanoma cell proliferation, delayed DNA repair, and cooperated with PARP inhibitors to induce melanoma cell death. This work was published in *Cell Reports* in 2023. I contributed to this study during the peer-review process by performing experiments investigating the synergy between BAHCC1 depletion and PARP inhibition.

Finally, in a third study closely related to my work on synthetic ecteinascidins, and on which I worked extensively during my Master 2 internship, we developed *in vitro* models of resistance to ecteinascidins and identified the drug efflux transporter ABCB1 as a major resistance mechanism associated with focal amplification and increased AP-1/TEAD activity. My contribution included the direct identification of ABCB1 upregulation by RNA-sequencing, validation at the protein level by western blotting, and functional siRNA-mediated knockdown experiments demonstrating reversal of resistance to ecteinascidins. This project constituted the major component of my Master 2 internship and later evolved into a longer-term study pursued by Clara Maréchal, a PhD student, under the supervision of Max Cigrang. The manuscript presented below, on which I am listed as second co-author, contains most of the *in vitro* findings and will be submitted upon completion of the ongoing *in vivo* validation experiments investigating the role of ABCB1 in ecteinascidin resistance in more physiological models.

Les ecteinascidines

Quand la pharmacologie marine cible la dépendance transcriptionnelle du cancer

Max Cigrang, Jolian Obid, Frédéric Coin

Institut de génétique et de biologie moléculaire et cellulaire, CNRS UMR7104, Inserm U1258, Université de Strasbourg, Illkirch, France.
cigrangm@igbmc.fr
obidj@igbmc.fr
fredr@igbmc.fr

› La plasticité phénotypique des cellules cancéreuses leur permet d'adopter divers états cellulaires afin de s'adapter à l'environnement et de développer une résistance aux thérapies anticancéreuses. Ce phénomène est particulièrement prévalent dans le mélanome cutané, un cancer très agressif et invasif. Malgré des avancées thérapeutiques majeures, notamment avec les thérapies ciblées (inhibiteurs de la voie MAPK) et les immunothérapies (inhibiteurs de points de contrôle immunitaire), la mortalité reste forte. En effet, plus de 50 % des mélanomes à un stade avancé développent des résistances aux traitements existants [1].

L'évasion thérapeutique des cellules tumorales repose sur leur capacité à osciller entre un état différencié, caractérisé par une prolifération accrue, et un état mésenchymateux ou indifférencié, leur conférant une forte capacité invasive et une résistance aux traitements [2]. Ces transitions phénotypiques sont orchestrées par des remaniements épigénétiques, où chaque état cellulaire est associé à l'activation de programmes transcriptionnels spécifiques [3]. Ainsi, les cellules différenciées du mélanome dépendent fortement de la surexpression d'oncogènes tels que *MITF (Microphtalmia-associated transcription factor)* et *SOX10 (SRY-box transcription factor 10)*, tandis que les cellules indifférenciées expriment préférentiellement *AXL*, qui code un récepteur à activité tyrosine kinase impliqué dans leur survie et leur agressivité. Actuellement, aucune stratégie thérapeutique efficace ne permet de cibler sélectivement les cellules cancéreuses indifférenciées. La « dépendance transcriptionnelle » désigne le concept selon lequel la survie des cellules cancéreuses repose sur la reprogrammation transcriptionnelle et l'expression constitutive de certains oncogènes [4]. Un des mécanismes impliqués est l'acquisition aberrante de super-amplificateurs (en anglais, *super-enhancers*). Ces structures chromatiniennes concentrent des facteurs transcriptionnels tels que CDK7, BRD4 et le complexe Médiateur, formant ainsi des condensats nucléaires à séparation de phase, qui favorisent l'expression forte d'oncogènes comme *MITF*, *SOX10* et *AXL* dans les cellules de mélanome [5, 6] (*Figure 1A*).

Les ecteinascidines synthétiques : une nouvelle classe d'inhibiteurs transcriptionnels ?

La dépendance des cellules cancéreuses à la machinerie transcriptionnelle a motivé le développement d'inhibiteurs qui ciblent des facteurs de transcription clés comme CDK7 et BRD4, mais dont l'efficacité thérapeutique est limitée en raison de leurs profils pharmacocinétiques défavorables et de leur courte durée d'action [7, 8]. Dans ce contexte, un intérêt croissant s'est porté sur les ecteinascidines, une famille de composés naturels dérivés des tuniciers marins[1], dont les propriétés anticancéreuses se révèlent particulièrement prometteuses. Les ecteinascidines synthétiques, conçues pour reproduire et améliorer les effets biologiques de ces composés naturels, offrent une sélectivité accrue et des propriétés pharmacocinétiques optimisées. Parmi elles, la lurbinectédine, dérivée de la trabectédine, a reçu l'approbation de la *Food and Drug Administration* américaine en 2020 pour le traitement du cancer du poumon à petites cellules en rechute, ce qui a constitué la première avancée thérapeutique majeure pour cette maladie depuis quinze ans [9]. Cependant, bien que la lurbinectédine soit identifiée comme un agent interagissant avec l'ADN [10, 11], son mode d'action précis et ses effets transcriptionnels restaient mal connus, notamment concernant son impact sur les mélanomes.

Évaluation de l'efficacité des ecteinascidines contre le mélanome

Nous avons créé des ecteinascidines synthétiques de nouvelle génération, dérivées de la lurbinectédine (ecubectédine et PM54), et avons évalué l'effet de ces composés sur des cellules de mélanome en raison de leur forte addiction transcriptionnelle et de leur propension à la résistance thérapeutique. Nous avons constaté que les ecteinascidines synthétiques exercent, à très faibles concentrations (de l'ordre du nanomolaire), une forte cytotoxicité sur toute une gamme de cellules de mélanomes (dérivées de patients), quel que soit leur statut mutationnel ou leur état phénotypique, différencié ou indifférencié. Ces ecteinascidines se démarquent ainsi des inhibiteurs de MAPK (*mitogen-activated protein kinase*) ou des médicaments de l'immunothérapie. Les traitements par

[1] Petits animaux marins invertébrés dont le corps est protégé par une enveloppe cellulosique appelée tunique.

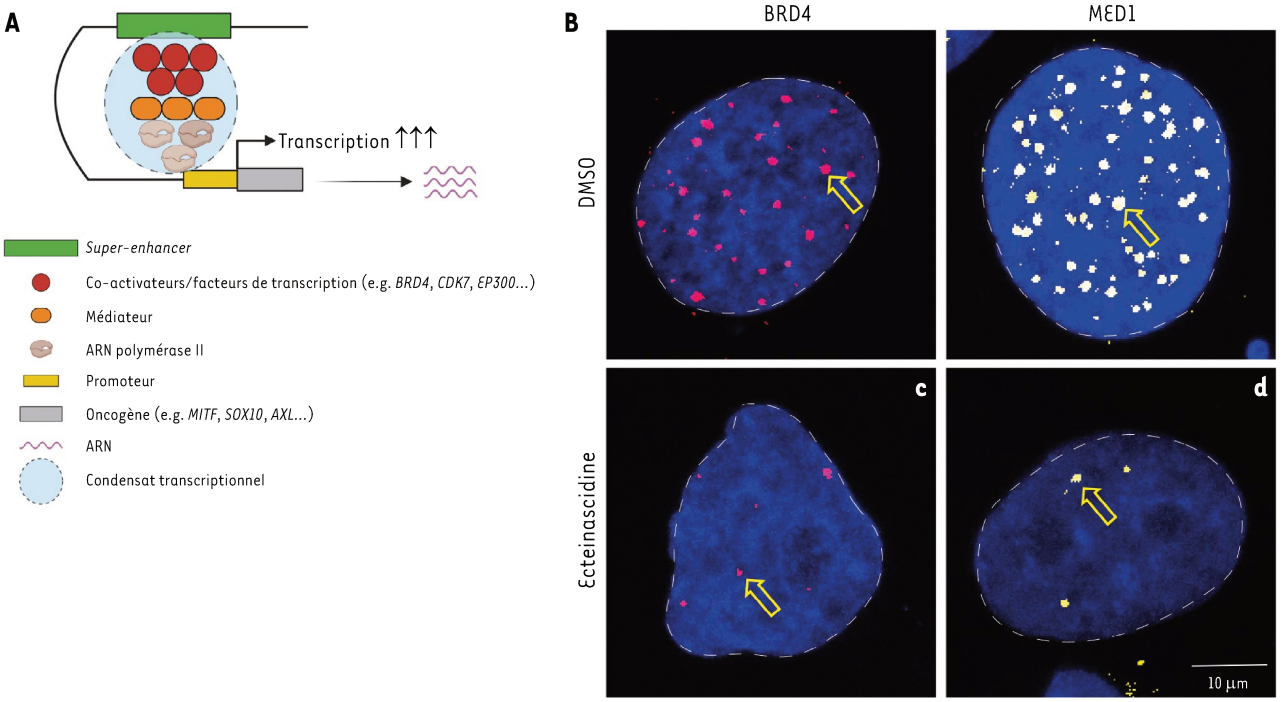

Figure 1. Perturbation des condensats transcriptionnels associés aux super-amplificateurs par les ecteinascidines synthétiques. **A.** Schéma représentant l'organisation d'un super-amplificateur (*super-enhancer*). Les régulateurs transcriptionnels (par exemple, BRD4, CDK7, EP300), le complexe Médiateur, et l'ARN polymérase II s'accumulent sur le super-amplificateur, formant un condensat transcriptionnel à séparation de phase, qui interagit avec le promoteur d'un oncogène cible et stimule fortement son expression. Figure créée avec le logiciel BioRender. **B.** Images de microscopie confocale après marquage par immunofluorescence, montrant le coactivateur BRD4 (en rouge) et la protéine MED1 du complexe Médiateur (en orange) dans des cellules de mélanome traitées avec du DMSO (diméthylsulfoxyde, témoin) ou avec des ecteinascidines synthétiques (lurbinectédine, écubectédine, PM54). Le traitement par les ecteinascidines synthétiques entraîne une inhibition de l'expression de *BRD4* et *MED1*, conduisant à la dispersion des condensats transcriptionnels associés aux super-amplificateurs et à l'inactivation des oncogènes qui en dépendent.

ecteinascidines synthétiques conduisent à la production de cassures double brin de l'ADN et à une forte apoptose. Leur effet cytotoxique a été confirmé *in vivo* sur des modèles murins de xénogreffes de mélanome : l'administration d'ecteinascidines synthétiques à ces souris par voie intraveineuse pendant trois semaines consécutives a entraîné une franche régression de la croissance tumorale.

Effets transcriptionnels des ecteinascidines

Afin de caractériser le mécanisme d'action des ecteinascidines synthétiques, nous avons effectué des analyses transcriptomiques par séquençage nucléotidique des ARN messagers, qui ont permis de constater que de nombreux gènes dépendants des super-amplificateurs étaient fortement sous-exprimés après traitement. Les ecteinascidines synthétiques semblaient surtout affecter l'expression des gènes surexprimés dans un type cellulaire donné : par exemple, l'expression des gènes *MITF* et *SOX10* était spécifiquement inhibée dans les cellules tumorales différenciées, alors que celle de *AXL* était uniquement inhibée dans les cellules tumorales indifférenciées. Cependant, il convient de souligner que seule l'expression d'un petit nombre de gènes était affectée par les ecteinascidines synthétiques dans chacun de ces deux types de cellules. Ces gènes se sont avérés coder essentiellement des protéines impliquées dans la régulation transcriptionnelle (*e.g. BRD4*, *CDK7*, *CDK12*, *CDK13*, *EP300*, *CBP*) ainsi que des protéines du complexe Médiateur (*e.g. CDK8*, *MED1* et *MED13*), qui sont impliquées dans le maintien des super-amplificateurs. La diminution de l'expression de ces gènes, qui se produit rapidement après le traitement par les ecteinascidines synthétiques, est suivie de celle des gènes dont la transcription dépend des super-amplificateurs.

Afin de mieux comprendre les effets transcriptionnels complexes des ecteinascidines synthétiques, nous en avons synthétisé une forme biotinylée afin de cartographier leurs sites de liaisons sur l'ADN par la méthode de Chem-Map (*chemical mapping*) [12]. Étonnamment, nous avons constaté que les ecteinascidines synthétiques ne se lient pas à tout le génome, contrairement à d'autres agents chimiothérapiques comme les

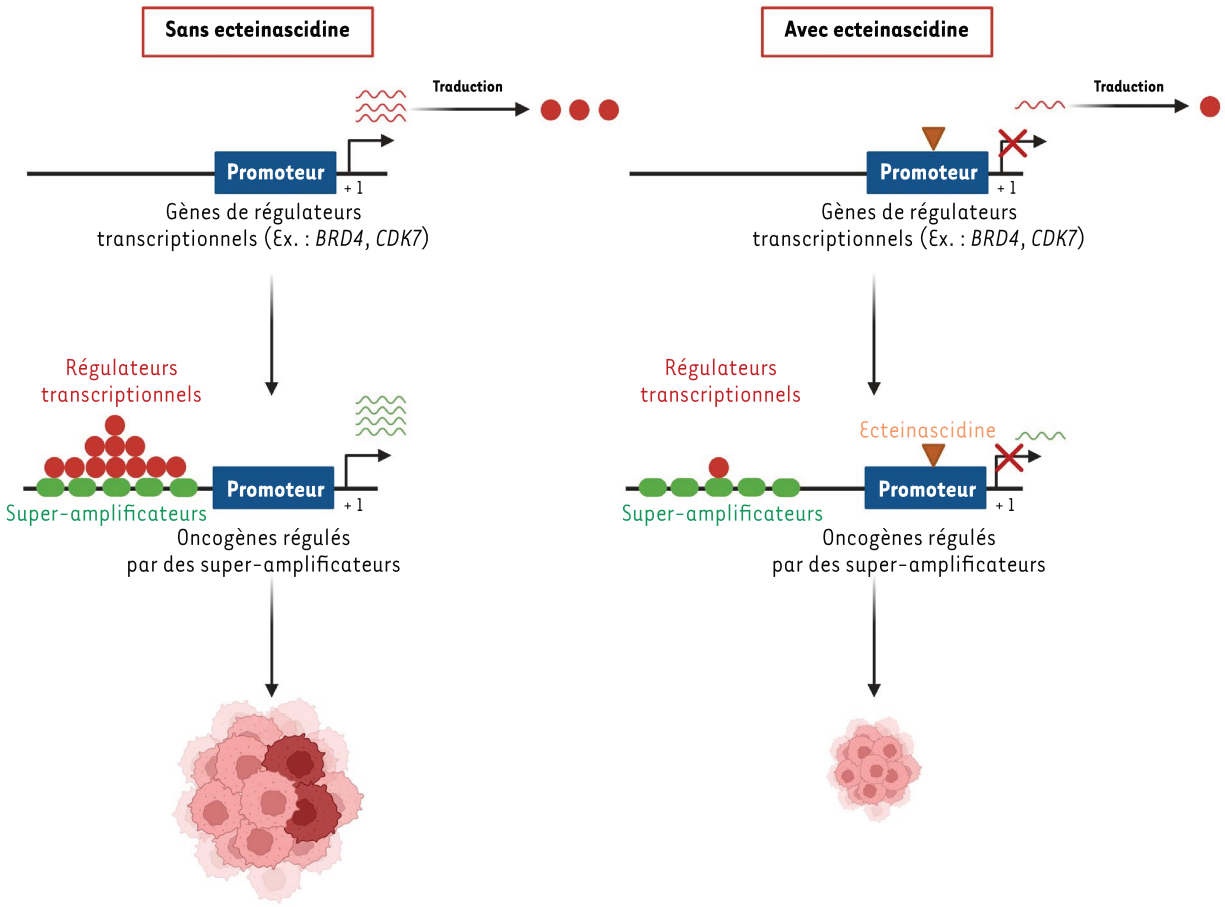

Figure 2. Mécanisme d'inhibition transcriptionnelle induite par les ecteinascidines synthétiques. En conditions normales, les régulateurs transcriptionnels s'accumulent sur les super-amplificateurs sous forme de condensats favorisant l'expression des oncogènes et la croissance tumorale. Après un traitement par une ecteinascidine synthétique, celle-ci se lie aux promoteurs des gènes codant des régulateurs transcriptionnels et inhibe ainsi leur transcription. Cette inhibition empêche le recrutement de ces régulateurs transcriptionnels aux super-amplificateurs et la formation des condensats transcriptionnels, entraînant ainsi la répression des oncogènes dépendant des super-amplificateurs et l'arrêt de la croissance tumorale. Figure créée avec le logiciel BioRender.

dérivés du platine, mais semblent se lier spécifiquement à des régions activement transcrites riches en îlots CpG, comme les super-amplificateurs ou les promoteurs d'oncogènes. De nouveau, nous avons observé une spécificité d'action des ecteinascidines synthétiques, qui se lient par exemple au promoteur et au super-amplificateur de l'oncogène *MITF* uniquement dans les cellules différenciées du mélanome, et non pas dans les cellules indifférenciées, qui n'expriment pas *MITF*. Cependant, les ecteinascidines synthétiques se lient systématiquement à des promoteurs de gènes codant des facteurs de transcription ou des coactivateurs exprimés ubiquitairement, pour inhiber leur transcription. Nous avons montré que la perte d'expression des gènes régulateurs de la transcription comme *BRD4* perturbe considérablement les condensats transcriptionnels (*Figure 1B*), et conduit en conséquence à l'inactivation des super-amplificateurs. Dans leur ensemble, ces résultats suggèrent que les ecteinascidines synthétiques provoquent initialement une inactivation des promoteurs contrôlant l'expression des gènes codant des facteurs de transcription et des coactivateurs, ce qui perturbe les condensats transcriptionnels et entraîne l'inactivation secondaire des promoteurs des oncogènes dépendant des super-amplificateurs, de concert avec la liaison directe des ecteinascidines synthétiques à ces oncogènes (*Figure 2*).

Vers une nouvelle classe d'inhibiteurs universels des super-amplificateurs ?

Ces mécanismes ont été validés dans d'autres modèles tumoraux, notamment dans le cancer du poumon à petites cellules, suggérant que les ecteinascidines synthétiques pourraient constituer des

inhibiteurs universels des super-amplificateurs, indépendamment de la nature phénotypique des cellules cancéreuses. Il importe de noter que les cellules non tumorales (fibroblastes, kératinocytes) sont beaucoup moins sensibles aux ecteinascidines synthétiques, probablement en raison de leur faible dépendance aux super-amplificateurs.

Nos travaux ont mis en lumière le mode d'action des ecteinascidines synthétiques dans l'inhibition de la transcription oncogénique, ouvrant la voie à une optimisation chimique de ces composés à visée thérapeutique [13]. Sur la base de ces résultats, des essais cliniques de phase I ont débuté pour évaluer leur efficacité contre divers cancers solides à des stades avancés, y compris les mélanomes (NCT05841563, EudraCT 2022-002031-65). ◊

Ecteinascidins: When marine pharmacology targets the transcriptional dependency of cancer

LIENS D'INTÉRÊT

Les auteurs déclarent n'avoir aucun lien d'intérêt concernant les données publiées dans cet article.

RÉFÉRENCES

1. Schadendorf D, Akkooi ACJ van, Berking C, *et al.* Melanoma. *Lancet* 2018 ; 392 : 971-84.
2. Kozar I, Margue C, Rothengatter S, *et al.* Many ways to resistance: How melanoma cells evade targeted therapies. *Biochim Biophys Acta Rev Cancer* 2019 ; 1871 : 313-22.
3. Wouters J, Kalender-Atak Z, Minnoye L, *et al.* Robust gene expression programs underlie recurrent cell states and phenotype switching in melanoma. *Nat Cell Biol* 2020 ; 22 : 986-98.
4. Bradner JE, Hnisz D, Young RA. Transcriptional addiction in cancer. *Cell* 2017 ; 168 : 629-43.
5. Berico P, Nogaret M, Cigrang M, *et al.* Super-enhancer-driven expression of *BAHCC1* promotes melanoma cell proliferation and genome stability. *Cell Rep* 2023 ; 42 : 113363.
6. Eliades P, Abraham BJ, Ji Z, *et al.* High *MITF* expression is associated with super-enhancers and suppressed by CDK7 inhibition in melanoma. *J Invest Dermatol* 2018 ; 138 : 1582-90.
7. Berico P, Cigrang M, Davidson G, *et al.* CDK7 and MITF repress a transcription program involved in survival and drug tolerance in melanoma. *EMBO Rep* 2021 ; 22 : e51683.
8. Donati B, Lorenzini E, Ciarrocchi A. BRD4 and cancer: going beyond transcriptional regulation. *Mol Cancer* 2018 ; 17 : 164.
9. Trigo J, Subbiah V, Besse B, *et al.* Lurbinectedin as second-line treatment for patients with small-cell lung cancer: a single-arm, open-label, phase 2 basket trial. *Lancet Oncol* 2020 ; 21 : 645-54.
10. Costanzo F, Martínez Diez M, Santamaría Nuñez G, *et al.* Promoters of ASCL1- and NEUROD1-dependent genes are specific targets of lurbinectedin in SCLC cells. *EMBO Mol Med* 2022 ; 14 : e14841.
11. Santamaría Nuñez G, Robles CMG, Giraudon C, *et al.* Lurbinectedin specifically triggers the degradation of phosphorylated RNA polymerase II and the formation of DNA breaks in cancer cells. *Mol Cancer Ther* 2016 ; 15 : 2399-412.
12. Yu Z, Spiegel J, Melidis L, et al. Chem-map profiles drug binding to chromatin in cells. *Nat Biotechnol* 2023 ; 41 : 1265-71.
13. Cigrang M, Obid J, Nogaret M, *et al.* Pan-inhibition of super-enhancer-driven oncogenic transcription by next-generation synthetic ecteinascidins yields potent anti-cancer activity. *Nat Commun* 2025 ; 16 : 512.

Cell Reports

Article

Super-enhancer-driven expression of BAHCC1 promotes melanoma cell proliferation and genome stability

Graphical abstract

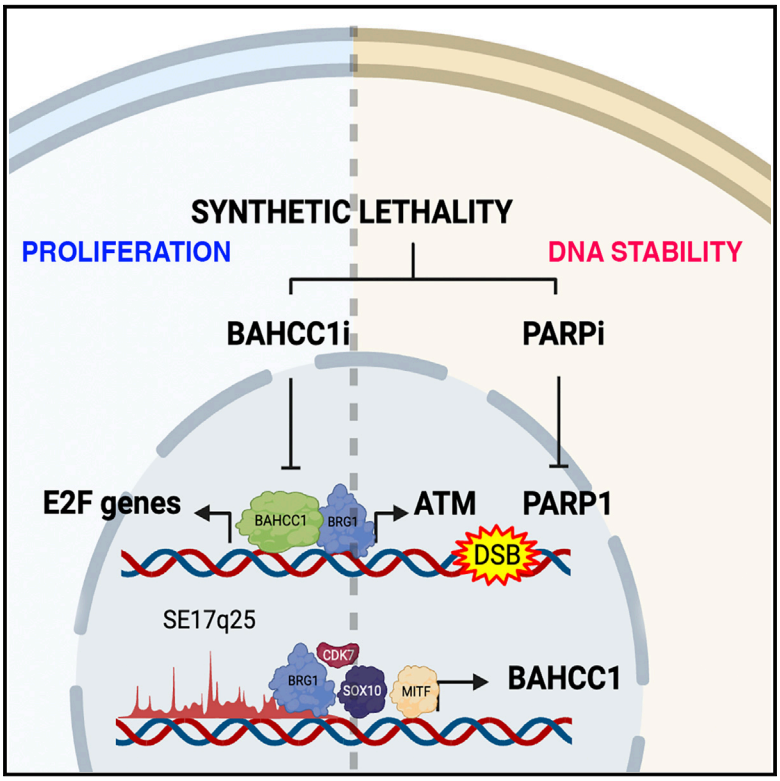

Highlights

- BAHCC1 is highly expressed in melanoma cells
- BAHCC1 regulates expression of DNA-repair and E2F/KLF-dependent cell-cycle genes
- BAHCC1 depletion impairs tumor engraftment, growth, and dissemination
- BAHCC1 deficiency cooperates with PARP inhibition to induce melanoma cell death

Authors

Pietro Berico, Maguelone Nogaret, Max Cigrang, ..., Eva Hernando, Irwin Davidson, Frédéric Coin

Correspondence

irwin@igbmc.fr (I.D.),
fredr@igbmc.fr (F.C.)

In brief

Berico et al. identify a MITF/SOX10/TFIIH-dependent super-enhancer promoting the expression of BAHCC1 in a broad panel of melanoma cells. Integrative genomics analyses reveal that BAHCC1 is a transcriptional regulator controlling expression of E2F/KLF-dependent cell-cycle and DNA-repair genes in melanoma.

Berico et al., 2023, Cell Reports *42*, 113363
November 28, 2023 © 2023 The Authors.
https://doi.org/10.1016/j.celrep.2023.113363

Cell Reports

CellPress
OPEN ACCESS

Article

Super-enhancer-driven expression of BAHCC1 promotes melanoma cell proliferation and genome stability

Pietro Berico,[1,2,3,4,7,8] Maguelone Nogaret,[1,2,3,4] Max Cigrang,[1,2,3,4] Antonin Lallement,[1,2,3,4] Fatemeh Vand-Rajabpour,[7,8] Amanda Flores-Yanke,[7,8] Giovanni Gambi,[1,2,3,4] Guillaume Davidson,[1,2,3,4] Leane Seno,[1,2,3,4] Julian Obid,[1,2,3,4] Bujamin H. Vokshi,[1,2,3,4] Stephanie Le Gras,[1,2,3,4] Gabrielle Mengus,[1,2,3,4] Tao Ye,[1,2,3,4] Carlos Fernandez Cordero,[7,8] Mélanie Dalmasso,[5,6] Emmanuel Compe,[1,2,3,4] Corine Bertolotto,[5,6] Eva Hernando,[7,8] Irwin Davidson,[1,2,3,4,*] and Frédéric Coin[1,2,3,4,9,*]

[1]Institut de Génétique et de Biologie Moléculaire et Cellulaire, Equipe Labéllisée, "Ligue contre le Cancer 2022", BP 163, 67404 Illkirch Cedex, C.U. Strasbourg, France
[2]Centre National de la Recherche Scientifique, UMR7104, 67404 Illkirch, France
[3]Institut National de la Santé et de la Recherche Médicale, U1258, 67404 Illkirch, France
[4]Université de Strasbourg, 67404 Illkirch, France
[5]Université Côte d'Azur, Nice, France
[6]INSERM, Biology and Pathologies of Melanocytes, Equipe labellisée "Ligue contre le Cancer 2020" and Equipe labellisée "Fondation ARC 2022", Centre Méditerranéen de Médecine Moléculaire, Nice, France
[7]Department of Pathology, New York University Grossman School of Medicine, New York, NY 10016, USA
[8]Interdisciplinary Melanoma Cooperative Group, Perlmutter Cancer Center, NYU Langone Health, New York, NY 10016, USA
[9]Lead contact
*Correspondence: irwin@igbmc.fr (I.D.), fredr@igbmc.fr (F.C.)
https://doi.org/10.1016/j.celrep.2023.113363

SUMMARY

Super-enhancers (SEs) are stretches of enhancers ensuring a high level of expression of key genes associated with cell function. The identification of cancer-specific SE-driven genes is a powerful means for the development of innovative therapeutic strategies. Here, we identify a MITF/SOX10/TFIIH-dependent SE promoting the expression of BAHCC1 in a broad panel of melanoma cells. BAHCC1 is highly expressed in metastatic melanoma and is required for tumor engraftment, growth, and dissemination. Integrative genomics analyses reveal that BAHCC1 is a transcriptional regulator controlling expression of E2F/KLF-dependent cell-cycle and DNA-repair genes. BAHCC1 associates with BRG1-containing remodeling complexes at the promoters of these genes. BAHCC1 silencing leads to decreased cell proliferation and delayed DNA repair. Consequently, BAHCC1 deficiency cooperates with PARP inhibition to induce melanoma cell death. Our study identifies BAHCC1 as an SE-driven gene expressed in melanoma and demonstrates how its inhibition can be exploited as a therapeutic target.

INTRODUCTION

Transcriptional deregulation represents a key mechanism for cancer initiation and progression.[1] A combination of somatic mutations and microenvironmental cues leads to the overexpression of transcription regulators promoting aberrant gene expression programs, ultimately resulting in cancer hallmarks.[2] A key mechanism promoting tumor-specific gene expression programs is the aberrant activation of super-enhancers (SEs), broad gene regulatory elements highly dependent on the activity of general co-activators compared to canonical enhancers.[3] Consequently, transcriptional inhibitors targeting co-activators such as BRD4 (bromodomain-containing protein 4) and the cyclin-dependent kinase 7 (CDK7) of the basal transcription factor TFIIH are widely used to disrupt SE-associated genes in cancer cells.[4,5] However, the presence of SE-associated genes in healthy cells, together with the poor pharmacokinetics and efficacy of transcriptional inhibitors in human clinical trials, underscores the need for alternative strategies[6,7] such as the identification of cancer-specific SE-driven genes.[8]

Cutaneous melanoma remains the most lethal skin cancer, with an incidence that has continued to increase over the past few decades.[9,10] Despite the significant improvement in 5-year overall survival provided by therapies targeting mitogen-activated protein kinase (MAPK) including vemurafenib and trametinib (BRAF and MEK inhibitors, respectively),[11,12] or by immune checkpoint inhibitors anti-PD1 and anti-CTLA4,[13] many patients still develop resistance, in part due to melanoma phenotypic plasticity, a dynamic and non-mutational mechanism of adaptation to microenvironmental changes and drug exposure.[14,15] Plasticity results in an important intratumor heterogeneity involving multiple cell states with distinct transcriptional

This is an open access article under the CC BY-NC-ND license (http://creativecommons.org/licenses/by-nc-nd/4.0/).

signatures and different proliferative, invasive, and drug-resistance phenotypes. Melanoma phenotype plasticity depends in part on two opposing gene expression programs, governed by the transcription factors MITF (microphthalmia-associated transcription factor) and SOX10 (SRY-box transcription factor 10) or AP-1 (activating protein 1) and TEAD (transcriptional enhancer associate domain), respectively, whose activities modulate melanoma cell-state transition.[16–19] Other forms of melanoma include uveal melanoma, the most common primary intraocular tumor in adults that is intrinsically different from cutaneous melanoma. In uveal melanoma, the most frequent driver mutations are those involving the heterotrimeric G-protein subunits GNAQ or GNA11.[20,21] Despite successful treatment of primary uveal melanoma, 50% of patients will develop metastases that are highly refractory to existing treatments.[22] Therefore, there is an urgent need to better understand the molecular mechanisms involved in these two cancers in order to develop efficient treatments.

Here, by using the global molecular features of SEs (enrichment in TFIIH/CDK7, BRG1, and H3K27ac) as well as those specific to melanoma cells (enrichment in MITF and SOX10), we characterized the SE landscapes of patient-derived short-term cutaneous melanoma cultures. Integrative epigenomic analyses revealed a melanoma-specific SE regulating the expression of the bromo-adjacent homology and coiled-coil domain-containing 1 (BAHCC1) protein in a broad panel of cutaneous, but also uveal, melanoma cells. BAHCC1 drives cutaneous and uveal melanoma cell proliferation and is required for tumor growth and engraftment of cutaneous melanoma cells *in vivo*. Loss-of-function and genomic profiling experiments show that BAHCC1 is a transcriptional regulator controlling the expression of a subset of E2F (E2 factor)/KLF (Krüppel-like factor)-dependent cell-cycle and DNA-repair genes in melanoma cells. BAHCC1 associates with BRG1 (BRM/SWI2-related gene 1)-containing remodeling complexes at the promoters of these genes. Consistent with the involvement of BAHCC1 in the regulation of DNA-repair genes, including the crucial cell-cycle kinase ATM (ataxia telangiectasia mutated), BAHCC1 depletion delays DNA repair and cooperates with PARP (poly ADP-ribose polymerase) inhibition to induce melanoma cell death. We thus identify BAHCC1 as an SE-dependent pan-melanoma expressed gene and demonstrate how its inhibition can be leveraged to impair melanoma cell proliferation, alone or in combination with DNA-damage-inducing agents.

RESULTS

SE17q25 regulates BAHCC1 expression in melanoma

To identify skin cutaneous melanoma (SKCM)-specific SEs, we performed *in silico* rank ordering of SE (ROSE)[23] analysis of H3K27ac chromatin immunoprecipitation sequencing (ChIP-seq) data from short-term melanoma cultures (MM)[16] and two normal human melanocyte (NHEM) samples (NHEM1 and -2).[8] The MM panel covered the two main phenotypes and most common driver mutations (Table S1). We further ranked SEs using DiffBind according to the enrichment in the binding of the lineage-specific transcription factors MITF and SOX10, which are recruited to long and short enhancers in melanocytic-like melanoma cells (Figure S1A).[24–27] Using these criteria, we identified a collection of potential SEs active in MM cells (Table S2). We further defined *bona fide* melanoma-specific SEs as active in at least 5 MM cell cultures. An SE at chr17q25.3 (hereafter referred to as SE17q25) met these criteria and was absent from NHEMs (Figures 1A, left, and S1B). The SE17q25 region measured around 20 kb and was recurrent not only in many of the MM cells but also in melanoma cell lines such as SK-MEL-5 and 501mel (Figure 1A, left and right; Table S2).

SE17q25 localized in close proximity to the promoter of the protein-coding gene BAHCC1 (Figure 1A). The Cancer Genome Atlas (TCGA) reports that high SE17q25 activity, as measured by the level of ATAC (assay for transposase-accessible chromatin)-seq signal, correlated with high BAHCC1 expression in several tumors and that the highest SE17q25 activity was observed in SKCM, with the highest BAHCC1 expression (Figure 1B). qRT-PCR and western blotting showed that BAHCC1 displayed higher RNA and protein levels in melanoma cells highly expressing MITF and SOX10, including melanocytic-like melanoma cells (501mel, MM117, IGR-37, SK-MEL-28, SK-MEL-5, MM011) and uveal melanoma (UVM) cells (OMM1, OMM1.3, OMM2.5) (Figures S1C and S1D). In agreement with these observations, analyses of the Cancer Cell Line Encyclopedia (CCLE) revealed that BAHCC1 expression correlated with that of MITF in melanoma cell lines (n = 49) (Figure 1C). Furthermore, depletion of SOX10 or MITF strongly reduced BAHCC1 mRNA and protein expression in melanocytic-like melanoma cells (Figures 1D and 1E). Note that MITF depletion reduced BRG1 recruitment at SE17q25, suggesting the decommission of this SE (Figure S1E).

Compared to melanocytic-like melanoma cells, BAHCC1 was less expressed in mesenchymal-like MITF^{LOW} melanoma cells (MM099, MM047, IGR-39, and MM029) (Figures S1C and S1D). Note, however, that BAHCC1 expression remained significantly higher in MITF/SOX10^{LOW} melanoma cells compared to non-transformed (but immortalized) Hermes3A melanocytes or the non-melanoma cell line U-2 OS (Figure S1D), arguing that activation of SE17q25 and BAHCC1 expression therefore requires not only MITF/SOX10 expression but additional events that accompany oncogenic transformation.

In addition to MITF and SOX10, the ATP-dependent chromatin remodeler BRG1 and the TFIIH kinase CDK7, which is known to associate with SEs,[28] also bound SE17q25 in 501mel cells (Figure 1A, right). Interestingly, treatment of 501mel cells for a short period of time with TFIIH inhibitors (the CDK7 inhibitor THZ1[5] or the TFIIH/XPB inhibitor triptolide[29,30]) significantly diminished BAHCC1 expression (Figure 1F). In parallel, CRISPR interference (CRISPRi) of SE17q25 in 501mel using a dead Cas9 (dCas9) fused with the repressive Krüppel-associated box (KRAB) domain (dCas9^{KRAB}) and guide RNAs targeting SE17q25 (gSE17q25) diminished BAHCC1 expression compared to GAPDH control gene (Figure 1G). Altogether these data link SE17q25 activity to BAHCC1 expression in melanoma cells.

BAHCC1 expression increases during melanoma progression

To explore BAHCC1 expression in tumors, we analyzed public transcriptional data and observed first that BAHCC1 was more strongly expressed in melanoma cell lines compared to other

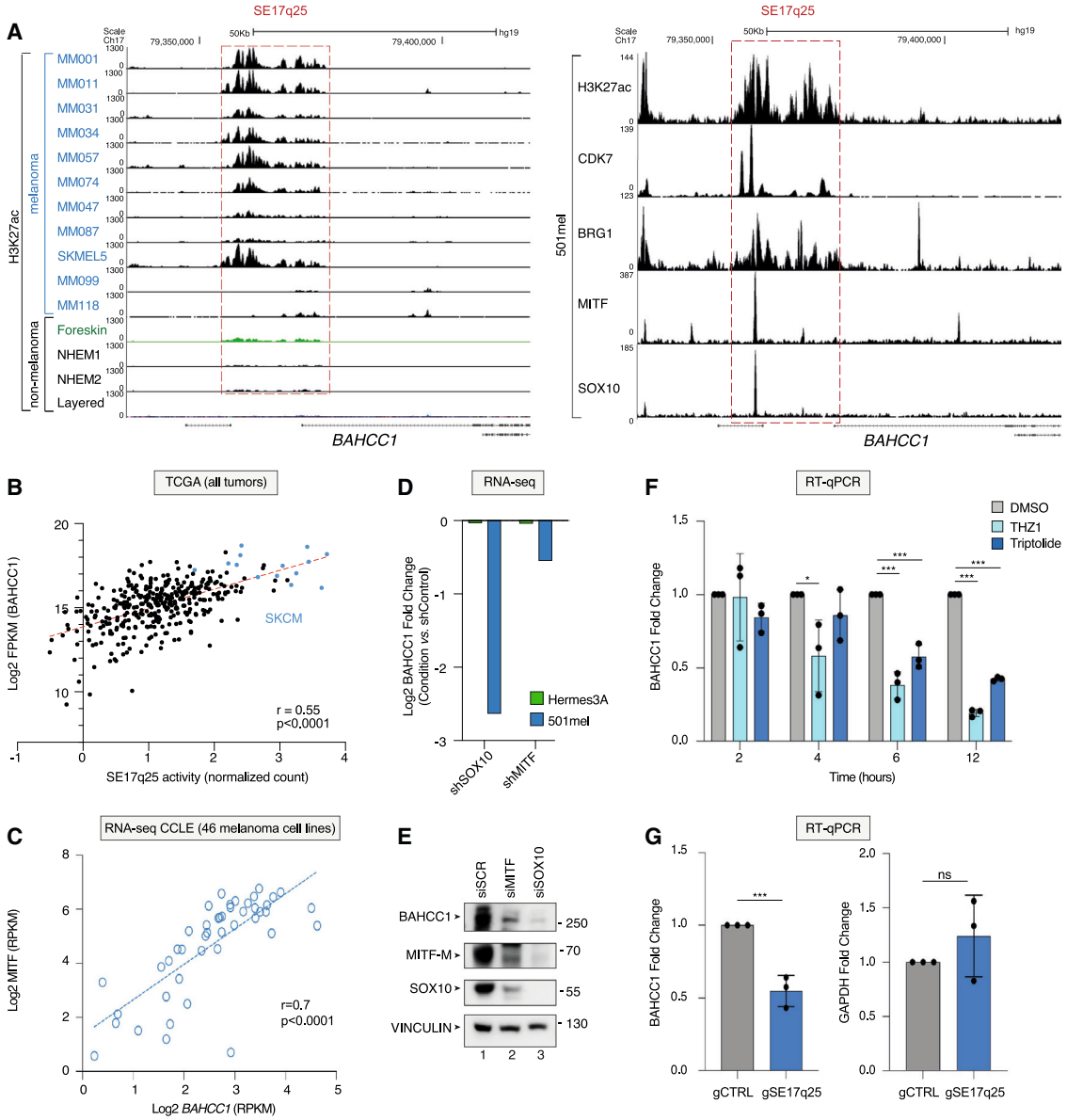

Figure 1. SE17q25 regulates BAHCC1 expression in melanoma

(A) Left: captures of the UCSC genome browser (GRCh38/hg19) showing the ChIP-seq profiles of H3K27ac in the genomic region of SE17q25 in several MM cell lines, healthy melanocytes (NHEM, normal human epidermal melanocytes; foreskin, human foreskin melanocytes) and other tumor and healthy cell lines (layered: H3K27ac mark on 7 cell lines from ENCODE project). Right: captures of the UCSC genome browser (GRCh38/hg19) showing the ChIP-seq profiles of H3K27ac, CDK7, BRG1, MITF, and SOX10 at SE17q25 in mel501 cells. RefSeq-annotated genes are displayed at the bottom.

(B) Spearman correlation between BAHCC1 RNA expression and SE17q25 activity, as defined by the ATAC-seq signal (normalized count), measured in different TCGA tumor samples (n = 399). The SKCM samples are highlighted in light blue and have the higher expression of BAHCC1 and SE17q25 activity. "Spearman r" and p value are shown on bottom right.

(C) Dot plot of BAHCC1 vs. MITF expression (RPKM) determined by RNA-seq from melanoma cell lines obtained from the CCLE datasets (n = 49). The linear regression curve is shown in blue. "Spearman r" and p value are shown on bottom right.

(D) BAHCC1 mRNA fold change (condition vs. shControl) upon SOX10 or MITF KD in healthy melanocytes (Hermes3A) or 501mel melanoma cells obtained from GEO: GSE61967.

(E) 501mel melanoma cells were transfected with siSCR, siMITF, and siSOX10 for 24 h. Total extracts were resolved by SDS-PAGE and immunoblotted against proteins as indicated. Molecular sizes are indicated.

(F) 501mel cells were treated with DMSO, THZ1, or triptolide for 2, 4, 6, and 12 h as indicated, and the relative amount of BAHCC1 mRNA was quantified by qRT-PCR. Bars represent mean values of three different experiments (biological triplicates) (±SEM), two-way ANOVA Šídák's multiple comparisons test.

(G) qRT-PCR for GAPDH and BAHCC1 in 501mel cells co-transfected with CRISPR-dCas9^{KRAB} and guide RNAs (gRNAs) against SE17q25 (gSE17q25) or a non-targeting genomic region (gCTRL). Bars represent mean values of three different experiments (biological triplicates) (±SEM); paired t test.

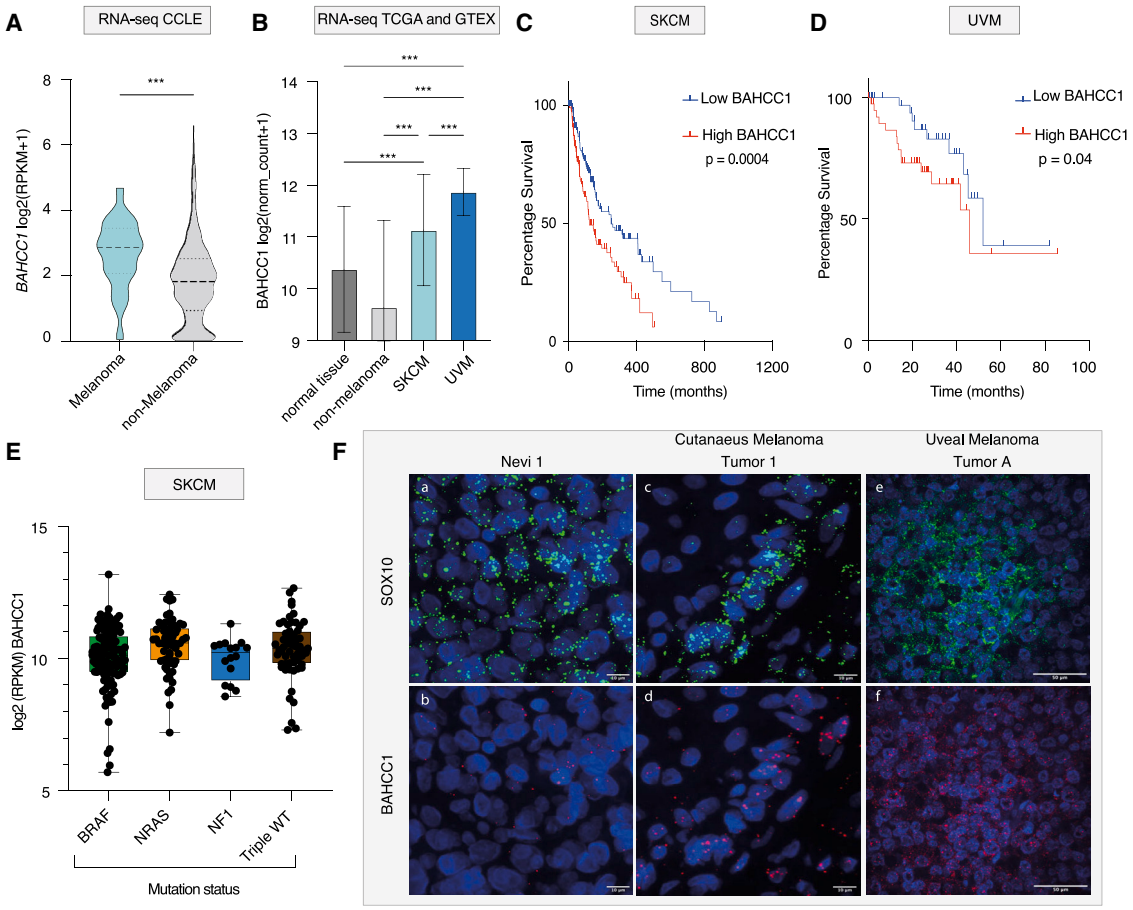

Figure 2. BAHCC1 is overexpressed in melanoma

(A) Violin plot of BAHCC1 levels in melanoma vs. non-melanoma cell lines (RPKM) obtained from CCLE (n = 1019); unpaired t test.

(B) Normalized RNA levels of BAHCC1 in healthy tissues (n = 8,156), non-melanoma tumors (n = 10,416), SKCM (n = 469), and UVM (n = 79) obtained from TCGA and The Genotype-Tissue Expression (GTEX) datasets. Ordinary one-way ANOVA using Dunnett's multiple comparisons test vs. all.

(C and D). Kaplan-Meier analysis of TCGA data from patients with SKCM (n = 302) (C) or UVM (n = 80) (D) with high or low BAHCC1 expression (lower and upper percentiles = 50); log-rank Mantel-Cox test.

(E) Box and whisker plot representation of BAHCC1 expression (RPKM) in TCGA data from patients with SKCM (n = 469) according to the BRAF, NRAS, and NF1 mutational status. Bars show the min and max values; box represent mean ± SEM.

(F) RNA fluorescence *in situ* hybridization (FISH) against BAHCC1 and SOX10 mRNA in naevus melanoma, cutaneous melanoma, and UVM tissue biopsies. Scale bars are indicated. Additional samples are shown in Figures S2E and S2F.

tumor cells (Figure 2A). In agreement, SKCM and UVM tumors from TCGA displayed higher levels of BAHCC1 compared to other tumors and healthy tissues (Figure 2B). Furthermore, BAHCC1 overexpression was a marker of poor prognosis in patients with SKCM or UVM (Figures 2C and 2D), and its expression was independent from the *BRAF*, *NRAS*, or *NF1* mutation status in patients with SKCM (Figure 2E).

To trace the evolution of BAHCC1 expression along melanoma initiation and progression, different published bulk and single-cell transcriptomic datasets from healthy cells and pre-malignant and malignant lesions were combined. Notably, we observed that BAHCC1 expression progressively increased going from healthy skin to primary melanoma and metastatic lesions specifically in malignant cells (Figures S2A–S2E) and that BAHCC1 levels were elevated in melanoma cells vs. melanocyte stem cells in BRAF mouse melanoma model (Figure S2F).[31] Using RNA *in situ* hybridization on a cohort of patient samples including benign nevi, cutaneous melanoma, and UVM, we confirmed the increased expression of BAHCC1 mRNA in SOX10-positive malignant cells (Figures 2F, S2G, and S2H). Overall, these results indicate that BAHCC1 expression progressively increases during melanoma progression from primary tumors to metastasis.

BAHCC1 is required for melanoma cell proliferation and tumor growth

To investigate the functional consequences of BAHCC1 knockdown (BAHCC1 KD), we transfected melanoma cells with two independent custom antisense oligonucleotides (ASOs; locked nucleic acid GapmeRs) targeting the BAHCC1 pre-mRNA ($GR^{\#1}$ and $GR^{\#2}$), which efficiently silenced BAHCC1 expression in 501mel cells (Figure S3A). BAHCC1 KD reduced

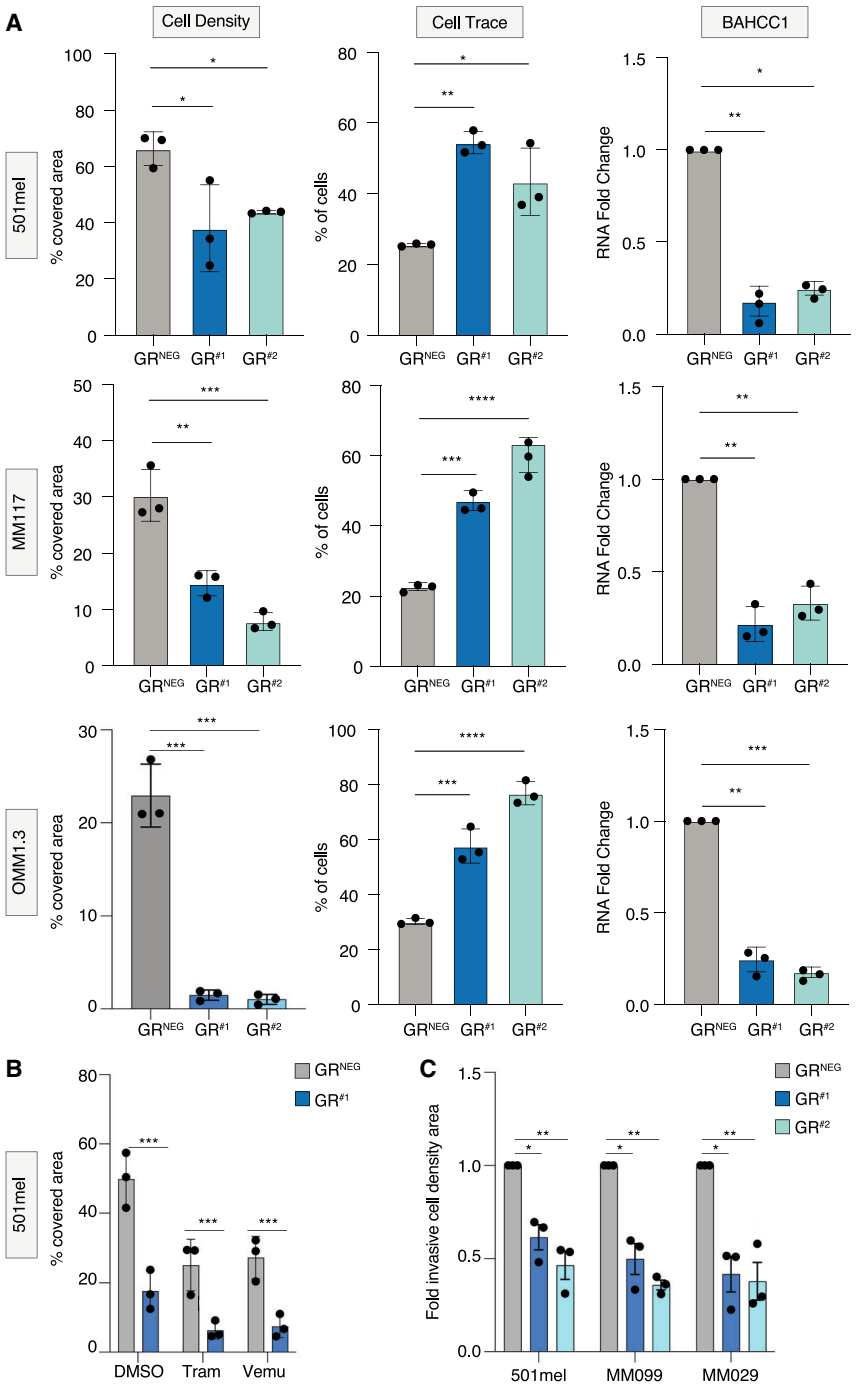

Figure 3. BAHCC1 depletion impairs melanoma cell proliferation

(A) Left: quantification of crystal violet staining of cells transfected with GapmeR^{NEG} (GR^{NEG}), GapmeR$^{\#1}$ (GR$^{\#1}$), and GapmeR$^{\#2}$ (GR$^{\#2}$) in SKCM cells (501mel and MM117) and UVM (OMM1.3) cells. Middle: CellTrace staining was measured by fluorescence-activated cell sorting (FACS) in the cells used on the left, and results are represented as a percentage of slow proliferative cells considering an arbitrary threshold between 20% and 30% in the GR^{NEG} control. Right: relative BAHCC1 expression upon transfection with GR^{NEG}, GR$^{\#1}$, and GR$^{\#2}$ were measured by qRT-PCR in the cells used on the left. Bars represent mean values of three different experiments (biological triplicates) (±SEM). Ordinary one-way ANOVA using Dunnett's multiple comparisons test.

(B) Cell coverage quantification of crystal violet staining of 501mel cells transfected with GR^{NEG} or GR$^{\#1}$ upon treatment with DMSO, trametinib (10 nM), or vemurafenib (5 μM). Bars represent mean values of three different experiments (biological triplicates) (±SEM). Ordinary one-way ANOVA using Dunnett's multiple comparisons test.

(C) Cell coverage quantification of the Boyden chamber Transwell after crystal violet staining of 501mel, MM099, and MM029 cells transfected with GR^{NEG}, GR$^{\#1}$, and GR$^{\#2}$. Bars represent mean values of three different experiments (biological triplicates) (±SEM). Two-way ANOVA using Tukey's multiple comparisons test.

proliferation of cutaneous melanocytic-like (501mel and MM117) and mesenchymal-like (MM047 and MM029) melanoma cells and also of UVM cell lines (OMM1.3 and OMM2.5) (Figures 3A and S3B). In contrast, BAHCC1 KD did not affect proliferation of U-2 OS cells excluding an off-target effect (Figure S3B). Given the anti-proliferative role of MAPK inhibitors (MAPKis) used in the clinic, we investigated whether BAHCC1 KD could exacerbate their effect. Indeed, BAHCC1 KD further reduced the proliferation of a melanocytic cell line upon treatment with trametinib or vemurafenib (Figure 3B). We also evaluated the effect of BAHCC1 KD on melanoma cell invasive capacity and observed that BAHCC1 KD significantly impaired migration of 501mel, MM099, and MM029 melanoma cells (Figure 3C). Altogether, these results highlight the importance of BAHCC1 for melanoma cell proliferation and invasion *in vitro*.

To test the effects of BAHCC1 silencing *in vivo*, we injected melanocytic 501mel melanoma cells engineered to constitutively express luciferase together with GFP and either a non-targeting short hairpin RNA (shRNA; SH^{NTC}) or two independent shRNAs against BAHCC1 (SH$^{\#1}$ and SH$^{\#2}$) in immunocompromised mice (Figure S4A). KD of BAHCC1 dramatically prevented cell-line-derived xenograft (CDX) tumor engraftment and growth compared to the SH^{NTC} (Figures 4A and 4B). In parallel, we also performed intracardiac injection of the 501mel cells to evaluate their capacity to disseminate and form lesions with or without BAHCC1 KD. Concordant with the *in vitro* proliferation and invasion assays, BAHCC1 KD completely prevented colonization in several organs, including the liver, as shown by bioluminescence and immunohistochemistry (IHC) (Figures 4C, 4D, and

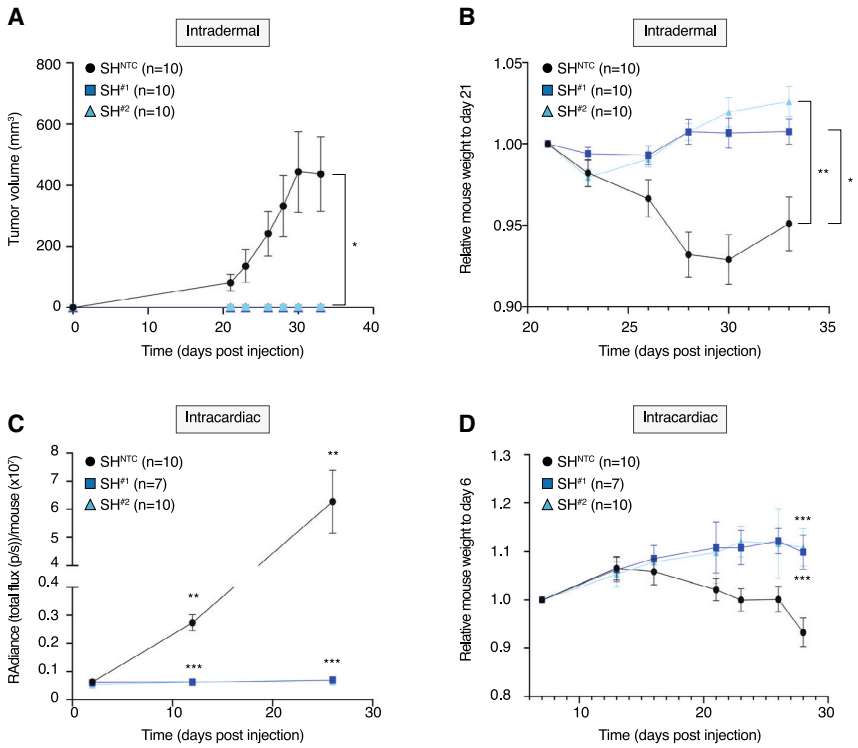

Figure 4. BAHCC1 depletion impairs melanoma tumor engraftment and metastatic growth

(A) Kinetics of tumor growth of 501mel melanoma cells stably expressing shNTC (SH^{NTC}) or shBAHCC1 ($SH^{\#1}$ and $SH^{\#2}$) injected intradermally in NSG mice (±SEM); number of mice per group are shown. Two-way ANOVA Dunnet's multiple comparisons test.

(B) Relative weights of mice after intracardiac injection of 501mel melanoma cells stably expressing SH^{NTC} or shBAHCC1 ($SH^{\#1}$ and $SH^{\#2}$), measured every 3 days after day 21 post-injection. Each mouse weight was normalized to day 21 weight. Two-way ANOVA Dunnet's multiple comparisons test.

(C) Bioluminescence was measured in the three intracardiac groups as indicated at days 2, 12, and 26 post-injection. Bioluminescence is expressed as total radiance per mouse. Number of animals per group are displayed. Two-way ANOVA Dunnet's multiple comparisons test.

(D) Animal weights were measured as indicated at days 7, 13, 16, 21, 23, 26, and 28 post-injection. Weight was scaled to day 7 for each mouse to evaluate the relative variations. Two-way ANOVA Dunnet's multiple comparisons test.

S4B–SD). These data demonstrate the critical role of BAHCC1 in melanoma tumor engraftment and growth *in vivo*.

BAHCC1 regulates E2F/KLF target genes involved in DNA repair and cell cycle

To better understand BAHCC1 function in melanoma cell proliferation, we first checked its localization by immunofluorescence in 501mel cells and observed its nuclear localization (Figure S5A). Analysis of subcellular protein fractions by immunoblot confirmed BAHCC1 accumulation in the nuclear soluble and insoluble fractions (Figure S5B). We then investigated the potential role of BAHCC1 to regulate melanoma gene expression first by transcriptome profiling of 501mel and MM047 cells before and after BAHCC1 KD. RNA-seq revealed that several hundred genes were deregulated in the absence of BAHCC1 (absolute log2 fold change > 0.5 and adjusted p value < 0.05) (Figure 5A), with a significant overlap of 200 genes between the 501mel and MM047 cells (Figure 5B; Table S3). Gene Ontology (GO) analyses of the 200 co-downregulated and 82 co-upregulated genes revealed their enrichment in cell cycle (MCM7, TOP2A, CNTRL), DNA repair (RAD51B, FANCG, ATM), and regulation of the MAPK pathway (MAP2K1, CDKN1B, CDKN2C), as well as mitochondria biogenesis (MTFR1, IMMP2L, DNA2) and cell migration (MMP2, COL18A1, BMP1) (Figures 5C and S5C), consistent with the anti-proliferative and anti-invasive effects of BAHCC1 KD observed above. Note that no modification of the melanocytic signature of 501mel nor the mesenchymal signature of MM047 was observed after BAHCC1 KD (Figure S5D).

To evaluate if BAHCC1 directly regulates gene expression by chromatin binding, we profiled endogenous BAHCC1 ($BAHCC1^{WT}$ [wild type]) genome-wide occupancy using CUT&Tag followed by deep sequencing in 501mel cells. We identified 31,280 peaks for endogenous $BAHCC1^{WT}$, localizing mostly in proximal gene promoters (37.62%) and distal intergenic (24.28%) regions (Figure S5E). Read density clustering of $BAHCC1^{WT}$, H3K27ac ChIP-seq, and ATAC-seq in the 31,280 BAHCC1-occupied regions demonstrated that $BAHCC1^{WT}$ mostly binds to active chromatin at the nucleosome-depleted regions between two H3K27ac-marked nucleosomes (Figure 5D). Moreover, a large fraction of the 41,088 annotated transcription start sites (TSSs) showed TSS-centered BAHCC1 and ATAC peaks flanked by H3K27ac chromatin marks (Figure 5E). Consistent with these data, analysis of the 1,000 best-scoring BAHCC1-occupied sites with RSAT to identify transcription factor DNA-binding motifs and transcription factors that may cooperate with or recruit BAHCC1 to regulate gene expression revealed strong enrichment of the NFY- and SP-family factors known to be enriched at proximal promoters (Table S4). Integrating BAHCC1 RNA-seq and CUT&Tag data, we observed that among the 11,385 genes associated with TSS-centered BAHCC1 peaks, 783 genes were deregulated upon BAHCC1 KD in 501mel cells, of which 539 (70%) were downregulated and 244 (30%) were upregulated (Figure 5F). RSAT analyses of the DNA motifs under the BAHCC1-bound sites at the downregulated promoters showed enrichment of NFY as above but also of motifs for KLF-family factors. Analyses of the promoters of upregulated genes showed KLF-family factors but also SOX10 (Table S4).

Further evidence for the role of BAHCC1 in cell-cycle gene regulation came from mining of single-cell RNA-seq (scRNA-seq)

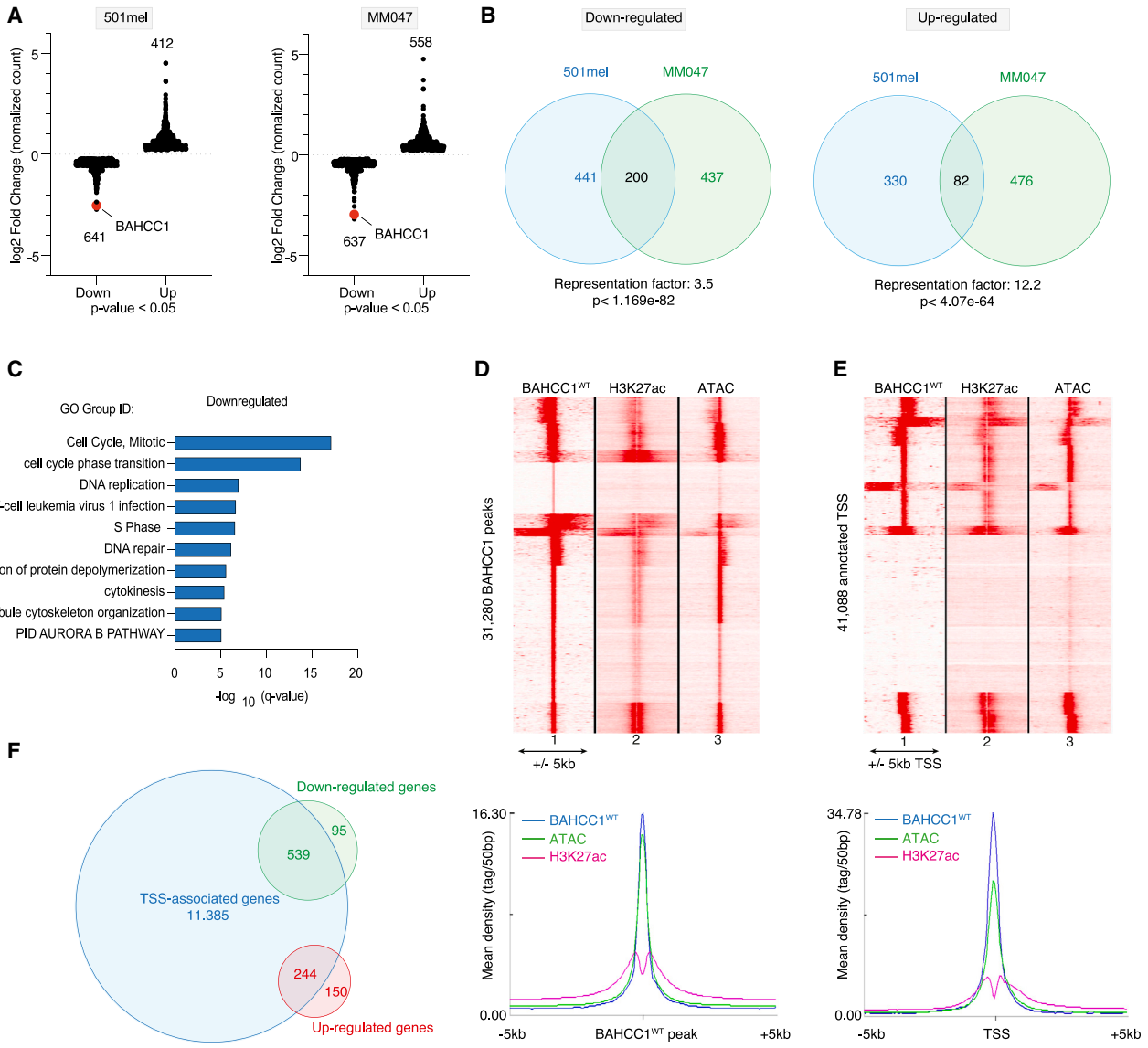

Figure 5. BAHCC1 is a transcriptional regulator

(A) Scatterplot of the significantly ($p < 0.05$) deregulated genes (normalized count) upon BAHCC1 KD in 501mel and MM047. Red dots highlight BAHCC1, which is one of the top downregulated genes.

(B) Venn diagram between significantly downregulated (top) and upregulated (bottom) genes identified by RNA-seq in 501mel and MM047 upon BAHCC1 KD. Representation factor and p values were calculated using hypergeometric test.

(C) GO analysis of the 200 co-downregulated genes between 501mel and MM047 upon BAHCC1 KD. The 10 most significant annotation groups are listed from top to bottom according to the −log10(q value).

(D) Top: read density clustering obtained with seqMINER for the 31,280 BAHCC1-occupied sites relative to BAHCC1, H3K27ac, and ATAC-seq signals in 501mel cells in a genomic window of 10 kb around the peaks. Bottom: merge meta-profile distribution of BAHCC1, H3K27ac, and ATAC enrichment relative to the 31,280 BAHCC1 peaks.

(E) Top: read density clustering obtained with seqMINER for BAHCC1, H3K27ac, and ATAC-seq signals relative to the 41,088 annotated TSSs. Bottom: merge meta-profile distribution of BAHCC1, H3K27ac, and ATAC in a ±5 kb window around the TSS.

(F) Venn diagram between genes showing a TSS-associated BAHCC1 protein and the significantly down- or upregulated genes following BAHCC1 KD, as determined by RNA-seq.

from melanoma patient-derived xenografts (PDXs)[17,26] where BAHCC1 seemed to be preferentially expressed in the "mitotic" melanoma cell subpopulation (Figure S5F) that was also significantly enriched in E2F and SP/KLF regulons (Figure S5G). Similarly, scRNA-seq from uveal and cutaneous tumors[32,33] were separated into "slow"- or "fast"-cycling cells according to the Tirosh cell-cycle signature (95 genes) (Table S5). We observed that BAHCC1 was significantly enriched in fast-cycling cells

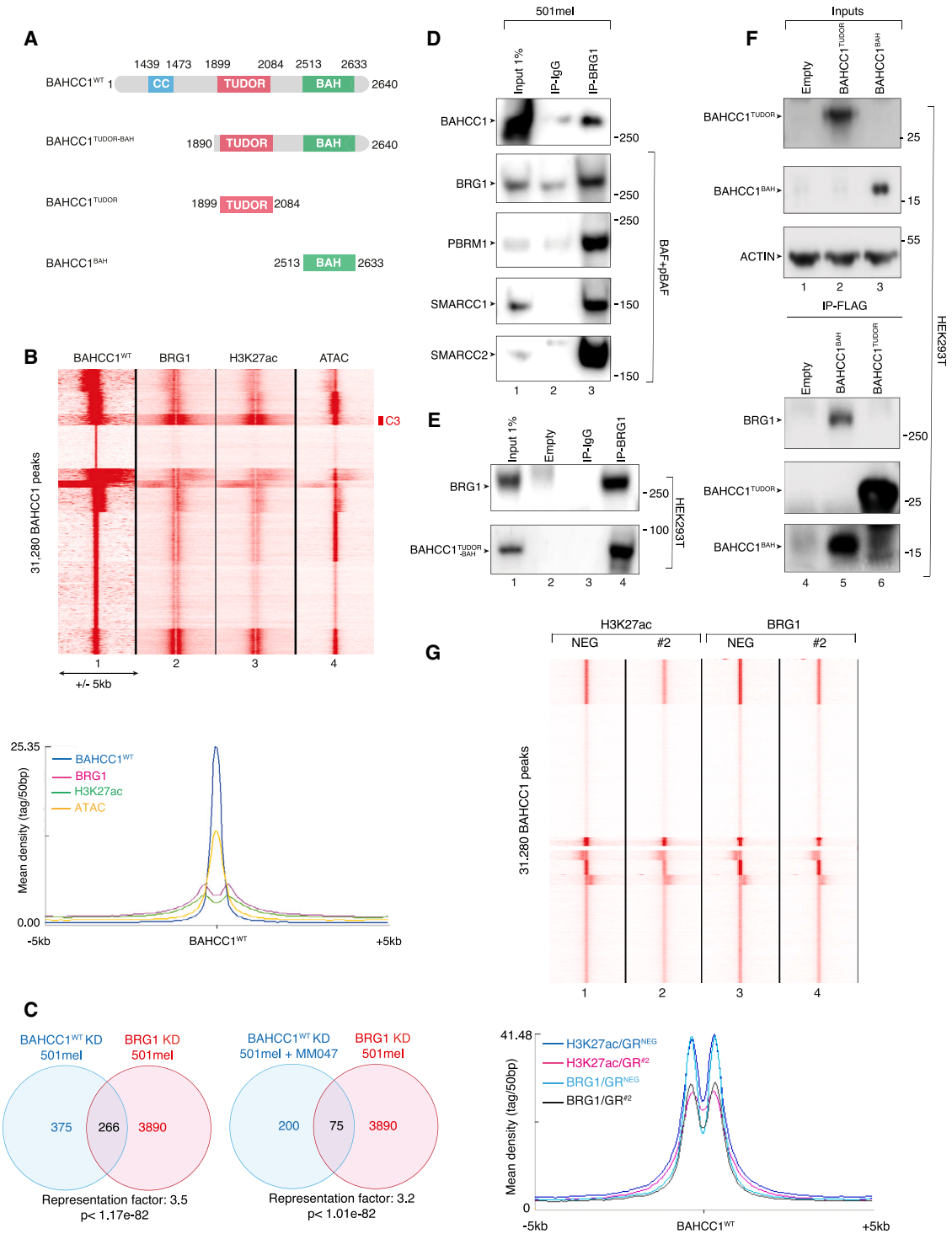

Figure 6. BAHCC1 interacts with BRG1-containing chromatin remodeler complexes

(A) Domain architecture of BAHCC1. CC, coiled coil. The deletion mutants used below are shown.

(B) Top: read density clustering using seqMINER showing the co-localization between BAHCC1^{WT}, BRG1, H3K27ac, and ATAC signals in the 31,280 BAHCC1-occupied sites. Cluster 3 (C3) is highlighted. Bottom: meta-profiles of BAHCC1, BRG1, H3K27ac and ATAC signals around the 31,280 BAHCC1 peaks.

(C) Left: Venn diagram showing the overlap between the downregulated genes in 501mel following either BRG1 or BAHCC1 KD. Right: Venn diagram showing the overlap between the downregulated genes in mel501 after BRG1 KD and the common downregulated genes in 501mel and MM047 after BAHCC1 KD. Representation factor and p values were calculated using hypergeometric test.

(legend continued on next page)

(Figure S5H), confirming its potential role in the control of the cell cycle in melanoma cells. Similar observations were made using TCGA datasets from patients with UVM or SKCM in which BAHCC1 expression significantly correlated with the Tirosh cell-cycle signature (Figure S5I). Together, these results demonstrate that BAHCC1 regulates the expression of a set of E2F/KLF-dependent genes involved in cell cycle and DNA repair.

BAHCC1 interacts with BRG1-containing complexes

Protein Blast and AlphaFold tools revealed the presence of a coiled-coil (CC) region in the central part of BAHCC1 together with two well-conserved TUDOR and BAH domains at the C terminus (Figure 6A). CCs are involved in protein-protein interactions, while BAH and TUDOR domains are found in a wide range of chromatin-binding proteins, where they are readers of histone modifications and act as chromatin co-activators/repressors.[34,35] We profiled genome occupancy of a FLAG-tagged truncated form of BAHCC1 missing the N-terminal CC domain and bearing only the short C-terminal region containing the TUDOR and BAH domains (BAHCC1$^{TUDOR-BAH}$) (Figure 6A). Genome-wide BAHCC1$^{TUDOR-BAH}$ occupancy pattern highly overlapped with endogenous BAHCC1^{WT}, as shown by seqMINER read density heatmap (Figure S6A), further validating the CUT&Tag data obtained above with the full-length endogenous protein. However, a limited cluster of sites was selectively occupied by endogenous BAHCC1^{WT} but not by the truncated form (Figure S6A; Table S6). This BAHCC1 N-terminal region-dependent cluster included 222 of the 539 genes downregulated after BAHCC1 KD, including DNA-repair or cell-cycle genes such as ATM or CDKN1A (Table S6). In agreement with this, RSAT analyses showed that N-terminal region-dependent sites were preferentially enriched in KLF-family DNA-binding motifs similar to the down-regulated promoters (Table S4).

We previously demonstrated that the BRG1 subunit of the PBAF chromatin remodeling complex occupied H3K27ac-marked nucleosomes in 501mel melanoma cells.[25] Comparison of genome-wide occupancy of both BRG1 and BAHCC1 showed that most BAHCC1 peaks were flanked by nucleosomes bound by BRG1 and marked by H3K27ac (Figure 6B). seqMINER read density clustering allowed the identification of several BAHCC1-BRG1 clusters, among which cluster 3 (C3) was associated with DNA-repair and cell-cycle genes including ATM, which was strongly enriched in BAHCC1, BRG1, and H3K27ac at its promoter (Figure S6B). Moreover, a significant fraction of genes downregulated upon BAHCC1 KD in 501mel were also downregulated by BRG1 silencing (Figure 6C, left), including 75 of the 200 genes downregulated in both 501mel and MM047 (Figure 6C, right). Most of these genes were found to be involved in mitosis and DNA repair, including ATM (Figures S6C and S6D; Table S3).

We next aimed to investigate whether a physical interaction could be observed between BAHCC1 and BRG1-containing complexes. BRG1 co-immunoprecipitated with endogenous BAHCC1, together with the BAF/pBAF subunits PBRM1, SMARCC1, and SMARCC2 in 501mel cells (Figure 6D). In parallel, pull-down of BRG1 co-precipitated the FLAG-tagged BAHCC1$^{TUDOR-BAH}$-deletion mutant overexpressed in HEK293T cells (Figure 6E). We further observed that BRG1 co-precipitated specifically with the BAH domain of BAHCC1 but not with the TUDOR domain (Figure 6F). The BAHCC1^{BAH}-BRG1 co-precipitation was confirmed in 501mel melanoma cells stably expressing the hemagglutinin (HA)-tagged BAHCC1^{BAH} domain (Figure S6E).

Moreover, both H3K27ac and BRG1 genomic occupancies were reduced around BAHCC1-binding sites following BAHCC1 KD (Figure 6G). Altogether, these data highlight a direct physical interaction between BAHCC1 and BRG1-containing BAF and PBAF complexes, which impacts BRG1 recruitment and H3K27ac deposition around BAHCC1-binding sites.

BAHCC1 KD cooperates with PARP inhibition to induce melanoma cell death

The above results suggested a role of BAHCC1 in genome stability through its regulation of DNA-repair proteins, including the master DNA damage repair sensor ATM. In agreement, qRT-PCR and immunoblotting showed that BAHCC1 KD decreased expression of ATM at the mRNA and protein levels (Figures 7A and 7B), which can be explained by a loss of H3K27ac deposition and BRG1 recruitment at its promoter (Figure S7A). Furthermore, BAHCC1 expression positively correlated with genome alteration frequencies in human melanoma tumors (Figure 7C). We then tested the effect of BAHCC1 KD on the ability of 501mel cells to repair DNA following treatment with neocarzinostatin (NCS), which induces DNA double-strand breaks (Figure 7D). Strikingly, BAHCC1 KD led to higher numbers of γH2AX foci during the repair time course, indicating a delay in the repair of DNA double-strand breaks in the absence of BAHCC1 (Figures 7E and S7B).

PARP1 is the main PARP-family protein involved in DNA damage response, where it acts as a DNA damage sensor. PARP1 inhibition (PARPi) has been shown to increase DNA replication fork destabilization, leading to accumulation of DNA breaks.[36] Since the PARP pathway acts independently from ATM, it has been postulated that ATM-deficient cancer cells become addicted to PARP-dependent DNA repair, making them highly sensitive to PARPi.[37] Therefore, we queried whether BAHCC1 KD might

(D) BRG1 was immunoprecipitated (IP-BRG1) from nuclear extracts of 501mel cells. Following SDS-PAGE, proteins were immunoblotted as indicated, including subunits of the pBAF/BAF complexes. IP-IgG was performed as a negative control. Molecular sizes are indicated.
(E) HEK293T cells were transfected to express HA-BAHCC1$^{TUDOR-BAH}$ protein and BRG1 was IP (IP-BRG1). Following SDS-PAGE, proteins were immunoblotted as indicated. IP-IgG was performed as a negative control. Molecular sizes are indicated.
(F) HEK293T cells were transfected to express FLAG-BAHCC1^{BAH} and FLAG-BAHCC1^{TUDOR} domains, and FLAG-IP was performed. Following SDS-PAGE, proteins were immunoblotted as indicated. Molecular sizes are indicated.
(G) Top: read density clustering using seqMINER showing the co-localization between H3K27ac and BRG1 signals in the 31,280 H3K27ac-deposition sites with (GR^{NEG}) or without BAHCC1 (GR$^{\#2}$). Bottom: meta-profiles of H3K27ac and BRG1 signals around the 31,280 H3K27ac peaks with (GR^{NEG}) or without (GR$^{\#2}$) BAHCC1.

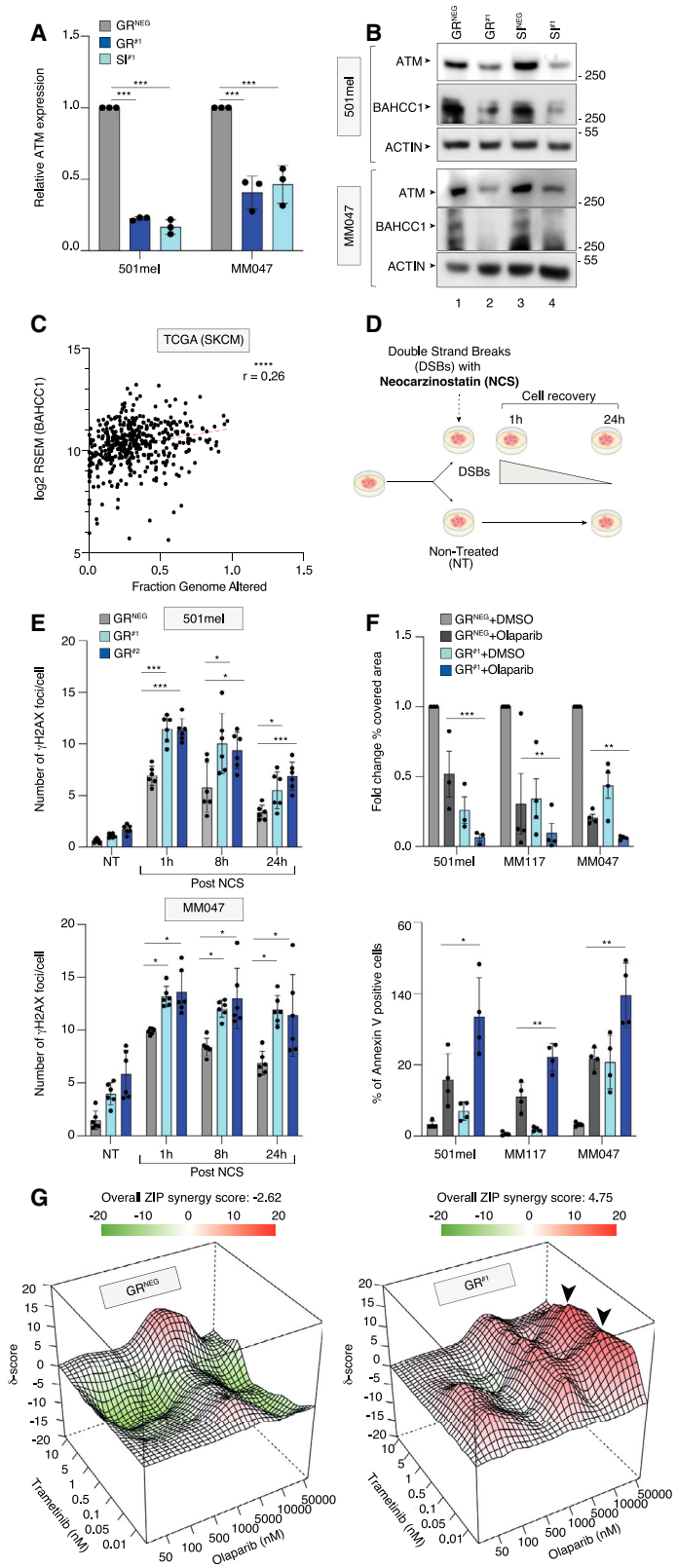

Figure 7. BAHCC1 depletion cooperates with PARPi to induce cell death

(A) Relative ATM expression upon transfection with GR^{NEG}, $GR^{\#1}$, and shBAHCC1 was measured by qRT-PCR in 501mel or MM047. Bars represent mean values of three different experiments (biological triplicates) (±SEM). Two-way ANOVA using Šídák's multiple comparisons test.

(B) 501mel or MM047 was transfected with GR^{NEG}, $GR^{\#1}$, siCTRL (SI^{NEG}), or shBAHCC1 ($SI^{\#1}$). Whole-cell extracts were resolved by SDS-PAGE, and proteins were immunoblotted as indicated.

(C) Spearman correlation between BAHCC1 expression and the fraction of genomic alteration (FGA) in TCGA melanoma samples (n = 443), where FGA is considered as the percentage of copy-number alterations found in the tumor compared to the healthy karyotype. The linear regression curve is shown in red.

(D) Schematic representation of the *in vitro* experiments using neocarzinostatin (NCS).

(E) Immunofluorescence quantification of the number of γH2AX foci per cell in 501mel and MM047 transfected either with GR^{NEG}, $GR^{\#1}$, or $GR^{\#2}$ and treated or not (NT) with NCS (1, 8, and 24 h recovery). Bars represent the means obtained from six biological replicates (±SEM) (501mel n1 = 45,338, n2 = 46,604, n3 = 47,365, n4 = 39,185, n5 = 61,975, n6 = 85,783; MM047 n1 = 26,535, n2 = 26,284, n3 = 28,105, n4 = 8,559, n5 = 13,342, n6 = 18,296). Two-way ANOVA test.

(F) Left: crystal violet quantification expressed as fold change relative to GR^{NEG}-transfected cells treated with DMSO. Bars represent mean values of three different experiments (biological triplicates) (±SEM). Two-way ANOVA using Dunnett's multiple comparisons test. Right: percentage of annexin V-positive cells in 501mel, MM117, and MM047 transfected with GR^{NEG} and $GR^{\#1}$ and treated for 96 h with DMSO or 10 μM olaparib. Bars represent mean values of three different experiments (biological triplicates) (±SEM). Two-way ANOVA using Dunnett's multiple comparisons test.

(G) Surface plot in three-dimensional views, showing synergy scores for impact of trametinib plus olaparib combination on 501mel cell viability. Cells were transfected with GR^{NEG} and $GR^{\#1}$. ZIP synergy scores (shown as d-scores) were calculated from the percentage of inhibition of 501mel cell viability in the dose combination matrix. Black arrows indicate the areas of the most synergistic scores (ZIP > 10). Areas in red, white, and green show regions of synergy, additivity, and antagonism, respectively.

potentiate the effect of PARPi in melanoma cells. Strikingly, co-treatment with the PARPi olaparib and BAHCC1 KD showed a significant cooperative effect on viability of 501mel (MITF^{HIGH}, BRAF^{V600E}), MM117 (MITF^{HIGH}, triple WT), and MM047 (MITF^{LOW}, NRAS^{Q61R}) melanoma cells due to increased apoptosis (Figure 7F). We additionally tested the impact of the combination of PARPi and targeted therapies on the viability of 501mel cells with or without BAHCC1 with SynergyFinder, using the Zero Interaction Potency (ZIP) model. In the absence of BAHCC1, the overall positive ZIP score of 4.45 suggested moderate synergy between the two drugs, which was highest at intermediate and high concentrations of olaparib (ZIP $\geq$ 10), regardless of the concentration of trametinib (Figure 7G, right). The negative ZIP score in the presence of BAHCC1 (Figure 7G, left) suggested that it was the absence of BAHCC1 that induced the moderate synergism observed above. Overall, these findings demonstrate the important role of BAHCC1 in the expression of DNA-repair genes such as ATM, and the kinetics of DNA repair are in line with the idea that melanoma cells may be sensitized to PARPi by BAHCC1 depletion.

DISCUSSION

Deregulation of gene expression in cancer cells is well established and cannot always be explained solely by genomic alterations such as mutations or copy-number variations. Cancer cells undergo significant changes in their transcriptional program through extensive rewiring that includes the acquisition of alternative gene regulatory elements such as SEs.[1,23,38] Using several H3K27ac ChIP-seq datasets from short-term patient-derived cutaneous melanoma cultures, we identified melanoma-specific SEs and their associated genes as potential targets for therapy. We further integrated the H3K27ac profile with the binding profiles of master regulators in melanoma cells such as SOX10 and MITF, which occupy long and short enhancers found in cutaneous melanocytic-like melanoma cells, with SOX10 being required to achieve high levels of activity.[27] Our analysis converged on the SE17q25 element that was activated in most melanocytic-like melanoma cells, regardless of driver mutation status. In cutaneous melanoma cells, the SE17q25 element was not only highly occupied by MITF and SOX10 but also by the TFIIH kinase CDK7 and BRG1, all of which are known to occupy relevant SEs.[5,39,40] Depletion of MITF or SOX10 as well as TFIIH inhibition decommissioned SE17q25 and reduced the expression of BAHCC1, a gene located in close vicinity to SE17q25. In addition, selective CRISPR-mediated silencing of SE17q25 significantly affected BAHCC1 expression, strongly supporting the idea that SE17q25 regulated BAHCC1 expression. These observations in cultured cells were validated using TCGA data on human tumors showing that SE17q25 activity positively correlates with BAHCC1 expression. Importantly, SE17q25 activity and BAHCC1 expression are highest in SKCM compared to other tumors.

In agreement with its dependency on MITF and SOX10 observed *in vitro*, high BAHCC1 expression correlated with high MITF and SOX10 expression in melanoma biopsies and with poor prognosis in both patients with SKCM and with UVM.[41] Consistent with these findings, an extensive analysis of single-cell transcriptomic data from melanoma PDXs demonstrated that BAHCC1 expression was the highest in "mitotic-like" cells.[26] "Mitotic-like" melanoma cells have been found in metastatic SKCM and UVM biopsies and are characterized by expression of E2F-dependent genes. E2F transcription factors are known to promote melanoma progression and metastasis.[42,43] These data are consistent with the fact that our *in vitro* and *in vivo* functional studies showed that BAHCC1 was essential for melanoma cell proliferation and tumor growth by regulating a set of E2F/KLF-dependent genes. Although MITF^{LOW} cells have significantly reduced SE17q25 activity and BAHCC1 expression, we observed that they also depend on SE17q25 and BAHCC1, whose expression may be differently regulated by other TFs important for the mesenchymal state such as TFAP2A, FOSL2, and TEAD4 that bind within SE17q25.[8,16,19,27]

BAH domains are known to bind post-translation modifications (PTMs) of histones such as H3K27me3[44,45] and H4K20me2.[46,47] A previous study characterized the BAHCC1 BAH domain, showing that it binds H3K27me3 and that BAHCC1 interacts with histone deacetylases (HDACs) and SAP30BP proteins of the polycomb repressor complex 1 (PRC1) in acute myeloid leukemia (AML) to repress a large number of genes involved in myeloid differentiation and to promote cell proliferation.[45] In melanoma, BAHCC1 did not show a predominant repressive role, as an equivalent number of genes were up- and downregulated after BAHCC1 KD. CUT&Tag performed on H3K27me3 in 501mel demonstrated that this mark was not present around the BAHCC1-binding sites (Figures S8A and S8B). These observations support the idea that BAHCC1 activity in melanoma does not depend on BAH-H3K27me3 interactions. Our data demonstrated an interaction between BAHCC1 and the SWI/SNF chromatin remodeling complexes, occurring through the BAHCC1^{BAH} domain. We postulate that BRG1 may act upstream to remodel the chromatin, creating the nucleosome-depleted regions to be occupied by BAHCC1. Alternatively, BAHCC1 may be recruited to chromatin via interaction with transcription factors such as those of the KLF/SP/E2F families to regulate their target genes. Moreover, the N-terminal region of BAHCC1, containing the CC domain, appears to be important for the recruitment of BAHCC1 to a set of genes involved in cell proliferation and DNA repair, again suggesting that the BAH domain is not the only determinant of genomic recruitment. We therefore propose that either or both of the above mechanisms drive BAHCC1 genomic recruitment in melanoma, in stark contrast to the BAH-H3K27me3 pathway in AML.

Metastatic melanoma is characterized by the overexpression of genes involved in the DNA damage response (DDR), which makes this tumor stage highly refractory to chemo- and radiotherapies.[48] DDR is essential for maintaining genomic stability to face genotoxic stress resulting from environmental and endogenous DNA damage. In the DDR, ATM, the pivotal mediator of genotoxic stress, phosphorylates histone H2AX to γH2AX to generate docking sites for proteins involved in DNA break repair. ATM also links DNA damage to the cell cycle by controlling key DNA damage checkpoints to regulate DNA break repair directly or indirectly though the control of cell-cycle

checkpoints. On the other hand, PARP1 is able to bind to damaged DNA sites to promote the PARylation of surrounding proteins, thus creating new scaffolds for the recruitment of DNA-repair proteins involved in an alternative DNA break repair pathway. This dual DNA-repair mechanism ensures that DNA breaks are repaired efficiently. However, the loss of one DNA-repair pathway results in increased reliance on the other, which is not essential under healthy settings. Therefore, a high response rate to the PARP inhibitor olaparib was found in patients with metastatic prostate[49] or gastric[50] cancers harboring low expression or mutations of ATM. Since ATM was one of the E2F-dependent genes strongly regulated by BAHCC1, we wondered if this dependence could be exploited therapeutically. Interestingly, BAHCC1 KD cooperates with PARP inhibition by olaparib to impact cell survival, associated with increased apoptosis. In addition to their potential clinical application, these data clearly demonstrate the involvement of BAHCC1 in the control of genes involved in DDR in melanoma cells and suggest that metastatic melanoma upregulates BAHCC1 to promote genomic stability and cellular fitness necessary to sustain high mitotic rates. Finally, the presence of a gene expressed in both cutaneous melanoma and UVM cells makes it possible to envisage common treatments for these two cancers.

Limitations of the study

Our study shows the involvement of BAHCC1 in melanoma growth and maintenance. We show that BAHCC1 is a transcription factor involved in regulating the expression of genes involved in cell-cycle progression and DNA repair. Although we have shown the link between BAHCC1 and BRG1-containing transcription complexes, we have not demonstrated the precise molecular role of BAHCC1 in melanoma. We assume that it interacts with BAF/pBAF complexes to facilitate their recruitment to the promoters of these genes, but we have not demonstrated this hypothesis.

STAR★METHODS

Detailed methods are provided in the online version of this paper and include the following:

- KEY RESOURCES TABLE
- RESOURCE AVAILABILITY
  - Lead contact
  - Materials availability
  - Data and code availability
- EXPERIMENTAL MODEL AND STUDY PARTICIPANT DETAILS
  - Human sample collection
  - Cell culture
  - Mouse xenograft studies
- METHOD DETAILS
  - Synergy assay
  - Identification of SEs
  - RNA FISH
  - Protein extraction
  - Co-immunoprecipitation
  - RNA extraction and qRT-PCR
  - Immunofluorescence
  - Cell proliferation assay
  - Cell death assay
  - Cell density assay
  - Cell invasion assay
  - CUT&Tag and deep sequencing
  - Deep sequencing analysis
  - Bulk RNA-seq analysis
  - Single cell data analysis
  - Other publicly available datasets used in this work
- QUANTIFICATION AND STATISTICAL ANALYSIS

SUPPLEMENTAL INFORMATION

Supplemental information can be found online at https://doi.org/10.1016/j.celrep.2023.113363.

ACKNOWLEDGMENTS

We thank the IGBMC facilities, in particular Paola Rossolillo and Karim Essabri for the isolation of BAHCC1 cDNA, and Dr. Catherine Birck and Dr. Nathalie Troffer-Charlier for the purification of the BAH and TUDOR domains. We thank Prof D. Lipsker and the staff of the Strasbourg University Hospital dermatology clinic for tumor sections and Prof. G. Ghanem and Prof. J.-C. Marine for providing us with the MM-series melanoma cultures. This study was supported by the Institut National Du Cancer (INCa) (INCa_18353, F.C. and I.D.); the Ligue Contre le Cancer (Equipe labélisée 2022, F.C. and I.D.); the Fondation ARC; and the ANR-10-LABX-0030-INRT, a French State fund managed by the Agence Nationale de la Recherche under the frame program Investissements d'Avenir ANR-10- IDEX-0002-02. Sequencing was performed by the IGBMC GenomEast platform, a member of the "France Génomique" consortium (ANR-10-INBS-0009). E.H. is funded by R01CA243446, R01CA274100, U54 CA263001, and R01CA277425 (NCI/NIH). P.B. has been supported by the Ligue contre le Cancer and the National Cancer Center. We thank the NYULH Preclinical imaging (Orlando Aristizabal), Experimental Pathology (Cindy Loomis, Mark Alu), and Microscopy Core facilities, all partially supported by the Cancer Center Support Grant (CCSG) from NCI/NIH to the Perlmutter Cancer Center P30CA016087 (PI: B. Nsel).

AUTHOR CONTRIBUTIONS

P.B., I.D., and F.C. conceived the study. P.B., I.D., and F.C. analyzed the data. P.B. performed most of the *in vitro* functional studies, RNA-seq, and RNAScope. P.B. and M.N. performed qRT-PCR and WB. S.L.G., G.D., T.Y., and P.B., performed bioinformatic analyses. B.H.V., A.L., and M.C. performed wet lab of CUT&Tag experiments. M.C. performed the Boyden chamber experiments. J.O. performed the SynergyFinder experiment. P.B., M.N., and L.S. performed immunoprecipitation. E.H. supervised the *in vivo* studies and provided feedback on the manuscript. P.B., F.V.-R., A.F.-Y., and C.F.C. performed *in vivo* experiments. G.M., G.G., M.D., E.C., and C.B. provided valuable materials. F.C., I.D., and P.B wrote the manuscript.

DECLARATION OF INTERESTS

The authors declare no competing interests.

Received: November 2, 2022
Revised: July 27, 2023
Accepted: October 16, 2023
Published: November 3, 2023

REFERENCES

1. Bradner, J.E., Hnisz, D., and Young, R.A. (2017). Transcriptional Addiction in Cancer. Cell *168*, 629–643. https://doi.org/10.1016/j.cell.2016.12.013.

2. Hnisz, D., Abraham, B.J., Lee, T.I., Lau, A., Saint-André, V., Sigova, A.A., Hoke, H.A., and Young, R.A. (2013). Super-enhancers in the control of cell identity and disease. Cell *155*, 934–947. https://doi.org/10.1016/j.cell.2013.09.053.

3. Pott, S., and Lieb, J.D. (2015). What are super-enhancers? Nat. Genet. *47*, 8–12. https://doi.org/10.1038/ng.3167.

4. Filippakopoulos, P., Qi, J., Picaud, S., Shen, Y., Smith, W.B., Fedorov, O., Morse, E.M., Keates, T., Hickman, T.T., Felletar, I., et al. (2010). Selective inhibition of BET bromodomains. Nature *468*, 1067–1073. https://doi.org/10.1038/nature09504.

5. Kwiatkowski, N., Zhang, T., Rahl, P.B., Abraham, B.J., Reddy, J., Ficarro, S.B., Dastur, A., Amzallag, A., Ramaswamy, S., Tesar, B., et al. (2014). Targeting transcription regulation in cancer with a covalent CDK7 inhibitor. Nature *511*, 616–620. https://doi.org/10.1038/nature13393.

6. Postel-Vinay, S., Herbschleb, K., Massard, C., Woodcock, V., Soria, J.-C., Walter, A.O., Ewerton, F., Poelman, M., Benson, N., Ocker, M., et al. (2019). First-in-human phase I study of the bromodomain and extraterminal motif inhibitor BAY 1238097: emerging pharmacokinetic/pharmacodynamic relationship and early termination due to unexpected toxicity. Eur. J. Cancer *109*, 103–110.

7. Ameratunga, M., Braña, I., Bono, P., Postel-Vinay, S., Plummer, R., Aspegren, J., Korjamo, T., Snapir, A., and de Bono, J.S. (2020). First-in-human Phase 1 open label study of the BET inhibitor ODM-207 in patients with selected solid tumours. Br. J. Cancer *123*, 1730–1736. https://doi.org/10.1038/s41416-020-01077-z.

8. Fontanals-Cirera, B., Hasson, D., Vardabasso, C., Di Micco, R., Agrawal, P., Chowdhury, A., Gantz, M., de Pablos-Aragoneses, A., Morgenstern, A., Wu, P., et al. (2017). Harnessing BET Inhibitor Sensitivity Reveals AMIGO2 as a Melanoma Survival Gene. Mol. Cell *68*, 731–744.e9. https://doi.org/10.1016/j.molcel.2017.11.004.

9. Ribas, A., Read, P., and Slingluff, C. (2015). Cutaneous Melanoma. In Rosenberg's Cancer: Principles and Practice of Oncology, H. DeVita, ed. (Wolters Kluwer).

10. Mitchell, T., Karakousis, G., and Schuchter, L. (2020). Melanoma. In Abeloff's Clinical Oncology Abeloff's Clinical Oncology, J.E. Niederhuber, J.O. Armitage, J.H. Doroshow, M.B. Kastan, and J.E. Tepper, eds. (Elsevier).

11. Chapman, P.B., Hauschild, A., Robert, C., Haanen, J.B., Ascierto, P., Larkin, J., Dummer, R., Garbe, C., Testori, A., Maio, M., et al. (2011). Improved Survival with Vemurafenib in Melanoma with BRAF V600E Mutation. N. Engl. J. Med. *364*, 2507–2516. https://doi.org/10.1056/NEJMoa1103782.

12. Robert, C., Grob, J.J., Stroyakovskiy, D., Karaszewska, B., Hauschild, A., Levchenko, E., Chiarion Sileni, V., Schachter, J., Garbe, C., Bondarenko, I., et al. (2019). Five-Year Outcomes with Dabrafenib plus Trametinib in Metastatic Melanoma. N. Engl. J. Med. *381*, 626–636. https://doi.org/10.1056/NEJMoa1904059.

13. Curti, B.D., and Faries, M.B. (2021). Recent Advances in the Treatment of Melanoma. N. Engl. J. Med. *384*, 2229–2240. https://doi.org/10.1056/NEJMra2034861.

14. Marin-Bejar, O., Rogiers, A., Dewaele, M., Femel, J., Karras, P., Pozniak, J., Bervoets, G., Van Raemdonck, N., Pedri, D., Swings, T., et al. (2021). Evolutionary predictability of genetic versus nongenetic resistance to anticancer drugs in melanoma. Cancer Cell *39*, 1135–1149.e8. https://doi.org/10.1016/j.ccell.2021.05.015.

15. Rubanov, A., Berico, P., and Hernando, E. (2022). Epigenetic Mechanisms Underlying Melanoma Resistance to Immune and Targeted Therapies. Cancers *14*, 5858. https://doi.org/10.3390/cancers14235858.

16. Verfaillie, A., Imrichova, H., Atak, Z.K., Dewaele, M., Rambow, F., Hulselmans, G., Christiaens, V., Svetlichnyy, D., Luciani, F., Van Den Mooter, L., et al. (2015). Decoding the regulatory landscape of melanoma reveals TEADS as regulators of the invasive cell state. Nat. Commun. *6*, 6683. https://doi.org/10.1038/ncomms7683.

17. Rambow, F., Rogiers, A., Marin-Bejar, O., Aibar, S., Femel, J., Dewaele, M., Karras, P., Brown, D., Chang, Y.H., Debiec-Rychter, M., et al. (2018). Toward Minimal Residual Disease-Directed Therapy in Melanoma. Cell *174*, 843–855.e19. https://doi.org/10.1016/j.cell.2018.06.025.

18. Rambow, F., Marine, J.C., and Goding, C.R. (2019). Melanoma plasticity and phenotypic diversity: Therapeutic barriers and opportunities. Genes Dev. *33*, 1295–1318. https://doi.org/10.1101/gad.329771.119.

19. Wouters, J., Kalender-Atak, Z., Minnoye, L., Spanier, K.I., De Waegeneer, M., Bravo González-Blas, C., Mauduit, D., Davie, K., Hulselmans, G., Najem, A., et al. (2020). Robust gene expression programs underlie recurrent cell states and phenotype switching in melanoma. Nat. Cell Biol. *22*, 986–998. https://doi.org/10.1038/s41556-020-0547-3.

20. Onken, M.D., Worley, L.A., Long, M.D., Duan, S., Council, M.L., Bowcock, A.M., and Harbour, J.W. (2008). Oncogenic Mutations in *GNAQ* Occur Early in Uveal Melanoma. Invest. Ophthalmol. Vis. Sci. *49*, 5230–5234. https://doi.org/10.1167/iovs.08-2145.

21. Van Raamsdonk, C.D., Griewank, K.G., Crosby, M.B., Garrido, M.C., Vemula, S., Wiesner, T., Obenauf, A.C., Wackernagel, W., Green, G., Bouvier, N., et al. (2010). Mutations in *GNA11* in Uveal Melanoma. N. Engl. J. Med. *363*, 2191–2199. https://doi.org/10.1056/NEJMoa1000584.

22. Yang, J., Manson, D.K., Marr, B.P., and Carvajal, R.D. (2018). Treatment of uveal melanoma: where are we now? Ther. Adv. Med. Oncol. *10*, 1758834018757175. https://doi.org/10.1177/1758834018757175.

23. Lovén, J., Hoke, H.A., Lin, C.Y., Lau, A., Orlando, D.A., Vakoc, C.R., Bradner, J.E., Lee, T.I., and Young, R.A. (2013). Selective inhibition of tumor oncogenes by disruption of super-enhancers. Cell *153*, 320–334. https://doi.org/10.1016/j.cell.2013.03.036.

24. Strub, T., Giuliano, S., Ye, T., Bonet, C., Keime, C., Kobi, D., Le Gras, S., Cormont, M., Ballotti, R., Bertolotto, C., and Davidson, I. (2011). Essential role of microphthalmia transcription factor for DNA replication, mitosis and genomic stability in melanoma. Oncogene *30*, 2319–2332. https://doi.org/10.1038/onc.2010.612.

25. Laurette, P., Strub, T., Koludrovic, D., Keime, C., Le Gras, S., Seberg, H., Van Otterloo, E., Imrichova, H., Siddaway, R., Aerts, S., et al. (2015). Transcription factor MITF and remodeller BRG1 define chromatin organisation at regulatory elements in melanoma cells. Elife *4*, e06857. https://doi.org/10.7554/eLife.06857.

26. Berico, P., Cigrang, M., Davidson, G., Braun, C., Sandoz, J., Legras, S., Vokshi, B.H., Slovic, N., Peyresaubes, F., Gene Robles, C.M., et al. (2021). CDK7 and MITF repress a transcription program involved in survival and drug tolerance in melanoma. EMBO Rep. *22*, e51683. https://doi.org/10.15252/embr.202051683.

27. Mauduit, D., Taskiran, I.I., Minnoye, L., de Waegeneer, M., Christiaens, V., Hulselmans, G., Demeulemeester, J., Wouters, J., and Aerts, S. (2021). Analysis of long and short enhancers in melanoma cell states. Elife *10*, e71735. https://doi.org/10.7554/eLife.71735.

28. Chipumuro, E., Marco, E., Christensen, C.L., Kwiatkowski, N., Zhang, T., Hatheway, C.M., Abraham, B.J., Sharma, B., Yeung, C., Altabef, A., et al. (2014). CDK7 inhibition suppresses super-enhancer-linked oncogenic transcription in MYCN-driven cancer. Cell *159*, 1126–1139. https://doi.org/10.1016/j.cell.2014.10.024.

29. Titov, D.V., Gilman, B., He, Q.L., Bhat, S., Low, W.K., Dang, Y., Smeaton, M., Demain, A.L., Miller, P.S., Kugel, J.F., et al. (2011). XPB, a subunit of TFIIH, is a target of the natural product triptolide. Nat. Chem. Biol. *7*, 182–188. https://doi.org/10.1038/nchembio.522.

30. Noel, P., Hussein, S., Ng, S., Antal, C.E., Lin, W., Rodela, E., Delgado, P., Naveed, S., Downes, M., Lin, Y., et al. (2020). Triptolide targets super-enhancer networks in pancreatic cancer cells and cancer-associated fibroblasts. Oncogenesis *9*, 100. https://doi.org/10.1038/s41389-020-00285-9.

31. Sun, Q., Lee, W., Mohri, Y., Takeo, M., Lim, C.H., Xu, X., Myung, P., Atit, R.P., Taketo, M.M., Moubarak, R.S., et al. (2019). A novel mouse model demonstrates that oncogenic melanocyte stem cells engender melanoma

resembling human disease. Nat. Commun. *10*, 5023. https://doi.org/10.1038/s41467-019-12733-1.

32. Tirosh, I., Izar, B., Prakadan, S.M., Wadsworth, M.H., Treacy, D., Trombetta, J.J., Rotem, A., Rodman, C., Lian, C., Murphy, G., et al. (2016). Dissecting the multicellular ecosystem of metastatic melanoma by single-cell RNA-seq. Science *352*, 189–196. https://doi.org/10.1126/science.aad0501.
33. Pandiani, C., Strub, T., Nottet, N., Cheli, Y., Gambi, G., Bille, K., Husser, C., Dalmasso, M., Béranger, G., Lassalle, S., et al. (2021). Single-cell RNA sequencing reveals intratumoral heterogeneity in primary uveal melanomas and identifies HES6 as a driver of the metastatic disease. Cell Death Differ. *28*, 1990–2000. https://doi.org/10.1038/s41418-020-00730-7.
34. Ciani, B., Bjelić, S., Honnappa, S., Jawhari, H., Jaussi, R., Payapilly, A., Jowitt, T., Steinmetz, M.O., and Kammerer, R.A. (2010). Molecular basis of coiled-coil oligomerization-state specificity. Proc. Natl. Acad. Sci. USA *107*, 19850–19855. https://doi.org/10.1073/pnas.1008502107.
35. Musselman, C.A., Lalonde, M.-E., Côté, J., and Kutateladze, T.G. (2012). Perceiving the epigenetic landscape through histone readers. Nat. Struct. Mol. Biol. *19*, 1218–1227. https://doi.org/10.1038/nsmb.2436.
36. Caron, M.C., Sharma, A.K., O'Sullivan, J., Myler, L.R., Ferreira, M.T., Rodrigue, A., Coulombe, Y., Ethier, C., Gagné, J.P., Langelier, M.F., et al. (2019). Poly(ADP-ribose) polymerase-1 antagonizes DNA resection at double-strand breaks. Nat. Commun. *10*, 2954. https://doi.org/10.1038/s41467-019-10741-9.
37. Pilié, P.G., Gay, C.M., Byers, L.A., O'Connor, M.J., and Yap, T.A. (2019). PARP Inhibitors: Extending Benefit Beyond *BRCA* -Mutant Cancers. Clin. Cancer Res. *25*, 3759–3771. https://doi.org/10.1158/1078-0432.CCR-18-0968.
38. Lee, T.I., and Young, R.A. (2013). Transcriptional regulation and its misregulation in disease. Cell *152*, 1237–1251. https://doi.org/10.1016/j.cell.2013.02.014.
39. Barutcu, A.R., Lajoie, B.R., Fritz, A.J., McCord, R.P., Nickerson, J.A., Van Wijnen, A.J., Lian, J.B., Stein, J.L., Dekker, J., Stein, G.S., and Imbalzano, A.N. (2016). SMARCA4 regulates gene expression and higherorder chromatin structure in proliferating mammary epithelial cells. Genome Res. *26*, 1188–1201. https://doi.org/10.1101/gr.201624.115.
40. Eliades, P., Abraham, B.J., Ji, Z., Miller, D.M., Christensen, C.L., Kwiatkowski, N., Kumar, R., Njauw, C.N., Taylor, M., Miao, B., et al. (2018). High MITF Expression Is Associated with Super-Enhancers and Suppressed by CDK7 Inhibition in Melanoma. J. Invest. Dermatol. *138*, 1582–1590. https://doi.org/10.1016/j.jid.2017.09.056.
41. Gao, Y., Li, Y., Niu, X., Wu, Y., Guan, X., Hong, Y., Chen, H., and Song, B. (2020). Identification and Validation of Prognostically Relevant Gene Signature in Melanoma. BioMed Res. Int. *2020*, 5323614. https://doi.org/10.1155/2020/5323614.
42. Ma, Y., Kurtyka, C.A., Boyapalle, S., Sung, S.-S., Lawrence, H., Guida, W., and Cress, W.D. (2008). A Small-Molecule E2F Inhibitor Blocks Growth in a Melanoma Culture Model. Cancer Res. *68*, 6292–6299. https://doi.org/10.1158/0008-5472.CAN-08-0121.
43. Alla, V., Engelmann, D., Niemetz, A., Pahnke, J., Schmidt, A., Kunz, M., Emmrich, S., Steder, M., Koczan, D., and Pützer, B.M. (2010). E2F1 in Melanoma Progression and Metastasis. J. Natl. Cancer Inst. *102*, 127–133. https://doi.org/10.1093/jnci/djp458.
44. Zhao, D., Zhang, X., Guan, H., Xiong, X., Shi, X., Deng, H., and Li, H. (2016). The BAH domain of BAHD1 is a histone H3K27me3 reader. Protein Cell *7*, 222–226. https://doi.org/10.1007/s13238-016-0243-z.
45. Fan, H., Lu, J., Guo, Y., Li, D., Zhang, Z.M., Tsai, Y.H., Pi, W.C., Ahn, J.H., Gong, W., Xiang, Y., et al. (2020). BAHCC1 binds H3K27me3 via a conserved BAH module to mediate gene silencing and oncogenesis. Nat. Genet. *52*, 1384–1396. https://doi.org/10.1038/s41588-020-00729-3.
46. Kuo, A.J., Song, J., Cheung, P., Ishibe-Murakami, S., Yamazoe, S., Chen, J.K., Patel, D.J., and Gozani, O. (2012). ORC1 BAH domain links H4K20 to DNA replication licensing and Meier-Gorlin syndome. Nature *484*, 115–119. https://doi.org/10.1038/nature10956.ORC1.
47. Dai, Y., Zhang, A., Shan, S., Gong, Z., and Zhou, Z. (2018). Structural basis for recognition of 53BP1 tandem Tudor domain by TIRR. Nat. Commun. *9*, 2123. https://doi.org/10.1038/s41467-018-04557-2.
48. Kauffmann, A., Rosselli, F., Lazar, V., Winnepenninckx, V., Mansuet-Lupo, A., Dessen, P., Van Den Oord, J.J., Spatz, A., and Sarasin, A. (2008). High expression of DNA repair pathways is associated with metastasis in melanoma patients. Oncogene *27*, 565–573. https://doi.org/10.1038/sj.onc.1210700.
49. Mateo, J., Carreira, S., Sandhu, S., Miranda, S., Mossop, H., Perez-Lopez, R., Nava Rodrigues, D., Robinson, D., Omlin, A., Tunariu, N., et al. (2015). DNA-Repair Defects and Olaparib in Metastatic Prostate Cancer. N. Engl. J. Med. *373*, 1697–1708. https://doi.org/10.1056/NEJMoa1506859.
50. Bang, Y.-J., Im, S.-A., Lee, K.-W., Cho, J.Y., Song, E.-K., Lee, K.H., Kim, Y.H., Park, J.O., Chun, H.G., Zang, D.Y., et al. (2015). Randomized, Double-Blind Phase II Trial With Prospective Classification by ATM Protein Level to Evaluate the Efficacy and Tolerability of Olaparib Plus Paclitaxel in Patients With Recurrent or Metastatic Gastric Cancer. J. Clin. Orthod. *33*, 3858–3865. https://doi.org/10.1200/JCO.2014.60.0320.
51. Badal, B., Solovyov, A., Di Cecilia, S., Chan, J.M., Chang, L.W., Iqbal, R., Aydin, I.T., Rajan, G.S., Chen, C., Abbate, F., et al. (2017). Transcriptional dissection of melanoma identifies a high-risk subtype underlying TP53 family genes and epigenome deregulation. JCI Insight *2*, e92102. https://doi.org/10.1172/jci.insight.92102.
52. Yan, B.Y., Garcet, S., Gulati, N., Kiecker, F., Fuentes-Duculan, J., Gilleaudeau, P., Sullivan-Whalen, M., Shemer, A., Mitsui, H., and Krueger, J.G. (2019). Novel immune signatures associated with dysplastic naevi and primary cutaneous melanoma in human skin. Exp. Dermatol. *28*, 35–44. https://doi.org/10.1111/exd.13805.
53. Kabbarah, O., Nogueira, C., Feng, B., Nazarian, R.M., Bosenberg, M., Wu, M., Scott, K.L., Kwong, L.N., Xiao, Y., Cordon-Cardo, C., et al. (2010). Integrative Genome Comparison of Primary and Metastatic Melanomas. PLoS One *5*, e10770. https://doi.org/10.1371/journal.pone.0010770.
54. Xu, L., Shen, S.S., Hoshida, Y., Subramanian, A., Ross, K., Brunet, J.P., Wagner, S.N., Ramaswamy, S., Mesirov, J.P., and Hynes, R.O. (2008). Gene expression changes in an animal melanoma model correlate with aggressiveness of human melanoma metastases. Mol. Cancer Res. *6*, 760–769. https://doi.org/10.1158/1541-7786.MCR-07-0344.
55. Scatolini, M., Grand, M.M., Grosso, E., Venesio, T., Pisacane, A., Balsamo, A., Sirovich, R., Risio, M., and Chiorino, G. (2010). Altered molecular pathways in melanocytic lesions: Altered Molecular Pathways in Melanocytic Lesions. Int. J. Cancer *126*, 1869–1881. https://doi.org/10.1002/ijc.24899.
56. Ross-Innes, C.S., Stark, R., Teschendorff, A.E., Holmes, K.A., Ali, H.R., Dunning, M.J., Brown, G.D., Gojis, O., Ellis, I.O., Green, A.R., et al. (2012). Differential oestrogen receptor binding is associated with clinical outcome in breast cancer. Nature *481*, 389–393. https://doi.org/10.1038/nature10730.
57. Ramírez, F., Ryan, D.P., Grüning, B., Bhardwaj, V., Kilpert, F., Richter, A.S., Heyne, S., Dündar, F., and Manke, T. (2016). deepTools2: a next generation web server for deep-sequencing data analysis. Nucleic Acids Res. *44*, W160–W165. https://doi.org/10.1093/nar/gkw257.
58. Ye, T., Krebs, A.R., Choukrallah, M.-A., Keime, C., Plewniak, F., Davidson, I., and Tora, L. (2011). seqMINER: an integrated ChIP-seq data interpretation platform. Nucleic Acids Res. *39*, e35. https://doi.org/10.1093/nar/gkq1287.
59. Bailey, T.L., and Grant, C.E. (2021). SEA: Simple Enrichment Analysis of motifs. Preprint at bioRxiv. https://doi.org/10.1101/2021.08.23.457422.
60. Dobin, A., Davis, C.A., Schlesinger, F., Drenkow, J., Zaleski, C., Jha, S., Batut, P., Chaisson, M., and Gingeras, T.R. (2013). STAR: ultrafast universal RNA-seq aligner. Bioinformatics *29*, 15–21. https://doi.org/10.1093/bioinformatics/bts635.

61. Anders, S., and Huber, W. (2010). Differential expression analysis for sequence count data. Genome Biol. *11*, R106–R112. https://doi.org/10.1186/GB-2010-11-10-R106/COMMENTS.

62. Langmead, B., Trapnell, C., Pop, M., and Salzberg, S.L. (2009). Ultrafast and memory-efficient alignment of short DNA sequences to the human genome. Genome Biol. *10*, R25. https://doi.org/10.1186/gb-2009-10-3-r25.

63. Ennen, M., Keime, C., Gambi, G., Kieny, A., Coassolo, S., Thibault-Carpentier, C., Margerin-Schaller, F., Davidson, G., Vagne, C., Lipsker, D., and Davidson, I. (2017). MITF-High and MITF-Low Cells and a Novel Subpopulation Expressing Genes of Both Cell States Contribute to Intra- and Intertumoral Heterogeneity of Primary Melanoma. Clin. Cancer Res. *23*, 7097–7107. https://doi.org/10.1158/1078-0432.Ccr-17-0010.

64. Ianevski, A., Giri, A.K., and Aittokallio, T. (2022). SynergyFinder 3.0: an interactive analysis and consensus interpretation of multi-drug synergies across multiple samples. Nucleic Acids Res. *50*, W739–W743. https://doi.org/10.1093/nar/gkac382.

65. Heinz, S., Benner, C., Spann, N., Bertolino, E., Lin, Y.C., Laslo, P., Cheng, J.X., Murre, C., Singh, H., and Glass, C.K. (2010). Simple Combinations of Lineage-Determining Transcription Factors Prime cis-Regulatory Elements Required for Macrophage and B Cell Identities. Mol. Cell *38*, 576–589. https://doi.org/10.1016/j.molcel.2010.05.004.

66. Zhang, Y., Liu, T., Meyer, C.A., Eeckhoute, J., Johnson, D.S., Bernstein, B.E., Nusbaum, C., Myers, R.M., Brown, M., Li, W., and Liu, X.S. (2008). Model-based analysis of ChIP-Seq (MACS). Genome Biol. *9*, R137–R139. https://doi.org/10.1186/GB-2008-9-9-R137/FIGURES/3.

67. Yu, G., Wang, L.-G., and He, Q.-Y. (2015). ChIPseeker: an R/Bioconductor package for ChIP peak annotation, comparison and visualization. Bioinformatics *31*, 2382–2383. https://doi.org/10.1093/bioinformatics/btv145.

68. Thomas-Chollier, M., Herrmann, C., Defrance, M., Sand, O., Thieffry, D., and Van Helden, J. (2012). RSAT peak-motifs: motif analysis in full-size ChIP-seq datasets. Nucleic Acids Res. *40*, e31. https://doi.org/10.1093/nar/gkr1104.

69. Love, M.I., Huber, W., and Anders, S. (2014). Moderated estimation of fold change and dispersion for RNA-seq data with DESeq2. Genome Biol. *15*, 550. https://doi.org/10.1186/S13059-014-0550-8/FIGURES/9.

70. Benjamini, Y., and Hochberg, Y. (1995). Controlling the False Discovery Rate: A Practical and Powerful Approach to Multiple Testing. J. Roy. Stat. Soc. B *57*, 289–300. https://doi.org/10.1111/J.2517-6161.1995.TB02031.X.

71. Butler, A., Hoffman, P., Smibert, P., Papalexi, E., and Satija, R. (2018). Integrating single-cell transcriptomic data across different conditions, technologies, and species. Nat. Biotechnol. *36*, 411–420. https://doi.org/10.1038/nbt.4096.

72. Tsoi, J., Robert, L., Paraiso, K., Galvan, C., Sheu, K.M., Lay, J., Wong, D.J.L., Atefi, M., Shirazi, R., Wang, X., et al. (2018). Multi-stage Differentiation Defines Melanoma Subtypes with Differential Vulnerability to Drug-Induced Iron-Dependent Oxidative Stress. Cancer Cell *33*, 890–904.e5. https://doi.org/10.1016/j.ccell.2018.03.017.

STAR★METHODS

KEY RESOURCES TABLE

REAGENT or RESOURCE	SOURCE	IDENTIFIER
Antibodies		
ACTB	IGBMC house-made	N/A
ATM	Cell Signaling Technology	Cat# 2873; RRID:AB_2062659
AXL	Proteintech	Cat# 13196-1-AP; RRID:AB_10642006
BAHCC1	Thermo Fisher Scientific	Cat# PA5-54785; RRID:AB_2638459
BRG1	Abcam	Cat# ab110641; RRID:AB_10861578
FLAG	Sigma-Aldrich	Cat#F7425; RRID:AB_439687
GFP	Abcam	Cat#ab290; RRID:AB_2313768
H3K27ac	Abcam	Cat#ab4729; RRID:AB_2118291
HA	Abcam	Cat#ab9110; RRID:AB_307019
γH2AX	Sigma-Aldrich	Cat#05–636; RRID:AB_309864
IgG control	Abcam	Cat#ab171870; RRID:AB_2687657
c-JUN	Cell Signaling Technology	Cat# 9165 (also 9165T, 9165S, 9165L), RRID:AB_2130165
Ki67	Abcam	Cat# ab15580; RRID:AB_443209
LUCIFERASE	Santa Cruz Biotechnology	Cat# sc-57604; RRID:AB_629896
MITF	Cell Signaling Technology	Cat# 12590, RRID:AB_2616024
SOX9	Cell Signaling Technology	Cat# 82630; RRID:AB_2665492
SOX10	Cell Signaling Technology	Cat# 89356 (also 89356S); RRID:AB_2792980
VINCULIN	Sigma-Aldrich	Cat# V4505; RRID:AB_477617
Biological samples		
Histological sections of nevi and cutaneous melanoma samples	Prof. B. Cribier, head of the *Laboratoire d'histopathologie et d'immunopathologie cutanees*, Strasbourg CHU hospital	N/A
Histological sections primary uveal melanoma tumor sections	Nice CHU hospital.	Pandiani et al.[33]
Chemicals, peptides, and recombinant proteins		
CellTrace™ Violet Proliferation Kit	Fisher Scientific	C34557
Doxycycline	ENVIGO	TD.00502
Fugene6	Roche Diagnostics	1815075
Lipofectamine 2000	Fisher Scientific	11668027
Lipofectamine RNAiMAX	Fisher Scientific	13778030
NCS	Sigma Aldrich	N9162
SYBR Green	Roche Diagnostics	4887352001
Critical commercial assays		
Affinity Gel FLAG M2 conjugated beads	Sigma Aldrich	M8823
AnnexinV-APC	BD Biosciences	88-8007-72
CUT&Tag-IT™ Assay Kit	Active motif	#53165, #53160
Culturex® Basement Membrane Extract	R&D systems	3434-001-02
GentleMACS C-tubes	Miltenyibiotec	130-096-334
Human Tumor dissociation kit	Miltenyibiotec	130-095-929
LAB-TEK II chamber slides	Thermo Fisher Scientific	154461
Matrigel	Corning	356231
NucleoSpin RNA Plus kit	Macherey-Nagel	740990

(*Continued on next page*)

Continued

REAGENT or RESOURCE	SOURCE	IDENTIFIER
ProLong™ Gold antifade reagent	Invitrogen	P36930
Reverse Transcriptase Superscript IV	Life Technologies	18090050
Deposited data		
CUT&Tag	This paper	GSE205462
RNA-seq	This paper	GSE201702
RNA-seq	Scatolini et al.[51]	GSE12391
RNA-seq	Tsoi et al.[52]	GSE80829
RNA-seq	Badal et al.[51]	GSE98394
RNA-seq	Yan et al.[52]	GSE114445
RNA-seq	Kabbarah et al.[53]	GSE46517
RNA-seq	Xu et al.[54]	GSE8401
Experimental models: Cell lines		
All MM melanoma cells	Dr. G. Ghanem (Institute Jules Bordet, Brussels, Belgium) and J-C Marine (VIB-KU Leuven, Belgium)	Verfaillie et al.[16]
OMM1.3	Pandiani et al.[33]	N/A
OMM2.5	Pandiani et al.[33]	RRID:CVCL_C307
Hermes3A	Dr. C Bennett, University of London (UK)	RRID:CVCL_VS10
U-2 OS	ATCC	RRID:CVCL_0042
501mel HA-BAHCC1^{BAH}	This paper	N/A
501mel	Dr. C Goding, University of Oxford (UK)	RRID:CVCL_4633
HEK293T	ATCC	RRID:CVCL_0063
SKMEL-28	Dr. L Larue, Institut Curie) (France)	RRID:CVCL_0526
IGR37	Dr. C Goding, University of Oxford (UK)	RRID:CVCL_2075
Experimental models: Organisms/strains		
NOD.Cg-Prkdc^{scid} IL2rg^{tm1Wjl}/SzJ (NSG)	Jackson Laboratories	RRID:BCBC_4142
Oligonucleotides		
GR^{NEG}: TCATACTATATGACAG	This study	N/A
GR$^{\#1}$: AGATTGGCGGTAGGAA	This study	N/A
GR$^{\#2}$: TCCGTGGAATTTAGAT	This study	N/A
gRNA SE17q25$^{\#1}$: GGCACGAGGCGCATAGCTA	This study	N/A
gRNA SE17q25$^{\#2}$: TGCACGCCCCTCTTGTTCAG	This study	N/A
gRNA SE17q25$^{\#3}$: CTGATTTCTACCCTTCCGTG	This study	N/A
SI^{NEG}	ON-TARGETplus SMARTpool L-001830-10	Orizon Discovery
SI$^{\#1}$	ON-TARGETplus SMARTpool L-023331-02	Orizon Discovery
siMITF	ON-TARGETplus SMARTpool L-008674-00	Orizon Discovery
siSOX10	ON-TARGETplus SMARTpool L-017192-00	Orizon Discovery
Recombinant DNA		
pcDNA-FLAG	This study	N/A
pX629_dCas9_KRAB_mScarlet	This study	N/A
pCDNA-GFP	This study	N/A
pcDNA-GFP-SE17q25	This study	N/A
pcDNA-FLAG-BAHCC1^{TUDOR}	This study	N/A
pcDNA-FLAG-BAHCC1^{BAH}	This study	N/A
pLT3_shCTRL	This study	N/A
pLT3_sh4 (shBAHCC1)	This study	N/A

(*Continued on next page*)

Continued

REAGENT or RESOURCE	SOURCE	IDENTIFIER
pGL4.10Luc2	This study	N/A
pLenti6-GFP	This study	N/A
pLenti-TET-3HA-BAHCC1^{BAH}	This study	N/A
pLenti6-3HA-BAHCC1$^{BAH-TUDOR}$	This study	N/A
Software and algorithms		
FlowJo software	https://www.flowjo.com/solutions/flowjo/downloads	N/A
Seurat software package version 3.1.4	Butler et al.[55]	N/A
Fiji	https://imagej.net/software/fiji/downloads	N/A
DeepTool2	Ramírez et al.[56]	N/A
DiffBind v1.12.3	Ross-Innes et al.[26]	N/A
ROSE	Lovén et al.[23]	N/A
Homer v4.9.1	Heinz et al.[57]	N/A
ChIPseeker	Yu et al.[58]	N/A
Seq-MINER	Ye et al.[59]	N/A
Homer makeUCSCfile v4.9.1	Heinz et al.[57]	N/A
Cutadapt version 1.10	https://cutadapt.readthedocs.io/en/v1.10/	N/A
Bowtie v 2.2.8	Langmead et al.[60]	N/A
STAR version 2.5.3a	Dobin et al.[61]	N/A
Scope	https://scope.aertslab.org	N/A
Bioconductor package AUCell v 1.6.1	https://www.bioconductor.org/packages/release/bioc/html/AUCell.html	N/A
Deeptools multiBamSummary v2.5.0	Ramírez et al.[56]	N/A
Htseq-count version 0.6.1p1	https://htseq.readthedocs.io/en/master/history.html	N/A
Bioconductor package DESeq2 version 1.16.1	https://bioconductor.org/packages/release/bioc/html/DESeq2.html	N/A
Prism 9	https://www.graphpad.com/scientific-software/prism/	N/A
iRegulon plugin of Cytoscape	https://apps.cytoscape.org/apps/iregulon	N/A
Graeber Lab software	https://systems.crump.ucla.edu/	N/A
CCLE portal	https://sites.broadinstitute.org/ccle	N/A
Regulatory Sequence Analysis Tools (RSAT) web server	Thomas-Chollier et al.[62]	N/A
Other		
High-throughput imaging system CX7	Thermofisher	N/A
EVOS xl Core microscope	Thermofisher	N/A
IVIS imager	Perkin Elmer	N/A
Q800R3 sonicator	Qsonica	N/A
LightCycler 480	Roche	N/A
Illumina HiSeq 4000	Illumina	N/A
gentleMACS^{TM} Dissociator	Miltenyibiotec	N/A

RESOURCE AVAILABILITY

Lead contact

Further information and requests for resources and reagents should be directed to and will be fulfilled by the Lead Contact, Frédéric Coin (fredr@igbmc.fr).

Materials availability

Reagents generated in this study will be made available on request, but we may require a payment and/or a completed Materials Transfer Agreement if there is potential for commercial application.

Data and code availability

- Next generation sequencing raw and processed data have been deposited at GEO: Accession numbers of these data are listed in the key resources table
- This paper analyzes existing, publicly available data. These accession numbers for the datasets are listed in the key resources table
- This paper does not report original code
- Any additional information required to reanalyze the data reported in this paper is available from the lead contact upon request

EXPERIMENTAL MODEL AND STUDY PARTICIPANT DETAILS

Human sample collection

Information about human tumor samples is provided in Ext. Table S7. Nevi 1; male/62yo, Nevi 2; female/45yo, Tumor 1; male/50yo, Tumor 2; female/66yo, Tumor 3; male/70yo, Tumor A; female/84yo, Tumor B; male/69yo, Tumor C; male/84yo, Tumor D, male/65yo.

Tumors for cutaneous melanoma were obtained after written informed consent from the University of Strasbourg Medical facutly ethics board and good clinical practice. Tumors 1, 2 and 3 are identical to tumors 4, 5 and 6 described in.[63] Tumors A, B, C and D for uveal melanoma were obtained after written informed consent from the Nice CHU hospital. They are identical to tumor A, B, C and D described in.[33]

Cell culture

Patient-derived short-term cultures MM cells have been grown in HAM-F10 (Gibco, Invitrogen) supplemented with 10% Fetal Calf Serum (FCS) and penicillin-streptomycin. 501mel and SK-MEL-28 cells were grown in RPMI w/o HEPES (Gibco, Invitrogen) supplemented with 10% FCS and gentamycin and IGR37 and IGR39 were grown in RPMI w/o HEPES supplemented with 15% of FCS and gentamycin. Uveal melanoma cells OMM1.3 and OMM2.5 were cultured respectively in DMEM (4.5 g/L glucose) supplemented with 10% FCS, penicillin-streptomycin, Sodium Pyruvate, MEM essential vitamin mixture, NEAA mixture and HEPES, and RPMI w/o HEPES supplemented with 2gr/l glucose, 10% FCS and penicillin-streptomycin. U-2 OS cells were grown in DMEM/Ham-F10 (1:1) supplemented with 10% FCS and gentamicin. HEK293T cell were grown in DMEM (1 g/L glucose) supplemented with 10% FCS and penicillin-streptomycin. All cell lines were grown in 5% CO_2 at 37°C. Melanocyte cell line Hermes3A was grown in 10% CO_2 at 37°C in RPMI w/o HEPES supplemented with 10% FCS, penicillin-streptomycin, 200nM TPA (Sigma Aldrich), 200p.m. Cholera Toxin (Sigma Aldrich), 10 ng/mL hSCF (Life Technologies), 10nM EDN-1 (Sigma Aldrich) and 2mM Glutamine (Invitrogen). All cell lines used were mycoplasma negative.

501mel for *in vivo* studies were generated by transducing cells first with lentiviral vector pEIGW-SK II Luc-GFP (kindly provided by Dr. Iannis Aifantis) followed by a second transduction with MISSION shRNA lentiviral vectors shNTC (Millipore Sigma, SHC002), shBAHCC1$^{\#1}$ (Millipore Sigma, TRCN0000230988) and shBAHCC1$^{\#2}$ (Millipore Sigma, TRCN0000217993).[45]

501mel HA-BAHCC1^{BAH} were generated by transducing cells with lentiviral vectors pLenti-TET-3HA-BAHCC1^{BAH} and selected with 0.5ug/mL of puromycin.

Cells carrying a doxycycline-inducible system were treated with 1ug/mL of doxycycline for at least 24h.

GapmeRs or siRNAs were transfected in cells with Lipofectamine RNAiMAX following the manufacture instructions using an oligos final concentration of 25nM and cells were harvested 48h and/or 72h after transfection.

For CRISPRi experiments, 501mel cells were co-transfected with pX629_dCas9_KRAB_mScarlet (plasmid obtained from the IGBMC BioMol service) and pCDNA-GFP (gCTRL) or pcDNA-GFP-SE17q25 (gSE17q25) using Fugene6 following manufacture instructions. Afterward, double-positive GFP+/mScarlet+ cells were sorted with a FACSaria Fusion BD Biosciences Cell sorter and RNA extraction was performed 72h post sorting.

BAHCC1^{TUDOR} and BAHCC1^{BAH} were cloned into a pcDNA-FLAG vector. pcDNA-FLAG, pcDNA-FLAG-BAHCC1^{TUDOR}, pcDNA-FLAG-BAHCC1^{BAH}, pLenti6-GFP and pLenti6-3HA-BAHCC1$^{BAH-TUDOR}$ vectors were transiently transfected in HEK293T cells with Lipofectamine 2000 following the manufacture instructions.

Mouse xenograft studies

Animal experiments were performed in NYU Langone Health and were approved by the Institutional Animal Care and Use Committee (IACUC) under the protocol number IA16-00051. All experiments conform to the relevant regulatory standards.

Immunodeficient 6 weeks-old male mice NOD.Cg-Prkdc^{scid} IL2rg^{tm1Wjl}/SzJ (NSG) were purchased from Jackson Laboratories and maintained in the NYU Langone Health SBCAF germ-free animal facility. For primary tumor formation, 1 × 10^5 501mel cells were resuspended in 50μL of PBS +50μL of Corning Matrigel Matrix Basement Membrane (ref. 354234) and injected intradermally in the flank of the animal.

Primary tumor volume was measured every 3 days after becoming palpable using two-dimensional caliper (volume = (π/6) × length × wide^2) and animals were euthanized when tumors reached 1cm^3 volume.

For *in vivo* metastasis assay, 1 × 10^5 501mel cells were resuspended in 100μL of PBS mice and injected in the heart left ventricle of NSG mice through ultrasound imaging-guided injection. Metastasis burden was quantified once per week through luciferase injection followed by bioluminescence measurement with *In Vivo* Imaging System (IVIS) imager at the NYULH Preclinical Imaging Core. Animals were euthanized when the body weight reached a 20% decrease.

After euthanasia, mouse organs were collected and analyzed by *ex vivo* GFP fluorescence using a Zeiss AxioObserver microscope in the NYULH Microscopy Laboratory. Organs were then fixed in 10% Formalin for 72hrs followed by 72hrs in ethanol 70% before paraffin inclusion, sectioning, hematoxylin & eosin staining and imaging at the NYULH Experimental Pathology Research Laboratory.

METHOD DETAILS

Synergy assay

24 h after transfection with GAPMERs, 501mel or MM047 cells were seeded into 96-well plates at 5.000 cells/well. 24 h later, cells were incubated with combinations of increasing concentrations of the MEK inhibitor Trametinib or the PARP inhibitor Olaparib, for 72 h. Cell viabilities were assessed using PrestoBlue reagent (ThermoFisher) according to the manufacturer's instructions. The absorbance was measured with a Cell-Insight CX5 microplate reader. Synergy scoring was then determined using the SynergyFinder software (https://synergyfinder.fimm.fi) and by implementing the ZIP calculation method.[64]

Identification of SEs

H3K27ac ChIP-seq data from 12 different melanoma cell lines (MM001, MM011, MM031, MM034, MM057, MM074, MM047, MM087, MM099, MM118, SK-MEL-5, 501mel) and 3 melanocytes cell lines (NHEM1, NHEM2, Foreskin) were retrieved from GEO GSE60666, GSM958157 and GSE94488 and mapped to the Homo Sapiens genome (assembly hg19) using Bowtie v1.0.0 with default parameters except for "-p 3 -m 1 –strata –best –chunkmbs 128". Normalized BigWig files were generated using Homer makeUCSCfile v4.9.1[65] with the following parameter'-norm 20e6′ meaning that data were normalized to 20M reads. The genome was divided into bins of 10Kb long with Deeptools multiBamSummary v2.5.0.[57] The number of reads for each bin was computed for each sample. The following figure was made with Deeptools plotCorrelation and shows the pairwise correlation values (Spearman) for all samples of this project. Peaks were called using MACS2 with default parameters except for "-g hs -f BAM –broad –broad-cutoff 0.1". Peaks falling into ENCODE blacklisted regions ("An Integrated Encyclopedia of DNA Elements in the Human Genome" 2012–9AD) were removed. Peaks were annotated relative to genomic features using Homer v4.9.1 (annotations got extracted from gtf file downloaded from ensembl v75). ROSE was used to differentiate SEs from typical enhancers (detected from H3K27ac data). SEs were annotated relative to genomic features using Homer v4.9.1 (annotations got extracted from gtf file downloaded from ensembl v75). Finally, SEs were filtered according to their position relative to the one of SOX10 and MITF (ChIP-seq tracks in 501mel)[24,25] using the bioconductor package DiffBind v1.12.3.[56]

RNA FISH

Assays were performed following the manufacturer's instructions (https://acdbio.com/manual-assays-rnascope). For the detection of BAHCC1 and SOX10, cells and paraffin tissue sections were treated following the RNAScope manufacture protocol. Cells and tissue samples were counterstained with DAPI and visualized using confocal microscope Spinning disk Leica CSU W1. The sequences of the probes were not provided by the manufacture.

Protein extraction

For the production of whole cell extracts, cells were washed once with cold PBS, rinsed with a cell scraper, pelleted and resuspended in LSDB 0.5M buffer (0.5M KCl, 50mM Tris HCl pH 7.9, 20% Glycerol, 1% NP40, 1mM DTT, PIC). Afterward cells were fully disrupted with 3 cycles of heat shock in liquid nitrogen and 37°C water bath and centrifugated 15 min at 14,000rpm to pellet cell debris.

To obtain cytoplasmic and nuclear protein fractions, cells were first lysed in hypotonic buffer (10 mM Tris–HCl at pH 7.65, 1.5 mM $MgCl_2$, 10 mM KCl) and disrupted by Dounce homogenizer. The cytosolic fraction was separated from the pellet by centrifugation at 4°C. The nuclear soluble fraction was obtained by incubation of the pellet in high salt buffer (final NaCl concentration of 300 mM) and then separated by centrifugation at 4°C. To obtain the nuclear insoluble fraction (chromatin fraction), the remaining pellet was digested with micrococcal nuclease and sonicated.

Co-immunoprecipitation

Whole cell extract was prepared by resuspending cells in LSDB buffer (50mM Tris HCl pH 7.9, 20% Glycerol, 1% NP40, 1mM DTT, PIC) containing 150mM KCl, followed by sonication in Q800R3 sonicator. Between 250ug-1mg of protein extract was used to performed IP with 1-10μg of primary antibody overnight at 4°C on rotation. Following, 50ul of Dynabeads protein A/G were added to the samples for 2h at 4°C. In alternative, FLAG-tagged proteins were immunoprecipitated directly using Affinity Gel FLAG M2 conjugated beads. Beads were washed five times with TGEN buffer (20mM Tris-HCl pH 7.65, 3mM $MgCl_2$, 0.1mM EDTA, 10% glycerol, 0.01% NP-40, PIC) containing 150mM NaCl. Samples were loaded on NuPage gel to perform Western blot.

RNA extraction and qRT-PCR

Total RNA isolation was performed according to the manufacture protocol with NucleoSpin RNA Plus kit. RNA was retrotranscribed with Reverse Transcriptase Superscript IV and qPCR was performed with SYBR Green and monitored by LightCycler 480. Gene expression results were normalized according to four housekeeping genes (HMBS, TBP, UBC and RPL13a). Primers for qRT-PCR and ChIP-qPCR were designed using Primer-BLAST.

Immunofluorescence

Human tissue sections were deparaffinized and dehydrated with Histosol and dilutions of ethanol 100%, 90%, 70% and 30% and rehydrated with demineralized water. Subsequently sections were boiled in Sodium Citrate buffer (0.1M Citric acid, 0.1M Sodium citrate) for 15min to unmask antigens. In parallel, 2D culture cells were grown on LAB-TEK II chamber slides and fixed with 4% formaldehyde or 100% methanol. Afterward, both tissues and cells were permeabilized and saturated in blocking buffer (1% BSA, PBS, 0.3% Triton X-100). Primary antibodies were diluted in blocking buffer and incubate ON at 4°C in wet chamber. Secondary antibody staining was carried out in blocking buffer for 1h and 30 min at room temperature. Nuclei were marked with DAPI and slides were mounted with ProLong Gold antifade reagent before microscope image acquisition.

For γH2AX foci quantification, transfected or naive cells were plated in 96 well plates OptiPlates-96 and eventually treated with NCS (150nM) for 1h at 37°C followed by 1h, 8h or 24h of recovery in complete medium. Afterward, cells were labeled for γH2AX following a classic immunofluorescence protocol. Image acquisition was done using high-throughput imaging system CX7 using 20X objective (50 fields per well). Image segmentation was done with HCS studio. Nuclei were identified using DAPI staining and γH2AX foci were identified within nuclei mask. Foci number and intensity were quantified automatically.

Cell proliferation assay

To measure cell proliferation, cells were incubated first with CellTrace Violet according to the manufacture instructions and analyzed by flow cytometry using a FORTESSA BD Biosciences Cytofluorometer. Data were analyzed with FlowJo software. To define slow proliferating cells, we considered that they represented the 30% of cells with the highest concentration of BV421 in the control treatment. We then calculated the % of cells that had a concentration greater than or equal to this value after treatment.

Cell death assay

To measure cell death, cells were rinsed and incubated 15min with AnnexinV-APC after treatment and analyzed by flow cytometry on a FORTESSA BD Biosciences Cytofluorometer. Data were analyzed with FlowJo software.

Cell density assay

Briefly, following transfection, between 5.10^4 to 1.10^5 cells were grown in 6 wells plate for up to 1 week. Afterward cells were fixed for 10min with 4% Formaldehyde solution, washed once with PBS and stained with Crystal Violet solution 0.2% for 15 min at room temperature. The wells were finally washed twice with deionized water, air dried, scanned and analyzed with Fiji considering the area occupancy of the cells.[26]

Cell invasion assay

Briefly, between 1 and 2.10^5 cells were seeded inside a Boyden Chamber insert covered with Serum free media and 4% Matrigel. The inserts were placed in 24 wells plate filled with complete medium. After 12-24h, the inserts were fixed with 4% Formaldehyde solution for 10min, gently cleaned inside with a cotton stick and stained for 15 min at room temperature with a Crystal Violet solution 0.2%. Afterward the inserts were washed twice in deionized water, air dried and photos were collected using an EVOS xl Core microscope. The pictures were analyzed with Fiji considering the area occupancy of the cells.

CUT&Tag and deep sequencing

Assays were performed following the manufacturer's instructions (https://www.activemotif.com/catalog/1318/cut-tag-it-kit). Briefly, 5.10^5 cells per condition were used. The cells were washed 2 time before the binding on Concavalin A beads and then incubated overnight with BAHCC1 ($BAHCC1^{WT}$) or HA ($BAHCC1^{TUDOR-BAH}$) primary antibodies at the recommended dilution (1:50) or without antibody (negative control). The next day the corresponding secondary antibody, a guinea pig Anti-rabbit antibody was used following a 1:100 dilution in digitonin buffer and incubated at room temperature for 1h. The CUT&Tag-IT Assembled pA-Tn5 Transposomes were incubated for 1h at room temperature before tagmentation. Cells were resuspended in Tagmentation buffer and incubated at 37°C for 1h, then the Tagmentation process was stopped by addition of EDTA and SDS. Protein digestion was performed by the addition of 80ug/mL of proteinase K and incubated at 55°C for 60min. DNA was retrieved on DNA purification columns provided by the manufacturer. Library preparation and PCR amplification were done using the Kit primers and purified by 2 successive washes with SPRI beads. Samples were subjected to paired-end sequencing by the IGBMC GenomEast platform on Illumina HiSeq 4000 instrument.

Deep sequencing analysis

ChIP-seq data for BRG1,[25] H3K27ac and ATAC-seq[8] and CUT&Tag-seq for BAHCC1 (this work) were analyzed as follows.[26] After reads mapping onto hg19 human genome, peak calling was performed using MACS2 according to specific negative control inputs.[66]

Peak annotation was carried out using HOMER[65] and ChIPseeker.[67] Peak genome distribution and correlation between BAHCC1 and BRG1, H3K27ac and ATAC was performed using deepTool2. Peak enrichment for BRG1, H3K27ac, ATAC and BAHCC1 was done using seq-MINER. Top 500 macs peaks summits for BAHCC1 alone or co-bound by BAHCC1 and BRG1 (identified with seq-MINER)[58] were subsequently extended of 100bp upstream and downstream using ''bedtools slop'' followed by extraction of FASTA format sequences with ''bedtools getfasta''. DNA binding motif analysis was carried out with Simple Enrichment Analysis (SEA)[59] and by the pipeline ''peak-motifs'' available online as part of the Regulatory Sequence Analysis Tools (RSAT)[68] using +/− 400bp around the center to cut peak sequences and the non-redundant vertebrate Jaspar core database for motif comparison.

Bulk RNA-seq analysis

Reads were preprocessed to remove adapter and low-quality sequences (Phred quality score below 20). After this preprocessing, reads shorter than 40 bases were discarded for further analysis. These preprocessing steps were performed using cutadapt version 1.10. Reads were mapped to rRNA sequences using bowtie version 2.2.8[62] and reads mapping to rRNA sequences were removed for further analysis. Reads were mapped onto the hg19 assembly of Homo sapiens genome using STAR version 2.5.3a.[60] Gene expression quantification was performed from uniquely aligned reads using htseq-count version 0.6.1p1, with annotations from Ensembl version 75 and ''union'' mode. Only non-ambiguously assigned reads have been retained for further analyses. Read counts have been normalized across samples with the median-of-ratios method proposed by Anders and Huber[61] to make these counts comparable between samples. Comparisons of interest were performed using the Wald test for differential expression proposed by Love[69] and implemented in the Bioconductor package DESeq2 version 1.16.1. Genes with high Cook's distance were filtered out and independent filtering based on the mean of normalized counts was performed. P-values were adjusted for multiple testing using the Benjamini and Hochberg method.[70] iRegulon plugin of Cytoscape was used to analyze the co-deregulated genes between iBAHCC1 and iBRG1.

Single cell data analysis

Expression matrix with row reads counts for the single cell experiment was retrieved from GEO GSE116237, GSE115978, GSE151091, GSE138665, GSE185386 and GSE113502 datasets. Then, data were normalized and clustered using the Seurat software package version 3.1.4 in R version 3.6.1.[71] Data were filtered and only genes detected in at least 3 cells and cells with at least 350 detected genes were kept for further analysis. Expression of 26,661 transcripts in single cells was quantified. To cluster cells, read counts were normalized using the method ''LogNormalize'' of the Seurat function NormalizeData. It divides gene expression counts by the total expression, multiplies this by a scale factor (10,000 was used), and log-transforms the result. Then, 2000 variable features were selected with the variance stabilizing transformation method using the Seurat function FindVariableGenes with default parameters. Integrated expression matrices were scaled (linear transformation) followed by principal component analysis (PCA) for linear dimensional reduction. The 20 principal components (PCs) were used to cluster the cells with a resolution of 0.5 and as input to tSNE to visualize the dataset in two dimensions. The Bioconductor package AUCell v 1.6.1 was used to assess whether some cells from the different datasets were enriched in gene sets of interest.

Other publicly available datasets used in this work

BAHCC1 RNA expression was quantified in available datasets including GEO GSE12391,[55] GSE80829,[72] GSE98394,[51] GSE114445,[52] GSE46517,[53] GSE8401[54] and in the CCLE portal. TCGA and GTEx data were obtained through UCSC Xena browser, cBioPortal and Gene Expression Profiling Interactive Analysis 2 (GEPIA2). PCA profile of TCGA and melanoma cell lines according to their phenotypic profile was obtained from the Graeber Lab software.

QUANTIFICATION AND STATISTICAL ANALYSIS

Statistical analysis was mostly performed using Prism 9. Briefly, for absolute quantification comparison, Student's t-test and ordinary one-way ANOVA unpaired were used; paired test was used for relative quantification comparisons. Grouped sample analysis was carried out through two-way ANOVA test. Kaplan-Meier survival curves were analyzed using Mantel-Cox test. For correlation analysis, Spearman analysis was performed together with linear regression curve fit. Statistical analysis on RNA-seq and ChIP-seq is listed in their dedicated sections. For Venn diagram statistic, hypergeometric test was performed using Nemates software (nemates.org). p values are represented as ns ($p > 0.05$), * ($p < 0.05$), ** ($p < 0.01$), *** ($p < 0.005$) and **** ($p < 0.001$).

Cell Reports, Volume *42*

Supplemental information

Super-enhancer-driven expression of BAHCC1 promotes melanoma cell proliferation and genome stability

Pietro Berico, Maguelone Nogaret, Max Cigrang, Antonin Lallement, Fatemeh Vand-Rajabpour, Amanda Flores-Yanke, Giovanni Gambi, Guillaume Davidson, Leane Seno, Julian Obid, Bujamin H. Vokshi, Stephanie Le Gras, Gabrielle Mengus, Tao Ye, Carlos Fernandez Cordero, Mélanie Dalmasso, Emmanuel Compe, Corine Bertolotto, Eva Hernando, Irwin Davidson, and Frédéric Coin

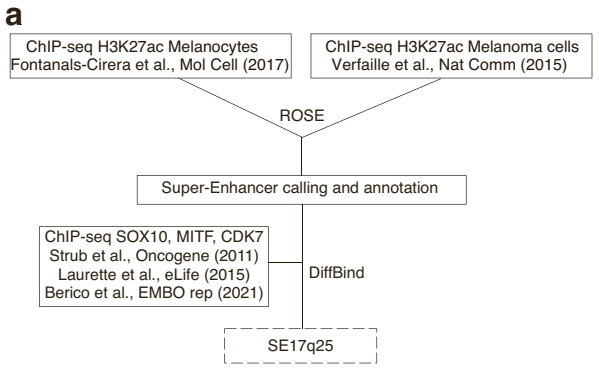
a
ChIP-seq H3K27ac Melanocytes
Fontanals-Cirera et al., Mol Cell (2017)
ChIP-seq H3K27ac Melanoma cells
Verfaille et al., Nat Comm (2015)
ROSE
Super-Enhancer calling and annotation
ChIP-seq SOX10, MITF, CDK7
Strub et al., Oncogene (2011)
Laurette et al., eLife (2015)
Berico et al., EMBO rep (2021)
DiffBind
SE17q25

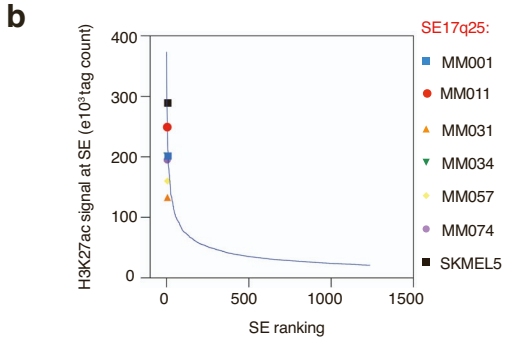
b
H3K27ac signal at SE (e10³tag count)
SE ranking
SE17q25:
MM001
MM011
MM031
MM034
MM057
MM074
SKMEL5

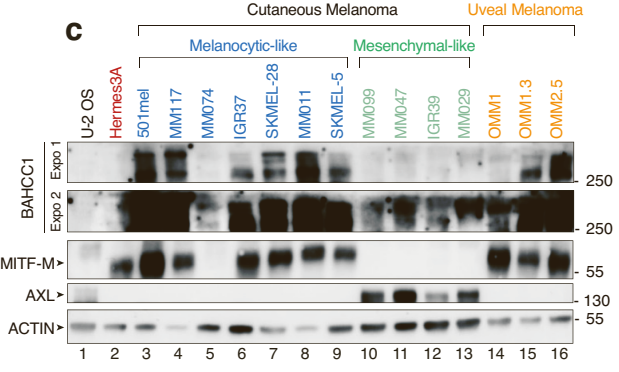
c
Cutaneous Melanoma
Uveal Melanoma
Melanocytic-like
Mesenchymal-like
U-2 OS
Hermes3A
501mel
MM117
MM074
IGR37
SKMEL-28
MM011
SKMEL-5
MM099
MM047
IGR39
MM029
OMM1
OMM1.3
OMM2.5
BAHCC1
Expo 1
Expo 2
MITF-M
AXL
ACTIN

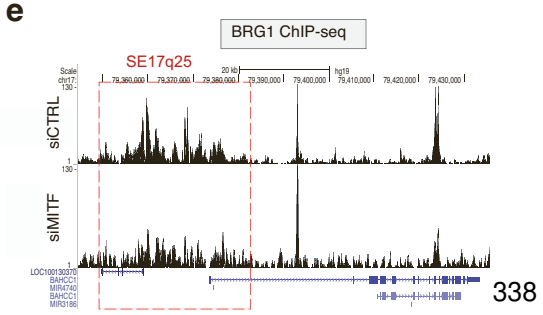
e
BRG1 ChIP-seq
SE17q25
siCTRL
siMITF

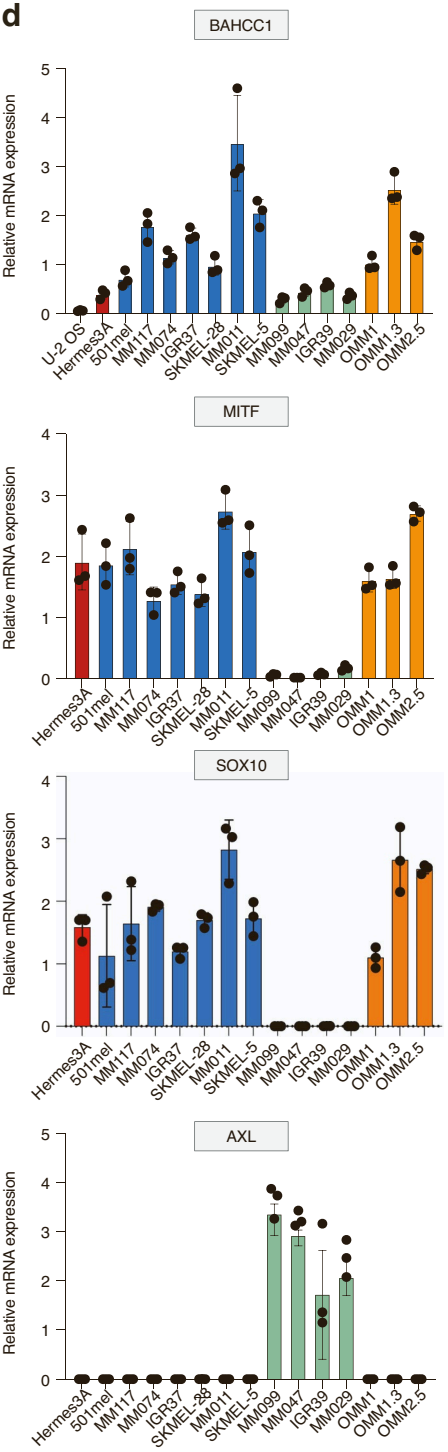
d
BAHCC1
MITF
SOX10
AXL
Relative mRNA expression
U-2 OS
Hermes3A
501mel
MM117
MM074
IGR37
SKMEL-28
MM011
SKMEL-5
MM099
MM047
IGR39
MM029
OMM1
OMM1.3
OMM2.5

Ext. Figure 1: BAHCC1 overexpression in melanoma cells

a. Schematic representation of the SE pipeline analysis used to identify SE17q25.

b. Dot plot representing the H3K27ac signal at SEs as a function of the ROSE ranking. We used the distribution of SEs in MM011 cells as a representative distribution. In different shape and colors are the specific positions of SE17q25 in the corresponding melanoma cell lines.

c. Immunoblot against BAHCC1, MITF, AXL and ACTIN in U-2 OS, immortalized melanocyte Hermes3A and several SKCM and UVM cell lines as indicated.

d. Relative expression of BAHCC1, MITF and AXL determined by RT-qPCR in a large panel of melanoma and non-melanoma cell lines as indicated. Bars represent mean values of three different experiments (Biological triplicates) (+/- SEM).

e. BRG1 ChIP-seq tracks in 501mel treated with siCTRL or siMITF, scaled in the region of SE17q25. The decommission of SE17q25 is illustrated by the loss of BRG1 binding. Values were retrieved from the GEO dataset GSE61967. The red box indicates the SE17q25 localization.

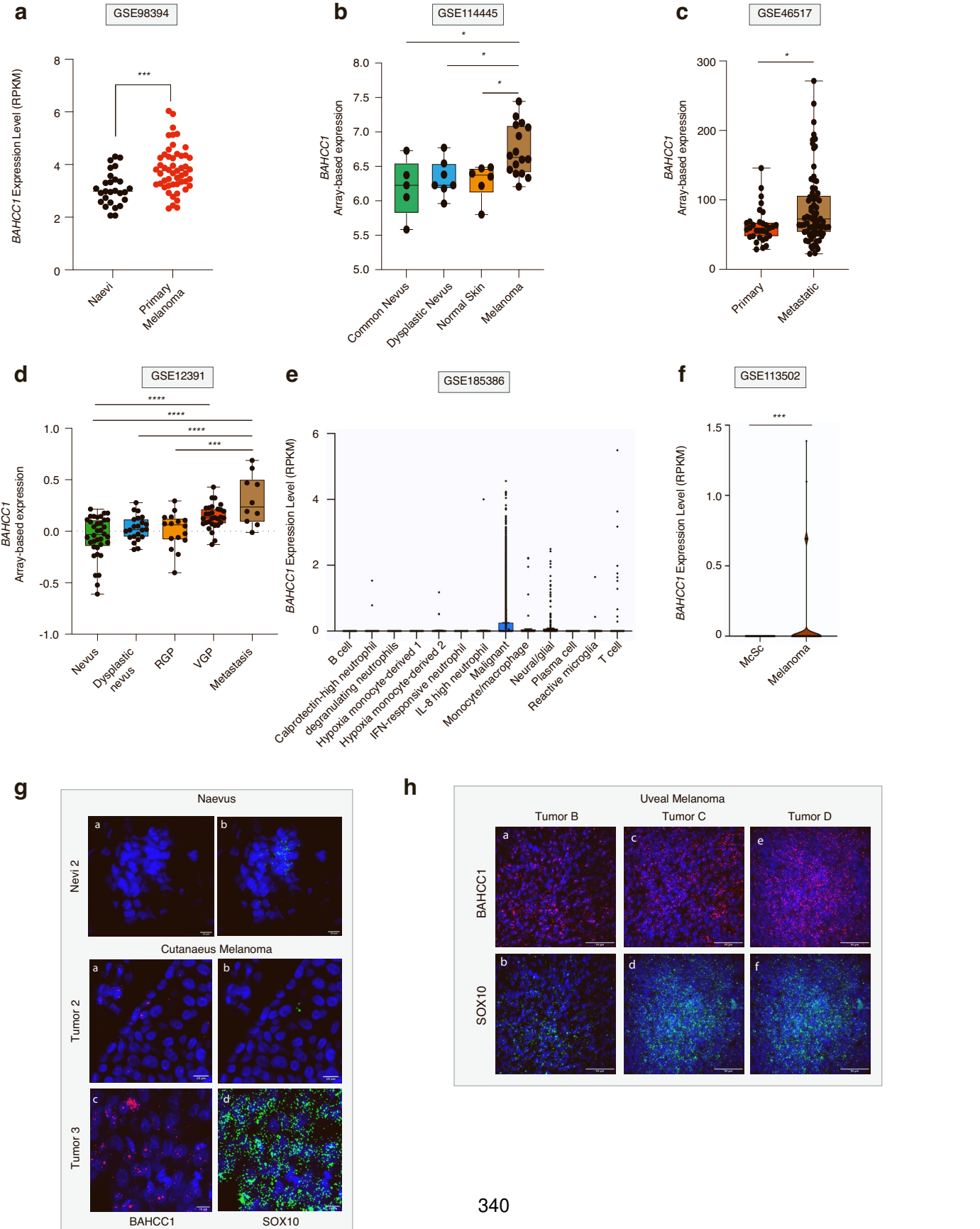
a
GSE98394
BAHCC1 Expression Level (RPKM)
Naevi
Primary Melanoma
b
GSE114445
BAHCC1 Array-based expression
Common Nevus
Dysplastic Nevus
Normal Skin
Melanoma
c
GSE46517
BAHCC1 Array-based expression
Primary
Metastatic
d
GSE12391
BAHCC1 Array-based expression
Nevus
Dysplastic nevus
RGP
VGP
Metastasis
e
GSE185386
BAHCC1 Expression Level (RPKM)
B cell
Calprotectin-high neutrophil
degranulating neutrophils
Hypoxia monocyte-derived 1
Hypoxia monocyte-derived 2
IFN-responsive neutrophil
IL-8 high neutrophil
Malignant
Monocyte/macrophage
Neural/glial
Plasma cell
Reactive microglia
T cell
f
GSE113502
BAHCC1 Expression Level (RPKM)
McSc
Melanoma
g
Naevus
Nevi 2
Cutanaeus Melanoma
Tumor 2
Tumor 3
BAHCC1
SOX10
h
Uveal Melanoma
Tumor B
Tumor C
Tumor D
BAHCC1
SOX10

Ext. Figure 2: BAHCC1 expression increases during melanoma progression

a. BAHCC1 expression in human nevi (n=27) and primary melanomas (n=51). Values were retrieved from the GEO dataset GSE98394 (Badal et al., 2017); unpaired t-test.

b. BAHCC1 expression in normal skin (n=6), common nevus (n=5), dysplastic nevus (n=7) and melanoma (n=16). Values were retrieved from the GEO dataset GSE114445; Ordinary One-Way ANOVA using Dunnett's multiple comparisons test all *vs.* all.

c. BAHCC1 expression in primary (n=31) and metastatic (n=73) melanoma. Values were retrieved from the GEO dataset GSE46517; unpaired t-test.

d. Expression levels of BAHCC1 in human biopsies of nevus (n=36), dysplastic nevus (n=22), melanoma radial growth phase (RGP) (n=16), vertical growth phase (VGP) (n=30) and metastatic melanoma (n=10). Values were retrieved from the GEO dataset GSE12391. Ordinary One-Way ANOVA using Dunnett's multiple comparisons test all *vs.* all.

e. BAHCC1 expression in the different cells identified in a melanoma brain metastasis. Values were retrieved from the GEO dataset GSE 185386.

f. BAHCC1 expression in melanocyte stem cells *vs.* melanoma cells in BRAF melanoma mouse model. Values were retrieved from the GEO dataset GSE113502; unpaired t-test.

g-h. RNA FISH for SOX10 and BAHCC1 in human tissue samples of nevi (n=1), cutaneous (n=2) and uveal melanomas (n=3). Scale bar is indicated for each image.

a

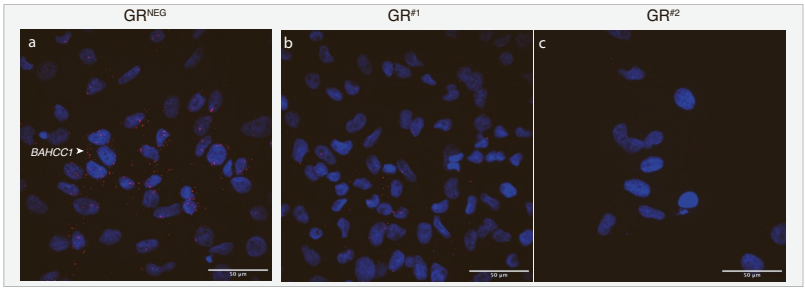
GR^NEG
GR^#1
GR^#2
a
b
c
BAHCC1

b

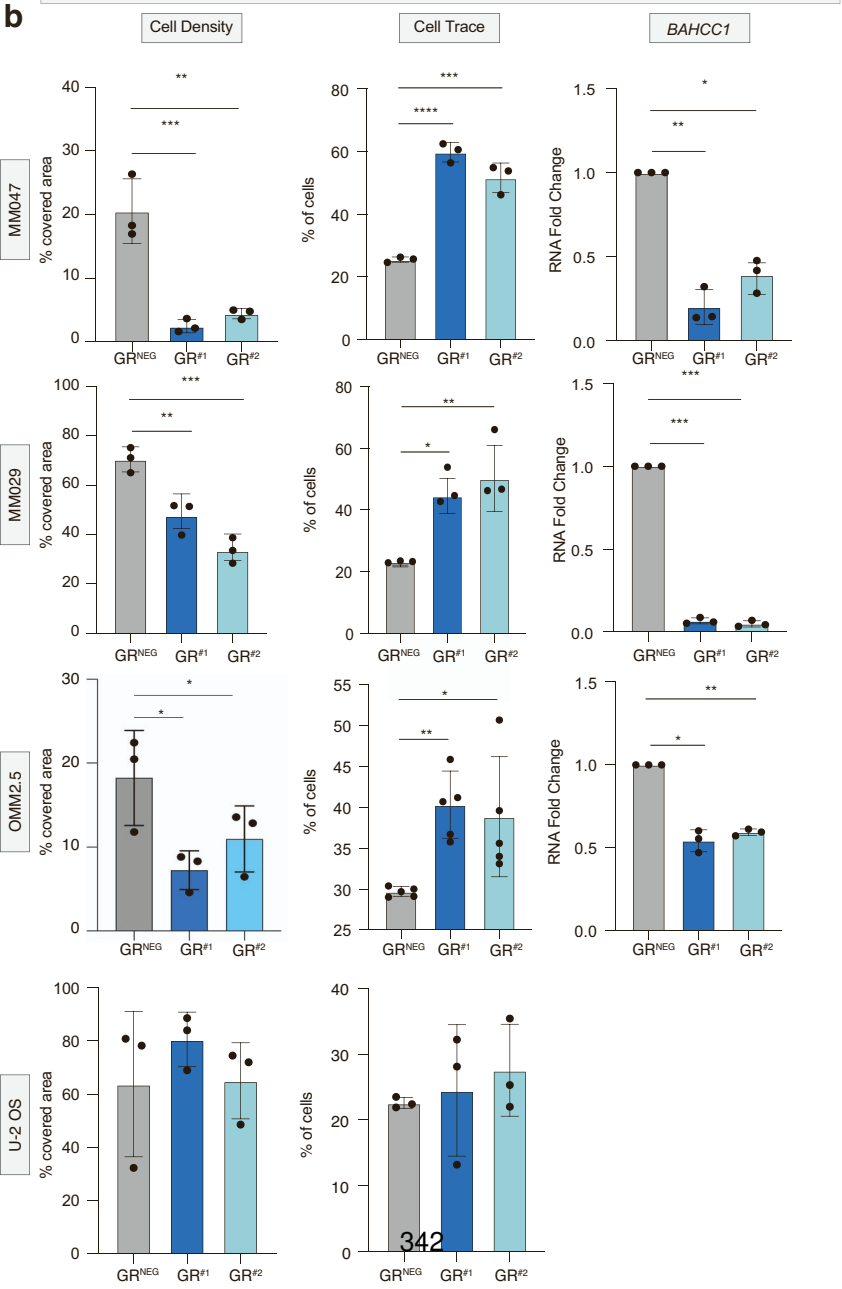
Cell Density
Cell Trace
BAHCC1
MM047
MM029
OMM2.5
U-2 OS
% covered area
% of cells
RNA Fold Change
GR^NEG
GR^#1
GR^#2

Ext. Figure 3: BAHCC1 depletion impairs SKCM and UVM cells proliferation

a. RNA FISH was performed for BAHCC1 in 501mel and MM047 transfected with GapmeR^{NEG} (GR^{NEG}), GapmeR$^{\#1}$ (GR$^{\#1}$) and GapmeR$^{\#2}$ (GR$^{\#2}$). Scale bars are indicated.

b. **Left panel**; Cell coverage quantification of crystal violet staining of cells transfected with GapmeR^{NEG} (GR^{NEG}), GapmeR$^{\#1}$ (GR$^{\#1}$) and GapmeR$^{\#2}$ (GR$^{\#2}$) in SKCM cells (MM047 and MM029) or UVM cells (OMM2.5). **Middle panel;** CellTrace staining was measured by FACS in the cells used in the left panel and results are represented as % of slow proliferative cells considering an arbitrary threshold between 20-30% in the GapmeR^{NEG} (NEG) control. **Right panel;** Relative BAHCC1 expressions upon transfection with GapmeR^{NEG} (NEG), GapmeR$^{\#1}$ (GR$^{\#1}$) and GapmeR$^{\#2}$ (GR$^{\#2}$) were measured by RT-qPCR in the cells used in the left panel (with the exception of U-2 OS cells that do not express BAHCC1). Bars represent mean values of three different experiments (Biological triplicates) (+/- SEM). Two-way ANOVA using Šídák's multiple comparisons test.

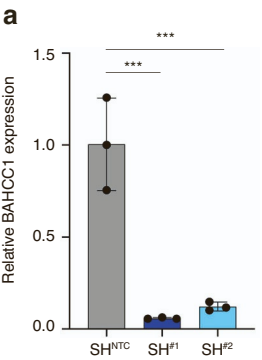
a
***
***
1.5
1.0
0.5
0.0
Relative BAHCC1 expression
SHNTC
SH#1
SH#2

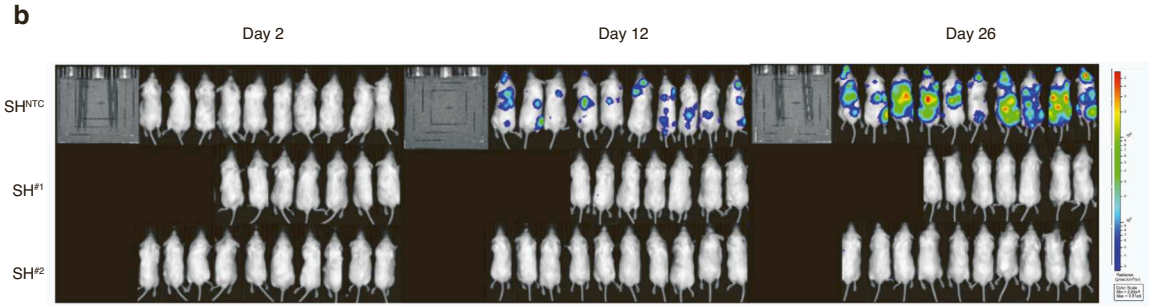
b
Day 2
Day 12
Day 26
SHNTC
SH#1
SH#2

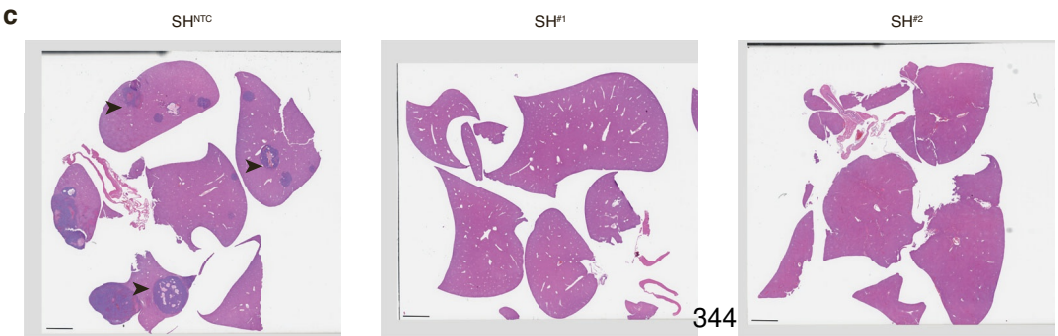
c
SHNTC
SH#1
SH#2

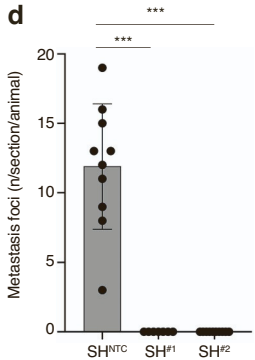
d
***
***
20
15
10
5
0
Metastasis foci (n/section/animal)
SHNTC
SH#1
SH#2

Ext Figure 4: Cell derived xenografts engraftment and metastases require BAHCC1.

a. Invalidation of BAHCC1 using $SH^{\#1}$ and $SH^{\#2}$ was evaluated in 501mel cells right before injection in animals through RT-qPCR, using shNTC as control. Two-way ANOVA Dunnet's multiple comparisons test.

b. Bioluminescence imaging with IVIS of intracardiac group mice at day 2, day 12 and day 26 post injection.

c. Representative H&E-stained liver tissue sections derived from NSG mice injected intracardiac with 501mel cells expressing SH^{NTC} (control) or $SH^{\#1}$ and $SH^{\#2}$(targeting BAHCC1). Black arrow marks some metastatic foci in the tissue. On the bottom left is represented the scale bar corresponding to 2mm.

d. Histogram showing the number of metastatic foci detectable in each tissue section per mouse which is significantly reduced in $SH^{\#1}$ and $SH^{\#2}$ compared to SH^{NTC}.

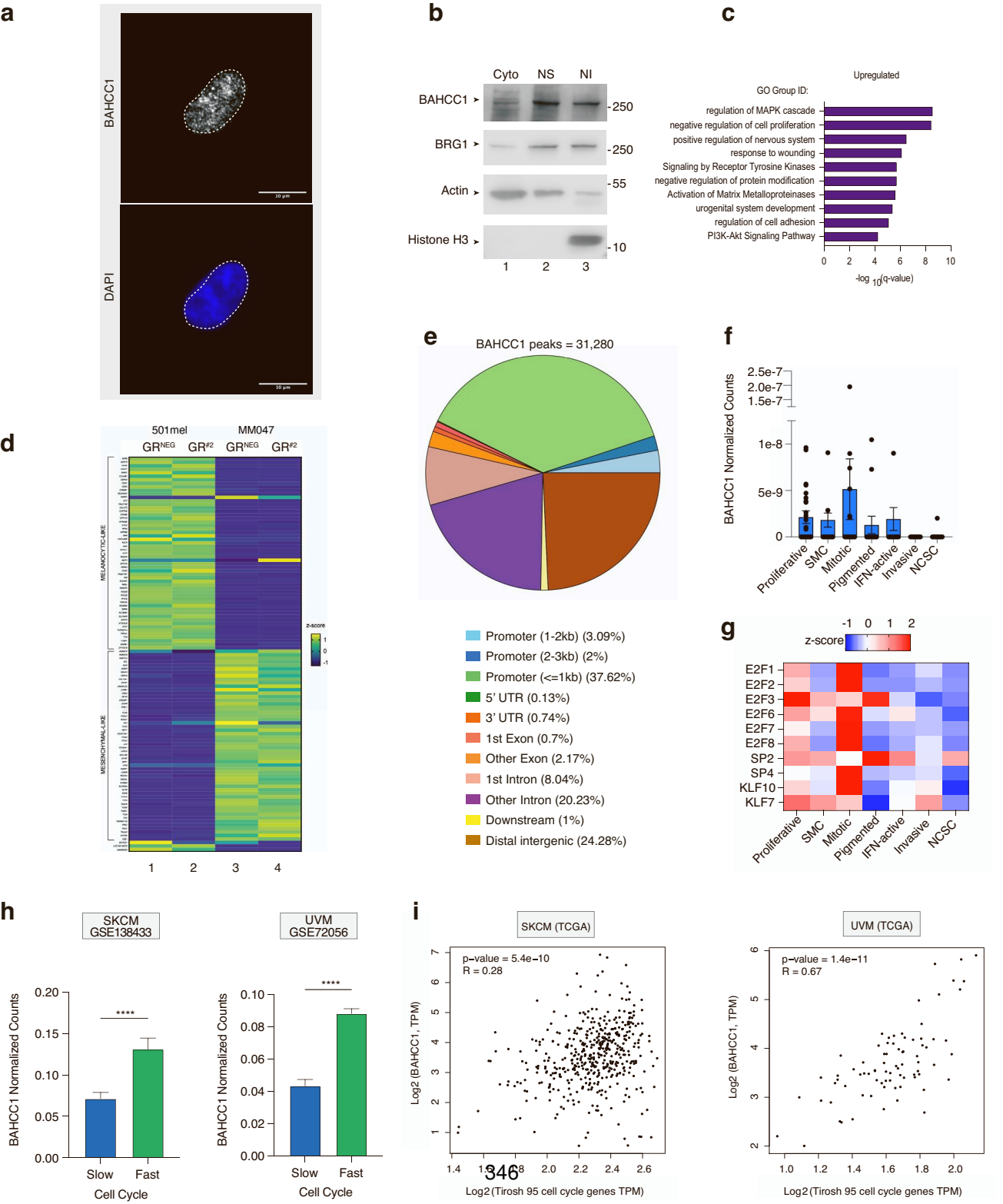
a
BAHCC1
DAPI
b
Cyto
NS
NI
BAHCC1
BRG1
Actin
Histone H3
250
250
55
10
1
2
3
c
Upregulated
GO Group ID:
regulation of MAPK cascade
negative regulation of cell proliferation
positive regulation of nervous system
response to wounding
Signaling by Receptor Tyrosine Kinases
negative regulation of protein modification
Activation of Matrix Metalloproteinases
urogenital system development
regulation of cell adhesion
PI3K-Akt Signaling Pathway
0
2
4
6
8
10
-log 10(q-value)
d
501mel
MM047
GRNEG
GR#2
GRNEG
GR#2
MELANOCYTIC-LIKE
MESENCHYMAL-LIKE
z-score
1
2
3
4
e
BAHCC1 peaks = 31,280
Promoter (1-2kb) (3.09%)
Promoter (2-3kb) (2%)
Promoter (<=1kb) (37.62%)
5' UTR (0.13%)
3' UTR (0.74%)
1st Exon (0.7%)
Other Exon (2.17%)
1st Intron (8.04%)
Other Intron (20.23%)
Downstream (1%)
Distal intergenic (24.28%)
f
BAHCC1 Normalized Counts
2.5e-7
2.0e-7
1.5e-7
1e-8
5e-9
0
Proliferative
SMC
Mitotic
Pigmented
IFN-active
Invasive
NCSC
g
-1
0
1
2
z-score
E2F1
E2F2
E2F3
E2F6
E2F7
E2F8
SP2
SP4
KLF10
KLF7
Proliferative
SMC
Mitotic
Pigmented
IFN-active
Invasive
NCSC
h
SKCM
GSE138433
UVM
GSE72056
BAHCC1 Normalized Counts
0.20
0.15
0.10
0.05
0.00
****
Slow
Fast
Cell Cycle
BAHCC1 Normalized Counts
0.10
0.08
0.06
0.04
0.02
0.00
****
Slow
Fast
Cell Cycle
i
SKCM (TCGA)
p-value = 5.4e-10
R = 0.28
Log2 (BAHCC1, TPM)
Log2 (Tirosh 95 cell cycle genes TPM)
UVM (TCGA)
p-value = 1.4e-11
R = 0.67
Log2 (BAHCC1, TPM)
Log2 (Tirosh 95 cell cycle genes TPM)

Ext. Figure 5: BAHCC1 localizes at the promoter of E2F/KLF dependent genes

a. Immunostaining of BAHCC1 in 501mel cells using an anti-BAHCC1 antibody together with DAPI staining. Scale bars are indicated.

b. Immunoblot of the indicated proteins in 501mel protein sub fractions corresponding to cytoplasm (Cyto), nuclear soluble (NS) and nuclear insoluble (NI). BRG1 and Actin were used as positive controls for NS/NI and Cyto respectively.

c. GO analysis of the 82 co-upregulated genes between 501mel and MM047 upon BAHCC1 KD. The first 10 most significant annotation groups are listed from top to bottom according to the -log10(q-value).

d. Genes characterizing the melanocytic-type and mesenchymal-like transcription signatures (Widmer et al., 2012) have been plotted on a heatmap and are shown in relation to their expression in 501mel or MM047 following expression of controlled or anti-BAHCC1 GAPMER. RPKM values are represented as z-score. The color key shows the $\log_2$ expression values. Green color stands for high expression and dark violet for low expression.

e. Pie chart displaying the distribution of 31,280 BAHCC1 peaks identified in this work with respect of genomic annotations.

f. BAHCC1 expression among the different transcriptional states previously identified in Rambow melanoma PDXs (n=674 cells).

g. Heatmap representing the regulon activity of E2F, Sp/KLF transcription factor family members obtained by SCENIC analysis in the different transcriptional states of Rambow PDX described in **(e)**.

h. BAHCC1 single cell expression retrieved from the GEO dataset GSE138433 and GSE72056 was separated in two groups of “Slow” and “Fast” cell cycle cells based on cell enrichment of 95 cell cycle genes identified by Tirosh and colleagues (4) (Ext. Table 6).

i. SKCM (n=469) and UVM (n=81) Spearman correlation between BAHCC1 expression and Tirosh cell cycle signature (95 genes). Values were retrieved from TCGA. Analysis was done using GEPIA2.

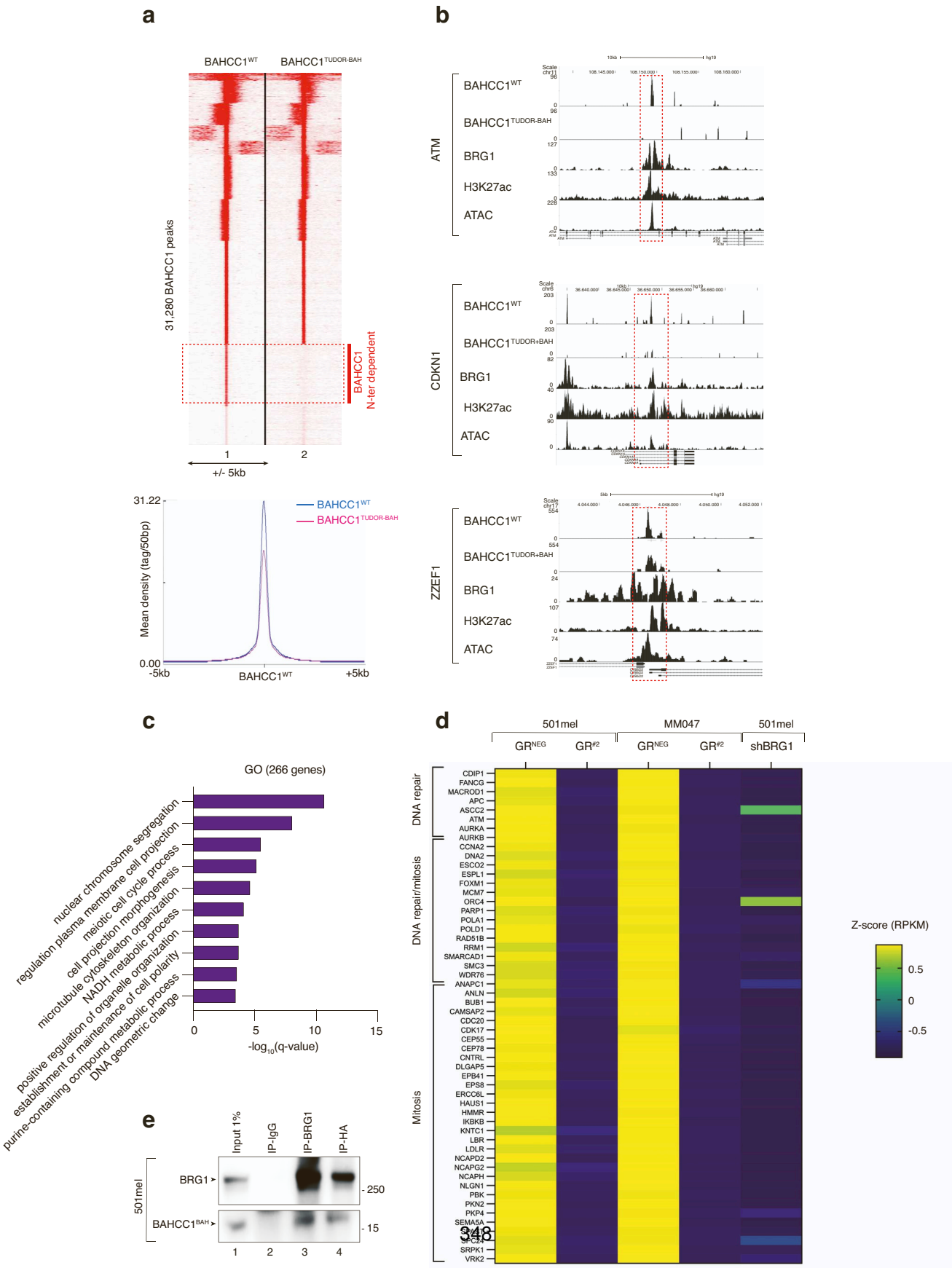
a
BAHCC1WT
BAHCC1TUDOR-BAH
31,280 BAHCC1 peaks
BAHCC1 N-ter dependent
1
2
+/- 5kb
31.22
0.00
Mean density (tag/50bp)
BAHCC1WT
BAHCC1TUDOR-BAH
-5kb
+5kb
b
ATM
CDKN1
ZZEF1
BAHCC1WT
BAHCC1TUDOR-BAH
BAHCC1TUDOR+BAH
BRG1
H3K27ac
ATAC
c
GO (266 genes)
nuclear chromosome segregation
regulation plasma membrane cell projection
meiotic cell cycle process
cell projection morphogenesis
microtubule cytoskeleton organization
NADH metabolic process
positive regulation of organelle organization
establishment or maintenance of cell polarity
purine-containing compound metabolic process
DNA geometric change
0
5
10
15
-log10(q-value)
d
501mel
MM047
501mel
GRNEG
GR#2
GRNEG
GR#2
shBRG1
DNA repair
DNA repair/mitosis
Mitosis
CDIP1
FANCG
MACROD1
APC
ASCC2
ATM
AURKA
AURKB
CCNA2
DNA2
ESCO2
ESPL1
FOXM1
MCM7
ORC4
PARP1
POLA1
POLD1
RAD51B
RRM1
SMARCAD1
SMC3
WDR76
ANAPC1
ANLN
BUB1
CAMSAP2
CDC20
CDK17
CEP55
CEP78
CNTRL
DLGAP5
EPB41
EPS8
ERCC6L
HAUS1
HMMR
IKBKB
KNTC1
LBR
LDLR
NCAPD2
NCAPG2
NCAPH
NLGN1
PBK
PKN2
PKP4
SEMA5A
SPC24
SRPK1
VRK2
Z-score (RPKM)
0.5
0
-0.5
e
Input 1%
IP-IgG
IP-BRG1
IP-HA
501mel
BRG1
BAHCC1BAH
250
15
1
2
3
4

Ext. Figure 6: BAHCC1 and BRG1 co-regulate expression of cell cycle and DNA repair genes

a. **Upper panel**; Read density clustering using SeqMINER showing the colocalization between $BAHCC1^{WT}$ and $BAHCC1^{TUDOR\text{-}BAH}$ in the 31,280 $BAHCC1^{WT}$ occupied sites. Red box indicates the cluster of BAHCC1 N-terminal region dependent peaks. **Lower panel**; Meta-profiles of $BAHCC1^{WT}$ and $BAHCC1^{TUDOR\text{-}BAH}$ signals around the 31,280 BAHCC1 peaks.

b. Captures of the UCSC genome browser (GRCh38/hg19) showing the ChIP-seq profiles for $BAHCC1^{WT}$, $BAHCC1^{TUDOR\text{-}BAH}$, BRG1, H3K27ac and ATAC-seq in 501mel corresponding to the promoter regions of ATM, ZZEF1 and CDKN1 genes. ZZEF1 is used as a control gene recruiting both $BAHCC1^{WT}$ and $BAHCC1^{TUDOR\text{-}BAH}$. RefSeq annotated genes are displayed at the bottom.

c. Gene annotation analysis of the 266 genes co-regulated by BRG1 and BAHCC1 in 501mel. The histogram shows the top 10 deregulated biological pathways according to the $-\log_{10}$(q-value).

d. Heatmap of the genes involved in DNA repair and/or mitosis and significantly co-regulated by BAHCC1 and BRG1 in melanoma cells as indicated. $GapmeR^{\#2}$ ($GR^{\#2}$) was used to knock-down BAHCC1. $GapmeR^{NEG}$ (GR^{NEG}) was used as negative control.

e. Following the stable overexpression of a $HA\text{-}BAHCC1^{BAH}$ domain in 501mel cells, immunoprecipitation was carried out using anti-IgG (control), anti-BRG1 and anti-HA antibodies. Following SDS-PAGE, proteins were immunoblotted as indicated. Molecular sizes are indicated.

a

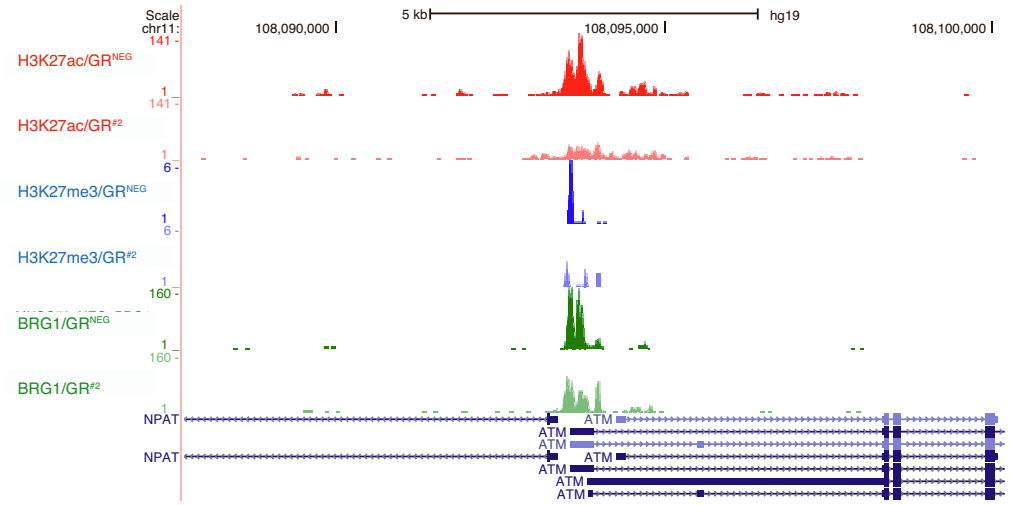
Scale
chr11:
5 kb
hg19
108,090,000
108,095,000
108,100,000
H3K27ac/GR^NEG
H3K27ac/GR^#2
H3K27me3/GR^NEG
H3K27me3/GR^#2
BRG1/GR^NEG
BRG1/GR^#2
NPAT
ATM

b

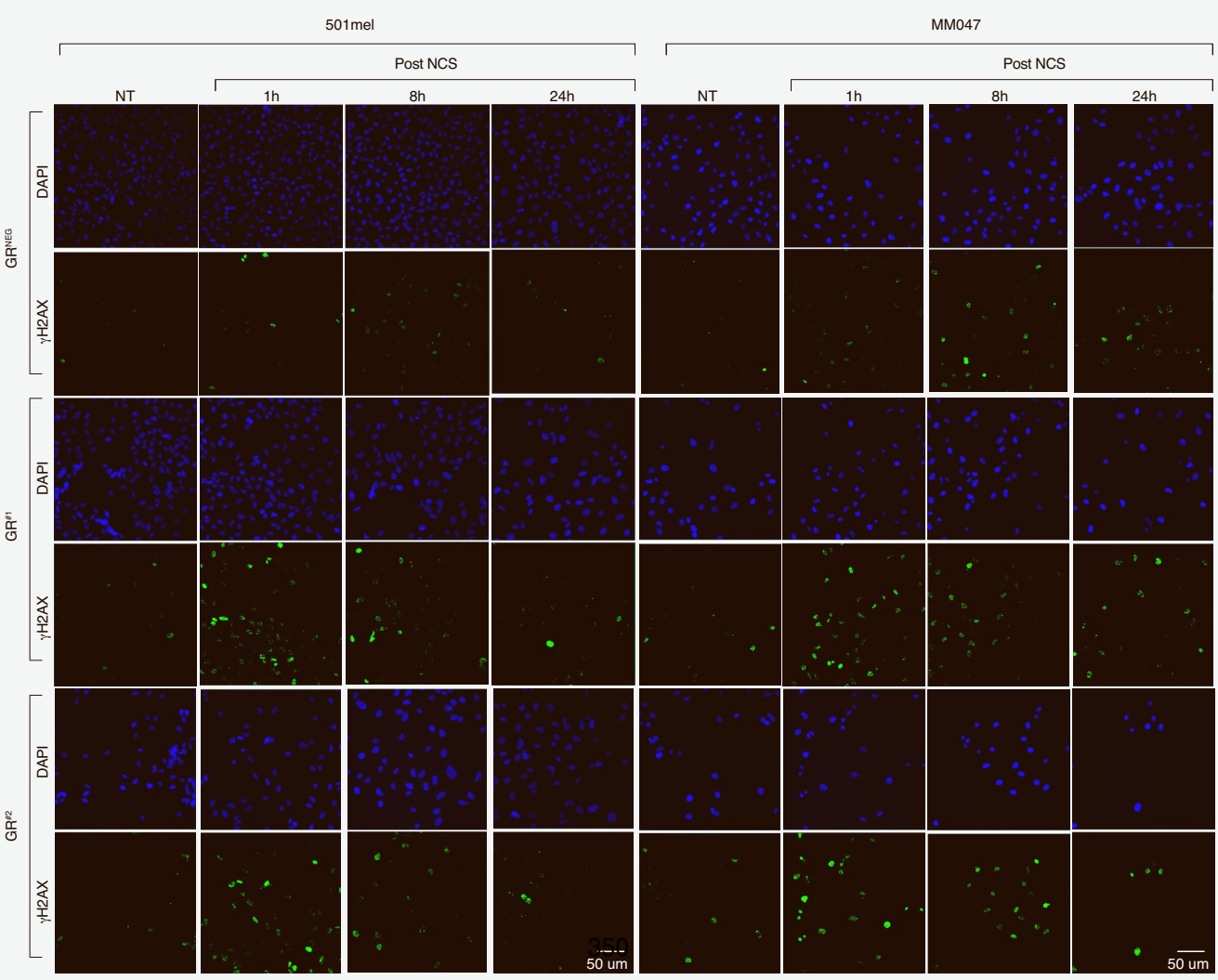
501mel
MM047
Post NCS
NT
1h
8h
24h
GR^NEG
GR^#1
GR^#2
DAPI
γH2AX
50 um

Ext. Figure 7: BAHCC1 depletion impairs double-stranded DNA repair

a. Genome Browser overview of H3K27ac, H3K27me3 and BRG1 at ATM's promoter. Overview obtained with GapmeR control (GR^{NEG}) was compared to that obtained with GapmeR against BAHCC1 ($GR^{\#2}$).

b. Immunofluorescence for γH2AX in 501mel and MM047 in basal conditions or upon DNA damage in presence or absence of BAHCC1. Images are representative of the quantification of Figure 7. DAPI staining is shown. Scale bars are shown.

a

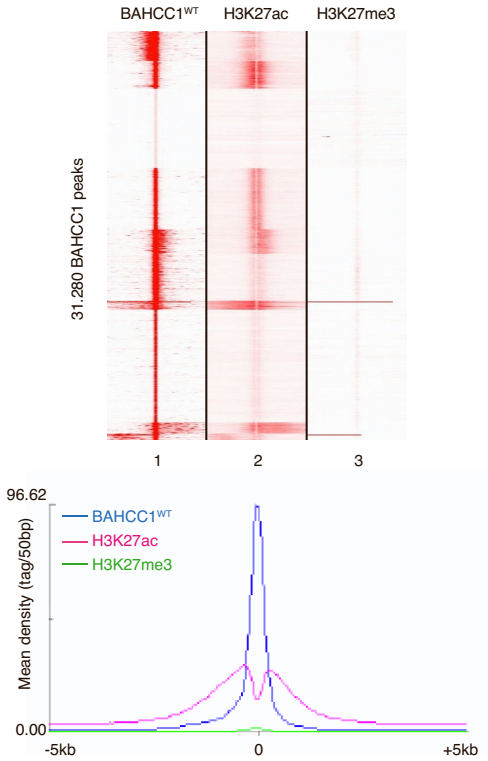
BAHCC1WT
H3K27ac
H3K27me3
31,280 BAHCC1 peaks
1
2
3
96.62
BAHCC1WT
H3K27ac
H3K27me3
Mean density (tag/50bp)
0.00
-5kb
0
+5kb

b

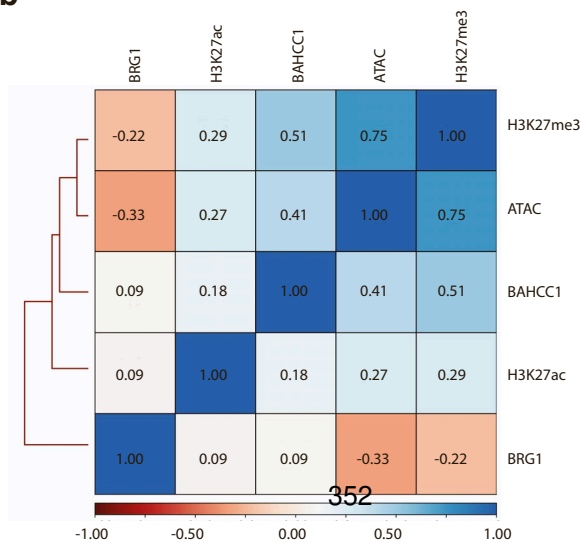
BRG1
H3K27ac
BAHCC1
ATAC
H3K27me3
-0.22
0.29
0.51
0.75
1.00
H3K27me3
-0.33
0.27
0.41
1.00
0.75
ATAC
0.09
0.18
1.00
0.41
0.51
BAHCC1
0.09
1.00
0.18
0.27
0.29
H3K27ac
1.00
0.09
0.09
-0.33
-0.22
BRG1
-1.00
-0.50
0.00
0.50
1.00

Ext. Figure 8: BAHCC1 does not co-localized with H3K27me3

a. **Upper panel**; Read density clustering using SeqMINER showing the colocalization between BAHCC^{WT}, H3K27me3 and H3K27ac at the 31,280 BAHCC1^{WT} occupied sites. Red box indicates the cluster of BAHCC1 N-terminal region dependent peaks. **Lower panel**; Meta-profiles of BAHCC^{WT}, H3K27me3 and H3K27ac around the 31,280 BAHCC1^{WT} occupied sites.

b. Heatmap representing the hierarchical clustering of Spearman's correlation between BAHCC1, H3K27ac, BRG1, ATAC and H3K27me3 genome wide multi bigwig summary distribution in 501mel cells.

Cells	Driver mutations	Cancer	Phenotypes
501mel	BRAF V600E	Cutaneous	Melanocyte-like
MM001	Triple-WT	Cutaneous	Melanocyte-like
MM117	Triple-WT	Cutaneous	Melanocyte-like
MM011	NRAS Q61L	Cutaneous	Melanocyte-like
MM029	BRAF V600K	Cutaneous	Mesenchymal-like
MM031	Triple-WT	Cutaneous	Melanocyte-like
MM034	BRAF V600E	Cutaneous	Melanocyte-like
MM047	NRAS Q61R	Cutaneous	Mesenchymal-like
MM057	NRAS Q61L	Cutaneous	Melanocyte-like
MM074	BRAF V600E	Cutaneous	Melanocyte-like
MM087	Triple-WT	Cutaneous	Melanocyte-like
MM099	BRAF V600E	Cutaneous	Mesenchymal-like
MM118	Triple-WT	Cutaneous	Melanocyte-like
SKMEL-28	BRAF V600E	Cutaneous	Melanocyte-like
SKMEL-5	BRAF V600E	Cutaneous	Melanocyte-like
OMM1.3	GNAQ Q209P	Uveal	
OMM2.5	GNAQ Q209P	Uveal	

Extended Table 1: Melanoma cells used in this study

The melanoma cells, their driver mutations and phenotypes are indicated.

N°	Histology/cell type	Age	Sex	
Nevi 1	Naevus	62yo	M	
Nevi 2	Naevus	45yo	F	
				Mutation
Tumor 1	Primary SSM melanoma	50yo	M	BRAF, NRAS & c-kit negative
Tumor 2	Melanoma hypodermal metastasis	66yo	F	BRAF V600E
Tumor 3	Primary SSM melanoma	70yo	M	BRAF V600E
Tumor A	Spindle	84yo	F	GNAQ Q209P
Tumor B	Epitheloid	69yo	M	GNA11 Q209L
Tumor C	Mixed	84yo	M	WT
Tumor D	Spindle	65yo	M	GNA11 Q209L

Extended Table 7: Human tumor samples

Information about human tumor samples are summarized in this table

<u>Preliminary draft:</u> Cancer cell transcriptional landscape primes the development of resistance to synthetic ecteinascidins

Clara Maréchal[1, 2, 3, 4], **Julian Obid**[1, 2, 3, 4], Maguelone Nogaret [1, 2, 3, 4], Philippe Catez[1, 2, 3, 4], Clara Capelli[1, 2, 3, 4], Max Cigrang[1, 2, 3, 4, 5] and Frédéric Coin [1, 2, 3, 4, 5]

[1]Institut de Génétique et de Biologie Moléculaire et Cellulaire Illkirch Cedex, C.U. Equipe Labélisée Ligue contre le Cancer 2022, Strasbourg, France

[2] Centre National de la Recherche Scientifique, UMR7104, 67404 Illkirch, France

[3] Institut National de la Santé et de la Recherche Médicale, U1258, 67404 Illkirch, France

[4] Université de Strasbourg, 67404 Illkirch, France

[5] Corresponding authors, fredr@igbmc.fr, cigrang@igbmc.fr

Tel: +33 3 88 65 34 49

Key words: Therapeutic Resistance, Lurbinectedin, Ecteinascidins, ABCB1, Melanoma

Abstract

Synthetic ecteinascidins are engineered analogs of marine-derived compounds with potent anticancer activity that induce DNA damage and disrupt oncogenic transcription. Lurbinectedin, the first FDA-approved compound in this class, is used to treat relapsed small cell lung cancer (SCLC). We recently demonstrated that lurbinectedin and its analogs, ecubectedin and PM54, currently undergoing clinical testing, induce apoptosis in differentiated and undifferentiated melanoma cells. However, no mechanisms of resistance to synthetic ecteinascidins have been functionally characterized, limiting the ability to anticipate or overcome therapeutic failure. Here, we establish the first in vitro models of acquired resistance by exposing undifferentiated melanoma cells to escalating concentrations of synthetic ecteinascidins. Resistant cells exhibit broad cross-resistance mediated by overexpression of the drug efflux transporter ABCB1, driven by focal amplification and elevated AP-1/TEAD activity, characteristic of the undifferentiated state. In contrast, differentiated melanoma cells were intrinsically unable to acquire resistance due to low AP-1/TEAD activity and FBXO21-mediated ABCB1 degradation, linked to the absence of its stabilizers CD44 and PIM1. ABCB1 overexpression conferred resistance across multiple clinically relevant cancer models, whereas pharmacological inhibition restored intracellular drug accumulation and cytotoxicity. These findings define a druggable, cell state-dependent resistance mechanism to synthetic ecteinascidins and support biomarker-guided strategies to improve clinical outcomes.

Introduction

Synthetic ecteinascidins are rationally engineered analogs of the marine-derived compound trabectedin, designed to enhance potency and improve pharmacokinetic properties (Le et al., 2015; Gadducci and Cosio, 2022; Povo-Retana et al., 2024). They constitute a relatively new class of DNA-interactive chemotherapeutic agents with significant anticancer activity. We previously elucidated their mechanism of action, which involves covalent binding to CpG-rich DNA regions within open chromatin, particularly at promoters of highly transcribed oncogenes. This binding stalls the transcriptional machinery and potently suppresses oncogene expression (Cigrang et al., 2025). Additionally, drug-induced DNA adducts are recognized by the XPG and XPF–ERCC1 endonucleases, triggering DNA double-strand breaks and apoptosis (Santamaría Nuñez et al., 2016; Costanzo et al., 2022).

Lurbinectedin, the first synthetic ecteinascidin approved for clinical use, received accelerated FDA approval in 2020 as second-line treatment for relapsed small cell lung cancer (SCLC) following platinum-based therapy, representing the first novel therapeutic option for SCLC in over two decades (Trigo et al., 2020; Manzo et al., 2022). Recently, we demonstrated the preclinical efficacy of lurbinectedin and two additional ecteinascidin analogs, ecubectedin/PM14 and PM54, in melanoma models resistant to both targeted therapies and immune checkpoint inhibitors (Cigrang et al., 2025). These promising results have spurred ongoing clinical trials of lurbinectedin and related analogs in diverse malignancies, including mesothelioma, breast cancer, and melanoma (Metaxas et al., 2020; Boni et al., 2022; Calles et al., 2025). Furthermore, multiple Phase III trials are evaluating combination regimens to enhance therapeutic benefits (Aix et al., 2023; Calles et al., 2025). For example, the IMforte Phase III study recently showed that combining PD-L1 blockade with lurbinectedin significantly improved clinical outcomes (Paz-Ares et al., 2025), highlighting the immunomodulatory potential of this drug class (Xie et al., 2019; Dumoulin et al., 2022; Chakraborty et al., 2024).

Despite these advances, the durability of response to synthetic ecteinascidins remains limited, underscoring the urgent need to anticipate and overcome resistance mechanisms. To date, no models of acquired resistance to synthetic ecteinascidins have been established in vitro or in vivo in any cancer type, leaving the molecular basis of resistance unresolved. Given that these compounds require nuclear access to exert their effects, drug efflux via ATP-binding cassette (ABC) transporters represents a plausible resistance mechanism, as observed with other chromatin-targeting agents (Berico et al., 2021; Kurimchak et al., 2022). Among these, the efflux transporter ABCB1 (also known as MDR1 or P-

glycoprotein, P-gp) has emerged as a key mediator of multidrug resistance through its ability to expel structurally diverse chemotherapeutic agents from cancer cells (Rees, Johnson, and Lewinson, 2009). Although first-generation ABCB1 inhibitors were limited by systemic toxicity, next-generation compounds with improved safety profiles are now advancing in preclinical and clinical development (Engle and Kumar, 2022; Moore et al., 2023).

The intrinsic phenotypic plasticity of melanoma cells enables dynamic transitions between differentiated and undifferentiated cell states, offering a robust model to dissect resistance mechanisms driven by transcriptional reprogramming (Rambow et al., 2019; Arozarena et al., 2019). While differentiated melanoma cells are highly proliferative and generally drug-sensitive, therapeutic stress induces phenotype switching, generating drug-tolerant, undifferentiated populations that seed relapse and exhibit broad chemoresistance and immune evasion. These transitions are governed by lineage-specific transcription factors MITF/SOX10 in the differentiated state, and by AP-1/TEAD-driven programs in the undifferentiated state (Verfaillie et al., 2015; Wouters et al., 2020; Jalil et al., 2024). Leveraging this phenotypic plasticity, we established the first in vitro models of acquired resistance to synthetic ecteinascidins in undifferentiated melanoma models and identified a cell state-specific resistance mechanism. Specifically, we demonstrate that undifferentiated melanoma cells, but not their differentiated counterparts, acquire cross-resistance to multiple synthetic ecteinascidins through genomic amplification and AP-1/TEAD-dependent transcriptional upregulation of ABCB1, coupled with enhanced stabilization mediated by the glycoprotein CD44 and the serine/threonine kinase PIM1. In contrast, differentiated melanoma cells, characterized by low AP-1/TEAD activity and reduced expression of these stabilizing factors, direct ABCB1 toward proteasomal degradation via the E3 ubiquitin ligase FBXO21, thereby preventing resistance acquisition. Functionally, ABCB1 overexpression impairs both ecteinascidin-induced DNA damage and oncogene repression, conferring resistance across melanoma, SCLC, and colorectal cancer models. However, pharmacologic inhibition of ABCB1 or its upstream regulators, including AP-1/TEAD, CD44, and PIM1, restores intracellular drug accumulation and resensitizes resistant cells to ecteinascidin-induced apoptosis.

Together, these findings define a multilayered, cell state-specific and targetable AP-1/TEAD–CD44/PIM1–ABCB1 resistance axis in melanoma and, more broadly, provide a mechanistic framework to anticipate and overcome ecteinascidin resistance, supporting biomarker-guided combination strategies to prolong clinical responses.

Results

Establishment of melanoma cells with acquired resistance to synthetic ecteinascidins

Although the synthetic ecteinascidin lurbinectedin is clinically approved for treating patients with SCLC, previous attempts to establish lurbinectedin-resistant SCLC cell lines have consistently failed (personal communications). Given our recent work showing the high cytotoxic impact of synthetic ecteinascidins on melanoma cells, irrespective of their cellular phenotype, but also the well-documented propensity of melanoma cells to develop therapeutic resistance through cellular plasticity (Arozarena et al., 2019; Rambow et al., 2019; Berico et al., 2021; Rubanov et al., 2022), we aimed to establish synthetic ecteinascidin-resistant cell lines using these cellular models. We chronically exposed three differentiated melanoma cell lines (SKMEL28, 501mel, IGR37), one differentiated patient-derived cell culture (MM074) and two undifferentiated melanoma patient-derived cell cultures (MM099, MM029) to gradually increasing doses of lurbinectedin (lurbi), ecubectedin (ecub), or PM54. Initial drug concentrations were set at one-third of their respective IC50 values (Cigrang et al., 2025) (**Figure 1a**). Five out of the six melanoma cell types failed to survive the treatments beyond a few weeks, and repeated attempts did not yield resistant cells. However, a subset of undifferentiated MM029 cells gradually acquired tolerance to the drugs. Resistance, defined as sustained cell proliferation in drug concentrations at least 10-fold higher than the initial IC50 values, was achieved after 6 to 8 months of chronic exposure. Ultimately, we successfully established three synthetic ecteinascidin-resistant MM029 cell lines, designated as $MM029^{lurbi\text{-}R}$, $MM029^{ecub\text{-}R}$, and $MM029^{PM54\text{-}R}$. Subsequent IC50 measurements indicated that these cells exhibited 20- to 100-fold increased resistance to their respective drugs compared to the parental, drug-naïve MM029 cell line (**Figures 1b-d and Supplemental Table 1**). Strikingly, all three resistant lines displayed significant cross-resistance (**Figures 1b-d and Supplemental Table 1**), and the acquisition of resistance was accompanied phenotypically by decreased proliferation rates (**Figure 1e**), increased cellular senescence (**Figure 1f**), and reduced invasive capacities (**Figure 1g**).

Our previous work demonstrated that synthetic ecteinascidins exert cytotoxic effects primarily by downregulating critical oncogenes and by inducing DNA double-strand breaks, culminating in apoptosis (Cigrang et al., 2025). Notably, treatment of the newly generated resistant cells with ecteinascidins no longer reduced the expression of oncogenes such as *AMIGO2, EGFR, FOSL1* or *MYC (***Figure 1h)**, and no longer induced any cytostatic effect (**Figure 1i**), in stark contrast to parental MM029 cells.

Immunoblot and flow cytometry analysis revealed that markers of DNA double-strand breaks (γH2AX) and apoptosis (cleaved Caspase-3, cleaved PARP and Annexin V) were no longer induced following drug treatment in ecteinascidin-resistant cells **(Figure 1j-k).** Conversely, drug-sensitive MM029 cells exhibited pronounced induction of apoptotic cell death and DNA damage markers.

Collectively, these findings demonstrate that in vitro resistance to synthetic ecteinascidins can indeed be acquired. Resistant cells exhibit a loss of both the transcriptional repression and the DNA-damaging effects that are characteristic of these compounds. Furthermore, the observed cross-resistance suggests that a common underlying mechanism may contribute to cross-resistance against the three synthetic ecteinascidins.

Acquired resistance to synthetic ecteinascidins is associated with transcriptional reprogramming in melanoma cells

To investigate the molecular mechanisms underlying the acquired resistance to synthetic ecteinascidins, we performed bulk RNA sequencing (RNA-seq). We observed substantial gene expression changes in all three resistant cell lines, with hundreds of genes significantly up- or downregulated compared to parental MM029 cells **(Figures 2a-c and Supplemental Table 2)**. Although the transcriptional alterations varied considerably among the individual resistant cell lines (**Supplemental Figure 1a**), we identified two distinct sets of commonly deregulated genes. Specifically, 244 genes were commonly upregulated and 678 genes commonly downregulated in $MM029^{lurbi\text{-}R}$, $MM029^{ecub\text{-}R}$, and $MM029^{PM54\text{-}R}$ cells **(Figure 2d and Supplemental Figure 1b)**. Gene Ontology and Gene Set Enrichment Analysis did not identify significant correlations among the commonly upregulated genes **(Supplemental Figures 1c and 1e**). However, among the commonly downregulated genes, we unexpectedly observed significant enrichments for gene sets associated with neuronal development/differentiation, cell migration, and epithelial-to-mesenchymal transition **(Supplemental Figures 1d-e**). Upon closer inspection of gene expression changes related to well-characterized transcriptomic melanoma cell-state signatures (Rambow et al., 2018; Pozniak et al., 2024), a notable loss of neural crest stem cell (NCSC) and invasive/mesenchymal markers in resistant cells emerged (**Supplemental Figure 1f-g**). Melanoma cells exhibiting an undifferentiated/mesenchymal phenotype, such as MM029 cells, typically emerge during therapy and have been shown to be the main drivers conferring resistance to MAPK inhibitors (MAPKi) and immune checkpoint inhibitors (ICI) (Rambow et

al., 2019; Pozniak et al., 2024). However, the MM029 cells resistant to synthetic ecteinascidins appeared to downregulate the transcriptional programs associated with this undifferentiated state, as evidenced by reduced expression of genes previously implicated in ICI resistance (Hugo et al., 2015, 2016) (**Supplemental Figure 1h**). Of note, the ecteinascidin-resistant cells also exhibited significantly reduced TIDE scores (a computational tool to model immune dysfunction and exclusion caused by cancer cells based on their transcriptome), thus predicting an enhanced sensitivity to ICIs compared to $MM029^{WT}$ cells (Jiang et al., 2018) (**Supplemental Figure 1i**). In conclusion, the acquired resistance of MM029 melanoma cells to synthetic ecteinascidins is associated with substantial transcriptomic reprogramming, characterized by reduced expression of undifferentiated/mesenchymal cell state markers and potentially increased immunogenicity and sensitivity to ICIs.

ABCB1 is overexpressed in melanoma cells resistant to synthetic ecteinascidins

Upon analyzing the 244 commonly upregulated genes, we observed *ABCB1* consistently ranked as the most prominently overexpressed gene across all three resistant cell lines, with relative enrichments ranging approximately from 60-fold in $MM029^{ecub\text{-}R}$ cells to 250-fold in $MM029^{lurbi\text{-}R}$ cells **(Figures 2a-d)**. *ABCB1* encodes an ATP-dependent efflux pump with broad substrate specificity, transporting a wide range of hydrophobic compounds typically ranging from 200 to 1900 Daltons (Da) in molecular mass (Chufan, Sim and Ambudkar, 2015; Kodan et al., 2021). Given their average mass of approximately 800 Da, lurbi, ecub, and PM54 could potentially serve as substrates for ABCB1. RT-qPCR and immunoblotting confirmed ABCB1 overexpression in resistant cells **(Figures 2e-f)**. Flow cytometry assays using fluorescent dye Rhodamine123, an established ABCB1 substrate (Webb et al., 1996), revealed significantly enhanced cellular efflux capacities in all three synthetic ecteinascidin-resistant cell lines **(Figure 2g and Supplemental Figure 2a)**. Immunofluorescence assays further demonstrated an inverse correlation between ABCB1 expression and DNA double-strand break induction by synthetic ecteinascidins, as $MM029^{lurbi\text{-}R}$ cells no longer exhibited increased γH2AX levels following lurbinectedin treatment **(Figures 2h-i)**. Notably, under drug-naïve conditions, parental MM029 cells already exhibited elevated ABCB1 protein levels compared to other melanoma cell lines tested for resistance development **(Supplemental Figures 2b-c)**. Cut&Tag data revealed that the promoter of ABCB1 displayed a more open chromatin profile and increased transcriptional activity in MM029 cells compared to differentiated 501mel cells. Indeed, MM029 cells displayed a distinctly undifferentiated phenotype,

indicated by high SOX9 and AP-1 transcription factor protein levels (Verfaillie et al., 2015; Comandante-Lou et al., 2022) (**Supplemental Figure 2d**). In conclusion, these results indicate that ABCB1 overexpression is a consistent feature across resistant cell lines, correlating with increased drug efflux activity and reduced susceptibility to drug-induced DNA damage. Additionally, an initial basal expression level of ABCB1 seems to be necessary for the subsequent development of ecteinascidin resistance.

ABCB1 overexpression is mediated by focal amplification and AP-1/TEAD activity

We next sought to elucidate the molecular mechanisms driving ABCB1 overexpression in our resistant cellular models. Transcriptomic analysis revealed that resistant cells overexpressed multiple genes located within the 7q21.12 genomic region, which harbours *ABCB1* and other MDR-associated genes (**Figure 3a**). Chromosomal amplifications at this locus have been previously linked to drug resistance (Genovese et al., 2017). Consistent with this, copy number variation assays demonstrated a ~30-fold increase in ABCB1 copy number in MM029$^{lurbi\text{-}R}$ and MM029$^{PM54\text{-}R}$ cells, and a ~5-fold increase in MM029$^{ecub\text{-}R}$ cells compared to parental MM029 cells (**Figure 3b**).

Gene amplification events alone were unlikely to fully account for the extensive transcriptional rewiring and degree of ABCB1 upregulation, suggesting the involvement of additional regulatory mechanisms. To explore this, we performed regulon analysis of differentially expressed genes between resistant and sensitive cells. iRegulon analysis (Janky et al., 2014) identified TEAD4 as a candidate transcriptional regulator driving resistance (**Figure 3c**). TEAD factors have been previously implicated in melanoma cell state regulation through cooperation with AP-1, both playing key roles in undifferentiated melanoma cells (Verfaillie et al., 2015, Mauduit et al., 2021; Comandante-Lou et al., 2022). Fittingly, when comparing the transcription factors commonly upregulated in resistant cells with those upregulated in parental MM029 cells upon short drug exposures (Cigrang et al. 2025), the AP-1 factor FOS was identified **(Figure 3d)**. We subsequently confirmed that various AP-1 and TEAD transcription factors were upregulated in drug-resistant cells **(Figure 3e-f)**, and RNA-Seq data revealed AP-1 factor induction upon short drug treatments to be a common phenomenon across melanoma cells (**Figure 3g**). Importantly, Cut&Tag assays demonstrated that the AP-1 factor JUN was enriched at the ABCB1 promoter, suggesting a regulatory role (**Figure 3h**). Consistent with these observations, treatment of synthetic ecteinascidin-resistant cells with the AP-1 inhibitors SR11302 and Veratramine, as well as the TEAD inhibitor MGH-CP1, resulted in the downregulation of *ABCB1* expression (**Figure 3i**). This was

accompanied by the reduced expression of established AP-1/TEAD target genes, including *AXL* and *JUN*, whereas expression of the housekeeping gene *GAPDH* remained unaffected. Co-treatment with AP-1 or TEAD inhibitors partly restored sensitivity of resistant cells to lurbinectedin (**Figures 3j-l, Supplemental Table 1**). Together, these findings demonstrate that ABCB1 overexpression in ecteinascidin-resistant melanoma cells results from the combined effects of focal genomic amplifications and transcriptional activation by AP-1 and TEAD factors, which cooperatively sustain the drug-resistant phenotype.

ABCB1 inhibition resensitizes resistant cells to synthetic ecteinascidins through restoration of DNA binding

Our data strongly suggested that ABCB1 is involved in resistance to synthetic ecteinascidins. To functionally confirm this hypothesis, we first performed siRNA-mediated knockdown of ABCB1 in synthetic ecteinascidin-resistant cells (**Supplemental Figure 3a**). Loss of ABCB1 expression led to significant resensitization of MM029$^{lurbi\text{-}R}$, MM029$^{ecub\text{-}R}$, and MM029$^{PM54\text{-}R}$ cells to all three drugs (**Supplemental Figure 3b–d, Supplemental Table 1**). Next, we assessed the effects of pharmacological ABCB1 inhibitors (ABCB1i) on resistant cells. Using Rhodamine123 efflux assays, we determined the inhibitor concentrations necessary to effectively block efflux in resistant cells. A brief 4-hour treatment with Tariquidar, a specific ABCB1 and ABCG2 inhibitor (Kannan et al., 2010), blocked Rhodamine efflux starting at 25 nM (**Supplemental Figure 3e**). Verapamil, a clinically available calcium channel blocker and nonspecific ABCB1 inhibitor (Wu, Calcagno, and Ambudkar, 2008), blocked efflux at concentrations starting from 100 µM (**Supplemental Figure 3f**). Strikingly, treatment of resistant cells with effective ABCB1 inhibitor concentrations fully restored sensitivity to synthetic ecteinascidins (**Figures 4a–f, Supplemental Table 1**), as evidenced by the total re-establishment of cytostatic (**Figure 4g**) and cytotoxic effects (**Figure 4h**).

Given these findings, we investigated whether ABCB1 inhibition enables synthetic ecteinascidins to re-enter the nucleus of resistant cells. Previously, by performing chemical mapping of biotinylated synthetic ecteinascidins, we identified their genomic binding sites in MM029 cells (Cigrang et al., 2025). Strong binding was detected at transcriptionally active regions, including cell state-specific marker genes such as *AXL* and *TEAD4* (**Supplemental Figures 3g-h**). CUT&Tag-qPCR assays confirmed the binding of biotinylated lurbinectedin (Bio-lurbi) to these loci in MM029 cells (**Figures 4i–j**). In contrast, MM029$^{lurbi\text{-}}$

^{R} cells treated with Bio-lurbi alone showed no significant genomic enrichment; however, co-treatment with Tariquidar restored drug binding to levels comparable to those observed in MM029 cells. Correspondingly, co-treatment of MM029$^{lurbi\text{-}R}$ cells with lurbinectedin and Tariquidar reinstated the downregulation of these oncogenes (**Figures 4k–l**). Collectively, these data indicate that ABCB1-mediated drug efflux is a major mechanism underlying resistance to synthetic ecteinascidins. Importantly, ABCB1 inhibition reversed this resistance, restoring drug accumulation, genomic binding, oncogene repression and subsequent apoptosis.

ABCB1 overexpression drives resistance to synthetic ecteinascidins in different cancer cell types

To further elucidate the role of ABCB1 in the resistance to synthetic ecteinascidins, we performed lentiviral overexpression of ABCB1. MM029 cells infected with an ABCB1-encoding lentivirus (MM029^{ABCB1}) exhibited an 1,800-fold increase in ABCB1 mRNA expression compared to MM029 or control mCherry-expressing cells (MM029^{CTL}) **(Figure 5a)**. Immunoblot analysis confirmed ABCB1 overexpression at the protein level **(Figure 5b)**. MM029^{ABCB1} cells showed a 10- to 20-fold increase in IC_{50} values for synthetic ecteinascidins relative to MM029 and MM029^{CTL} cells **(Figures 5c-e)**. Notably, in all ABCB1-overexpressing cell lines (MM029$^{lurbi\text{-}R}$, MM029$^{ecub\text{-}R}$, MM029$^{PM54\text{-}R}$, and MM029^{ABCB1}), lurbi treatment failed to induce γH2AX accumulation, an effect that was restored by co-treatment with tariquidar **(Figure 5f)**. Considering the clinical use of lurbinectedin in SCLC patients, we also performed lentivirus-mediated overexpression of ABCB1 in DMS53 SCLC cells (DMS53^{ABCB1}) (**Figures g-h**). Once again, we observed that these cells exhibited reduced DNA damage induction (**Figure 5i**) and demonstrated approximately 10- to 20-fold increased resistance to synthetic ecteinascidin treatment (**Figure 5j**).

Given the well-established role of ABCB1 in mediating cross-resistance to multiple chemotherapeutics, including doxorubicin (Doxo) (Yin et al., 2021; Adorni et al., 2023), we next examined whether acquisition of resistance to an unrelated drug could confer cross-resistance to synthetic ecteinascidins. Because melanoma and SCLC cells are intrinsically refractory to Doxo, we used the initially Doxo-sensitive colorectal carcinoma cell line LoVo and rendered it resistant through chronic drug exposure (**Figure 6a**). The resulting LoVo$^{Doxo\text{-}R}$ cells exhibited robust ABCB1 overexpression at both the mRNA and protein levels (**Figures 6b–c**) and displayed increased cross-resistance to lurbi, ecub, and PM54

(**Figure 6d**). siRNA-mediated knockdown, and pharmacological inhibition of ABCB1 in LoVo$^{Doxo\text{-}R}$ cells significantly restored sensitivity to synthetic ecteinascidins (**Figures 6e–g**) and reinstated drug-induced DNA damage, as evidenced by γH2AX accumulation (**Figure 6h**). Of note, while Tariquidar treatment and *ABCB1* knockout fully restored ecteinascidin sensitivity in LoVo$^{Doxo\text{-}R}$ cells (**Figures 6e-g**), doxorubicin sensitivity was only partially restored (**Figure 6i**), suggesting that while ABCB1 is the exclusive mediator of ecteinascidin resistance, additional mechanisms contribute to doxorubicin resistance in this model. Collectively, these findings demonstrate that ABCB1 overexpression is sufficient to confer resistance to synthetic ecteinascidins across cancer types, including clinically relevant SCLC models, and that acquisition of resistance to other chemotherapeutics via ABCB1 upregulation can confer cross-resistance to synthetic ecteinascidins.

AP-1/TEAD-driven CD44 and PIM1 expression stabilizes ABCB1 in undifferentiated melanoma cells

Because differentiated/melanocytic melanoma cells failed to develop resistance to synthetic ecteinascidins, we next investigated the molecular basis for their inability to develop drug insensitivity. Differentiated IGR37 and SKMEL28 melanoma cells were transduced with an ABCB1-encoding lentivirus (IGR37^{ABCB1} and SKMEL28^{ABCB1}). Although ABCB1 mRNA levels were upregulated in both cell lines (**Figure 7a**), ABCB1 protein expression remained undetectable (**Figure 7b**). Treatment with the proteasome inhibitor MG132 restored ABCB1 protein accumulation in IGR37^{ABCB1} and SKMEL28^{ABCB1} cells (**Figure 7c**), whereas MG132 had no effect in undifferentiated MM029^{ABCB1} cells (**Figure 7d**). Consistently, immunoprecipitation analysis revealed robust ABCB1 ubiquitination in SKMEL28^{ABCB1} cells (**Figure 7e**), indicating that differentiated melanoma cells target ABCB1 for proteasomal degradation.

Although the regulation of ABCB1 stability is incompletely understood in melanoma cells, several E3 ubiquitin ligases, including FBXO21, have been reported to mediate ABCB1 degradation in other contexts (Ravindranath et al. 2015). Strikingly, FBXO21 knockdown increased ABCB1 protein levels in SKMEL28^{ABCB1} cells (**Figure 7f and Supplemental Figure 4a-b**), implicating FBXO21 as a mediator of ABCB1 degradation in differentiated melanoma cells. However, despite increased ABCB1 protein levels following FBXO21 silencing, we observed no corresponding increase in efflux activity (**Supplemental Figure 4c**) or drug resistance (**Supplemental Figure 4d**), suggesting that additional defects in ABCB1

trafficking, regulation, or maturation constrain its functional activity in differentiated cells. We further observed that FBXO21 was ubiquitously expressed across both differentiated and undifferentiated melanoma cell lines (**Supplemental Figure 4e**), indicating that FBXO21 expression levels alone are insufficient to account for the selective ABCB1 degradation observed in differentiated cells, or for the apparent stabilization in undifferentiated counterparts. Interestingly, the stemness-associated surface marker CD44 has been reported to protect ABCB1 from FBXO21-mediated ubiquitination and degradation (Ravindranath et al., 2015; Chen et al., 2018). In line with this, we found CD44 expression restricted to undifferentiated melanoma cells (**Supplemental Figures 4e-f**), suggesting a role in ABCB1 stabilization in this cell state. siRNA-mediated knockdown of CD44, combined with cycloheximide treatment to block de novo protein synthesis, markedly accelerated ABCB1 depletion relative to controls, consistent with enhanced protein degradation (**Supplemental Figures 4g-h**).

To identify potential additional modulators of ABCB1 stability, we compared the expression of other known ABCB1 regulators between differentiated and undifferentiated melanoma cells (**Supplemental Figure 5a**). This analysis revealed that the kinase PIM1, previously shown to protect ABCB1 from proteasomal degradation and promote its maturation (Xie et al., 2010; Natarajan et al., 2013), was likewise selectively expressed in undifferentiated cells (**Supplemental Figures 5a–b**). Notably, both CD44 and PIM1 were found to be components of the mesenchymal melanoma transcriptional signature, the gene regulatory network underlying the undifferentiated cell state (Wouters et al., 2020) (**Supplemental Figure 5c**). Given the established role of AP-1/TEAD in enforcing this state (Verfaillie et al., 2015; Comandante-Lou et al., 2022) and in regulating ABCB1 expression (**Figure 4f**), we next investigated whether they also influence CD44 and PIM1 expression. CUT&Tag profiling revealed strong JUN enrichment at the prompters of both *CD44* and *PIM1* (**Supplemental Figure 5d**), and pharmacological inhibition of AP-1 or TEADs led to marked downregulation of both factors in MM029 cells (**Supplemental Figure 5e**). Previously published RNA-Seq data of differentiated 501mel melanoma cells (Laurette et al., 2015), revealed the concurrent gain of of expression of ABCB1, PIM1, and AP-1 factors upon loss of MITF and SOX10, the master transcription factors underlying the melanocytic state (**Supplemental Figure 5f**). These observations suggested that besides direct transcriptional control of *ABCB1*, AP-1/TEAD factors maintain ABCB1 function in undifferentiated melanoma cells by coordinately upregulating stabilizing factors in a cell-state dependent manner. To functionally validate the contributions of CD44 and PIM1 to drug transport–dependent resistance, we

perturbed each factor in MM029^{ABCB1} and MM029$^{lurbi-R}$ cells. siRNA-mediated knockdown of CD44 or pharmacological inhibition of PIM1 with the selective inhibitor SGI-1776 (Chen et al., 2009) significantly reduced efflux capacity (**Figures 7g–h and Supplemental Figure 5g**) and partially resensitized MM029^{ABCB1} cells to lurbinectedin (**Figure 7i**). Notably, an even more pronounced effect was observed in MM029$^{lurbi-R}$ cells, where PIM1 inhibition nearly completely restored lurbinectedin sensitivity (**Figure 7j).** Similarly, PIM1 inhibition significantly resensitized LoVo^{Doxo-R} cells to synthetic ecteinascidins (**Figure 7k**).

Together, these findings delineate a transcriptionally controlled resistance axis in undifferentiated melanoma cells, wherein AP-1/TEAD activity sustains the expression of ABCB1-stabilizing factors, including CD44 and PIM1. This axis protects ABCB1 from proteasomal degradation, thereby enabling functional drug efflux and resistance to ecteinascidins. By contrast, in differentiated cells, ABCB1 remains functionally impaired despite ectopic expression, likely due to the absence of these stabilizing factors. The lack of AP-1/TEAD activity results in reduced PIM1 and CD44 expression, permitting FBXO21-dependent degradation and collectively rendering differentiated cells incapable of acquiring drug resistance (**Supplemental Figure 6**).

Discussion

Here, we describe a unique cellular model of acquired resistance to synthetic ecteinascidins (lurbinectedin, ecubectedin, and PM54), generated by chronic exposure of an undifferentiated melanoma cell line. In these models, ABCB1 overexpression consistently emerged as the dominant, recurrent resistance mechanism. To our knowledge, molecular mechanisms of acquired resistance to this drug class have not been defined previously, likely reflecting both the recent nature of the clinical approval of lurbinectedin for SCLC and the difficulty of establishing ecteinascidin-resistant in vitro models. Despite repeated attempts, we were unable to derive resistant lines from SCLC models or from most melanoma lines tested, underscoring the pronounced cell-state specificity of this phenomenon. Resistant cells arose exclusively from MM029 melanoma cells, which display a highly undifferentiated phenotype and uniquely exhibit detectable baseline ABCB1 expression in the absence of drug pressure. These findings suggest that only a subset of transcriptionally and epigenetically primed cells, marked by high plasticity and baseline efflux capacity, can stably acquire resistance through further ABCB1 upregulation. Moreover, enforced ABCB1 overexpression markedly diminished the antitumor activity of synthetic ecteinascidins, demonstrating that ABCB1 overexpression is sufficient, on its own, to confer resistance.

Interestingly, the acquisition of resistance to synthetic ecteinascidins was accompanied by profound transcriptional reprogramming in melanoma cells, characterized by the downregulation of invasive, mesenchymal, and neural crest stem cell (NCSC) signatures previously associated with therapeutic resistance (Rambow et al., 2018; Wouters et al., 2020). Notably, these cell states are linked to immune evasion and poor response to immunotherapy (Hugo et al., 2016; Auslander et al., 2018). Our data thus suggest that, paradoxically, upregulation of ABCB1 and acquisition of resistance to ecteinascidins in undifferentiated melanoma cells necessitate a shift away from a mesenchymal/NCSC-like program. This phenotypic adaptation may expose new vulnerabilities, including potentially increased immunogenicity and sensitivity to immune checkpoint inhibitors, as predicted by the reduced TIDE scores observed in our resistant models. Such cell state trade-offs have been proposed as evolutionary constraints in therapy resistance, wherein acquisition of resistance to one treatment confers susceptibility to another (Shaffer et al., 2017; Rambow et al., 2019). Future studies should investigate whether such collateral vulnerabilities can be therapeutically exploited to overcome or prevent resistance to ecteinascidin-based therapies.

Mechanistically, we demonstrate that ABCB1 overexpression in resistant cells arises from a combination of focal genomic amplification and transcriptional activation by TEAD and AP-1 factors, both master regulators of melanoma cell state plasticity (Verfaillie et al., 2015; Rambow et al., 2019). Critically, our data reveal that AP-1 and TEAD not only directly drive ABCB1 transcription but also sustain the expression of ABCB1-stabilizing factors CD44 and PIM1, which in turn inhibit the proteasomal degradation of ABCB1 in undifferentiated melanoma cells. In contrast, differentiated melanoma cells, characterized by low AP-1/TEAD activity, fail to maintain CD44 and PIM1 expression, resulting in FBXO21-mediated ABCB1 ubiquitination and degradation **(Supplemental Figure 6).** These findings provide a mechanistic explanation for why resistance to ecteinascidins remains confined to a specific melanoma cell state. Notably, CD44, PIM1, and FBXO21 have been previously implicated in regulating ABCB1 stability and trafficking in other cancer contexts (Xie et al., 2010; Natarajan et al., 2013; Ravindranath et al., 2015; Chen et al., 2018). Our study extends these observations by demonstrating their functional roles in melanoma and by integrating them into a unified resistance axis controlled by AP-1 and TEAD, thereby linking melanoma cell heterogeneity and dedifferentiation to drug efflux. In doing so, we define a multilayered mechanism integrating transcriptional and post-translational regulation that governs the cell state-dependent emergence of resistance to synthetic ecteinascidins, highlighting the therapeutic potential of targeting the AP-1/TEAD–CD44/PIM1–ABCB1 axis.

Functionally, ABCB1 upregulation inhibited nuclear drug accumulation, impaired the binding of ecteinascidins to their genomic targets, and prevented the repression of oncogenes and induction of DNA damage. Notably, ABCB1 inhibition, via siRNA or clinically tested pharmacological inhibitors such as tariquidar and verapamil, restored drug sensitivity, genomic occupancy, and downstream cytotoxic effects. We further confirmed that ABCB1 overexpression was sufficient to confer resistance in other cancer models, underscoring the translational relevance of this resistance mechanism. Given that lurbinectedin is approved for use in SCLC, biopsies obtained from patients at relapse should be evaluated for ABCB1 expression to further assess its contribution to therapeutic resistance. Although systemic toxicity has historically limited the development of ABCB1 inhibitors, renewed interest in overcoming transporter-mediated resistance, particularly through tumor-targeted delivery strategies or combination therapies, is driving the development of next-generation inhibitors with improved therapeutic windows (Engle and Kumar, 2022). Our findings also highlight PIM1 as a promising therapeutic target. In addition to its role in ABCB1 stabilization, PIM1 is a proto-oncogenic kinase with

established functions in cancer cell survival and proliferation, and several inhibitors are currently undergoing clinical evaluation (Bellon and Nicot, 2023; Chen et al., 2024). We observed that pharmacological inhibition of PIM1 markedly impaired ABCB1 efflux activity across different resistant cancer models, thereby resensitizing them to ecteinascidins. These results warrant further investigation into the mechanistic interplay between PIM1 and ABCB1 stability and may support the repurposing of PIM1 inhibitors as alternative or complementary strategies to overcome drug efflux–mediated resistance.

Taken together, our findings define a transcriptionally and post-translationally regulated resistance axis centered on the efflux pump ABCB1, constrained by melanoma cell state, and sufficient to abrogate the therapeutic effects of synthetic ecteinascidins. These results provide a compelling rationale for assessing ABCB1 status, potentially together with CD44 and other stemness-associated factors, as predictive biomarkers of drug response in patients prior to ecteinascidin treatment. In parallel, they support the development of therapeutic strategies aimed at targeting ABCB1 itself, its regulators such as CD44 or PIM1, and cell state determinants including AP-1 and TEADs, to overcome or prevent resistance. More broadly, our study highlights that beyond pharmacological inhibition of ABC transporters, rational chemical modifications of next-generation synthetic ecteinascidins to evade efflux or leverage selective uptake mechanisms may represent promising avenues to overcome resistance. Combined with biomarker-driven patient stratification, these strategies could significantly enhance the durability of response to chromatin-targeting therapeutics across a broad spectrum of cancers.

Material and methods

Resource availability:

Lead contact: Further information and requests for resources and reagents should be directed to and will be fulfilled by the Lead Contact, Frédéric Coin (fredr@igbmc.fr).

Extended resource table: An extended resource table with antibodies, oligonucleotide sequences, chemicals and reagents used in this work is provided in **Supplemental Table 3**.

Cell culture, generation of resistant cells, and drug treatments

Cells were cultured at 37 °C in a humidified atmosphere with 5% CO_2 and regularly tested for mycoplasma contamination. Patient-derived short-term melanoma cultures MM074, MM029, and MM099 were grown in HAM-F10 medium (Gibco, Invitrogen) supplemented with 10% fetal calf serum (FCS), 25 mM HEPES, 5.2 mM GlutaMAX, and penicillin–streptomycin. Melanoma cell lines 501mel (RRID: CVCL_4633) and SKMEL28 (RRID:CVCL_0526) were maintained in RPMI 1640 medium without HEPES (Gibco, Invitrogen) supplemented with 10% FCS and gentamicin, while IGR37 (RRID:CVCL_2075) and IGR39 (RRID:CVCL_2076) were cultured in RPMI 1640 without HEPES supplemented with 15% FCS and gentamicin. The SCLC cell line DMS53 (RRID:CVCL_1177) was cultured in Waymouth MB 752/1 medium supplemented with 10% FCS and gentamicin. The LoVo (RRID:CVCL_0399) colorectal cancer cell line was cultured in DMEM medium without HEPES supplemented with 10% FCS, and gentamicin. Lentivirus-infected cells were selected in puromycin-containing medium. 501mel, SKMEL28, IGR37, IGR39, and DMS53 were obtained from ATCC; MM074, MM029, and MM099 were provided by Dr. Ghanem Ghanem (Université Libre de Bruxelles). Ecteinascidin-resistant cells were maintained in the presence of 30 nM lurbinectedin, ecubectedin, or PM54 to ensure stable resistance. To generate resistant lines, differentiated melanocytic-like (SKMEL28, 501mel, MM074, IGR37) and undifferentiated mesenchymal-like (MM029, MM099) melanoma cells were chronically exposed to escalating doses of lurbinectedin, ecubectedin, or PM54, starting at one-third of the respective IC_{50} values. In most cases, cells were eliminated within 1–2 weeks; however, MM029 cells were treated continuously for over eight months, yielding stable, resistant populations proliferating at drug concentrations ≥10-fold higher than the initial IC_{50}.

Lurbinectedin (PM1183), ecubectedin, and PM54 were provided by PharmaMar S.A. Rhodamine 123 (HY-D0816), tariquidar (XR9576), verapamil (HY-14275), veratramine (HY-N0837), SR11302 (HY-15870), MGH-CP1 (HY-139330), MG132 (HY-13259), SGI-1776 (HY-13287A), puromycin (HY-B1743), cycloheximide (HY-12320) and doxorubicin (HY-15142) were purchased from MedChemExpress.

IC_{50} Determination and re-sensitization Assays

Cells were seeded at 5,000 cells per well in 96-well plates and treated with increasing concentrations of lurbinectedin, ecubectedin, or PM54. After 72 hours, cell viability was assessed using PrestoBlue reagent (Thermo Fisher Scientific) according to the manufacturer's instructions. Absorbance was measured using a CellInsight CX5 microplate reader (Thermo Fisher Scientific). IC_{50} values were calculated by nonlinear curve fitting using Prism 10 software (GraphPad).

For re-sensitization experiments, cells were transfected with siRNAs 48 hours prior to ecteinascidin treatment. Combined treatments with ABCB1, AP-1/TEAD, or PIM inhibitors were performed concurrently with ecteinascidin exposure; the inhibitor concentrations used are indicated in the corresponding figure legends.

siRNA Transfection

Cells were transfected with 25 nM siRNA using Lipofectamine™ RNAiMAX (Thermo Fisher Scientific) according to the manufacturer's protocol. ON-TARGETplus SMARTpool siRNAs (Horizon Discovery) were used for gene silencing. Cells were harvested 48 hours after transfection for subsequent analyses.

Proliferation and Senescence Assays

For proliferation and senescence analyses, 2×10^5 cells were seeded in 6-well plates and labeled with CellTrace™ reagent (Thermo Fisher Scientific) according to the manufacturer's instructions. Cells were subsequently treated with ecteinascidins for 72 hours. Following treatment, cells were stained with C_{12}FDG (Thermo Fisher Scientific) following the manufacturer's protocol. Fluorescence was acquired on a BD LSRFortessa™ flow cytometer and analyzed using FlowJo software (BD Biosciences).

Rhodamine 123 Efflux Assays

For Rho123 efflux assays, 2×10^5 cells were seeded in 6-well plates and treated with either CD44-targeting siRNA or inhibitors of ABCB1 or PIM1 for 48 hours. Cells were then incubated with 1 µg/mL

Rhodamine 123 in PBS for 90 minutes at 37 °C, washed twice with PBS (5 minutes per wash), and immediately analyzed by flow cytometry (BD LSRFortessa™). Rho123 fluorescence intensity was used as an inverse readout of ABCB1 activity, with high intracellular Rho123 indicating impaired efflux and low intracellular fluorescence reflecting active ABCB1-mediated efflux.

Immunofluorescence assays

Cells grown on glass coverslips were rinsed with PBS and fixed in 4% paraformaldehyde for 15 min at room temperature. Following fixation, cells were permeabilized with 0.1% Triton X-100 in PBS and blocked with 5% BSA for 1 h. Primary antibodies were incubated overnight at 4°C in blocking solution. The next day, cells were incubated with Alexa Fluor–conjugated secondary antibodies diluted in PBS containing 5% BSA for 1 h at room temperature. Nuclei were counterstained with DAPI. For γH2AX quantification, foci were manually counted using the Cell Counter plugin in Fiji. For ABCB1 quantification, cell boundaries were manually defined using the β-tubulin signal as a reference in Fiji. The fluorescence intensity of ABCB1 was measured within the corresponding regions of interest (ROIs), and values were normalized to the cell area.

Boyden Chamber Invasion Assay

For invasion assays, 2×10^6 cells were seeded into Boyden chamber inserts (Fisher Scientific) precoated with 4% Matrigel (Corning) and overlaid with serum-free medium. Inserts were placed into 24-well plates containing complete growth medium as a chemoattractant. After 24 hours, cells were fixed with 4% formaldehyde for 10 minutes, washed once with PBS, and stained with 0.2% crystal violet solution for 15 minutes. Inserts were subsequently washed twice with deionized water, air-dried, and imaged using an EVOS XL Core microscope (Thermo Fisher Scientific). Images were analyzed using Fiji software (ImageJ) by quantifying the area occupied by the invading cells.Bulk RNA-Sequencing and analysis.

RNA Extraction and RT-qPCR

Total RNA was extracted using the NucleoSpin RNA Plus kit (Macherey-Nagel) following the manufacturer’s instructions. Complementary DNA (cDNA) was synthesized using SuperScript™ IV Reverse Transcriptase (Invitrogen, Thermo Fisher Scientific). Quantitative PCR (qPCR) was performed

using SYBR Green Master Mix (Roche) on a LightCycler® 480 Instrument II (Roche). Primers were designed using Primer-BLAST (NCBI).

Copy Number Assays

Copy number variations were assessed using qBiomarker Copy Number PCR Assays (Qiagen) according to the manufacturer's instructions. qPCR was performed to quantify gene copy number changes.

Protein Extraction and Western Blotting

For whole-cell extracts, cells were rinsed once with cold PBS, pelleted, and resuspended in LSDB 0.5 M buffer (500 mM KCl, 50 mM Tris-HCl pH 7.9, 20% glycerol, 1% NP-40, 1 mM DTT, and protease inhibitor cocktail [Roche]). Cells were lysed by three cycles of heat shock (immersion in liquid nitrogen followed by thawing in a 37 °C water bath). Lysates were centrifuged at 14,000 × g for 15 minutes at 4 °C to remove debris. Protein extraction using CHAPSO was also performed to gently solubilize ABCB1, aiming to improve signal intensity and ensure its detection at the expected molecular weight. Cells were first homogenized in twice its volume of a buffer containing 5 mM HEPES pH 7.4, 1 mM EDTA, 0.25 M sucrose, and protease inhibitor cocktail. The homogenate was then centrifuged at 1,000 g for 5 minutes at 4°C. After removing the supernatant, the pellet was re-homogenized in twice its volume of a buffer containing 25 mM HEPES, 150 mM NaCl, 2 mM EDTA, 1% CHAPSO and protease inhibitor cocktail. The extract was subsequently ultracentrifuged at 60,000 rpm for 1 hour at 4°C. Finally, the supernatant was collected.

Protein extracts were separated on 4%-12% Bis-Tris gradient gels (Invitrogen) using SDS–polyacrylamide gel electrophoresis (SDS–PAGE) and transferred to nitrocellulose membranes. Membranes were blocked in PBS containing 5% non-fat dry milk and 0.01% Tween-20, and incubated overnight at 4 °C with primary antibodies diluted in blocking solution. After washing, membranes were incubated for 1 hour at room temperature with HRP-conjugated secondary antibodies (Jackson ImmunoResearch). Protein bands were visualized using an enhanced chemiluminescence (ECL) detection system (GE Healthcare). Western blot signal intensities were quantified using ImageJ software.

ABCB1 overexpression

MM029, IGR37, SKMEL28, and DMS53 cells stably overexpressing ABCB1 were generated by lentiviral transduction. Cells were transduced with pLenti-pCMV-ABCB1 vectors encoding untagged ABCB1 (Origene, SC119584) in the presence of polybrene (8 μg/mL), followed by selection with 3 μg/mL puromycin. As a control, cells expressing mCherry were generated using pLenti-pCMV-mCherry vectors under the same conditions.

Lentiviral shRNA transduction

Lentiviral particles were generated in HEK293T cells by co-transfecting the pGFP-C-shLenti vector encoding shFBXO21 (Origene, TL313039) with packaging plasmids using a standard calcium phosphate or lipid-based transfection protocol. After 48 h, viral supernatants were harvested, filtered, and used to transduce SKMEL28-ABCB1 cells. Following a 24 h incubation, the medium was replaced, and cells were selected with puromycin (3 μg/mL) for 7 days. The shRNA was expressed constitutively under the control of the U6 promoter. Transduction efficiency was assessed by GFP fluorescence.

CUT&Tag

Cells were treated with either DMSO or 30 nM biotinylated lurbinectedin (Bio-Lurbi) for 6 h. For co-treatment experiments, cells were pre-treated with 1 μM Tariquidar for 90 min prior to the addition of 30 nM Bio-Lurbi. CUT&Tag assays were performed in biological duplicates using the CUT&Tag-IT Assay Kit (Active Motif, 53160 and 53165) according to the manufacturer's protocol. Briefly, 5×10^5 cells per condition were harvested, washed twice with wash buffer, and bound to Concanavalin A–coated magnetic beads. Cells were then incubated overnight at 4°C with primary antibodies (1:50 dilution). The following day, secondary antibodies were added at 1:100 dilution in digitonin buffer and incubated for 1 h at room temperature. Next, cells were incubated with CUT&Tag-IT Assembled pA-Tn5 Transposomes for 1 h at room temperature, followed by incubation in tagmentation buffer at 37°C for 1 h. The reaction was stopped with EDTA and SDS, and proteins were digested with Proteinase K (10 mg/mL) at 55°C for 1 h. DNA was purified and subsequently amplified by PCR. Amplified DNA was purified with two rounds of SPRI bead cleanup and eluted in 200 μL of nuclease-free water. DNA enrichment was quantified by qPCR, and fold enrichment was calculated relative to the DMSO control.

Immunoprecipitation

Thirty microliters of a 1:1 mix of Magnetic Protein A/G beads (Thermo Fisher) were washed with PBS and incubated for 2 hours at 4 °C with 5 µg of anti-ubiquitin antibody per sample. After two additional PBS washes, 30 µL of the antibody–Protein A/G complex was added to 500 µg of total protein lysate per sample and incubated overnight at 4 °C with gentle rotation. Twenty micrograms of lysate were kept aside as input. The beads were then washed twice with LSDB buffer (as described above) supplemented with either 300 mM or 150 mM NaCl. Bound proteins were eluted in 1× Laemmli sample buffer by heating at 70 °C for 10 minutes and analyzed by SDS–PAGE and immunoblotting.

RNA-seq library preparation, sequencing and analysis

Library preparation was performed at the GenomEast platform at the Institute of Genetics and Molecular and Cellular Biology using the RiboPOOL Kit Manual v1 + Modified TruSeq Stranded mRNA Reference Guide – PN 1000000040498. Total RNA-seq libraries were generated from 500 ng of total RNA. Before cDNA synthesis, cytoplasmic and mitochondrial ribosomal RNA (rRNA) were removed using a biotin-streptavidin magnetic bead-based procedure with the riboPOOL kit targeting HMR ribosomal rRNA (siTOOLs Biotech, Planegg/Martinsried, DE) according to the manufacturer's instructions. Total RNA-seq libraries were then generated using the TruSeq Stranded mRNA Library Prep Kit and TruSeq RNA Single Indexes Kits A and B (Illumina, San Diego, USA), omitting the poly-A selection step and starting from the fragmentation step. Briefly, following clean-up by ethanol precipitation, the depleted RNA was fragmented into small pieces using divalent cations at 94°C for 8 minutes. Cleaved RNA fragments were then copied into first-strand cDNA using reverse transcriptase and random primers, followed by second-strand cDNA synthesis using DNA Polymerase I and RNase H. Strand specificity was achieved by replacing dTTP with dUTP during second-strand synthesis. The double-stranded cDNA fragments were blunted using T4 DNA polymerase, Klenow DNA polymerase, and T4 PNK. A single A-nucleotide was added to the 3' ends of the blunt DNA fragments using a Klenow fragment (3' to 5' exo minus) enzyme. The cDNA fragments were ligated to double-stranded adapters using T4 DNA Ligase. The ligated products were enriched by PCR amplification (30 s at 98°C; [10 s at 98°C, 30 s at 60°C, 30 s at 72°C] ×12 cycles; 5 min at 72°C). Surplus PCR primers were further removed by purification using AMPure XP beads (Beckman-Coulter, Villepinte, France), and the final cDNA libraries were checked for quality and quantified using capillary electrophoresis. Libraries were sequenced on an Illumina HiSeq 4000 sequencer as single-read 50 base reads. Image analysis and base calling were performed using RTA version 2.7.7 and bcl2fastq version 2.20.0.422.

Reads were preprocessed to remove adapter and low-quality sequences (Phred quality score below 20). After this preprocessing, reads shorter than 40 bases were discarded for further analysis. These preprocessing steps were performed using cutadapt version 1.10. Reads were mapped to rRNA sequences using bowtie version 2.2.8 and reads mapping to rRNA sequences were removed for further analysis. Reads were mapped onto the hg19 assembly of Homo sapiens genome using STAR version 2.5.3a. Gene expression quantification was performed from uniquely aligned reads using htseq-count version 0.6.1p1, with annotations from Ensembl version 75 and ‘’union" mode. Only non-ambiguously assigned reads have been retained for further analyses. Read counts have been normalized across samples with the median-of-ratios method proposed by Anders and Huber (Anders and Huber, 2010) to make these counts comparable between samples. Comparisons of interest were performed using the Wald test for differential expression proposed by Love et al. (Love et al., 2014) and implemented in the Bioconductor package DESeq2 version 1.16.1. Genes with high Cook’s distance were filtered out and independent filtering based on the mean of normalized counts was performed. P-values were adjusted for multiple testing using the Benjamini and Hochberg method (Benjamini and Hochberg, 1995). Deregulated genes were defined as genes with log2(Fold change) > 1 or < 1 and adjusted P-value < 0.05.

Volcano plots were generated using the Prism10 statistical software (GraphPad). Heatmaps were generated using Morpheus (https://software.broadinstitute.org/morpheus). Gene Ontology Analysis was performed using ShinyGO (Ge SX, Jung D & Yao, 2020). Venn diagrams were generated using DeepVenn (https://www.deepvenn.com/). iRegulon analysis was performed using the iRegulon Cytoscape 3 plugin (Janky et al. 2014). TIDE analysis was performed using the TIDE website (http://tide.dfci.harvard.edu/).

Data availability

The publicly available datasets used in this study can be accessed from the Gene Expression Omnibus (GEO) under the following accession codes: RNA-seq of MM029 cells after short-term drug exposure and Chem-mapping of Bio-Lurbi and Bio-PM54 binding sites in MM029 cells, GSE256103; melanoma phenotype and resistance signatures, GSE65186, GSE78220, and GSE116237. Raw and processed RNA-seq data generated in this study have been deposited in the Gene Expression Omnibus (GEO) under accession number GSE294646.

Author contributions:

Conceptualization: MC, FC

Methodology: MC, FC

Investigation: CM, MN, JO, PC, MC

Analysis of data: CM, MC, FC, JO

Funding acquisition: FC

Supervision: FC

Writing – original draft: MC, FC

Writing – review & editing: MC, FC

References

1. Adorni, M. P. et al. A New ABCB1 Inhibitor Enhances the Anticancer Effect of Doxorubicin in Both In Vitro and In Vivo Models of NSCLC. Int J Mol Sci 24, 989 (2023).

2. Aix, S. P. et al. Combination lurbinectedin and doxorubicin versus physician's choice of chemotherapy in patients with relapsed small-cell lung cancer (ATLANTIS): a multicentre, randomised, open-label, phase 3 trial. Lancet Respir Med 11, 74–86 (2023).

3. Arozarena, I. & Wellbrock, C. Phenotype plasticity as enabler of melanoma progression and therapy resistance. Nat Rev Cancer 19, 377–391 (2019).

4. Auslander, N. et al. Robust prediction of response to immune checkpoint blockade therapy in metastatic melanoma. Nat Med 24, 1545–1549 (2018).

5. Bellon, M. & Nicot, C. Targeting Pim kinases in hematological cancers: molecular and clinical review. Mol Cancer 22, 18 (2023).

6. Berico, P. et al. CDK7 and MITF repress a transcription program involved in survival and drug tolerance in melanoma. EMBO Rep 22, e51683 (2021).

7. Boni, V. et al. Lurbinectedin, a selective inhibitor of oncogenic transcription, in patients with pretreated germline BRCA1/2 metastatic breast cancer: results from a phase II basket study. ESMO Open 7, 100571 (2022).

8. Calles, A. et al. Unveiling the Mechanism of Lurbinectedin's Action and Its Potential in Combination Therapies in Small Cell Lung Cancer. Mol Cancer Ther 24, 828–839 (2025).

9. Calles, A. et al. Lurbinectedin Plus Pembrolizumab in Relapsed SCLC: The Phase I/II LUPER Study. Journal of Thoracic Oncology 20, 969–982 (2025).

10. Chakraborty, S. et al. Lurbinectedin sensitizes PD-L1 blockade therapy by activating STING-IFN signaling in small-cell lung cancer. Cell Rep Med 5, 101852 (2024).

11. Chen, C., Zhao, S., Karnad, A. & Freeman, J. W. The biology and role of CD44 in cancer progression: therapeutic implications. J Hematol Oncol 11, 64 (2018).

12. Chen, L. S., Redkar, S., Bearss, D., Wierda, W. G. & Gandhi, V. Pim kinase inhibitor, SGI-1776, induces apoptosis in chronic lymphocytic leukemia cells. Blood 114, 4150–4157 (2009).

13. Chen, S., Yang, Y., Yuan, Y. & Bo Liu, null. Targeting PIM kinases in cancer therapy: An update on pharmacological small-molecule inhibitors. Eur J Med Chem 264, 116016 (2024).

14. Chufan, E. E., Sim, H.-M. & Ambudkar, S. V. Molecular basis of the polyspecificity of P-glycoprotein (ABCB1): recent biochemical and structural studies. Adv Cancer Res 125, 71–96 (2015).

15. Cigrang, M. et al. Pan-inhibition of super-enhancer-driven oncogenic transcription by next-generation synthetic ecteinascidins yields potent anti-cancer activity. Nat Commun 16, 512 (2025).

16. Comandante-Lou, N., Baumann, D. G. & Fallahi-Sichani, M. AP-1 transcription factor network explains diverse patterns of cellular plasticity in melanoma cells. Cell Rep 40, 111147 (2022).

17. Costanzo, F. et al. Promoters of ASCL1- and NEUROD1-dependent genes are specific targets of lurbinectedin in SCLC cells. EMBO Mol Med 14, e14841 (2022).

18. Dumoulin, D. W. et al. Lurbinectedin shows clinical activity and immune-modulatory functions in patients with pre-treated small cell lung cancer and malignant pleural mesothelioma. Eur J Cancer 172, 357–366 (2022).

19. Engle, K. & Kumar, G. Cancer multidrug-resistance reversal by ABCB1 inhibition: A recent update. Eur J Med Chem 239, 114542 (2022).

20. Gadducci, A. & Cosio, S. Trabectedin and lurbinectedin: Mechanisms of action, clinical impact, and future perspectives in uterine and soft tissue sarcoma, ovarian carcinoma, and endometrial carcinoma. Front Oncol 12, 914342 (2022).

21. Genovese, I., Ilari, A., Assaraf, Y. G., Fazi, F. & Colotti, G. Not only P-glycoprotein: Amplification of the ABCB1-containing chromosome region 7q21 confers multidrug resistance upon cancer cells by coordinated overexpression of an assortment of resistance-related proteins. Drug Resist Updat 32, 23–46 (2017).

22. Hugo, W. et al. Non-genomic and Immune Evolution of Melanoma Acquiring MAPKi Resistance. Cell 162, 1271–1285 (2015).

23. Hugo, W. et al. Genomic and Transcriptomic Features of Response to Anti-PD-1 Therapy in Metastatic Melanoma. Cell 165, 35–44 (2016).

24. Jalil, A., Donate, M. M. & Mattei, J. Exploring resistance to immune checkpoint inhibitors and targeted therapies in melanoma. Cancer Drug Resist 7, 42 (2024).

25. Janky, R. et al. iRegulon: From a Gene List to a Gene Regulatory Network Using Large Motif and Track Collections. PLOS Computational Biology 10, e1003731 (2014).

26. Jiang, P. et al. Signatures of T cell dysfunction and exclusion predict cancer immunotherapy response. Nat Med 24, 1550–1558 (2018).

27. Kannan, P. et al. The “Specific” P-Glycoprotein Inhibitor Tariquidar Is Also a Substrate and an Inhibitor for Breast Cancer Resistance Protein (BCRP/ABCG2). ACS Chem Neurosci 2, 82–89 (2010).

28. Kodan, A. et al. ABCB1/MDR1/P-gp employs an ATP-dependent twist-and-squeeze mechanism to export hydrophobic drugs. FEBS Lett 595, 707–716 (2021).

29. Kurimchak, A. M. et al. The drug efflux pump MDR1 promotes intrinsic and acquired resistance to PROTACs in cancer cells. Sci Signal 15, eabn2707 (2022).

30. Laurette P, Strub T et al. Transcription factor MITF and remodeller BRG1 define chromatin organisation at regulatory elements in melanoma cells. Elife. 2015 Mar 24;4:e06857. doi: 10.7554/eLife.06857. PMID: 25803486; PMCID: PMC4407272.

31. Le, V. H., Inai, M., Williams, R. M. & Kan, T. Ecteinascidins. A review of the chemistry, biology and clinical utility of potent tetrahydroisoquinoline antitumor antibiotics. Nat Prod Rep 32, 328–347 (2015).

32. Manzo, A. et al. Lurbinectedin in small cell lung cancer. Front Oncol 12, 932105 (2022).

33. Mauduit, D. et al. Analysis of long and short enhancers in melanoma cell states. Elife 10, e71735 (2021).

34. Metaxas, Y. et al. Lurbinectedin as second- or third-line palliative therapy in malignant pleural mesothelioma: an international, multi-centre, single-arm, phase II trial (SAKK 17/16). Ann Oncol 31, 495–500 (2020).

35. Moore, J. M., Bell, E. L., Hughes, R. O. & Garfield, A. S. ABC transporters: human disease and pharmacotherapeutic potential. Trends Mol Med 29, 152–172 (2023).

36. Natarajan, K. et al. The Pim kinase inhibitor SGI-1776 decreases cell surface expression of P-glycoprotein (ABCB1) and breast cancer resistance protein (ABCG2) and drug transport by Pim-1-dependent and -independent mechanisms. Biochem Pharmacol 85, 514–524 (2013).

37. Paz-Ares, L. et al. Efficacy and safety of first-line maintenance therapy with lurbinectedin plus atezolizumab in extensive-stage small-cell lung cancer (IMforte): a randomised, multicentre, open-label, phase 3 trial. Lancet 405, 2129–2143 (2025).

38. Povo-Retana, A., Landauro-Vera, R., Alvarez-Lucena, C., Cascante, M. & Boscá, L. Trabectedin and Lurbinectedin Modulate the Interplay between Cells in the Tumour Microenvironment-Progresses in Their Use in Combined Cancer Therapy. Molecules 29, 331 (2024).

39. Pozniak, J. et al. A TCF4-dependent gene regulatory network confers resistance to immunotherapy in melanoma. Cell 187, 166-183.e25 (2024).

40. Rambow, F., Marine, J.-C. & Goding, C. R. Melanoma plasticity and phenotypic diversity: therapeutic barriers and opportunities. Genes Dev 33, 1295–1318 (2019).

41. Rambow, F. et al. Toward Minimal Residual Disease-Directed Therapy in Melanoma. Cell 174, 843-855.e19 (2018).

42. Ravindranath, A. K. et al. CD44 promotes multi-drug resistance by protecting P-glycoprotein from FBXO21-mediated ubiquitination. Oncotarget 6, 26308–26321 (2015).

43. Rees, D. C., Johnson, E. & Lewinson, O. ABC transporters: the power to change. Nat Rev Mol Cell Biol 10, 218–227 (2009).

44. Rubanov, A., Berico, P. & Hernando, E. Epigenetic Mechanisms Underlying Melanoma Resistance to Immune and Targeted Therapies. Cancers (Basel) 14, 5858 (2022).

45. Santamaría Nuñez, G. et al. Lurbinectedin Specifically Triggers the Degradation of Phosphorylated RNA Polymerase II and the Formation of DNA Breaks in Cancer Cells. Mol Cancer Ther 15, 2399–2412 (2016).

46. Shaffer, S. M. et al. Rare cell variability and drug-induced reprogramming as a mode of cancer drug resistance. Nature 546, 431–435 (2017).

47. Trigo, J. et al. Lurbinectedin as second-line treatment for patients with small-cell lung cancer: a single-arm, open-label, phase 2 basket trial. Lancet Oncol 21, 645–654 (2020).

48. Verfaillie, A. et al. Decoding the regulatory landscape of melanoma reveals TEADS as regulators of the invasive cell state. Nat Commun 6, 6683 (2015).

49. Webb, M., Raphael, C. L., Asbahr, H., Erber, W. N. & Meyer, B. F. The detection of rhodamine 123 efflux at low levels of drug resistance. Br J Haematol 93, 650–655 (1996).

50. Wouters, J. et al. Robust gene expression programs underlie recurrent cell states and phenotype switching in melanoma. Nat Cell Biol 22, 986–998 (2020).

51. Wu, C.-P., Calcagno, A. M. & Ambudkar, S. V. Reversal of ABC drug transporter-mediated multidrug resistance in cancer cells: evaluation of current strategies. Curr Mol Pharmacol 1, 93–105 (2008).

52. Xie, W. et al. Lurbinectedin synergizes with immune checkpoint blockade to generate anticancer immunity. Oncoimmunology 8, e1656502 (2019).

53. Xie, Y., Burcu, M., Linn, D. E., Qiu, Y. & Baer, M. R. Pim-1 kinase protects P-glycoprotein from degradation and enables its glycosylation and cell surface expression. Mol Pharmacol 78, 310–318 (2010).

54. Yin, W. et al. The inhibition of ABCB1/MDR1 or ABCG2/BCRP enables doxorubicin to eliminate liver cancer stem cells. Sci Rep 11, 10791 (2021).

Figure Legends

Figure 1: Generation of undifferentiated melanoma cells resistant to synthetic ecteinascidins

a. Four differentiated and two undifferentiated melanoma cell types were chronically exposed to escalating concentrations of lurbinectedin (Lurbi), ecubectedin (Ecub), or PM54. Relative melanocytic differentiation levels and baseline IC_{50} values, previously determined in Cigrang et al. (2025), are shown. Initial treatment concentrations were set at one-third of the baseline IC_{50} values. Drug resistance, defined as sustained cell proliferation at $10\times IC_{50}$, was only successfully achieved in undifferentiated MM029 cells.

b-d. Dose–response curves for MM029, $MM029^{lurbi\text{-}R}$, $MM029^{ecub\text{-}R}$, and $MM029^{PM54\text{-}R}$ cells treated for 72 h with increasing concentrations of lurbi (**b**), ecub (**c**), or PM54 (**d**). Viability is shown relative to DMSO-treated controls; IC_{50} values are indicated. Data represent mean ± SD of three biological replicates.

e. Cell proliferation was assessed by CellTrace staining (72 hours). Populations with low CellTrace signal (indicating higher proliferation) were quantified by flow cytometry. Data represent mean ± SD of three biological replicates; *P*-values were calculated via one-way ANOVA with Dunnett's multiple comparisons test (vs. MM029).

f. Senescence was quantified by C_{12}FDG staining and flow cytometry. High C_{12}FDG signal denotes increased senescence. Data represent mean ± SD of three biological replicates; *P*-values were calculated via one-way ANOVA with Dunnett's multiple comparisons test (vs. MM029).

g. Invasion was quantified using Boyden chamber assays. Surface coverage index is represented as mean ± SD for three biological replicates; *P*-values were calculated via one-way ANOVA with Dunnett's multiple comparisons test (vs. MM029).

h. RT–qPCR analysis for *AMIGO2*, *EGFR*, *FOSL1*, and *MYC* in MM029 and resistant derivatives cells treated with DMSO or lurbi (5 nM, 24 h). Results are shown as expression fold changes of lurbi-treated cells vs. DMSO-treated cells. Expression normalized to 18S. Data represent mean ± SD of three biological replicates; *P*-values were calculated via one-way ANOVA with Dunnett's multiple comparisons test (vs. MM029).

i. Cell proliferation was assessed by CellTrace staining in indicated cells and treatments (72 hours, 1xIC50 of MM029). Populations with low CellTrace signal (indicating higher proliferation) were quantified by flow cytometry. Data represent mean ± SD of three biological replicates; *P*-values were calculated via one-way ANOVA with Dunnett's multiple comparisons test (vs. MM029).

j. Immunoblot analysis of indicated proteins from cells treated with Lurbi (5 nM, 24h) or DMSO control. Molecular weights (kDa) are shown. Source data are available.

k. Apoptosis was assessed by Annexin V staining in indicated cells and treatments (72 hours, 1xIC50 of MM029) and quantified by flow cytometry. Data represent mean ± SD of three biological replicates; *P*-values were calculated via one-way ANOVA with Dunnett's multiple comparisons test (vs. MM029).

Figure 2: ABCB1 overexpression enhances efflux and reduces drug-induced DNA damage in resistant cells

a–c. Volcano plots displaying differentially expressed genes in $MM029^{lurbi\text{-}R}$ (**a**), $MM029^{ecub\text{-}R}$ (**b**), and $MM029^{PM54\text{-}R}$ cells (**c**) compared to MM029 cells, from bulk RNA-seq analysis. Genes with $|\log_2(\text{fold change})| > 1$ and adjusted $P < 0.05$ were considered significant; numbers of significantly deregulated genes are indicated.

d. Venn diagram illustrating overlap of significantly upregulated genes among $MM029^{lurbi\text{-}R}$, $MM029^{ecub\text{-}R}$, and $MM029^{PM54\text{-}R}$ cells compared to MM029 cells.

e. RT–qPCR analysis showing *ABCB1* expression in indicated cells. Expression is 18S-normalized. Data represent mean ± SD of three biological replicates; *P*-values were calculated via one-way ANOVA with Dunnett's multiple comparisons test (vs. MM029).

f. Immunoblot of indicated proteins in MM029 and resistant cells. Molecular weights (kDa) are shown. Source data are available.

g. Efflux capacity was assessed by Rhodamine123 staining and flow cytometry. Reduced Rhodamine123 signal corresponds to higher efflux capacity. Data represent mean ± SD of three biological replicates; *P*-values were calculated via one-way ANOVA with Dunnett's multiple comparisons test (vs. MM029).

h. Representative immunofluorescence images of γH2AX, Tubulin and ABCB1 in MM029 and $MM029^{lurbi\text{-}R}$ cells treated with either DMSO or Lurbi (10 nM, 8 h). Mixed-cell images (bottom panels) represent a 1:1 co-culture of MM029 and $MM029^{lurbi\text{-}R}$ cells.

i. Quantification of γH2AX intensity from (**d**). 200 nuclei/condition were analyzed across three biological replicates. Statistical analysis by one-way ANOVA with Dunnett's multiple comparisons test.

Figure 3: ABCB1 overexpression is driven by genomic amplification and AP-1/TEAD-driven transcriptional mechanisms

a. Heatmap of relative mRNA expression for genes within the 7q21.12 amplicon (harboring ABCB1 and other MDR-related genes) in MM029 and resistant cells, as determined by RNA-seq.

b. ABCB1 copy number variations assessed by qPCR with genomic DNA. Data represent mean ± SD of three biological replicates; *P*-values were calculated via one-way ANOVA with Dunnett's multiple comparisons test (vs. MM029).

c. Venn diagram showing TEAD4 as the only shared iRegulon-predicted master regulator of overexpressed genes in $MM029^{lurbi\text{-}R}$, $MM029^{ecub\text{-}R}$, and $MM029^{PM54\text{-}R}$ cells.

d. Overlap between transcription factors upregulated upon short drug exposure (Cigrang et al., 2025) and those constitutively upregulated in resistant cell lines.

e. Heatmap depicting relative expression levels of indicated AP-1 and TEAD factors, shown as log2(Fold change) in resistant vs MM029 parental cells, as determined by RNA-seq. Highlighted genes are commonly and significantly upregulated (Adj. $P < 0.05$) in resistant cells.

f. RT–qPCR analysis of AP-1 and TEAD factors in MM029 and resistant cells. Expression normalized to 18S and shown as z-score heatmap. Data represent mean of three biological replicates. Highlighted genes are commonly upregulated in resistant cells.

g. Heatmap depicting relative expression levels of indicated AP-1 factors, shown as log2(Fold change) in short-term ecteinascidin-treated (10xIC50, 8h) vs DMSO-treated cells, as determined by RNA-seq in Cigrang et al., 2025.

h. Gene track of JUN occupancy at the *ABCB1* promoter in MM029 cells, as determined by CUT&Tag.

i. RT–qPCR analysis for *ABCB1*, *AXL*, *JUN*, and *GAPDH* in MM029$^{lurbi\text{-}R}$ cells treated for 72 h with either DMSO or inhibitors of AP-1 (10 μM for SR11302, 5 μM for Veratramine) or TEAD (10 μM for MGH-CP1). Data represent mean ± SD of three biological replicates; *P*-values were calculated via one-way ANOVA with Dunnett's multiple comparisons test (vs. DMSO).

j–l. Dose-response curves for MM029$^{lurbi\text{-}R}$ (g), MM029$^{ecub\text{-}R}$ (h), and MM029$^{PM54\text{-}R}$ (i) treated with increasing concentrations of lurbi ± inhibitors of AP-1 (10 μM for SR11302, 5 μM for Veratramine) or TEAD (10 μM for MGH-CP1). Viability is shown relative to DMSO-treated controls; IC_{50} values are indicated. Data represent mean ± SD of three biological replicates.

Figure 4: ABCB1 inhibition restores ecteinascidin binding and sensitivity

a–f. Dose–response curves for indicated cells treated with lurbi (a, d), ecub (b, e), or PM54 (c, f) in the presence or absence of ABCB1 inhibitors. Cells were treated with respective synthetic ecteinascidins for 72 h with or without 100 nM Tariquidar (a–c) or 150 μM Verapamil (d–f). Viability is shown relative to DMSO-treated controls; IC_{50} values are indicated. Data represent mean ± SD of three biological replicates.

g-h. Flow cytometry assessment of cell proliferation (**g**) and apoptosis (**h**) by CellTrace and Annexin V staining, respectively, in indicated cells and treatments (72 hours, 1xIC50 of MM029), with or without 100 nM Tariquidar or 150 μM Verapamil. Data represent mean ± SD of three biological replicates; *P*-values were calculated via one-way ANOVA with Dunnett's multiple comparisons test (vs. MM029).

i–j. MM029 and MM029$^{lurbi\text{-}R}$ cells were incubated with either DMSO or biotinylated lurbinectedin (Bio-lurbi; 30 nM, 8 h), ± Tariquidar (100 nM). Enrichment of Bio-lurbi at previously identified drug-binding sites in the *AXL* (i) and *TEAD4* (j) genes was assessed by CUT&Tag–qPCR. Data represent mean ± SD of three biological replicates; *P*-values were calculated via one-way ANOVA with Dunnett's multiple comparisons test.

k–l. RT–qPCR for AXL (k) and TEAD4 (l) expression in MM029 and MM029$^{Lurbi\text{-}R}$ cells treated with either DMSO or Lurbi (5 nM, 24 h) ± Tariquidar (100 nM). Expression is 18S-normalized. Data shown as mean ± SD of three replicates; statistical analysis by one-way ANOVA with Dunnett's multiple comparisons test.

Figure 5: ABCB1 overexpression confers resistance in melanoma and SCLC models

a. RT–qPCR analysis for ABCB1 in MM029 cells transduced with mCherry control ($MM029^{CTL}$) or ABCB1-expressing lentivirus ($MM029^{ABCB1}$). Expression is 18S-normalized. Data shown as mean ± SD of three replicates; statistical analysis by one-way ANOVA with Dunnett's multiple comparisons test.

b. Immunoblot of indicated proteins in $MM029^{CTL}$, resistant cells and $MM029^{ABCB1}$ cells. Molecular weights (kDa) are shown. Source data are available.

c–e. Dose–response curves for indicated cells treated for 72 h with increasing concentrations of lurbi (c), ecub (d), or PM54 (e). Viability is shown relative to DMSO-treated controls; IC_{50} values are indicated. Data represent mean ± SD of three biological replicates.

f. Indicated cells were treated with lurbi (5 nM, 24h) ± Tariquidar (100 nM). Protein lysates were immuno-blotted for proteins as indicated. Molecular mass of the proteins is shown (kDa). Source data are available.

g. RT–qPCR analysis for ABCB1 in DMS53 cells transduced with ABCB1-expressing lentivirus ($DMS53^{ABCB1}$) vs control DMS53 cells. Expression is 18S-normalized. Data shown as mean ± SD of three replicates; statistical analysis by one-way ANOVA with Dunnett's multiple comparisons test.

h. Immunoblot of indicated proteins in DMS53 and $DMS53^{ABCB1}$ cells. Molecular weights (kDa) are shown. Source data are available.

i. Immunoblot of indicated proteins in DMS53 and $DMS53^{ABCB1}$ cells treated with DMSO, lurbi or PM54 (5 nM, 24h). Molecular weights (kDa) are shown. Source data are available.

j. Dose–response curves for indicated cells treated for 72 h with increasing concentrations of lurbi, ecub, or PM54. Viability is shown relative to DMSO-treated controls; IC_{50} values are indicated. Data represent mean ± SD of three biological replicates.

Figure 6: Insensitivity to Doxorubicin through ABCB1 upregulation leads to cross-resistance with synthetic ecteinascidins

a. Dose–response curves for indicated cells treated for 72 h with increasing concentrations of Doxorubicin. Viability is shown relative to DMSO-treated controls; IC_{50} values are indicated. Data represent mean ± SD of three biological replicates.

b. RT–qPCR analysis for ABCB1 and others ABC transporters in $LoVo^{Doxo\text{-}R}$ vs control LoVo cells. Expression is 18S-normalized. Data shown as mean ± SD of three replicates; statistical analysis by one-way ANOVA with Dunnett's multiple comparisons test.

c. Immunoblot of indicated proteins in LoVo WT and $LoVo^{Doxo\text{-}R}$ cells. Molecular mass of the proteins is shown (kDa). Source data are available.

d. Dose–response curves for indicated cells treated for 72 h with increasing concentrations of indicated synthetic ecteinascidins. Viability is shown relative to DMSO-treated controls; IC_{50} values are indicated. Data represent mean ± SD of three biological replicates.

e-g. Dose–response curves of the indicated cells treated with lurbi (**e**), ecub (**f**), or PM54 (**g**) in the presence of ABCB1 inhibitor Tariquidar or following ABCB1 knockdown. Cells were exposed to the respective synthetic ecteinascidins for 72 h in the presence of 100 nM Tariquidar or transfected with siABCB1 for 72 h. Cell viability is expressed relative to DMSO-treated controls, and IC_{50} values are shown. Data represent mean ± SD from three biological replicates.

h. Immunoblot of indicated proteins in LOVO WT and $LoVo^{Doxo\text{-}R}$ cells. Molecular mass of the proteins is shown (kDa). Source data are available.

i. Dose–response curves for $LoVo^{Doxo\text{-}R}$ cells treated for 72 h with increasing concentrations of Doxorubicin in the presence of ABCB1 inhibitor Tariquidar. Viability is shown relative to DMSO-treated controls; IC_{50} values are indicated. Data represent mean ± SD of three biological replicates.

Figure 7: ABCB1 is degraded in differentiated melanoma cells but stabilized by CD44 and PIM1 in undifferentiated cells

a. RT–qPCR analysis for ABCB1 in IGR37 and SKMEL28 cells transduced with ABCB1-expressing lentivirus ($IGR37^{ABCB1}$ and $SKMEL28^{ABCB1}$) vs control cells. Expression is 18S-normalized. Data shown

as mean ± SD of three replicates; statistical analysis by one-way ANOVA with Dunnett's multiple comparisons test.

b. Immunoblot for ABCB1 and GAPDH in indicated cells. Molecular weights (kDa) are shown. Source data are available.

c. IGR37^{ABCB1} and SKMEL28^{ABCB1} cells were treated with MG132 (24h, 1uM) and protein extracts were then immunoblotted for ABCB1 and GAPDH. Molecular weights (kDa) are shown. Source data are available.

d. MM029^{ABCB1} cells (upper panel) or MM099^{ABCB1} cells (lower panel) were treated with MG132 (24h, 1uM) and protein extracts were then immunoblotted for indicated proteins. Molecular weights (kDa) are shown. Source data are available.

e. Protein extracts were isolated from SKMEL28^{ABCB1} cells treated with DMSO or MG132 (24h, 1uM). After immunoprecipitation with anti-ubiquitin (IP: Ubiquitin), the immunoprecipitated proteins were resolved by SDS-PAGE and blotted with anti-ABCB1 antibody. Source data are available.

f. Protein extracts from SKMEL28^{ABCB1} cells transduced with lentivirus expressing shRNA targeting FBXO21 or non-targeting control were subjected to immunoblotting for the indicated proteins. Molecular weights (kDa) are indicated. Source data are available.

g-h. MM029^{ABCB1} cells were treated with 5 uM SGI-1776 for 24h (**g**), or 48h with siSCR or siCD44 (**h**) before Rhodamine123 staining and efflux quantification by flow cytometry. Reduced Rhodamine123 signal corresponds to higher efflux capacity. Data represent mean ± SD of three biological replicates; *P*-values were calculated via one-way ANOVA with Dunnett's multiple comparisons test.

i-j. Dose-response curves for MM029^{ABCB1} cells (**i**) or MM029$^{lurbi\text{-}R}$ cells (**j**) treated with increasing concentrations of lurbi ± DMSO, SGI-1776 (5 uM), siSCR, or siCD44 for 72h. Viability is shown relative to DMSO-treated controls; IC_{50} values are indicated. Data represent mean ± SD of three biological replicates.

k. Dose-response curves for LoVo$^{Doxo\text{-}R}$ cells treated with increasing concentrations of ecteinascidins ± DMSO or SGI-1776 (5 μM). Viability is shown relative to DMSO-treated controls; IC_{50} values are indicated. Data represent mean ± SD of three biological replicates.

Supplemental Figure Legends

Supplemental Figure 1: Resistant cells display decreased expression of mesenchymal and neural-crest melanoma signatures

a. Heatmap showing z-score–normalized expression of all significantly deregulated genes across resistant cell lines compared to MM029 cells.

b. Venn diagram comparing significantly downregulated genes between $MM029^{lurbi\text{-}R}$, $MM029^{ecub\text{-}R}$, and $MM029^{PM54\text{-}R}$ cells, as determined by bulk RNA-seq.

c-d. Gene Ontology analysis of the commonly upregulated (**c**) or downregulated (**d**) genes between $MM029^{lurbi\text{-}R}$, $MM029^{ecub\text{-}R}$, and $MM029^{PM54\text{-}R}$ cells.

e. Gene set enrichment analysis hallmarks commonly affected (either significantly negative or positive correlations) between $MM029^{lurbi\text{-}R}$, $MM029^{ecub\text{-}R}$, and $MM029^{PM54\text{-}R}$ cells.

f-g. Graph depicting average log2(Fold Change) of melanoma cell state signature genes, identified in Rambow et al., 2018 (**f**), and Pozniak et al., 2024 (**g**), between $MM029^{lurbi\text{-}R}$, $MM029^{ecub\text{-}R}$, or $MM029^{PM54\text{-}R}$ cells vs. MM029 cells. Error bars indicate mean ± SD between signature genes. *P*-values were determined using ordinary one-way ANOVA with Dunnett's multiple comparisons test (vs. MM029).

h. Graph depicting average log2(Fold Change) of genes upregulated upon ICI resistance or genes upregulated upon MAPKi resistance, identified in Hugo et al., 2015, 2016, between $MM029^{lurbi\text{-}R}$, $MM029^{ecub\text{-}R}$, or $MM029^{PM54\text{-}R}$ cells vs. MM029 cells. Error bars indicate mean ± SD between signature genes. *P*-values were determined using ordinary one-way ANOVA with Dunnett's multiple comparisons test (vs. MM029) .

i. TIDE prediction scores based on differentially expressed genes between $MM029^{lurbi\text{-}R}$, $MM029^{ecub\text{-}R}$, or $MM029^{PM54\text{-}R}$ cells vs. MM029 cells. Lower TIDE scores predict decreased tumor immune dysfunction and exclusion and improved ICI response.

Supplemental Figure 2: Undifferentiated MM029 cells display basal rates of ABCB1 expression

a. Representative gating strategies for MM029, $MM029^{lurbi\text{-}R}$, $MM029^{ecub\text{-}R}$, and $MM029^{PM54\text{-}R}$ cells treated with either DMSO or Rhodamine123.

b. RT–qPCR analysis for ABCB1 in indicated melanoma cells. Expression normalized to 18S. Data represent mean ± SD of three biological replicates; *P*-values were calculated via one-way ANOVA with Dunnett's multiple comparisons test (vs. MM029).

c. Protein lysates of different melanoma cell types were immuno-blotted for proteins as indicated. Molecular weights (kDa) are shown. Source data are available.

d. Gene tracks of ATAC-Seq, H3K27ac, BRD4, RNA polymerase II (RNAPII) occupancy, and RNA-Seq signals at the *ABCB1* promoter in differentiated 501mel or undifferentiated MM029 cells. Data from Cigrang et al., 2025.

Supplemental Figure 3: ABCB1 inhibition resensitizes resistant cells to synthetic ecteinascidins in vitro

a. Protein lysates from the indicated cells were immuno-blotted for ABCB1 and ACTb, after 48h treatment of siSCR or siABCB1. Molecular mass of the proteins is shown (kDa). Source data are available.

b-d. Indicated cells were treated with siSCR or siABCB1 for 48h, before being treated with increasing concentrations of lurbi (b), ecub (c) or PM54 (d) for 72h. Cell viability is shown relative to DMSO-treated controls and IC_{50} values are indicated. Error bars indicate mean values +/- Standard Deviation (SD) for three biological replicates.

e-f. Indicated cells were incubated with increasing concentrations of Tariquidar (**e**) or Verapamil (**f**) for 24h, before Rhodamine efflux essays were performed by Flow cytometry. % of Rhodamine123 positive cells are indicated. Cells positive for Rhodamine123 signal display reduced efflux activity.

g-h. Gene tracks showing relative enrichments of Bio-Lurbi, Bio-PM54, RNA polymerase II (RNAPII), BRD4, H3K27ac, as well as ATAC-Seq signal, at the *AXL* (**g**) and *TEAD4* (**h**) loci, as identified in Cigrang et al., 2025. The red square indicates region targeted by primers for CUT&Tag-qPCR.

Supplemental Figure 4: Knockdown of FBXO21 increases ABCB1 levels but is insufficient to induce resistance in differentiated melanoma cells

a. Representative immunofluorescence images of ABCB1 and Tubulin in MM029^{ABCB1}, SKMEL28^{ABCB1} and SKMEL28^{ABCB1} shFBXO21 cells.

b. Quantification of ABCB1 intensity from 40 cells/condition were analyzed across three biological replicates. Intensities within each ROI were measured and normalized to cell area. Statistical analysis by one-way ANOVA with Dunnett's multiple comparisons test.

c. SKMEL28^{ABCB1} cells transduced with lentivirus expressing shRNA targeting FBXO21 or non-targeting control were stained with Rhodamine123 and efflux quantification was performed by flow cytometry. Data represent mean ± SD of three biological replicates; P-values were calculated via one-way ANOVA with Dunnett's multiple comparisons test. Representative gating strategies are indicated vs MM029$^{lurbi-R}$ cells.

d. Dose-response curves for SKMEL28^{ABCB1} cells transduced with lentivirus expressing shRNA targeting FBXO21 or non-targeting control were treated with increasing concentrations of lurbi for 72h. Viability is shown relative to DMSO-treated controls; IC_{50} values are indicated. Data represent mean ± SD of three biological replicates.

e. Protein lysates of different melanoma cell types were immuno-blotted for proteins as indicated. Molecular weights (kDa) are shown. Source data are available.

f. Gene tracks of ATAC-Seq, H3K27ac, BRD4, RNA polymerase II (RNAPII) occupancy, and RNA-Seq signals at the *CD44* promoter in differentiated 501mel or undifferentiated MM029 cells. Data from Cigrang et al., 2025.

g. MM029^{ABCB1} cells were transfected with siSCR or siCD44 for 72 h, followed by treatment with cycloheximide (100 µg/mL) for 0, 8, or 16 h. Protein extracts were subjected to immunoblotting for the indicated proteins. Molecular weights (kDa) are indicated. Source data are available.

h. Relative *ABCB1* levels from (**f**) were quantified, normalized to ACTB, and are presented as mean ± SD of three biological replicates. Statistical analysis was performed using one-way ANOVA with Dunnett's multiple comparisons test.

Supplemental Figure 5: ABCB1 stabilizers CD44 and PIM1 are overexpressed in undifferentiated melanoma cells due to AP-1/TEAD activity

a. RT–qPCR analysis of genes implicated in ABCB1 degradation or stabilization across three differentiated and three undifferentiated melanoma cell lines. Expression values were normalized to 18S and visualized as a z-score heatmap. Data represent the mean of three biological replicates. Highlighted genes are differentially expressed between cell states.

b. Relative expression (z-scores) of *CD44* and *PIM1* from (a). Data represent mean ± SD of three biological replicates. Statistical analysis was performed using one-way ANOVA with Dunnett's multiple comparisons test.

c. Venn diagram showing the overlap between ABCB1 stabilizers (**a**) with melanoma cell state-associated gene signatures (Wouters et al., 2020).

d. Gene track of JUN occupancy at the *CD44* and *PIM1* promoters in MM029 cells, as determined by CUT&Tag.

e. RT–qPCR analysis for PIM1 and CD44 in MM029 cells treated for 24 h with either DMSO or inhibitors of AP-1 (10 μM for SR11302, 5 μM for Veratramine) or TEAD (10 μM for MGH-CP1). Data represent mean ± SD of three biological replicates; P-values were calculated via one-way ANOVA with Dunnett's multiple comparisons test (vs. DMSO).

f. Histogram showing mean expression level (log2(FC) vs respective controls) of indicated factors in 501mel shMITF and 501mel siSOX10 cells. Data from Laurette et al., 2015.

g. Representative gating strategies for MM029^{ABCB1} pre-treated with 5 μM SGI-1776 for 24h or transfected for 48h with siSCR or siCD44, followed by DMSO or Rhodamine123 treatment.

Supplemental Figure 6: Working model illustrating the cell state-dependent regulation of *ABCB1*-mediated drug resistance

Undifferentiated melanoma cells exhibit high AP-1/TEAD transcriptional activity, which drives the expression of *ABCB1* and its stabilizers, including CD44 and PIM1, enabling drug efflux and resistance acquisition. In contrast, differentiated melanoma cells, characterized by low AP-1/TEAD activity, fail to

produce functional ABCB1 due to reduced gene transcription and enhanced proteasomal degradation. In the absence of ABCB1, synthetic ecteinascidins accumulate in the nucleus, bind to DNA, and induce DNA damage and transcriptional repression.

Figure 1

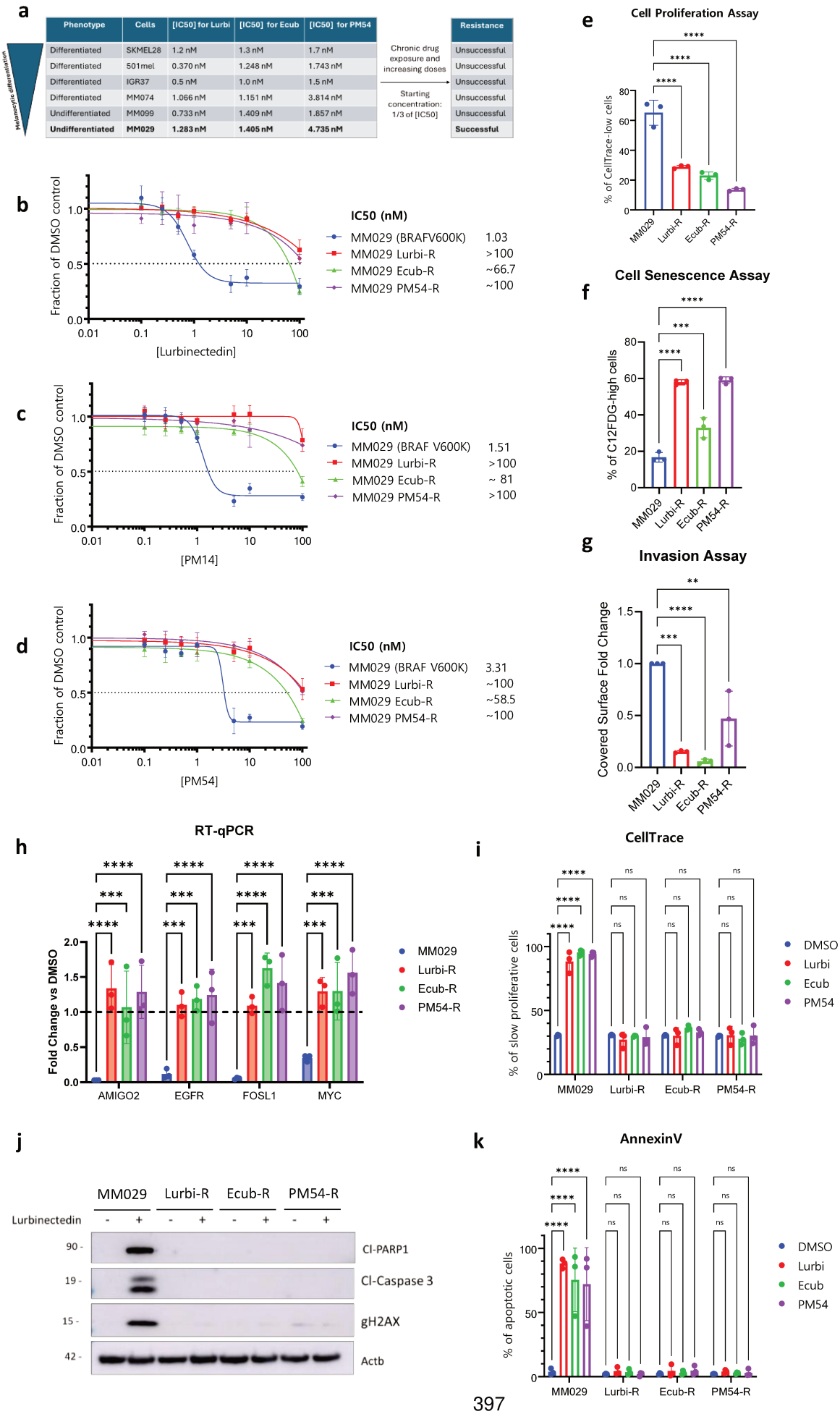
a
Phenotype
Cells
[IC50] for Lurbi
[IC50] for Ecub
[IC50] for PM54
Resistance
Differentiated SKMEL28 1.2 nM 1.3 nM 1.7 nM Unsuccessful
Differentiated 501mel 0.370 nM 1.248 nM 1.743 nM Unsuccessful
Differentiated IGR37 0.5 nM 1.0 nM 1.5 nM Unsuccessful
Differentiated MM074 1.066 nM 1.151 nM 3.814 nM Unsuccessful
Undifferentiated MM099 0.733 nM 1.409 nM 1.857 nM Unsuccessful
Undifferentiated MM029 1.283 nM 1.405 nM 4.735 nM Successful
Melanocytic differentiation
Chronic drug exposure and increasing doses
Starting concentration: 1/3 of [IC50]
b
Fraction of DMSO control
[Lurbinectedin]
IC50 (nM)
MM029 (BRAFV600K) 1.03
MM029 Lurbi-R >100
MM029 Ecub-R ~66.7
MM029 PM54-R ~100
c
Fraction of DMSO control
[PM14]
IC50 (nM)
MM029 (BRAF V600K) 1.51
MM029 Lurbi-R >100
MM029 Ecub-R ~ 81
MM029 PM54-R >100
d
Fraction of DMSO control
[PM54]
IC50 (nM)
MM029 (BRAF V600K) 3.31
MM029 Lurbi-R ~100
MM029 Ecub-R ~58.5
MM029 PM54-R ~100
e
Cell Proliferation Assay
% of CellTrace-low cells
MM029
Lurbi-R
Ecub-R
PM54-R
f
Cell Senescence Assay
% of C12FDG-high cells
g
Invasion Assay
Covered Surface Fold Change
h
RT-qPCR
Fold Change vs DMSO
AMIGO2
EGFR
FOSL1
MYC
MM029
Lurbi-R
Ecub-R
PM54-R
i
CellTrace
% of slow proliferative cells
DMSO
Lurbi
Ecub
PM54
j
MM029
Lurbi-R
Ecub-R
PM54-R
Lurbinectedin
Cl-PARP1
Cl-Caspase 3
gH2AX
Actb
k
AnnexinV
% of apoptotic cells
DMSO
Lurbi
Ecub
PM54

Figure 2

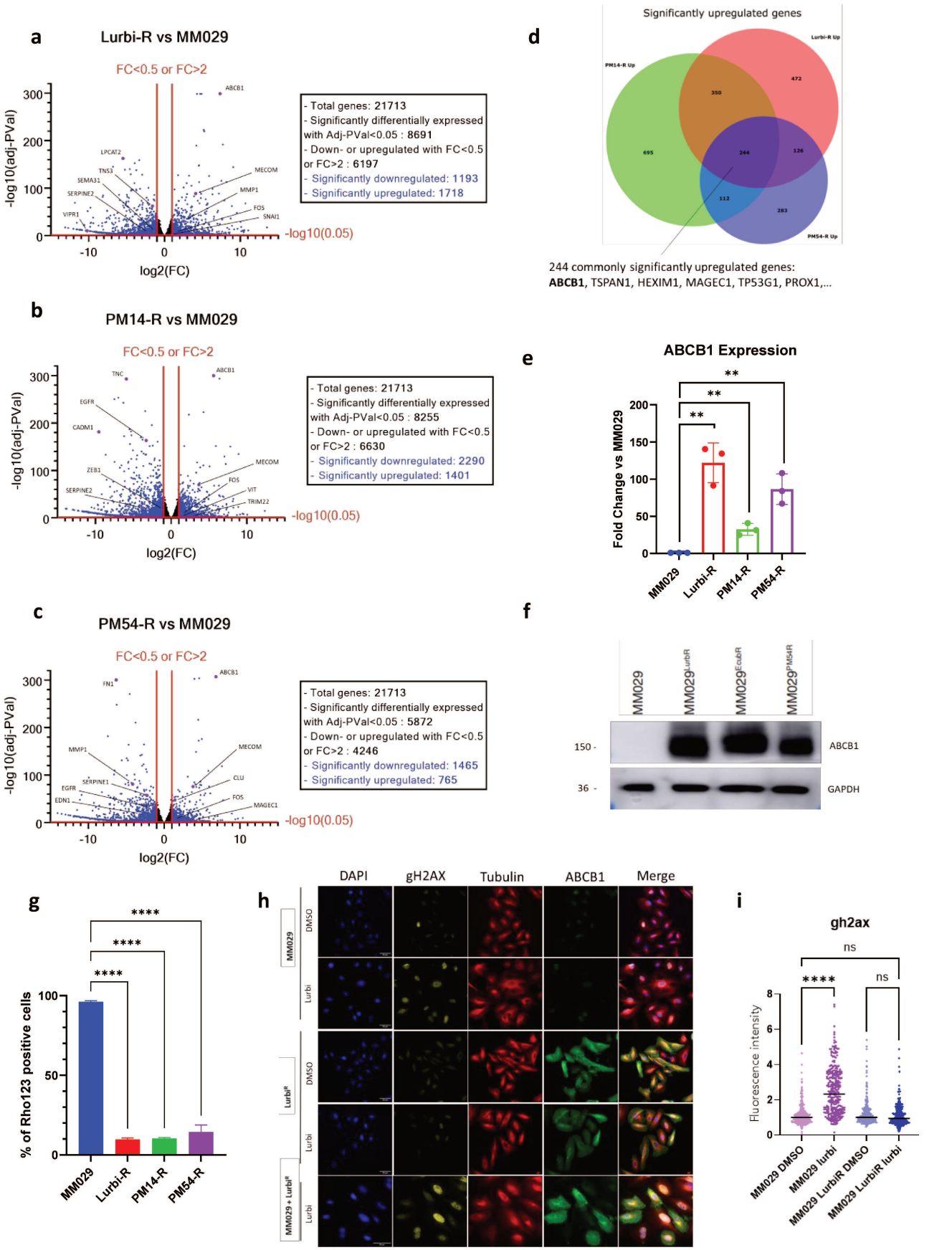
a
Lurbi-R vs MM029
FC<0.5 or FC>2
-log10(adj-PVal)
log2(FC)
-log10(0.05)
- Total genes: 21713
- Significantly differentially expressed with Adj-PVal<0.05 : 8691
- Down- or upregulated with FC<0.5 or FC>2 : 6197
- Significantly downregulated: 1193
- Significantly upregulated: 1718
ABCB1
LPCAT2
TNS3
SEMA3I
SERPINE2
VIPR1
MECOM
MMP1
FOS
SNAI1
b
PM14-R vs MM029
FC<0.5 or FC>2
- Total genes: 21713
- Significantly differentially expressed with Adj-PVal<0.05 : 8255
- Down- or upregulated with FC<0.5 or FC>2 : 6630
- Significantly downregulated: 2290
- Significantly upregulated: 1401
TNC
EGFR
CADM1
ZEB1
SERPINE2
VIT
TRIM22
c
PM54-R vs MM029
FC<0.5 or FC>2
- Total genes: 21713
- Significantly differentially expressed with Adj-PVal<0.05 : 5872
- Down- or upregulated with FC<0.5 or FC>2 : 4246
- Significantly downregulated: 1465
- Significantly upregulated: 765
FN1
MMP1
SERPINE1
EGFR
EDN1
CLU
MAGEC1
d
Significantly upregulated genes
Lurbi-R Up
PM14-R Up
PM54-R Up
472
350
695
244
126
112
283
244 commonly significantly upregulated genes:
ABCB1, TSPAN1, HEXIM1, MAGEC1, TP53G1, PROX1,...
e
ABCB1 Expression
Fold Change vs MM029
MM029
Lurbi-R
PM14-R
PM54-R
f
MM029
MM029LurbR
MM029EcabR
MM029PM54R
150 -
36 -
ABCB1
GAPDH
g
% of Rho123 positive cells
MM029
Lurbi-R
PM14-R
PM54-R
h
DAPI
gH2AX
Tubulin
ABCB1
Merge
MM029
DMSO
Lurbi
MM029 + LurbiR
i
gh2ax
Fluorescence intensity
MM029 DMSO
MM029 lurbi
MM029 LurbiR DMSO
MM029 LurbiR lurbi

Supplemental Figure 1



a

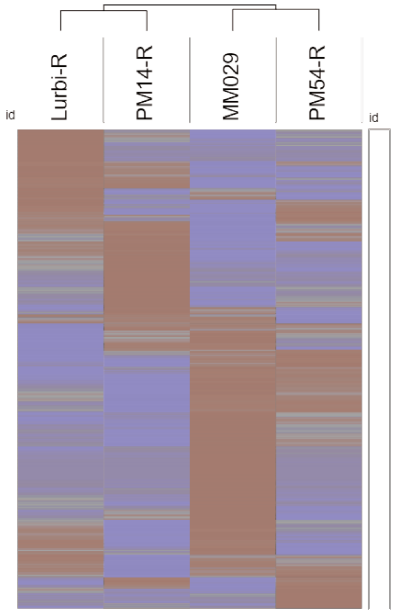

b

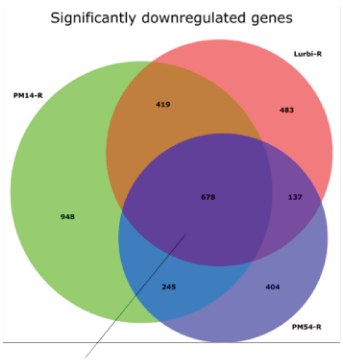

678 commonly significantly downregulated genes:
TNS3, EGFR, NGFR, NGF, VIPR1, AR, KIT, ...

c

244 commonly significantly upregulated genes

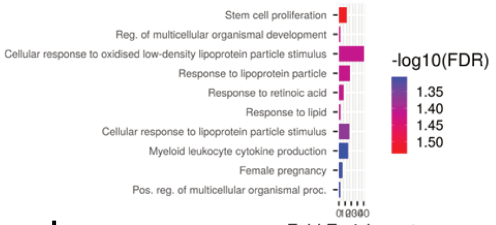

d

678 commonly significantly downregulated genes

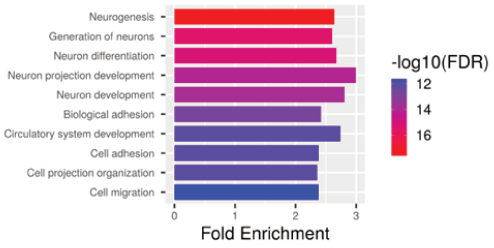

e

GSEA: Common positive correlation (Nom. P-val < 0.05)

No significant correlation found

GSEA: Common negative correlation (Nom. P-val < 0.05)

HALLMARK_EPITHELIAL_MESENCHYMAL_TRANSITION
HALLMARK_TNFA_SIGNALING_VIA_NFKB
HALLMARK_INFLAMMATORY_RESPONSE
HALLMARK_UV_RESPONSE_DN
HALLMARK_APICAL_JUNCTION
HALLMARK_HEDGEHOG_SIGNALING
HALLMARK_KRAS_SIGNALING_UP
HALLMARK_TGF_BETA_SIGNALING
HALLMARK_ALLOGRAFT_REJECTION
HALLMARK_MYOGENESIS
HALLMARK_ESTROGEN_RESPONSE_LATE
HALLMARK_MITOTIC_SPINDLE
HALLMARK_ESTROGEN_RESPONSE_EARLY
HALLMARK_P53_PATHWAY
HALLMARK_PI3K_AKT_MTOR_SIGNALING
HALLMARK_IL6_JAK_STAT3_SIGNALING
HALLMARK_UV_RESPONSE_UP
HALLMARK_APICAL_SURFACE

f

Melanoma phenotype signatures (Rambow et al. 2018)

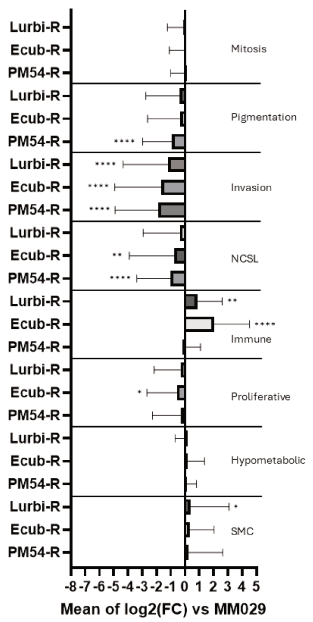

g

Melanoma phenotype signatures (Pozniak et al. 2024)

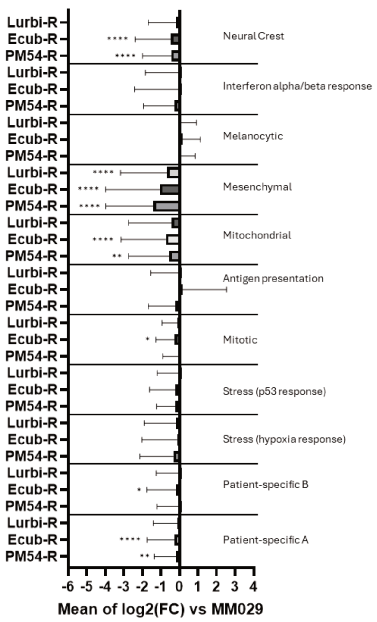

h

ICI-R upregulated + MAPKi-R upregulated (Hugo et al. 2015, 2016)

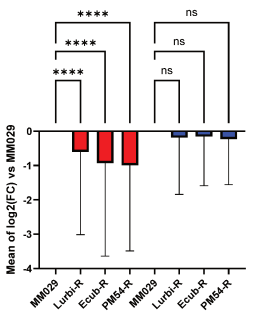

i

ICI resistance signature

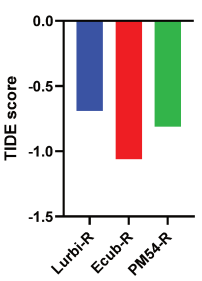

Supplemental Figure 2

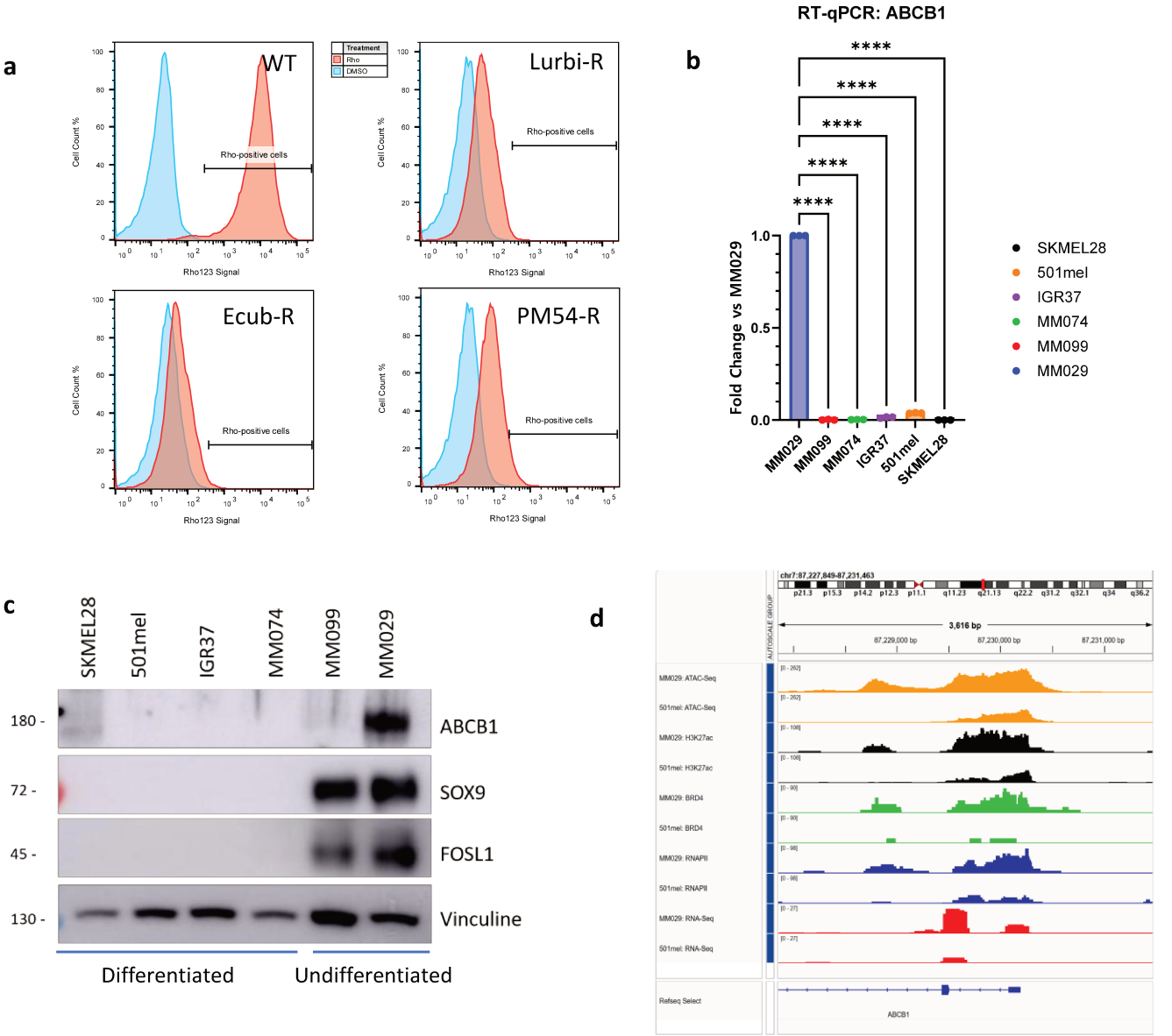

Figure 3

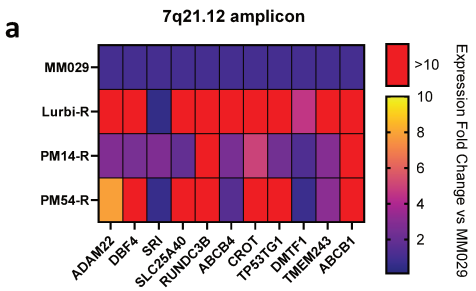
a
7q21.12 amplicon
MM029
Lurbi-R
PM14-R
PM54-R
ADAM22
DBF4
SRI
SLC25A40
RUNDC3B
ABCB4
CROT
TP53TG1
DMTF1
TMEM243
ABCB1
>10
10
8
6
4
2
Expression Fold Change vs MM029

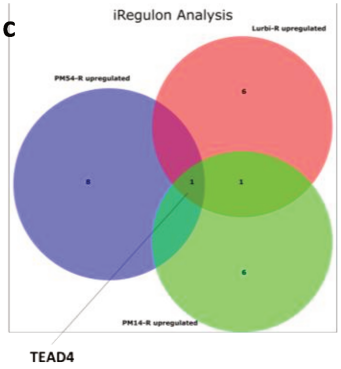
c
iRegulon Analysis
Lurbi-R upregulated
PM54-R upregulated
PM14-R upregulated
TEAD4

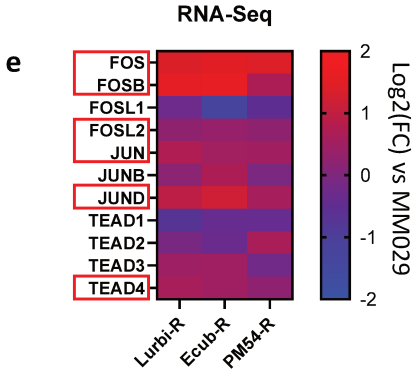
e
RNA-Seq
FOS
FOSB
FOSL1
FOSL2
JUN
JUNB
JUND
TEAD1
TEAD2
TEAD3
TEAD4
Lurbi-R
Ecub-R
PM54-R
Log2(FC) vs MM029

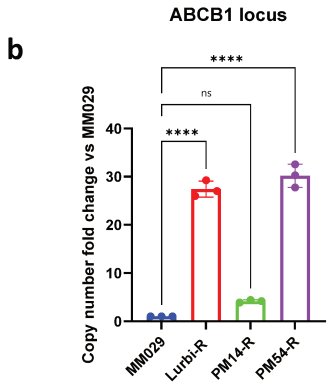
b
ABCB1 locus
Copy number fold change vs MM029
MM029
Lurbi-R
PM14-R
PM54-R
****
ns

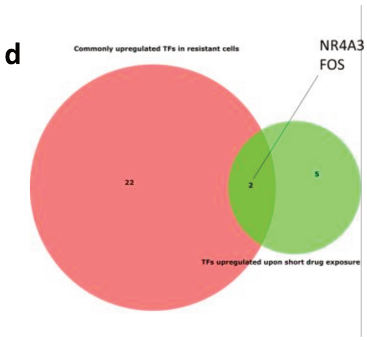
d
Commonly upregulated TFs in resistant cells
NR4A3
FOS
TFs upregulated upon short drug exposure

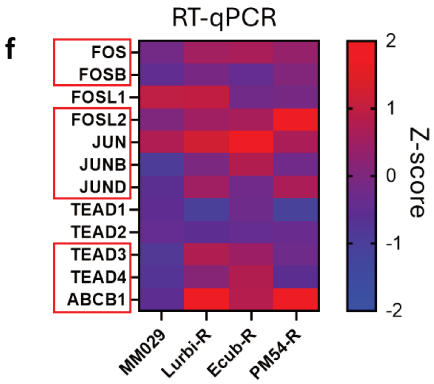
f
RT-qPCR
FOS
FOSB
FOSL1
FOSL2
JUN
JUNB
JUND
TEAD1
TEAD2
TEAD3
TEAD4
ABCB1
MM029
Lurbi-R
Ecub-R
PM54-R
Z-score

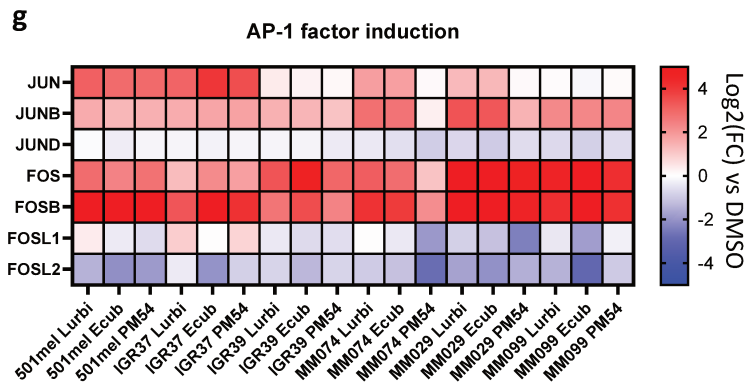
g
AP-1 factor induction
JUN
JUNB
JUND
FOS
FOSB
FOSL1
FOSL2
501mel Lurbi
501mel Ecub
501mel PM54
IGR37 Lurbi
IGR37 Ecub
IGR37 PM54
IGR39 Lurbi
IGR39 Ecub
IGR39 PM54
MM074 Lurbi
MM074 Ecub
MM074 PM54
MM029 Lurbi
MM029 Ecub
MM029 PM54
MM099 Lurbi
MM099 Ecub
MM099 PM54
Log2(FC) vs DMSO

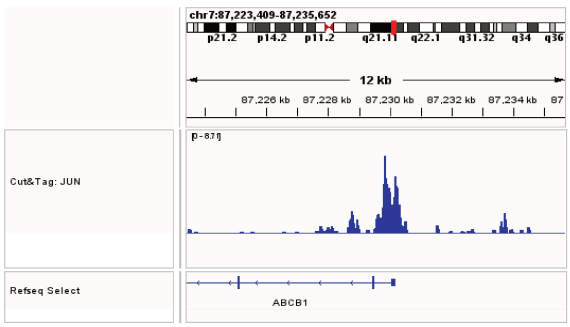
h
chr7:87,223,409-87,235,652
12 kb
Cut&Tag: JUN
Refseq Select
ABCB1

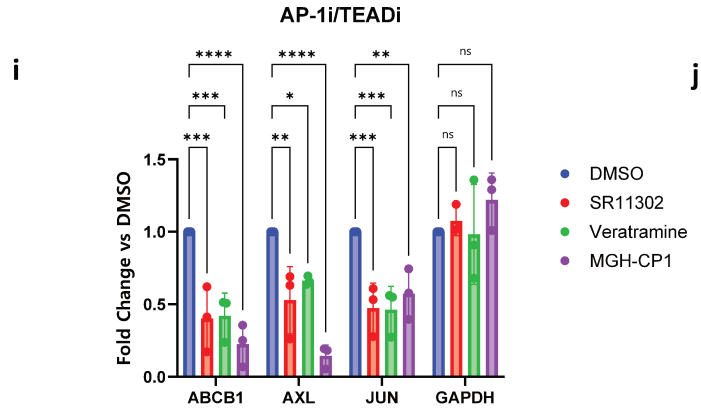
i
AP-1i/TEADi
Fold Change vs DMSO
ABCB1
AXL
JUN
GAPDH
DMSO
SR11302
Veratramine
MGH-CP1

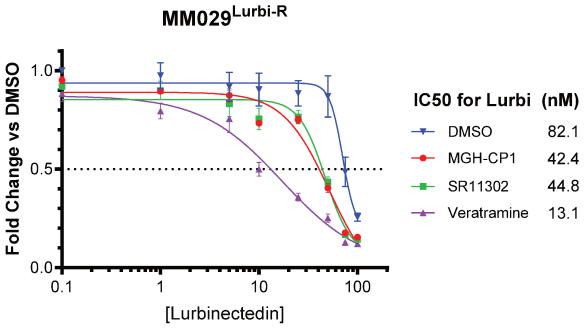
j
MM029Lurbi-R
Fold Change vs DMSO
[Lurbinectedin]
IC50 for Lurbi (nM)
DMSO 82.1
MGH-CP1 42.4
SR11302 44.8
Veratramine 13.1

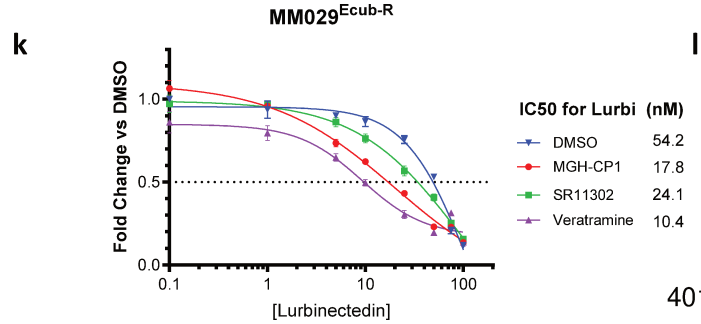
k
MM029Ecub-R
Fold Change vs DMSO
[Lurbinectedin]
IC50 for Lurbi (nM)
DMSO 54.2
MGH-CP1 17.8
SR11302 24.1
Veratramine 10.4

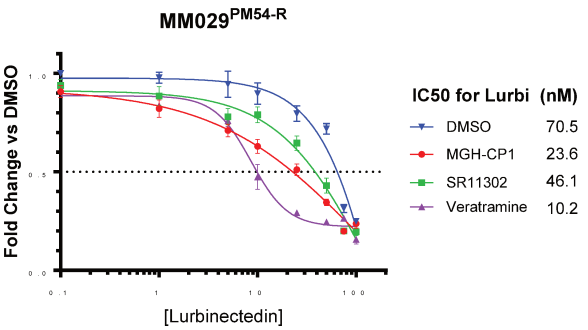
l
MM029PM54-R
Fold Change vs DMSO
[Lurbinectedin]
IC50 for Lurbi (nM)
DMSO 70.5
MGH-CP1 23.6
SR11302 46.1
Veratramine 10.2

Supplemental Figure 3

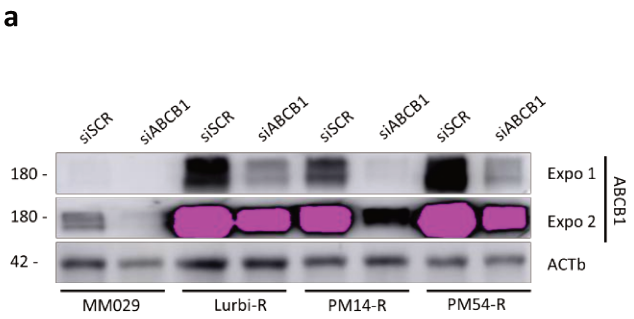

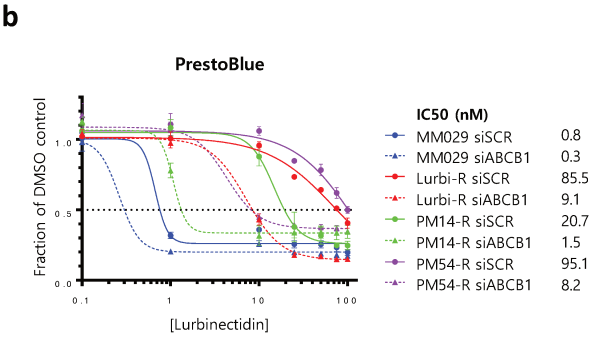

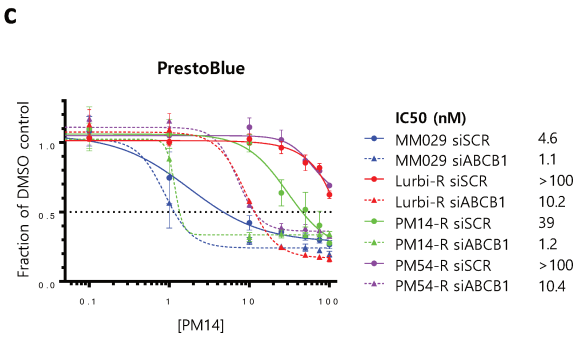

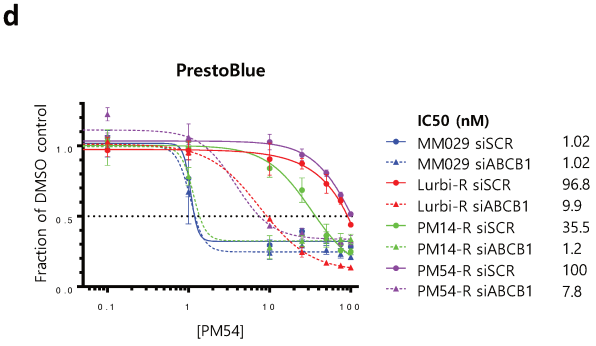

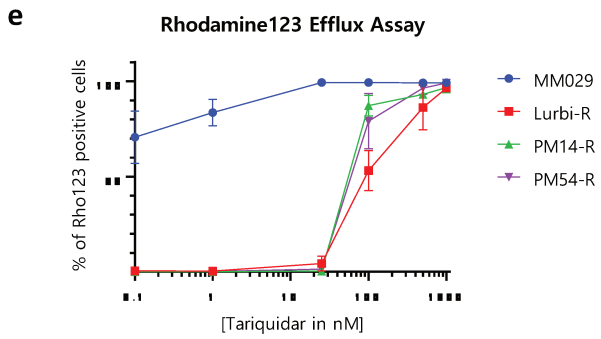

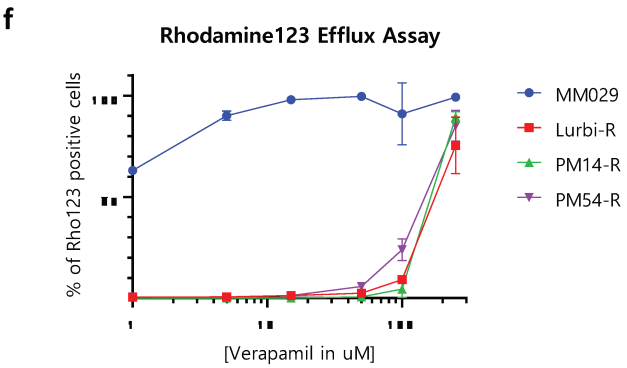

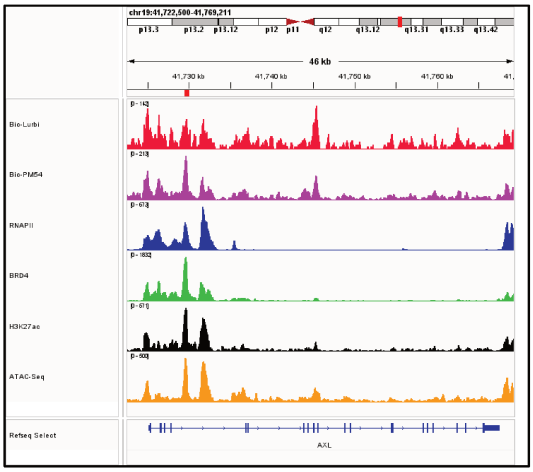

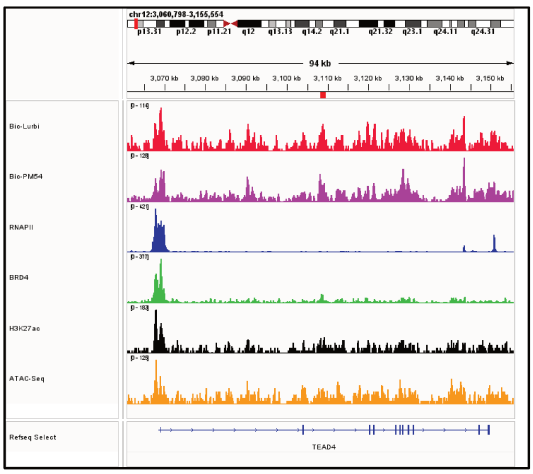

Figure 4

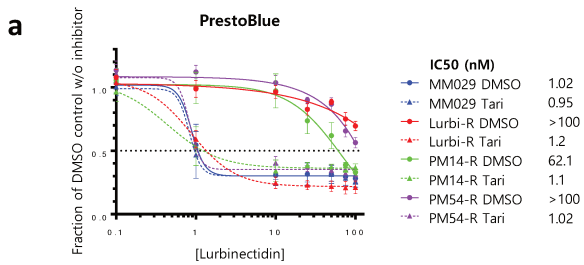
a
PrestoBlue
Fraction of DMSO control w/o inhibitor
[Lurbinectidin]
IC50 (nM)
MM029 DMSO 1.02
MM029 Tari 0.95
Lurbi-R DMSO >100
Lurbi-R Tari 1.2
PM14-R DMSO 62.1
PM14-R Tari 1.1
PM54-R DMSO >100
PM54-R Tari 1.02

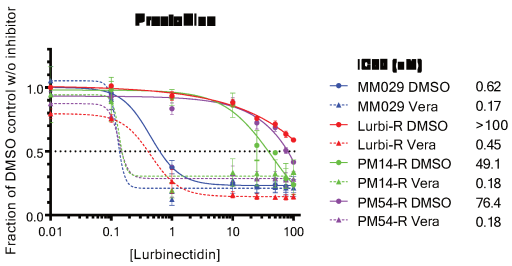
d
Fraction of DMSO control w/o inhibitor
[Lurbinectidin]
MM029 DMSO 0.62
MM029 Vera 0.17
Lurbi-R DMSO >100
Lurbi-R Vera 0.45
PM14-R DMSO 49.1
PM14-R Vera 0.18
PM54-R DMSO 76.4
PM54-R Vera 0.18

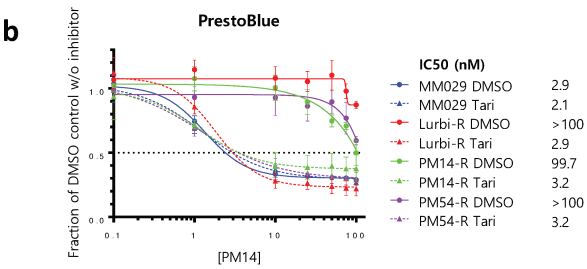
b
PrestoBlue
Fraction of DMSO control w/o inhibitor
[PM14]
IC50 (nM)
MM029 DMSO 2.9
MM029 Tari 2.1
Lurbi-R DMSO >100
Lurbi-R Tari 2.9
PM14-R DMSO 99.7
PM14-R Tari 3.2
PM54-R DMSO >100
PM54-R Tari 3.2

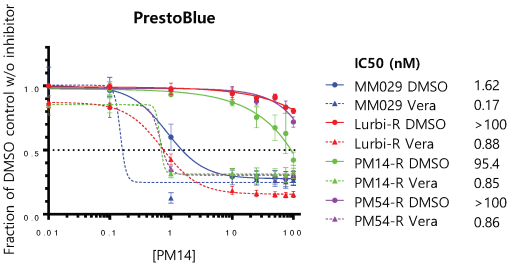
e
PrestoBlue
Fraction of DMSO control w/o inhibitor
[PM14]
IC50 (nM)
MM029 DMSO 1.62
MM029 Vera 0.17
Lurbi-R DMSO >100
Lurbi-R Vera 0.88
PM14-R DMSO 95.4
PM14-R Vera 0.85
PM54-R DMSO >100
PM54-R Vera 0.86

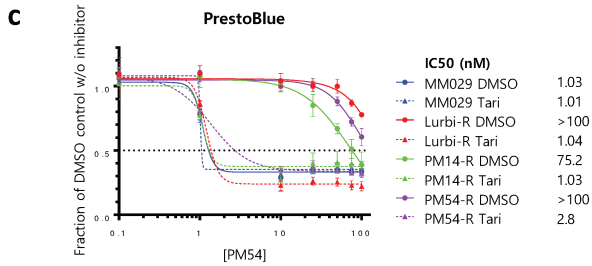
c
PrestoBlue
Fraction of DMSO control w/o inhibitor
[PM54]
IC50 (nM)
MM029 DMSO 1.03
MM029 Tari 1.01
Lurbi-R DMSO >100
Lurbi-R Tari 1.04
PM14-R DMSO 75.2
PM14-R Tari 1.03
PM54-R DMSO >100
PM54-R Tari 2.8

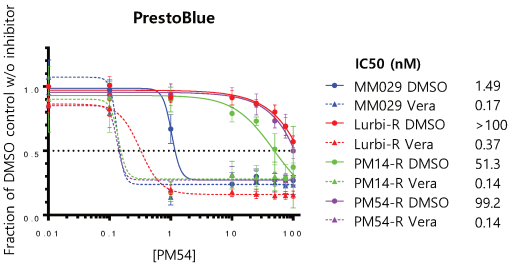
f
PrestoBlue
Fraction of DMSO control w/o inhibitor
[PM54]
IC50 (nM)
MM029 DMSO 1.49
MM029 Vera 0.17
Lurbi-R DMSO >100
Lurbi-R Vera 0.37
PM14-R DMSO 51.3
PM14-R Vera 0.14
PM54-R DMSO 99.2
PM54-R Vera 0.14

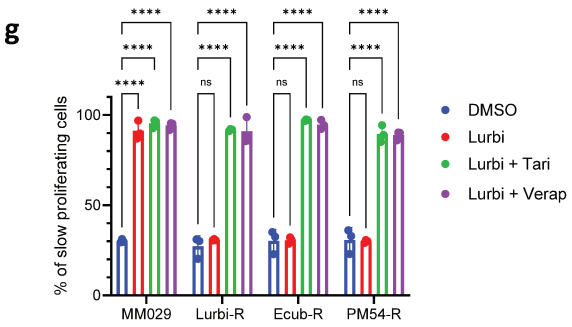
g
% of slow proliferating cells
MM029
Lurbi-R
Ecub-R
PM54-R
DMSO
Lurbi
Lurbi + Tari
Lurbi + Verap

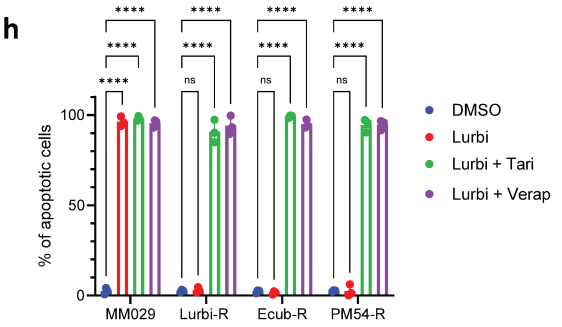
h
% of apoptotic cells
MM029
Lurbi-R
Ecub-R
PM54-R
DMSO
Lurbi
Lurbi + Tari
Lurbi + Verap

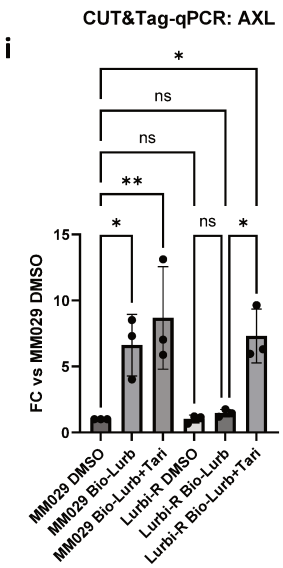
i
CUT&Tag-qPCR: AXL
FC vs MM029 DMSO
MM029 DMSO
MM029 Bio-Lurb
MM029 Bio-Lurb+Tari
Lurbi-R DMSO
Lurbi-R Bio-Lurb
Lurbi-R Bio-Lurb+Tari

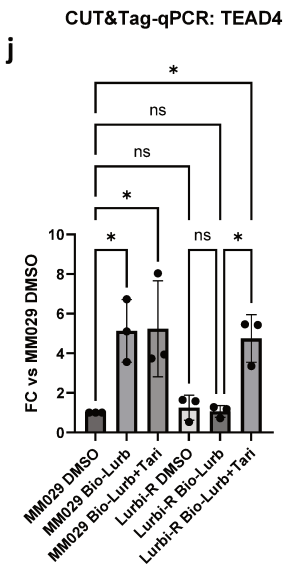
j
CUT&Tag-qPCR: TEAD4
FC vs MM029 DMSO
MM029 DMSO
MM029 Bio-Lurb
MM029 Bio-Lurb+Tari
Lurbi-R DMSO
Lurbi-R Bio-Lurb
Lurbi-R Bio-Lurb+Tari

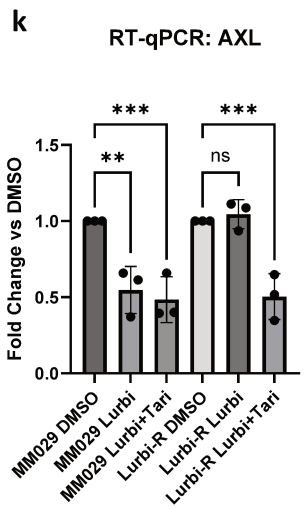
k
RT-qPCR: AXL
Fold Change vs DMSO
MM029 DMSO
MM029 Lurbi
MM029 Lurbi+Tari
Lurbi-R DMSO
Lurbi-R Lurbi
Lurbi-R Lurbi+Tari

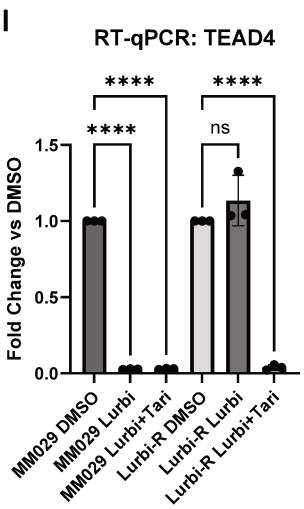
l
RT-qPCR: TEAD4
Fold Change vs DMSO
MM029 DMSO
MM029 Lurbi
MM029 Lurbi+Tari
Lurbi-R DMSO
Lurbi-R Lurbi
Lurbi-R Lurbi+Tari

Figure 5

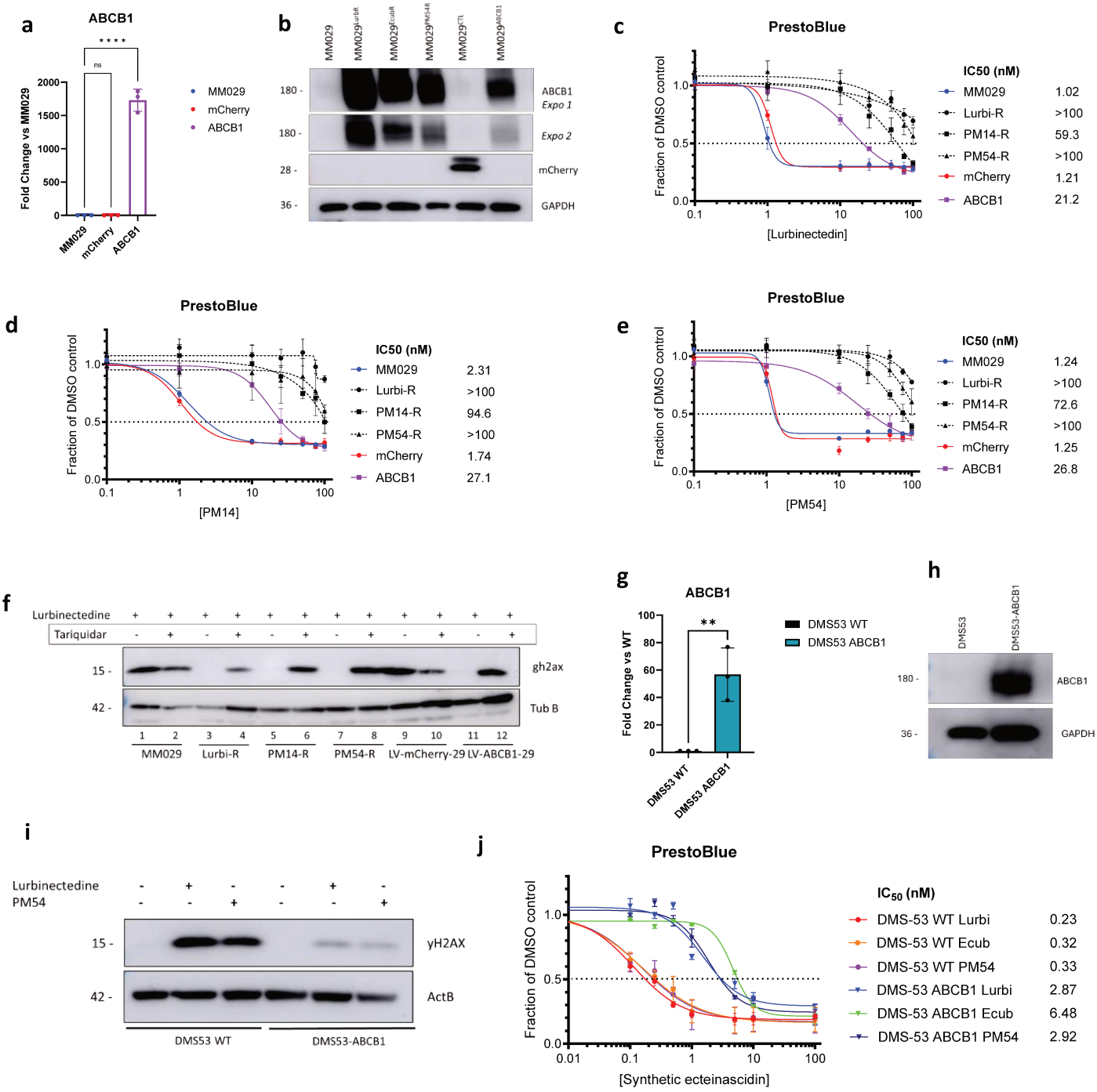
a
ABCB1
****
ns
Fold Change vs MM029
2000
1500
1000
500
0
MM029
mCherry
ABCB1
b
MM029
MM029LurbR
MM029EcubR
MM029PM54R
MM029cTL
MM029ABCB1
180 -
180 -
28 -
36 -
ABCB1 Expo 1
Expo 2
mCherry
GAPDH
c
PrestoBlue
Fraction of DMSO control
[Lurbinectedin]
IC50 (nM)
MM029 1.02
Lurbi-R >100
PM14-R 59.3
PM54-R >100
mCherry 1.21
ABCB1 21.2
d
PrestoBlue
Fraction of DMSO control
[PM14]
IC50 (nM)
MM029 2.31
Lurbi-R >100
PM14-R 94.6
PM54-R >100
mCherry 1.74
ABCB1 27.1
e
PrestoBlue
Fraction of DMSO control
[PM54]
IC50 (nM)
MM029 1.24
Lurbi-R >100
PM14-R 72.6
PM54-R >100
mCherry 1.25
ABCB1 26.8
f
Lurbinectedine
Tariquidar
15 -
42 -
gh2ax
Tub B
MM029
Lurbi-R
PM14-R
PM54-R
LV-mCherry-29
LV-ABCB1-29
g
ABCB1
**
Fold Change vs WT
DMS53 WT
DMS53 ABCB1
h
DMS53
DMS53-ABCB1
180 -
36 -
ABCB1
GAPDH
i
Lurbinectedine
PM54
15 -
42 -
yH2AX
ActB
DMS53 WT
DMS53-ABCB1
j
PrestoBlue
Fraction of DMSO control
[Synthetic ecteinascidin]
IC50 (nM)
DMS-53 WT Lurbi 0.23
DMS-53 WT Ecub 0.32
DMS-53 WT PM54 0.33
DMS-53 ABCB1 Lurbi 2.87
DMS-53 ABCB1 Ecub 6.48
DMS-53 ABCB1 PM54 2.92

Figure 6

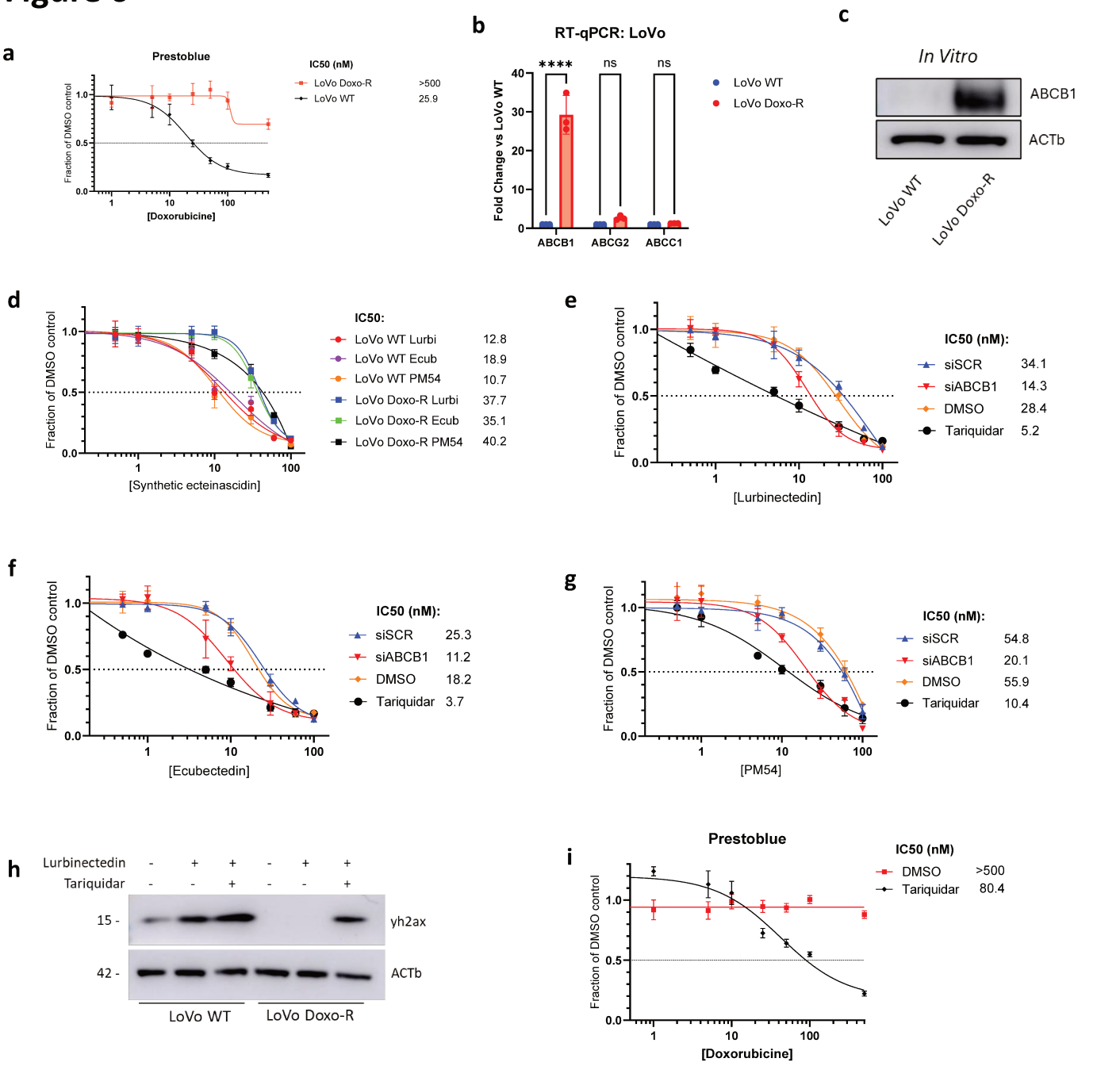
a
Prestoblue
IC50 (nM)
LoVo Doxo-R >500
LoVo WT 25.9
Fraction of DMSO control
[Doxorubicine]
b
RT-qPCR: LoVo
Fold Change vs LoVo WT
****
ns
ns
LoVo WT
LoVo Doxo-R
ABCB1
ABCG2
ABCC1
c
In Vitro
ABCB1
ACTb
LoVo WT
LoVo Doxo-R
d
IC50:
LoVo WT Lurbi 12.8
LoVo WT Ecub 18.9
LoVo WT PM54 10.7
LoVo Doxo-R Lurbi 37.7
LoVo Doxo-R Ecub 35.1
LoVo Doxo-R PM54 40.2
Fraction of DMSO control
[Synthetic ecteinascidin]
e
IC50 (nM):
siSCR 34.1
siABCB1 14.3
DMSO 28.4
Tariquidar 5.2
Fraction of DMSO control
[Lurbinectedin]
f
IC50 (nM):
siSCR 25.3
siABCB1 11.2
DMSO 18.2
Tariquidar 3.7
Fraction of DMSO control
[Ecubectedin]
g
IC50 (nM):
siSCR 54.8
siABCB1 20.1
DMSO 55.9
Tariquidar 10.4
Fraction of DMSO control
[PM54]
h
Lurbinectedin - + + - + +
Tariquidar - - + - - +
15 -
42 -
yh2ax
ACTb
LoVo WT
LoVo Doxo-R
i
Prestoblue
IC50 (nM)
DMSO >500
Tariquidar 80.4
Fraction of DMSO control
[Doxorubicine]

Figure 7

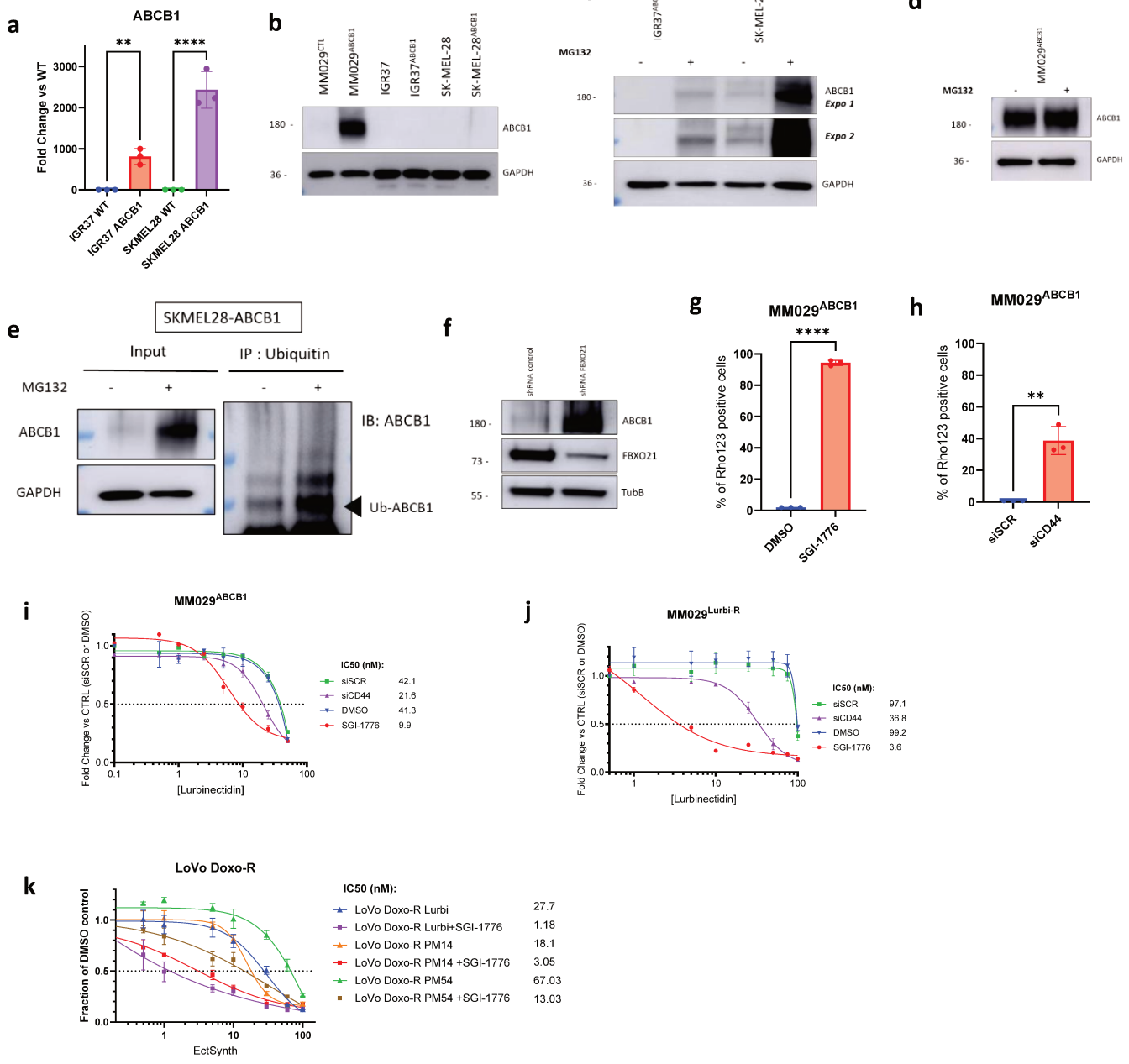
a
ABCB1
**
****
Fold Change vs WT
3000
2000
1000
0
IGR37 WT
IGR37 ABCB1
SKMEL28 WT
SKMEL28 ABCB1
b
MM029CTL
MM029ABCB1
IGR37
IGR37ABCB1
SK-MEL-28
SK-MEL-28ABCB1
180 -
36 -
ABCB1
GAPDH
c
IGR37ABCB1
SK-MEL-28ABCB1
MG132
- + - +
180 -
36 -
ABCB1
Expo 1
Expo 2
GAPDH
d
MM029ABCB1
MG132
- +
180 -
36 -
ABCB1
GAPDH
e
SKMEL28-ABCB1
Input
IP : Ubiquitin
MG132
- + - +
ABCB1
GAPDH
IB: ABCB1
Ub-ABCB1
f
shRNA control
shRNA FBXO21
180 -
73 -
55 -
ABCB1
FBXO21
TubB
g
MM029ABCB1
****
% of Rho123 positive cells
100
80
60
40
20
0
DMSO
SGI-1776
h
MM029ABCB1
**
% of Rho123 positive cells
100
80
60
40
20
0
siSCR
siCD44
i
MM029ABCB1
Fold Change vs CTRL (siSCR or DMSO)
1.0
0.5
0.0
0.1
1
10
100
[Lurbinectidin]
IC50 (nM):
siSCR 42.1
siCD44 21.6
DMSO 41.3
SGI-1776 9.9
j
MM029Lurbi-R
Fold Change vs CTRL (siSCR or DMSO)
1.0
0.5
0.0
1
10
100
[Lurbinectidin]
IC50 (nM):
siSCR 97.1
siCD44 36.8
DMSO 99.2
SGI-1776 3.6
k
LoVo Doxo-R
Fraction of DMSO control
1.0
0.5
0.0
1
10
100
EctSynth
IC50 (nM):
LoVo Doxo-R Lurbi 27.7
LoVo Doxo-R Lurbi+SGI-1776 1.18
LoVo Doxo-R PM14 18.1
LoVo Doxo-R PM14 +SGI-1776 3.05
LoVo Doxo-R PM54 67.03
LoVo Doxo-R PM54 +SGI-1776 13.03

Supplemental Figure 4

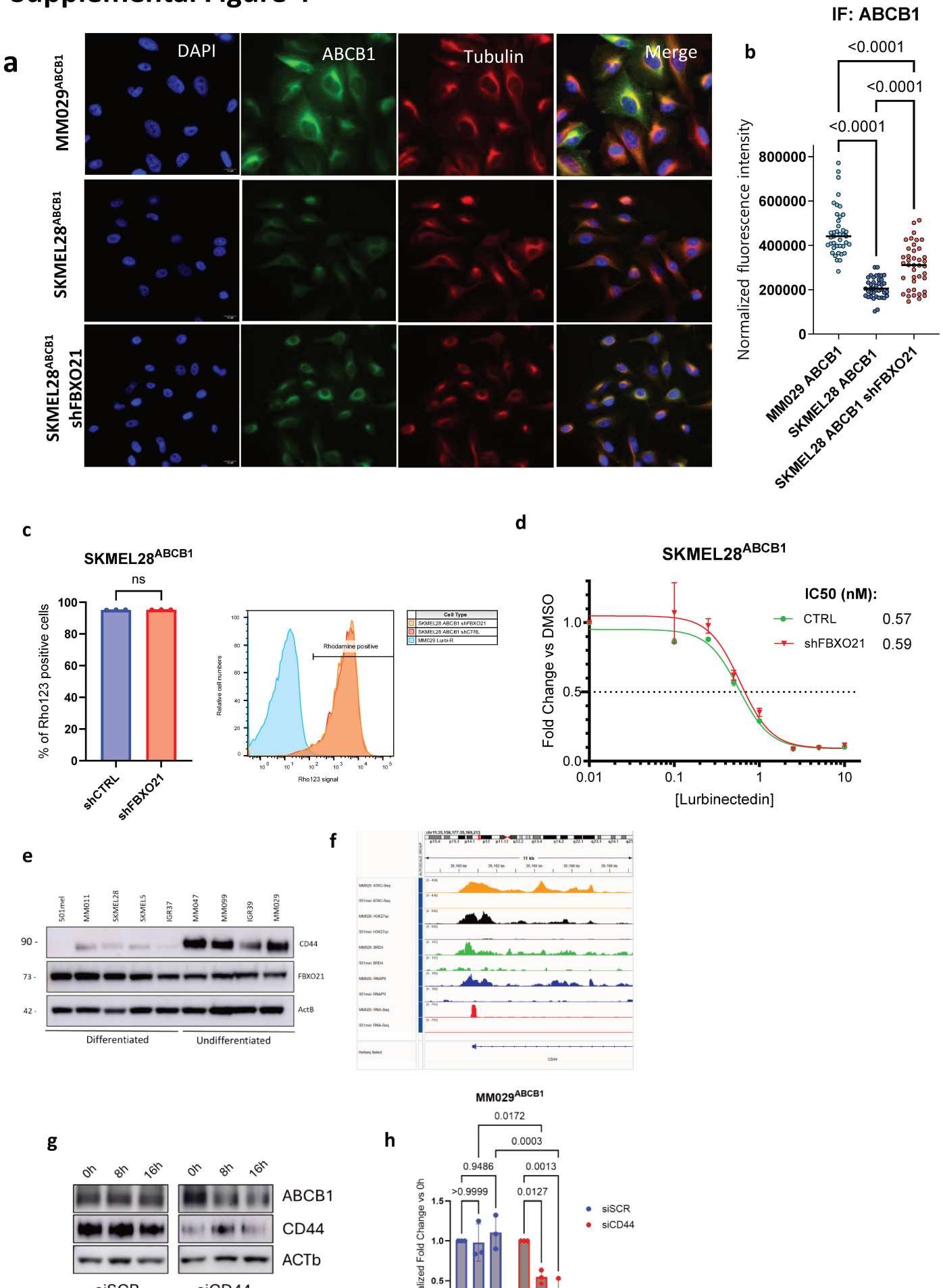

Supplemental Figure 5

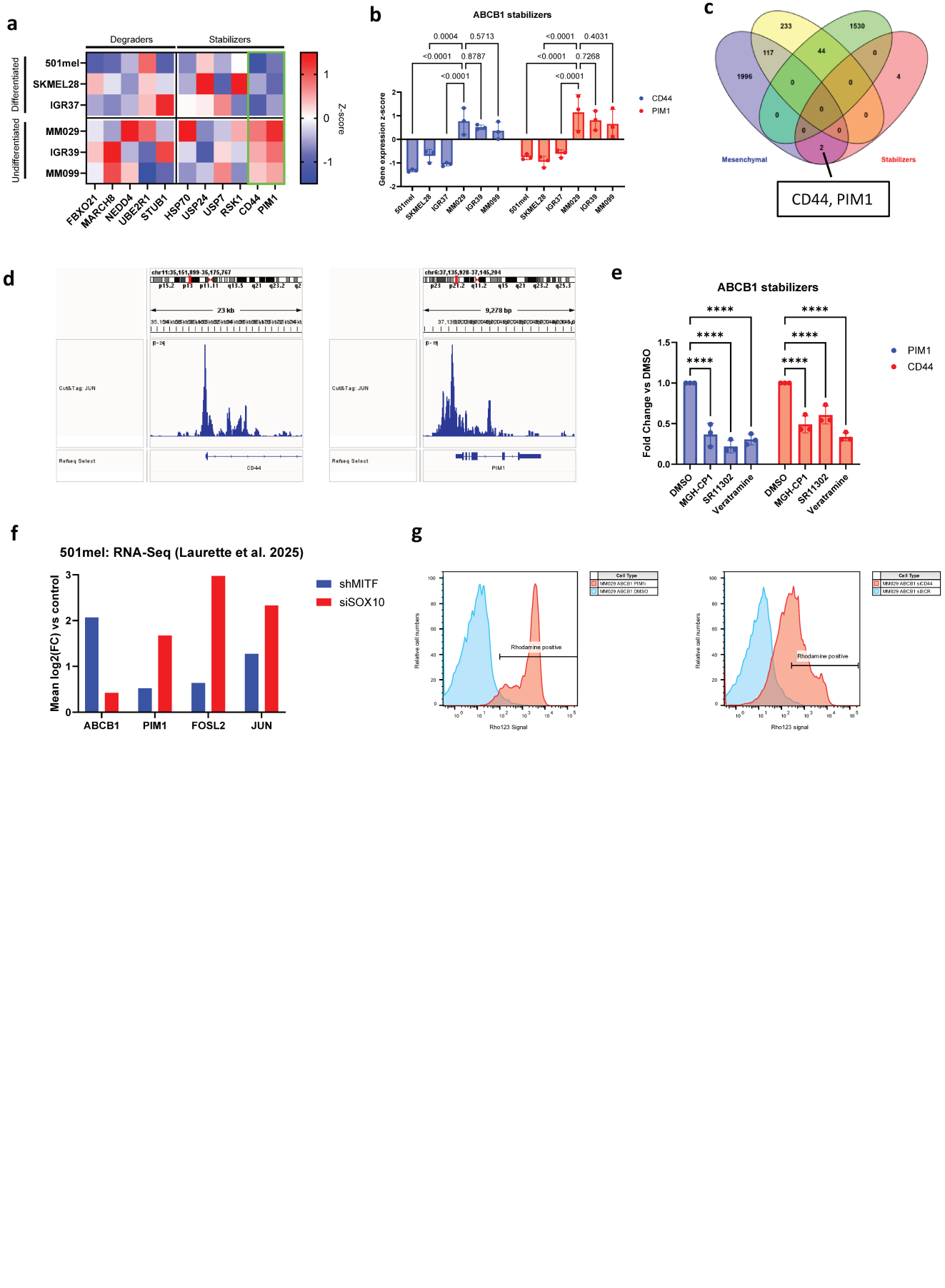

Supplemental Figure 6

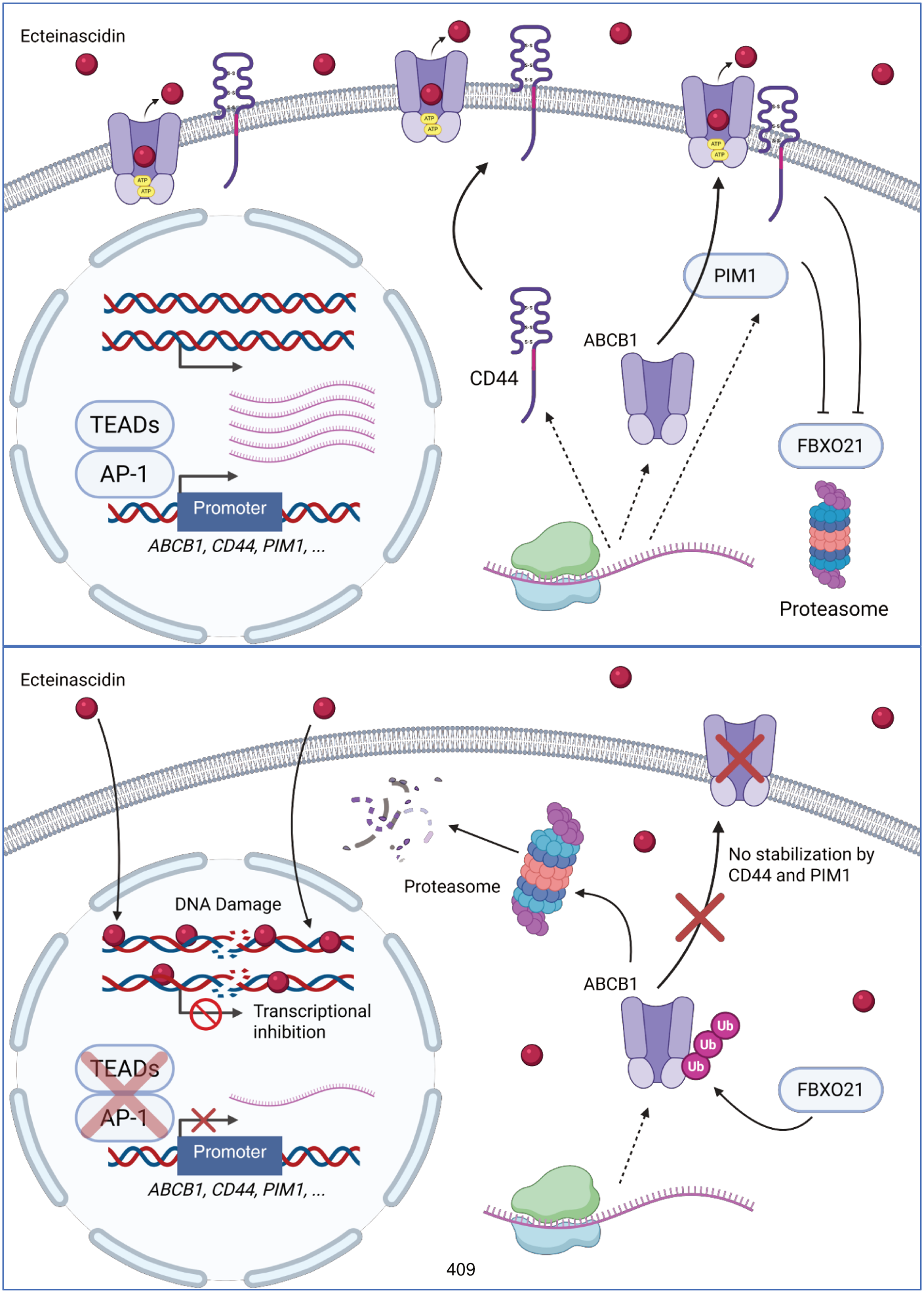

References

1. Abbotts R, Dellomo AJ & Rassool FV (2022) Pharmacologic Induction of BRCAness in BRCA-Proficient Cancers: Expanding PARP Inhibitor Use. *Cancers (Basel)* 14: 2640

2. Ackermann J, Frutschi M, Kaloulis K, McKee T, Trumpp A & Beermann F (2005) Metastasizing melanoma formation caused by expression of activated N-RasQ61K on an INK4a-deficient background. *Cancer Res* 65: 4005–4011

3. Agudo J, Park ES, Rose SA, Alibo E, Sweeney R, Dhainaut M, Kobayashi KS, Sachidanandam R, Baccarini A, Merad M, *et al* (2018) Quiescent Tissue Stem Cells Evade Immune Surveillance. *Immunity* 48: 271-285.e5

4. Ahnesorg P, Smith P & Jackson SP (2006) XLF interacts with the XRCC4-DNA ligase IV complex to promote DNA nonhomologous end-joining. *Cell* 124: 301–313

5. Alam H, Tang M, Maitituoheti M, Dhar SS, Kumar M, Han CY, Ambati CR, Amin SB, Gu B, Chen T-Y, *et al* (2020) KMT2D Deficiency Impairs Super-Enhancers to Confer a Glycolytic Vulnerability in Lung Cancer. *Cancer Cell* 37: 599-617.e7

6. Alexandrov LB, Nik-Zainal S, Wedge DC, Aparicio SAJR, Behjati S, Biankin AV, Bignell GR, Bolli N, Borg A, Børresen-Dale A-L, *et al* (2013) Signatures of mutational processes in human cancer. *Nature* 500: 415–421

7. Alkallas R, Lajoie M, Moldoveanu D, Hoang KV, Lefrançois P, Lingrand M, Ahanfeshar-Adams M, Watters K, Spatz A, Zippin JH, *et al* (2020) Multi-omic analysis reveals significantly mutated genes and DDX3X as a sex-specific tumor suppressor in cutaneous melanoma. *Nat Cancer* 1: 635–652

8. Anand R, Ranjha L, Cannavo E & Cejka P (2016) Phosphorylated CtIP Functions as a Co-factor of the MRE11-RAD50-NBS1 Endonuclease in DNA End Resection. *Mol Cell* 64: 940–950

9. Antoniou AC, Casadei S, Heikkinen T, Barrowdale D, Pylkäs K, Roberts J, Lee A, Subramanian D, De Leeneer K, Fostira F, *et al* (2014) Breast-cancer risk in families with mutations in PALB2. *N Engl J Med* 371: 497–506

10. Aoi Y & Shilatifard A (2023) Transcriptional elongation control in developmental gene expression, aging, and disease. *Mol Cell* 83: 3972–3999

11. Armstrong N, Ryder S, Forbes C, Ross J & Quek RG (2019) A systematic review of the international prevalence of BRCA mutation in breast cancer. *CLEP* Volume 11: 543–561

12. Arnold M, Singh D, Laversanne M, Vignat J, Vaccarella S, Meheus F, Cust AE, de Vries E, Whiteman DC & Bray F (2022) Global Burden of Cutaneous Melanoma in 2020 and Projections to 2040. *JAMA Dermatol* 158: 495–503

13. Arnold M, de Vries E, Whiteman DC, Jemal A, Bray F, Parkin DM & Soerjomataram I (2018) Global burden of cutaneous melanoma attributable to ultraviolet radiation in 2012. *Int J Cancer* 143: 1305–1314

14. Arnould C, Rocher V, Saur F, Bader AS, Muzzopappa F, Collins S, Lesage E, Le Bozec B, Puget N, Clouaire T, *et al* (2023) Chromatin compartmentalization regulates the response to DNA damage. *Nature* 623: 183–192

15. Arozarena I & Wellbrock C (2019) Phenotype plasticity as enabler of melanoma progression and therapy resistance. *Nat Rev Cancer* 19: 377–391

16. Ascierto PA, Dréno B, Larkin J, Ribas A, Liszkay G, Maio M, Mandalà M, Demidov L, Stroyakovskiy D, Thomas L, *et al* (2021) 5-Year Outcomes with Cobimetinib plus Vemurafenib in BRAFV600 Mutation-Positive Advanced Melanoma: Extended Follow-up of the coBRIM Study. *Clin Cancer Res* 27: 5225–5235

17. Atkins MB, Lee SJ, Chmielowski B, Tarhini AA, Cohen GI, Truong T-G, Moon HH, Davar D, O'Rourke M, Stephenson JJ, *et al* (2023) Combination Dabrafenib and Trametinib Versus Combination Nivolumab and Ipilimumab for Patients With Advanced BRAF-Mutant Melanoma: The DREAMseq Trial-ECOG-ACRIN EA6134. *J Clin Oncol* 41: 186–197

18. Audeh MW, Carmichael J, Penson RT, Friedlander M, Powell B, Bell-McGuinn KM, Scott C, Weitzel JN, Oaknin A, Loman N, *et al* (2010) Oral poly(ADP-ribose) polymerase inhibitor olaparib in patients with *BRCA1* or *BRCA2* mutations and recurrent ovarian cancer: a proof-of-concept trial. *The Lancet* 376: 245–251

19. Aylon Y, Liefshitz B & Kupiec M (2004) The CDK regulates repair of double-strand breaks by homologous recombination during the cell cycle. *EMBO J* 23: 4868–4875

20. Aymard F, Bugler B, Schmidt CK, Guillou E, Caron P, Briois S, Iacovoni JS, Daburon V, Miller KM, Jackson SP, *et al* (2014) Transcriptionally active chromatin recruits homologous recombination at DNA double-strand breaks. *Nat Struct Mol Biol* 21: 366–374

21. Bagati A, Kumar S, Jiang P, Pyrdol J, Zou AE, Godicelj A, Mathewson ND, Cartwright ANR, Cejas P, Brown M, *et al* (2021) Integrin αvβ6-TGFβ-SOX4 Pathway Drives Immune Evasion in Triple-Negative Breast Cancer. *Cancer Cell* 39: 54-67.e9

22. Bajrami I, Frankum JR, Konde A, Miller RE, Rehman FL, Brough R, Campbell J, Sims D, Rafiq R, Hooper S, *et al* (2014) Genome-wide profiling of genetic synthetic lethality identifies CDK12 as a novel determinant of PARP1/2 inhibitor sensitivity. *Cancer Res* 74: 287–297

23. Bakhoum SF & Landau DA (2017) Chromosomal Instability as a Driver of Tumor Heterogeneity and Evolution. *Cold Spring Harb Perspect Med* 7: a029611

24. Bakr A, Oing C, Köcher S, Borgmann K, Dornreiter I, Petersen C, Dikomey E & Mansour WY (2015) Involvement of ATM in homologous recombination after end resection and RAD51 nucleofilament formation. *Nucleic Acids Res* 43: 3154–3166

25. Bal E, Kumar R, Hadigol M, Holmes AB, Hilton LK, Loh JW, Dreval K, Wong JCH, Vlasevska S, Corinaldesi C, *et al* (2022) Super-Enhancer Hypermutation Alters Oncogene Expression in B-cell Lymphoma. *Nature* 607: 808–815

26. Ballotti R, Cheli Y & Bertolotto C (2020) The complex relationship between MITF and the immune system: a Melanoma ImmunoTherapy (response) Factor? *Mol Cancer* 19: 170

27. Banani SF, Lee HO, Hyman AA & Rosen MK (2017) Biomolecular condensates: organizers of cellular biochemistry. *Nat Rev Mol Cell Biol* 18: 285–298

28. Banerji J, Rusconi S & Schaffner W (1981) Expression of a beta-globin gene is enhanced by remote SV40 DNA sequences. *Cell* 27: 299–308

29. Barbieri CE, Baca SC, Lawrence MS, Demichelis F, Blattner M, Theurillat J-P, White TA, Stojanov P, Van Allen E, Stransky N, *et al* (2012) Exome sequencing identifies recurrent SPOP, FOXA1 and MED12 mutations in prostate cancer. *Nat Genet* 44: 685–689

30. Barnum KJ & O'Connell MJ (2014) Cell cycle regulation by checkpoints. *Methods Mol Biol* 1170: 29–40

31. Barone A, Chi D-C, Theoret MR, Chen H, He K, Kufrin D, Helms WS, Subramaniam S, Zhao H, Patel A, *et al* (2017) FDA Approval Summary: Trabectedin for Unresectable or Metastatic Liposarcoma or Leiomyosarcoma Following an Anthracycline-Containing Regimen. *Clin Cancer Res* 23: 7448–7453

32. Bartkowiak B, Liu P, Phatnani HP, Fuda NJ, Cooper JJ, Price DH, Adelman K, Lis JT & Greenleaf AL (2010) CDK12 is a transcription elongation-associated CTD kinase, the metazoan ortholog of yeast Ctk1. *Genes Dev* 24: 2303–2316

33. Bassi C, Ho J, Srikumar T, Dowling RJO, Gorrini C, Miller SJ, Mak TW, Neel BG, Raught B & Stambolic V (2013) Nuclear PTEN controls DNA repair and sensitivity to genotoxic stress. *Science* 341: 395–399

34. Bastian BC (2014) The molecular pathology of melanoma: an integrated taxonomy of melanocytic neoplasia. *Annu Rev Pathol* 9: 239–271

35. Bauer J & Bastian BC (2006) Distinguishing melanocytic nevi from melanoma by DNA copy number changes: comparative genomic hybridization as a research and diagnostic tool. *Dermatol Ther* 19: 40–49

36. Baylin SB & Jones PA (2011) A decade of exploring the cancer epigenome — biological and translational implications. *Nat Rev Cancer* 11: 726–734

37. Baylin SB & Jones PA (2016) Epigenetic Determinants of Cancer. *Cold Spring Harb Perspect Biol* 8: a019505

38. Bębenek A & Ziuzia-Graczyk I (2018) Fidelity of DNA replication-a matter of proofreading. *Curr Genet* 64: 985–996

39. Belgiovine C, Bello E, Liguori M, Craparotta I, Mannarino L, Paracchini L, Beltrame L, Marchini S, Galmarini CM, Mantovani A, *et al* (2017) Lurbinectedin reduces tumour-associated macrophages and the inflammatory tumour microenvironment in preclinical models. *Br J Cancer* 117: 628–638

40. Bell RJA, Rube HT, Kreig A, Mancini A, Fouse SD, Nagarajan RP, Choi S, Hong C, He D, Pekmezci M, *et al* (2015) Cancer. The transcription factor GABP selectively binds and activates the mutant TERT promoter in cancer. *Science* 348: 1036–1039

41. Benito-Martínez S, Salavessa L, Raposo G, Marks MS & Delevoye C (2021) Melanin Transfer and Fate within Keratinocytes in Human Skin Pigmentation. *Integr Comp Biol* 61: 1546–1555

42. Benton CB, Chien KS, Tefferi A, Rodriguez J, Ravandi F, Daver N, Jabbour E, Jain N, Alvarado Y, Kwari M, *et al* (2019) Safety and tolerability of lurbinectedin (PM01183) in patients with acute myeloid leukemia and myelodysplastic syndrome. *Hematol Oncol* 37: 96–102

43. Berico P, Cigrang M, Davidson G, Braun C, Sandoz J, Legras S, Vokshi BH, Slovic N, Peyresaubes F, Gene Robles CM, *et al* (2021) CDK7 and MITF repress a transcription program involved in survival and drug tolerance in melanoma. *EMBO Rep* 22: e51683

44. Berico P, Nogaret M, Cigrang M, Lallement A, Vand-Rajabpour F, Flores-Yanke A, Gambi G, Davidson G, Seno L, Obid J, *et al* (2023a) Super-enhancer-driven expression of BAHCC1 promotes melanoma cell proliferation and genome stability. *Cell Reports* 42

45. Berico P, Nogaret M, Cigrang M, Lallement A, Vand-Rajabpour F, Flores-Yanke A, Gambi G, Davidson G, Seno L, Obid J, *et al* (2023b) Super-enhancer-driven expression of BAHCC1 promotes melanoma cell proliferation and genome stability. *Cell Rep* 42: 113363

46. Berk-Krauss J, Stein JA, Weber J, Polsky D & Geller AC (2020) New Systematic Therapies and Trends in Cutaneous Melanoma Deaths Among US Whites, 1986-2016. *Am J Public Health* 110: 731–733

47. Bester AC, Roniger M, Oren YS, Im MM, Sarni D, Chaoat M, Bensimon A, Zamir G, Shewach DS & Kerem B (2011) Nucleotide Deficiency Promotes Genomic Instability in Early Stages of Cancer Development. *Cell* 145: 435–446

48. Bevill SM, Casaní-Galdón S, El Farran CA, Cytrynbaum EG, Macias KA, Oldeman SE, Oliveira KJ, Moore MM, Hegazi E, Adriaens C, *et al* (2023) Impact of supraphysiologic MDM2 expression on chromatin networks and therapeutic responses in sarcoma. *Cell Genom* 3: 100321

49. Bhagwat AS, Roe J-S, Mok BYL, Hohmann AF, Shi J & Vakoc CR (2016) BET Bromodomain Inhibition Releases the Mediator Complex from Select cis-Regulatory Elements. *Cell Rep* 15: 519–530

50. Bhamidipati D, Haro-Silerio JI, Yap TA & Ngoi N (2023) PARP inhibitors: enhancing efficacy through rational combinations. *Br J Cancer* 129: 904–916

51. Bindra RS, Gibson SL, Meng A, Westermark U, Jasin M, Pierce AJ, Bristow RG, Classon MK & Glazer PM (2005) Hypoxia-induced down-regulation of BRCA1 expression by E2Fs. *Cancer Res* 65: 11597–11604

52. Bittner M, Meltzer P, Chen Y, Jiang Y, Seftor E, Hendrix M, Radmacher M, Simon R, Yakhini Z, Ben-Dor A, *et al* (2000) Molecular classification of cutaneous malignant melanoma by gene expression profiling. *Nature* 406: 536–540

53. Bizuayehu HM, Ahmed KY, Kibret GD, Dadi AF, Belachew SA, Bagade T, Tegegne TK, Venchiarutti RL, Kibret KT, Hailegebireal AH, *et al* (2024) Global Disparities of Cancer and Its Projected Burden in 2050. *JAMA Netw Open* 7: e2443198

54. Bizzaro F, Fuso Nerini I, Taylor MA, Anastasia A, Russo M, Damia G, Guffanti F, Guana F, Ostano P, Minoli L, *et al* (2021) VEGF pathway inhibition potentiates PARP inhibitor efficacy in ovarian cancer independent of BRCA status. *J Hematol Oncol* 14: 186

55. Blackford AN & Jackson SP (2017) ATM, ATR, and DNA-PK: The Trinity at the Heart of the DNA Damage Response. *Mol Cell* 66: 801–817

56. Blayney JW, Francis H, Rampasekova A, Camellato B, Mitchell L, Stolper R, Cornell L, Babbs C, Boeke JD, Higgs DR, *et al* (2023) Super-enhancers include classical enhancers and facilitators to fully activate gene expression. *Cell* 186: 5826-5839.e18

57. Blazek D, Kohoutek J, Bartholomeeusen K, Johansen E, Hulinkova P, Luo Z, Cimermancic P, Ule J & Peterlin BM (2011) The Cyclin K/Cdk12 complex maintains genomic stability via regulation of expression of DNA damage response genes. *Genes Dev* 25: 2158–2172

58. Blobel GA, Higgs DR, Mitchell JA, Notani D & Young RA (2021) Testing the super-enhancer concept. *Nat Rev Genet* 22: 749–755

59. Boija A, Klein IA, Sabari BR, Dall'Agnese A, Coffey EL, Zamudio AV, Li CH, Shrinivas K, Manteiga JC, Hannett NM, *et al* (2018) Transcription Factors Activate Genes through the Phase-Separation Capacity of Their Activation Domains. *Cell* 175: 1842-1855.e16

60. Boija A, Klein IA & Young RA (2021) Biomolecular Condensates and Cancer. *Cancer Cell* 39: 174–192

61. Boija A, Mahat DB, Zare A, Holmqvist P-H, Philip P, Meyers DJ, Cole PA, Lis JT, Stenberg P & Mannervik M (2017) CBP Regulates Recruitment and Release of Promoter-Proximal RNA Polymerase II. *Mol Cell* 68: 491-503.e5

62. Bondeson DP, Mares A, Smith IED, Ko E, Campos S, Miah AH, Mulholland KE, Routly N, Buckley DL, Gustafson JL, *et al* (2015) Catalytic in vivo protein knockdown by small-molecule PROTACs. *Nat Chem Biol* 11: 611–617

63. Bonfanti M, La Valle E, Fernandez Sousa Faro JM, Faircloth G, Caretti G, Mantovani R & D'Incalci M (1999) Effect of ecteinascidin-743 on the interaction between DNA binding proteins and DNA. *Anticancer Drug Des* 14: 179–186

64. Bonilla B, Hengel SR, Grundy MK & Bernstein KA (2020) RAD51 Gene Family Structure and Function. *Annu Rev Genet* 54: 25–46

65. de Bono J, Mateo J, Fizazi K, Saad F, Shore N, Sandhu S, Chi KN, Sartor O, Agarwal N, Olmos D, *et al* (2020) Olaparib for Metastatic Castration-Resistant Prostate Cancer. *N Engl J Med* 382: 2091–2102

66. de Bono J, Ramanathan RK, Mina L, Chugh R, Glaspy J, Rafii S, Kaye S, Sachdev J, Heymach J, Smith DC, *et al* (2017) Phase I, Dose-Escalation, Two-Part Trial of the PARP

Inhibitor Talazoparib in Patients with Advanced Germline BRCA1/2 Mutations and Selected Sporadic Cancers. *Cancer Discov* 7: 620–629

67. Borkin D, He S, Miao H, Kempinska K, Pollock J, Chase J, Purohit T, Malik B, Zhao T, Wang J, *et al* (2015) Pharmacologic inhibition of the Menin-MLL interaction blocks progression of MLL leukemia in vivo. *Cancer Cell* 27: 589–602

68. Boshuizen J, Koopman LA, Krijgsman O, Shahrabi A, van den Heuvel EG-, Ligtenberg MA, Vredevoogd DW, Kemper K, Kuilman T, Song J-Y, *et al* (2018) Cooperative targeting of melanoma heterogeneity with an AXL antibody-drug conjugate and BRAF/MEK inhibitors. *Nat Med* 24: 203–212

69. Boukouris AE, Michaelidou K, Joosse SA, Charpidou A, Mavroudis D, Syrigos KN & Agelaki S (2025) A comprehensive overview of minimal residual disease in the management of early-stage and locally advanced non-small cell lung cancer. *NPJ Precis Oncol* 9: 178

70. Boumahdi S, Driessens G, Lapouge G, Rorive S, Nassar D, Le Mercier M, Delatte B, Caauwe A, Lenglez S, Nkusi E, *et al* (2014) SOX2 controls tumour initiation and cancer stem-cell functions in squamous-cell carcinoma. *Nature* 511: 246–250

71. Boutros A, Croce E, Ferrari M, Gili R, Massaro G, Marconcini R, Arecco L, Tanda ET & Spagnolo F (2024) The treatment of advanced melanoma: Current approaches and new challenges. *Crit Rev Oncol Hematol* 196: 104276

72. Bouwman P, Aly A, Escandell JM, Pieterse M, Bartkova J, van der Gulden H, Hiddingh S, Thanasoula M, Kulkarni A, Yang Q, *et al* (2010) 53BP1 loss rescues BRCA1 deficiency and is associated with triple-negative and BRCA-mutated breast cancers. *Nat Struct Mol Biol* 17: 688–695

73. Boyce RP & Howard-Flanders P (1964) RELEASE OF ULTRAVIOLET LIGHT-INDUCED THYMINE DIMERS FROM DNA IN E. COLI K-12. *Proc Natl Acad Sci U S A* 51: 293–300

74. Bozic I & Nowak MA (2014) Timing and heterogeneity of mutations associated with drug resistance in metastatic cancers. *Proceedings of the National Academy of Sciences* 111: 15964–15968

75. Bradford PT, Goldstein AM, Tamura D, Khan SG, Ueda T, Boyle J, Oh K-S, Imoto K, Inui H, Moriwaki S-I, *et al* (2011) Cancer and neurologic degeneration in xeroderma pigmentosum: long term follow-up characterises the role of DNA repair. *J Med Genet* 48: 168–176

76. Bradner JE, Hnisz D & Young RA (2017) Transcriptional Addiction in Cancer. *Cell* 168: 629–643

77. Bray F, Laversanne M, Sung H, Ferlay J, Siegel RL, Soerjomataram I & Jemal A (2024) Global cancer statistics 2022: GLOBOCAN estimates of incidence and mortality worldwide for 36 cancers in 185 countries. *CA Cancer J Clin* 74: 229–263

78. Brown D, Kogan S, Lagasse E, Weissman I, Alcalay M, Pelicci PG, Atwater S & Bishop JM (1997) A PMLRARalpha transgene initiates murine acute promyelocytic leukemia. *Proc Natl Acad Sci U S A* 94: 2551–2556

79. Brown JS, Amend SR, Austin RH, Gatenby RA, Hammarlund EU & Pienta KJ (2023) Updating the Definition of Cancer. *Mol Cancer Res* 21: 1142–1147

80. Bryant HE, Schultz N, Thomas HD, Parker KM, Flower D, Lopez E, Kyle S, Meuth M, Curtin NJ & Helleday T (2005) Specific killing of BRCA2-deficient tumours with inhibitors of poly(ADP-ribose) polymerase. *Nature* 434: 913–917

81. Bunting SF, Callén E, Wong N, Chen H-T, Polato F, Gunn A, Bothmer A, Feldhahn N, Fernandez-Capetillo O, Cao L, *et al* (2010) 53BP1 inhibits homologous recombination in Brca1-deficient cells by blocking resection of DNA breaks. *Cell* 141: 243–254

82. Bunz F, Fauth C, Speicher MR, Dutriaux A, Sedivy JM, Kinzler KW, Vogelstein B & Lengauer C (2002) Targeted Inactivation of p53 in Human Cells Does Not Result in Aneuploidy1. *Cancer Res* 62: 1129–1133

83. Burr ML, Sparbier CE, Chan KL, Chan Y-C, Kersbergen A, Lam EYN, Azidis-Yates E, Vassiliadis D, Bell CC, Gilan O, *et al* (2019) An Evolutionarily Conserved Function of Polycomb Silences the MHC Class I Antigen Presentation Pathway and Enables Immune Evasion in Cancer. *Cancer Cell* 36: 385-401.e8

84. Bushweller JH (2019) Targeting transcription factors in cancer - from undruggable to reality. *Nat Rev Cancer* 19: 611–624

85. Byrum AK, Vindigni A & Mosammaparast N (2019) Defining and Modulating 'BRCAness'. *Trends in Cell Biology* 29: 740–751

86. Caksa S, Baqai U & Aplin AE (2022) The future of targeted kinase inhibitors in melanoma. *Pharmacol Ther* 239: 108200

87. Caldecott KW (2003) DNA single-strand break repair and spinocerebellar ataxia. *Cell* 112: 7–10

88. Caldecott KW (2008) Single-strand break repair and genetic disease. *Nat Rev Genet* 9: 619–631

89. Caldecott KW (2022) DNA single-strand break repair and human genetic disease. *Trends Cell Biol* 32: 733–745

90. Caldecott KW (2024) Causes and consequences of DNA single-strand breaks. *Trends in Biochemical Sciences* 49: 68–78

91. Calles A, Calvo E, Santamaría Nuñez G, Costanzo F, Guillén MJ, Martinez Diez M, Gupta A, Cuevas C, Egly J-M & Avilés P (2025) Unveiling the Mechanism of Lurbinectedin's Action and Its Potential in Combination Therapies in Small Cell Lung Cancer. *Mol Cancer Ther* 24: 828–839

92. Cancer Genome Atlas Network (2015) Genomic Classification of Cutaneous Melanoma. *Cell* 161: 1681–1696

93. Carcamo S, Nguyen CB, Grossi E, Filipescu D, Alpsoy A, Dhiman A, Sun D, Narang S, Imig J, Martin TC, *et al* (2022) Altered BAF occupancy and transcription factor dynamics in PBAF-deficient melanoma. *Cell Rep* 39: 110637

94. Carracedo A & Pandolfi PP (2008) The PTEN–PI3K pathway: of feedbacks and cross-talks. *Oncogene* 27: 5527–5541

95. Carroll JS (2016) Mechanisms of oestrogen receptor (ER) gene regulation in breast cancer. *Eur J Endocrinol* 175: R41–R49

96. Ceccaldi R, Liu JC, Amunugama R, Hajdu I, Primack B, Petalcorin MIR, O'Connor KW, Konstantinopoulos PA, Elledge SJ, Boulton SJ, *et al* (2015) Homologous-recombination-deficient tumours are dependent on Polθ-mediated repair. *Nature* 518: 258–262

97. Ceccaldi R, Rondinelli B & D'Andrea AD (2016a) Repair Pathway Choices and Consequences at the Double-Strand Break. *Trends Cell Biol* 26: 52–64

98. Ceccaldi R, Sarangi P & D'Andrea AD (2016b) The Fanconi anaemia pathway: new players and new functions. *Nat Rev Mol Cell Biol* 17: 337–349

99. Centeno PP, Pavet V & Marais R (2023) The journey from melanocytes to melanoma. *Nat Rev Cancer* 23: 372–390

100. Centore RC, Sandoval GJ, Soares LMM, Kadoch C & Chan HM (2020) Mammalian SWI/SNF Chromatin Remodeling Complexes: Emerging Mechanisms and Therapeutic Strategies. *Trends in Genetics* 36: 936–950

101. Chae YK, Anker JF, Carneiro BA, Chandra S, Kaplan J, Kalyan A, Santa-Maria CA, Platanias LC & Giles FJ (2016) Genomic landscape of DNA repair genes in cancer. *Oncotarget* 7: 23312–23321

102. Chakraborty S, Sen U, Ventura K, Jethalia V, Coleman C, Sridhar S, Banerjee A, Ozakinci H, Mahendravarman Y, Snioch K, *et al* (2024) Lurbinectedin sensitizes PD-L1 blockade therapy by activating STING-IFN signaling in small-cell lung cancer. *Cell Rep Med* 5: 101852

103. Chambon P, Weill JD, Doly J, Strosser MT & Mandel P (1966) On the formation of a novel adenylic compound by enzymatic extracts of liver nuclei. *Biochemical and Biophysical Research Communications* 25: 638–643

104. Chambon P, Weill JD & Mandel P (1963) Nicotinamide mononucleotide activation of new DNA-dependent polyadenylic acid synthesizing nuclear enzyme. *Biochem Biophys Res Commun* 11: 39–43

105. Chang HHY, Pannunzio NR, Adachi N & Lieber MR (2017) Non-homologous DNA end joining and alternative pathways to double-strand break repair. *Nat Rev Mol Cell Biol* 18: 495–506

106. Chapman PB, Hauschild A, Robert C, Haanen JB, Ascierto P, Larkin J, Dummer R, Garbe C, Testori A, Maio M, *et al* (2011) Improved survival with vemurafenib in melanoma with BRAF V600E mutation. *N Engl J Med* 364: 2507–2516

107. Chapuy B, McKeown MR, Lin CY, Monti S, Roemer MGM, Qi J, Rahl PB, Sun HH, Yeda KT, Doench JG, *et al* (2013) Discovery and characterization of super-enhancer-associated dependencies in diffuse large B cell lymphoma. *Cancer Cell* 24: 777–790

108. Chatterjee N & Walker GC (2017) Mechanisms of DNA damage, repair, and mutagenesis. *Environ Mol Mutagen* 58: 235–263

109. Chemla Y, Itzhaki O, Melamed S, Weller C, Sade Y, Manich P, Reshef K, Xenidis N, Maliah A, Levy G, *et al* (2026) HLA export by melanoma cells decoys cytotoxic T cells to promote immune evasion. *Cell* 189: 233-251.e29

110. Chen G, Chen J, Qiao Y, Shi Y, Liu W, Zeng Q, Xie H, Shi X, Sun Y, Liu X, *et al* (2018) ZNF830 mediates cancer chemoresistance through promoting homologous-recombination repair. *Nucleic Acids Res* 46: 1266–1279

111. Chen X, Zhang T, Su W, Dou Z, Zhao D, Jin X, Lei H, Wang J, Xie X, Cheng B, *et al* (2022) Mutant p53 in cancer: from molecular mechanism to therapeutic modulation. *Cell Death Dis* 13: 974

112. Chipumuro E, Marco E, Christensen CL, Kwiatkowski N, Zhang T, Hatheway CM, Abraham BJ, Sharma B, Yeung C, Altabef A, *et al* (2014) CDK7 inhibition suppresses super-enhancer-linked oncogenic transcription in MYCN-driven cancer. *Cell* 159: 1126–1139

113. Cho W-K, Spille J-H, Hecht M, Lee C, Li C, Grube V & Cisse II (2018) Mediator and RNA polymerase II clusters associate in transcription-dependent condensates. *Science* 361: 412–415

114. Christie EL, Fereday S, Doig K, Pattnaik S, Dawson S-J & Bowtell DDL (2017) Reversion of BRCA1/2 Germline Mutations Detected in Circulating Tumor DNA From Patients With High-Grade Serous Ovarian Cancer. *J Clin Oncol* 35: 1274–1280

115. Chu X, Tian W, Ning J, Xiao G, Zhou Y, Wang Z, Zhai Z, Tanzhu G, Yang J & Zhou R (2024) Cancer stem cells: advances in knowledge and implications for cancer therapy. *Sig Transduct Target Ther* 9: 170

116. Chu Y-Y, Chen M-K, Wei Y, Lee H-H, Xia W, Wang Y-N, Yam C, Hsu JL, Wang H-L, Chang W-C, *et al* (2022) Targeting the ALK–CDK9-Tyr19 kinase cascade sensitizes ovarian and breast tumors to PARP inhibition via destabilization of the P-TEFb complex. *Nat Cancer* 3: 1211–1227

117. Cichorek M, Wachulska M, Stasiewicz A & Tymińska A (2013) Skin melanocytes: biology and development. *Postepy Dermatol Alergol* 30: 30–41

118. Clairmont CS, Sarangi P, Ponnienselvan K, Galli LD, Csete I, Moreau L, Adelmant G, Chowdhury D, Marto JA & D'Andrea AD (2020) TRIP13 regulates DNA repair pathway choice through REV7 conformational change. *Nat Cell Biol* 22: 87–96

119. Clapier CR, Iwasa J, Cairns BR & Peterson CL (2017) Mechanisms of action and regulation of ATP-dependent chromatin-remodelling complexes. *Nat Rev Mol Cell Biol* 18: 407–422

120. Cleaver JE (1968) Defective repair replication of DNA in xeroderma pigmentosum. *Nature* 218: 652–656

121. Clements PM, Breslin C, Deeks ED, Byrd PJ, Ju L, Bieganowski P, Brenner C, Moreira M-C, Taylor AMR & Caldecott KW (2004) The ataxia-oculomotor apraxia 1 gene product has a role distinct from ATM and interacts with the DNA strand break repair proteins XRCC1 and XRCC4. *DNA Repair (Amst)* 3: 1493–1502

122. Clouaire T, Rocher V, Lashgari A, Arnould C, Aguirrebengoa M, Biernacka A, Skrzypczak M, Aymard F, Fongang B, Dojer N, *et al* (2018) Comprehensive Mapping of Histone Modifications at DNA Double-Strand Breaks Deciphers Repair Pathway Chromatin Signatures. *Mol Cell* 72: 250-262.e6

123. Coin F, Oksenych V, Mocquet V, Groh S, Blattner C & Egly JM (2008) Nucleotide excision repair driven by the dissociation of CAK from TFIIH. *Mol Cell* 31: 9–20

124. Coleman RL, Fleming GF, Brady MF, Swisher EM, Steffensen KD, Friedlander M, Okamoto A, Moore KN, Ben-Baruch NE, Werner TL, *et al* (2019) Veliparib with First-Line Chemotherapy and as Maintenance Therapy in Ovarian Cancer. *New England Journal of Medicine* 381: 2403–2415

125. Collet L, Hanvic B, Turinetto M, Treilleux I, Chopin N, Le Saux O & Ray-Coquard I (2024) BRCA1/2 alterations and reversion mutations in the area of PARP inhibitors in high grade ovarian cancer: state of the art and forthcoming challenges. *Front Oncol* 14: 1354427

126. Compe E & Egly J-M (2012) TFIIH: when transcription met DNA repair. *Nat Rev Mol Cell Biol* 13: 343–354

127. Conroy M & Naidoo J (2022) Immune-related adverse events and the balancing act of immunotherapy. *Nat Commun* 13: 392

128. Conte M, Fontana E, Nebbioso A & Altucci L (2020) Marine-Derived Secondary Metabolites as Promising Epigenetic Bio-Compounds for Anticancer Therapy. *Mar Drugs* 19: 15

129. Cortes-Ciriano I, Lee S, Park W-Y, Kim T-M & Park PJ (2017) A molecular portrait of microsatellite instability across multiple cancers. *Nat Commun* 8: 15180

130. Costanzo F, Martínez Diez M, Santamaría Nuñez G, Díaz-Hernandéz JI, Genes Robles CM, Díez Pérez J, Compe E, Ricci R, Li T, Coin F, *et al* (2022) Promoters of ASCL1- and NEUROD1-dependent genes are specific targets of lurbinectedin in SCLC cells. *EMBO Molecular Medicine* 14: e14841

131. Cramer P (2019) Organization and regulation of gene transcription. *Nature* 573: 45–54

132. Cremer T & Cremer M (2010) Chromosome territories. *Cold Spring Harb Perspect Biol* 2: a003889

133. Crews ST & Pearson JC (2009) Transcriptional autoregulation in development. *Curr Biol* 19: R241-246

134. Cruz C, Castroviejo-Bermejo M, Gutiérrez-Enríquez S, Llop-Guevara A, Ibrahim YH, Gris-Oliver A, Bonache S, Morancho B, Bruna A, Rueda OM, *et al* (2018) RAD51 foci as a functional biomarker of homologous recombination repair and PARP inhibitor resistance in germline BRCA-mutated breast cancer. *Ann Oncol* 29: 1203–1210

135. Cui R, Widlund HR, Feige E, Lin JY, Wilensky DL, Igras VE, D'Orazio J, Fung CY, Schanbacher CF, Granter SR, *et al* (2007) Central role of p53 in the suntan response and pathologic hyperpigmentation. *Cell* 128: 853–864

136. Curtin JA, Fridlyand J, Kageshita T, Patel HN, Busam KJ, Kutzner H, Cho K-H, Aiba S, Bröcker E-B, LeBoit PE, *et al* (2005) Distinct sets of genetic alterations in melanoma. *N Engl J Med* 353: 2135–2147

137. Dai W, Wu J, Peng X, Hou W, Huang H, Cheng Q, Liu Z, Luyten W, Schoofs L, Zhou J, *et al* (2022) CDK12 orchestrates super-enhancer-associated CCDC137 transcription to direct hepatic metastasis in colorectal cancer. *Clin Transl Med* 12: e1087

138. Damsky WE, Curley DP, Santhanakrishnan M, Rosenbaum LE, Platt JT, Gould Rothberg BE, Taketo MM, Dankort D, Rimm DL, McMahon M, *et al* (2011) β-catenin signaling controls metastasis in Braf-activated Pten-deficient melanomas. *Cancer Cell* 20: 741–754

139. Dankort D, Curley DP, Cartlidge RA, Nelson B, Karnezis AN, Damsky WE, You MJ, DePinho RA, McMahon M & Bosenberg M (2009) Braf(V600E) cooperates with Pten loss to induce metastatic melanoma. *Nat Genet* 41: 544–552

140. Dantzer F, de La Rubia G, Ménissier-De Murcia J, Hostomsky Z, de Murcia G & Schreiber V (2000) Base excision repair is impaired in mammalian cells lacking Poly(ADP-ribose) polymerase-1. *Biochemistry* 39: 7559–7569

141. Dantzer F, Schreiber V, Niedergang C, Trucco C, Flatter E, De La Rubia G, Oliver J, Rolli V, Ménissier-de Murcia J & de Murcia G (1999) Involvement of poly(ADP-ribose) polymerase in base excision repair. *Biochimie* 81: 69–75

142. Darnell JE (2002) Transcription factors as targets for cancer therapy. *Nat Rev Cancer* 2: 740–749

143. Davies MA & Samuels Y (2010) Analysis of the genome to personalize therapy for melanoma. *Oncogene* 29: 5545–5555

144. Dawson MA, Prinjha RK, Dittmann A, Giotopoulos G, Bantscheff M, Chan W-I, Robson SC, Chung C, Hopf C, Savitski MM, *et al* (2011) Inhibition of BET recruitment to chromatin as an effective treatment for MLL-fusion leukaemia. *Nature* 478: 529–533

145. De Vos M, Schreiber V & Dantzer F (2012) The diverse roles and clinical relevance of PARPs in DNA damage repair: current state of the art. *Biochem Pharmacol* 84: 137–146

146. Dean JL, Thangavel C, McClendon AK, Reed CA & Knudsen ES (2010) Therapeutic CDK4/6 inhibition in breast cancer: key mechanisms of response and failure. *Oncogene* 29: 4018–4032

147. Deaton AM & Bird A (2011) CpG islands and the regulation of transcription. *Genes Dev* 25: 1010–1022

148. Dekker J & Mirny L (2016) The 3D Genome as Moderator of Chromosomal Communication. *Cell* 164: 1110–1121

149. Dekker J & Misteli T (2015) Long-Range Chromatin Interactions. *Cold Spring Harb Perspect Biol* 7: a019356

150. Di Leo L, Pagliuca C, Kishk A, Rizza S, Tsiavou C, Pecorari C, Dahl C, Pacheco MP, Tholstrup R, Brewer JR, *et al* (2024) AMBRA1 levels predict resistance to MAPK inhibitors in melanoma. *Proceedings of the National Academy of Sciences* 121: e2400566121

151. Dias MP, Moser SC, Ganesan S & Jonkers J (2021) Understanding and overcoming resistance to PARP inhibitors in cancer therapy. *Nat Rev Clin Oncol* 18: 773–791

152. Ding L, Kim M, Kanchi KL, Dees ND, Lu C, Griffith M, Fenstermacher D, Sung H, Miller CA, Goetz B, *et al* (2014) Clonal architectures and driver mutations in metastatic melanomas. *PLoS One* 9: e111153

153. Dixon JR, Selvaraj S, Yue F, Kim A, Li Y, Shen Y, Hu M, Liu JS & Ren B (2012) Topological domains in mammalian genomes identified by analysis of chromatin interactions. *Nature* 485: 376–380

154. D'Mello SAN, Finlay GJ, Baguley BC & Askarian-Amiri ME (2016) Signaling Pathways in Melanogenesis. *Int J Mol Sci* 17: 1144

155. Dobosz P & Dzieciątkowski T (2019) The Intriguing History of Cancer Immunotherapy. *Front Immunol* 10: 2965

156. Dongre A & Weinberg RA (2019) New insights into the mechanisms of epithelial–mesenchymal transition and implications for cancer. *Nat Rev Mol Cell Biol* 20: 69–84

157. Doudican NA & Orlow SJ (2017) Inhibition of the CRAF/prohibitin interaction reverses CRAF-dependent resistance to vemurafenib. *Oncogene* 36: 423–428

158. Drier Y, Cotton MJ, Williamson KE, Gillespie SM, Ryan RJH, Kluk MJ, Carey CD, Rodig SJ, Sholl LM, Afrogheh AH, *et al* (2016) An oncogenic MYB feedback loop drives alternate cell fates in adenoid cystic carcinoma. *Nat Genet* 48: 265–272

159. Du M, Stitzinger SH, Spille J-H, Cho W-K, Lee C, Hijaz M, Quintana A & Cissé II (2024) Direct observation of a condensate effect on super-enhancer controlled gene bursting. *Cell* 187: 331-344.e17

160. Dubbury SJ, Boutz PL & Sharp PA (2018) CDK12 regulates DNA repair genes by suppressing intronic polyadenylation. *Nature* 564: 141–145

161. Ducy M, Sesma-Sanz L, Guitton-Sert L, Lashgari A, Gao Y, Brahiti N, Rodrigue A, Margaillan G, Caron M-C, Côté J, *et al* (2019) The Tumor Suppressor PALB2: Inside Out. *Trends Biochem Sci* 44: 226–240

162. Durbin AD, Zimmerman MW, Dharia NV, Abraham BJ, Iniguez AB, Weichert-Leahey N, He S, Krill-Burger JM, Root DE, Vazquez F, *et al* (2018) Selective gene dependencies in

MYCN-amplified neuroblastoma include the core transcriptional regulatory circuitry. *Nat Genet* 50: 1240–1246

163. Durkacz BW, Omidiji O, Gray DA & Shall S (1980) (ADP-ribose)n participates in DNA excision repair. *Nature* 283: 593–596

164. Eaton JD, Francis L, Davidson L & West S (2020) A unified allosteric/torpedo mechanism for transcriptional termination on human protein-coding genes. *Genes Dev* 34: 132–145

165. Edelbrock MA, Kaliyaperumal S & Williams KJ (2013) Structural, molecular and cellular functions of MSH2 and MSH6 during DNA mismatch repair, damage signaling and other noncanonical activities. *Mutat Res* 743–744: 53–66

166. Edwards SL, Brough R, Lord CJ, Natrajan R, Vatcheva R, Levine DA, Boyd J, Reis-Filho JS & Ashworth A (2008) Resistance to therapy caused by intragenic deletion in BRCA2. *Nature* 451: 1111–1115

167. Egly J-M & Coin F (2011) A history of TFIIH: Two decades of molecular biology on a pivotal transcription/repair factor. *DNA Repair* 10: 714–721

168. Elder DE, Bastian BC, Cree IA, Massi D & Scolyer RA (2020) The 2018 World Health Organization Classification of Cutaneous, Mucosal, and Uveal Melanoma: Detailed Analysis of 9 Distinct Subtypes Defined by Their Evolutionary Pathway. *Archives of Pathology & Laboratory Medicine* 144: 500–522

169. Eliades P, Abraham BJ, Ji Z, Miller DM, Christensen CL, Kwiatkowski N, Kumar R, Njauw CN, Taylor M, Miao B, *et al* (2018) High MITF Expression Is Associated with Super-Enhancers and Suppressed by CDK7 Inhibition in Melanoma. *J Invest Dermatol* 138: 1582–1590

170. El-Khamisy SF, Masutani M, Suzuki H & Caldecott KW (2003) A requirement for PARP-1 for the assembly or stability of XRCC1 nuclear foci at sites of oxidative DNA damage. *Nucleic Acids Res* 31: 5526–5533

171. Elliott K, Singh VK, Bäckerholm A, Ögren L, Lindberg M, Soczek KM, Hoberg E, Luijts T, Van den Eynden J, Falkenberg M, *et al* (2024) Mechanistic basis of atypical TERT promoter mutations. *Nat Commun* 15: 9965

172. ENCODE Project Consortium (2012) An integrated encyclopedia of DNA elements in the human genome. *Nature* 489: 57–74

173. Eychenne T, Novikova E, Barrault M-B, Alibert O, Boschiero C, Peixeiro N, Cornu D, Redeker V, Kuras L, Nicolas P, *et al* (2016) Functional interplay between Mediator and TFIIB in preinitiation complex assembly in relation to promoter architecture. *Genes Dev* 30: 2119–2132

174. Falkson CI, Ibrahim J, Kirkwood JM, Coates AS, Atkins MB & Blum RH (1998) Phase III trial of dacarbazine versus dacarbazine with interferon alpha-2b versus dacarbazine with tamoxifen versus dacarbazine with interferon alpha-2b and tamoxifen in patients with metastatic malignant melanoma: an Eastern Cooperative Oncology Group study. *J Clin Oncol* 16: 1743–1751

175. Farmer H, McCabe N, Lord CJ, Tutt ANJ, Johnson DA, Richardson TB, Santarosa M, Dillon KJ, Hickson I, Knights C, *et al* (2005) Targeting the DNA repair defect in BRCA mutant cells as a therapeutic strategy. *Nature* 434: 917–921

176. Feige E, Yokoyama S, Levy C, Khaled M, Igras V, Lin RJ, Lee S, Widlund HR, Granter SR, Kung AL, *et al* (2011) Hypoxia-induced transcriptional repression of the melanoma-associated oncogene MITF. *Proc Natl Acad Sci U S A* 108: E924-933

177. Filippakopoulos P, Qi J, Picaud S, Shen Y, Smith WB, Fedorov O, Morse EM, Keates T, Hickman TT, Felletar I, *et al* (2010) Selective inhibition of BET bromodomains. *Nature* 468: 1067–1073

178. Firestein R, Bass AJ, Kim SY, Dunn IF, Silver SJ, Guney I, Freed E, Ligon AH, Vena N, Ogino S, *et al* (2008) CDK8 is a colorectal cancer oncogene that regulates beta-catenin activity. *Nature* 455: 547–551

179. Fischer M, Schade AE, Branigan TB, Müller GA & DeCaprio JA (2022) Coordinating gene expression during the cell cycle. *Trends Biochem Sci* 47: 1009–1022

180. Flavahan WA, Drier Y, Johnstone SE, Hemming ML, Tarjan DR, Hegazi E, Shareef SJ, Javed NM, Raut CP, Eschle BK, *et al* (2019) Altered chromosomal topology drives oncogenic programs in SDH-deficient GISTs. *Nature* 575: 229–233

181. Fok JHL, Ramos-Montoya A, Vazquez-Chantada M, Wijnhoven PWG, Follia V, James N, Farrington PM, Karmokar A, Willis SE, Cairns J, *et al* (2019) AZD7648 is a potent and selective DNA-PK inhibitor that enhances radiation, chemotherapy and olaparib activity. *Nat Commun* 10: 5065

182. Fong CY, Gilan O, Lam EYN, Rubin AF, Ftouni S, Tyler D, Stanley K, Sinha D, Yeh P, Morison J, *et al* (2015) BET inhibitor resistance emerges from leukaemia stem cells. *Nature* 525: 538–542

183. Fong PC, Yap TA, Boss DS, Carden CP, Mergui-Roelvink M, Gourley C, De Greve J, Lubinski J, Shanley S, Messiou C, *et al* (2010) Poly(ADP)-Ribose Polymerase Inhibition: Frequent Durable Responses in BRCA Carrier Ovarian Cancer Correlating With Platinum-Free Interval. *JCO* 28: 2512–2519

184. Fontanals-Cirera B, Hasson D, Vardabasso C, Di Micco R, Agrawal P, Chowdhury A, Gantz M, de Pablos-Aragoneses A, Morgenstern A, Wu P, *et al* (2017) Harnessing BET Inhibitor Sensitivity Reveals AMIGO2 as a Melanoma Survival Gene. *Mol Cell* 68: 731-744.e9

185. Forni A & Moreo L (1969) Chromosome studies in a case of benzene-induced erythro-leukaemia. *European Journal of Cancer (1965)* 5: IN13

186. Fradet-Turcotte A, Canny MD, Escribano-Díaz C, Orthwein A, Leung CCY, Huang H, Landry M-C, Kitevski-LeBlanc J, Noordermeer SM, Sicheri F, *et al* (2013) 53BP1 is a reader of the DNA-damage-induced H2A Lys 15 ubiquitin mark. *Nature* 499: 50–54

187. França GS, Baron M, King BR, Bossowski JP, Bjornberg A, Pour M, Rao A, Patel AS, Misirlioglu S, Barkley D, *et al* (2024) Cellular adaptation to cancer therapy along a resistance continuum. *Nature* 631: 876–883

188. Fransson Å, Glaessgen D, Alfredsson J, Wiman KG, Bajalica-Lagercrantz S & Mohell N (2016) Strong synergy with APR-246 and DNA-damaging drugs in primary cancer cells from patients with TP53 mutant High-Grade Serous ovarian cancer. *J Ovarian Res* 9: 27

189. French CA, Miyoshi I, Kubonishi I, Grier HE, Perez-Atayde AR & Fletcher JA (2003) BRD4-NUT fusion oncogene: a novel mechanism in aggressive carcinoma. *Cancer Res* 63: 304–307

190. French CA, Ramirez CL, Kolmakova J, Hickman TT, Cameron MJ, Thyne ME, Kutok JL, Toretsky JA, Tadavarthy AK, Kees UR, *et al* (2008) BRD-NUT oncoproteins: a family of closely related nuclear proteins that block epithelial differentiation and maintain the growth of carcinoma cells. *Oncogene* 27: 2237–2242

191. Friedberg EC (2008) A brief history of the DNA repair field. *Cell Res* 18: 3–7

192. Fu H, Liu R, Jia Z, Li R, Zhu F, Zhu W, Shao Y, Jin Y, Xue Y, Huang J, *et al* (2022) Poly(ADP-ribosylation) of P-TEFb by PARP1 disrupts phase separation to inhibit global transcription after DNA damage. *Nat Cell Biol* 24: 513–525

193. Gadducci A & Cosio S (2022) Trabectedin and lurbinectedin: Mechanisms of action, clinical impact, and future perspectives in uterine and soft tissue sarcoma, ovarian carcinoma, and endometrial carcinoma. *Front Oncol* 12: 914342

194. Gao Y, Zhang T, Terai H, Ficarro SB, Kwiatkowski N, Hao M-F, Sharma B, Christensen CL, Chipumuro E, Wong K-K, *et al* (2018) Overcoming Resistance to the THZ Series of Covalent Transcriptional CDK Inhibitors. *Cell Chem Biol* 25: 135-142.e5

195. Garralda E, Schram AM, Bedard PL, Schwartz GK, Yuen E, McNeely SC, Ribeiro S, Cunningham J, Wang Y, Urunuela A, *et al* (2024) A Phase I Dose-Escalation Study of LY3405105, a Covalent Inhibitor of Cyclin-Dependent Kinase 7, Administered to Patients With Advanced Solid Tumors. *Oncologist* 29: e131–e140

196. Gaszner M & Felsenfeld G (2006) Insulators: exploiting transcriptional and epigenetic mechanisms. *Nat Rev Genet* 7: 703–713

197. Genschel J, Bazemore LR & Modrich P (2002) Human exonuclease I is required for 5' and 3' mismatch repair. *J Biol Chem* 277: 13302–13311

198. Germano G, Frapolli R, Belgiovine C, Anselmo A, Pesce S, Liguori M, Erba E, Uboldi S, Zucchetti M, Pasqualini F, *et al* (2013) Role of macrophage targeting in the antitumor activity of trabectedin. *Cancer Cell* 23: 249–262

199. Germano G, Frapolli R, Simone M, Tavecchio M, Erba E, Pesce S, Pasqualini F, Grosso F, Sanfilippo R, Casali PG, *et al* (2010) Antitumor and anti-inflammatory effects of trabectedin on human myxoid liposarcoma cells. *Cancer Res* 70: 2235–2244

200. Ghavi-Helm Y, Jankowski A, Meiers S, Viales RR, Korbel JO & Furlong EEM (2019) Highly rearranged chromosomes reveal uncoupling between genome topology and gene expression. *Nat Genet* 51: 1272–1282

201. Gibson BA, Zhang Y, Jiang H, Hussey KM, Shrimp JH, Lin H, Schwede F, Yu Y & Kraus WL (2016) Chemical genetic discovery of PARP targets reveals a role for PARP-1 in transcription elongation. *Science* 353: 45–50

202. Gide TN, Wilmott JS, Scolyer RA & Long GV (2018) Primary and Acquired Resistance to Immune Checkpoint Inhibitors in Metastatic Melanoma. *Clin Cancer Res* 24: 1260–1270

203. Gilad O, Nabet BY, Ragland RL, Schoppy DW, Smith KD, Durham AC & Brown EJ (2010) Combining ATR Suppression with Oncogenic Ras Synergistically Increases Genomic Instability, Causing Synthetic Lethality or Tumorigenesis in a Dosage-Dependent Manner. *Cancer Res* 70: 9693–9702

204. Glatz K, Hartmann C, Antic M & Kutzner H (2010) Frequent mitotic activity in banal melanocytic nevi uncovered by immunohistochemical analysis. *Am J Dermatopathol* 32: 643–649

205. Gogola E, Duarte AA, de Ruiter JR, Wiegant WW, Schmid JA, de Bruijn R, James DI, Guerrero Llobet S, Vis DJ, Annunziato S, *et al* (2018) Selective Loss of PARG Restores PARylation and Counteracts PARP Inhibitor-Mediated Synthetic Lethality. *Cancer Cell* 33: 1078-1093.e12

206. Golan T, Hammel P, Reni M, Van Cutsem E, Macarulla T, Hall MJ, Park J-O, Hochhauser D, Arnold D, Oh D-Y, *et al* (2019) Maintenance Olaparib for Germline BRCA-Mutated Metastatic Pancreatic Cancer. *N Engl J Med* 381: 317–327

207. Gonçalves E, Ryan CJ & Adams DJ (2026) Synthetic lethality in cancer drug discovery: challenges and opportunities. *Nat Rev Drug Discov* 25: 22–38

208. Gottlieb TM & Jackson SP (1993) The DNA-dependent protein kinase: requirement for DNA ends and association with Ku antigen. *Cell* 72: 131–142

209. Gracia B, Zhang X-H, Montes P, Pham TC, Huang M, Chen J & Karras GI (2025) HSP90 buffers deleterious genetic variations in BRCA1. *Mol Cell* 85: 4365-4378.e10

210. Greenberg MVC & Bourc'his D (2019) The diverse roles of DNA methylation in mammalian development and disease. *Nat Rev Mol Cell Biol* 20: 590–607

211. Grellety T, Peyraud F, Sevenet N, Tredan O, Dohollou N, Barouk-Simonet E, Kind M, Longy M, Blay J-Y & Italiano A (2020) Dramatic response to PARP inhibition in a PALB2-mutated breast cancer: moving beyond BRCA. *Ann Oncol* 31: 822–823

212. Grivennikov SI, Greten FR & Karin M (2010) Immunity, Inflammation, and Cancer. *Cell* 140: 883–899

213. Groelly FJ, Fawkes M, Dagg RA, Blackford AN & Tarsounas M (2023) Targeting DNA damage response pathways in cancer. *Nat Rev Cancer* 23: 78–94

214. Grossi E, Nguyen CB, Carcamo S, Callaú VK, Moran S, Filipescu D, Tagore S, Firestone TM, Keogh M-C, Sun L, *et al* (2025) The SWI/SNF PBAF complex facilitates REST occupancy at repressive chromatin. *Molecular Cell* 85: 1714-1729.e7

215. Grundy GJ & Parsons JL (2020) Base excision repair and its implications to cancer therapy. *Essays Biochem* 64: 831–843

216. Gui F, Jiang B, Jiang J, He Z, Tsujino T, Takai T, Arai S, Pana C, Köllermann J, Bradshaw GA, *et al* (2025) Acute BRCAness induction and AR pathway blockage through CDK12/7/9 degradation enhances PARP inhibitor sensitivity in prostate cancer. *Science Advances* 11: eadu0847

217. Guo W, Wang H & Li C (2021) Signal pathways of melanoma and targeted therapy. *Signal Transduct Target Ther* 6: 424

218. Guo Y-J, Pan W-W, Liu S-B, Shen Z-F, Xu Y & Hu L-L (2020) ERK/MAPK signalling pathway and tumorigenesis. *Exp Ther Med* 19: 1997–2007

219. Ha K, Fiskus W, Choi DS, Bhaskara S, Cerchietti L, Devaraj SGT, Shah B, Sharma S, Chang JC, Melnick AM, *et al* (2014) Histone deacetylase inhibitor treatment induces 'BRCAness' and synergistic lethality with PARP inhibitor and cisplatin against human triple negative breast cancer cells. *Oncotarget* 5: 5637–5650

220. Haas L, Elewaut A, Gerard CL, Umkehrer C, Leiendecker L, Pedersen M, Krecioch I, Hoffmann D, Novatchkova M, Kuttke M, *et al* (2021) Acquired resistance to anti-MAPK targeted therapy confers an immune-evasive tumor microenvironment and cross-resistance to immunotherapy in melanoma. *Nat Cancer* 2: 693–708

221. Haberle V & Lenhard B (2016) Promoter architectures and developmental gene regulation. *Seminars in Cell & Developmental Biology* 57: 11–23

222. Haberle V & Stark A (2018) Eukaryotic core promoters and the functional basis of transcription initiation. *Nat Rev Mol Cell Biol* 19: 621–637

223. Hajdu SI (2011) A note from history: Landmarks in history of cancer, part 1. *Cancer* 117: 1097–1102

224. Han J, Zhao Y, Shirai K, Molodtsov A, Kolling FW, Fisher JL, Zhang P, Yan S, Searles TG, Bader JM, *et al* (2021) Resident and circulating memory T cells persist for years in melanoma patients with durable responses to immunotherapy. *Nat Cancer* 2: 300–311

225. Hanahan D (2022) Hallmarks of Cancer: New Dimensions. *Cancer Discov* 12: 31–46

226. Hanahan D & Weinberg RA (2000) The hallmarks of cancer. *Cell* 100: 57–70

227. Hanahan D & Weinberg RA (2011) Hallmarks of Cancer: The Next Generation. *Cell* 144: 646–674

228. Hauschild A, Grob J-J, Demidov LV, Jouary T, Gutzmer R, Millward M, Rutkowski P, Blank CU, Miller WH, Kaempgen E, *et al* (2012) Dabrafenib in BRAF-mutated metastatic melanoma: a multicentre, open-label, phase 3 randomised controlled trial. *Lancet* 380: 358–365

229. He J, Kang X, Yin Y, Chao KSC & Shen WH (2015) PTEN regulates DNA replication progression and stalled fork recovery. *Nat Commun* 6: 7620

230. Hegde ML, Hazra TK & Mitra S (2008) Early steps in the DNA base excision/single-strand interruption repair pathway in mammalian cells. *Cell Res* 18: 27–47

231. Hendriks HR, Fiebig HH, Giavazzi R, Langdon SP, Jimeno JM & Faircloth GT (1999) High antitumour activity of ET743 against human tumour xenografts from melanoma, non-small-cell lung and ovarian cancer. *Ann Oncol* 10: 1233–1240

232. Hennessy A, Oh C, Diffey B, Wakamatsu K, Ito S & Rees J (2005) Eumelanin and pheomelanin concentrations in human epidermis before and after UVB irradiation. *Pigment Cell Res* 18: 220–223

233. Henriques T, Gilchrist DA, Nechaev S, Bern M, Muse GW, Burkholder A, Fargo DC & Adelman K (2013) Stable pausing by RNA polymerase II provides an opportunity to target and integrate regulatory signals. *Mol Cell* 52: 517–528

234. Hickson I, Zhao Y, Richardson CJ, Green SJ, Martin NMB, Orr AI, Reaper PM, Jackson SP, Curtin NJ & Smith GCM (2004) Identification and characterization of a novel and specific inhibitor of the ataxia-telangiectasia mutated kinase ATM. *Cancer Res* 64: 9152–9159

235. Hindi NN, Elsakrmy N & Ramotar D (2021) The base excision repair process: comparison between higher and lower eukaryotes. *Cell Mol Life Sci* 78: 7943–7965

236. Hnisz D, Abraham BJ, Lee TI, Lau A, Saint-André V, Sigova AA, Hoke HA & Young RA (2013) Super-Enhancers in the Control of Cell Identity and Disease. *Cell* 155: 934–947

237. Hnisz D, Schuijers J, Lin CY, Weintraub AS, Abraham BJ, Lee TI, Bradner JE & Young RA (2015) Convergence of developmental and oncogenic signaling pathways at transcriptional super-enhancers. *Mol Cell* 58: 362–370

238. Hnisz D, Shrinivas K, Young RA, Chakraborty AK & Sharp PA (2017) A Phase Separation Model for Transcriptional Control. *Cell* 169: 13–23

239. Hodi FS, O'Day SJ, McDermott DF, Weber RW, Sosman JA, Haanen JB, Gonzalez R, Robert C, Schadendorf D, Hassel JC, *et al* (2010) Improved survival with ipilimumab in patients with metastatic melanoma. *N Engl J Med* 363: 711–723

240. Hodis E, Watson IR, Kryukov GV, Arold ST, Imielinski M, Theurillat J-P, Nickerson E, Auclair D, Li L, Place C, *et al* (2012) A landscape of driver mutations in melanoma. *Cell* 150: 251–263

241. Hoek KS, Eichhoff OM, Schlegel NC, Döbbeling U, Kobert N, Schaerer L, Hemmi S & Dummer R (2008) In vivo switching of human melanoma cells between proliferative and invasive states. *Cancer Res* 68: 650–656

242. Hoek KS, Schlegel NC, Brafford P, Sucker A, Ugurel S, Kumar R, Weber BL, Nathanson KL, Phillips DJ, Herlyn M, *et al* (2006) Metastatic potential of melanomas defined by specific gene expression profiles with no BRAF signature. *Pigment Cell Res* 19: 290–302

243. Hollaender A & Duggar BM (1938) The Effects of Sublethal Doses of Monochromatic Ultraviolet Radiation on the Growth Properties of Bacteria. *J Bacteriol* 36: 17–37

244. Hoppe MM, Jaynes P, Wardyn JD, Upadhyayula SS, Tan TZ, Lie S, Lim DGZ, Pang BNK, Lim S, P S Yeong J, *et al* (2021) Quantitative imaging of RAD51 expression as a marker of platinum resistance in ovarian cancer. *EMBO Mol Med* 13: e13366

245. Horn S, Figl A, Rachakonda PS, Fischer C, Sucker A, Gast A, Kadel S, Moll I, Nagore E, Hemminki K, *et al* (2013) TERT promoter mutations in familial and sporadic melanoma. *Science* 339: 959–961

246. Hosea R, Hillary S, Naqvi S, Wu S & Kasim V (2024) The two sides of chromosomal instability: drivers and brakes in cancer. *Sig Transduct Target Ther* 9: 75

247. Howell A & Howell SJ (2023) Tamoxifen evolution. *Br J Cancer* 128: 421–425

248. Huang FW, Hodis E, Xu MJ, Kryukov GV, Chin L & Garraway LA (2013) Highly recurrent TERT promoter mutations in human melanoma. *Science* 339: 957–959

249. Huang R & Zhou P-K (2021) DNA damage repair: historical perspectives, mechanistic pathways and clinical translation for targeted cancer therapy. *Signal Transduct Target Ther* 6: 254

250. Hubbard GK, Mutton LN, Khalili M, McMullin RP, Hicks JL, Bianchi-Frias D, Horn LA, Kulac I, Moubarek MS, Nelson PS, *et al* (2016) Combined MYC Activation and Pten Loss Are Sufficient to Create Genomic Instability and Lethal Metastatic Prostate Cancer. *Cancer Res* 76: 283–292

251. Huen MSY, Grant R, Manke I, Minn K, Yu X, Yaffe MB & Chen J (2007) RNF8 transduces the DNA-damage signal via histone ubiquitylation and checkpoint protein assembly. *Cell* 131: 901–914

252. Hugo W, Zaretsky JM, Sun L, Song C, Moreno BH, Hu-Lieskovan S, Berent-Maoz B, Pang J, Chmielowski B, Cherry G, *et al* (2016) Genomic and Transcriptomic Features of Response to Anti-PD-1 Therapy in Metastatic Melanoma. *Cell* 165: 35–44

253. Hunter MV, Joshi E, Bowker S, Montal E, Ma Y, Kim YH, Yang Z, Tuffery L, Li Z, Rosiek E, *et al* (2025) Mechanical confinement governs phenotypic plasticity in melanoma. *Nature* 647: 517–527

254. Iqbal J, Ragone A, Lubinski J, Lynch HT, Moller P, Ghadirian P, Foulkes WD, Armel S, Eisen A, Neuhausen SL, *et al* (2012) The incidence of pancreatic cancer in BRCA1 and BRCA2 mutation carriers. *Br J Cancer* 107: 2005–2009

255. Ira G, Pellicioli A, Balijja A, Wang X, Fiorani S, Carotenuto W, Liberi G, Bressan D, Wan L, Hollingsworth NM, *et al* (2004) DNA end resection, homologous recombination and DNA damage checkpoint activation require CDK1. *Nature* 431: 1011–1017

256. Irvine M, Stewart A, Pedersen B, Boyd S, Kefford R & Rizos H (2018) Oncogenic PI3K/AKT promotes the step-wise evolution of combination BRAF/MEK inhibitor resistance in melanoma. *Oncogenesis* 7: 72

257. Jacob F & Monod J (1961) Genetic regulatory mechanisms in the synthesis of proteins. *J Mol Biol* 3: 318–356

258. Jacobs AL & Schär P (2012) DNA glycosylases: in DNA repair and beyond. *Chromosoma* 121: 1–20

259. Jaffray DA, Knaul F, Baumann M & Gospodarowicz M (2023) Harnessing progress in radiotherapy for global cancer control. *Nat Cancer* 4: 1228–1238

260. Jang JE, Eom J-I, Jeung H-K, Cheong J-W, Lee JY, Kim JS & Min YH (2017) AMPK-ULK1-Mediated Autophagy Confers Resistance to BET Inhibitor JQ1 in Acute Myeloid Leukemia Stem Cells. *Clin Cancer Res* 23: 2781–2794

261. Jang MK, Mochizuki K, Zhou M, Jeong H-S, Brady JN & Ozato K (2005) The bromodomain protein Brd4 is a positive regulatory component of P-TEFb and stimulates RNA polymerase II-dependent transcription. *Mol Cell* 19: 523–534

262. Jaspers JE, Kersbergen A, Boon U, Sol W, van Deemter L, Zander SA, Drost R, Wientjens E, Ji J, Aly A, *et al* (2013) Loss of 53BP1 causes PARP inhibitor resistance in Brca1-mutated mouse mammary tumors. *Cancer Discov* 3: 68–81

263. Jaspers JE, Sol W, Kersbergen A, Schlicker A, Guyader C, Xu G, Wessels L, Borst P, Jonkers J & Rottenberg S (2015) BRCA2-deficient sarcomatoid mammary tumors exhibit multidrug resistance. *Cancer Res* 75: 732–741

264. Jensen RB, Carreira A & Kowalczykowski SC (2010) Purified human BRCA2 stimulates RAD51-mediated recombination. *Nature* 467: 678–683

265. Jerby-Arnon L, Shah P, Cuoco MS, Rodman C, Su M-J, Melms JC, Leeson R, Kanodia A, Mei S, Lin J-R, *et al* (2018) A Cancer Cell Program Promotes T Cell Exclusion and Resistance to Checkpoint Blockade. *Cell* 175: 984-997.e24

266. Jiang M, Azevedo-Pouly AC, Deering TG, Hoang CQ, DiRenzo D, Hess DA, Konieczny SF, Swift GH & MacDonald RJ (2016) MIST1 and PTF1 Collaborate in Feed-Forward Regulatory Loops That Maintain the Pancreatic Acinar Phenotype in Adult Mice. *Mol Cell Biol* 36: 2945–2955

267. Johannessen CM, Boehm JS, Kim SY, Thomas SR, Wardwell L, Johnson LA, Emery CM, Stransky N, Cogdill AP, Barretina J, *et al* (2010) COT drives resistance to RAF inhibition through MAP kinase pathway reactivation. *Nature* 468: 968–972

268. Johannet P, Rousseau B, Aghajanian C, Foote MB & Diaz LA (2025) Therapeutic targeting of mismatch repair-deficient cancers. *Nat Rev Clin Oncol* 22: 734–759

269. Johnson SF, Cruz C, Greifenberg AK, Dust S, Stover DG, Chi D, Primack B, Cao S, Bernhardy AJ, Coulson R, *et al* (2016) CDK12 Inhibition Reverses De Novo and Acquired PARP Inhibitor Resistance in BRCA Wild-Type and Mutated Models of Triple-Negative Breast Cancer. *Cell Reports* 17: 2367–2381

270. Johnstone SE, Reyes A, Qi Y, Adriaens C, Hegazi E, Pelka K, Chen JH, Zou LS, Drier Y, Hecht V, *et al* (2020) Large-Scale Topological Changes Restrain Malignant Progression in Colorectal Cancer. *Cell* 182: 1474-1489.e23

271. Kadauke S & Blobel GA (2009) Chromatin loops in gene regulation. *Biochim Biophys Acta* 1789: 17–25

272. Kadoch C, Hargreaves DC, Hodges C, Elias L, Ho L, Ranish J & Crabtree GR (2013) Proteomic and bioinformatic analysis of mammalian SWI/SNF complexes identifies extensive roles in human malignancy. *Nat Genet* 45: 592–601

273. Kais Z, Rondinelli B, Holmes A, O'Leary C, Kozono D, D'Andrea AD & Ceccaldi R (2016) FANCD2 maintains fork stability in BRCA1/2-deficient tumors and promotes alternative end-joining DNA repair. *Cell Rep* 15: 2488–2499

274. Kapoor A, Goldberg MS, Cumberland LK, Ratnakumar K, Segura MF, Emanuel PO, Menendez S, Vardabasso C, Leroy G, Vidal CI, *et al* (2010) The histone variant macroH2A suppresses melanoma progression through regulation of CDK8. *Nature* 468: 1105–1109

275. Karakashev S, Fukumoto T, Zhao B, Lin J, Wu S, Fatkhutdinov N, Park P-H, Semenova G, Jean S, Cadungog MG, *et al* (2020) EZH2 Inhibition Sensitizes CARM1-High, Homologous Recombination Proficient Ovarian Cancers to PARP Inhibition. *Cancer Cell* 37: 157-167.e6

276. Karponis D, Joshy J, Stratigos IA, Craig PJ, Mistry K, van Bodegraven B, Venables ZC & Levell NJ (2025) Cutaneous melanoma in situ: a review. *Clin Exp Dermatol* 50: 529–536

277. Karras P, Black JRM, McGranahan N & Marine J-C (2024) Decoding the interplay between genetic and non-genetic drivers of metastasis. *Nature* 629: 543–554

278. Karras P, Bordeu I, Pozniak J, Nowosad A, Pazzi C, Van Raemdonck N, Landeloos E, Van Herck Y, Pedri D, Bervoets G, *et al* (2022) A cellular hierarchy in melanoma uncouples growth and metastasis. *Nature* 610: 190–198

279. Katainen R, Dave K, Pitkänen E, Palin K, Kivioja T, Välimäki N, Gylfe AE, Ristolainen H, Hänninen UA, Cajuso T, *et al* (2015) CTCF/cohesin-binding sites are frequently mutated in cancer. *Nat Genet* 47: 818–821

280. Kaufman B, Shapira-Frommer R, Schmutzler RK, Audeh MW, Friedlander M, Balmaña J, Mitchell G, Fried G, Stemmer SM, Hubert A, *et al* (2015) Olaparib monotherapy in patients with advanced cancer and a germline BRCA1/2 mutation. *J Clin Oncol* 33: 244–250

281. Kaufman CK, Mosimann C, Fan ZP, Yang S, Thomas AJ, Ablain J, Tan JL, Fogley RD, van Rooijen E, Hagedorn EJ, *et al* (2016) A zebrafish melanoma model reveals emergence of neural crest identity during melanoma initiation. *Science* 351: aad2197

282. Keilholz U, Conradt C, Legha SS, Khayat D, Scheibenbogen C, Thatcher N, Goey SH, Gore M, Dorval T, Hancock B, *et al* (1998) Results of interleukin-2-based treatment in advanced melanoma: a case record-based analysis of 631 patients. *J Clin Oncol* 16: 2921–2929

283. Kemp CJ, Moore JM, Moser R, Bernard B, Teater M, Smith LE, Rabaia NA, Gurley KE, Guinney J, Busch SE, *et al* (2014) CTCF haploinsufficiency destabilizes DNA methylation and predisposes to cancer. *Cell Rep* 7: 1020–1029

284. Khaliq M, Manikkam M, Martinez ED & Fallahi-Sichani M (2021) Epigenetic modulation reveals differentiation state specificity of oncogene addiction. *Nat Commun* 12: 1536

285. Killela PJ, Reitman ZJ, Jiao Y, Bettegowda C, Agrawal N, Diaz LA, Friedman AH, Friedman H, Gallia GL, Giovanella BC, *et al* (2013) TERT promoter mutations occur frequently in gliomas and a subset of tumors derived from cells with low rates of self-renewal. *Proc Natl Acad Sci U S A* 110: 6021–6026

286. Kim IS, Heilmann S, Kansler ER, Zhang Y, Zimmer M, Ratnakumar K, Bowman RL, Simon-Vermot T, Fennell M, Garippa R, *et al* (2017) Microenvironment-derived factors driving metastatic plasticity in melanoma. *Nat Commun* 8: 14343

287. Kinde I, Munari E, Faraj SF, Hruban RH, Schoenberg M, Bivalacqua T, Allaf M, Springer S, Wang Y, Diaz LA, *et al* (2013) TERT promoter mutations occur early in urothelial neoplasia and are biomarkers of early disease and disease recurrence in urine. *Cancer Res* 73: 7162–7167

288. King M-C, Marks JH & Mandell JB (2003) Breast and Ovarian Cancer Risks Due to Inherited Mutations in BRCA1 and BRCA2. *Science* 302: 643–646

289. Kjeldsen JW, Lorentzen CL, Martinenaite E, Ellebaek E, Donia M, Holmstroem RB, Klausen TW, Madsen CO, Ahmed SM, Weis-Banke SE, *et al* (2021) A phase 1/2 trial of an immune-modulatory vaccine against IDO/PD-L1 in combination with nivolumab in metastatic melanoma. *Nat Med* 27: 2212–2223

290. Klein IA, Boija A, Afeyan LK, Hawken SW, Fan M, Dall'Agnese A, Oksuz O, Henninger JE, Shrinivas K, Sabari BR, *et al* (2020) Partitioning of cancer therapeutics in nuclear condensates. *Science* 368: 1386–1392

291. Kondrashova O, Nguyen M, Shield-Artin K, Tinker AV, Teng NNH, Harrell MI, Kuiper MJ, Ho G-Y, Barker H, Jasin M, *et al* (2017) Secondary Somatic Mutations Restoring RAD51C and RAD51D Associated with Acquired Resistance to the PARP Inhibitor Rucaparib in High-Grade Ovarian Carcinoma. *Cancer Discov* 7: 984–998

292. Kondrashova O, Topp M, Nesic K, Lieschke E, Ho G-Y, Harrell MI, Zapparoli GV, Hadley A, Holian R, Boehm E, *et al* (2018) Methylation of all BRCA1 copies predicts response to the PARP inhibitor rucaparib in ovarian carcinoma. *Nat Commun* 9: 3970

293. Konieczkowski DJ, Johannessen CM, Abudayyeh O, Kim JW, Cooper ZA, Piris A, Frederick DT, Barzily-Rokni M, Straussman R, Haq R, *et al* (2014) A melanoma cell state distinction influences sensitivity to MAPK pathway inhibitors. *Cancer Discov* 4: 816–827

294. Konstantinopoulos PA, Spentzos D, Karlan BY, Taniguchi T, Fountzilas E, Francoeur N, Levine DA & Cannistra SA (2010) Gene expression profile of BRCAness that correlates with responsiveness to chemotherapy and with outcome in patients with epithelial ovarian cancer. *J Clin Oncol* 28: 3555–3561

295. Koo CW, Xiao J, Coassolo S, Liu J, Yu C, Azumaya C, Gore SK, Cheung TK, Brillantes B, Rose CM, *et al* (2026) BCDX2–CX3 and DX2–CX3 complexes assemble and stabilize RAD51 filaments. *Nature*: 1–3

296. Kottemann MC & Smogorzewska A (2013) Fanconi anaemia and the repair of Watson and Crick DNA crosslinks. *Nature* 493: 356–363

297. Kozar I, Margue C, Rothengatter S, Haan C & Kreis S (2019) Many ways to resistance: How melanoma cells evade targeted therapies. *Biochim Biophys Acta Rev Cancer* 1871: 313–322

298. Krajewska M, Dries R, Grassetti AV, Dust S, Gao Y, Huang H, Sharma B, Day DS, Kwiatkowski N, Pomaville M, *et al* (2019) CDK12 loss in cancer cells affects DNA damage response genes through premature cleavage and polyadenylation. *Nat Commun* 10: 1757

299. Krastev DB, Li S, Sun Y, Wicks AJ, Hoslett G, Weekes D, Badder LM, Knight EG, Marlow R, Pardo MC, *et al* (2022) The ubiquitin-dependent ATPase p97 removes cytotoxic trapped PARP1 from chromatin. *Nat Cell Biol* 24: 62–73

300. Kraus WL (2015) PARPs and ADP-Ribosylation: 50 Years … and Counting. *Mol Cell* 58: 902–910

301. Krokan HE & Bjørås M (2013) Base Excision Repair. *Cold Spring Harb Perspect Biol* 5: a012583

302. Kuilman T, Michaloglou C, Vredeveld LCW, Douma S, van Doorn R, Desmet CJ, Aarden LA, Mooi WJ & Peeper DS (2008) Oncogene-induced senescence relayed by an interleukin-dependent inflammatory network. *Cell* 133: 1019–1031

303. Kunkel TA & Erie DA (2005) DNA MISMATCH REPAIR*. *Annual Review of Biochemistry* 74: 681–710

304. Kuzminov A (2001) Single-strand interruptions in replicating chromosomes cause double-strand breaks. *Proc Natl Acad Sci U S A* 98: 8241–8246

305. Kwiatkowski N, Zhang T, Rahl PB, Abraham BJ, Reddy J, Ficarro SB, Dastur A, Amzallag A, Ramaswamy S, Tesar B, *et al* (2014) Targeting transcription regulation in cancer with a covalent CDK7 inhibitor. *Nature* 511: 616–620

306. Lahiri S, Hamilton G, Moore G, Goehring L, Huang TT, Jensen RB & Rothenberg E (2025) BRCA2 prevents PARPi-mediated PARP1 retention to protect RAD51 filaments. *Nature* 640: 1103–1111

307. Lam LT, Pickeral OK, Peng AC, Rosenwald A, Hurt EM, Giltnane JM, Averett LM, Zhao H, Davis RE, Sathyamoorthy M, *et al* (2001) Genomic-scale measurement of mRNA turnover and the mechanisms of action of the anti-cancer drug flavopiridol. *Genome Biol* 2: RESEARCH0041

308. Lambert SA, Jolma A, Campitelli LF, Das PK, Yin Y, Albu M, Chen X, Taipale J, Hughes TR & Weirauch MT (2018) The Human Transcription Factors. *Cell* 172: 650–665

309. Landsberg J, Kohlmeyer J, Renn M, Bald T, Rogava M, Cron M, Fatho M, Lennerz V, Wölfel T, Hölzel M, *et al* (2012) Melanomas resist T-cell therapy through inflammation-induced reversible dedifferentiation. *Nature* 490: 412–416

310. Larkin J, Ascierto PA, Dréno B, Atkinson V, Liszkay G, Maio M, Mandalà M, Demidov L, Stroyakovskiy D, Thomas L, *et al* (2014) Combined vemurafenib and cobimetinib in BRAF-mutated melanoma. *N Engl J Med* 371: 1867–1876

311. Larkin J, Chiarion-Sileni V, Gonzalez R, Grob J-J, Rutkowski P, Lao CD, Cowey CL, Schadendorf D, Wagstaff J, Dummer R, *et al* (2019) Five-Year Survival with Combined Nivolumab and Ipilimumab in Advanced Melanoma. *N Engl J Med* 381: 1535–1546

312. Laughery MF, Brown AJ, Bohm KA, Sivapragasam S, Morris HS, Tchmola M, Washington AD, Mitchell D, Mather S, Malc EP, *et al* (2020) Atypical UV Photoproducts Induce Non-canonical Mutation Classes Associated with Driver Mutations in Melanoma. *Cell Rep* 33: 108401

313. Lauss M, Phung B, Borch TH, Harbst K, Kaminska K, Ebbesson A, Hedenfalk I, Yuan J, Nielsen K, Ingvar C, *et al* (2024) Molecular patterns of resistance to immune checkpoint blockade in melanoma. *Nat Commun* 15: 3075

314. Le DT, Durham JN, Smith KN, Wang H, Bartlett BR, Aulakh LK, Lu S, Kemberling H, Wilt C, Luber BS, *et al* (2017) Mismatch repair deficiency predicts response of solid tumors to PD-1 blockade. *Science* 357: 409–413

315. Le DT, Uram JN, Wang H, Bartlett BR, Kemberling H, Eyring AD, Skora AD, Luber BS, Azad NS, Laheru D, *et al* (2015a) PD-1 Blockade in Tumors with Mismatch-Repair Deficiency. *N Engl J Med* 372: 2509–2520

316. Le VH, Inai M, Williams RM & Kan T (2015b) Ecteinascidins. A Review of the Chemistry, Biology and Clinical Utility of Potent Tetrahydroisoquinoline Antitumor Antibiotics. *Nat Prod Rep* 32: 328–347

317. Leal JFM, Martínez-Díez M, García-Hernández V, Moneo V, Domingo A, Bueren-Calabuig JA, Negri A, Gago F, Guillén-Navarro MJ, Avilés P, *et al* (2010) PM01183, a new DNA minor groove covalent binder with potent in vitro and in vivo anti-tumour activity. *Br J Pharmacol* 161: 1099–1110

318. Ledermann J, Harter P, Gourley C, Friedlander M, Vergote I, Rustin G, Scott C, Meier W, Shapira-Frommer R, Safra T, *et al* (2012) Olaparib maintenance therapy in platinum-sensitive relapsed ovarian cancer. *N Engl J Med* 366: 1382–1392

319. Lee J, Ledermann JA & Kohn EC (2014) PARP Inhibitors for BRCA1/2 mutation-associated and BRCA-like malignancies. *Ann Oncol* 25: 32–40

320. Lee J-H & Paull TT (2004) Direct activation of the ATM protein kinase by the Mre11/Rad50/Nbs1 complex. *Science* 304: 93–96

321. Lee TI & Young RA (2013) Transcriptional regulation and its misregulation in disease. *Cell* 152: 1237–1251

322. Lee Y-R, Chen M & Pandolfi PP (2018) The functions and regulation of the PTEN tumour suppressor: new modes and prospects. *Nat Rev Mol Cell Biol* 19: 547–562

323. Leung AKL (2017) PARPs. *Curr Biol* 27: R1256–R1258

324. Li F, MacKenzie KR, Jain P, Santini C, Young DW & Matzuk MM (2020) Metabolism of JQ1, an inhibitor of bromodomain and extra terminal bromodomain proteins, in human and mouse liver microsomes†. *Biol Reprod* 103: 427–436

325. Li J, Dong A, Saydaminova K, Chang H, Wang G, Ochiai H, Yamamoto T & Pertsinidis A (2019) Single-Molecule Nanoscopy Elucidates RNA Polymerase II Transcription at Single Genes in Live Cells. *Cell* 178: 491-506.e28

326. Liang K, Gao X, Gilmore JM, Florens L, Washburn MP, Smith E & Shilatifard A (2015) Characterization of human cyclin-dependent kinase 12 (CDK12) and CDK13 complexes in C-terminal domain phosphorylation, gene transcription, and RNA processing. *Mol Cell Biol* 35: 928–938

327. Lieberman-Aiden E, van Berkum NL, Williams L, Imakaev M, Ragoczy T, Telling A, Amit I, Lajoie BR, Sabo PJ, Dorschner MO, *et al* (2009) Comprehensive mapping of long-range interactions reveals folding principles of the human genome. *Science* 326: 289–293

328. Lim SY, Shklovskaya E, Lee JH, Pedersen B, Stewart A, Ming Z, Irvine M, Shivalingam B, Saw RPM, Menzies AM, *et al* (2023) The molecular and functional landscape of resistance to immune checkpoint blockade in melanoma. *Nat Commun* 14: 1516

329. Lim WK, Ong CK, Tan J, Thike AA, Ng CCY, Rajasegaran V, Myint SS, Nagarajan S, Nasir NDM, McPherson JR, *et al* (2014) Exome sequencing identifies highly recurrent MED12 somatic mutations in breast fibroadenoma. *Nat Genet* 46: 877–880

330. Lima M, Bouzid H, Soares DG, Selle F, Morel C, Galmarini CM, Henriques JAP, Larsen AK & Escargueil AE (2016) Dual inhibition of ATR and ATM potentiates the activity of trabectedin and lurbinectedin by perturbing the DNA damage response and homologous recombination repair. *Oncotarget* 7: 25885–25901

331. Lin CY, Lovén J, Rahl PB, Paranal RM, Burge CB, Bradner JE, Lee TI & Young RA (2012) Transcriptional amplification in tumor cells with elevated c-Myc. *Cell* 151: 56–67

332. Lin KK, Harrell MI, Oza AM, Oaknin A, Ray-Coquard I, Tinker AV, Helman E, Radke MR, Say C, Vo L-T, *et al* (2019) BRCA Reversion Mutations in Circulating Tumor DNA Predict Primary and Acquired Resistance to the PARP Inhibitor Rucaparib in High-Grade Ovarian Carcinoma. *Cancer Discov* 9: 210–219

333. Lin YL, Shivji MK, Chen C, Kolodner R, Wood RD & Dutta A (1998) The evolutionarily conserved zinc finger motif in the largest subunit of human replication protein A is required for DNA replication and mismatch repair but not for nucleotide excision repair. *J Biol Chem* 273: 1453–1461

334. Lindahl T (1974) An N-glycosidase from Escherichia coli that releases free uracil from DNA containing deaminated cytosine residues. *Proc Natl Acad Sci U S A* 71: 3649–3653

335. Lisby M, Barlow JH, Burgess RC & Rothstein R (2004) Choreography of the DNA damage response: spatiotemporal relationships among checkpoint and repair proteins. *Cell* 118: 699–713

336. Litton JK, Rugo HS, Ettl J, Hurvitz SA, Gonçalves A, Lee K-H, Fehrenbacher L, Yerushalmi R, Mina LA, Martin M, *et al* (2018) Talazoparib in Patients with Advanced Breast Cancer and a Germline BRCA Mutation. *N Engl J Med* 379: 753–763

337. Liu X, Bushnell DA & Kornberg RD (2011) Lock and key to transcription: σ-DNA interaction. *Cell* 147: 1218–1219

338. Long GV, Flaherty KT, Stroyakovskiy D, Gogas H, Levchenko E, de Braud F, Larkin J, Garbe C, Jouary T, Hauschild A, *et al* (2017) Dabrafenib plus trametinib versus dabrafenib monotherapy in patients with metastatic BRAF V600E/K-mutant melanoma: long-term survival and safety analysis of a phase 3 study. *Ann Oncol* 28: 1631–1639

339. Long GV, Stroyakovskiy D, Gogas H, Levchenko E, de Braud F, Larkin J, Garbe C, Jouary T, Hauschild A, Grob JJ, *et al* (2014) Combined BRAF and MEK inhibition versus BRAF inhibition alone in melanoma. *N Engl J Med* 371: 1877–1888

340. Long GV, Swetter SM, Menzies AM, Gershenwald JE & Scolyer RA (2023) Cutaneous melanoma. *Lancet* 402: 485–502

341. Lorch Y, LaPointe JW & Kornberg RD (1987) Nucleosomes inhibit the initiation of transcription but allow chain elongation with the displacement of histones. *Cell* 49: 203–210

342. Lord CJ & Ashworth A (2016) BRCAness revisited. *Nat Rev Cancer* 16: 110–120

343. Louder RK, He Y, López-Blanco JR, Fang J, Chacón P & Nogales E (2016) Structure of promoter-bound TFIID and model of human pre-initiation complex assembly. *Nature* 531: 604–609

344. Lovén J, Hoke HA, Lin CY, Lau A, Orlando DA, Vakoc CR, Bradner JE, Lee TI & Young RA (2013) Selective Inhibition of Tumor Oncogenes by Disruption of Super-Enhancers. *Cell* 153: 320–334

345. Lubrano S, Cervantes-Villagrana RD, Faraji F, Ramirez S, Sato K, Adame-Garcia SR, Officer A, Arang N, Rigiracciolo DC, Anguiano Quiroz PY, *et al* (2025) FAK inhibition combined with the RAF-MEK clamp avutometinib overcomes resistance to targeted and immune therapies in BRAF V600E melanoma. *Cancer Cell* 43: 428-445.e6

346. Luo J, Chen Z, Qiao Y, Tien JC-Y, Young E, Mannan R, Mahapatra S, Bhattacharyya R, Xiao L, He T, *et al* (2025) Targeting histone H2B acetylated enhanceosomes via p300/CBP degradation in prostate cancer. *Nat Genet* 57: 2468–2481

347. Luo K, Li L, Li Y, Wu C, Yin Y, Chen Y, Deng M, Nowsheen S, Yuan J & Lou Z (2016) A phosphorylation-deubiquitination cascade regulates the BRCA2-RAD51 axis in homologous recombination. *Genes Dev* 30: 2581–2595

348. Lynce F, Shajahan-Haq AN & Swain SM (2018) CDK4/6 inhibitors in breast cancer therapy: Current practice and future opportunities. *Pharmacology & Therapeutics* 191: 65–73

349. Mabuchi S, Hisamatsu T, Kawase C, Hayashi M, Sawada K, Mimura K, Takahashi K, Takahashi T, Kurachi H & Kimura T (2011) The activity of trabectedin as a single agent

or in combination with everolimus for clear cell carcinoma of the ovary. *Clin Cancer Res* 17: 4462–4473

350. Machacova Z, Chroma K, Lukac D, Protivankova I & Moudry P (2024) DNA polymerase α-primase facilitates PARP inhibitor-induced fork acceleration and protects BRCA1-deficient cells against ssDNA gaps. *Nat Commun* 15: 7375

351. Mäkinen N, Mehine M, Tolvanen J, Kaasinen E, Li Y, Lehtonen HJ, Gentile M, Yan J, Enge M, Taipale M, *et al* (2011) MED12, the mediator complex subunit 12 gene, is mutated at high frequency in uterine leiomyomas. *Science* 334: 252–255

352. Malik S & Roeder RG (2023) Regulation of the RNA polymerase II pre-initiation complex by its associated coactivators. *Nat Rev Genet* 24: 767–782

353. Mansour MR, Abraham BJ, Anders L, Berezovskaya A, Gutierrez A, Durbin AD, Etchin J, Lawton L, Sallan SE, Silverman LB, *et al* (2014) An oncogenic super-enhancer formed through somatic mutation of a noncoding intergenic element. *Science* 346: 1373–1377

354. Mao Y, Gide TN, Maher NG, Vignati D, Boutros A, Cornejo-Páramo P, Potter AJ, Carlino MS, Paver EC, Burke H, *et al* (2026) Prospective tumour mutation burden and neoantigen profiling predicts immunotherapy response in metastatic melanoma. *NPJ Precis Oncol* 10: 55

355. Marei HE (2025) Epigenetic regulators in cancer therapy and progression. *npj Precis Onc* 9: 206

356. Mariathasan S, Turley SJ, Nickles D, Castiglioni A, Yuen K, Wang Y, Kadel EE, Koeppen H, Astarita JL, Cubas R, *et al* (2018) TGFβ attenuates tumour response to PD-L1 blockade by contributing to exclusion of T cells. *Nature* 554: 544–548

357. Marin-Gonzalez A, Rybczynski AT, Nilavar NM, Nguyen D, Li AG, Karwacki-Neisius V, Zou RS, Avilés-Vázquez FJ, Kanemaki MT, Scully R, *et al* (2025) Cohesin drives chromatin scanning during the RAD51-mediated homology search. *Science* 390: eadw1928

358. Mark KG & Rape M (2021) Ubiquitin-dependent regulation of transcription in development and disease. *EMBO Rep* 22: e51078

359. Marshall AD, Bailey CG, Champ K, Vellozzi M, O'Young P, Metierre C, Feng Y, Thoeng A, Richards AM, Schmitz U, *et al* (2017) CTCF genetic alterations in endometrial carcinoma are pro-tumorigenic. *Oncogene* 36: 4100–4110

360. Marteijn JA, Lans H, Vermeulen W & Hoeijmakers JHJ (2014) Understanding nucleotide excision repair and its roles in cancer and ageing. *Nat Rev Mol Cell Biol* 15: 465–481

361. Martinez EJ & Corey EJ (2000) A New, More Efficient, and Effective Process for the Synthesis of a Key Pentacyclic Intermediate for Production of Ecteinascidin and Phthalascidin Antitumor Agents. *Org Lett* 2: 993–996

362. Martínez-Jiménez F, Muiños F, Sentís I, Deu-Pons J, Reyes-Salazar I, Arnedo-Pac C, Mularoni L, Pich O, Bonet J, Kranas H, *et al* (2020) A compendium of mutational cancer driver genes. *Nat Rev Cancer* 20: 555–572

363. Martire S & Banaszynski LA (2020) The roles of histone variants in fine-tuning chromatin organization and function. *Nat Rev Mol Cell Biol* 21: 522–541

364. Matthews HK, Bertoli C & de Bruin RAM (2022) Cell cycle control in cancer. *Nat Rev Mol Cell Biol* 23: 74–88

365. Maya-Mendoza A, Moudry P, Merchut-Maya JM, Lee M, Strauss R & Bartek J (2018) High speed of fork progression induces DNA replication stress and genomic instability. *Nature* 559: 279–284

366. Mazón G, Mimitou EP & Symington LS (2010) SnapShot: Homologous recombination in DNA double-strand break repair. *Cell* 142: 646, 646.e1

367. Mazumdar C, Shen Y, Xavy S, Zhao F, Reinisch A, Li R, Corces MR, Flynn RA, Buenrostro JD, Chan SM, *et al* (2015) Leukemia-Associated Cohesin Mutants Dominantly Enforce Stem Cell Programs and Impair Human Hematopoietic Progenitor Differentiation. *Cell Stem Cell* 17: 675–688

368. McCabe N, Turner NC, Lord CJ, Kluzek K, Białkowska A, Swift S, Giavara S, O'Connor MJ, Tutt AN, Zdzienicka MZ, *et al* (2006) Deficiency in the Repair of DNA Damage by Homologous Recombination and Sensitivity to Poly(ADP-Ribose) Polymerase Inhibition. *Cancer Research* 66: 8109–8115

369. McGranahan N & Swanton C (2017) Clonal Heterogeneity and Tumor Evolution: Past, Present, and the Future. *Cell* 168: 613–628

370. Mehta A & Haber JE (2014) Sources of DNA double-strand breaks and models of recombinational DNA repair. *Cold Spring Harb Perspect Biol* 6: a016428

371. Mehta S & Zhang J (2022) Liquid–liquid phase separation drives cellular function and dysfunction in cancer. *Nat Rev Cancer* 22: 239–252

372. Melanoma of the Skin - Cancer Stat Facts *SEER*

373. Mendes-Pereira AM, Martin SA, Brough R, McCarthy A, Taylor JR, Kim J-S, Waldman T, Lord CJ & Ashworth A (2009) Synthetic lethal targeting of PTEN mutant cells with PARP inhibitors. *EMBO Mol Med* 1: 315–322

374. Ménissier-de Murcia J, Molinete M, Gradwohl G, Simonin F & de Murcia G (1989) Zinc-binding domain of poly(ADP-ribose)polymerase participates in the recognition of single strand breaks on DNA. *J Mol Biol* 210: 229–233

375. Michaloglou C, Vredeveld LCW, Soengas MS, Denoyelle C, Kuilman T, van der Horst CMAM, Majoor DM, Shay JW, Mooi WJ & Peeper DS (2005) BRAFE600-associated senescence-like cell cycle arrest of human naevi. *Nature* 436: 720–724

376. de Miguel FJ, Gentile C, Feng WW, Silva SJ, Sankar A, Exposito F, Cai WL, Melnick MA, Robles-Oteiza C, Hinkley MM, *et al* (2023) Mammalian SWI/SNF chromatin remodeling complexes promote tyrosine kinase inhibitor resistance in EGFR-mutant lung cancer. *Cancer Cell* 41: 1516-1534.e9

377. Min H-Y & Lee H-Y (2022) Molecular targeted therapy for anticancer treatment. *Exp Mol Med* 54: 1670–1694

378. Mirza MR, Åvall Lundqvist E, Birrer MJ, dePont Christensen R, Nyvang G-B, Malander S, Anttila M, Werner TL, Lund B, Lindahl G, *et al* (2019) Niraparib plus bevacizumab versus niraparib alone for platinum-sensitive recurrent ovarian cancer (NSGO-AVANOVA2/ENGOT-ov24): a randomised, phase 2, superiority trial. *Lancet Oncol* 20: 1409–1419

379. Mirza MR, Monk BJ, Herrstedt J, Oza AM, Mahner S, Redondo A, Fabbro M, Ledermann JA, Lorusso D, Vergote I, *et al* (2016) Niraparib Maintenance Therapy in Platinum-Sensitive, Recurrent Ovarian Cancer. *New England Journal of Medicine* 375: 2154–2164

380. Misteli T (2020) The Self-Organizing Genome: Principles of Genome Architecture and Function. *Cell* 183: 28–45

381. Mittal P & Roberts CWM (2020) The SWI/SNF complex in cancer — biology, biomarkers and therapy. *Nat Rev Clin Oncol* 17: 435–448

382. Mol CD, Izumi T, Mitra S & Tainer JA (2000) DNA-bound structures and mutants reveal abasic DNA binding by APE1 and DNA repair coordination [corrected]. *Nature* 403: 451–456

383. Monteran L, Zait Y & Erez N (2024) It's all about the base: stromal cells are central orchestrators of metastasis. *Trends in Cancer* 10: 208–229

384. Moriceau G, Hugo W, Hong A, Shi H, Kong X, Yu CC, Koya RC, Samatar AA, Khanlou N, Braun J, *et al* (2015) Tunable-combinatorial mechanisms of acquired resistance limit the efficacy of BRAF/MEK cotargeting but result in melanoma drug addiction. *Cancer Cell* 27: 240–256

385. Moser SC, Khalizieva A, Roehsner J, Pottendorfer E, Kaptein ML, Ricci G, Bhardwaj V, Bleijerveld OB, Hoekman L, van der Heijden I, *et al* (2025) NASP modulates histone turnover to drive PARP inhibitor resistance. *Nature* 645: 1071–1080

386. Müller J, Krijgsman O, Tsoi J, Robert L, Hugo W, Song C, Kong X, Possik PA, Cornelissen-Steijger PDM, Geukes Foppen MH, *et al* (2014) Low MITF/AXL ratio predicts early resistance to multiple targeted drugs in melanoma. *Nat Commun* 5: 5712

387. Murai J, Huang SN, Das BB, Renaud A, Zhang Y, Doroshow JH, Ji J, Takeda S & Pommier Y (2012) Trapping of PARP1 and PARP2 by Clinical PARP Inhibitors. *Cancer Res* 72: 5588–5599

388. de Murcia JM, Niedergang C, Trucco C, Ricoul M, Dutrillaux B, Mark M, Oliver FJ, Masson M, Dierich A, LeMeur M, *et al* (1997) Requirement of poly(ADP-ribose) polymerase in recovery from DNA damage in mice and in cells. *Proc Natl Acad Sci U S A* 94: 7303–7307

389. Nada H, Choi Y, Kim S, Jeong KS, Meanwell NA & Lee K (2024) New insights into protein-protein interaction modulators in drug discovery and therapeutic advance. *Signal Transduct Target Ther* 9: 341

390. Narita T, Ito S, Higashijima Y, Chu WK, Neumann K, Walter J, Satpathy S, Liebner T, Hamilton WB, Maskey E, *et al* (2021) Enhancers are activated by p300/CBP activity-dependent PIC assembly, RNAPII recruitment, and pause release. *Mol Cell* 81: 2166-2182.e6

391. Nasti TH & Timares L (2015) MC1R, eumelanin and pheomelanin: their role in determining the susceptibility to skin cancer. *Photochem Photobiol* 91: 188–200

392. Nazarova M & Sexton T (2026) The Dance of Promoters and Enhancers in Gene Regulation: Fast or Slow, Entwined or Distant? *Journal of Molecular Biology* 438: 169223

393. Negrini S, Gorgoulis VG & Halazonetis TD (2010) Genomic instability — an evolving hallmark of cancer. *Nat Rev Mol Cell Biol* 11: 220–228

394. Nesic K, Kondrashova O, Hurley RM, McGehee CD, Vandenberg CJ, Ho G-Y, Lieschke E, Dall G, Bound N, Shield-Artin K, *et al* (2021) Acquired RAD51C Promoter Methylation Loss Causes PARP Inhibitor Resistance in High-Grade Serous Ovarian Carcinoma. *Cancer Res* 81: 4709–4722

395. Newell F, Pires da Silva I, Johansson PA, Menzies AM, Wilmott JS, Addala V, Carlino MS, Rizos H, Nones K, Edwards JJ, *et al* (2022) Multiomic profiling of checkpoint inhibitor-treated melanoma: Identifying predictors of response and resistance, and markers of biological discordance. *Cancer Cell* 40: 88-102.e7

396. Ng JM-K & Yu J (2015) Promoter Hypermethylation of Tumour Suppressor Genes as Potential Biomarkers in Colorectal Cancer. *Int J Mol Sci* 16: 2472–2496

397. Nick McElhinny SA, Snowden CM, McCarville J & Ramsden DA (2000) Ku recruits the XRCC4-ligase IV complex to DNA ends. *Mol Cell Biol* 20: 2996–3003

398. Nimonkar AV, Genschel J, Kinoshita E, Polaczek P, Campbell JL, Wyman C, Modrich P & Kowalczykowski SC (2011) BLM-DNA2-RPA-MRN and EXO1-BLM-RPA-MRN constitute two DNA end resection machineries for human DNA break repair. *Genes Dev* 25: 350–362

399. Nishiyama A & Nakanishi M (2021) Navigating the DNA methylation landscape of cancer. *Trends in Genetics* 37: 1012–1027

400. Noordermeer SM & van Attikum H (2019) PARP Inhibitor Resistance: A Tug-of-War in BRCA-Mutated Cells. *Trends Cell Biol* 29: 820–834

401. Ochi T, Blackford AN, Coates J, Jhujh S, Mehmood S, Tamura N, Travers J, Wu Q, Draviam VM, Robinson CV, *et al* (2015) DNA repair. PAXX, a paralog of XRCC4 and XLF, interacts with Ku to promote DNA double-strand break repair. *Science* 347: 185–188

402. O'Connell MP, Marchbank K, Webster MR, Valiga AA, Kaur A, Vultur A, Li L, Herlyn M, Villanueva J, Liu Q, *et al* (2013) Hypoxia induces phenotypic plasticity and therapy resistance in melanoma via the tyrosine kinase receptors ROR1 and ROR2. *Cancer Discov* 3: 1378–1393

403. Oh M, Alkhushaym N, Fallatah S, Althagafi A, Aljadeed R, Alsowaida Y, Jeter J, Martin JR, Babiker HM, McBride A, *et al* (2019) The association of BRCA1 and BRCA2 mutations with prostate cancer risk, frequency, and mortality: A meta-analysis. *Prostate* 79: 880–895

404. Oldridge DA, Wood AC, Weichert-Leahey N, Crimmins I, Sussman R, Winter C, McDaniel LD, Diamond M, Hart LS, Zhu S, *et al* (2015) Genetic predisposition to neuroblastoma mediated by a LMO1 super-enhancer polymorphism. *Nature* 528: 418–421

405. Ooi WF, Xing M, Xu C, Yao X, Ramlee MK, Lim MC, Cao F, Lim K, Babu D, Poon L-F, *et al* (2016) Epigenomic profiling of primary gastric adenocarcinoma reveals super-enhancer heterogeneity. *Nat Commun* 7: 12983

406. Ordóñez-Morán P, Dafflon C, Imajo M, Nishida E & Huelsken J (2015) HOXA5 Counteracts Stem Cell Traits by Inhibiting Wnt Signaling in Colorectal Cancer. *Cancer Cell* 28: 815–829

407. Oreskovic E, Wheeler EC, Mengwasser KE, Fujimura E, Martin TD, Tothova Z & Elledge SJ (2022) Genetic analysis of cancer drivers reveals cohesin and CTCF as suppressors of PD-L1. *Proc Natl Acad Sci U S A* 119: e2120540119

408. Panagopoulos A & Altmeyer M (2021) The Hammer and the Dance of Cell Cycle Control. *Trends Biochem Sci* 46: 301–314

409. Pandey N & Black BE (2021) Rapid Detection and Signaling of DNA Damage by PARP-1. *Trends Biochem Sci* 46: 744–757

410. Pastushenko I, Brisebarre A, Sifrim A, Fioramonti M, Revenco T, Boumahdi S, Van Keymeulen A, Brown D, Moers V, Lemaire S, *et al* (2018) Identification of the tumour transition states occurring during EMT. *Nature* 556: 463–468

411. Patel AG, Sarkaria JN & Kaufmann SH (2011) Nonhomologous end joining drives poly(ADP-ribose) polymerase (PARP) inhibitor lethality in homologous recombination-deficient cells. *Proc Natl Acad Sci U S A* 108: 3406–3411

412. Pattabiraman DR, Bierie B, Kober KI, Thiru P, Krall JA, Zill C, Reinhardt F, Tam WL & Weinberg RA (2016) Activation of PKA leads to mesenchymal-to-epithelial transition and loss of tumor-initiating ability. *Science* 351: aad3680

413. Paz-Ares L, Borghaei H, Liu SV, Peters S, Herbst RS, Stencel K, Majem M, Şendur MAN, Czyżewicz G, Caro RB, *et al* (2025) Efficacy and safety of first-line maintenance therapy with lurbinectedin plus atezolizumab in extensive-stage small-cell lung cancer (IMforte): a randomised, multicentre, open-label, phase 3 trial. *Lancet* 405: 2129–2143

414. Pećina-Šlaus N, Kafka A, Salamon I & Bukovac A (2020) Mismatch Repair Pathway, Genome Stability and Cancer. *Front Mol Biosci* 7: 122

415. Pedretti F, Abdalfttah M, Pellegrino B, Mateo F, Martínez-Sanz P, Herencia-Ropero A, Òdena A, Clavell-Revelles P, Casali G, Domènech H, *et al* (2025) Harnessing STING Signaling and Natural Killer Cells Overcomes PARP Inhibitor Resistance in Homologous Recombination-Deficient Breast Cancer. *Cancer Res* 85: 1888–1908

416. Pelish HE, Liau BB, Nitulescu II, Tangpeerachaikul A, Poss ZC, Da Silva DH, Caruso BT, Arefolov A, Fadeyi O, Christie AL, *et al* (2015) Mediator kinase inhibition further activates super-enhancer-associated genes in AML. *Nature* 526: 273–276

417. Pellegrini L, Yu DS, Lo T, Anand S, Lee M, Blundell TL & Venkitaraman AR (2002) Insights into DNA recombination from the structure of a RAD51-BRCA2 complex. *Nature* 420: 287–293

418. Peng G, Chun-Jen Lin C, Mo W, Dai H, Park Y-Y, Kim SM, Peng Y, Mo Q, Siwko S, Hu R, *et al* (2014) Genome-wide transcriptome profiling of homologous recombination DNA repair. *Nat Commun* 5: 3361

419. Peng M, Lee S, Nair HG, MacGilvary N, Cong K, Kraemer M, Li R, McConnell J, Baer C, Deng B, *et al* (2025) RAD51 is chromatin enriched and targetable in BRCA1-deficient cells. *Mol Cell* 85: 3373-3387.e6

420. Pérez-González A, Bévant K & Blanpain C (2023) Cancer cell plasticity during tumor progression, metastasis and response to therapy. *Nat Cancer* 4: 1063–1082

421. Petropoulos M, Karamichali A, Rossetti GG, Freudenmann A, Iacovino LG, Dionellis VS, Sotiriou SK & Halazonetis TD (2024) Transcription–replication conflicts underlie sensitivity to PARP inhibitors. *Nature* 628: 433–441

422. Petrucelli N, Daly MB & Pal T (1993) BRCA1- and BRCA2-Associated Hereditary Breast and Ovarian Cancer. In *GeneReviews®*, Adam MP Bick S Mirzaa GM Pagon RA Wallace SE & Amemiya A (eds) Seattle (WA): University of Washington, Seattle

423. Pettitt SJ, Frankum JR, Punta M, Lise S, Alexander J, Chen Y, Yap TA, Haider S, Tutt ANJ & Lord CJ (2020) Clinical BRCA1/2 Reversion Analysis Identifies Hotspot Mutations and Predicted Neoantigens Associated with Therapy Resistance. *Cancer Discov* 10: 1475–1488

424. Pettitt SJ, Krastev DB, Brandsma I, Dréan A, Song F, Aleksandrov R, Harrell MI, Menon M, Brough R, Campbell J, *et al* (2018) Genome-wide and high-density CRISPR-Cas9 screens identify point mutations in PARP1 causing PARP inhibitor resistance. *Nat Commun* 9: 1849

425. Pfeifer GP (2020) Mechanisms of UV-induced mutations and skin cancer. *Genome Instab Dis* 1: 99–113

426. Pinner S, Jordan P, Sharrock K, Bazley L, Collinson L, Marais R, Bonvin E, Goding C & Sahai E (2009) Intravital imaging reveals transient changes in pigment production and Brn2 expression during metastatic melanoma dissemination. *Cancer Res* 69: 7969–7977

427. Pitter KL, Casey DL, Lu YC, Hannum M, Zhang Z, Song X, Pecorari I, McMillan B, Ma J, Samstein RM, *et al* (2021) Pathogenic ATM Mutations in Cancer and a Genetic Basis for Radiotherapeutic Efficacy. *J Natl Cancer Inst* 113: 266–273

428. Plo I, Liao ZY, Barceló JM, Kohlhagen G, Caldecott KW, Weinfeld M & Pommier Y (2003) Association of XRCC1 and tyrosyl DNA phosphodiesterase (Tdp1) for the repair of topoisomerase I-mediated DNA lesions. *DNA Repair (Amst)* 2: 1087–1100

429. Polo SE & Jackson SP (2011) Dynamics of DNA damage response proteins at DNA breaks: a focus on protein modifications. *Genes Dev* 25: 409–433

430. Pott S & Lieb JD (2015) What are super-enhancers? *Nat Genet* 47: 8–12

431. Povo-Retana A, Landauro-Vera R, Alvarez-Lucena C, Cascante M & Boscá L (2024) Trabectedin and Lurbinectedin Modulate the Interplay between Cells in the Tumour Microenvironment-Progresses in Their Use in Combined Cancer Therapy. *Molecules* 29: 331

432. Pozniak J, Pedri D, Landeloos E, Herck YV, Antoranz A, Vanwynsberghe L, Nowosad A, Roda N, Makhzami S, Bervoets G, *et al* (2024) A TCF4-dependent gene regulatory network confers resistance to immunotherapy in melanoma. *Cell* 187: 166-183.e25

433. Prabhu KS, Kuttikrishnan S, Ahmad N, Habeeba U, Mariyam Z, Suleman M, Bhat AA & Uddin S (2024) H2AX: A key player in DNA damage response and a promising target for cancer therapy. *Biomed Pharmacother* 175: 116663

434. Preiss J, Schlaeger R & Hilz H (1971) Specific inhibition of poly adpribose polymerase by thymidine and nicotinamide in HeLa cells. *FEBS Lett* 19: 244–246

435. Priya B, Ravi S & Kirubakaran S (2023) Targeting ATM and ATR for cancer therapeutics: Inhibitors in clinic. *Drug Discov Today* 28: 103662

436. Puissant A, Frumm SM, Alexe G, Bassil CF, Qi J, Chanthery YH, Nekritz EA, Zeid R, Gustafson WC, Greninger P, *et al* (2013) Targeting MYCN in neuroblastoma by BET bromodomain inhibition. *Cancer Discov* 3: 308–323

437. Quereda V, Bayle S, Vena F, Frydman SM, Monastyrskyi A, Roush WR & Duckett DR (2019) Therapeutic Targeting of CDK12/CDK13 in Triple-Negative Breast Cancer. *Cancer Cell* 36: 545-558.e7

438. Rambow F, Marine J-C & Goding CR (2019) Melanoma plasticity and phenotypic diversity: therapeutic barriers and opportunities. *Genes Dev* 33: 1295–1318

439. Rambow F, Rogiers A, Marin-Bejar O, Aibar S, Femel J, Dewaele M, Karras P, Brown D, Chang YH, Debiec-Rychter M, *et al* (2018) Toward Minimal Residual Disease-Directed Therapy in Melanoma. *Cell* 174: 843-855.e19

440. Rasool RU, Natesan R, Deng Q, Aras S, Lal P, Sander Effron S, Mitchell-Velasquez E, Posimo JM, Carskadon S, Baca SC, *et al* (2019) CDK7 Inhibition Suppresses Castration-Resistant Prostate Cancer through MED1 Inactivation. *Cancer Discov* 9: 1538–1555

441. Ray Chaudhuri A & Nussenzweig A (2017a) The multifaceted roles of PARP1 in DNA repair and chromatin remodelling. *Nat Rev Mol Cell Biol* 18: 610–621

442. Ray Chaudhuri A & Nussenzweig A (2017b) The multifaceted roles of PARP1 in DNA repair and chromatin remodelling. *Nat Rev Mol Cell Biol* 18: 610–621

443. Raymond JH, Aktary Z, Pouteaux M, Petit V, Luciani F, Wehbe M, Gizzi P, Bourban C, Decaudin D, Nemati F, *et al* (2025) Publisher Correction: Targeting GRPR for sex hormone-dependent cancer after loss of E-cadherin. *Nature* 643: E28

444. Reaper PM, Griffiths MR, Long JM, Charrier J-D, Maccormick S, Charlton PA, Golec JMC & Pollard JR (2011) Selective killing of ATM- or p53-deficient cancer cells through inhibition of ATR. *Nat Chem Biol* 7: 428–430

445. Regan JD, Trosko JE & Carrier WL (1968) Evidence for excision of ultraviolet-induced pyrimidine dimers from the DNA of human cells in vitro. *Biophys J* 8: 319–325

446. Ribeiro J, Hansen K, van Beek L, Stubbs C, Frigola J, Talbot S, Bentouati S, Hall J, Wijnhoven PWG, Armenia J, *et al* (2025) Genetic evidence for PARP1 trapping as a driver of PARP inhibitor efficacy in BRCA mutant cancer cells. *Nucleic Acids Res* 53: gkaf1398

447. Richter WF, Nayak S, Iwasa J & Taatjes DJ (2022) The Mediator complex as a master regulator of transcription by RNA polymerase II. *Nat Rev Mol Cell Biol* 23: 732–749

448. Riesenberg S, Groetchen A, Siddaway R, Bald T, Reinhardt J, Smorra D, Kohlmeyer J, Renn M, Phung B, Aymans P, *et al* (2015) MITF and c-Jun antagonism interconnects melanoma dedifferentiation with pro-inflammatory cytokine responsiveness and myeloid cell recruitment. *Nat Commun* 6: 8755

449. Rinehart KL (2000) Antitumor compounds from tunicates. *Medicinal Research Reviews* 20: 1–27

450. Rinehart KL, Holt TG, Fregeau NL, Stroh JG, Keifer PA, Sun F, Li LH & Martin DG (1990) Ecteinascidins 729, 743, 745, 759A, 759B, and 770: Potent Antitumor Agents from the Caribbean Tunicate Ecteinascidia turbinata. *Journal of Organic Chemistry* 55: 4512–4515

451. Rittenhouse NL & Dowen JM (2024) Cohesin regulation and roles in chromosome structure and function. *Curr Opin Genet Dev* 85: 102159

452. Robert C, Grob JJ, Stroyakovskiy D, Karaszewska B, Hauschild A, Levchenko E, Chiarion Sileni V, Schachter J, Garbe C, Bondarenko I, *et al* (2019) Five-Year Outcomes with Dabrafenib plus Trametinib in Metastatic Melanoma. *N Engl J Med* 381: 626–636

453. Robert C, Long GV, Brady B, Dutriaux C, Maio M, Mortier L, Hassel JC, Rutkowski P, McNeil C, Kalinka-Warzocha E, *et al* (2015a) Nivolumab in previously untreated melanoma without BRAF mutation. *N Engl J Med* 372: 320–330

454. Robert C, Schachter J, Long GV, Arance A, Grob JJ, Mortier L, Daud A, Carlino MS, McNeil C, Lotem M, *et al* (2015b) Pembrolizumab versus Ipilimumab in Advanced Melanoma. *N Engl J Med* 372: 2521–2532

455. Robertson BM, Fane ME, Weeraratna AT & Rebecca VW (2024) Determinants of resistance and response to melanoma therapy. *Nat Cancer* 5: 964–982

456. Robson M, Im S-A, Senkus E, Xu B, Domchek SM, Masuda N, Delaloge S, Li W, Tung N, Armstrong A, *et al* (2017) Olaparib for Metastatic Breast Cancer in Patients with a Germline BRCA Mutation. *New England Journal of Medicine* 377: 523–533

457. Rodriguez J, Ren G, Day CR, Zhao K, Chow CC & Larson DR (2019) Intrinsic dynamics of a human gene reveal the basis of expression heterogeneity. *Cell* 176: 213-226.e18

458. Rodriguez-Baena FJ, Marquez-Galera A, Ballesteros-Martinez P, Castillo A, Diaz E, Moreno-Bueno G, Lopez-Atalaya JP & Sanchez-Laorden B (2025) Microglial reprogramming enhances antitumor immunity and immunotherapy response in melanoma brain metastases. *Cancer Cell* 43: 413-427.e9

459. Rodríguez-Molina JB, West S & Passmore LA (2023) Knowing when to stop: Transcription termination on protein-coding genes by eukaryotic RNAPII. *Mol Cell* 83: 404–415

460. Romano M, Frapolli R, Zangarini M, Bello E, Porcu L, Galmarini CM, García-Fernández LF, Cuevas C, Allavena P, Erba E, *et al* (2013) Comparison of in vitro and in vivo biological effects of trabectedin, lurbinectedin (PM01183) and Zalypsis® (PM00104). *Int J Cancer* 133: 2024–2033

461. Rondinelli B, Gogola E, Yücel H, Duarte AA, van de Ven M, van der Sluijs R, Konstantinopoulos PA, Jonkers J, Ceccaldi R, Rottenberg S, *et al* (2017) EZH2 promotes degradation of stalled replication forks by recruiting MUS81 through histone H3 trimethylation. *Nat Cell Biol* 19: 1371–1378

462. Rose M, Burgess JT, O'Byrne K, Richard DJ & Bolderson E (2020) PARP Inhibitors: Clinical Relevance, Mechanisms of Action and Tumor Resistance. *Front Cell Dev Biol* 8: 564601

463. Rossi M, Pellegrini C, Cardelli L, Ciciarelli V, Di Nardo L & Fargnoli MC (2019) Familial Melanoma: Diagnostic and Management Implications. *Dermatol Pract Concept* 9: 10–16

464. Rouault CD, Bansard L, Martínez-Balsalobre E, Bonnet C, Wicinski J, Lin S, Colombeau L, Debieu S, Pinna G, Vandamme M, *et al* (2025a) Inhibition of the STAT3/Fanconi anemia axis is synthetic lethal with PARP inhibition in breast cancer. *Nat Commun* 16: 2159

465. Rouault CD, Charafe-Jauffret E & Ginestier C (2025b) The interplay of DNA damage, epigenetics and tumour heterogeneity in driving cancer cell fitness. *Nat Commun* 16: 8733

466. Ryan DP, Supko JG, Eder JP, Seiden MV, Demetri G, Lynch TJ, Fischman AJ, Davis J, Jimeno J & Clark JW (2001) Phase I and pharmacokinetic study of ecteinascidin 743 administered as a 72-hour continuous intravenous infusion in patients with solid malignancies. *Clin Cancer Res* 7: 231–242

467. Sabari BR, Dall'Agnese A, Boija A, Klein IA, Coffey EL, Shrinivas K, Abraham BJ, Hannett NM, Zamudio AV, Manteiga JC, *et al* (2018) Coactivator condensation at super-enhancers links phase separation and gene control. *Science* 361: eaar3958

468. Sabnis AJ & Bivona TG (2019) Principles of Resistance to Targeted Cancer Therapy: Lessons from Basic and Translational Cancer Biology. *Trends Mol Med* 25: 185–197

469. Sade-Feldman M, Yizhak K, Bjorgaard SL, Ray JP, de Boer CG, Jenkins RW, Lieb DJ, Chen JH, Frederick DT, Barzily-Rokni M, *et al* (2018) Defining T Cell States Associated with Response to Checkpoint Immunotherapy in Melanoma. *Cell* 175: 998-1013.e20

470. Saginala K, Barsouk A, Aluru JS, Rawla P & Barsouk A (2021) Epidemiology of Melanoma. *Med Sci (Basel)* 9: 63

471. Sahin U, Oehm P, Derhovanessian E, Jabulowsky RA, Vormehr M, Gold M, Maurus D, Schwarck-Kokarakis D, Kuhn AN, Omokoko T, *et al* (2020) An RNA vaccine drives immunity in checkpoint-inhibitor-treated melanoma. *Nature* 585: 107–112

472. Sainsbury S, Niesser J & Cramer P (2013) Structure and function of the initially transcribing RNA polymerase II-TFIIB complex. *Nature* 493: 437–440

473. Sakai R, Rinehart KL, Guan Y & Wang AH (1992) Additional antitumor ecteinascidins from a Caribbean tunicate: crystal structures and activities in vivo. *Proc Natl Acad Sci U S A* 89: 11456–11460

474. Sakai W, Swisher EM, Karlan BY, Agarwal MK, Higgins J, Friedman C, Villegas E, Jacquemont C, Farrugia DJ, Couch FJ, *et al* (2008) Secondary mutations as a mechanism of cisplatin resistance in BRCA2-mutated cancers. *Nature* 451: 1116–1120

475. Sampathi S, Acharya P, Zhao Y, Wang J, Stengel KR, Liu Q, Savona MR & Hiebert SW (2019) The CDK7 inhibitor THZ1 alters RNA polymerase dynamics at the 5' and 3' ends of genes. *Nucleic Acids Res* 47: 3921–3936

476. Samstein RM, Lee C-H, Shoushtari AN, Hellmann MD, Shen R, Janjigian YY, Barron DA, Zehir A, Jordan EJ, Omuro A, *et al* (2019) Tumor mutational load predicts survival after immunotherapy across multiple cancer types. *Nat Genet* 51: 202–206

477. Sanborn JZ, Chung J, Purdom E, Wang NJ, Kakavand H, Wilmott JS, Butler T, Thompson JF, Mann GJ, Haydu LE, *et al* (2015) Phylogenetic analyses of melanoma reveal complex patterns of metastatic dissemination. *Proc Natl Acad Sci U S A* 112: 10995–11000

478. Sanchez-Vega F, Mina M, Armenia J, Chatila WK, Luna A, La KC, Dimitriadoy S, Liu DL, Kantheti HS, Saghafinia S, *et al* (2018) Oncogenic Signaling Pathways in The Cancer Genome Atlas. *Cell* 173: 321-337.e10

479. Sandhu SK, Schelman WR, Wilding G, Moreno V, Baird RD, Miranda S, Hylands L, Riisnaes R, Forster M, Omlin A, *et al* (2013) The poly(ADP-ribose) polymerase inhibitor niraparib (MK4827) in BRCA mutation carriers and patients with sporadic cancer: a phase 1 dose-escalation trial. *Lancet Oncol* 14: 882–892

480. Santamaría Nuñez G, Robles CMG, Giraudon C, Martínez-Leal JF, Compe E, Coin F, Aviles P, Galmarini CM & Egly J-M (2016) Lurbinectedin Specifically Triggers the Degradation of Phosphorylated RNA Polymerase II and the Formation of DNA Breaks in Cancer Cells. *Molecular Cancer Therapeutics* 15: 2399–2412

481. Sartori AA, Lukas C, Coates J, Mistrik M, Fu S, Bartek J, Baer R, Lukas J & Jackson SP (2007) Human CtIP promotes DNA end resection. *Nature* 450: 509–514

482. Satoh MS & Lindahl T (1992) Role of poly(ADP-ribose) formation in DNA repair. *Nature* 356: 356–358

483. Sava GP, Fan H, Fisher RA, Lusvarghi S, Pancholi S, Ambudkar SV, Martin L-A, Charles Coombes R, Buluwela L & Ali S (2020) ABC-transporter upregulation mediates resistance to the CDK7 inhibitors THZ1 and ICEC0942. *Oncogene* 39: 651–663

484. Schiantarelli J, Benamar M, Park J, Sax HE, Oliveira G, Bosma-Moody A, Campbell KM, Liu D, Johnson DB, Rodig S, *et al* (2025) Genomic mediators of acquired resistance to immunotherapy in metastatic melanoma. *Cancer Cell* 43: 308-316.e6

485. Schreiber V, Dantzer F, Ame J-C & de Murcia G (2006) Poly(ADP-ribose): novel functions for an old molecule. *Nat Rev Mol Cell Biol* 7: 517–528

486. Schultz CW, Zhang Y, Elmeskini R, Zimmermann A, Fu H, Murai Y, Wangsa D, Kumar S, Takahashi N, Atkinson D, *et al* (2023) ATR inhibition augments the efficacy of lurbinectedin in small-cell lung cancer. *EMBO Mol Med* 15: e17313

487. Schuster RC (1964) DARK REPAIR OF ULTRAVIOLET INJURY IN E. COLI DURING DEPRIVATION OF THYMINE. *Nature* 202: 614–615

488. Schwartz MR, Luo L & Berwick M (2019) Sex Differences in Melanoma. *Curr Epidemiol Rep* 6: 112–118

489. Scully R, Panday A, Elango R & Willis NA (2019) DNA double-strand break repair-pathway choice in somatic mammalian cells. *Nat Rev Mol Cell Biol* 20: 698–714

490. Seaman FC & Hurley LH (1998) Molecular Basis for the DNA Sequence Selectivity of Ecteinascidin 736 and 743: Evidence for the Dominant Role of Direct Readout via Hydrogen Bonding. *J Am Chem Soc* 120: 13028–13041

491. Seip K, Fleten KG, Barkovskaya A, Nygaard V, Haugen MH, Engesæter BØ, Mælandsmo GM & Prasmickaite L (2016) Fibroblast-induced switching to the mesenchymal-like phenotype and PI3K/mTOR signaling protects melanoma cells from BRAF inhibitors. *Oncotarget* 7: 19997–20015

492. Sengupta S & George RE (2017) Super-Enhancer-Driven Transcriptional Dependencies in Cancer. *Trends Cancer* 3: 269–281

493. Sensi M, Catani M, Castellano G, Nicolini G, Alciato F, Tragni G, De Santis G, Bersani I, Avanzi G, Tomassetti A, *et al* (2011) Human cutaneous melanomas lacking MITF and melanocyte differentiation antigens express a functional Axl receptor kinase. *J Invest Dermatol* 131: 2448–2457

494. Setlow RB & Carrier WL (1964) The disappearance of thymine dimers from dna: an error-correcting mechanism. *Proceedings of the National Academy of Sciences* 51: 226–231

495. Setlow RB, Regan JD, German J & Carrier WL (1969) Evidence that xeroderma pigmentosum cells do not perform the first step in the repair of ultraviolet damage to their DNA. *Proc Natl Acad Sci U S A* 64: 1035–1041

496. Sfeir A, Tijsterman M & McVey M (2024) Microhomology-Mediated End-Joining Chronicles: Tracing the Evolutionary Footprints of Genome Protection. *Annu Rev Cell Dev Biol* 40: 195–218

497. Shaffer SM, Dunagin MC, Torborg SR, Torre EA, Emert B, Krepler C, Beqiri M, Sproesser K, Brafford PA, Xiao M, *et al* (2017) Rare cell variability and drug-induced reprogramming as a mode of cancer drug resistance. *Nature* 546: 431–435

498. Shah S, Takei Y, Zhou W, Lubeck E, Yun J, Eng C-HL, Koulena N, Cronin C, Karp C, Liaw EJ, *et al* (2018) Dynamics and Spatial Genomics of the Nascent Transcriptome by Intron seqFISH. *Cell* 174: 363-376.e16

499. Shain AH & Bastian BC (2016) From melanocytes to melanomas. *Nat Rev Cancer* 16: 345–358

500. Shain AH, Yeh I, Kovalyshyn I, Sriharan A, Talevich E, Gagnon A, Dummer R, North J, Pincus L, Ruben B, *et al* (2015) The Genetic Evolution of Melanoma from Precursor Lesions. *N Engl J Med* 373: 1926–1936

501. Shan W, Yuan J, Hu Z, Jiang J, Wang Y, Loo N, Fan L, Tang Z, Zhang T, Xu M, *et al* (2020) Systematic Characterization of Recurrent Genomic Alterations in Cyclin-Dependent Kinases Reveals Potential Therapeutic Strategies for Cancer Treatment. *Cell Reports* 32: 107884

502. Shanbhag NM, Rafalska-Metcalf IU, Balane-Bolivar C, Janicki SM & Greenberg RA (2010) ATM-dependent chromatin changes silence transcription in cis to DNA double-strand breaks. *Cell* 141: 970–981

503. Sharma P, Goswami S, Raychaudhuri D, Siddiqui BA, Singh P, Nagarajan A, Liu J, Subudhi SK, Poon C, Gant KL, *et al* (2023) Immune checkpoint therapy—current perspectives and future directions. *Cell* 186: 1652–1669

504. Sharma P, Hu-Lieskovan S, Wargo JA & Ribas A (2017) Primary, Adaptive, and Acquired Resistance to Cancer Immunotherapy. *Cell* 168: 707–723

505. Sharova LV, Sharov AA, Nedorezov T, Piao Y, Shaik N & Ko MSH (2009) Database for mRNA half-life of 19 977 genes obtained by DNA microarray analysis of pluripotent and differentiating mouse embryonic stem cells. *DNA Res* 16: 45–58

506. Shen S, Vagner S & Robert C (2020) Persistent Cancer Cells: The Deadly Survivors. *Cell* 183: 860–874

507. Shen WH, Balajee AS, Wang J, Wu H, Eng C, Pandolfi PP & Yin Y (2007) Essential role for nuclear PTEN in maintaining chromosomal integrity. *Cell* 128: 157–170

508. Shi H, Hong A, Kong X, Koya RC, Song C, Moriceau G, Hugo W, Yu CC, Ng C, Chodon T, *et al* (2014a) A novel AKT1 mutant amplifies an adaptive melanoma response to BRAF inhibition. *Cancer Discov* 4: 69–79

509. Shi H, Hugo W, Kong X, Hong A, Koya RC, Moriceau G, Chodon T, Guo R, Johnson DB, Dahlman KB, *et al* (2014b) Acquired resistance and clonal evolution in melanoma during BRAF inhibitor therapy. *Cancer Discov* 4: 80–93

510. Shi Y, Liao Y, Liu Q, Ni Z, Zhang Z, Shi M, Li P, Li H & Rao Y (2023) BRD4-targeting PROTAC as a unique tool to study biomolecular condensates. *Cell Discov* 9: 47

511. Shiau AK, Barstad D, Loria PM, Cheng L, Kushner PJ, Agard DA & Greene GL (1998) The structural basis of estrogen receptor/coactivator recognition and the antagonism of this interaction by tamoxifen. *Cell* 95: 927–937

512. Shibata A, Conrad S, Birraux J, Geuting V, Barton O, Ismail A, Kakarougkas A, Meek K, Taucher-Scholz G, Löbrich M, *et al* (2011) Factors determining DNA double-strand break repair pathway choice in G2 phase. *EMBO J* 30: 1079–1092

513. Shibata A, Moiani D, Arvai AS, Perry J, Harding SM, Genois M-M, Maity R, van Rossum-Fikkert S, Kertokalio A, Romoli F, *et al* (2014) DNA double-strand break repair pathway choice is directed by distinct MRE11 nuclease activities. *Mol Cell* 53: 7–18

514. Shors AR, Kim S, White E, Argenyi Z, Barnhill RL, Duray P, Erickson L, Guitart J, Horenstein MG, Lowe L, *et al* (2006) Dysplastic naevi with moderate to severe histological dysplasia: a risk factor for melanoma. *Br J Dermatol* 155: 988–993

515. Shrinivas K, Sabari BR, Coffey EL, Klein IA, Boija A, Zamudio AV, Schuijers J, Hannett NM, Sharp PA, Young RA, *et al* (2019) Enhancer Features that Drive Formation of Transcriptional Condensates. *Mol Cell* 75: 549-561.e7

516. Shu S, Lin CY, He HH, Witwicki RM, Tabassum DP, Roberts JM, Janiszewska M, Huh SJ, Liang Y, Ryan J, *et al* (2016) Response and resistance to BET bromodomain inhibitors in triple-negative breast cancer. *Nature* 529: 413–417

517. Shu S, Wu H-J, Ge JY, Zeid R, Harris IS, Jovanović B, Murphy K, Wang B, Qiu X, Endress JE, *et al* (2020) Synthetic Lethal and Resistance Interactions with BET Bromodomain Inhibitors in Triple-Negative Breast Cancer. *Mol Cell* 78: 1096-1113.e8

518. Simeonov KP, Byrns CN, Clark ML, Norgard RJ, Martin B, Stanger BZ, Shendure J, McKenna A & Lengner CJ (2021) Single-cell lineage tracing of metastatic cancer reveals selection of hybrid EMT states. *Cancer Cell* 39: 1150-1162.e9

519. Singh S, Jaigirdar AA, Mulkey F, Cheng J, Hamed SS, Li Y, Liu J, Zhao H, Goheer A, Helms WS, *et al* (2021) FDA Approval Summary: Lurbinectedin for the Treatment of Metastatic Small Cell Lung Cancer. *Clin Cancer Res* 27: 2378–2382

520. Skoulidis F, Li BT, Dy GK, Price TJ, Falchook GS, Wolf J, Italiano A, Schuler M, Borghaei H, Barlesi F, *et al* (2021) Sotorasib for Lung Cancers with KRAS p.G12C Mutation. *N Engl J Med* 384: 2371–2381

521. Smith MP, Brunton H, Rowling EJ, Ferguson J, Arozarena I, Miskolczi Z, Lee JL, Girotti MR, Marais R, Levesque MP, *et al* (2016) Inhibiting Drivers of Non-mutational Drug Tolerance Is a Salvage Strategy for Targeted Melanoma Therapy. *Cancer Cell* 29: 270–284

522. Smith MP, Ferguson J, Arozarena I, Hayward R, Marais R, Chapman A, Hurlstone A & Wellbrock C (2013) Effect of SMURF2 targeting on susceptibility to MEK inhibitors in melanoma. *J Natl Cancer Inst* 105: 33–46

523. Smith SL (2017) War! What is it good for? Mustard gas medicine. *CMAJ* 189: E321–E322

524. Soares DG, Escargueil AE, Poindessous V, Sarasin A, de Gramont A, Bonatto D, Henriques JAP & Larsen AK (2007) Replication and homologous recombination repair regulate DNA double-strand break formation by the antitumor alkylator ecteinascidin 743. *Proc Natl Acad Sci U S A* 104: 13062–13067

525. Sobol RW, Prasad R, Evenski A, Baker A, Yang XP, Horton JK & Wilson SH (2000) The lyase activity of the DNA repair protein beta-polymerase protects from DNA-damage-induced cytotoxicity. *Nature* 405: 807–810

526. Solomon DA, Kim T, Diaz-Martinez LA, Fair J, Elkahloun AG, Harris BT, Toretsky JA, Rosenberg SA, Shukla N, Ladanyi M, *et al* (2011) Mutational inactivation of STAG2 causes aneuploidy in human cancer. *Science* 333: 1039–1043

527. Son K, Takhaveev V, Mor V, Yu H, Dillier E, Zilio N, Püllen NJL, Ivanov D, Ulrich HD, Sturla SJ, *et al* (2024) Trabectedin derails transcription-coupled nucleotide excision repair to induce DNA breaks in highly transcribed genes. *Nat Commun* 15: 1388

528. de Sousa e Melo F, Kurtova AV, Harnoss JM, Kljavin N, Hoeck JD, Hung J, Anderson JE, Storm EE, Modrusan Z, Koeppen H, *et al* (2017) A distinct role for Lgr5+ stem cells in primary and metastatic colon cancer. *Nature* 543: 676–680

529. Soutourina J (2018) Transcription regulation by the Mediator complex. *Nat Rev Mol Cell Biol* 19: 262–274

530. Spranger S, Bao R & Gajewski TF (2015) Melanoma-intrinsic β-catenin signalling prevents anti-tumour immunity. *Nature* 523: 231–235

531. Stoppa-Lyonnet D (2016) The biological effects and clinical implications of BRCA mutations: where do we go from here? *Eur J Hum Genet* 24: S3–S9

532. Straume O, Sviland L & Akslen LA (2000) Loss of nuclear p16 protein expression correlates with increased tumor cell proliferation (Ki-67) and poor prognosis in patients with vertical growth phase melanoma. *Clin Cancer Res* 6: 1845–1853

533. Straussman R, Morikawa T, Shee K, Barzily-Rokni M, Qian ZR, Du J, Davis A, Mongare MM, Gould J, Frederick DT, *et al* (2012) Tumour micro-environment elicits innate resistance to RAF inhibitors through HGF secretion. *Nature* 487: 500–504

534. Strebhardt K & Ullrich A (2008) Paul Ehrlich's magic bullet concept: 100 years of progress. *Nat Rev Cancer* 8: 473–480

535. Strickler JH, Hanks BA & Khasraw M (2021) Tumor Mutational Burden as a Predictor of Immunotherapy Response: Is More Always Better? *Clin Cancer Res* 27: 1236–1241

536. Ström CE, Johansson F, Uhlén M, Szigyarto CA-K, Erixon K & Helleday T (2011) Poly (ADP-ribose) polymerase (PARP) is not involved in base excision repair but PARP inhibition traps a single-strand intermediate. *Nucleic Acids Res* 39: 3166–3175

537. Stucki M, Clapperton JA, Mohammad D, Yaffe MB, Smerdon SJ & Jackson SP (2005) MDC1 directly binds phosphorylated histone H2AX to regulate cellular responses to DNA double-strand breaks. *Cell* 123: 1213–1226

538. Su J, Morgani SM, David CJ, Wang Q, Er EE, Huang Y-H, Basnet H, Zou Y, Shu W, Soni RK, *et al* (2020) TGF-β orchestrates fibrogenic and developmental EMTs via the RAS effector RREB1. *Nature* 577: 566–571

539. Su Y, Wei W, Robert L, Xue M, Tsoi J, Garcia-Diaz A, Homet Moreno B, Kim J, Ng RH, Lee JW, *et al* (2017) Single-cell analysis resolves the cell state transition and signaling dynamics associated with melanoma drug-induced resistance. *Proc Natl Acad Sci U S A* 114: 13679–13684

540. Sun C, Yin J, Fang Y, Chen J, Jeong KJ, Chen X, Vellano CP, Ju Z, Zhao W, Zhang D, *et al* (2018) BRD4 Inhibition Is Synthetic Lethal with PARP Inhibitors through the Induction of Homologous Recombination Deficiency. *Cancer Cell* 33: 401-416.e8

541. Sundararajan S, Thida AM, Yadlapati S, Mukkamalla SKR & Koya S (2026) Metastatic Melanoma. In *StatPearls* Treasure Island (FL): StatPearls Publishing

542. Sung P, Krejci L, Van Komen S & Sehorn MG (2003) Rad51 recombinase and recombination mediators. *J Biol Chem* 278: 42729–42732

543. Swanton C, Bernard E, Abbosh C, André F, Auwerx J, Balmain A, Bar-Sagi D, Bernards R, Bullman S, DeGregori J, *et al* (2024) Embracing cancer complexity: Hallmarks of systemic disease. *Cell* 187: 1589–1616

544. Sweasy JB, Lang T & DiMaio D (2006) Is base excision repair a tumor suppressor mechanism? *Cell Cycle* 5: 250–259

545. Swisher EM, Harrell MI, Lin K, Coleman RL, Konecny GE, Tinker AV, O'Malley DM, McNeish I & Kaufmann SH (2017a) BRCA1 and RAD51C promoter hypermethylation confer sensitivity to the PARP inhibitor rucaparib in patients with relapsed, platinum-sensitive ovarian carcinoma in ARIEL2 Part 1. *Gynecologic Oncology* 145: 5

546. Swisher EM, Lin KK, Oza AM, Scott CL, Giordano H, Sun J, Konecny GE, Coleman RL, Tinker AV, O'Malley DM, *et al* (2017b) Rucaparib in relapsed, platinum-sensitive high-grade ovarian carcinoma (ARIEL2 Part 1): an international, multicentre, open-label, phase 2 trial. *Lancet Oncol* 18: 75–87

547. Sy SMH, Huen MSY & Chen J (2009) PALB2 is an integral component of the BRCA complex required for homologous recombination repair. *Proc Natl Acad Sci U S A* 106: 7155–7160

548. Taghbalout A, Tung C-H, Clow PA, Tjong H, Wang P, Wong CH, Mao DD, Maurya R, Huang M-F, Ngan CY, *et al* (2025) Extrachromosomal DNA associates with nuclear condensates and reorganizes chromatin structures to enhance oncogenic transcription. *Cancer Cell* 43: 2191-2205.e6

549. Taglialatela A, Alvarez S, Leuzzi G, Sannino V, Ranjha L, Huang J-W, Madubata C, Anand R, Levy B, Rabadan R, *et al* (2017) Restoration of Replication Fork Stability in BRCA1- and BRCA2-Deficient Cells by Inactivation of SNF2-Family Fork Remodelers. *Mol Cell* 68: 414-430.e8

550. Takata M, Sasaki MS, Sonoda E, Morrison C, Hashimoto M, Utsumi H, Yamaguchi-Iwai Y, Shinohara A & Takeda S (1998) Homologous recombination and non-homologous end-joining pathways of DNA double-strand break repair have overlapping roles in the maintenance of chromosomal integrity in vertebrate cells. *EMBO J* 17: 5497–5508

551. Takebayashi Y, Pourquier P, Zimonjic DB, Nakayama K, Emmert S, Ueda T, Urasaki Y, Kanzaki A, Akiyama S, Popescu N, *et al* (2001) Antiproliferative activity of ecteinascidin 743 is dependent upon transcription-coupled nucleotide-excision repair. *Nat Med* 7: 961–966

552. Taub R, Kirsch I, Morton C, Lenoir G, Swan D, Tronick S, Aaronson S & Leder P (1982) Translocation of the c-myc gene into the immunoglobulin heavy chain locus in human Burkitt lymphoma and murine plasmacytoma cells. *Proc Natl Acad Sci U S A* 79: 7837–7841

553. Tavecchio M, Natoli C, Ubezio P, Erba E & D'Incalci M (2007) Dynamics of cell cycle phase perturbations by trabectedin (ET-743) in nucleotide excision repair (NER)-deficient and NER-proficient cells, unravelled by a novel mathematical simulation approach. *Cell Prolif* 40: 885–904

554. Telli ML, Timms KM, Reid J, Hennessy B, Mills GB, Jensen KC, Szallasi Z, Barry WT, Winer EP, Tung NM, *et al* (2016) Homologous Recombination Deficiency (HRD) Score Predicts Response to Platinum-Containing Neoadjuvant Chemotherapy in Patients with Triple-Negative Breast Cancer. *Clin Cancer Res* 22: 3764–3773

555. Teloni F, Takacs Z, Mitter M, Langer CCH, Prlesi I, Steinacker TL, Reuter VP, Mylarshchikov D & Gerlich DW (2025) Cohesin guides homology search during DNA repair using loops and sister chromatid linkages. *Science* 390: eadw0566

556. Thomas HF, Kotova E, Jayaram S, Pilz A, Romeike M, Lackner A, Penz T, Bock C, Leeb M, Halbritter F, *et al* (2021) Temporal dissection of an enhancer cluster reveals distinct temporal and functional contributions of individual elements. *Mol Cell* 81: 969-982.e13

557. Thomas NE, Berwick M & Cordeiro-Stone M (2006) Could BRAF mutations in melanocytic lesions arise from DNA damage induced by ultraviolet radiation? *J Invest Dermatol* 126: 1693–1696

558. Tirosh I, Izar B, Prakadan SM, Wadsworth MH, Treacy D, Trombetta JJ, Rotem A, Rodman C, Lian C, Murphy G, *et al* (2016) Dissecting the multicellular ecosystem of metastatic melanoma by single-cell RNA-seq. *Science* 352: 189–196

559. Toh M & Ngeow J (2021) Homologous Recombination Deficiency: Cancer Predispositions and Treatment Implications. *Oncologist* 26: e1526–e1537

560. Tovar C, Graves B, Packman K, Filipovic Z, Higgins B, Xia M, Tardell C, Garrido R, Lee E, Kolinsky K, *et al* (2013) MDM2 small-molecule antagonist RG7112 activates p53 signaling and regresses human tumors in preclinical cancer models. *Cancer Res* 73: 2587–2597

561. Trabucco SE, Gerstein RM, Evens AM, Bradner JE, Shultz LD, Greiner DL & Zhang H (2015) Inhibition of bromodomain proteins for the treatment of human diffuse large B-cell lymphoma. *Clin Cancer Res* 21: 113–122

562. Trigo J, Subbiah V, Besse B, Moreno V, López R, Sala MA, Peters S, Ponce S, Fernández C, Alfaro V, *et al* (2020) Lurbinectedin as second-line treatment for patients with small-cell lung cancer: a single-arm, open-label, phase 2 basket trial. *The Lancet Oncology* 21: 645–654

563. Tsoi J, Robert L, Paraiso K, Galvan C, Sheu KM, Lay J, Wong DJL, Atefi M, Shirazi R, Wang X, *et al* (2018) Multi-stage Differentiation Defines Melanoma Subtypes with Differential Vulnerability to Drug-Induced Iron-Dependent Oxidative Stress. *Cancer Cell* 33: 890-904.e5

564. Tubbs A & Nussenzweig A (2017) Endogenous DNA Damage as a Source of Genomic Instability in Cancer. *Cell* 168: 644–656

565. Tucker MA, Fraser MC, Goldstein AM, Struewing JP, King MA, Crawford JT, Chiazze EA, Zametkin DP, Fontaine LS & Clark WH (2002) A natural history of melanomas and dysplastic nevi: an atlas of lesions in melanoma-prone families. *Cancer* 94: 3192–3209

566. Tufail M, Hu J-J, Liang J, He C-Y, Wan W-D, Huang Y-Q, Jiang C-H, Wu H & Li N (2024) Hallmarks of cancer resistance. *iScience* 27: 109979

567. Tung NM, Robson ME, Ventz S, Santa-Maria CA, Nanda R, Marcom PK, Shah PD, Ballinger TJ, Yang ES, Vinayak S, *et al* (2020) TBCRC 048: Phase II Study of Olaparib for Metastatic Breast Cancer and Mutations in Homologous Recombination-Related Genes. *J Clin Oncol* 38: 4274–4282

568. Turajlic S, Furney SJ, Lambros MB, Mitsopoulos C, Kozarewa I, Geyer FC, Mackay A, Hakas J, Zvelebil M, Lord CJ, *et al* (2012) Whole genome sequencing of matched primary and metastatic acral melanomas. *Genome Res* 22: 196–207

569. Turner N, Tutt A & Ashworth A (2004) Hallmarks of 'BRCAness' in sporadic cancers. *Nat Rev Cancer* 4: 814–819

570. Tutt A, Robson M, Garber JE, Domchek SM, Audeh MW, Weitzel JN, Friedlander M, Arun B, Loman N, Schmutzler RK, *et al* (2010) Oral poly(ADP-ribose) polymerase inhibitor olaparib in patients with BRCA1 or BRCA2 mutations and advanced breast cancer: a proof-of-concept trial. *Lancet* 376: 235–244

571. Vaidyanathan A, Sawers L, Gannon A-L, Chakravarty P, Scott AL, Bray SE, Ferguson MJ & Smith G (2016) ABCB1 (MDR1) induction defines a common resistance mechanism in paclitaxel- and olaparib-resistant ovarian cancer cells. *Br J Cancer* 115: 431–441

572. Van Allen EM, Wagle N, Sucker A, Treacy DJ, Johannessen CM, Goetz EM, Place CS, Taylor-Weiner A, Whittaker S, Kryukov GV, *et al* (2014) The genetic landscape of clinical resistance to RAF inhibition in metastatic melanoma. *Cancer Discov* 4: 94–109

573. Verdegaal EME, de Miranda NFCC, Visser M, Harryvan T, van Buuren MM, Andersen RS, Hadrup SR, van der Minne CE, Schotte R, Spits H, *et al* (2016) Neoantigen landscape dynamics during human melanoma-T cell interactions. *Nature* 536: 91–95

574. Verfaillie A, Imrichova H, Atak ZK, Dewaele M, Rambow F, Hulselmans G, Christiaens V, Svetlichnyy D, Luciani F, Van den Mooter L, *et al* (2015) Decoding the regulatory landscape of melanoma reveals TEADS as regulators of the invasive cell state. *Nat Commun* 6: 6683

575. Verma P, Zhou Y, Cao Z, Deraska PV, Deb M, Arai E, Li W, Shao Y, Puentes L, Li Y, *et al* (2021) ALC1 links chromatin accessibility to PARP inhibitor response in homologous recombination-deficient cells. *Nat Cell Biol* 23: 160–171

576. Vido MJ, Le K, Hartsough EJ & Aplin AE (2018) BRAF Splice Variant Resistance to RAF Inhibitor Requires Enhanced MEK Association. *Cell Rep* 25: 1501-1510.e3

577. Vilenchik MM & Knudson AG (2003) Endogenous DNA double-strand breaks: Production, fidelity of repair, and induction of cancer. *Proceedings of the National Academy of Sciences* 100: 12871–12876

578. Villanueva J, Vultur A, Lee JT, Somasundaram R, Fukunaga-Kalabis M, Cipolla AK, Wubbenhorst B, Xu X, Gimotty PA, Kee D, *et al* (2010) Acquired resistance to BRAF inhibitors mediated by a RAF kinase switch in melanoma can be overcome by cotargeting MEK and IGF-1R/PI3K. *Cancer Cell* 18: 683–695

579. Viny AD, Ott CJ, Spitzer B, Rivas M, Meydan C, Papalexi E, Yelin D, Shank K, Reyes J, Chiu A, *et al* (2015) Dose-dependent role of the cohesin complex in normal and malignant hematopoiesis. *J Exp Med* 212: 1819–1832

580. Viros A, Sanchez-Laorden B, Pedersen M, Furney SJ, Rae J, Hogan K, Ejiama S, Girotti MR, Cook M, Dhomen N, *et al* (2014) Ultraviolet radiation accelerates BRAF-driven melanomagenesis by targeting TP53. *Nature* 511: 478–482

581. Vodenicharov MD, Sallmann FR, Satoh MS & Poirier GG (2000) Base excision repair is efficient in cells lacking poly(ADP-ribose) polymerase 1. *Nucleic Acids Res* 28: 3887–3896

582. Wagner R & Meselson M (1976) Repair tracts in mismatched DNA heteroduplexes. *Proc Natl Acad Sci U S A* 73: 4135–4139

583. Wallace SS, Murphy DL & Sweasy JB (2012) Base Excision Repair and Cancer. *Cancer Lett* 327: 73–89

584. Wang C, Jette N, Moussienko D, Bebb DG & Lees-Miller SP (2017) ATM-Deficient Colorectal Cancer Cells Are Sensitive to the PARP Inhibitor Olaparib. *Transl Oncol* 10: 190–196

585. Wang D, Li C, Zhang Y, Wang M, Jiang N, Xiang L, Li T, Roberts TM, Zhao JJ, Cheng H, *et al* (2016) Combined inhibition of PI3K and PARP is effective in the treatment of ovarian cancer cells with wild-type PIK3CA genes. *Gynecol Oncol* 142: 548–556

586. Wang E, Sorolla MA, Krishnan PDG & Sorolla A (2020a) From Seabed to Bedside: A Review on Promising Marine Anticancer Compounds. *Biomolecules* 10: 248

587. Wang L, Xu M, Kao C-Y, Tsai SY & Tsai M-J (2020b) Small molecule JQ1 promotes prostate cancer invasion via BET-independent inactivation of FOXA1. *J Clin Invest* 130: 1782–1792

588. Wang W, Albadari N, Du Y, Fowler JF, Sang HT, Xian W, McKeon F, Li W, Zhou J & Zhang R (2024) MDM2 Inhibitors for Cancer Therapy: The Past, Present, and Future. *Pharmacol Rev* 76: 414–453

589. Wang Y, Zhang T, Kwiatkowski N, Abraham BJ, Lee TI, Xie S, Yuzugullu H, Von T, Li H, Lin Z, *et al* (2015) CDK7-Dependent Transcriptional Addiction in Triple-Negative Breast Cancer. *Cell* 163: 174–186

590. Wang Z-Q, Zhang Z-C, Wu Y-Y, Pi Y-N, Lou S-H, Liu T-B, Lou G & Yang C (2023) Bromodomain and extraterminal (BET) proteins: biological functions, diseases, and targeted therapy. *Signal Transduct Target Ther* 8: 420

591. Weber JS, Carlino MS, Khattak A, Meniawy T, Ansstas G, Taylor MH, Kim KB, McKean M, Long GV, Sullivan RJ, *et al* (2024) Individualised neoantigen therapy mRNA-4157 (V940) plus pembrolizumab versus pembrolizumab monotherapy in resected melanoma (KEYNOTE-942): a randomised, phase 2b study. *The Lancet* 403: 632–644

592. Weinstein IB & Joe AK (2006) Mechanisms of disease: Oncogene addiction--a rationale for molecular targeting in cancer therapy. *Nat Clin Pract Oncol* 3: 448–457

593. Whalen JM, Earley J, Silva C, Mercurio AM & Cantor SB (2025) Targeting BRCA1-deficient PARP inhibitor-resistant cells with nickases reveals nick resection as a cancer vulnerability. *Nat Cancer* 6: 278–291

594. Whitehouse CJ, Taylor RM, Thistlethwaite A, Zhang H, Karimi-Busheri F, Lasko DD, Weinfeld M & Caldecott KW (2001) XRCC1 stimulates human polynucleotide kinase activity at damaged DNA termini and accelerates DNA single-strand break repair. *Cell* 104: 107–117

595. Whiteman DC, Green AC & Olsen CM (2016) The Growing Burden of Invasive Melanoma: Projections of Incidence Rates and Numbers of New Cases in Six Susceptible Populations through 2031. *J Invest Dermatol* 136: 1161–1171

596. Whyte WA, Orlando DA, Hnisz D, Abraham BJ, Lin CY, Kagey MH, Rahl PB, Lee TI & Young RA (2013) Master Transcription Factors and Mediator Establish Super-Enhancers at Key Cell Identity Genes. *Cell* 153: 307–319

597. Winter GE, Buckley DL, Paulk J, Roberts JM, Souza A, Dhe-Paganon S & Bradner JE (2015) Phthalimide conjugation as a strategy for in vivo target protein degradation. *Science* 348: 1376–1381

598. Wolchok JD, Chiarion-Sileni V, Rutkowski P, Cowey CL, Schadendorf D, Wagstaff J, Queirolo P, Dummer R, Butler MO, Hill AG, *et al* (2025) Final, 10-Year Outcomes with Nivolumab plus Ipilimumab in Advanced Melanoma. *N Engl J Med* 392: 11–22

599. Wolf Y, Bartok O, Patkar S, Eli GB, Cohen S, Litchfield K, Levy R, Jiménez-Sánchez A, Trabish S, Lee JS, *et al* (2019) UVB-Induced Tumor Heterogeneity Diminishes Immune Response in Melanoma. *Cell* 179: 219-235.e21

600. Wrenn ED, Harris JC, Apfelbaum AA, Valenti JR, Lipson PA, Walter SI, Garcia NM, Miyaki A, Chen SC, Olson JM, *et al* (2026) Autocrine TGFβ2 enforces a transcriptionally hybrid cell state in Ewing sarcoma. *Science Advances* 12: eady0550

601. Wright WD, Shah SS & Heyer W-D (2018) Homologous recombination and the repair of DNA double-strand breaks. *Journal of Biological Chemistry* 293: 10524–10535

602. Wu B, Zhang B, Li B, Wu H & Jiang M (2024) Cold and hot tumors: from molecular mechanisms to targeted therapy. *Signal Transduct Target Ther* 9: 274

603. Wu S-Y & Chiang C-M (2007) The double bromodomain-containing chromatin adaptor Brd4 and transcriptional regulation. *J Biol Chem* 282: 13141–13145

604. Wu Y, Song Y, Wang R & Wang T (2023) Molecular mechanisms of tumor resistance to radiotherapy. *Mol Cancer* 22: 96

605. Xia B, Sheng Q, Nakanishi K, Ohashi A, Wu J, Christ N, Liu X, Jasin M, Couch FJ & Livingston DM (2006) Control of BRCA2 cellular and clinical functions by a nuclear partner, PALB2. *Mol Cell* 22: 719–729

606. Xiao D, Yao J, Yang X, Xie Y, Zhou X, Li D, Peng M, Wang W, Zou H & Yang X (2026) Repression of EGFR by new biguanide 4C potentiated ovarian cancer to PARP inhibitors through down-regulation of BRCA2 and Rad51. *Cell Death Dis*

607. Xie Z, Sokolov I, Osmala M, Yue X, Bower G, Pett JP, Chen Y, Wang K, Cavga AD, Popov A, *et al* (2025) DNA-guided transcription factor interactions extend human gene regulatory code. *Nature* 641: 1329–1338

608. Xing F, Persaud Y, Pratilas CA, Taylor BS, Janakiraman M, She Q-B, Gallardo H, Liu C, Merghoub T, Hefter B, *et al* (2012) Concurrent loss of the PTEN and RB1 tumor suppressors attenuates RAF dependence in melanomas harboring (V600E)BRAF. *Oncogene* 31: 446–457

609. Xu G, Chapman JR, Brandsma I, Yuan J, Mistrik M, Bouwman P, Bartkova J, Gogola E, Warmerdam D, Barazas M, *et al* (2015) REV7 counteracts DNA double-strand break resection and affects PARP inhibition. *Nature* 521: 541–544

610. Yang J, Antin P, Berx G, Blanpain C, Brabletz T, Bronner M, Campbell K, Cano A, Casanova J, Christofori G, *et al* (2020) Guidelines and definitions for research on epithelial–mesenchymal transition. *Nat Rev Mol Cell Biol* 21: 341–352

611. Yang JH & Hansen AS (2024) Enhancer selectivity in space and time: from enhancer-promoter interactions to promoter activation. *Nat Rev Mol Cell Biol* 25: 574–591

612. Yang L, Zhang Y, Shan W, Hu Z, Yuan J, Pi J, Wang Y, Fan L, Tang Z, Li C, *et al* (2017) Repression of BET activity sensitizes homologous recombination–proficient cancers to PARP inhibition. *Science Translational Medicine* 9: eaal1645

613. Yang Y, Zhang M & Wang Y (2022) The roles of histone modifications in tumorigenesis and associated inhibitors in cancer therapy. *Journal of the National Cancer Center* 2: 277–290

614. Yardman-Frank JM & Fisher DE (2021) Skin pigmentation and its control: From ultraviolet radiation to stem cells. *Exp Dermatol* 30: 560–571

615. Yazinski SA, Comaills V, Buisson R, Genois M-M, Nguyen HD, Ho CK, Todorova Kwan T, Morris R, Lauffer S, Nussenzweig A, *et al* (2017) ATR inhibition disrupts rewired homologous recombination and fork protection pathways in PARP inhibitor-resistant BRCA-deficient cancer cells. *Genes Dev* 31: 318–332

616. Yh I, C G-G, V S, L H, K T-L, A P, P A, P C, M G, J G, *et al* (2012) PI3K inhibition impairs BRCA1/2 expression and sensitizes BRCA-proficient triple-negative breast cancer to PARP inhibition. *Cancer discovery* 2

617. Yilmaz D, Furst A, Meaburn K, Lezaja A, Wen Y, Altmeyer M, Reina-San-Martin B & Soutoglou E (2021) Activation of homologous recombination in G1 preserves centromeric integrity. *Nature* 600: 748–753

618. Young RA (2011) Control of the embryonic stem cell state. *Cell* 144: 940–954

619. Youssef KK, Narwade N, Arcas A, Marquez-Galera A, Jiménez-Castaño R, Lopez-Blau C, Fazilaty H, García-Gutierrez D, Cano A, Galcerán J, *et al* (2024) Two distinct epithelial-to-mesenchymal transition programs control invasion and inflammation in segregated tumor cell populations. *Nat Cancer* 5: 1660–1680

620. Yurchenko AA, Rajabi F, Braz-Petta T, Fassihi H, Lehmann A, Nishigori C, Wang J, Padioleau I, Gunbin K, Panunzi L, *et al* (2023) Genomic mutation landscape of skin cancers from DNA repair-deficient xeroderma pigmentosum patients. *Nat Commun* 14: 2561

621. Zafar A, Khatoon S, Khan MJ, Abu J & Naeem A (2025) Advancements and limitations in traditional anti-cancer therapies: a comprehensive review of surgery, chemotherapy, radiation therapy, and hormonal therapy. *Discov Oncol* 16: 607

622. Zandarashvili L, Langelier M-F, Velagapudi UK, Hancock MA, Steffen JD, Billur R, Hannan ZM, Wicks AJ, Krastev DB, Pettitt SJ, *et al* (2020) Structural basis for allosteric PARP-1 retention on DNA breaks. *Science* 368: eaax6367

623. Zaretsky JM, Garcia-Diaz A, Shin DS, Escuin-Ordinas H, Hugo W, Hu-Lieskovan S, Torrejon DY, Abril-Rodriguez G, Sandoval S, Barthly L, *et al* (2016) Mutations Associated with Acquired Resistance to PD-1 Blockade in Melanoma. *New England Journal of Medicine* 375: 819–829

624. Zeng Y, Arisa O, Peer CJ, Fojo A & Figg WD (2024) PARP inhibitors: A review of the pharmacology, pharmacokinetics, and pharmacogenetics. *Seminars in Oncology* 51: 19–24

625. Zewail-Foote M & Hurley LH (1999) Ecteinascidin 743: a minor groove alkylator that bends DNA toward the major groove. *J Med Chem* 42: 2493–2497

626. Zhang M, Liu C, Tu J, Tang M, Ashrafizadeh M, Nabavi N, Sethi G, Zhao P & Liu S (2025) Advances in cancer immunotherapy: historical perspectives, current developments, and future directions. *Mol Cancer* 24: 136

627. Zhang P, Wei Y, Wang L, Debeb BG, Yuan Y, Zhang J, Yuan J, Wang M, Chen D, Sun Y, *et al* (2014) ATM-mediated stabilization of ZEB1 promotes DNA damage response and radioresistance through CHK1. *Nat Cell Biol* 16: 864–875

628. Zhang S, O'Regan R & Xu W (2020) The emerging role of mediator complex subunit 12 in tumorigenesis and response to chemotherapeutics. *Cancer* 126: 939–948

629. Zhang S, Royer R, Li S, McLaughlin JR, Rosen B, Risch HA, Fan I, Bradley L, Shaw PA & Narod SA (2011) Frequencies of BRCA1 and BRCA2 mutations among 1,342 unselected patients with invasive ovarian cancer. *Gynecologic Oncology* 121: 353–357

630. Zhang T, Kwiatkowski N, Olson CM, Dixon-Clarke SE, Abraham BJ, Greifenberg AK, Ficarro SB, Elkins JM, Liang Y, Hannett NM, *et al* (2016) Covalent targeting of remote cysteine residues to develop CDK12 and CDK13 inhibitors. *Nat Chem Biol* 12: 876–884

631. Zhao D, Wang A, Li Y, Cai X, Zhao J, Zhang T, Zhao Y, Dong Y, Zhou F, Li Y, *et al* (2024) Establishing the homologous recombination score threshold in metastatic prostate cancer patients to predict the efficacy of PARP inhibitors. *J Natl Cancer Cent* 4: 280–287

632. Zhou B, Wang L, Zhang S, Bennett BD, He F, Zhang Y, Xiong C, Han L, Diao L, Li P, *et al* (2016) INO80 governs superenhancer-mediated oncogenic transcription and tumor growth in melanoma. *Genes Dev* 30: 1440–1453

633. Zhou J, Tison K, Zhou H, Bai L, Acharyya RK, McEachern D, Metwally H, Wang Y, Pitter M, Choi JE, *et al* (2025) STAT5 and STAT3 balance shapes dendritic cell function and tumour immunity. *Nature* 643: 519–528

634. Zhou Q, Huang J, Zhang C, Zhao F, Kim W, Tu X, Zhang Y, Nowsheen S, Zhu Q, Deng M, *et al* (2020) The bromodomain containing protein BRD-9 orchestrates RAD51–RAD54 complex formation and regulates homologous recombination-mediated repair. *Nat Commun* 11: 2639

635. Zhu S, Gao H, Jiang D, Guo G, Hou J, Han Y, Zhang C, Hu X, Indulkar S, Kloeber JA, *et al* (2025) Isoform-specific function of NSD3 in DNA replication stress confers resistance to PARP inhibitors in prostate cancer. *Mol Cell* 85: 2673-2687.e8

636. Zimmermann M, Lottersberger F, Buonomo SB, Sfeir A & de Lange T (2013) 53BP1 regulates DSB repair using Rif1 to control 5' end resection. *Science* 339: 700–704

637. Zimmermann M, Murina O, Reijns MAM, Agathanggelou A, Challis R, Tarnauskaitė Ž, Muir M, Fluteau A, Aregger M, McEwan A, *et al* (2018) CRISPR screens identify genomic ribonucleotides as a source of PARP-trapping lesions. *Nature* 559: 285–289

638. Zou L & Elledge SJ (2003) Sensing DNA damage through ATRIP recognition of RPA-ssDNA complexes. *Science* 300: 1542–1548

Université de Strasbourg

Julian Obid
Targeting transcriptional addiction and DNA repair in cancer: From super-enhancer inhibition to synthetic lethality

École Doctorale des Sciences de la Vie et de la Santé STRASBOURG

Résumé

Le cancer reste un défi thérapeutique majeur en raison de l'hétérogénéité tumorale, de l'adaptation cellulaire et de l'émergence de résistances aux traitements. Parmi les vulnérabilités exploitables, la dépendance transcriptionnelle des cellules cancéreuses et leurs altérations des voies de réparation de l'ADN représentent deux axes thérapeutiques particulièrement prometteurs. Dans cette thèse, nous avons étudié le potentiel des ectéinascidines synthétiques, notamment la lurbinectédine et ses dérivés PM14 et PM54, comme inhibiteurs transcriptionnels liant l'ADN capables de cibler ces deux dépendances. Dans un premier temps, nous avons montré que ces molécules perturbent les programmes oncogéniques dépendants des super-enhancers dans le mélanome. En se liant préférentiellement à des promoteurs actifs, riches en CpG et associés à une chromatine ouverte, les ectéinascidines répriment rapidement l'expression de facteurs de transcription et de coactivateurs essentiels, entraînant l'inhibition de programmes oncogéniques spécifiques des états cellulaires du mélanome, y compris ceux associés à la résistance thérapeutique. Dans un second temps, nous avons démontré que ces composés induisent un état fonctionnel de BRCAness dans plusieurs modèles tumoraux BRCA-proficients. Ce mécanisme repose sur une perturbation de l'élongation transcriptionnelle, conduisant à la répression préférentielle de longs gènes impliqués dans la recombinaison homologue et la voie de Fanconi. Cette déficience fonctionnelle de la réparation de l'ADN sensibilise les cellules cancéreuses aux inhibiteurs de PARP et peut restaurer leur efficacité dans des modèles résistants. Ainsi, ce travail met en évidence les ectéinascidines synthétiques comme une classe prometteuse de molécules capables de cibler simultanément l'addiction transcriptionnelle et les vulnérabilités de réparation de l'ADN dans le cancer.

Mots-clés : Cancer, Addiction transcriptionnelle, Super-enhancers, Réparation de l'ADN, Inhibiteurs de PARP

Abstract

Cancer remains a major therapeutic challenge due to tumor heterogeneity, cellular adaptation, and the emergence of treatment resistance. Among exploitable vulnerabilities, transcriptional addiction and defects in DNA repair pathways represent two particularly promising therapeutic axes. In this thesis, we investigated the potential of synthetic ecteinascidins, including lurbinectedin and its derivatives PM14 and PM54, as DNA-binding transcriptional inhibitors capable of targeting these two dependencies. First, we showed that these molecules disrupt super-enhancer-dependent oncogenic programs in melanoma. By preferentially binding active CpG-rich promoters associated with open chromatin, ecteinascidins rapidly repress the expression of key transcription factors and coactivators, leading to the inhibition of melanoma state-specific oncogenic programs, including those associated with therapeutic resistance. Second, we demonstrated that these compounds induce a functional BRCAness state in multiple BRCA-proficient cancer models. Mechanistically, this effect is associated with impaired transcription elongation, resulting in the preferential repression of long genes involved in homologous recombination and the Fanconi anemia pathway. This functional DNA repair deficiency sensitizes cancer cells to PARP inhibitors and can restore PARP inhibitor efficacy in resistant models. Overall, this work identifies synthetic ecteinascidins as a promising class of DNA-binding transcriptional inhibitors capable of simultaneously targeting transcriptional addiction and DNA repair vulnerabilities in cancer. These findings provide a conceptual and therapeutic framework for exploiting transcriptional perturbation to induce DNA repair deficiency and expand the clinical potential of PARP inhibitor-based combinations beyond classical BRCA-mutated tumors.

Keywords: Cancer, Transcriptional Addiction, Super-Enhancers, DNA Repair, PARP Inhibitors